

Oil & Natural Gas Technology

DOE Award No.: DE-FC26-05NT42660

Final Scientific/Technical Report

Analysis Of Critical Permeability, Capillary Pressure And Electrical Properties For Mesaverde Tight Gas Sandstones From Western U.S. Basins

Submitted by:

University of Kansas Center for Research, Inc.
2385 Irving Hill Road
Lawrence, KS 66044

Prepared for:

United States Department of Energy
National Energy Technology Laboratory

June 30, 2009



Office of Fossil Energy

***Solicitation Number: DE-PS26-04NT42072
Subtopic Area: 1-Understanding Tight Gas Resources***

U.S. DOE Contract Number: DE-FC26-05NT42660

***University of Kansas Center for Research, Inc.
and the Kansas Geological Survey
2385 Irving Hill Road
Lawrence, KS 66044-7552***

***Technical Point of Contact - Alan P. Byrnes
voice: 785-864-3965, Fax: 785-864-5317, e-mail: apbyrnes@cox.net
Budgetary/Contractual Point of Contact- Tracie Watkins
voice: 785-864-7288, Fax: 785-864-5025, e-mail: twatkins@ku.edu***

Title of Project:

***Analysis of Critical Permeability, Capillary and Electrical
Properties for Mesaverde Tight Gas Sandstones
from Western U.S. Basins***

***University of Kansas-Kansas Geological Survey
Alan P. Byrnes (Principal Investigator)***

***The Discovery Group, Inc.
Robert M. Cluff, John C. Webb***

Supporting Team Members:

***Kansas Geological Survey– John Victorine, Ken Stalder, Daniel S. Osburn, Andrew
Knoderer, Owen Metheny, Troy Hommertzhaim, and Joshua P. Byrnes***

The Discovery Group Inc. – Daniel A. Krygowski and Stefani Whittaker

ACKNOWLEDGEMENT:

This material is based upon work support by the Department of Energy (National Nuclear Security Administration) under Contract Number DE-FC26-05NT042660

DISCLAIMER:

This report was prepared as an account of work sponsored by an agency of the United States Government. Neither the United States Government nor any agency thereof, nor any of their employees, makes any warranty, express or implied, or assumes any legal liability or responsibility for the accuracy, completeness, or usefulness of any information, apparatus, product, or process disclosed, or represents that its use would not infringe privately owned rights. Reference herein to any specific commercial product, process, or service by trade name, trademark, manufacturer, or otherwise does not necessarily constitute or imply its endorsement, recommendation, or favoring by the United States Government or any agency thereof. The views and opinions of authors herein do not necessarily state or reflect those of the United States Government or any agency thereof.

TABLE OF CONTENTS

TITLE PAGE
DISCLAIMER	i
TABLE OF CONTENTS	ii
LIST OF TABLES	vi
LIST OF FIGURES	vii
LIST OF ACRONYMS	x
EXECUTIVE SUMMARY	xiii
INTRODUCTION	1
I.1 Statement of Problem	1
I.2 Statement of Study Objectives	6
I.3 Report Organization	7
RESULTS AND DISCUSSION	8
Task 1. Research Management Plan	8
Task 1.1 Discussion	8
Task 2. Technology Status Assessment	9
Task 2.1 Result	9
Task 2.1.1 Current State of Information	9
<i>Task 2.1.1.1 Prior studies of Mesaverde Tight Gas Sandstones (TGS)</i>	9
<i>Task 2.1.1.1.1 Porosity</i>	9
<i>Task 2.1.1.1.2 Permeability</i>	10
<i>Task 2.1.1.1.3 Relative Permeability and Critical Gas Saturation</i>	10
<i>Task 2.1.1.1.4 Capillary Pressure</i>	10
<i>Task 2.1.1.1.5 Water Saturation and Cation Exchange Capacity</i>	11
<i>Task 2.1.1.1.6 Scale Dependence of Sgc and Relative Permeability</i>	11
<i>Task 2.1.1.2 Technology/Methodology Being Used</i>	12
<i>Task 2.1.1.3 Limitations of Present Knowledge</i>	12
Task 3. Acquire Data and Materials	13
Task 3.1 Compile Published Advanced Properties Data	13
Task 3.1.1 Task Statement	13
Task 3.1.2 Methods	13
Task 3.1.3 Results	14
Task 3.2 Compile Representative Lithofacies Core and Logs from Major Basins	23
Task 3.2.1 Task Statement	23
Task 3.2.2 Methods	23
Task 3.2.3 Results	24
Task 3.3 Acquire Logs from Sample Wells and Digitize	31
Task 3.3.1 Task Statement	31
Task 3.3.2 Methods	31
Task 3.3.3 Results	31
Task 4. Measure Rock Properties	33
Task 4.1 Measure Basic Rock Properties (k, ϕ , ρ_g) and Select Population	33
Task 4.1.1 Task Statement	33
Task 4.1.2 Methods	33
<i>Task 4.1.2.1 Sample Preparation</i>	33

Task 4.1.2.2 <i>In situ Porosity and Pore Volume Compressibility</i>	33
Task 4.1.2.3 <i>Routine Helium Porosity and Grain Density</i>	35
Task 4.1.2.4 <i>Routine Air and In Situ Klinkenberg Permeability</i>	35
Task 4.1.2.5 <i>Impact of Drying vs. Native State or Restored State Analysis on k</i> ...	36
Task 4.1.3 Results	38
Task 4.1.3.1 <i>Grain Density</i>	39
Task 4.1.3.2 <i>Porosity</i>	40
Task 4.1.3.2.1 <i>In situ Porosity and Pore Volume Compressibility</i>	43
Task 4.1.3.3 <i>Permeability</i>	53
Task 4.1.3.4 <i>Permeability-Stress Dependence</i>	58
Task 4.1.3.5 <i>Porosity-Permeability Relationship</i>	63
Task 4.1.3.5.1 <i>Predictive equations for porosity-permeability</i>	64
Task 4.2 Measure Critical Gas Saturation	70
Task 4.2.1 Task Statement.....	70
Task 4.2.2 Methods.....	70
Task 4.2.2.1 <i>Air-Mercury Critical Nonwetting Phase Saturation</i>	70
Task 4.2.2.2 <i>Air-Brine Critical Gas Saturation Measurement</i>	74
Task 4.2.3 Results and Discussion	77
Task 4.2.3.1 <i>Executive Summary</i>	77
Task 4.2.3.2 <i>Introduction</i>	78
Task 4.2.3.3 <i>Previous Work</i>	80
Task 4.2.3.3.1 <i>Gas Relative Permeability</i>	80
Task 4.2.3.3.2 <i>Critical-Gas Saturation</i>	85
Task 4.2.3.3.3 <i>Percolation Theory</i>	86
Task 4.2.3.4 <i>Critical Non-wetting Phase Saturation</i>	88
Task 4.2.3.5 <i>Critical Gas Saturation</i>	91
Task 4.2.3.6 <i>Discussion</i>	95
Task 4.2.3.6.1 <i>Pore Networks and k_{rg}, S_{gc}</i>	96
Task 4.2.3.7 <i>Conclusions</i>	101
Task 4.3 Measure <i>In situ</i> and Routine Capillary Pressure.....	103
Task 4.3.1 Task Statement.....	103
Task 4.3.2 Methods.....	104
Task 4.3.2.1 <i>Unconfined Capillary Pressure</i>	104
Task 4.3.2.2 <i>Confined Capillary Pressure</i>	104
Task 4.3.2.3 <i>Unconfined, Cycling Drainage-Imbibition Capillary Pressure</i>	106
Task 4.3.3 Results.....	108
Task 4.3.3.1 <i>Capillary Pressure Drainage-Imbibition Hysteresis</i>	110
Task 4.3.3.2 <i>Unconfined and Confined Capillary Pressure</i>	118
Task 4.4 Measure Electrical Properties	127
Task 4.4.1 Task Statement.....	127
Task 4.4.2 Methods.....	127
Task 4.4.3 Results.....	130
Task 4.4.3.1 <i>Archie Porosity Exponent versus Porosity</i>	130
Task 4.4.3.2 <i>Salinity Dependence of Archie Porosity Exponent and CEC</i>	136
Task 4.5 Measure Geologic and Petrologic Properties.....	141
Task 4.5.1 Task Statement	141

Task 4.5.2 Methods.....	141
<i>Task 4.5.2.1 Core and Sample Description</i>	143
<i>Task 4.5.2.2 Thin Section Petrography</i>	145
Task 4.5.3 Results.....	147
<i>Task 4.5.3.1 Lithofacies and Sedimentary Structures</i>	151
<i>Task 4.5.3.2 Depositional Environment</i>	151
<i>Task 4.5.3.3 Mineralogy</i>	152
<i>Task 4.5.3.4 Diagenesis</i>	153
<i>Task 4.5.3.5 Lithologic Influence on Porosity and Permeability</i>	154
<i>Task 4.5.3.6 Porosity in the Mesaverde Group</i>	154
Task 4.6 Perform Standard Log Analysis.....	167
Task 4.6.1 Task Statement.....	167
Task 4.6.2 Methods.....	167
<i>Task 4.6.2.1 Basic Log Analysis Parameters</i>	167
<i>Task 4.6.2.2 Shale Volume</i>	168
<i>Task 4.6.2.4 Effective Porosity</i>	170
<i>Task 4.6.2.5 Water Saturation Computation</i>	172
<i>Task 4.6.2.6 Permeability</i>	174
<i>Task 4.6.2.7 Filter results for Coals and Bad Hole</i>	175
Task 4.6.3 Results.....	176
Task 5. Build Database and Web-Based Rock Catalog	178
Task 5.1 Compile Published and Measured Data into Database	178
Task 5.1.1 Task Description.....	178
Task 5.1.2 Methods	178
Task 5.1.3 Results	178
Task 5.2 Modify Existing Web-Based Software to Provide Data Access.....	180
Task 5.2.1 Task Description.....	180
Task 5.2.2 Methods	180
Task 5.2.3 Results	180
Task 6. Analyze Wireline-Log Signatures and Analysis Algorithms	181
Task 6.1 Compare Log and Core Properties.....	181
Task 6.1.1 Task Statement.....	181
Task 6.1.2 Methods.....	181
Task 6.1.3 Results.....	182
<i>Task 6.1.3.1 Log-Core Porosity Comparisons</i>	184
<i>Task 6.1.3.2 Core Permeability vs. Log Permeability Comparisons</i>	186
<i>Task 6.1.3.3 Permeability from NMR Logs</i>	188
<i>Task 6.1.3.4 Water Saturation</i>	192
<i>Task 6.1.3.5 Rock Type Identification from Log Data</i>	195
<i>Task 6.1.3.5.1 Gamma Ray and Vshale</i>	195
<i>Task 6.1.3.5.2 Deep Resistivity</i>	196
<i>Task 6.1.3.5.3 Bulk Density, neutron Porosity, and Photoelectric Factor</i>	196
Task 6.2 Evaluate Results and Determine Log-Analysis Algorithm Inputs.....	200
Task 6.2.1 Methods	200
<i>Task 6.2.1.1 Porosity Models</i>	200
<i>Task 6.2.1.2 Permeability Modeling Using Basin-Specific Phi-K Relations</i>	200

<i>Task 6.2.1.3 Advanced Water Saturation Model</i>	202
<i>Task 6.2.1.4 Stepwise Log Analysis Procedure</i>	203
Task 6.2.2 Results	205
Task 7. Simulate Scale-Dependence of Relative Permeability	207
Task 7.1 Construct Basic Bedform Architecture Simulation Models	207
Task 7.2 Perform Numerical Simulation of Flow for Basic Bedform Architectures	209
Task 8. Technology Transfer	218
Task 8.1 Technology Transfer	218
Task 8.1.1 Early Project Presentations	218
Task 8.1.2 Project Website	218
Task 8.1.3 Technical Presentations	218
Task 8.2 Reporting Requirements	228
REFERENCES	229
APPENDICES	248
Porosity, Permeability and Grain Density Data	A1-1
Pore Volume Compressibility Data	A2-1
Critical Gas Saturation Data	A3-1
Capillary Pressure Data	A4-1
Electrical Resistivity Data	A5-1

LIST OF TABLES

Table 3.1.3.1 List of 88 references relevant to Mesaverde low-permeability geologic and petrophysical properties	16
Table 3.2.1 List of wells sampled	25
Table 3.3.1 List of wells with LAS files and used in study	32
Table 4.1.1 Summary statistics for grain density by basin	39
Table 4.1.2 Summary statistics for routine helium by basin	42
Table 4.1.3 Summary statistics for porosity by basins	52
Table 4.1.4 Summary statistics for <i>in situ</i> Klinkenberg Permeability by basins	55
Table 4.1.5 Permeability stress dependence relationships.....	59
Table 4.1.6 ANN parameters for permeability prediction	68
Table 4.1.7 Summary of Klinkenberg permeability equations by basin	69
Table 4.2.1 List of abbreviations and symbols in critical gas analysis	79
Table 4.2.2 General increase of average S_{gc} with decreasing PSS RC4 values	94
Table 4.3.1 Land C values for selected sample populations	115
Table 4.5.1 List of wells with core descriptions	142
Table 4.5.2 Macroscopic rock digital classification system	144
Table 4.5.3 Depth of epoxy impregnation for various conditions	146
Table 4.5.4 Porosity network types of the Mesaverde Group.....	156
Table 6.1.1 Core to log comparison plots included in Excel	182
Table 6.2.1 Porosity-permeability regression parameters determined by basin	201
Table 7.2.1 Reservoir simulation base model parameters	211

LIST OF FIGURES

Figure 1.1	EIA estimate of future natural gas supply	2
Figure 1.2	EIA estimate of future unconventional natural gas supply	2
Figure 3.1.1	Gas relative permeability vs. water saturation – published studies.....	18
Figure 3.1.2	Gas relative perm curves from published studies	19
Figure 3.1.3	Piceance Basin core porosity vs. water saturation	20
Figure 3.1.4	Piceance Basin core porosity vs. water saturation MWX2	21
Figure 3.1.5	Routine core analysis water saturation vs. cation exchange capacity	22
Figure 3.2.1	Sampled well locations.....	26
Figure 3.2.2	Number of wells sampled by basin and source	27
Figure 3.2.3	Number of core plugs by basin	28
Figure 3.2.4	Distribution of core sample depths by basin	29
Figure 3.2.5	Routine helium porosity distribution by basin	30
Figure 4.1.1	Grain density distribution for all basins	39
Figure 4.1.2	Grain density distribution by basin	40
Figure 4.1.3	Porosity distribution for all samples	41
Figure 4.1.4	Porosity distribution by basin	41
Figure 4.1.5	Histogram of ratio of paired plug porosities.....	43
Figure 4.1.6	Cross-plot of in situ/ambient pore volume versus confining pressure	45
Figure 4.1.7	Cross-plot of slope of log-linear curves in Fig. 4.1.6.....	46
Figure 4.1.8	Cross-plot of intercept of log-linear curves in Fig. 4.1.6	46
Figure 4.1.9	Cross-plot of pore volume compressibility slope function.....	47
Figure 4.1.10	Cross-plot of pore volume compressibility intercept function.....	47
Figure 4.1.11	Pore volume compressibility vs. net stress.....	48
Figure 4.1.12	Cross-plot of routine porosity and <i>in situ</i> porosity	49
Figure 4.1.13	Cross-plot of estimated <i>in situ</i> porosity versus routine porosity	51
Figure 4.1.14	Distribution of <i>in situ</i> Klinkenberg permeability for all samples.....	54
Figure 4.1.15	Distribution of <i>in situ</i> Klinkenberg permeability by basin.....	54
Figure 4.1.16	Cross-plot Klinkenberg constant, <i>b</i> , vs. Klinkenberg permeability	57
Figure 4.1.17	Histogram of ratio of paired plug <i>in situ</i> Klinkenberg permeability	58
Figure 4.1.18	Cross-plot of <i>in situ</i> Klinkenberg permeability vs. routine air permeability...62	
Figure 4.1.19	Cross-plot of <i>in situ</i> Klinkenberg permeability vs. routine air permeability...63	
Figure 4.1.20	Cross-plot of <i>in situ</i> Klinkenberg permeability vs. calculated <i>in situ</i>	64
Figure 4.1.21	Cross-plot of <i>in situ</i> Klinkenberg permeability vs. calculated <i>in situ</i>	66
Figure 4.1.22	Cross-plot of measured vs. ANN-predicted permeability	67
Figure 4.1.23	Cross-plot of <i>in situ</i> Klinkenberg permeability vs. calculated <i>in situ</i>	68
Figure 4.2.1	Capillary pressure samples' cross-plot of permeability vs. porosity.....	71
Figure 4.2.2	Schematics of high-pressured mercury intrusion apparatus.....	73
Figure 4.2.3	Illustration of the estimation of critical mercury saturation	74
Figure 4.2.4	Schematic of high pressure air-brine critical gas apparatus	76
Figure 4.2.5	Relative gas permeability curves for 43 samples	82
Figure 4.2.6	Gas relative permeability measured at a single water saturation	83
Figure 4.2.7	Relative gas permeability curves.....	85
Figure 4.2.8	Critical mercury saturation vs. Klinkenberg permeability	89
Figure 4.2.9	Cross-plot of contained S from capillary pressure curves.....	91

Figure 4.2.10 Distribution histogram of critical air-brine saturation.....	92
Figure 4.2.11 Cross-plot of air-brine critical gas saturation vs. <i>in situ</i> permeability	93
Figure 4.2.12 Conceptual pore network models	97
Figure 4.2.13 Example of critical saturation in a cross-bedded sandstone.....	100
Figure 4.3.1 Flow schematic of confined and unconfined mercury intrusion apparatus	107
Figure 4.3.2 Air-mercury capillary pressure curves for selected samples.....	109
Figure 4.3.3 Air-mercury capillary pressure curves for selected samples.....	110
Figure 4.3.4 Air-mercury successive drainage and imbibition.....	111
Figure 4.3.5 Example air-mercury successive drainage and imbibition curves	112
Figure 4.3.6 Cross-plot of residual vs. initial non-wetting saturation	114
Figure 4.3.7 Cross-plot of residual and initial non-wetting phase saturation	116
Figure 4.3.8 Cross-plot of residual and initial non-wetting phase saturation	117
Figure 4.3.9 Example of <i>in situ</i> and unconfined air-mercury capillary pressure curves	121
Figure 4.3.10 Cross-plot of entry pore diameter, air-mercury and gas column height.....	125
Figure 4.3.11 Cross-plot of air-mercury threshold vs. permeability.....	126
Figure 4.4.1 Schematic of resistivity apparatus.....	129
Figure 4.4.2 Archie porosity exponent vs. <i>in situ</i> porosity.....	132
Figure 4.4.3 Cross-plot of <i>in situ</i> Archie porosity exponent vs. <i>in situ</i> porosity	133
Figure 4.4.4 Cross-plot of <i>in situ</i> Archie porosity exponent vs. log <i>in situ</i> porosity	134
Figure 4.4.5 Relationship of Waxman-Smits model parameters	137
Figure 4.4.6 Core conductivity vs. saturating brine core conductivity	138
Figure 4.4.7 Cation Exchange Capacity, Qv, versus permeability	138
Figure 4.4.8 Salinity-independent m^* versus porosity	139
Figure 4.4.9 Cross-plot of Archie porosity exponent vs. brine resistivity.....	140
Figure 4.5.1 Correlation of digital rock type with wireline by response.....	148
Figure 4.5.2 Example of core description of coastal mudstones in the Mesaverde.....	149
Figure 4.5.3 Example of core description of fluvial sandstones in the Mesaverde	150
Figure 4.5.4 Mesaverde lithofacies with rock type digital classification	157
Figure 4.5.5 Lithic (QFL) ternary plot comparing sandstones composition between basins	158
Figure 4.5.6 QFL vs environment of deposition, Uinta and Piceance Basins	158
Figure 4.5.7 Ternary plot of lithic fragment composition for Uinta and Piceance Basin.....	159
Figure 4.5.8 Example from Piceance Basin illustrating influence of grain size.....	159
Figure 4.5.9 Ternary plot of porosity distribution for sandstones of the Mesaverde Group	160
Figure 4.5.10 Mesaverde thin section photomicrographs of type I porosity	161
Figure 4.5.11 Mesaverde thin section photomicrographs of type II porosity	162
Figure 4.5.12 Mesaverde thin section photomicrographs of type III porosity	163
Figure 4.5.13 Mesaverde thin section photomicrographs of type IV porosity	164
Figure 4.5.14 Mesaverde thin section photomicrographs of type V porosity	165
Figure 4.5.15 Example from Piceance basin influence of pore type	166
Figure 4.6.1 Example of plot where clean and shale values of the GR are chosen	168
Figure 4.6.2 Neutron-density cross-plot used to calculate a cross-plot porosity PHIDN.....	169
Figure 4.6.3 Multiple cross-plots to visually choose the locally determined shale porosity	170
Figure 4.6.4 Example of porosity comparison plot from standard log analysis	172
Figure 4.6.5 Example of an interactive Pickett plot used to calculate R_w	173
Figure 4.6.6 Depth plot showing the BVWI value that was chosen.....	174
Figure 4.6.7 Examples of wireline log presenting standard log analysis interpretation.....	176

Figure 4.6.8 Example of porosity comparison plot from standard log analysis	177
Figure 6.1.1 Total density porosity vs. core porosity	185
Figure 6.1.2 Effective density porosity vs. core porosity	185
Figure 6.1.3 Effective neutron-density vs. core porosity	186
Figure 6.1.4 Depth plot comparison of log-predicted and core properties	188
Figure 6.1.5 CMR porosity and permeability compared to standard density-neutron	190
Figure 6.1.6 CMR porosity and permeability compared to PHINDE	191
Figure 6.1.7 Cross-plot of water saturation vs. iso-bulk volume water	193
Figure 6.1.8 Pressure-depth plot for the MWX site	194
Figure 6.1.9 Volume of shale vs. rock type number	197
Figure 6.1.10 Log of deep resistivity vs. rock type number	198
Figure 6.1.11 NHPI-DHPI separation vs. rock type number	199
Figure 6.2.1 Example of water saturation computed using variable m	205
Figure 6.2.2 Example of water saturation computed using the variable m	206
Figure 7.1.1 Conceptual pore network models	208
Figure 7.2.1 Flow end member upscaling equations	209
Figure 7.2.2 CMG IMEX s simulation model	214
Figure 7.2.3 Cumulative gas recovery vs. time for models with varying permeability	215
Figure 7.2.4 Cross-plot of the cumulative gas and gas production rate	216
Figure 7.2.5 Cross-plot showing the dependence of incremental cumulative gas	217

LIST OF ACRONYMS

a = Archie equation constant, dimensionless
AAPG = American Association of Petroleum Geologists
C = Land equation constant
cc = cubic centimeter, cm^3
CEC = Cation exchange capacity (mequivalents/liter)
D = Fractal dimension
 D = pore throat diameter (microns)
DOE = Department of Energy
 D_{te} = Threshold entry pore diameter (microns)
E = Euclidean dimension
 F = Fraction of total network sites where gas nucleation occurs
g = gram
GD = grain density (g/cm^3)
GUI = graphical user interface
Hg = mercury
 H_{te} = Threshold entry gas column height (ft)
 K = Permeability, mD
K = thousands, x1000
KGS = Kansas Geological Survey
kPa = Kilo Pascal, 1 kPa = 0.001 MPa =
 k_{ik} = *in situ* Klinkenberg permeability, millidarcies
 k_{mk} = geometric mean of *in situ* and routine Klinkenberg permeability (mD)
 k_{rg} = Relative permeability to gas, fraction (v/v)
 k_{rg,S_w} = Relative permeability to gas at a specific water saturation S_w , fraction (v/v)
KU = University of Kansas
KUCR = University of Kansas Center for Research, Inc.
KUERC = University of Kansas Energy Research Center
L = Network size, number of nodes
ln = natural logarithm
 $\log R_{wX}$ = log10 of resistivity of brine at salinity X
 $\log R_{w40K}$ = log10 of resistivity of 40K ppm NaCl = 0.758.
 m = Archie cementation (porosity) exponent, (dimensionless)
 m_1 = matrix porosity exponent
 m_2 = fracture or touching vug porosity exponent
 m_{40K} = Archie porosity exponent at 40,000 ppm NaCl,
mD = millidarcy, 1 mD = $9.87 \times 10^{-4} \mu\text{m}^2$
Mesaverde = Mesaverde Group
MICP = mercury intrusion capillary pressure
MPa = Mega Pascal, 1 MPa = 1000 kPa =
 $m_x = m$ at salinity X
 n = Archie saturation exponent, dimensionless
n = number
 N_{\perp} = Series network
 $N_{\perp d}$ = Discontinuous series network

$N_{//}$ = Parallel network
 NaCl = sodium chloride
 NCS = net confining stress
 nD = nanodarcy, 1×10^{-6} mD
 NETL = National Energy Technology Laboratory
 NMR = nuclear magnetic resonance
 N_p = Percolation network, random
 $^{\circ}\text{F}$ = temperature degrees Fahrenheit
 P = average net effective confining pressure (psi)
 P_c = capillary pressure, psia
 $P_{c_{S_{gc,high}}}$ = Capillary pressure at $S_{gc,high}$
 $P_{c_{lab}}$ = laboratory-measured capillary pressure (psia)
 $P_{c_{res}}$ = capillary pressure (psia) at reservoir conditions
 pdf = Adobe Acrobat portable document file
 ppm = parts per million
 PTTC = Petroleum Technology Transfer Council
 PPTD = Principal pore throat diameter
 psi = pound per square inch, 1 psi = 6.89 kPa = 0.00689 MPa
 psia = pound per square inch absolute
 P_{te} = Capillary pressure threshold entry pressure, psi
 P_{te} = threshold entry pressure, psi
 R_o = resistivity of brine saturated rock, ohm-m²/m
 R_w = resistivity of brine, ohm-m²/m
 scc = standard cubic centimeter
 $S_{g,Pc-Sgc,high}$ = Gas saturation at $P_{c_{S_{gc,high}}}$
 S_{gc} = Critical gas saturation, expressed as a fractional (v/v) hydrocarbon saturation ($1-S_w$), saturation below which $k_{rg} = 0$
 $S_{gc,low}$ = Lowest critical gas saturation in parallel network, fraction (v/v)
 $S_{gc,high}$ = Highest critical gas saturation in series network, fraction (v/v)
 Slope_{m-Rw} = slope of m_{Rw} versus $\log R_w$ for an individual sample
 S_{nwc} = critical non-wetting phase saturation
 S_{nwi} = initial non-wetting phase saturation
 S_{nwi} = non-wetting saturation initial, fractional percent of pore volume
 S_{nwr} = non-wetting saturation residual to imbibition, fractional percent of pore volume
 SPE = Society of Petroleum Engineers
 S_w = Water (or more generally wetting phase) saturation, fraction (v/v) or percent depending on context
 S_{wc} = Critical water saturation, fraction (v/v), saturation below which $k_{rw} = 0$
 $S_{wc,g}$ = Critical water saturation, fraction (v/v) with respect to gas drainage, saturation at which $k_{rg} = 1$ and below which $k_{rg} = 1$
 S_{wirr} = “irreducible” wetting phase saturation
 S_{wirr} = “irreducible” wetting saturation, fraction of pore volume
 Tcf = trillion cubic feet
 TDG = The Discovery Group Inc.
 TGS = tight gas sandstone(s)
 USDOE = United States Department of Energy

USEIA = United States Energy Information Administration
V = System volume (v)
XML = Extensible Mark-up Language

β = pore volume compressibility ($10^{-6}/\text{psi}$)

β_0 = linear regression intercept

β_1 = linear regression slope

ϕ = porosity, percent or fraction of bulk volume depending on context

ϕ_1 = matrix porosity

ϕ_2 = fracture or touching vug porosity

σ = interfacial tension (dyne/cm)

θ = contact angle, degrees

EXECUTIVE SUMMARY

U.S. Energy Information Administration gas supply estimates predict that Unconventional gas sources will be the dominant source of U.S. natural gas supply for at least the next two decades. Mesaverde Group tight gas sandstones will play an important role. To understand the reservoir properties accurate tools for formation evaluation are needed. This project provides petrophysical formation evaluation tools. Tasks involved included a review of the research plan by DOE (Task 1); initial technology assessment for DOE (Task 2); collection and consolidation of published advanced rock properties data into a publicly accessible digital database (Task 3.1); collection of 2216 (300 in original proposal) rock samples, with digital wireline logs, where available, from 44 wells in six basins (Washakie - 11; Uinta - 8; Piceance - 8; Greater Green River - 7; Wind River - 4; Powder River - 6; Sand Wash - 2) including seven cores and wells contributed by six petroleum companies (3.2). Measurement of basic petrophysical properties (Task 4.1). Measurements on selected samples included: 1) drainage critical gas saturation (4.2); routine and *in situ* mercury intrusion capillary pressure analysis (4.3); porosity exponent and multi-salinity electrical conductivity measurements (4.4); geologic properties including core description, thin-section microscopy, including diagenetic and point-count analysis (4.5); and standard wireline log analysis (4.6). The compiled published data and data measured in the study were input in a database (Task 5.1); and are provided online as a web-based database (5.2). Core and wireline log-calculated properties were compared and algorithms developed for improved calculation of reservoir properties from log response (Task 6). The scale dependence of critical gas saturation was evaluated (Task 7). An active web-based, publication, and short-course technology transfer program was conducted (Task 8) including presentation of all data on the project website (<http://www.kgs.ku.edu/mesaverde>).

Advanced rock properties data were compiled from 88 published studies. A total of 2216 core plugs were obtained representing 1182 original plugs (A), 776 paired plugs (B), and 258 additional pair plugs (C). This sampling represents approximately four times more original plugs than the 300 core plugs proposed and six times as many paired plugs (proposed n=150). Core samples range in depth from 124-16,723 ft, reflecting the range in depth of the Mesaverde for the basins studied. The cores also represented the range of porosity, 0-25%, and *in situ* Klinkenberg permeability, 0.000001 mD-200 mD.

Grain density distribution averages 2.653 ± 0.04 g/cc exhibiting a slight difference in distribution among basins. *In situ* porosity was correlated with routine porosity and shown to follow a crack compressibility model ($\phi_i/\phi_o = A \log P_e + B$) with compressibility increasing with decreasing porosity. The Klinkenberg constant, b , increases with decreasing permeability and *in situ* Klinkenberg permeability (mD) can be related to routine air permeability using either $\log k_{ik} = 1.34 \log k_{air} - 0.6$ or $\log k_{ik} = -0.0088(\log k_{air})^3 - 0.0716(\log k_{air})^2 + 1.366 \log k_{air} - 0.4574$. Permeability can be predicted within an approximate standard error of $\pm 3.5X$ using: $\log k_{ik} = C_1 \phi_i + C_2 R C_{2 \log} + C_3$ where the coefficients are defined for three major lithofacies by basin.

Critical gas saturation measurements, performed on 150 lithologically diverse samples of variable porosity and permeability, support the commonly applied assumption that $S_{gc} < 0.05$ at core scale but is scale dependent. Heterolithic samples indicate the dependence of S_{gc} on pore network architecture. Concepts from percolation theory and upscaling indicate that S_{gc} varies among four pore network architecture models: 1) percolation (N_p); 2) parallel ($N_{//}$); 3) series (N_{\perp}); and 4) discontinuous series ($N_{\perp d}$). Analysis suggests that S_{gc} is scale- and bedding-architecture dependent in cores and in the field. The models suggest that S_{gc} is likely to be low in

laminated and massive-bedded sandstones but in cross-bedded lithologies exhibiting series network properties, S_{gc} can range widely but can reach high values (e.g., $S_{gc} < 0.6$).

Hysteresis drainage and imbibition capillary pressure measurements on 33 samples show that residual and initial non-wetting phase saturation can be related by a Land-type relation ($1/S_{nwr}^* - 1/S_{nwi}^* = C$). Routine and *in situ* mercury injection capillary pressure analysis on 81 core pairs show that capillary pressure measurements on low-permeability sandstones are significantly influenced by confining stress, consistent with observed permeability changes. Threshold entry pressure increases with decreasing permeability. *In situ* and unconfined curves for high-permeability cores ($k_{ik} > 1$ mD) are nearly identical. With decreasing permeability the difference between unconfined and *in situ* threshold entry pressure increases. For all pairs this difference is greatest at the threshold entry pressure and decreases with decreasing wetting-phase saturation. It can be interpreted that confining stress exerts principal influence on the largest pore throats and that pore throats accessed at non-wetting phase saturations below approximately 50% are not significantly affected by confining stress.

A total of 907 resistivity measurements on 308 core samples were performed at various salinities. These data indicate that resistivity in these rocks is influenced by both conductive clays and pore architecture. Contrary to conventional models, the Archie porosity exponent decreases for all salinities with decreasing porosity below approximately $\phi_i=6\%$.

Over 550 core images were obtained and 150 thin sections micro-photographed and analyzed. Point-count data provided the basis for lithologic characterization and porosity typing. Rock lithologic properties were shown to correlate (and probably control/influence) petrophysical properties. Differences between properties of marine and fluvial rocks are evident.

Both Standard and advanced log analysis was performed on all the primary wells. Wireline log-calculated properties (ϕ , S_w , Lithology) were compared with core-derived properties. A zoned grain density model based on geologic knowledge of the section, tied to core grain densities, offers the best approach for single-log porosity determination. Overall, the shale corrected density-neutron cross-plot porosity is the best predictor of *in situ* porosity.

A series of models were analyzed that parametrically investigate the role of total bed thickness, thin high permeability bed permeability, and vertical permeability on cumulative gas recovery. The influence of a single 1-foot (0.3 m) thick higher permeability bed on cumulative gas production can be very significant.

Over 9 gigabytes of data are available for download from the Project Website (<http://www.kgs.ku.edu/mesaverde/>) comprising 1) Excel workbooks containing tables of data from previous studies; 2) Excel workbooks containing data for all petrophysical measurements performed in this study including: 2,102 helium porosity, 2,075 routine air permeability, 2,062 *in situ* Klinkenberg permeability, 2,101 grain density measurements, 907 electrical resistivity measurements, 301 mercury intrusion capillary pressure analyses, 150 air-brine critical gas saturation measurements, 113 pore volume compressibility analyses, 310 air-brine *in situ* porosity measurements; 550 core slab images representing the range of lithofacies exhibited by the Mesaverde in the six basins studied; 750 thin-section photomicrographs from 41 wells; 6,447 feet (2,054 m) of digital core descriptions presented both in Excel workbook format and in graphical core descriptions for 42 wells from 6 basins; graphical core descriptions of core from 42 wells; 21 standard wireline log analyses; 21 advanced wireline log analyses; pdf files of all technical slide and poster presentations; pdf files of all technical quarterly reports. Two publications, seven technical presentations, a one-day workshop at the AAPG Annual Convention, and technical talks at several society lunches were presented.

INTRODUCTION

I.1 Statement of Problem

Although prediction of future natural gas supply is complicated by uncertainty in such variables as demand, liquefied natural gas supply price and availability, coalbed methane and gas shale development rate, and pipeline availability, all U.S. Energy Information Administration gas supply estimates to date have predicted that Unconventional gas sources will be the dominant source of U.S. natural gas supply for at least the next two decades (Fig. 1.1; the period of estimation). Among the Unconventional gas supply sources, Tight Gas Sandstones (TGS) will represent 50-70% of the Unconventional gas supply in this time period (Fig. 1.2). Rocky Mountain TGS are estimated to be approximately 70% of the total TGS resource base ([USEIA, 2005](#)) and the Mesaverde Group (Mesaverde) sandstones represent the principal gas productive sandstone unit in the largest Western U.S. TGS basins including the basins that are the focus of this study (Washakie, Uinta, Piceance, northern Greater Green River, Wind River, Powder River). Industry assessment of the regional gas resource, projection of future gas supply, and exploration programs require an understanding of reservoir properties and accurate tools for formation evaluation. The goal of this study is to provide petrophysical formation evaluation tools related to relative permeability, capillary pressure, electrical properties and algorithms for wireline log analysis. Detailed and accurate moveable gas-in-place resource assessment is most critical in marginal gas plays and there is need for quantitative tools for definition of limits on gas producibility due to technology and rock physics and for defining water saturation.

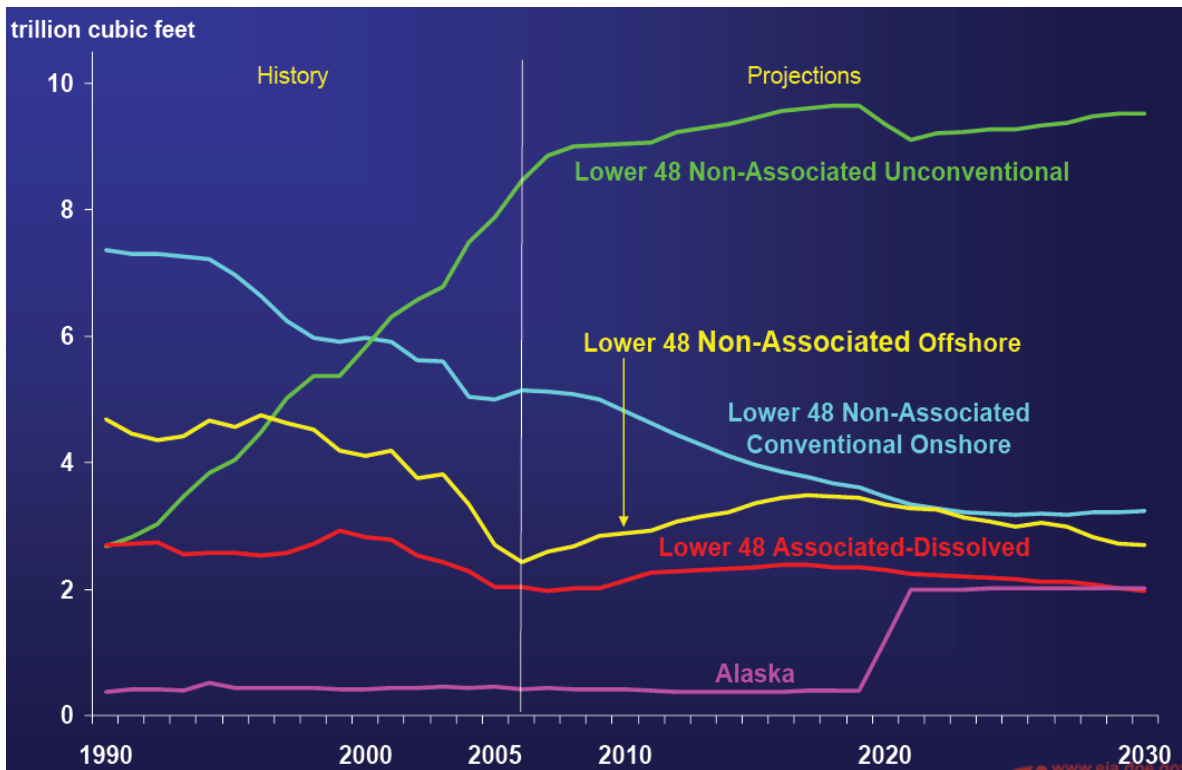


Figure 1.1 – Energy Information Administration prediction of future natural gas supply sources showing Lower 48 Unconventional sources will represent nearly 50% of consumption ([Caruso, 2008](#)).

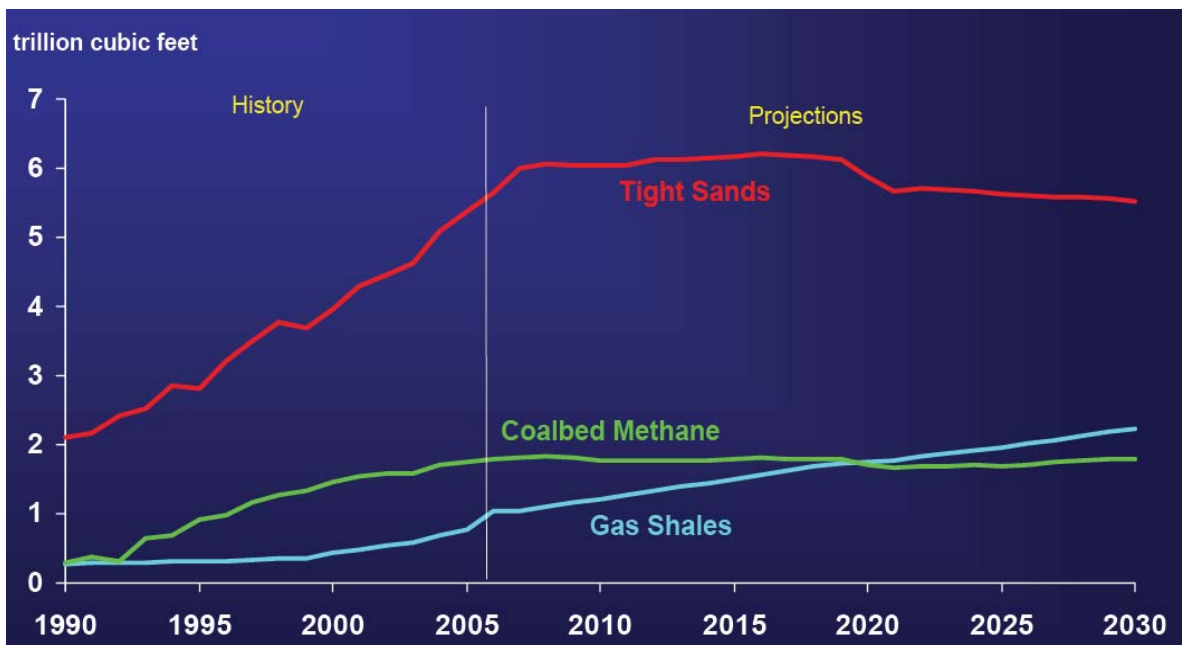


Figure 1.2 – Energy Information Administration prediction of future natural gas unconventional supply sources showing tight gas sandstones represent over half of unconventional supply ([Caruso, 2008](#)).

The results of this study address fundamental questions concerning: 1) gas storage; 2) gas flow; 3) capillary pressure; 4) electrical properties; 5) facies and upscaling issues; 6) wireline log interpretation algorithms; and 7) providing a web-accessible database of advanced rock properties. The following text briefly discusses the nature of these questions. Section I.2 briefly discusses the objective of the study with respect to the problems reviewed.

1) Gas Storage - Issues with gas volume or storage are principally related to porosity, gas saturation, and fluid properties. Fluid properties have been characterized in previous studies and gas saturation is defined by capillary pressure properties and wireline log response interpretation which are discussed separately. Routine (under no confining stress) porosity measurement in TGS is performed by commercial laboratories meeting quality control standards. Although routine helium porosity is commonly measured, the influence of confining stress on porosity has not been thoroughly investigated. Further, the pore volume compressibility, or change in pore volume with change in net effective confining stress, has not been widely reported nor well characterized for the Mesaverde. This issue is important because it is necessary to know: 1) how to correct higher routine porosity to reservoir (*in situ*) conditions; and 2) how *in situ* porosity changes with net effective stress increase associated with reservoir pore pressure decrease as the result of gas production.

2) Gas Flow - All assessments of gas resource are based on assumptions concerning gas relative permeability and, implicitly, the critical gas saturation (S_{gc}) or the minimum gas saturation at which gas flows. This saturation defines the beginning of the gas relative permeability curve. Some assessments have assumed that if gas is present, its' recovery is only a matter of price and/or technology. This premise is not valid if gas saturations are less than or near critical saturation. Gas saturation less than or equal to S_{gc} can be achieved in nature by: 1) highly local microscopic gas generation, such as from organic macerals, that have generated gas but the gas never formed a continuous phase across the pore system; 2) the rock has undergone water imbibition, either due to gas pressure decrease or water pressure increase, and the gas phase is trapped and represents a residual phase to water imbibition; 3) the gas entered the pore system under capillary pressure conditions existing during the gas entry but the rock has since undergone further compaction or diagenetic alteration and now exhibits different capillary

pressure properties; or 4) the gas is mobile but is near S_{gc} rather than at a gas saturation (S_g) significantly greater than S_{gc} . If S_{gc} is incorrectly interpreted to be low (e.g., $S_{gc} = 2\%$), when it is actually high (e.g., $S_{gc} = 30\%$) then for a measured gas saturation near 30% the reservoir would be incorrectly interpreted to contain significant mobile gas when the gas would be only incipiently mobile. Limited research has been done in this area and published data can be interpreted to indicate that S_{gc} increases with decreasing permeability. This would eliminate some gas from being produced and from resource base estimates. Understanding the minimum gas saturation necessary for gas flow (S_{gc}) is fundamental to defining the tight gas sandstone resource and is particularly critical to quantify in marginal resources.

3) Capillary Pressure - While there is some published work on the influence of confining stress on permeability and porosity in tight gas sandstones, little work has been done on the impact of confining stress on capillary pressure. In addition, most capillary pressure studies of TGS focus on the drainage capillary pressure curve and have not investigated or reported on the imbibition capillary pressure or on capillary pressure hysteresis where saturations change under a series of drainage and imbibition cycles beginning and ending at different initial and final saturations. There is a substantial body of work on conventional reservoirs that suggests the effects are substantial.

4) Electrical Properties - Extensive work has been done defining regional water composition, but there is less published work characterizing the effect of excess surface conductance or cation exchange (Waxman-Smits) effects on the conductivity of partially saturated Mesaverde rocks. In Mesaverde reservoirs diagenetic clays with high cation exchange capacity can be common and water salinities can often be fresh (<25,000 ppmw total dissolved solids). These conditions can lead to low resistivity for which the standard Archie ([1942](#)) analysis of wireline electric log response must be modified with some type of shaly sandstone approach. Mesaverde studies published to date have focused primarily on the Multiwell Experiment (MWX) in the Piceance Basin. In addition, work has been presented results for rocks with porosity generally greater than 6% porosity but little has been reported for rocks with porosity less than 6%. These rocks are generally considered to not be “pay” but reservoir flow simulation shows that these rocks represent storage for vertically adjacent beds where flow is significant. Therefore the accurate

determination of water and gas saturation in these rocks is important to resource assessment. To measure this using wireline logs it is necessary to both understand the porosity exponent of these rocks and how electrical conduction changes with salinity.

5) *Facies and Upscaling* - Beyond investigating the above fundamental properties for representative lithofacies in the Mesaverde, it is necessary to know how critical gas saturation, capillary pressure, electrical properties, upscaling issues, and wireline log response and analysis change with more easily measured Mesaverde rock properties such as lithofacies, porosity, and permeability; and how flow properties, particularly critical gas saturation, upscale with lithofacies bedding architecture. In addition, accuracy and variance of petrophysical relationships are premised on sampling, the scale of sampling, measurement methodology, and the geostatistical or spatial distribution of the properties. Little published work is available that addresses how porosity or permeability change over short length scales (2.5-5 cm; 1-2 inches)

6) *Wireline Log Interpretation* – Petrophysical properties and relationships measured on core and at the core scale can provide critical reservoir characterization information, but core cannot reasonably, or economically, be obtained for most wells over entire intervals of interest. For this reason, core are used for calibration of wireline log response interpretation so that log algorithms can be used where core are unavailable. This requires that the wireline log response curves be correlated with core-measured petrophysical properties. These relationships can vary with such properties as rock lithology, petrophysical property, *in situ* conditions, log vendor, log vintage, log traces available in the logging suite, and the log algorithms developed and used. Algorithms can sometimes be developed that meet reasonable accuracy and precision standards but that require a suite of input logs that are unavailable for historical wells and/or are prohibitively expensive for new wells. Determining the number of unique lithofacies classes and the criteria for defining classes can involve four principal criteria: (1) maximum number of lithofacies recognizable using the available petrophysical wireline log curves and other variables; (2) minimum number of lithofacies needed to accurately represent lithologic and petrophysical heterogeneity; (3) maximum distinction of core petrophysical properties among classes; and 4) the relative contribution of a lithofacies class to storage and flow.

7) **Data access** – The body of data concerning TGS advanced rock properties is extensive but few companies have been able to devote the time or resources to compiling the data and making the data digitally accessible. An internet-accessible database is needed to provide access to the library of both published and newly acquired data on TGS in general and specifically the Mesaverde.

I.2 Statement of Study Objectives

Major aspects of the study involved a series of tasks to reveal the nature of critical gas saturation, capillary pressure, and electrical properties, and how these change with basic petrophysical properties such as porosity and permeability. Principal goals were to measure critical gas saturation (S_{gc}) and capillary pressure (P_c), using at least 150 rocks selected to represent the range of lithofacies, porosity and permeability in the Mesaverde in five major TGS basins (Washakie, Uinta, Piceance, northern Greater Green River, and Wind River). Representative samples were to be obtained from at least 4-5 wells in each basin and the advanced properties samples selected from a set of 300 or more core samples to obtain the distribution of properties needed. The investigation was designed to discern the relationships among the independent geologic and petrophysical variables, lithology, and between basins. As noted, in Mesaverde reservoirs diagenetic clays with high cation exchange capacity can be common and water salinities can often be fresh leading to excess surface conductance effects. A secondary objective of the project was to evaluate this for the select samples to both determine the nature of conductive solids and develop algorithms for wireline log analysis of water saturation.

Tasks involved with meeting the project objectives included a clarification and review of the research plan by DOE (Task 1); initial technology assessment for DOE (Task 2); collection and consolidation of published advanced rock properties data into a publicly accessible digital database (Task 3.1); and collection of >2200 (300 proposed) rock samples, with digital wireline logs where available, from 44 wells in six basins that represent the range of lithofacies present in the Mesaverde Group in these basins (3.2). Measurement of basic properties (including routine and *in situ* porosity, permeability, and grain density) of these rocks and, based on these properties, selection of 150 samples to represent the range of porosity, permeability, and lithofacies in the wells and basins (Task 4.1). Measurements on these selected samples included:

1) drainage critical gas saturation (4.2); routine and *in situ* mercury intrusion capillary pressure analysis (4.3); porosity exponent and Co-Cw using multi-salinity method (4.4); geologic properties including core description, thin-section microscopy, including diagenetic and point-count analysis (4.5); and standard wireline log analysis (4.6). The compiled published data and data measured in the study were input in a database (Task 5.1); and are provided online as a web-based database (5.2). Core and wireline log-calculated properties were compared and algorithms developed for improved calculation of reservoir properties from log response (Task 6). The scale dependence of critical gas saturation was evaluated using bedform-scale reservoir simulation models that represent the basic bedform architectures found in the Mesaverde sandstones. Simulations were performed that would parametrically analyze how critical gas saturation and relative permeability scale with size and bedding architecture (Task 7). An active web-based, publication, and short-course technology transfer program was conducted (Task 8).

I.3. Report Organization

The following Results and Discussion section of this report will present the results for each of the tasks as defined above. The study involved the collection and organization of too much data, including core and log images, to appropriately present in a printed report format or even digitally as an Adobe Acrobat portable document (pdf) file. In particular, core slab and rock thin section images were preserved at high image resolution rather than reduced to lower resolution web presentation format so that future users can use the images quantitatively. Where appropriate data tables and figures are presented in the associated Task sections that follow. Where data tables or figures cannot be presented within this report due to size the study web archive location for these is cited. In addition to being archived on the KGS Mesaverde Project website, all data will be archived as a Kansas Geological Survey Open File Report in electronic format including this report and all associated databases, tables, and figures. Though technical in nature, the project administration involved tasks related to reporting and administration, such as Task 1. Details of these tasks and not summarized in this technical final report.

RESULTS AND DISCUSSION

Task 1. Research Management Plan

The objectives of this task were to develop a work breakdown structure and supporting narrative that concisely addresses the overall project as set forth in the agreement for the USDOE to review and accept according to the following guidelines: 1) The Recipient shall provide a concise summary of the objectives and approach for each Task and, where appropriate, for each subtask. 2) Recipient shall provide detailed schedules and planned expenditures for each Task including any necessary charts and tables, and all major milestones and decision points. This report is to be submitted within 30 days of the award. The DOE Contacting Officer's Technical Representative (COR) shall have 20 calendar days from receipt of the Research Management Plan to review and provide comments to the Recipient. Within 15 calendar days after receipt of the DOE's comments, the Recipient shall submit a final Research Management Plan to the DOE COR for review and approval.

1.1 Discussion

A revised research management plan including Work Breakdown Structure was drafted, submitted and approved. The approved management plan mirrored the proposal with minor modification. Based on initial contacts with gas companies that agreed to contribute core to the study but would not commence drilling and coring wells until the Spring of 2006, the schedule for acquiring core material was modified from the proposal to allow more time for sample acquisition. Task Statements from the revised Research Management Plan are presented at the beginning of each Task and Subtask below.

Task 2. Technology Status Assessment

The objectives of this task were to perform a Technology Status Assessment and submit a summary report describing the state of information and/or technology relevant to the proposed work. The report was to include both positive and negative aspects of each existing approach or technology. The report was to not exceed five typewritten pages in length. The report was not to contain any proprietary or confidential data, as the report was to be posted on the NETL website for public viewing.

The report submitted contained the following sections:

Current state of information or technology

- Summary Background of Industry/Sector
- Technologies/Tools/Approached/Data Being Used
- Benefits and Inadequacies of Current Information or Technology

Development Strategies

- Why New Approach is Required
- Problems to Address in this Research Project

Future

- What Barriers will the Research Overcome and the Impact on the U.S. Domestic Gas Supply

The following discussion presents pertinent excerpts from the interim report.

2.1 Results

2.1.1. Current State of Information

2.1.1.1 Prior studies of Mesaverde Tight Gas Sandstones (TGS)

Extensive work has been performed over several decades measuring TGS properties. Understanding of basic properties to date is reviewed below.

2.1.1.1.1 Porosity - The stress dependence of porosity and the laboratory conditions necessary for proper measurements are now widely recognized. Walsh and Grosenbaugh ([1979](#)) developed a model for fracture compressibility and Ostensen ([1983](#)) illustrated for low-permeability rock data from Jones and Owens ([1980](#)) and Sampath ([1982](#)) that these data conformed to the model of compressing cracks. Byrnes ([1997](#), 2000, [2003](#), [2005](#)) illustrated a relationship between routine and reservoir (*in situ*) porosity for Mesaverde/Frontier rocks.

2.1.1.1.2 Permeability - Extensive work has shown that the difference between permeabilities measured at routine conditions (k_{air}) and those measured at confining stress increases progressively with decreasing permeability and increasing confining stress ([Vairogs et al, 1971](#); [Thomas and Ward, 1972](#); [Byrnes et al, 1979](#); [Jones and Owens, 1980](#); [Sampath and Keighin, 1981](#); [Walls et al, 1982](#); [Ostensen, 1983](#); [Wei et al, 1986](#); [Luffel et al, 1991](#); [Byrnes, 1997](#); [Castle and Byrnes, 1998](#); [Byrnes et al, 2001](#), [Byrnes, 2005](#)). Byrnes et al (2001) presented a relationship between *in situ* Klinkenberg gas permeability (k_i) and routine air permeability (k_{air}): $\log k_{ik} = 0.059 (\log k_{air})^3 - 0.187 (\log k_{air})^2 + 1.154 \log k_{air} - 0.159$ (where k is in millidarcies) and illustrated the relationship between k_i and pore throat size in TGS. Mesaverde sandstones can be characterized as exhibiting either a log-linear k - ϕ relationship ([Dutton et al., 1993](#); [Byrnes 1997](#)) or, for subpopulations may exhibit a power-law trend ([Castle and Byrnes, 1998](#); [Byrnes and Castle, 2000](#); [Webb et al, 2008](#)).

2.1.1.1.3 Relative Permeability and Critical Gas Saturation - Relative gas permeability (k_{rg}) data for tight gas sandstones, have been reported in several studies ([Thomas and Ward, 1972](#); [Byrnes et al, 1979](#); [Jones and Owens, 1980](#); [Sampath and Keighin, 1981](#); [Walls, 1981](#); [Ward and Morrow, 1987](#); [Byrnes, 1997](#); [Castle and Byrnes, 1998](#); [Byrnes and Castle, 2000](#); [Byrnes, 2005](#)). Byrnes et al (1979) utilized a modified Corey (1954) equation to predict k_{rg} in low-permeability sandstones: $k_{rg} = (1 - (S_w - S_{wc,g}) / (1 - S_{gc} - S_{wc,g}))^p (1 - ((S_w - S_{wc,g}) / (1 - S_{wc,g})))^q$; where S_w is fractional water saturation, S_{gc} is the fractional critical gas saturation, $S_{wc,g}$ is the fractional critical water saturation relevant to the gas phase, and p and q are exponents expressing pore size distribution influence. Byrnes (2005) discussed the uncertainties in the end-point properties of TGS relative permeability curves and particularly the issues with S_{gc} . Critical gas saturation studies have primarily addressed solution gas drive gas connectivity (i.e., gas bubbles develop in pore space) and only a limited number address drainage gas displacement ([Closmann, 1987](#); [Li and Yortsos, 1993](#); [Kamath and Boyer, 1995](#)). Measured values of S_{gc} in the literature range from 0.2-38% and a function of such variables as core length, injection or pressure depletion rate, and interfacial tension. Byrnes (2005) presented results for S_{gc} in Mesaverde TGS that ranged from 10-45% and varied with pore architecture.

2.1.1.1.4 Capillary Pressure - Because of small pore-throat size, low-permeability gas-producing sandstones are typically characterized by high water saturation and high capillary pressure ([Thomas and Ward, 1972](#); [Dutton et al., 1993](#); [Byrnes, 1997, 2005](#)). Relationships

between “irreducible” water saturation and permeability ([Byrnes, 1997](#); [Byrnes and Castle, 2000](#)) and between threshold entry pressure or principal pore throat diameter (PPTD) and permeability ([Byrnes and Keighin, 1993](#); [Keighin, 1997](#); [Byrnes, 1997](#); [Byrnes, 2003](#)) have been published. The relationship between threshold entry pressure and permeability and between permeability and lithofacies at any given porosity requires that capillary pressure change with lithofacies at any given porosity. With change in both the threshold entry pressure, the critical or percolating pore throat size capillary pressure and pore throat size distribution with decreasing permeability, Byrnes ([2003](#), [2005](#)) illustrated generalized capillary pressure shapes for western tight gas sandstones. Byrnes and Keighin ([1993](#)) and Keighin ([1997](#)) showed that the *in situ* P_{pc} values range from 15-84% of unconfined P_{te} values illustrating the change in capillary pressure with confining stress.

2.1.1.1.5 Water Saturation and Cation Exchange Capacity – Wireline log determination of water saturation and identification of pay in tight gas sandstones is complicated by the low porosity, argillaceousness, and, in some rocks, the high cation exchange capacity (CEC) of the clays in the sandstones and the low salinity of the formation brines ([Kukul et al., 1983](#)). The problems of wireline log analysis in shaly sands is well recognized ([Fertl and Frost, 1980](#); [Worthington, 1985](#)) and numerous algorithms have been proposed for calculating water saturations in shaly sands including the empirical Simandoux ([1963](#)) and Indonesia ([Poupon and Leveaux, 1971](#)) equations and the more theoretical Dual Water ([Clavier, Coates, and Dumanoir, 1984](#)) and Waxman-Smits models ([Waxman and Smits, 1968](#); [Waxman and Thomas, 1974](#)). To calculate water saturation, accurate values of formation factor, saturation exponent, and excess surface conductivity effects are needed. The DOE has supported a study by Advanced Resources International to catalogue water composition data for the Greater Green River and Wind River basins. These data are critical to log-calculated water saturation, but significant saturation error can exist if CEC effects are present and are not accounted for in water saturation calculations. Isolated CEC data are available for Mesaverde ([Volk et al., 1979](#)) but no comprehensive study has been published.

2.1.1.1.6 Scale Dependence of S_{gc} and Relative Permeability - Even if relative permeability curves are known it is important to understand how to utilize them in reservoir modeling and simulation and have an understanding of how properties upscale. Analytically rigorous solutions for upscaling of permeability and relative permeability exist only for the

simplest architectural geometries such as layered beds (e.g., [Weber, 1982](#); [Craft and Hawkins, 1991](#); [Corey and Rathjens, 1956](#)) or for specific permeability architectures ([Kortekaas, 1985](#); [Honarpour et al., 1995](#); [Ringrose et al., 1996](#)). The most accurate, but most computationally intensive, method for calculation of pseudo-functions is to use flow simulations performed for representative architectures ([Warren and Price, 1961](#); [Desbarats, 1987](#)).

2.1.1.2 Technology/Methodology Being Used

This section of the interim report was summarized in the Introduction to this report, section I.2.

2.1.1.3 Limitations of Present Knowledge

The significant body of literature on TGS has helped define the TGS resource base. However, fundamental aspects of the properties discussed above are not fully understood including: **1) Gas Flow**- All assessments of gas resource are premised on assumptions concerning gas relative permeability and implicitly, the critical gas saturation (S_{gc}), which no published studies have measured for TGS. Understanding the minimum gas saturation necessary for gas flow (S_{gc}) is fundamental to defining the tight gas sandstone resource and is particularly critical to quantify in marginal resources; **2) Capillary Pressure** – Though work has been done on capillary pressure of low-permeability sandstones little work has been published on the lithofacies or pressure-dependence of capillary pressure; **3) Electrical Properties** - Extensive work has been done defining regional water composition, but there is little published work characterizing surface conduction effects on calculated water saturations from wireline log response for Mesaverde rocks; **4) Facies and Upscaling** – Most published studies of TGS properties are tied to location but are not distinguished by lithofacies. This places potential, and sometimes unknown, limits on application or results. The proposed project will investigate how properties, upscaling issues, and wireline log response and analysis change with Mesaverde rock properties such as lithofacies, porosity, and permeability and how flow properties upscale with lithofacies bedding architecture; and **5) Data access** – The body of data concerning TGS advanced rock properties is extensive but few companies have been able to devote the time or resources to compiling the data and make the data digitally accessible.

Task 3. Acquire Data and Materials

Subtask 3.1. Compile Published Advanced Properties Data

3.1.1 Task Statement

Advanced rock properties data, comprising compressibility, effects of confining pressure, capillary pressure, relative permeability, and electrical properties, shall be compiled from published studies and DOE reports. These data shall be digitized and entered into a fully integrated digital data system accessible to external users.

3.1.2 Methods

Reference searches were performed in the following databases: Georef, NTIS, DAI, GPO, Compendex, USBM, WorldCat, FSProc, SPE. Of the over nearly 2,000 references that are flagged for appropriate search criteria relevant to low-permeability sandstones and the Mesaverde, over 230 geologic and engineering technical publications were identified that pertain to Mesaverde geologic or petrophysical properties or to the properties of non-Mesaverde low-permeability sandstones which appear to be geologically and petrophysically relevant. Of the 230 publications, approximately 88 publications were considered to be geologically or petrophysically relevant to the issues addressed by this study (Table 3.1.2.1). Physical or electronic copies were obtained for the publications identified. Of these 88 references, more than 75% did not contain useful tabular data. Data in the publications most relevant to Mesaverde rocks or needed for relative permeability or critical gas saturation analysis were entered into a database either from tables in the publication or digitally interpreted from figures. Obtaining data from figures potentially introduces some error, as a function of the figure image quality and scales, but was within acceptable quality criteria (which generally ranged from an interpreted independent and dependent variable accuracy of 1%-5% of the true value used to create the figure). The significant figures reported reflect the accuracy of the figure interpretation process but may be one significant figure greater for some data (e.g., for a value with an error of 1% values above 10% might be reported with no decimal places whereas values less than 10% might be reported with a single decimal place). Where data were obtained directly from published

tables the number of significant figures reported were the same as in the publication, even if the number of significant figures shown in the publication was inappropriate for the data accuracy (e.g., reporting of routine porosity to two decimal places) .

Original plans were to present data in a single database format. However, it was found that the nature of publication reporting format and the diverse nature of the data was not conducive to the use of a single database. An Excel format for data presentation was used, with each publication presented on a separate worksheet within workbooks organized by data type.

It is important to note that the search and data capture was not comprehensive. There are publications in major journals, regional society publications, academic dissertation or theses, government-sponsored studies that were not found in the search process or were identified but from which data were not obtained because it was not considered sufficiently relevant. Also some figures in some publications, though important, were not in a format appropriate to accurate digitization either because of the scale of presentation or the quality of the reproduction. It was not the purpose of this task to analyze the data, only to compile the data.

3.1.3 Results

Table 3.1.2.1 presents the 88 references that were interpreted to be relevant to Mesaverde petrophysical properties important to this study or that addressed properties measured in this study in other low-permeability sandstones. The majority of publications do not include tables of data but include figures. Figures 3.1.1-3.1.5 provide examples of compiled data presented on the website.

Figure 3.1.1 illustrates a plot of gas relative permeability measured for individual saturations compiled from sources listed in Table 3.1.1. These gas relative permeabilities were obtained using a wide range of sample preparation and permeability measurement methods including oven and relative-humidity oven drying; as-received saturations; water saturation achieved by evaporation, centrifuge, porous plate; permeability measured by steady-state and pressure-pulse decay; permeability representing air permeability and Klinkenberg permeability; cores under varying net effective stress conditions; and including a very wide range of lithofacies (often unspecified).

In addition to single-point data complete gas relative permeability curves have been measured on cores in several studies using the single-phase stationary techniques where water is

stationary and gas flow measurement is performed at a low flow rate that does not change the water saturation. Figure 3.1.2 illustrates compiled curves from studies that reported complete gas relative permeability curves. As with the single-point data, these curves represent a range of experimental conditions including: core drying, core desaturation method, “reference” state of absolute permeability, net effective stress, variable rock lithology, and variable notably clay type and content.

Table 3.1.2.1 List of 88 references relevant to Mesaverde low-permeability geologic and petrophysical properties.

<i>Author</i>	<i>Author</i>	<i>Author</i>	<i>Year</i>
Fatt, I.	Davis, D.H.		1952
Cornell, D.	Katz, D.L.		1953
McLatchie, A.S.	Hemstock, R.A.	et al	1958
White, E.J.	Baptist, C.C.	et al	1960
Jones, F.O. Jr.			1964
Sloat, B.	Brown, M.		1968
Harville, D.W.	Hawkins, M.F. Jr.		1969
Bush, D.C.	Jenkins, R.E.		1970
Morrow, N.R.			1971
Vairogs, J.	Hearn, C.L.	et al	1971
Jones, S.C.			1972
Thomas, R.D.	Ward, D.C.		1972
Newman, G.H.			1973
Berg, R.R.			1975
Donaldson, E.C.	Kendall, R.F.	et al	1975
Gregory, A.R.			1976
Simon, D.E.	McDaniel, B.W.	et al	1976
Kern, J.W.	Hoyer, W.A.	et al	1977
Neasham, J.W.			1977
Newman, G.H.	Martin, J.C.		1977
Wilson, M.D.	Pittman, E.D.		1977
Byrnes, A. P.	Sampath, K.	et al	1979
Byrnes, A.P.	Sampath, K.	et al	1979
Hill, H.J.	Shirley, O.J.	et al	1979
Holditch, S.A.			1979
Juhasz, I.			1979
Patchett, J.G.	Coalson, E.B.		1979
Strickland, F.G.	Feves, M.L.	et al	1979
Volk, L.J.	Carroll, H.B.	et al	1979
Jones, F.O. Jr.	Owens, W.W.		1980
Keighin, W.C.			1980
Volk, L.J.	Raible, C.J.	et al	1980
Walls, J. D.	Nur, A.M.	et al	1980
Greenwald, R.F.	Somerton, W.H.		1981
Greenwald, R.F.	Somerton, W.H.		1981
Greenwald, R.F.			1981
McPeek, L.A.			1981
Rose, W.	Sampath, K.		1981
Rosepiler, M.J.			1981
Sampath, K.	Keighin, C.W.		1981
Wilson, M.D.			1981
Keighin, W.C.	Sampath, K.		1982
Mian, M.A.	Hilchie, D.W.		1982
Ruhovets, N.	Fertl, W.H.		1982

Sampath, K.			1982
Walls, J. D.			1982
Faris, S.R.	Woessner, D.E.	et al	1983
Kukal, G.C.	Biddison, C.L.	et al	1983
Ostensen, R.W.			1983
Finley R.J.			1984
Randolph, P.L.	Soeder, D.J.	et al	1984
Baldwin, B.	Butler, C.O.		1985
Brower, K.R.	Morrow, N.R.		1985
Robinson, B.M.	Holditch, S.A.	et al	1986
Wie, K.K.	Morrow, N.R.	et al	1986
Ward, J. S.	Morrow, N. R.		1987
Soeder, D.J.	Chowdiah, P.		1988
Logan, W.D.			1989
Spencer, C.W.			1989
Lerner, D.B.	Dacy, J.M.	et al	1990
Hyman, L.A.	Malek, D.J.	et al	1991
Luffel, D.L.	Howard, W.E.	et al	1991
Sattler, A.R.			1991
Hartmann, D.J.	MacMillan, L.		1992
Pittman, E.D.			1992
Byrnes, A.P.	Keighin, C.W.		1993
Dutton, S.P.			1993
Maloney, D.	Doggett, K.	et al	1993
Lee, W.J.	Hopkins, C.W.		1994
Lomax, J.	Howard, A.		1994
Nelson, P.H.			1994
Plumb, R.A.			1994
Cluff, R.M.	Byrnes, A.P.	et al	1995
Byrnes, A.P.			1997
Worthington, P.F.	Daines, J.M.	et al	1997
Castle, J.W.	Byrnes, A.P.		1998
Ohirhian, P.U.			1998
Craig, D.P.	Brown, T.D.		1999
Revil, A.	Cathles, L.M. III		1999
Byrnes, A.P.	Castle, J.W.		2000
Aguilera, R.			2002
Law, B.E.			2002
Mahadevan, J.	Sharma, M.M.		2003
Webb, J.C.	Cluff, S.G.	et al	2003
Wu, T.	Berg, R.R.		2003
Chen, J.	Petersen, M.E.	et al	2004
Shanley, K.W.	Robinson, J.	et al	2004
Byrnes, A.P.			2005

Table 3.1.2.1 List of 88 references relevant to Mesaverde low-permeability geologic and petrophysical properties.

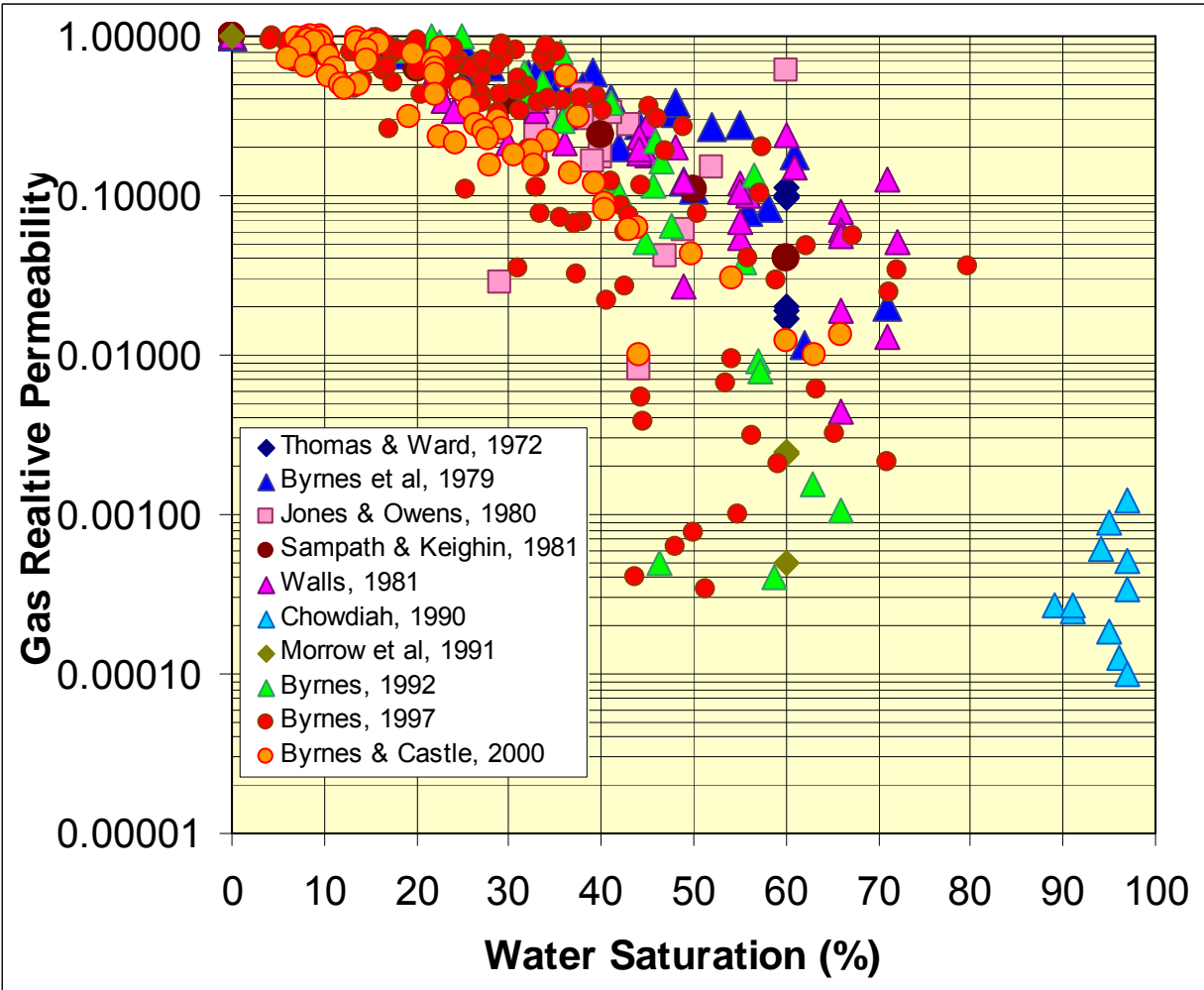


Figure 3.1.1 Gas relative permeability versus water saturation from published studies. Measurement methods and conditions including methods used to achieve saturation, measure gas relative permeability, and net effective confining stress vary among studies.

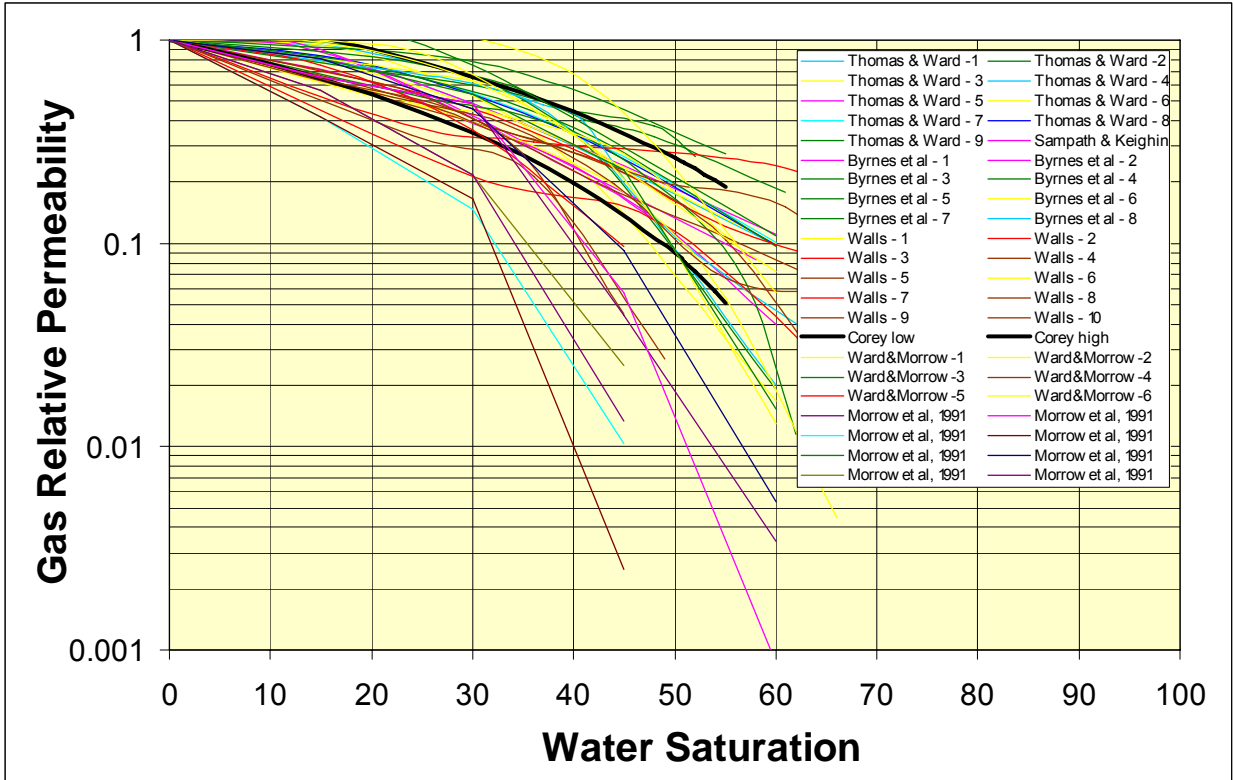


Figure 3.1.2 Gas relative permeability curves versus water saturation from published studies. Measurement methods and conditions including methods used to achieve saturation, measure gas relative permeability, and net effective confining stress vary among studies.

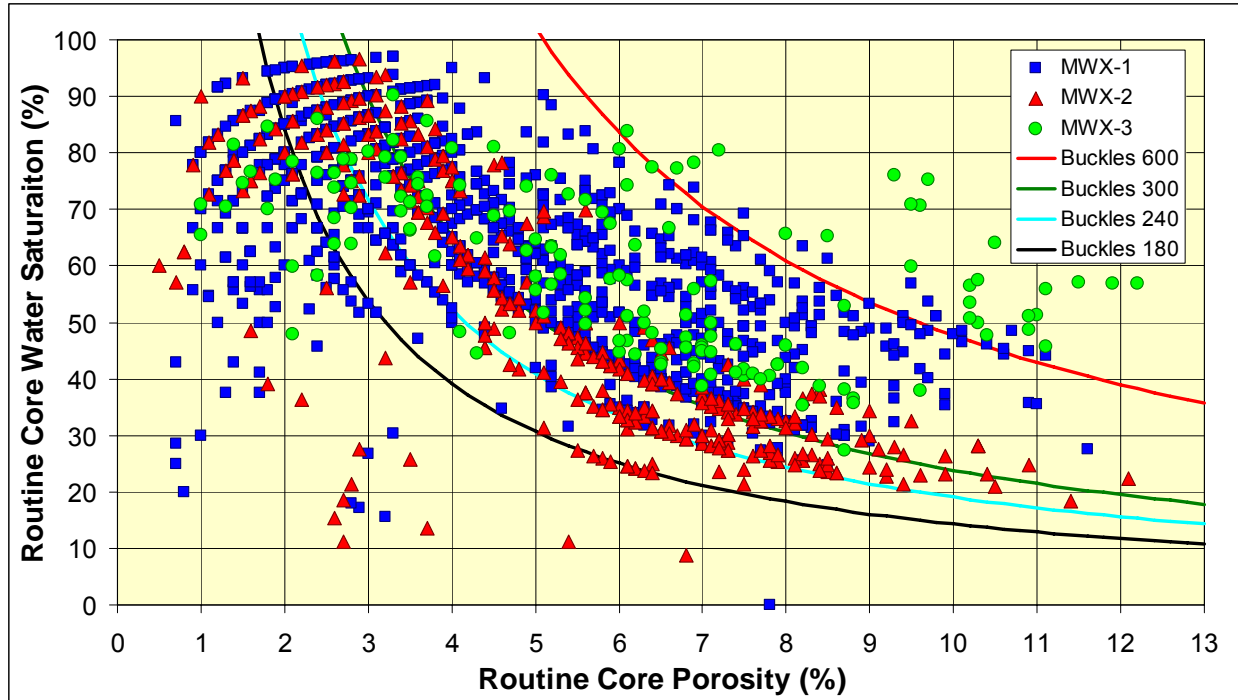


Figure 3.1.3 Routine core analysis porosity versus water saturation for the Piceance Basin MWX-1 through MWX-3 wells. Saturation versus porosity trends exhibit commonly observed Buckles power-law relationship. General trend lines shown represent $S_w = A\phi^{-1.1}$ where $A = 180, 240, 300,$ and 600 . In some basins differences in trend line result from height within hydrocarbon column but here differences are interpreted to primarily reflect lithologic differences.

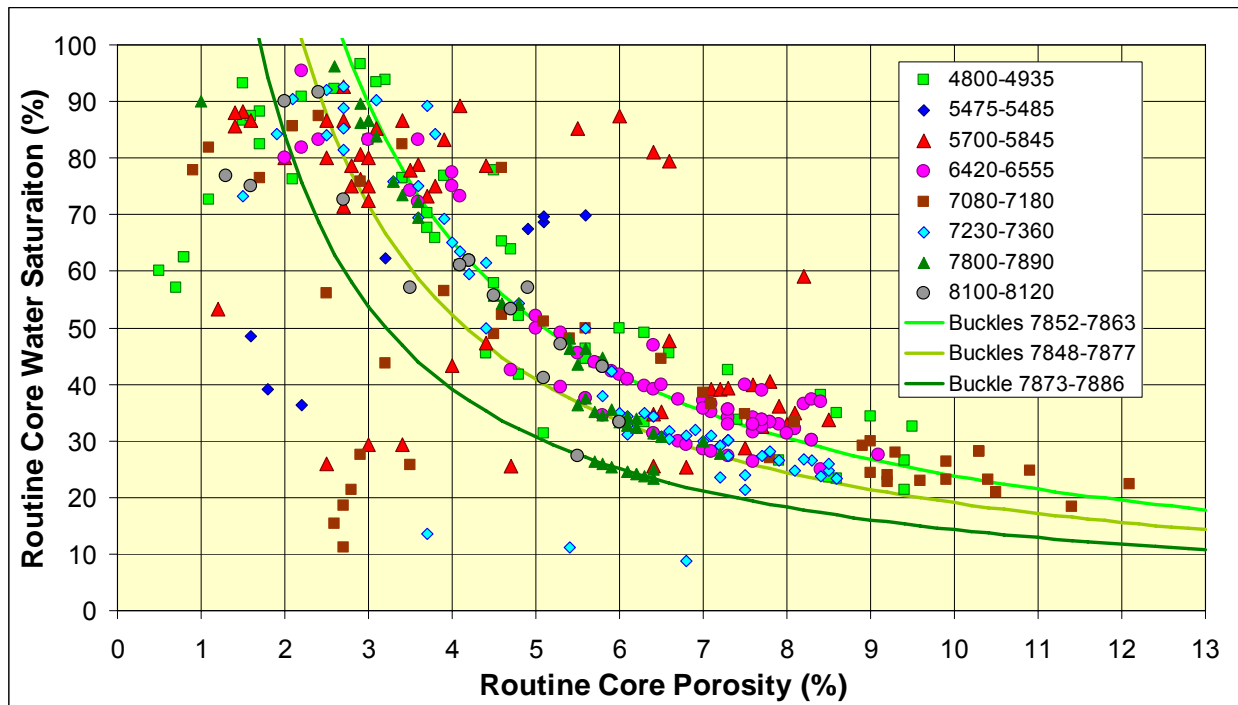


Figure 3.1.4 Routine core analysis porosity versus water saturation for the Piceance Basin MWX-2 well. Saturation versus porosity trends exhibit commonly observed Buckles power-law relationship. Trend lines for depth intervals 7852-7886 shown represent $S_w = A\phi^{-1.1}$ where $A = 180, 240,$ and $300,$ respectively. Differences in trends can be postulated to be due to differences in grain size and/or clay type/content.

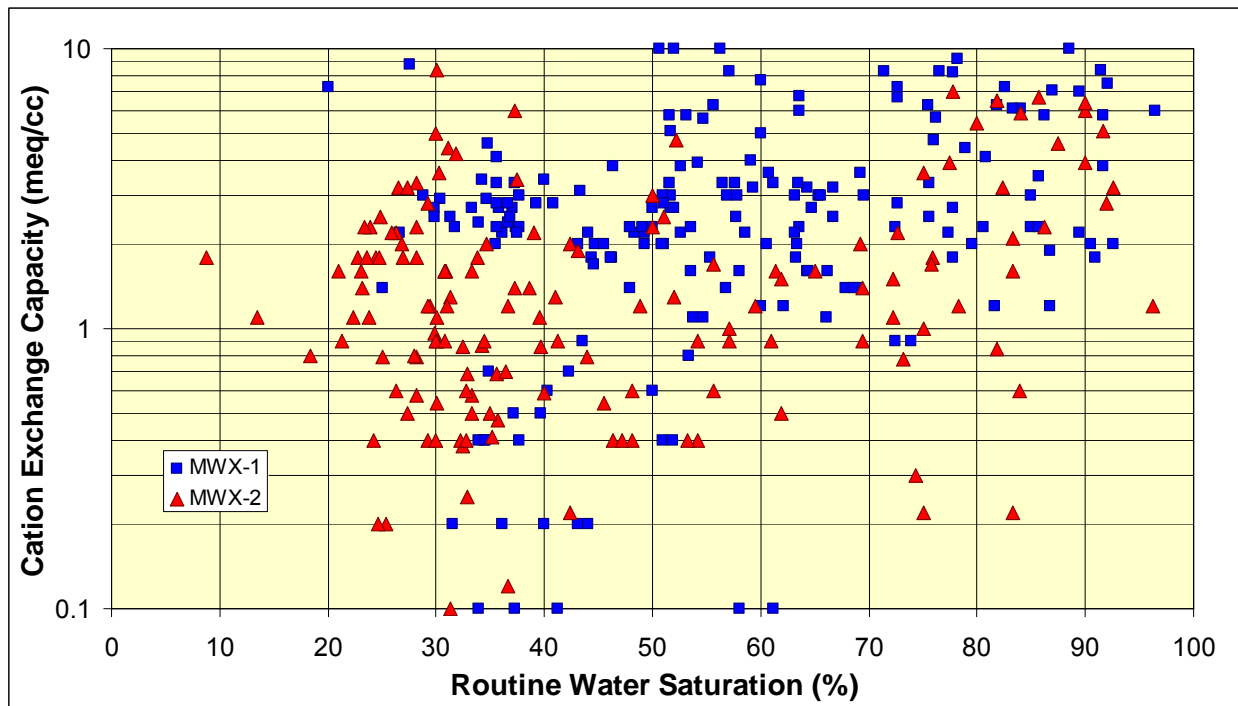


Figure 3.1.5 Routine core analysis water saturation versus cation exchange capacity for Piceance Basin MWX-1 and MWX-2 wells showing weak positive correlation.

Subtask 3.2. Compile Representative Lithofacies Core and Logs from Major Basins

3.2.1 Task Statement

Not less than a total of 300 rock samples shall be obtained from 4-5 wells in each of the five basins in the project (Washakie, Uinta, Piceance, Upper Greater Green River, and Wind River). The 4-5 wells in each basin shall be selected to provide a wide geographic distribution and shall be limited to wells that have adequate wireline log suites and core. Possible industry sponsors have been identified in each of the basins. For areas that need to be sampled but industry contribution cannot be obtained, wells shall be selected that have core available in the USGS core repository in Denver, Colorado, or other public core libraries. Cores and wells shall be selected that provide a comprehensive range in lithofacies, both reservoir and non-reservoir, characteristic of the Mesaverde in the area and basin and that serve both the objectives of the study and assessment needs of the industry participants.

3.2.2 Methods

A principal goal of this task was to obtain a sample population of Mesaverde cores that would provide a wide range in the following properties: 1) geographic location by basin; 2) depth; 3) rock lithology; 4) porosity; and 5) permeability. To achieve this goal: 1) companies were contacted to contribute core; and 2) the United States Geological Survey (USGS) Core library in Littleton, Colorado database was searched. The drilling schedules of most of the companies did not provide core to the project until late in the first year of the project. For this reason it was decided to obtain a complete sampling of each basin from the USGS core library and supplement this with the industry cores.

Core plugs measuring approximately 2.54-cm (1-inch) in diameter and 1.9-7.6 cm (0.75-3 inches) long were cut from slabbed or full-diameter core using a diamond core drill cooled with tap water either at the United States Geological Survey (USGS) Core library in Denver, Colorado or at service company facilities for industry-contributed core. Subsequent to coring the plugs were immediately towel dried. For two industry-contribution wells 3.8-cm (1.5-inch) diameter cores were

submitted; 2.54-cm (1-inch) diameter cores were cut from these to accommodate laboratory equipment sample size constraints.

Core plug ends were trimmed to make right cylinders using tap water as coolant at the Kansas Geological Survey. The core plug ends were subsequently used for geologic analysis, including rock thin sections.

3.2.3 Results

Table 3.2.1 lists the 44 wells sampled in the six basins, comprising for each basin: Washakie - 11; Uinta - 8; Piceance - 8; Greater Green River - 7; Wind River - 4; Powder River - 6; Sand Wash – 2. Contributed cores from industry by basin included: Bill Barrett Corp. – Piceance; BP America Production – Washakie; Exxon-Mobil – Piceance; Kerr-McGee Oil & Gas Onshore – Uinta; Shell Exploration & Production – Green River; Williams Exploration & Production – Piceance. Figure 3.2.1 shows the locations of the wells sampled and Figure 3.2.2 shows the distribution of wells by basin. The addition of the Powder River and Sand Wash basins to the sampling and the geographic distribution of wells within each basin provided a comprehensive Mesaverde sampling for the size of the sampling program.

API STATE CODE	API COUNTY CODE	API WELL #	BASIN	FIELD	WELL	OPERATOR	Twn	Rng	Sec
49	035	20622	GREEN RIVER	WILDCAT	1 OLD ROAD	AMERICAN HUNTER EXPL	27	N	108 W 27
49	013	08024	GREEN RIVER	PINEDALE	5 PINEDALE	EL PASO NATURAL GAS	30	N	108 W 5
49	035	20088	GREEN RIVER	MERNA	A-1 WASP	INEXCO OIL COMPANY	36	N	112 W 28
49	035	06020	GREEN RIVER	BIG PINEY	B-54 BIG PINEY	BELCO PETROLEUM	29	N	113 W 26
49	035	05742	GREEN RIVER	TIP TOP SHALLOW	C-47 TIP TOP SHALLOW	BELCO PETROLEUM	28	N	113 W 22
49	035	06200	GREEN RIVER	MASON	K-2 MASON	BELCO PETROLEUM	31	N	113 W 13
49	035	24198	GREEN RIVER	PINEDALE	Vible 1B-11D	SHELL E&P	31	N	109 W 11
05	045		PICEANCE		1 BOOK CLIFFS-DRILL HOLE	USGS-CG	7	S	104 W 17
05	103		PICEANCE	LOWER WHITE RIVER	21011-5 MOON LAKE	WESTERN FUELS ASSOC	2	N	101 W 1
05	103	10391	PICEANCE	WILLOW RIDGE	EM T63X-2G	EXXON-MOBIL	3	S	97 W 2
05	045	11402	PICEANCE	MAMM CREEK	LAST DANCE 43C-3-792	BILL BARRETT CORP.	5	7	92 W 3
05	103	09406	PICEANCE	WHITE RIVER DOME	M-30-2-96W /D-037934	FUEL RESOURCES DEV	2	N	96 W 30
05	045	06578	PICEANCE	GRAND VALLEY	MV 24-20 CHEVRON	BARRETT ENERGY	6	S	96 W 20
05	045	06001	PICEANCE	RULISON	MWX-2 SUPERIOR	CER CORPORATION	6	S	94 W 34
05	045	10927	PICEANCE	PARACHUTE	PUCKETT/TOSCO PA 424-34	WILLIAMS E&P	6	S	95 W 34
49	005	25627	POWDER RIVER	BRIDGE DRAW	1 BARLOW 21-20	LOUISIANA LAND & EXP	48	N	75 W 20
49	009	21513	POWDER RIVER	MIKES DRAW	2 FRED STATE	DAVIS OIL COMPANY	35	N	70 W 36
49	009	06335	POWDER RIVER	FLAT TOP	2 SHAWNEE	BELCO PETROLEUM	33	N	69 W 2
49	009	05481	POWDER RIVER	FLAT TOP	3 SHAWNEE	BELCO PETROLEUM	33	N	69 W 23
05	081	06718	SAND WASH	WEST CRAIG	1-691-0513	COCKRELL OIL CORP	6	N	91 W 5
05	081	06724	SAND WASH	CRAIG DOME	1-791-2613	COCKRELL OIL CORP	7	N	91 W 26
43	047	30584	UINTA	NATURAL BUTTES	11-17F RIVER BEND UNIT	MAPCO INCOPORATED	10	S	20 E 17
43	047	30545	UINTA	BONANZA	2-7 FLAT MESA FEDERAL	ENSERCH EXPLORATION	10	S	23 E 7
43	019		UINTA		3 BOOK CLIFFS	USGS-CG	17	S	24 E 3
43	047	30860	UINTA	WILDCAT	3-24 US LAMCO	CHAMPLIN PETROLEUM	13	S	20 E 24
43	019		UINTA		4 BOOK CLIFFS	USGS-CG	17	S	24 E 31
43	047	30584	UINTA	AGENCY DRAW	4-5 US LAMCO	ENSERCH EXPLORATION	13	S	20 E 5
43	047	36565	UINTA	NATURAL BUTTES	NBU 1022-1A	KERR-MCGEE OIL&GAS ONSHORE	10	S	22 E 1
46	047	36401	UINTA	NATURAL BUTTES	NBU 920-360	KERR-MCGEE OIL&GAS ONSHORE	9	S	22 E 36
49	037	21075	WASHAKIE		WILD ROSE 1	AMOCO PRODUCTION	17	N	94 W 5
49	037	05405	WASHAKIE	CHIMNEY ROCK	1 CHIMNEY ROCK	MOUNTAIN FUEL SUPPLY	18	N	102 W 12
49	037	21053	WASHAKIE	FIVE MILE GULCH	3 UNIT	AMOCO PRODUCTION	21	N	93 W 35
49	037	23956	WASHAKIE	SIBERIA RIDGE	5-2 SIBERIA RIDGE UNIT	AMOCO PRODUCTION	21	N	94 W 5
49	037	05683	WASHAKIE	PATRICK DRAW	65-1-7 ARCH UNIT	FOREST OIL CORP	19	N	99 W 1
49	037	05577	WASHAKIE	ARCH	ARCH UNIT UPRR #102-7-10	ANADARKO E&P CO. LP	19	N	98 W 7
49	037	05349	WASHAKIE		B-2A SPIDER CREEK	HUMBLE OIL & REF	18	N	110 W 27
49	007	21170	WASHAKIE	SAVERY	C-11 /FEE	FUEL RESOURCES DEV	12	N	90 W 11
49	037	22304	WASHAKIE	DRIPPING ROCK	DRIPPING ROCK #3	CELSIUS	14	N	94 W 8
49	037	22355	WASHAKIE	DRIPPING ROCK	DRIPPING ROCK #5	CELSIUS	14	N	94 W 19
49	037	99999	WASHAKIE		WILD ROSE	BP AMERICA PRODUCTION, INC.	18	N	94 W 33
49	013	20836	WIND RIVER	MADDEN	1-27 LOOKOUT	MONSANTO OIL	39	N	91 W 27
49	013	20786	WIND RIVER	LYSITE	1-9 LYSITE	MICH WISC PIPELINE	38	N	91 W 9
49	013	20966	WIND RIVER	MADDEN	2-1 CHEVRON	MONSANTO OIL	38	N	91 W 1
49	013	20724	WIND RIVER		31-22 TRIBAL PHILLIPS	BROWN TOM INC	4	N	31 E 31

Table 3.2.1 List of wells sampled.

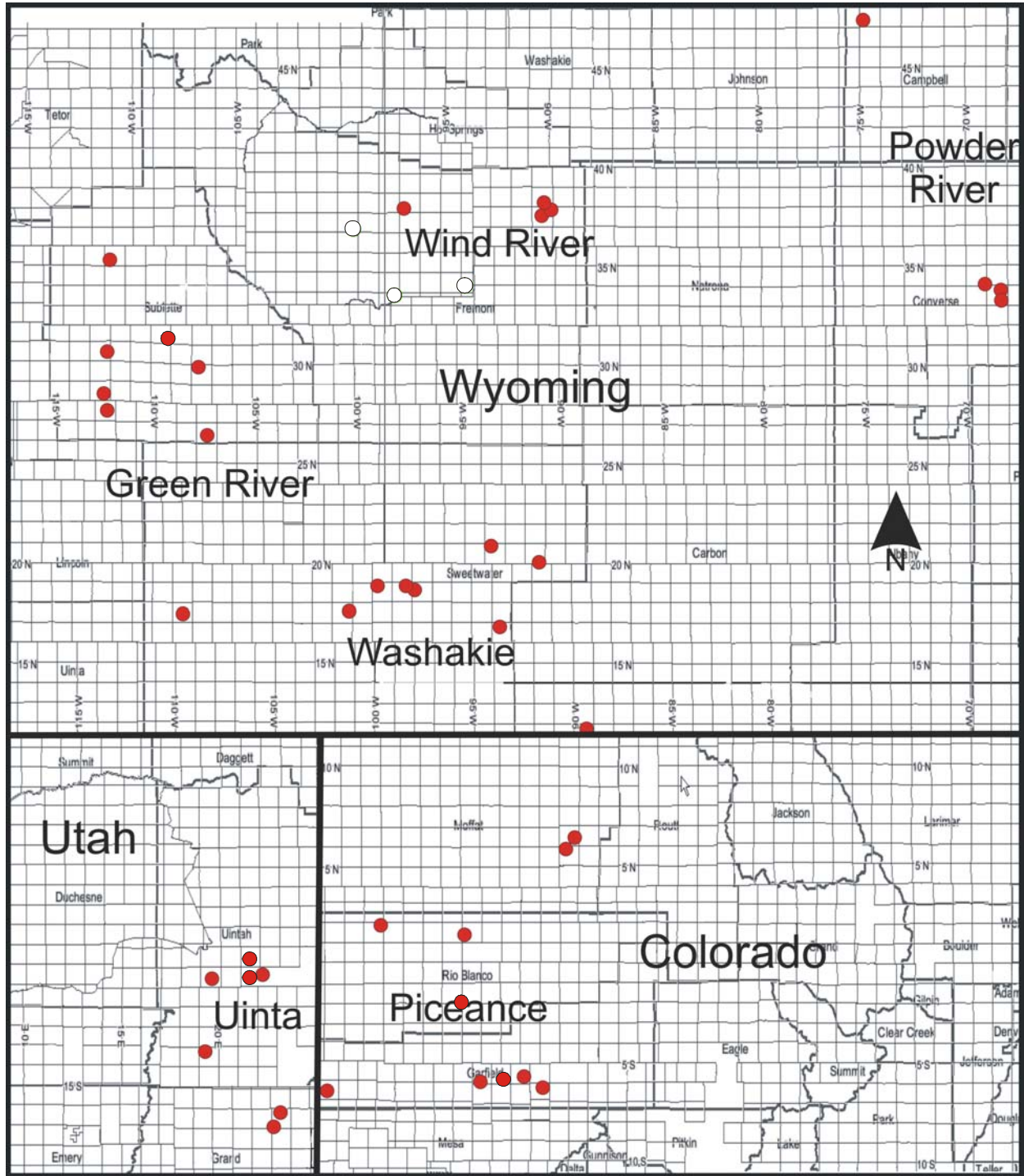


Figure 3.2.1 Location of wells sampled in study.

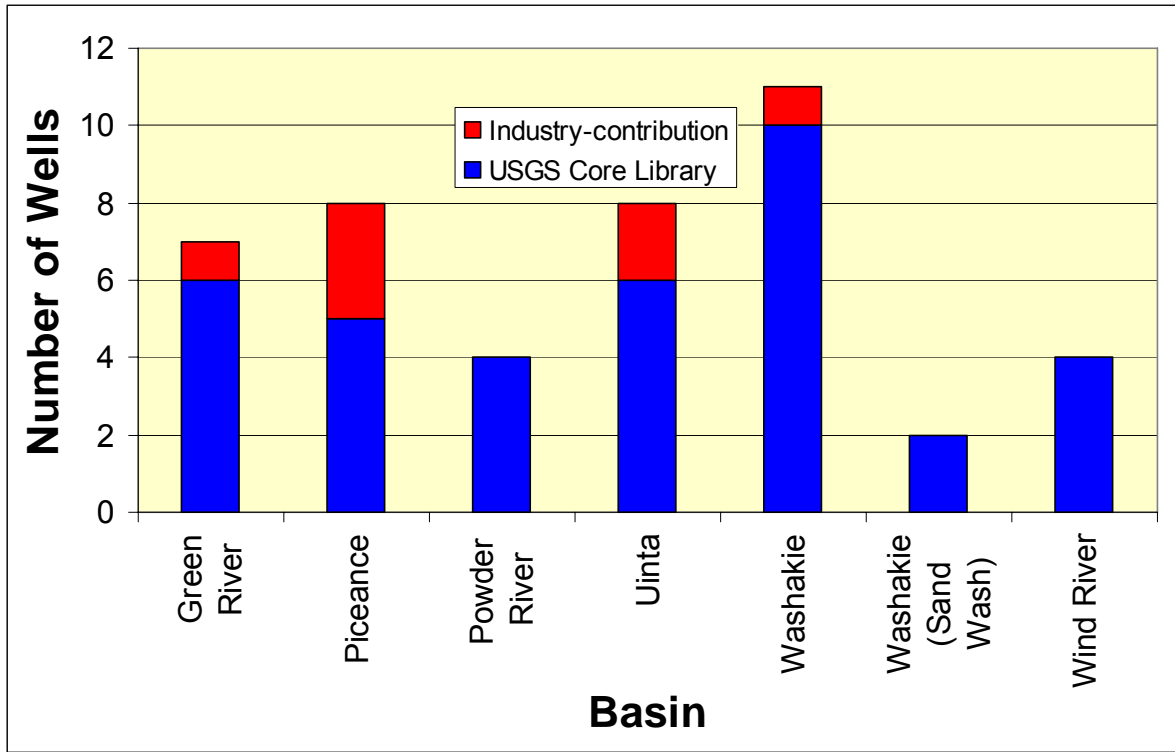


Figure 3.2.2 Number of wells sampled by basin and source.

A total of 2216 core plugs were obtained representing 1182 original plugs (A), 776 paired plugs (B), and 258 additional pair plugs (C) (Appendix 1). This sampling represents approximately four times more original plugs than the 300 core plugs proposed and six times as many paired plugs (proposed n=150). The decision to devote the greater effort in sampling was based on the observed variation in rock lithofacies encountered in the wells during the sampling process. To appropriately represent the lithofacies observed in core a greater number of samples were considered necessary. Intervals sampled in wells represent the range of lithofacies and porosity exhibited by the Mesaverde in each well. Figure 3.2.3 shows the number of core plugs, original and duplicate, for each basin.

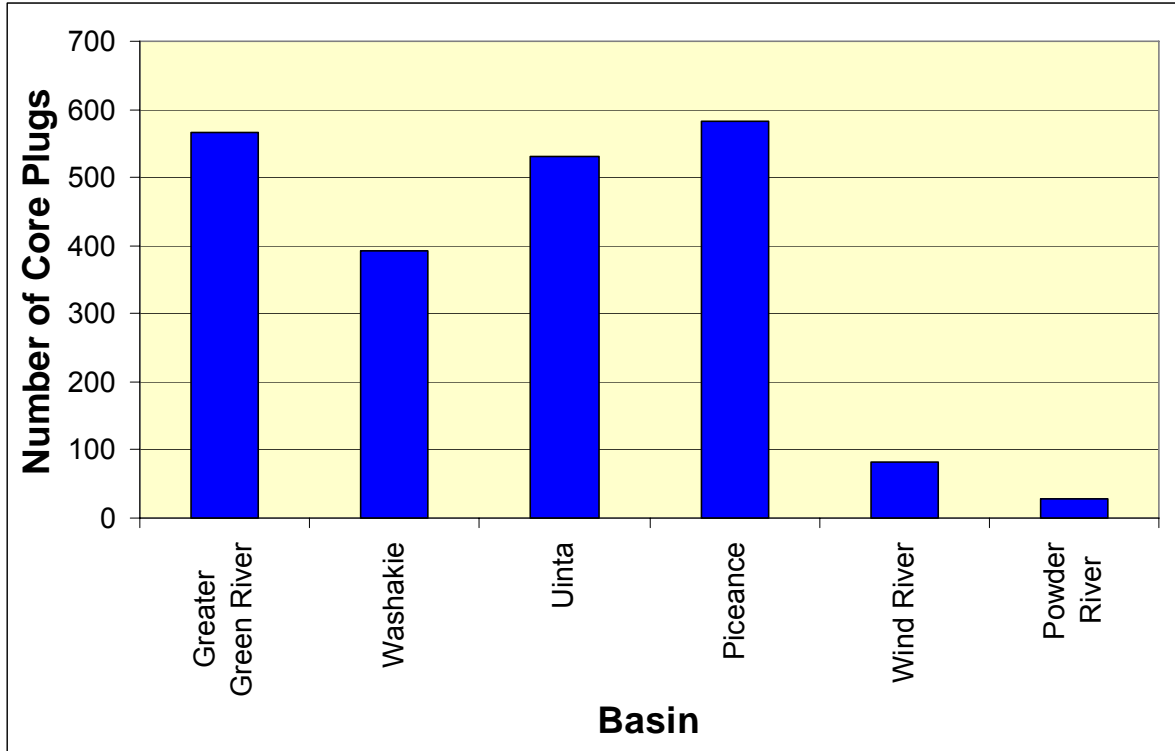


Figure 3.2.3 Number of core plugs (original and duplicate) by basin.

Core samples range in depth from 124-16,723 ft (Fig. 3.2.4). The distribution for the sample depths reflects the approximate complete range in depth of the Mesaverde for the basins studied.

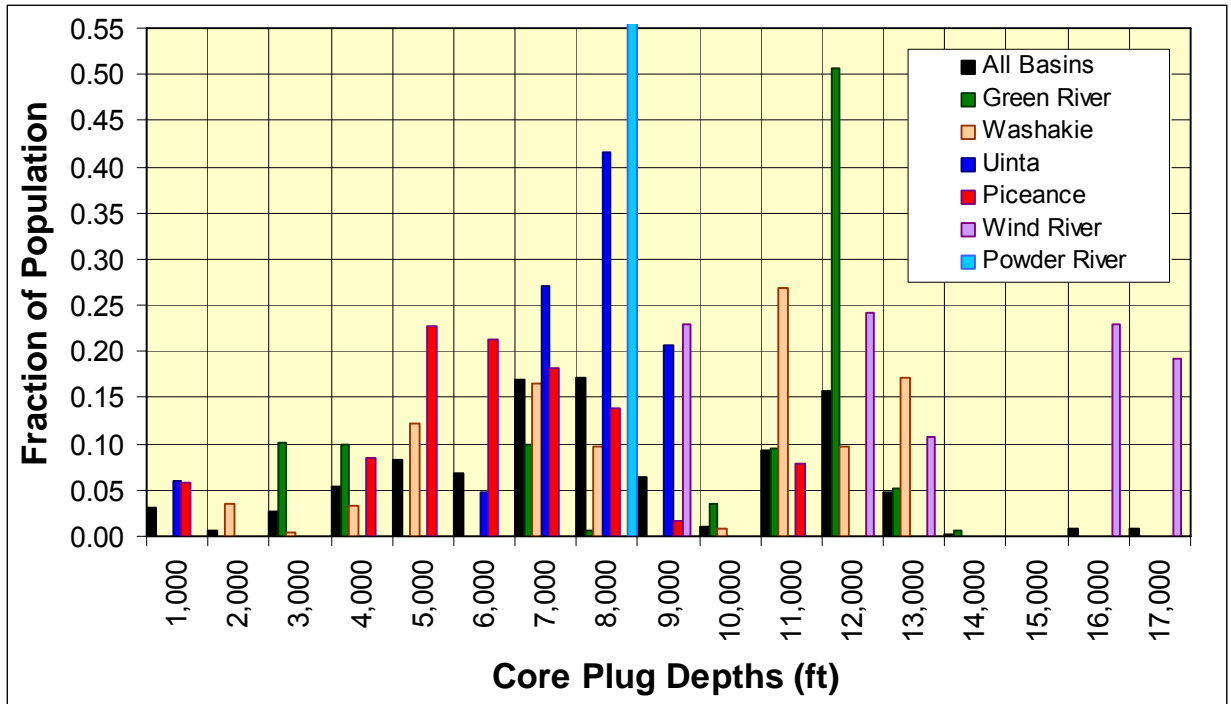


Figure 3.2.4 Distribution of core sample depths by basin.

Figure 3.2.5 illustrates that nearly the complete range in porosity exhibited by Mesaverde sandstones is present in all basins. Samples with higher porosity ($\phi > 12\%$) were not sampled in the Wind River Basin or $\phi > 16\%$ in the Powder River Basin. Based on examination of wireline logs this absence in the core samples reflects sampling and not absence of this range in porosity within the basins.

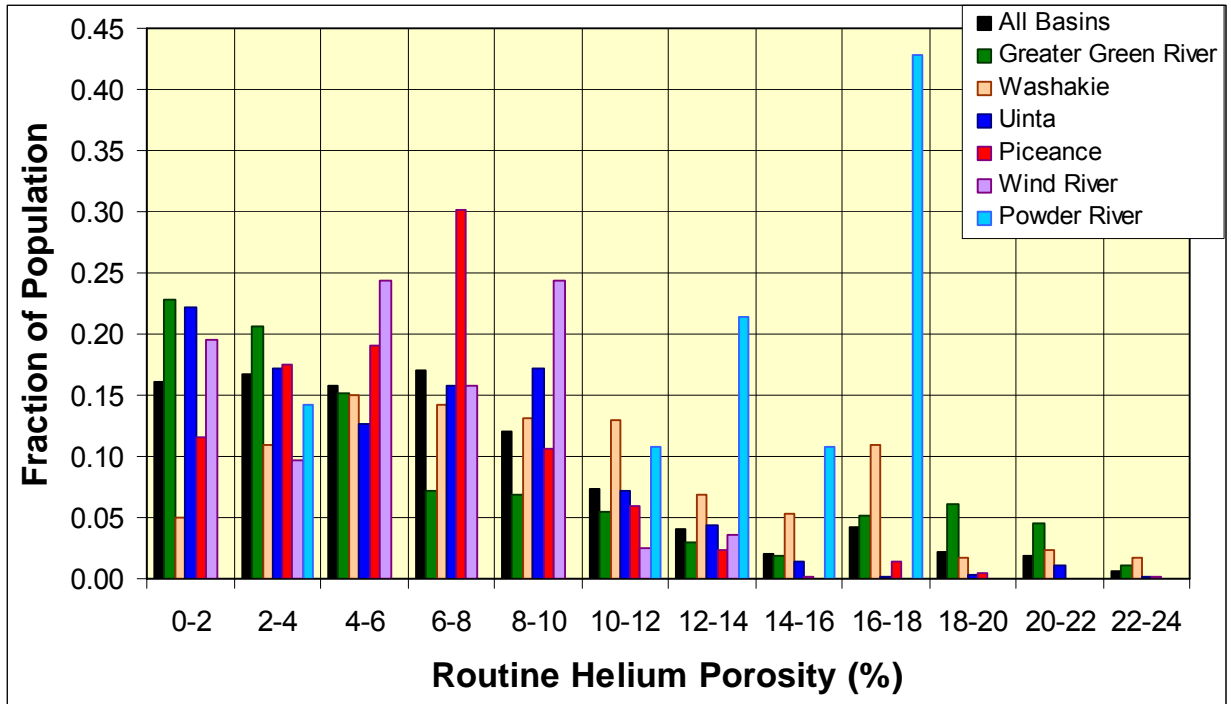


Figure 3.2.5 Routine helium porosity distribution by basin.

Subtask 3.3. Acquire logs from sample wells and digitize

3.3.1 Task Statement

A complete suite of available wireline logs shall be obtained for each of the wells from which core is obtained in Subtask 3.2. Only wells where an adequate suite of wireline logs is available shall be selected for sampling. For wells where logs are not available digitally, paper copies shall be digitized by a commercial service company.

3.3.2 Methods

Although attempts were made to select wells for which both core and a modern suite of wireline logs was available, wireline logs were not available for many of the wells for which it was important to sample the core. For industry-contributed wells, wireline logs were provided in Log ASCII Standard (LAS) format. For several of the USGS core wells LAS files were obtained from the Wyoming Oil & Gas Conservation Commission. Where digital LAS files were not available paper copies were obtained and the log traces digitized.

3.3.3 Results

Wells shown in Table 3.3.1 were utilized for routine and advanced log analysis in Task 6. LAS files for these wells are available at <http://www.kgs.ku.edu/mesaverde/reports.html>.

Basin	Field	Well	Operator	Township		Range		Section
Green River	Merna	Wasp A-1	Inexco Oil Company	36	n	112	w	28
Green River	Wildcat	1 Old Road	American Hunter Exploration	27	n	108	w	27
Green River	Pinedale	Vible 1D-11D	Shell E&P	31	n	109	w	11
Piceance	Parachute	Puckett/Tosco PA 424-34	Williams Production	6	s	95	w	34
Piceance	Mamm Creek	Last Dance 43C-3-792	Bill Barrett Corporation	7	s	92	w	3
Piceance	Rulison	MWX-2 Superior	CER Corporation	6	s	94	w	34
Piceance	Piceance Creek	EM T63X-2G	Exxon-Mobil Corporation	3	s	97	w	2
Powder River	Bridge Draw	1 Barlow 21-20	Louisiana Land & Exploration	48	n	75	w	20
Sand Wash	Craig Dome	1-791-2613	Cockrell Oil Corp	7	n	91	w	26
Uinta	Bonanza	2-7 Flat Mesa Federal	Enserch Expolration	10	s	23	e	7
Uinta	Natural Buttes	11-17F River Bend Unit	Mapco Inc.	10	s	20	e	17
Uinta	Natural Buttes	NBU 9-20-360	Kerr McGee	9	s	20	e	36
Uinta	Natural Buttes	NBU 1022-1A	Enserch Exploration	10	s	22	e	1
Washakie	Savery	C-11 / Fee	Fuel Resources Development	12	n	90	w	11
Washakie	Five Mile Gulch	3 Unit	Amoco Production	21	n	93	w	35
Washakie	Dripping Rock	Dripping Rock 3	Celsius	14	n	94	w	8
Washakie	Dripping Rock	Dripping Rock 5	Celsius	14	n	94	w	19
Washakie	Siberia Ridge	5-2 Siberia Ridge Unit	Amoco Production	21	n	94	w	5
Washakie	Wildrose	Wild Rose 1	----- Confidential -----					
Wind River	Madden	1-27 Lookout	Monsanto Oil	39	n	91	w	27

Table 3.3.1 List of wells for which LAS files were obtained or created and are used for routine and advanced log analysis (n = 20).

Task 4. Measure Rock Properties

Subtask 4.1. Measure Basic Properties (K, ϕ , Grain Density) and Select Advanced Population

4.1.1 Task Statement

Objectives of this task are to perform routine core analysis on not less than a total of 300 core samples. Data to be obtained include: whole-core porosity, permeability and grain density where previously measured and publicly available; routine helium porosity, routine air and *in situ* Klinkenberg permeability, and grain density. These measurements are intended to provide a basis for selecting the representative 150 samples for more advanced testing.

4.1.2 Methods

4.1.2.1 Sample Preparation

Plug collection methods are described in Section 3.2.2.

The first core samples obtained, from the Amoco Five Mile Gulch Unit 3 and American Hunter Old Road #1 wells, were vacuum/pressure saturated with a toluene/methyl alcohol azeotrope, and then soxhlet extracted with toluene/methyl alcohol to remove any remnant oil and salts. They were dried in an oven at 60°C to a constant weight within ± 0.003 g. Subsequent to these two wells, cores from the remaining wells were vacuum saturated with methyl alcohol, maintained in the methyl alcohol bath for not less than 3 days, air dried for approximately 3 days, immersed again in methyl alcohol to rinse off any salts precipitated from surface evaporation, and then dried in a convection oven at 60°C to a constant weight within 0.003 g. Cores were generally left in the oven for 3 to 6 days. This sample preparation procedure allowed the processing of many hundreds of core plugs. The potential impact of convection oven drying to constant weight is discussed below in section 4.1.2.5.

4.1.2.2 In situ Porosity and Pore Volume Compressibility –

Although pore volume compressibility was not a stated objective of this study it is necessary to understand how pore volume changes with increasing confining pressure because the *in situ* permeability, electrical properties, critical gas saturation, and MICP measurements are

all measured with the core under confining pressure. To better understand how pore volume changes with confining stress, pore volume compressibility measurements were performed on 113 representative samples. To measure *in situ* porosity the cores were evacuated for a period of eight (8) hours and then saturated with a deaerated 200,000 parts per million by weight sodium chloride (ppmw NaCl) brine solution. After vacuum saturation, complete saturation was obtained by applying a pressure of 7 MPa (1,000 psi) for a period of 24 hours to the saturating brine and samples. Complete saturation was confirmed by agreement between helium-measured porosity and gravimetric-saturation porosity values within 0.1 porosity percent. The cores were left immersed in deaerated brine for a period of 1 week.

After the cores had reached equilibrium with the brine, each was placed in a biaxial Hassler-type core holder and subjected to a series of increasing hydrostatic confining stresses of 1.38, 2.76, 6.9, 13.8, and 27.6 MPa (200, 400, 1000, 2000 and 4000 psi) approximating a range of reservoir stress conditions. For the Hassler cell used the porosity change from unconfined conditions to the first confining pressure of 1.38 MPa (200 psi) could not be measured. This is because the rubber confining sleeve had to be “set” to make full contact with the outer surface of the sample to prevent expulsion of brine in open gaps between the core and sleeve from being incorrectly interpreted as expelled pore water. This pressure varies with the core diameter and surface roughness. Calibration measurements indicate that the sleeve is set for most regular core samples with diameter of 2.50-2.54 cm (0.98-1.00 inches) at 0.35±0.17 MPa (50 ± 25 psi). Based on this sleeve response to stress, the hydrostatic confining pressures were estimated to induce the following net effective confining pressure on the core: 1.0, 2.4, 6.7, 13.4, and 27.2 MPa (150, 350 950, 1950, 3950 psi).

Pore volume decrease was determined by measuring the brine displaced from the core by compression using a micropipette, correcting for system compressibility changes. Pore pressure was at atmospheric pressure. Porosity calculations were performed assuming that the grains of the rock are incompressible and hence the bulk volume decreased by the same amount as the pore volume. Porosity was referenced to an assumed condition that at 0.35 MPa (50 psi) the pore volume equaled the routine helium pore volume. Pore volume change from 0.35 MPa (50 psi) to 1.38 MPa (200 psi) confining pressure was estimated by extrapolation of the pore volume compressibility trend from 1.39 – 27.6 MPa (200-4,000 psi). Equilibrium at pressure was assumed if pore volume change was less than 0.001 cc for a ten (10) minute period.

In addition to the compressibility measurements, *in situ* porosity measurement was obtained on 310 core samples during the electrical resistivity measurements. The complete experimental method for the electrical properties measurement is described under Task 4.4. For the *in situ* porosity aspect of the resistivity measurement, the core pore volume change was measured as described above for compressibility except that only a zero reading at 1.38 MPa (200 psi) and the expelled brine at 27.2 MPa (3950 psi) were recorded. The total porosity change was calculated as described above. A key difference in this measurement is that equilibrium was established when the electrical resistance was stable and not necessarily when pore volume change met compressibility equilibrium conditions. Electrical equilibrium was generally established within 10±5 minutes which represented only 10%-15% of the time for compressibility analysis.

4.1.2.3 Routine Helium Porosity and Grain Density

Routine helium porosities were determined using a Boyle's Law technique. Dry sample weights were measured to ±0.001 g and bulk volume was determined by Archimedes's Principle method by immersion in mercury and by caliper to an accuracy of ±0.02 cc. Ambient Helium porosity was measured to an accuracy and precision of better than ± 0.1 porosity percent. Grain density was calculated from the helium-measured grain volume and dry weight to an accuracy and precision of better than ±0.01 g/cc.

4.1.2.4 Routine Air and In Situ Klinkenberg Permeability

To measure routine air permeability each core was placed in a biaxial Hassler-type core holder and subjected to a hydrostatic confining stress of 4.14 MPa (600 psi). Permeability was measured from steady-state Nitrogen-gas flow measured at a constant upstream pressure of 20 psi to 400 psi, depending on the core permeability, with the downstream pressure at atmospheric pressure. Gas flow rate was measured using a high- or ultra-low flow range electronic mass flow meter for gas flow rates down to 0.05 scc/min and a bubble tube with a stop watch for flow rates less than 0.05 scc/min.

It is well recognized that it is necessary to restore low-permeability core samples to *in situ* stress conditions to obtain permeability values that are representative of the reservoir ([Vairogs et al., 1971](#); [Thomas and Ward, 1972](#); [Byrnes et al., 1979](#); [Jones and Owens, 1980](#); [Walls et al., 1982](#); [Sampath and Keighin, 1981](#); [Ostensen, 1983](#); [Wei et al., 1986](#); [Luffel et al.,](#)

[1991](#); [Byrnes, 1997](#); [Byrnes and Castle, 2000](#); [Byrnes, 2005](#)). To achieve uniformly constant approximate *in situ* conditions, subsequent to the routine air permeability measurement, the hydrostatic confining pressure was increased to 27.6 MPa (4,000 psi) greater than the mean pore pressure in the core. *In situ* Klinkenberg permeability was determined by measurement of permeability to nitrogen at two pore pressures and extrapolation of the k vs. $1/P$ trend to infinite pore pressure to obtain the Klinkenberg permeability at the intercept. The Klinkenberg gas permeability, which is equivalent to single-phase inert liquid or high pressure gas absolute permeability, increases with decreasing pore size. Equilibrium times ranged from 2 to 30 minutes with decreasing permeability.

4.1.2.5 Impact of Drying vs. Native State or Restored State Analysis on Permeability

Both low-humidity and humidity-oven drying at a relative humidity of 45% have been used for low-permeability sandstones. Experimental methodology in low-permeability sandstone core preparation is complicated by uncertainties in microscopic properties including water distribution, clay mineral hydration state, and salt distribution. Studies by Soeder ([1986](#)) and Morrow et al ([1991](#)) concluded that preserved core provide more accurate effective gas permeability values. However, although porosity and saturation differences were not reported, saturation differences between the dry and hydrated samples can be estimated to be $S_w=10\pm 5\%$. For these saturation differences the observed decrease in hydrated sample gas permeability of 57-96% of dry permeability is consistent with relative permeability decreases observed in Figure 3.1.1 and 3.1.2. That is, the observed lower permeability for hydrated samples can be interpreted to have been the result of relative permeability effects instead of drying.

Morrow et al ([1991](#)) hypothesized that the original salt content of the brine that originally occupied the pore space remained in the pores because the present lower water saturation was achieved by evaporation. Though possible, this hypothesis was not tested. To resaturate the cores Morrow et al used fresh water and, therefore, implicitly hypothesized that: 1) the remnant salt was uniformly distributed in the pore space; 2) remnant salt would dissolve in the injected fresh water in the pore resulting in a uniform brine concentration that was compatible with the clays; 3) during the process of cutting the core plug with fresh tap water no significant flushing occurred to remove the dried salts; 4) the fresh water did not damage any clays prior to dissolving the remnant salt; and 5)

confining stress hysteresis effects were negligible as required by their comparison of stressed preserved core effective gas permeabilities to subsequently dried and stressed dried core effective gas permeabilities.

In the Morrow et al ([1991](#)) study, comparison of the relative role of confining pressure and preservation versus drying (their Figure 7) shows that differences of +1,000 psi confining pressure result in a greater difference in effective gas permeability than differences resulting from preservation state for all saturation levels ($S_w = 0\%-60\%$). This strong influence of stress sensitivity implies that error associated with stress sensitivity hysteresis has to be removed for quantitative analysis of the relative influence of preservation. Further, it is recognized that core containing swelling clays is sensitive to fresh water. If the remnant dry salts are either: 1) no longer at the correct salinity; or 2) not uniformly distributed throughout the pore space such that imbibing fresh water would mix to form a uniform brine of the correct salinity in equilibrium with the pore-lining or pore-bridging expansive clay; then imbibition of fresh water is likely to cause clay swelling and permeability decrease, consistent with the decrease Morrow et al ([1991](#)) attributed to clay states resulting from preservation versus drying.

Soeder ([1986](#)) presents differences in preserved state and dry permeabilities but did not report porosity and saturations to provide a basis for quantitatively estimating possible relative permeability influence. Soeder ([1986](#)) also presents Scanning Electron Microscope (SEM) images of dry and preserved pores noting damage in the dried samples. It is important to note that all SEM images shown were of dried samples because the SEM images presented were not obtained in an environmental SEM (commonly used for biologic SEM imaging). In fact, nearly all SEM images of tight gas sandstone clays presented in publications are from dried samples that are conventionally gold coated. The preservation of delicate clay structure in all these images can be interpreted to indicate that moderate drying does not damage clays.

The above discussion does not reject the hypothesis that gas permeabilities are most accurately measured on preserved core. To the contrary, it can be reasonably argued that the closer to native-state conditions a core remains the more accurate the measured properties will remain. However, the above discussion illustrates that a given experimental procedure does not always guarantee that the microscopic properties of the core have been perfectly preserved nor that any change in environmental conditions results in “significant” and unacceptable change to key properties. It is also clear that gas permeabilities measured on core are always influenced by a wide

range of environmental variables to which the core has been subjected and is subjected to for a given measurement including principally: 1) stress history; 2) draining and imbibing fluid composition and history; 3) testing history; and 4) pore-lining or pore-bridging mineral (e.g., clay) composition. Beyond these considerations there are considerations concerning the nature of the property for which data are needed. Preserved core may provide more accurate effective gas permeabilities but not absolute permeability. If helium porosity is measured on the cores in this state the measured grain density and total porosity values are affected. The extent to which these are affected can only be quantitatively determined by subsequently drying the core and retesting. Further, accurate mercury intrusion capillary pressure analysis requires a clean dry surface for the general mercury-mercury vapor interfacial tension and contact angle to apply. Therefore this measurement requires a dried core and initial pore volume measured at dry conditions.

The primary purpose of this research was to provide a database of basic properties and to use the observed values to select samples for mercury intrusion capillary pressure analysis, and electrical properties analysis and critical-gas permeability measurement on resaturated cores. Given: 1) the unpreserved state of 38 of the 44 cores; 2) the need for accurate total porosity; 3) the large population of cores; 4) the need for cores that do not contain significant content of remnant salt; and 5) the need for clean dry cores for MICP, it was decided to clean and dry the cores, recognizing that some modification to gas permeability might result.

4.1.3 Results and Discussion

Appendix 1 summarizes all routine helium porosity, grain density, routine air permeability, *in situ* Klinkenberg permeability, and sample lithologic digital description data for all core plugs in the project. These data are also presented in Excel workbook form on the Project Website at <http://www.kgs.ku.edu/mesaverde/reports.html>.

4.1.3.1 Grain Density

Grain density distribution averages 2.653 ± 0.04 g/cc (error bar is 1 standard deviation; Fig. 4.1.1). Grain density distribution is skewed slightly to high density reflecting variable concentration of calcite, dolomite, and rare pyrite cement. Grain densities for the wells sampled exhibit a slight difference in distribution among basins (Fig 4.1.2, Table 4.1.1). It is important to note the small sample population of the Powder and Wind River Basin samples and these may be biased for conditions in the few wells and intervals sampled.

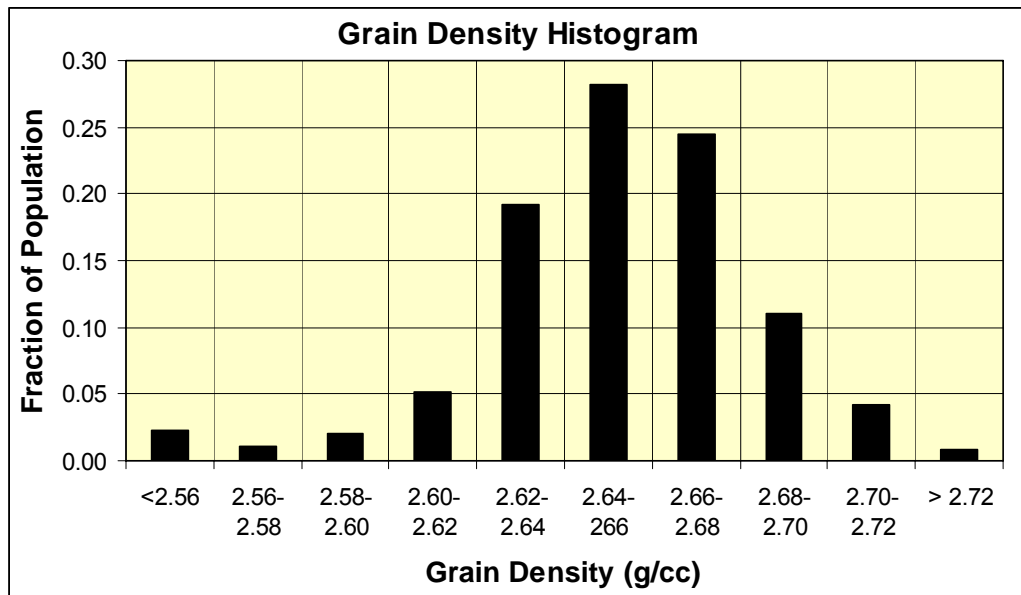


Figure 4.1.1. Grain density distribution for all basins and all samples (n=2200). Distribution is near normal with mean = 2.653 ± 0.04 g/cc. Slight skewness to higher values primarily reflects variable concentration of carbonate cement (n = 2184).

	All Basins	Greater Green River	Washakie	Uinta	Piceance	Wind River	Powder River
Mean	2.653	2.648	2.660	2.639	2.660	2.673	2.679
Median	2.654	2.645	2.662	2.649	2.661	2.673	2.674
St Dev	0.040	0.029	0.034	0.052	0.038	0.029	0.026
Minimum	2.30	2.50	2.47	2.30	2.35	2.51	2.60
Maximum	2.84	2.77	2.79	2.80	2.84	2.73	2.75
Kurtosis	15.1	2.6	3.7	13.2	14.0	10.2	3.9
Skewness	-2.00	0.28	-0.18	-2.82	-1.19	-1.87	-0.28
Count	2184	566	393	532	583	82	28

Table 4.1.1. Summary statistics for grain density for all original and duplicate cores by basin.

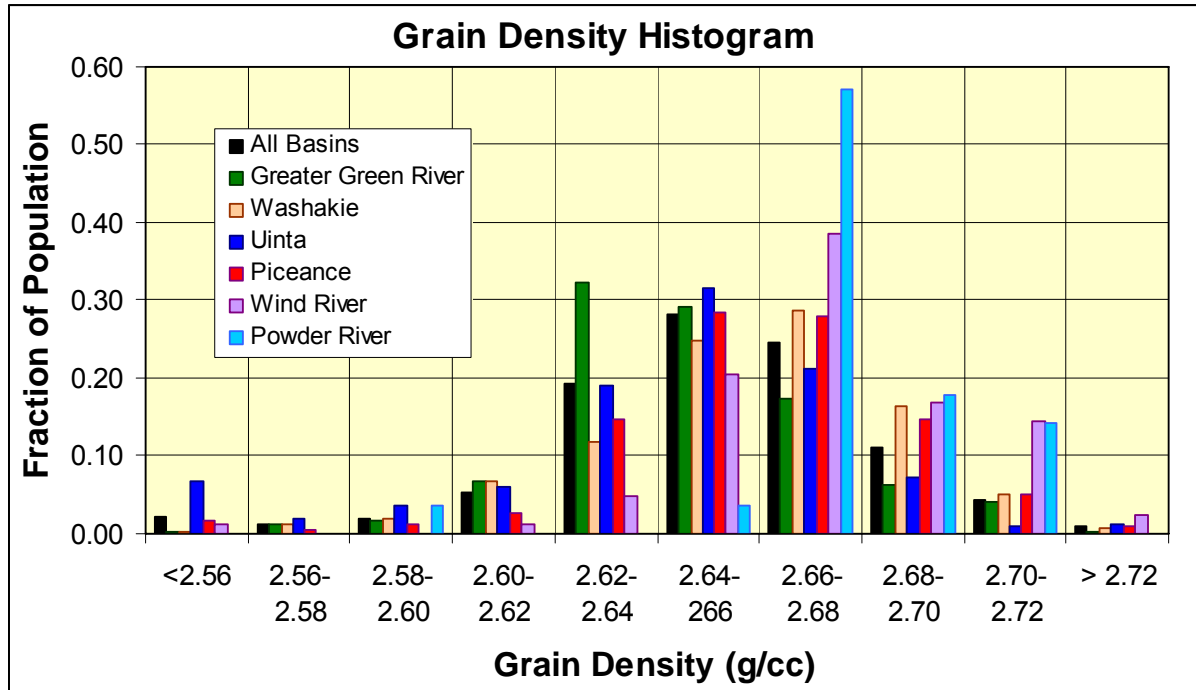


Figure 4.1.2. Grain density distribution by basin showing differences among basins (n = 2184).

4.1.3.2 Porosity

The porosity distribution is skewed to lower porosity (Fig. 4.1.3) consistent with general porosity distribution in the Mesaverde sandstone (Table 4.1.2). The large population of cores with porosity of $\phi = 0-2\%$ partially reflects a heavy sampling of low porosity intervals in two Green River Basin wells (Fig. 4.1.4).

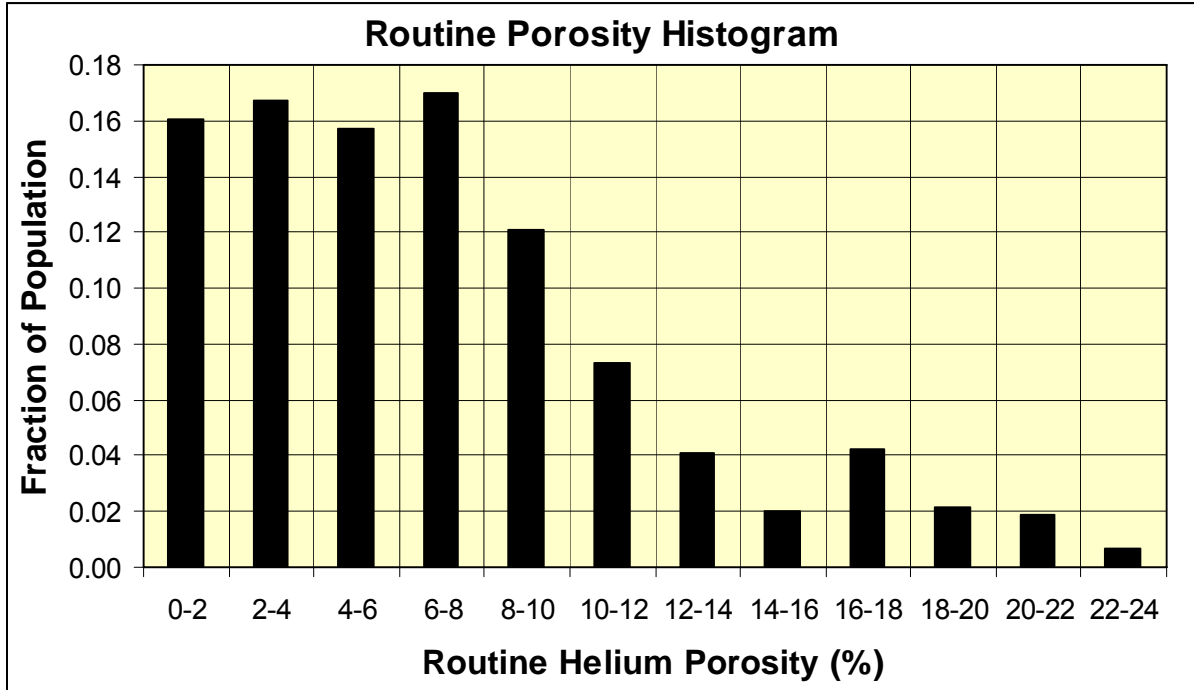


Figure 4.1.3. Porosity distribution for all samples (n = 2209).

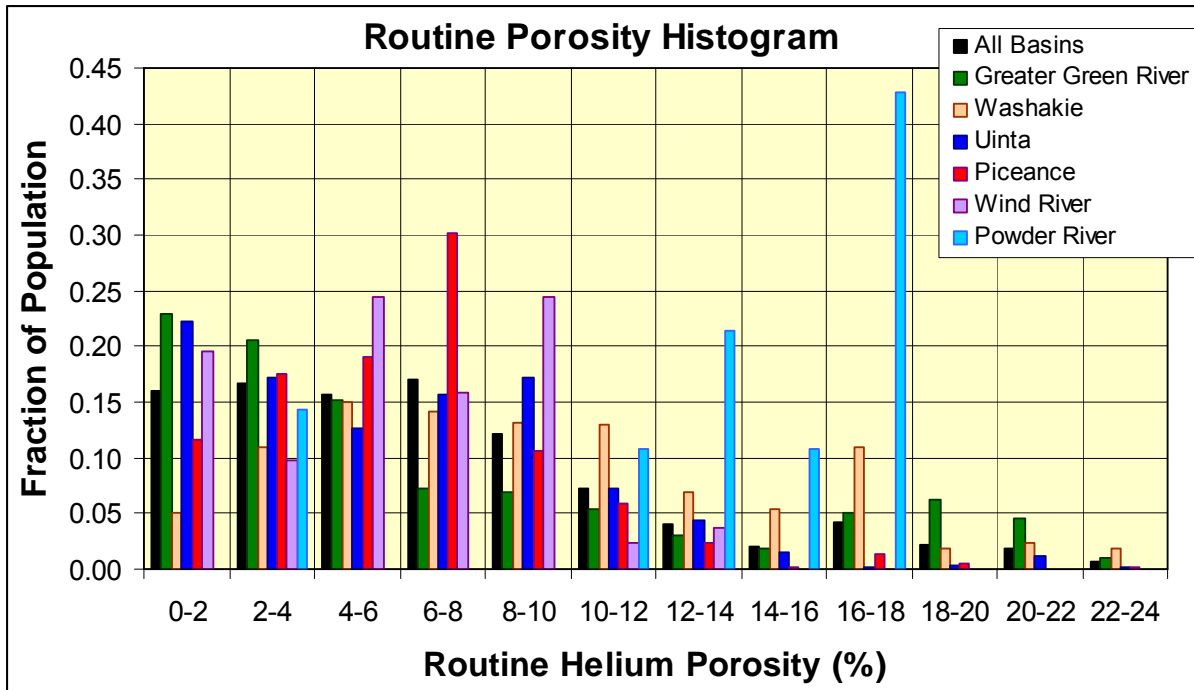


Figure 4.1.4. Porosity distribution by basin.

	All Basins	Greater Green River	Washakie	Uinta	Piceance	Wind River	Powder River
Mean	7.1	7.3	9.5	6.1	6.1	5.8	13.2
Median	6.2	4.6	8.7	5.9	6.1	5.5	15.1
St Dev	5.1	6.4	5.4	4.2	3.8	3.3	4.5
Minimum	0.0	0.0	0.0	0.0	0.0	0.0	2.6
Maximum	24.9	23.6	23.8	22.2	24.9	13.2	16.9
Kurtosis	0.7	-0.4	-0.4	1.1	4.5	-0.8	1.0
Skewness	1.0	1.0	0.5	0.9	1.4	0.1	-1.5
Count	2209	568	395	539	596	83	28

Table 4.1.2. Summary statistics for routine helium porosity for all samples by basin.

For 776 core plugs greater than 7.5 cm (3-inch) in length, the cores were cut in half to provide two paired core plugs for advanced properties measurements. Figure 4.1.5 illustrates the ratio of helium porosities of samples to the mean porosity of the sample pair. Over 75% of all samples exhibit porosity within 10% of the mean porosity of the porosity pair, and 88% exhibit porosities within 20%. For a rock with 10% porosity this distribution translates to 75% of adjacent cores would exhibit a porosity of 9-11% and an additional 13% of the population would exhibit porosities of 8-9% or 11-12%.

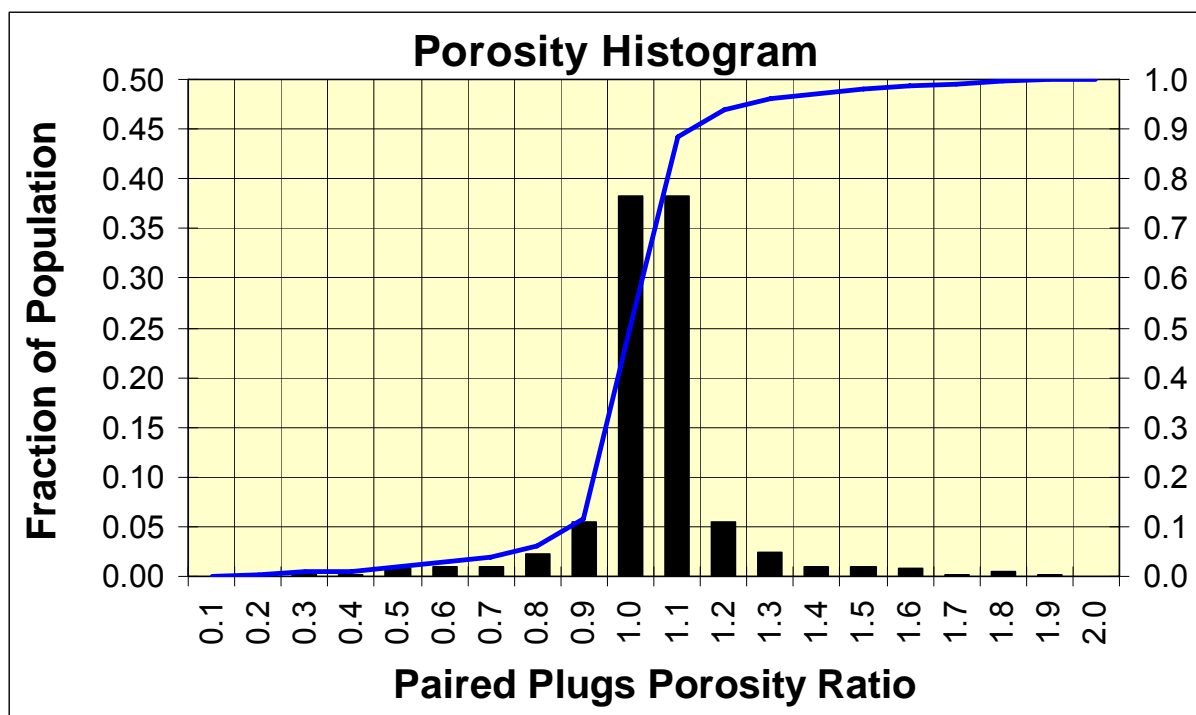


Figure 4.1.5. Histogram of ratio of paired plug porosities to mean porosity of plug pair. n = 652 pairs (n= 1304)

4.1.3.2.1 *In situ Porosity and Pore Volume Compressibility –*

Previous studies have investigated the effect of confining pressure on porosity and pore volume compressibility in sandstones, carbonates, and siltstones ([Carpenter and Spencer, 1940](#); [Hall, 1953](#); [Fatt, 1958](#); [McLatchie et al, 1958](#); [Mann and Fatt, 1960](#); [Dobrynin, 1962](#); [Knutson and Bohor, 1962](#); [Newman, 1973](#); [Mattax et al, 1975](#); [Newman and Martin, 1977](#); [Somerton and Matherson, 1978](#); and [Greenwald and Somerton, 1981a, 1981b](#)). The nature of pore volume change to confining stress has been shown to be a function of a range of variables most notably including; stress history ([Mattax et al, 1975](#)), two- and three-dimensional stress distribution ([Keelan, 1986](#); [Anderson, 1985](#); [Worthington et al, 1997](#)), degree of consolidation ([Newman, 1973](#); [Yale et al, 1993](#)), water saturation ([Mann and Fatt, 1960](#)), temperature and pore geometry ([Toksoz et al, 1976](#); [Cheng and Toksoz, 1979](#); [Walsh and Grosenbaugh, 1979](#); [Ostensen, 1983](#); [Katsube et al, 1992](#)). The modeling of Cheng and Toksoz ([1979](#)) shows that the pressure dependence of pores is highly sensitive to pore aspect ratio (α). Based on this, Katsube et al ([1992](#)) divided pores into three types: elastically rigid ($\alpha > 0.1$), elastically flexible ($\alpha = 0.001$ –

0.1), and highly stress sensitive sheet-like or crack-like pores ($\alpha < 0.001$). The work of Walsh and Grosenbaugh (1979) and Ostensen (1983) defined the nature of stress dependence of cracks and Jones and Owens (1980) showed that low-permeability sandstones had thin, sheet-like tabular pores based on their response to stress. The crack-compression model of Walsh and Grosenbaugh (1979) expresses the relationship between porosity and stress as:

$$\phi_i/\phi_o = A \log Pe + B \quad [4.1.1]$$

Where ϕ_i = porosity at defined effective *in situ* stress P_e , ϕ_o = reference initial porosity, P_e = effective confining stress, A and B are empirical constants that vary with rock properties.

The work of Jones and Owens (1980) and Sampath (1982) on the pore volume compressibility of low-permeability sandstones demonstrated that pore-volume compressibility values are generally low ($\beta < 6 \times 10^{-6} \text{ psi}^{-1}$). A population of 113 core samples representing a range of lithofacies and porosity was selected to measure pore volume compressibility (Appendix 2). Figure 4.1.6 illustrates the measured pore volume change from 1.0 – 27.2 MPa (150-3,950 psi) net effective confining pressure and estimated from 1.0 MPa down to a confining pressure predicted by the log-linear trend where the pore volume equals the routine helium porosity. In general this pressure was at a net effective stress of approximately 69 kPa (10 psi). Every sample exhibits a log-linear relationship between the fraction of initial pore volume (unconfined pore volume) at confining stress and the confining stress. The average correlation coefficient of the log-linear relationships is 0.99 ± 0.031 (error range is 2 standard deviations). Data are presented in Appendix 2.

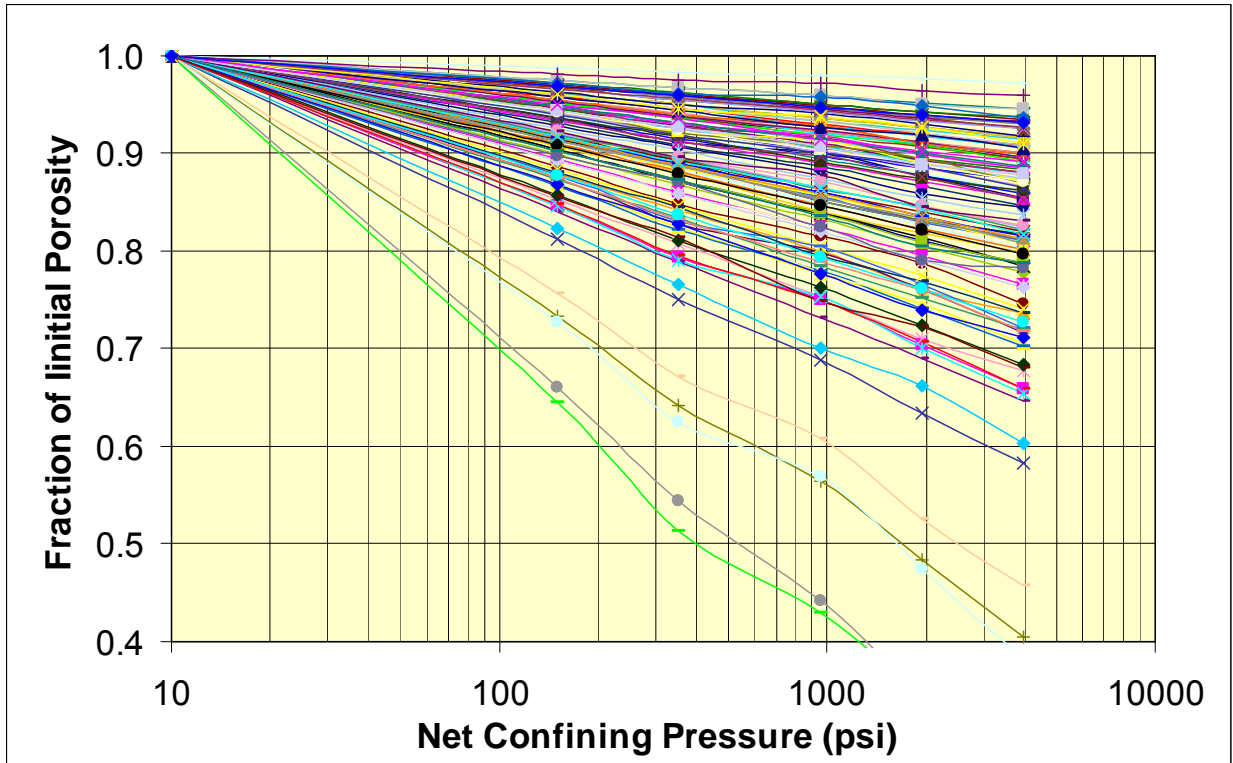


Figure 4.1.6. Cross-plot of fraction of initial pore volume versus net confining stress for 113 Mesaverde samples. Every sample exhibits a log-linear relationship though slopes and intercepts differ.

To develop an approximate predictive model of pore volume and pore volume compressibility change the slopes and intercepts of the curves in Figure 4.1.6 were correlated with porosity (Figs. 4.1.7 and 4.1.8). The slope and intercept of the curves shown in Figure 4.1.6 can be predicted using:

$$\phi_i/\phi_o \text{ Slope} = A = -0.00549 - 0.155/\phi^{0.5} \quad [4.1.2]$$

$$\phi_i/\phi_o \text{ Intercept} = B = 1.045 + 0.128/\phi \quad [4.1.3]$$

as shown in Figures 4.1.7 and 4.1.8.

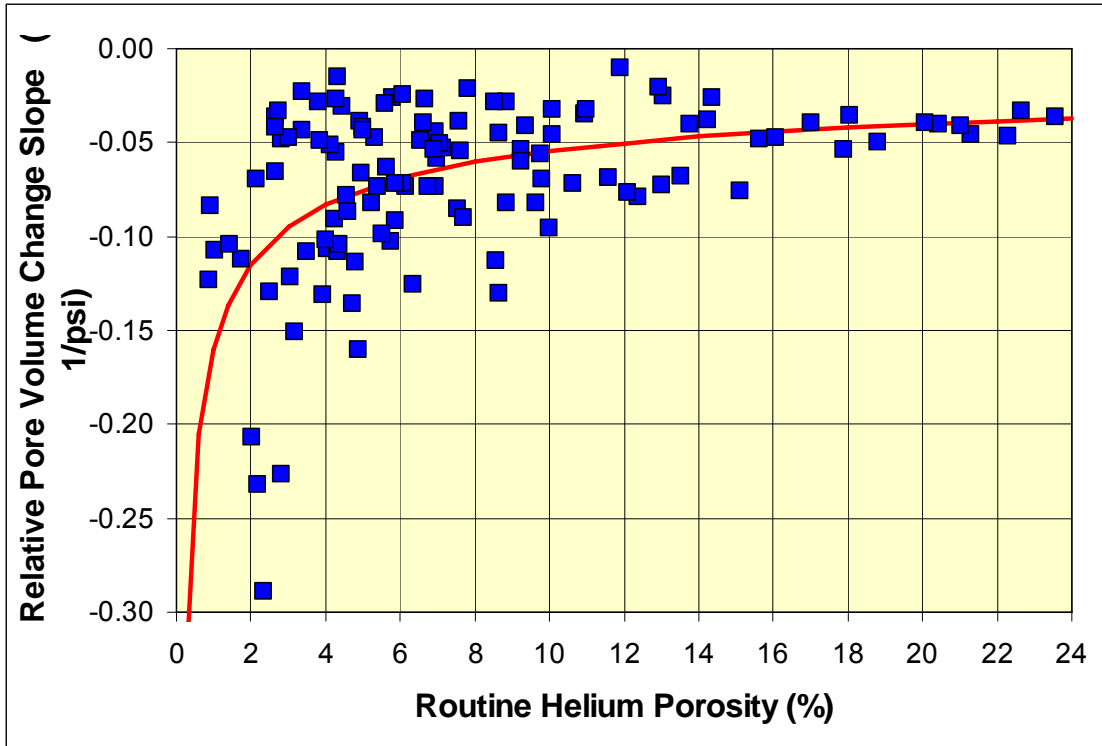


Figure 4.1.7. Cross-plot of slope of log-linear curves in Figure 4.1.6 with porosity. The relationship between the slope and porosity can be expressed: $\text{Slope} = -0.00549 - 0.155/\phi^{0.5}$

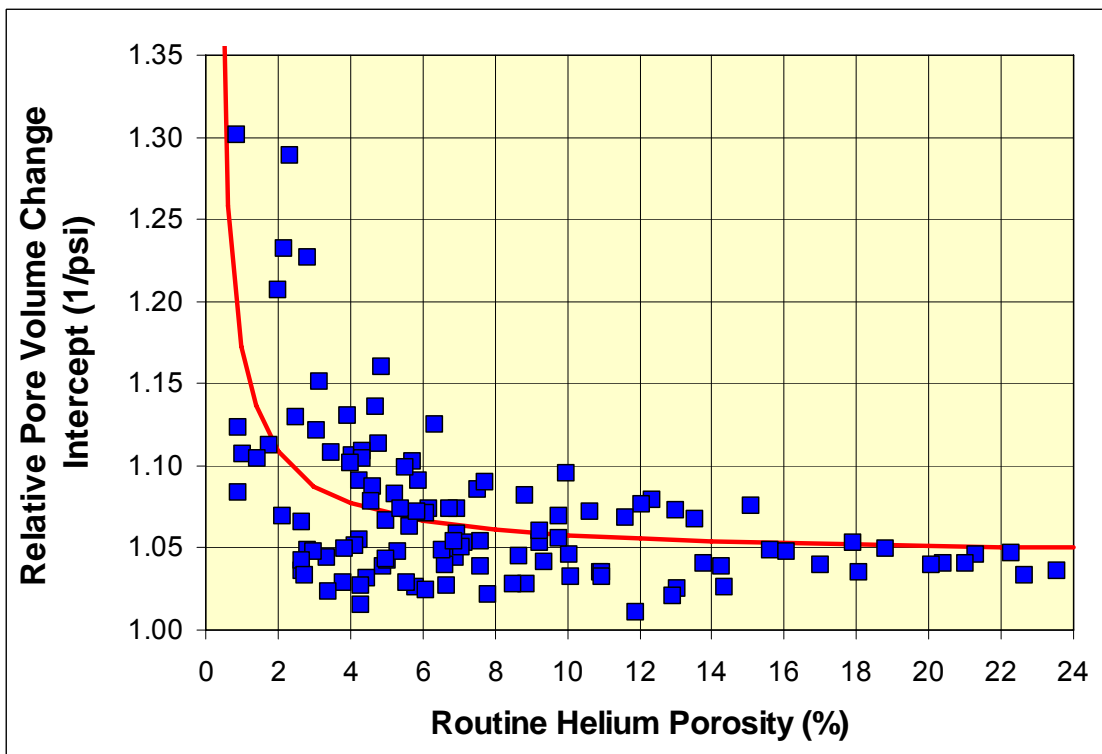


Figure 4.1.8. Cross-plot of intercept of log-linear curves in Figure 4.1.6 with porosity. The relationship between the intercept and porosity can be expressed: $\text{Intercept} = 0.128 \phi + 1.0045$

Utilizing equations 4.1.2 and 4.1.3 to calculate slopes and intercepts for rocks of different porosity, the fraction of initial pore volume relationship can be transformed to pore volume compressibility (change in volume/ unit volume/ change in pressure; β , 1/psi or 1/MPa). The above equations result in a power-law relationship between pore volume compressibility and net effective confining pressure of a form:

$$\log_{10} \beta = C \log_{10} P_e + D \quad [4.1.4]$$

Figures 4.1.9 and 4.1.10 show the slope and intercept relationships for prediction of pore volume compressibility of low-permeability sandstones that conform to equations 4.1.2 and 4.1.3. The slope and intercept of the pore volume compressibility relations can be predicted using:

$$C = -1.035 + 0.106/\phi^{0.5} \quad [4.1.5]$$

$$D = 4.857 \phi^{-0.038} \quad [4.1.6]$$

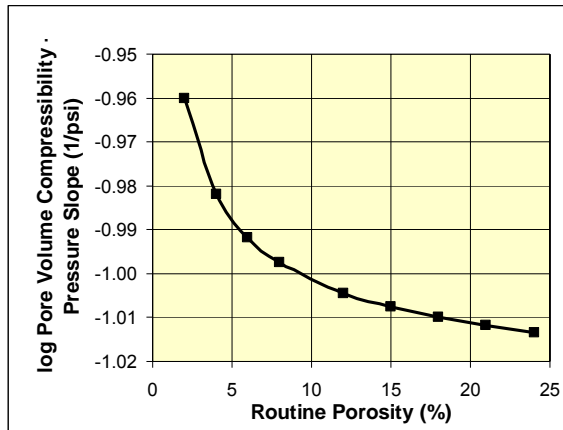


Figure 4.1.9. Cross-plot of pore volume compressibility slope function versus porosity.

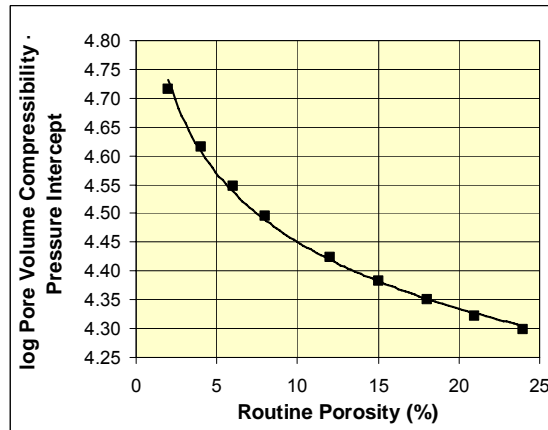


Figure 4.1.10. Cross-plot of pore volume compressibility intercept function versus porosity.

Inserting equations 4.1.5 and 4.1.6 into equation 4.1.4 and taking the antilog of both sides:

$$\beta = 10^{[(-1.035+0.106/\phi^{0.5})\log_{10} P_e+(4.857\phi^{-0.038})]} \quad [4.1.7]$$

where β is the pore volume compressibility ($10^{-6}/\text{psi}$), P_e is the average net effective confining pressure at which β applies, and ϕ is the unconfined routine porosity (%). From equation 4.1.7 it is evident that compressibility changes with sandstone porosity and the net effective stress. Figure 4.1.11 illustrates general compressibility curves for different porosity Mesaverde sandstones and siltstones.

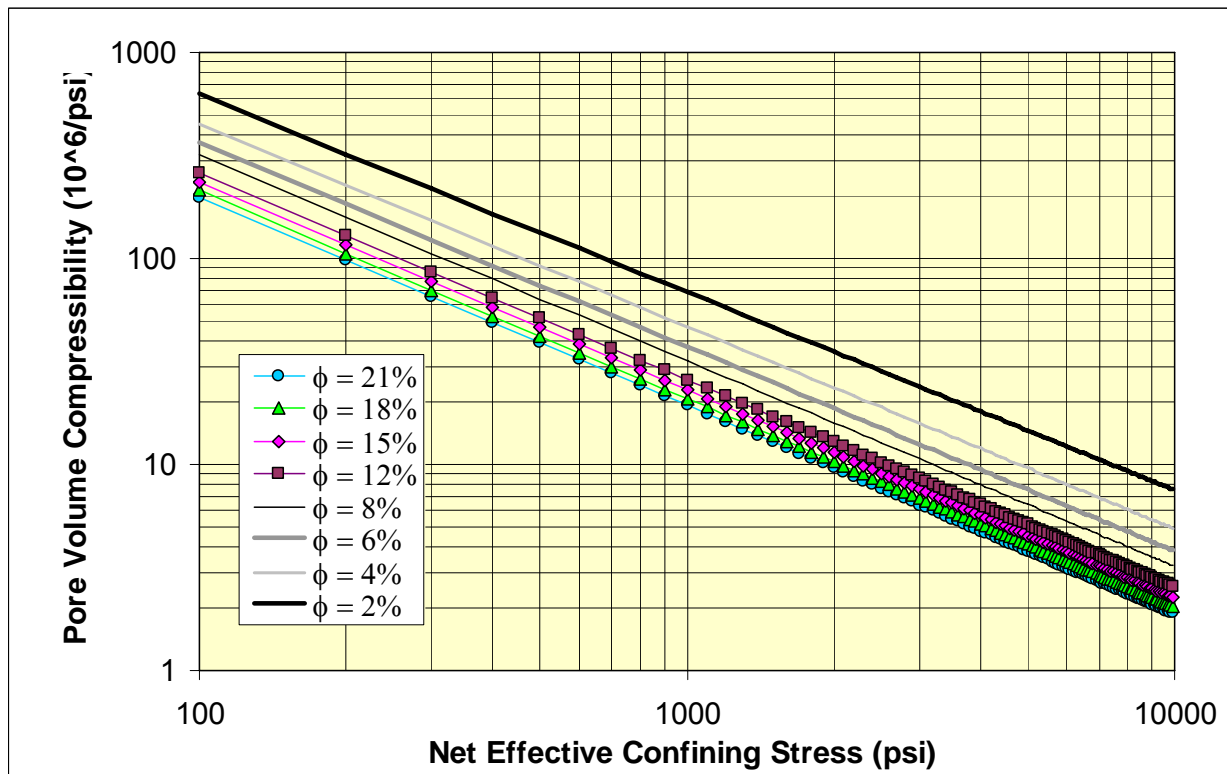


Figure 4.1.11. Pore volume compressibility versus net effective stress for Mesaverde sandstones and siltstones of various porosity as predicted using equation 4.1.7.

Pore volume compressibilities predicted using equation 4.1.7 are generally consistent with values published in the literature (e.g., [Jones and Owens, 1980](#)) for individual samples, usually reported at a single net effective stress. It is important to note that compressibility increases with decreasing confining stress and with decreasing porosity (Figure 4.1.11).

To compare *in situ* and routine porosity it is necessary to correct the bulk volume of the sample for the pore volume change, assuming that grain compressibility is negligible. In this study both the compressibility and the pore volume change during electrical properties measurement provided a basis for comparison of routine and *in situ* porosity. Figure 4.1.12

illustrates the relationship between the measured *in situ* porosity (at 26.7 MPa (4,000 psi) net effective stress) and the routine porosity. Reduced major axis analysis of this relationship can be expressed:

$$\phi_i = 0.943 \phi_{\text{routine}} - 0.23 \quad [4.1.8]$$

where ϕ_i = *in situ* porosity (%) at 26.7 MPa (4,000 psi) net effective stress and ϕ_{routine} = unconfined routine porosity (in %).

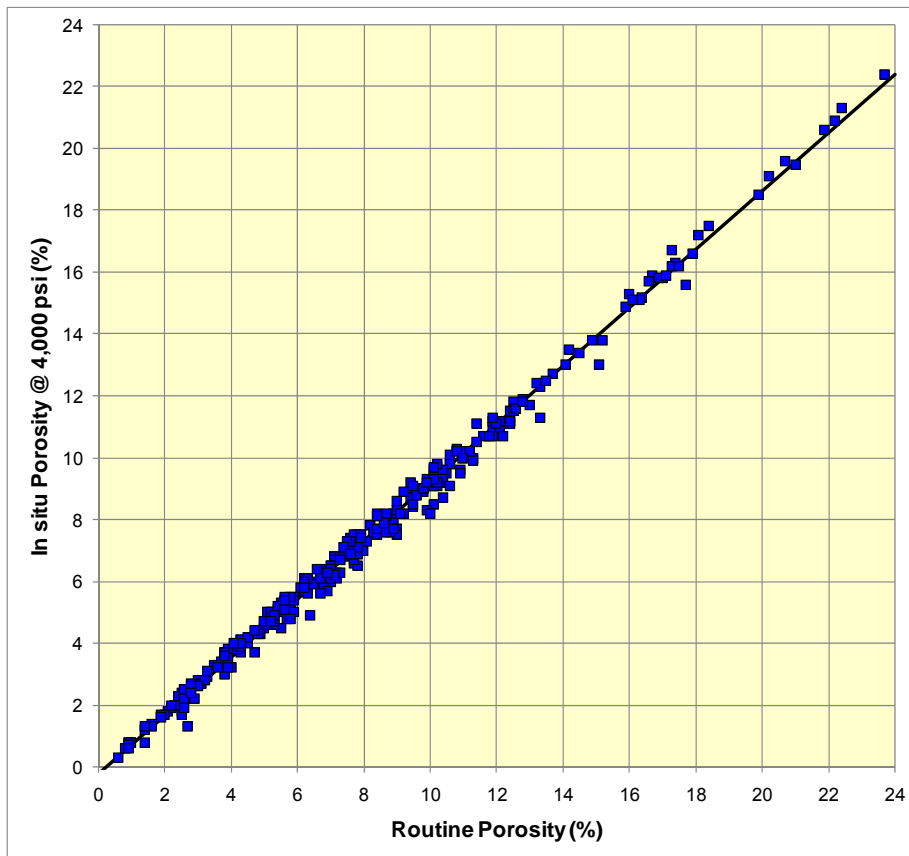


Figure 4.1.12. Cross-plot of routine porosity and *in situ* porosity measured at 26.7 MPa (4,000 psi) net effective hydrostatic confining stress for 310 cores during electrical resistivity measurement. Correlation line represents equation 4.1.8.

Applying equation 4.1.7 at $P_e = 26.7 \text{ MPa (4,000 psi)}$ we can estimate the pore volume change and calculate the corresponding *in situ* porosity for any given initial porosity. Figure 4.1.13 illustrates a comparison of the estimated porosity at $P_e = 26.7 \text{ MPa (4,000 psi)}$ compared to the initial, “routine,” porosity. Equation 4.1.9 illustrates the general form of an *in situ* versus

routine porosity trend and equations 4.1.10 through 4.1.14 show models from this study (Mesaverde Study) for the compressibility measurements, for porosity change measured in conjunction with electrical properties measurement, and from other previously published low-permeability sandstone studies including the Travis Peak ([Luffel et al, 1991](#)), Mesaverde/Frontier ([Byrnes, 1997](#)), and Clinton/Medina ([Byrnes and Castle, 2000](#)):

All Studies:	$\phi_i = A \phi_{\text{routine}} + B$	[4.1.9]
Mesaverde Study Compressibility:	$\phi_i = 0.96 \phi_{\text{routine}} - 0.73$	[4.1.10]
Mesaverde Study Electrical Properties:	$\phi_i = 0.943 \phi_{\text{routine}} - 0.23$	[4.1.11]
Travis Peak:	$\phi_i = 0.95 \phi_{\text{routine}} - 0.3$	[4.1.12]
Mesaverde/Frontier:	$\phi_i = 0.998 \phi_{\text{routine}} - 0.8$	[4.1.13]
Clinton/Medina: (Porosity is in %)	$\phi_i = 0.966 \phi_{\text{routine}} + 0.02$	[4.1.14]

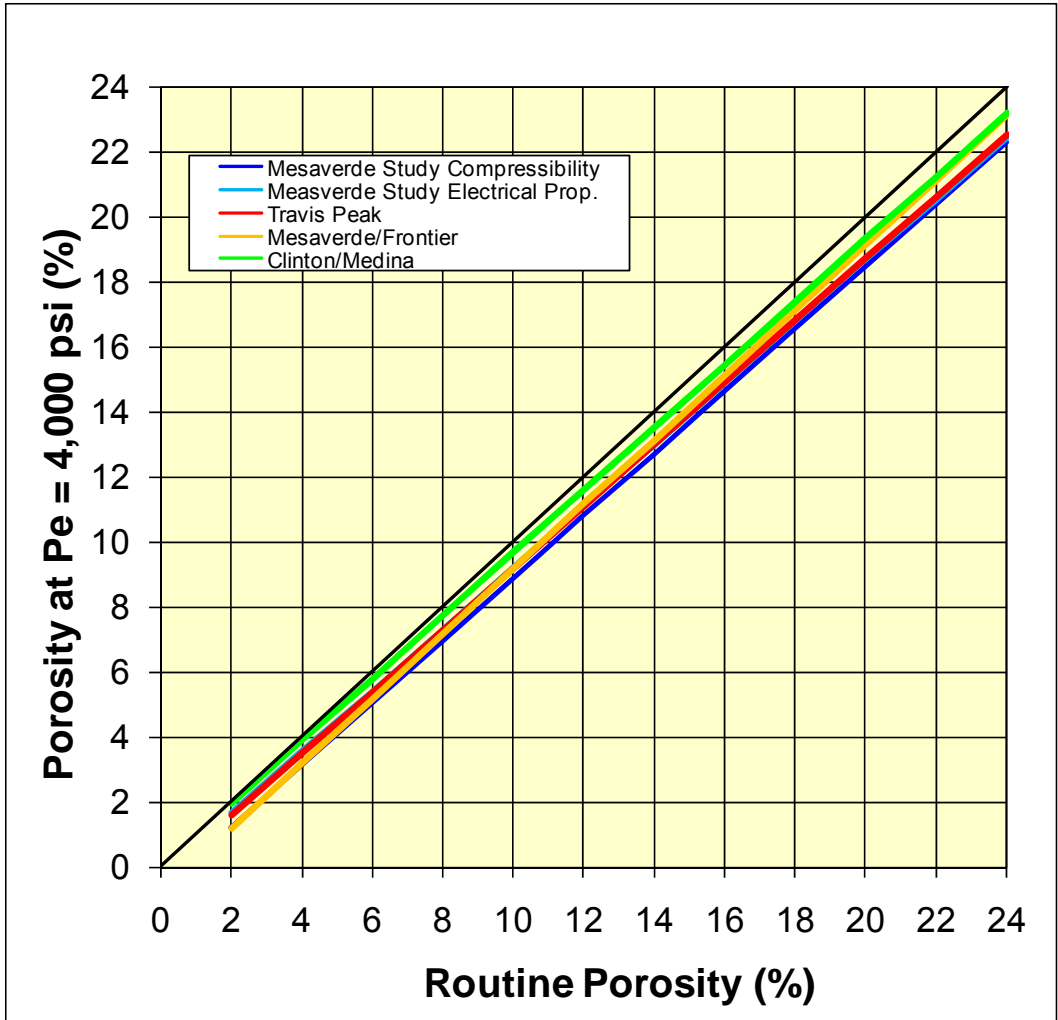


Figure 4.1.13. Cross-plot of estimated *in situ* porosity (at $P_e = 4,000$ psi) versus routine porosity, based on equation 4.1.8 assuming that pore volume change also represents bulk volume change, versus unconfined (e.g., routine) porosity. The slope and intercept are similar to values reported from low-permeability sandstones.

Predicted values can be compared for high and low porosity (Table 4.1.3) illustrating differences between the rocks and models.

	Travis Peak	Mesaverde/ Frontier	Clinton/ Medina	Mesaverde Study-Comp	Mesaverde Study-Elec
A >	0.950	0.998	0.966	0.960	0.943
B >	-0.300	-0.800	0.020	-0.73	-0.226
Routine Porosity	<i>In situ</i> Porosity (%)				
2	1.6	1.2	2.0	1.2	1.7
4	3.5	3.2	3.9	3.1	3.5
6	5.4	5.2	5.8	5.0	5.4
8	7.3	7.2	7.7	6.9	7.3
10	9.2	9.2	9.7	8.9	9.2
12	11.1	11.2	11.6	10.8	11.1
14	13.0	13.2	13.5	12.7	13.0
16	14.9	15.2	15.5	14.6	14.9
18	16.8	17.2	17.4	16.5	16.7
20	18.7	19.2	19.3	18.5	18.6
22	20.6	21.2	21.3	20.4	20.5
24	22.5	23.2	23.2	22.3	22.4

Table 4.1.3. Comparison of predicted porosity for present study (Mesaverde Study) from both the compressibility measurements and measurements performed in conjunction with electrical properties and previously published low-permeability sandstone studies cited in text.

Comparing predicted *in situ* porosity values for the different studies and measurements illustrates that the Clinton/Medina quartzose tight gas sandstones are the least compressible. Porosity changes for the Travis Peak and as measured with electrical properties for the Mesaverde are statistically identical. The greatest porosity decrease from routine conditions is exhibited by the Mesaverde samples measured in the compressibility analysis. The greater compressibility for these samples may be attributed to several causes including: 1) lithologic differences; 2) correction for sleeve effects; 3) wet versus dry; and 4) equilibration time under stress. For the samples measured in this study, because the compressibilities were measured in the same apparatus, it is interpreted that the two variables influencing the differences between the compressibility and electrical properties porosity changes are: 1) equilibration time; and, to a small degree 2) correction for sleeve effects. Given that the porosity changes observed during the compressibility measurements conformed to equilibrium criteria that would produce data for pore volume change that are more accurate, the compressibility data are interpreted to be most accurate. The increasing difference between the compressibility and electrical properties *in situ* porosities with decreasing porosity can be interpreted to indicate that pore volume compression equilibration time increase with decreasing porosity.

It is important to note that pore volume compressibility represents the elastic response to stress-field changes and does not necessarily exhibit the same pressure-dependence exhibited by porosity versus depth trends or compaction curve models ([Athy, 1930](#); [Dickinson, 1953](#)):

$$\phi_i/\phi_o = \exp[-\beta(Pe-Po)] \quad [4.1.15]$$

Where ϕ_i = porosity at defined effective *in situ* stress P_e , ϕ_o = reference initial porosity, P_e = effective confining stress, P_o = effective confining stress for ϕ_o and β is an empirical constant that varies with rock properties.

4.1.3.3 Permeability

Permeability for the core samples from all basins is approximately log-normally distributed (Fig. 4.1.14) with 52% of the samples exhibiting *in situ* Klinkenberg permeability in the range 0.0001-0.01 mD (1×10^{-7} - $1 \times 10^{-5} \mu\text{m}^2$) and 18% of the samples exhibiting $k_{ik} < 0.0001$ mD ($1 \times 10^{-7} \mu\text{m}^2$) and 30% exhibiting $k_{ik} > 0.01$ mD ($1 \times 10^{-5} \mu\text{m}^2$). The distribution of permeability for samples from different basins is generally similar (Fig. 4.1.15; Table 4.1.4) though slight differences in the mean and standard deviation exist. It is important to note that these distributions are for the sample set and may not reflect actual distributions within the basins.

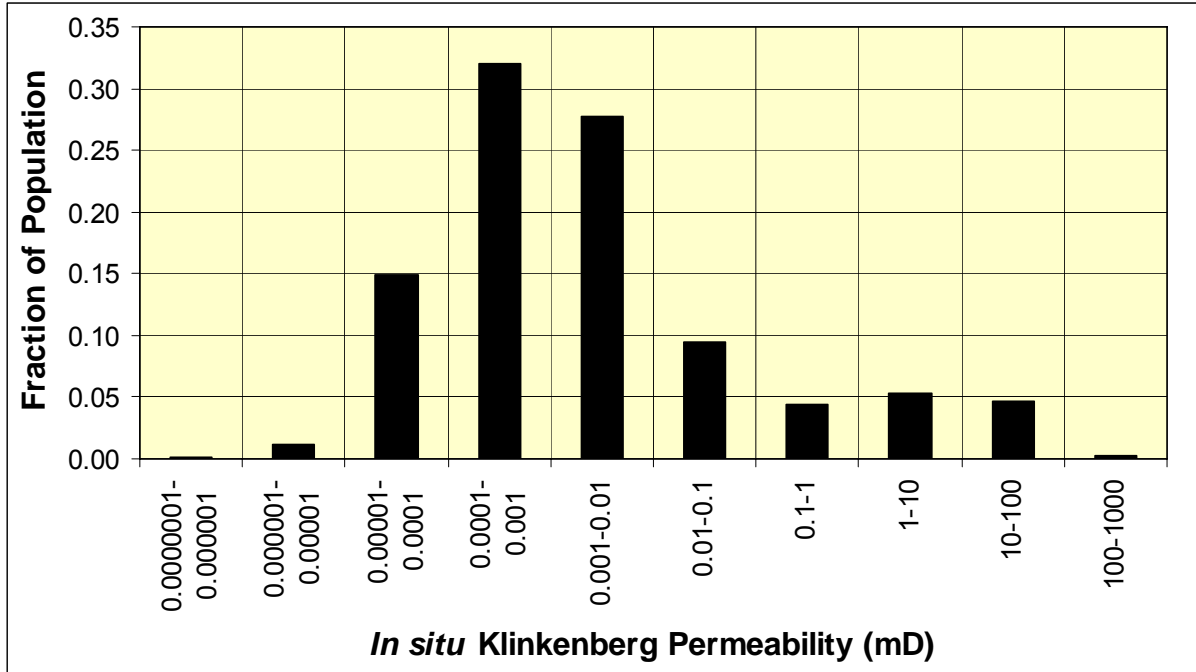


Figure 4.1.14. Distribution of *in situ* Klinkenberg permeability measured at 26.7 MPa (4,000 psi) net effective stress for all samples.

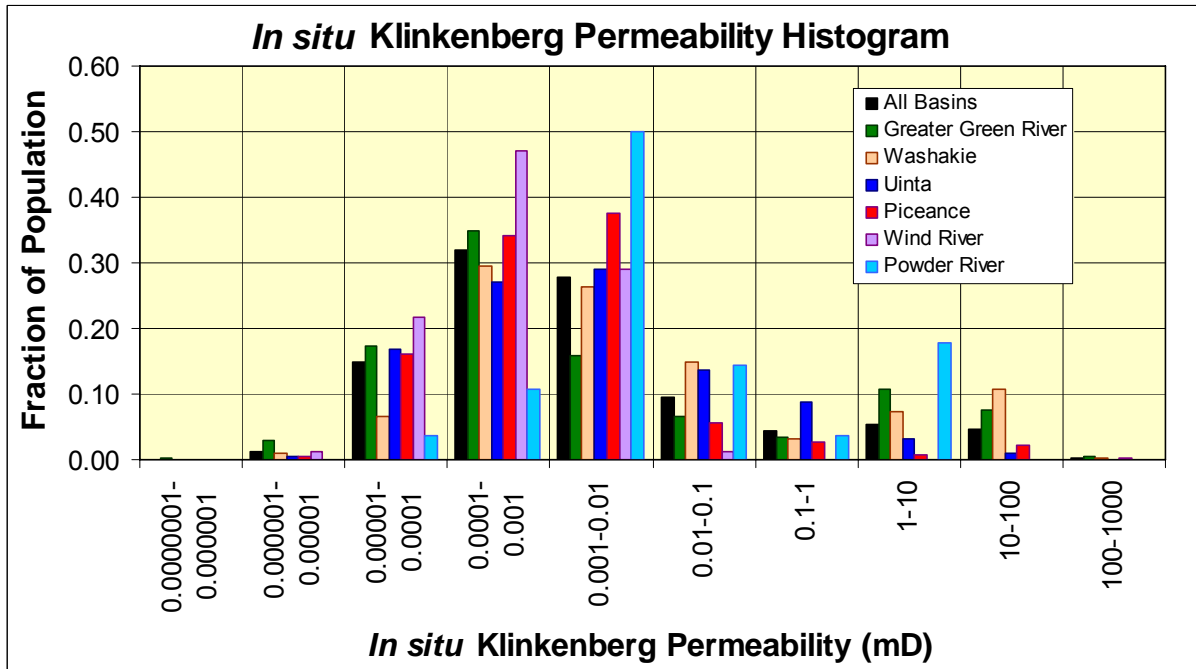


Figure 4.1.15. Distribution of *in situ* Klinkenberg permeability measured at 26.7 MPa (4,000 psi) net effective stress by basin.

	All Basins	Greater Green River	Washakie	Uinta	Piceance	Wind River	Powder River
Mean logk	-2.60	-2.49	-2.03	-2.66	-2.95	-3.44	-1.88
Median logk	-2.93	-3.15	-2.46	-2.86	-3.03	-3.36	-2.21
St Dev log	1.58	1.94	1.78	1.36	1.13	0.69	1.39
Minimum logk	-6.19	-6.19	-5.66	-5.33	-5.23	-5.11	-4.29
Maximum logk	2.31	2.31	2.08	1.88	2.05	-1.98	0.55
Kurtosis	0.62	-0.54	-0.39	0.17	4.02	-0.49	-0.38
Skewness	1.05	0.79	0.76	0.74	1.48	-0.01	0.50
Count	2143	555	373	529	577	81	28
Mean	0.0025	0.0032	0.0094	0.0022	0.0011	0.0004	0.0133
Median	0.0012	0.0007	0.0035	0.0014	0.0009	0.0004	0.0062
St Dev	37.9	87.4	59.9	23.0	13.4	4.9	24.5
Minimum	0.000001	0.000001	0.000002	0.000005	0.000006	0.000008	0.000051
Maximum	206.0	206.0	121.0	76.2	112.2	0.010	3.53
Kurtosis	0.62	-0.54	-0.39	0.17	4.02	-0.49	-0.38
Skewness	1.05	0.79	0.76	0.74	1.48	-0.01	0.50
Count	2143	555	373	529	577	81	28

Table 4.1.4. Summary statistics for *in situ* Klinkenberg Permeability for all samples by basin.

To provide a common reference stress reference frame, *in situ* Klinkenberg permeability was measured at 4,000 psi net overburden. *In situ* Klinkenberg permeability was determined by measurement of permeability to nitrogen at two pore pressures and extrapolation of the k vs. $1/P$ trend to infinite pore pressure to obtain the Klinkenberg permeability at the intercept. The Klinkenberg gas permeability, which is equivalent to single-phase inert liquid or high pressure gas absolute permeability, increases with decreasing pore size.

The influence of Klinkenberg gas slippage, which results from greater gas movement due to decreased molecule-molecule interactions at lower pressure, was characterized by Klinkenberg (1941) as:

$$k_{\text{gas}} = k_{\text{liquid}} (1 + 4cL/r) = k_{\text{liquid}} (1 + b/P) \quad [4.1.16]$$

where k_{gas} = gas permeability at pore pressure, k_{liquid} is liquid permeability and is equal to the Klinkenberg permeability k_{klink} , c = proportionality constant ($\simeq 1$), L = mean free path of gas molecule at pore pressure, r = pore radius, b = proportionality constant ($=f(c, L, r)$), and P = pore pressure (atm).

Because b is a function of pore radius distribution it can vary between rock samples. However, general values for b can be estimated from the relation presented by (Heid et al, 1950):

$$b = 0.777 k_{\text{klink}}^{-0.39} \quad [4.1.17]$$

and Jones and Owens ([1980](#)):

$$b = 0.867 k_{\text{klink}}^{-0.33} \quad [4.1.18]$$

Figure 4.1.16 shows the Klinkenberg proportionality constant b values measured on core in this study. Reduced major axis analysis predicts a slope and coefficient intermediate between values reported by Jones and Owens ([1980](#)) and Heid et al ([1950](#)):

$$b = 0.851 k_{\text{klink}}^{-0.341} \quad [4.1.19]$$

The b term is expressed in atmospheres to be consistent with previous studies. This figure extends the published trend to permeabilities below 0.001 mD and supplements the public data for the trend for permeabilities less than 0.01 mD. The variance in b at any given permeability is interpreted to result from several possible conditions including; 1) variance in lithology and corresponding pore throat size and size distribution for the same permeability; 2) heterogeneity of samples resulting in variable b within a sample and resulting averaging of the measured b during measurement; 3) variable b from one end of the sample to the other due to pressure drop across sample; and 4) error in one or both gas permeability measurements.

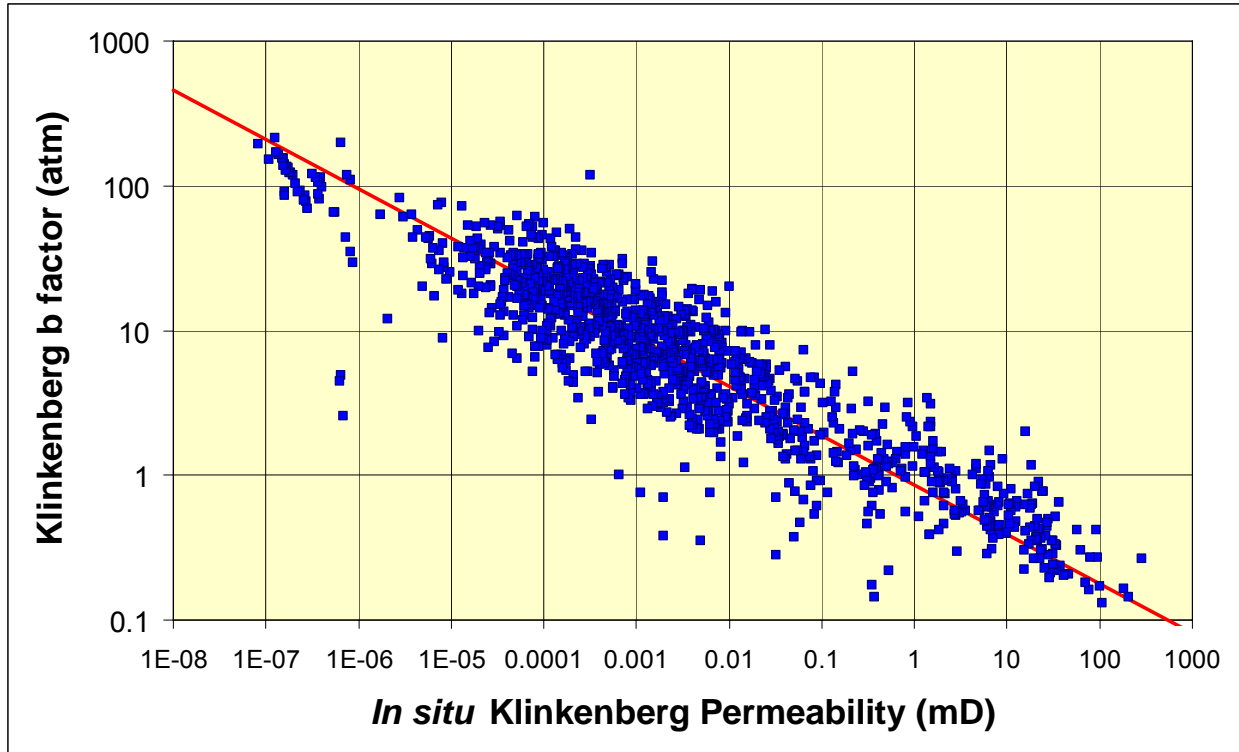


Figure 4.1.16. Cross-plot of Klinkenberg proportionality constant, b , versus *in situ* Klinkenberg permeability measured at 26.7 MPa (4,000 psi) net effective stress using nitrogen gas. Reduced major axis analysis indicates the correlation can be expressed as $b(\text{atm}) = 0.851 k_{ik}^{-0.341}$, $n = 1264$.

As described previously, 776 core plugs greater than 7.6 cm (3-inch) in length were cut in half to provide two paired core plugs for advanced properties measurements. Figure 4.1.17 illustrates the ratio of *in situ* Klinkenberg permeabilities of samples to the geometric mean permeability of the sample pair. Approximately 35% of all samples exhibit permeabilities within 10% of the mean, 55% within 20%, 70% within 30%, and 80% within 40%.

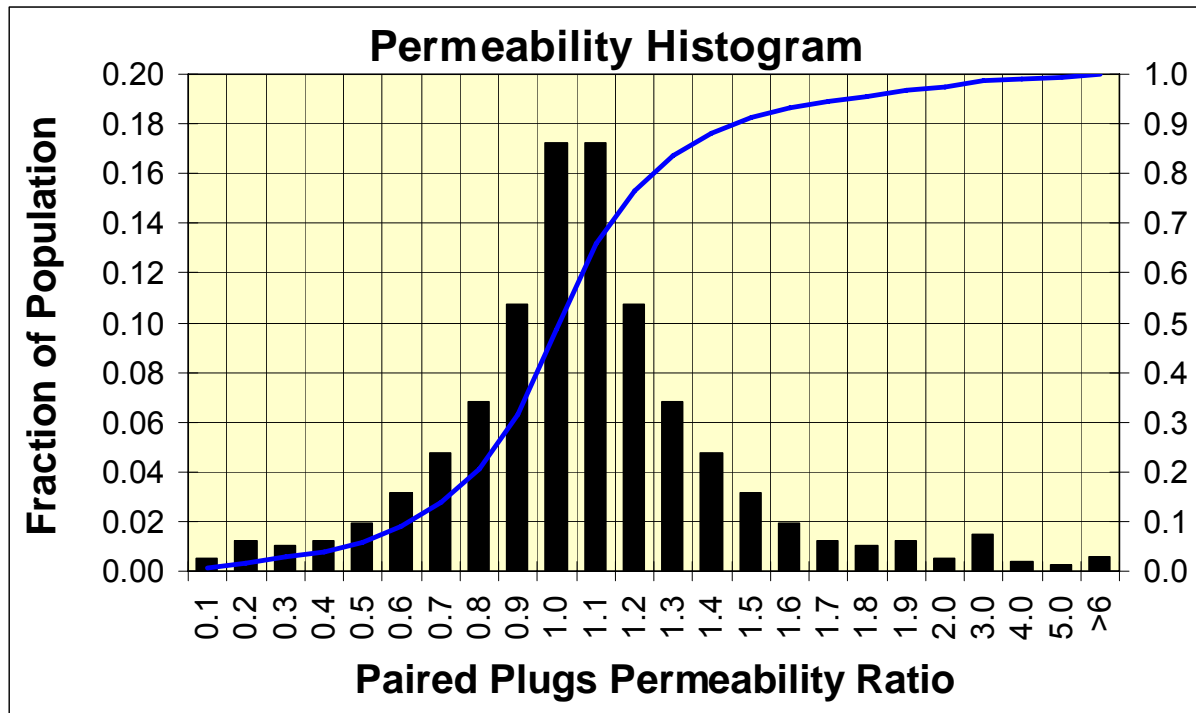


Figure 4.1.17. Histogram of ratio of paired plug *in situ* Klinkenberg permeabilities to mean permeability of plug pair. $n = 634 \times 2 = 1268$.

4.1.3.4 Permeability-Stress Dependence

In most low-permeability sandstones and siltstones, routine air permeability values range from 10 to 1,000 times greater than *in situ* gas and liquid permeability values. Previous studies of low-permeability sandstones and siltstones have shown that the difference between permeabilities measured at routine conditions and those measured at confining stress increases progressively with decreasing permeability and increasing confining pressure ([Vairogs et al, 1971](#); [Thomas and Ward, 1972](#); [Byrnes et al, 1979](#); [Jones and Owens, 1980](#); [Ostensen, 1983](#); [Luffel et al, 1991](#); [Thomas and Ward, 1972](#); [Walls et al, 1982](#); [Sampath and Keighin, 1981](#); [Wei et al, 1986](#); [Byrnes, 1997](#); [Castle and Byrnes, 1997](#); [Byrnes and Castle, 2000](#); [Byrnes, 2003](#); [Byrnes, 2005](#)). In a key study, Jones and Owens ([1980](#)) quantified these effects and concluded that the presence of a thin, sheet-like, tabular pore structure could explain the response to confining stress. This result was consistent with the modeling work of Cheng and Toksoz ([1979](#)). Ostensen ([1983](#)) provided a comprehensive theoretical analysis of the relationship between crack or thin sheet-like pore permeability and the response of rock properties to confining stress. Byrnes ([1997](#)) summarized *in situ* rock properties for low-permeability sandstones in Rocky

Mountain basins. Byrnes and Castle (2000) compared eastern and western tight gas sandstone rock properties.

Within low-permeability shales, siltstones, and sandstones three empirical models have been proposed for the stress dependence of permeability. These can be categorized as: 1) crack, 2) three-stage exponential, and 3) power-law.

Crack Model

The crack models fundamentally model the stress dependence of permeability dependence as resulting principally from the closure of the thin, sheet-like, or crack-like pores in the rocks. Stress dependence of cracks has been extensively studied (Table 4.1.5).

Model Type	Model	Equation
Noncrack	Capillary tube	$k/k_i = (1-2\sigma/E)^4$
Noncrack	Gangi, grain, 1978	$k/k_i = \{1-2\{3\pi(1-\nu^2)\sigma/4E\}^{2/3}\}^4$
Crack	Jones & Owens, 1980	$k/k_i = \{1-S\log(P_k/1000)\}^3$
Crack	Brower & Morrow, 1983	$k/k_i = \{1-(16(1-\nu^2)cL_c)/(9(1-2\nu)\pi w_i)\sigma\}^3$
Asperity	Gangi, bed of nails, 1978	$k/k_i = \{1-(\sigma/IE)^e\}^3$
Asperity	Walsh, exp. dist., 1981	$k = Ls^3/12 \{ \ln[(\nu E(\pi r_c \sigma^3)^{1/2})/(2(1-\nu^2)\sigma)] \}^3$
Asperity	Ostensen, Gauss., 1983	$k = 0.76Ls^3/12 \{ \ln[(2.48E(\sigma/r_c)^{1/2})/(3\pi^{1.5}(1-n^2)\sigma)] \}^2$

Table 4.1.5. Permeability stress dependence relationships (After Ostensen, 1983)

Exponential Model

Exponential relationships have been proposed for describing the effective confining pressure dependent permeability ([Athy, 1930](#); [Dickinson, 1953](#); [Brace et al., 1968](#); [Schmoker and Halley, 1982](#); [Hoholick et al., 1984](#); [Debschutz et al., 1989](#); [David et al., 1994](#); [Evans et al., 1997](#)). Katsube et al ([1991](#), [1992](#)) and Katsube and Coyner ([1994](#)) in studies of the stress-dependence of shales from the Canadian Scotian Shelf proposed that their permeability (k) versus stress (Pe) results suggested that the k-Pe relationship consists of three sequential exponential curves that change slope with increasing stress: 1) (smallest Pe values) represents restoration of widened pores resulting from stress release of rock samples brought to surface; 2) represents compacting deposits in widened pores, resulting from overpressure development

subsequent to compaction at higher stresses, and 3) (at highest Pe values) represents elastic and inelastic reduction of pores resulting from increasing effective stress (Pe).

Power-law Model

Based on the re-evaluation of the measurements of Morrow et al (1984), Shi and Wang (1986) proposed that the relation between effective pressure and permeability should follow a power-law relationship.

Routine Air versus in situ Klinkenberg Permeability

The goal in this study was not to characterize the permeability-stress dependence curve but to define the relationship between routine and *in situ* Klinkenberg permeability which can be obtained by measuring just routine air permeability and an *in situ* Klinkenberg permeability on the same core plug.

Byrnes (1997) presented the following relationship between k_{ik} and k_{air} for Mesaverde and Frontier low-permeability sandstones, undifferentiated:

$$\log k_{ik} = 1.34 \log k_{air} - 0.6 \quad [4.1.20]$$

The standard error of prediction of this relationship was a factor of 3.2 (i.e., a predicted value of 1 mD may be 3.2 mD or 0.32 mD, 1 standard deviation). This relationship was limited to rocks with routine permeability less than 1 mD. Byrnes (2003) extended the relationship up to 300 mD and showed that a generalized routine- *in situ* Klinkenberg permeability relationship for both low-permeability carbonates and sandstones could be represented by:

$$\log k_{ik} = 0.0588 (\log k_{air})^3 - 0.187 (\log k_{air})^2 + 1.154 \log k_{air} - 0.159 \quad [4.1.21]$$

where permeabilities are in millidarcies (mD). The trend is due both to the increase in effect of confining stress on pore-throat size with decreasing permeability and to the increase in gas slippage (i.e., Klinkenberg effect) with decreasing pore-throat size and decreasing permeability.

The present study provides a comprehensive data set to re-evaluate the relationship presented in equations 4.1.20 and 4.1.21 with specific application to Mesaverde sandstones. Figure 4.1.18 illustrates the relationship between k_{ik} and k_{air} for 2030 cores samples in this study. This relationship can be characterized by:

$$\log k_{ik} = -0.0088 (\log k_{air})^3 - 0.0716 (\log k_{air})^2 + 1.366 \log k_{air} - 0.4574 \quad [4.1.22]$$

The standard error of prediction of this relationship was a factor of 2.4 (i.e., a predicted value of 1 mD may be 2.42 mD or 0.42 mD, 1 standard deviation). It is evident in Figure 4.1.18 that a single polynomial equation like Eqn. 4.1.21 may not characterize the relationship for all permeability values as well as individual relationships for specified permeability ranges and for specific lithofacies.

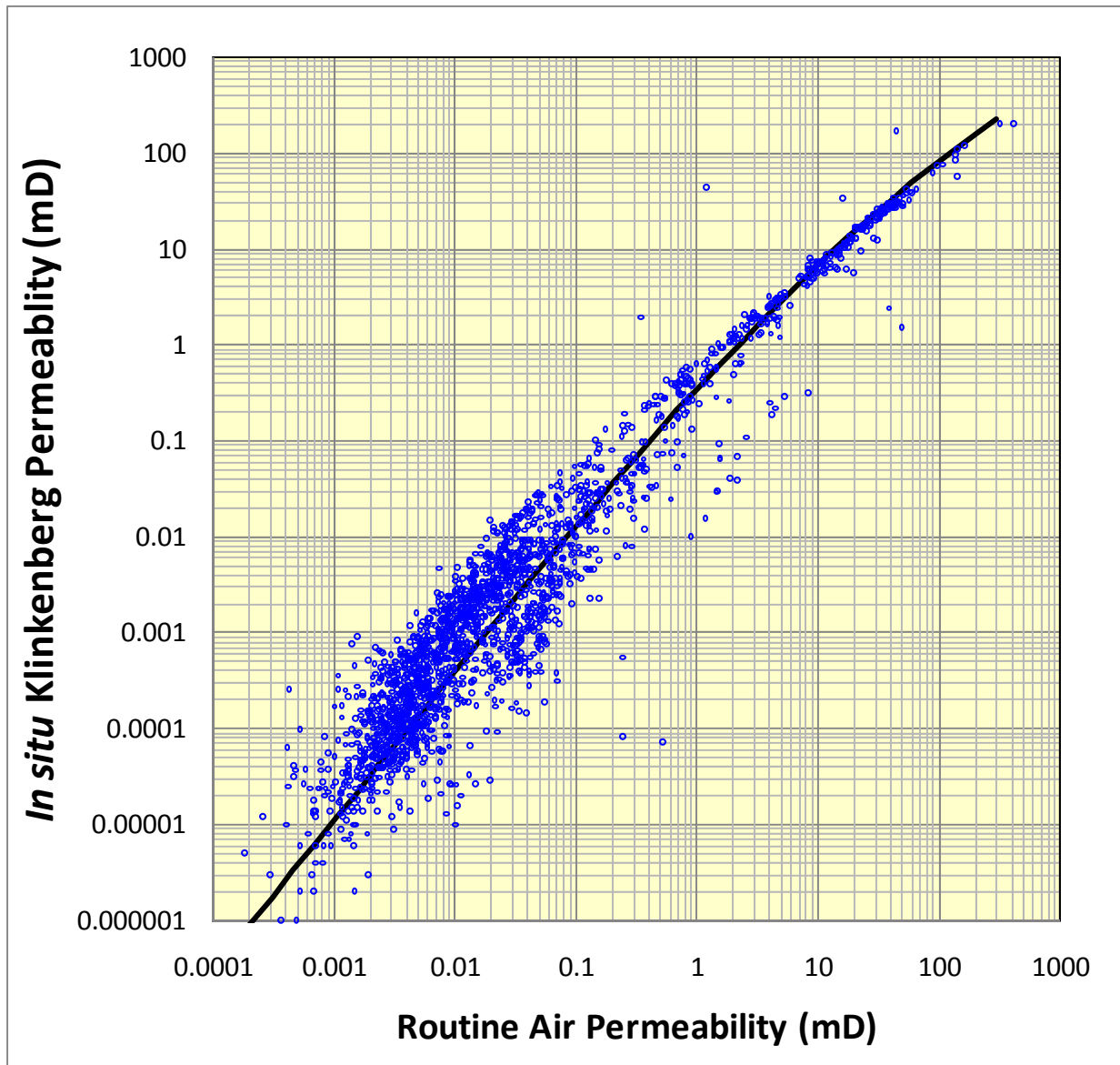


Figure 4.1.18. *In situ* Klinkenberg permeability (as measured at 4,000 psi net effective stress) versus routine air permeability (as measured at 100 psi mean pore pressure and 800 psi net effective stress). The polynomial relationship shown by the curve represents $\log k_{ik} = -0.0088 (\log k_{air})^3 - 0.0716 (\log k_{air})^2 + 1.366 \log k_{air} - 0.4574$ (Eqn. 4.1.22).

Comparing the predicted values of equations 4.1.20 through 4.1.22 (Figure 4.1.19) shows that equations 4.1.20 and 4.1.22 are within standard error of prediction similar for permeability values less than 10 mD (which was the approximate upper range for equation 4.1.20). Both of these equations were developed using Mesaverde rocks. Equation 4.1.21 represented both tight gas sandstones and carbonates undifferentiated. Equation 4.1.21 predicts higher and lower *in situ* Klinkenberg permeabilities for routine air permeability values greater than and less than 0.01

mD, respectively. This difference from equations 4.1.20 and 4.1.22 can be interpreted to reflect the influence of tight gas carbonates on equation 4.1.21.

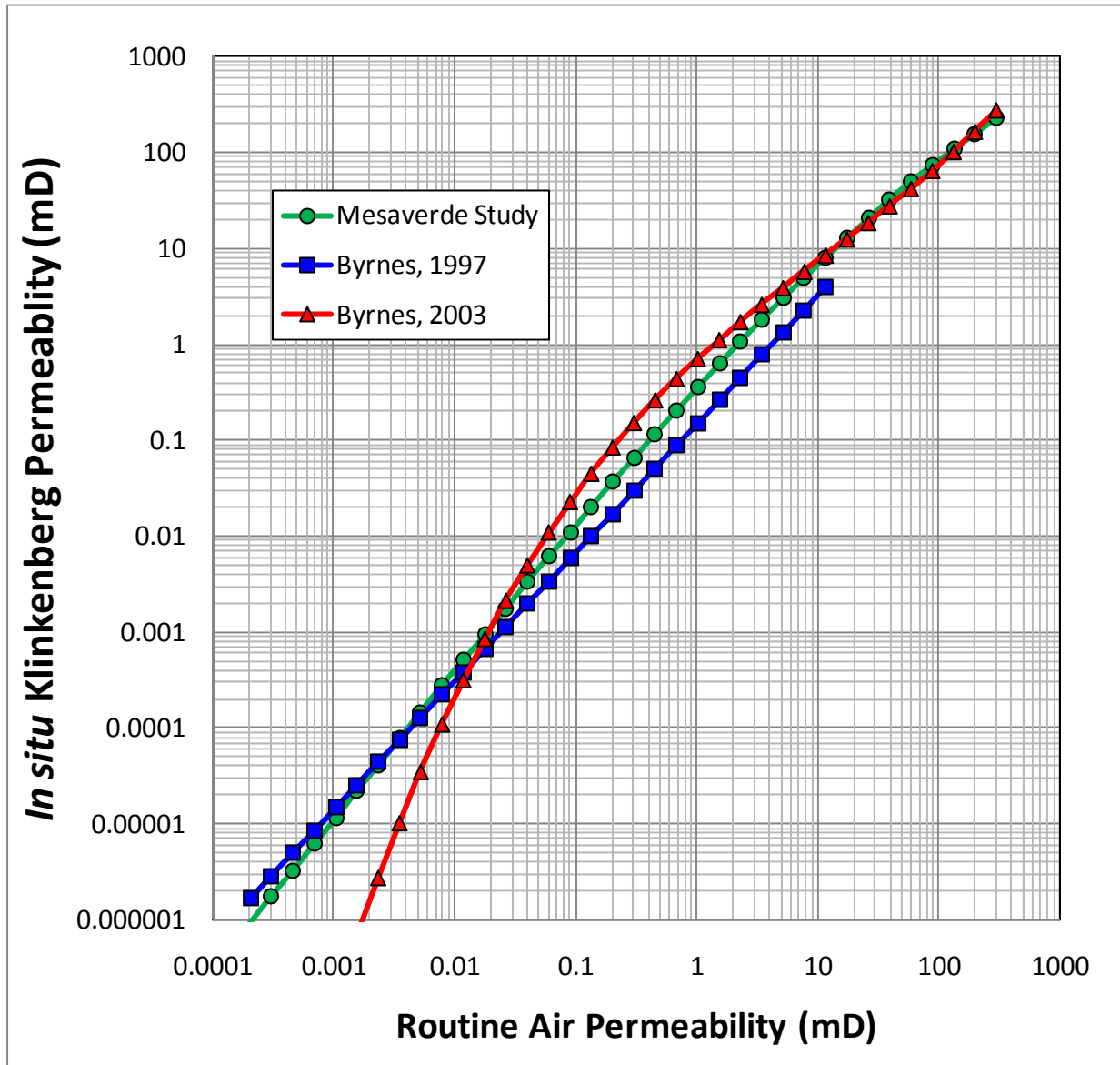


Figure 4.1.19. Crossplot of predicted *in situ* Klinkenberg permeability versus routine air permeability as expressed by equations 4.1.20 through 4.1.22.

4.1.3.5 Porosity-Permeability Relationship

Comparison of measured *in situ* Klinkenberg permeability versus an estimated approximate *in situ* porosity (routine porosity – 0.6%) for 2200 Mesaverde sandstones (Figure 4.1.20) shows that the present sample population exhibits higher permeability than previously published

Mesaverde/Frontier studies (e.g., [Byrnes, 1997](#)). This is interpreted as due in part to the absence of argillaceous Frontier samples and to the high fraction of less argillaceous sandstones in the analyzed sample set.

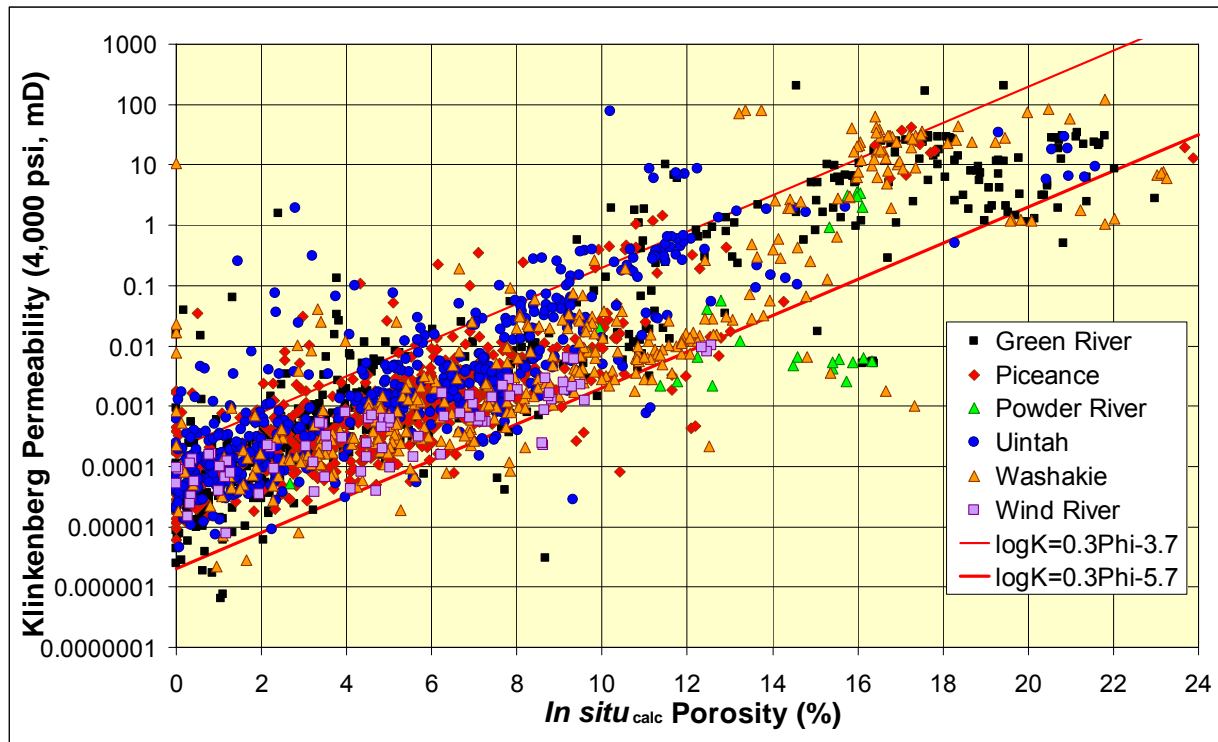


Figure 4.1.20. *In situ* Klinkenberg permeability versus calculated *in situ* porosity for all core samples coded by basin. Range of porosity and permeability of Mesaverde sandstones is generally exhibited by all basins.

4.1.3.5.1 Predictive equations for porosity-permeability

Figure 4.1.21 illustrates the relationship between permeability and porosity parametric with the second rock classification digit which represents size-sorting (see Subtask 4.5). Characteristic of most sandstones, permeability at any given porosity increases with increasing grain size and increasing sorting though this relationship is further influenced by sedimentary structure (rock digit 4) and the nature of cementation (rock digit 5). Samples exhibiting permeability greater than the empirically defined high limit generally exhibit an anomalous lithologic property that influences core plug permeability such as microfracturing along fine shale lamination, microfractures, or lithologic heterogeneity parallel to bedding with the presence of high permeability laminae in a core plug dominantly composed of a lower permeability-porosity rock.

Conversely, cores exhibiting permeability below the lower limit can exhibit such lithologic properties as churned-bioturbated texture, cross-bedding with fine-grained or shaly bed boundaries that are sub-parallel or perpendicular to flow and act as restrictions to flow, or high clay content. Permeability in low porosity samples and particularly below approximately 1% is generally a complex function of final pore architecture after cementation and is only weakly correlated with original grain size.

The estimated range in permeability at any given porosity increases with porosity and can be as great as four orders of magnitude for $\phi > 12\%$ but decreases to approximately 20X near $\phi=0\%$. Though in unconsolidated grain packs the influence of size and sorting can be quantified, in consolidated porous media the influence of these variables and particularly the influence of sedimentary structure can be non-linear and non-continuous. For example coarse grain size results in high permeability but if the sand was deposited in a trough cross-bedded structure and there is some orientation of bedding in the core that is not parallel to flow then the permeability can be significantly reduced. The rock classification system used works to both quantify and make continuous these parameters but has limits.

Excluding samples exhibiting permeability outside the limits shown in Figure 4.1.20 the relationship between the porosity and lithologic variables and permeability was explored. Multivariate linear regression analysis provides a predictive relationship:

$$\log k_{ik} = 0.282 \phi_i + 0.18 \text{RC2} - 5.13 \quad [4.1.23]$$

where k_{ik} is the *in situ* Klinkenberg permeability at 4,000 psi net confining stress (mD), ϕ_i is the approximate *in situ* porosity (%) and RC2 is the second digit of the rock classification representing size-sorting. Standard error of prediction for this equation is a factor of 4.5X (1 standard deviation).

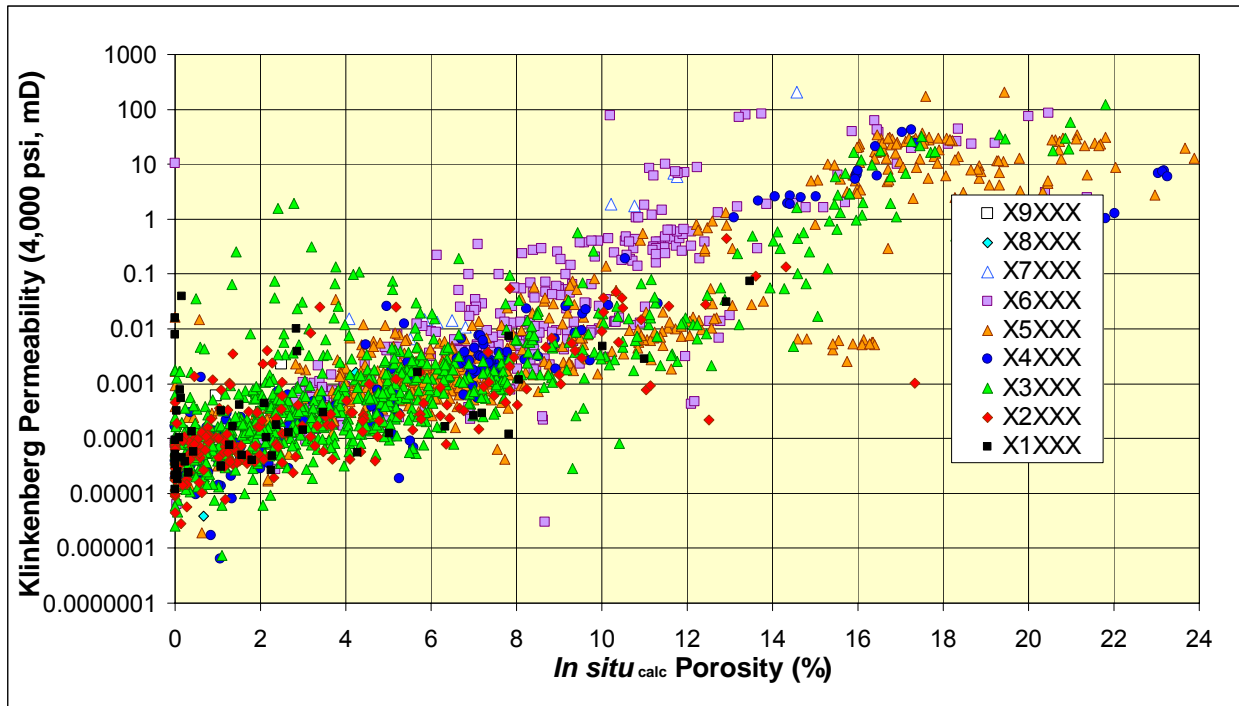


Figure 4.1.21. Cross-plot of *in situ* Klinkenberg permeability (k_{ik} , mD, measured at 27.6 MPa (4,000 psi) net effective stress) versus calculated *in situ* porosity ($\phi_{routine}-0.6$) coded by second rock type digit 2 (representing size-sorting). The high limit generally defines the upper range for medium-coarse grained rocks. The lower limit generally represents the limit for siltstone rocks.

The simplest non-linear relation is:

$$\log k_{ik} = 0.034 \phi_i^2 - 0.00109 \phi_i^3 + 0.0032 RC2 - 4.13 \quad [4.1.24]$$

which exhibits a standard error of prediction of 4.1X (1 std dev).

Because of the non-linear nature of the influence of the independent variable, an Artificial Neural Network (ANN) approach was also examined. A single hidden layer, 10 node network was used where the output from the hidden layer was a sigmoidal function ($1/1+\exp(-x)$) of the hidden-layer output. Table 4.1.6 shows the ANN parameters. The ANN, using *in situ* porosity (Φ_{ii}), RC2 and RC4 provides prediction of k_{ik} with a standard error of prediction of 3.3X (1 std dev, Fig. 4.1.22). Although Artificial Neural Network (ANN) methods are capable of predicting permeability within a factor of 3.3X, the ease of sharing and applying an ANN model is not as great as simpler algebraic equations.

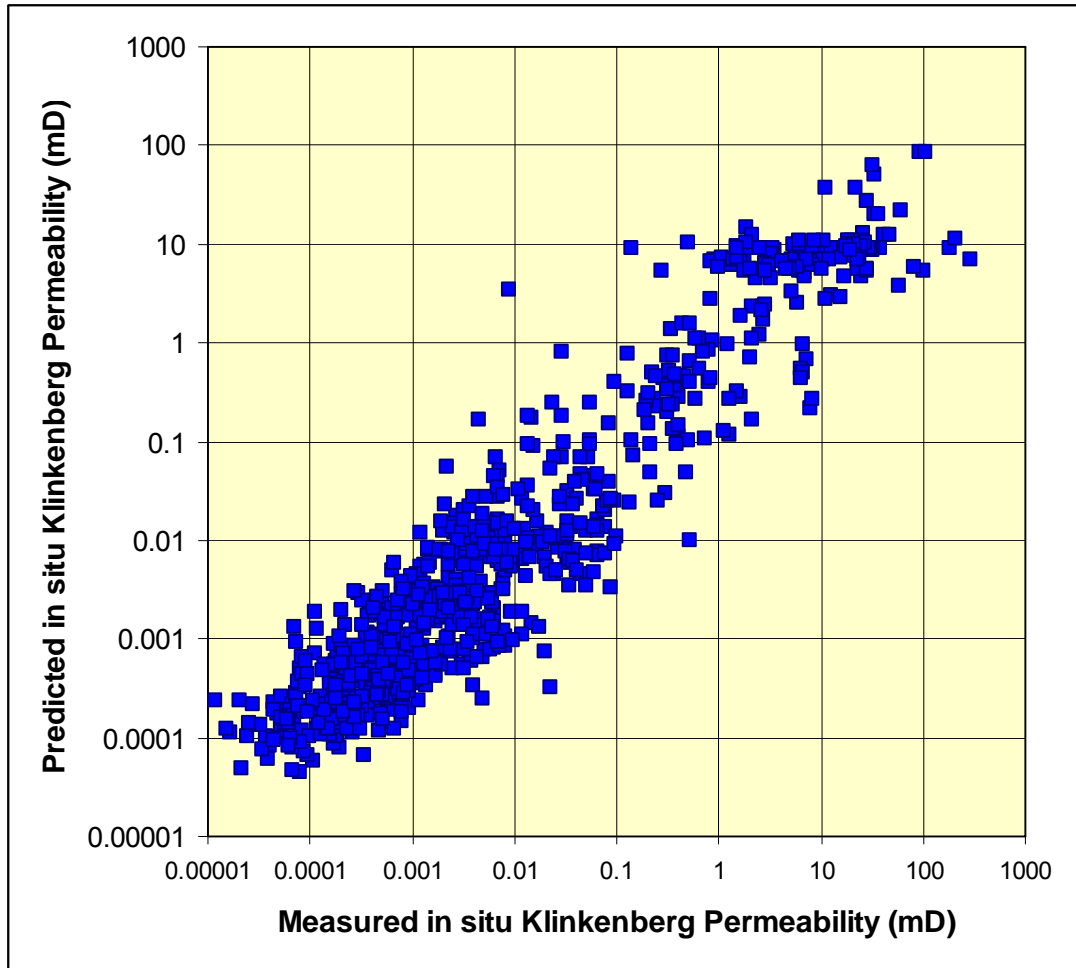


Figure 4.1.22. Cross-plot of measured versus predicted *in situ* Klinkenberg permeability using Artificial Neural Network (ANN) with parameters shown in Table 4.1.6. Correlation standard error is 3.5X.

Although inclusion of a term for size/sorting significantly improves permeability prediction, a unique wireline log signature for predicting the size/sorting rock digit 2 was not identified that could be applied universally. The difficulty in identifying the unique log signature is interpreted to be the result of lack of log normalization. Within a given well wireline response can predict Rock Digit 2 with appropriate accuracy but the nature of the relationship changes from one well to another. It was, however, found that three classes of size/sorting could be reliably identified from all wireline log response. These three classes comprise: 1) shales/mudstones, silty shales, siltstones, and very shaly sandstones with digit X(0-2)XXX; 2) moderately shaly sandstones X3XXX; and 3) very fine – coarse grained sandstones X(4-9)XXX. The relationship between permeability and porosity for the three classes of rock is shown in Figure 4.1.23.

hidden layer: 1						
Hidden layer nodes: 10						
		Mean>	8.239	4.280	6.294	hidden layer- to-output weights
		Std Dev>	5.260	1.335	2.527	
Input-to-hidden layer weights						
Node	Constant	Phii	RC2	RC4		
Constant						-0.388
1	-0.760	2.946	-2.027	-6.438	-0.885	
2	-2.155	4.637	1.279	0.895	2.323	
3	-4.999	7.901	0.957	3.167	-2.583	
4	-1.484	-0.307	-1.695	6.175	-0.154	
5	-4.597	4.582	1.568	0.730	4.022	
6	-2.609	0.320	-2.201	-2.257	-2.495	
7	-1.765	-1.843	-1.122	0.145	-3.859	
8	2.839	-3.146	-9.237	0.264	0.789	
9	-1.566	1.029	-1.588	-3.390	2.400	
10	2.951	0.778	3.316	0.179	-2.136	

Table 4.1.6. Artificial neural network parameters for k_{ik} prediction using ϕ_i , RC2 and RC4 as input variables. ANN utilized was a single hidden layer with 10 nodes and sigmoidal base function.

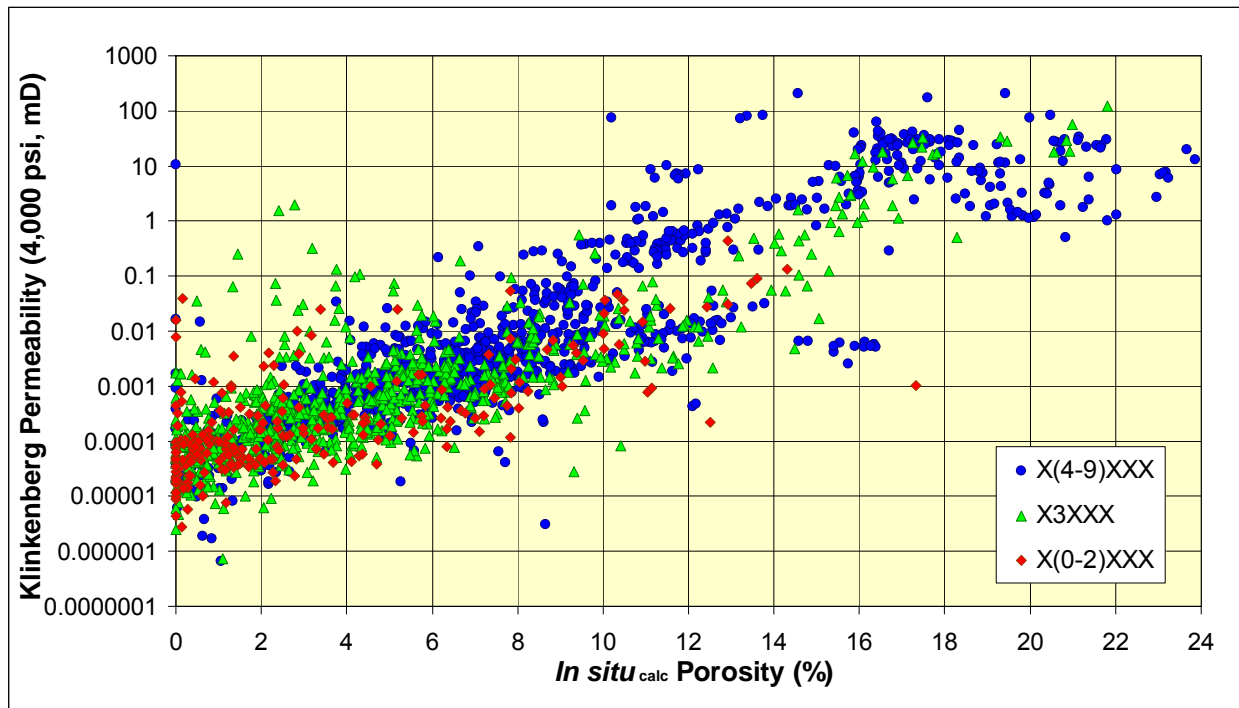


Figure 4.1.23. Cross-plot of *in situ* Klinkenberg permeability (k_{ik} , mD, measured at 4,000 psi net effective stress) versus calculated *in situ* porosity ($f_{routine}-0.8$) coded by clustered second rock type digit representing size-sorting classes that are identifiable by wireline gamma ray log response.

Utilizing a multivariate linear equation similar to Eq. 4.1.23, regression analysis provides a predictive relationship:

$$\log k_{ik} = C_1 \phi_i + C_2 RC2_{log} + C_3 \quad [4.1.25]$$

where k_{ik} is the *in situ* Klinkenberg permeability at 4,000 psi net confining stress (mD), ϕ_i is the approximate *in situ* porosity (%), $RC2_{log}$ is the log-predicted 3-class second digit of the rock classification representing size-sorting. C_1 is the porosity coefficient, C_2 is the RC2 coefficient and C_3 is the intercept. Examination of Figure 4.1.23 shows that the permeability-porosity trend exhibits different relationships for the porosity ranges; 0-12%, 12-18%, and > 18%. Multivariate equations using: 1) porosity; 2) rock class (1-3); and for each of these three porosity classes separately (0-12%, 12-18%, >18%); and also performed separately for each basin provided equations that exhibit an average standard error of prediction of: 0-12%: 3.8±1X; 12-18%: 3.8±1X; >18%: 3.1X (for all basins undifferentiated; Table 4.1.7).

	All Mesaverde	Green River	Piceance	Powder River	Uinta	Washakie	Wind River
Porosity < 24%							
Porosity Coefficient	0.266	0.278	0.252	0.210	0.255	0.298	0.159
RC2 Coefficient	0.148	0.085	0.108	0.000	0.357	0.078	0.249
Intercept	-4.713	-4.612	-4.615	-4.515	-4.891	-4.950	-4.863
Count	1983	536	553	28	504	283	79
Std Error of Prediction	5.4	5.3	4.2	10.8	4.8	7.4	2.1
Porosity ≤ 12%							
Porosity Coefficient	0.241	0.273	0.215	0.193	0.247	0.221	0.152
RC2 Coefficient	0.174	0.069	0.206	0.000	0.365	0.039	0.260
Intercept	-4.678	-4.573	-4.669	-4.382	-4.877	-4.546	-4.860
Count	1691	418	528	8	486	175	76
Std Error of Prediction	4.6	4.7	3.8	3	4.8	3.5	2.1
12% < Porosity < 18%							
Porosity Coefficient	0.464	0.282	0.555	0.547	0.108	0.638	
RC2 Coefficient	0.681	0.548	0.013	0.689	0.584	0.229	
Intercept	-8.614	-5.366	-8.382	-10.282	-3.178	-10.082	
Count	184	56	18	12	13	74	
Std Error of Prediction	5.4	2.4	4.3	4.3	3.6	2.9	
Porosity ≥ 18%							
Porosity Coefficient	0.264						
RC2 Coefficient	0.000						
Intercept	-4.596						
Count	35						
Std Error of Prediction	3.1						

Table 4.1.7. Summary of *in situ* Klinkenberg permeability equations for each basin separated by porosity class. The standard error of prediction is expressed as a factor (e.g. 5.4 = ±5.4X).

Subtask 4.2. Measure Critical Gas Saturation

4.2.1 Task Statement

The objective of this task was to measure critical non-wetting phase and gas saturation using air-mercury capillary pressure analysis and air-brine displacement.

4.2.2 Methods

Both air-mercury critical non-wetting phase saturation measurements and air-brine critical gas were performed. All mercury capillary pressure data are posted on the Project Website.

4.2.2.1 Air-Mercury Critical Nonwetting Phase Saturation

Both unconfined mercury intrusion capillary pressure (MICP) analysis and confined MICP analysis was performed. Samples ranged widely in lithology with samples representing arkose to sub-litharenite composition, grain sizes ranging from siltstone to upper medium-grained, argillaceousness ranging from clean to shaly, and sedimentary structures comprising massive, laminar, low-angle cross, ripple-laminated, and convolute or bioturbated bedding. The low-permeability sandstones analyzed exhibited a range in porosity and permeability characteristic of the sampled population of Mesaverde sandstones (Figure 4.2.1).

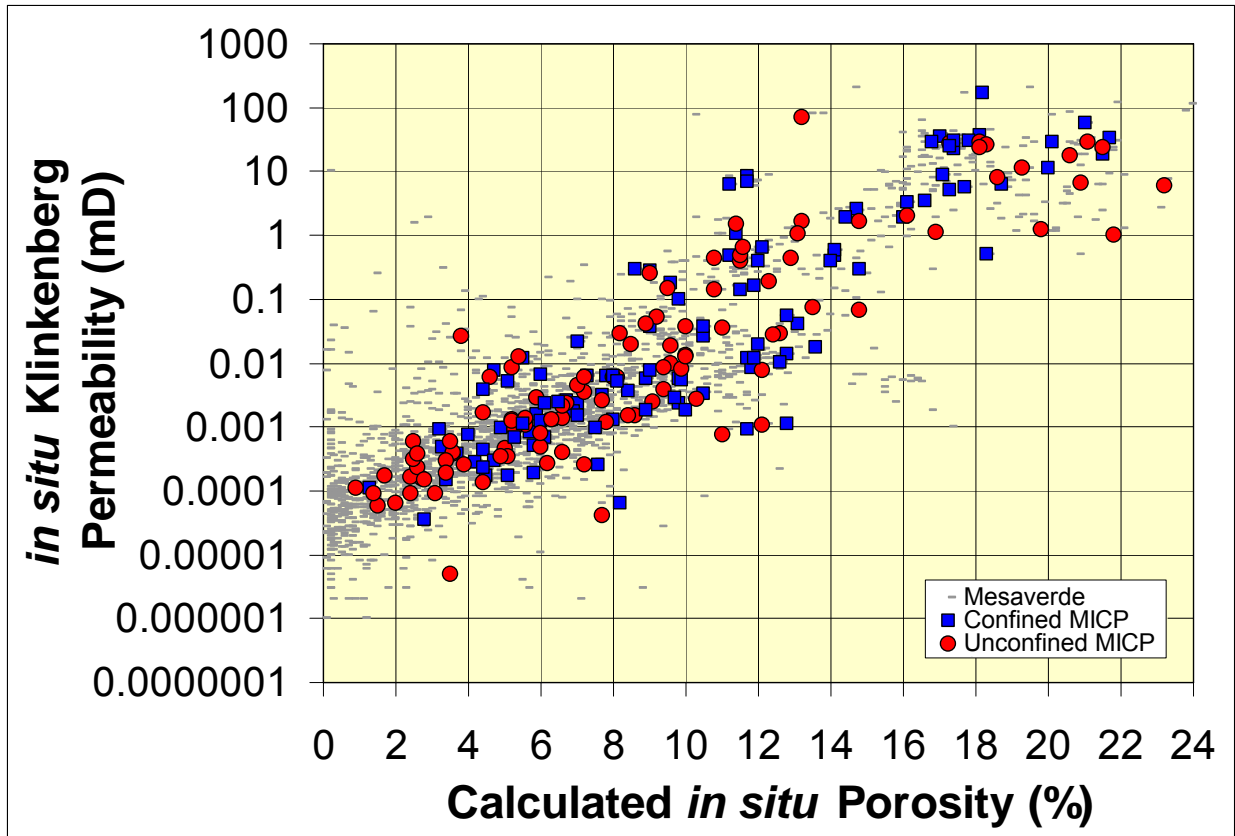


Figure 4.2.1. Cross-plot of *in situ* Klinkenberg permeability versus *in situ* porosity for low-permeability sandstones for which unconfined (red circles) and confined (blue squares) mercury intrusion capillary pressure analysis was performed to determine the critical mercury (non-wetting phase) saturation. Samples range widely in lithology from siltstone to lower-, medium-grained sandstone with varying clay content and different sedimentary structures.

The mercury intrusion method was selected both to approximately reproduce the methodology of Thompson et al. (1987) and Schowalter (1979) and because mercury allows examination of empty pores, volumes can be measured with accuracy, equilibration times are brief because there is no wetting phase displacement, it is possible to investigate properties of the porous network at saturations greater than the percolation threshold, it allows electrical conductance of the nonwetting phase to be measured, and it allows establishment of capillary equilibrium in association with percolation threshold measurements. Though useful, this method does present the significant limitation that a water wetting-phase is not present which can influence results compared to MICP. To measure *in situ* porosity and permeability the cores were subjected to a hydrostatic confining stress of 0.0113 MPa/m depth (0.5 psi/foot depth) to simulate *in situ*

stress. Helium porosities were measured using a Boyle's Law method and Klinkenberg permeabilities were determined using a pressure pulse decay method.

For unconfined mercury intrusion analysis each sample was subjected to step-wise, increasing, mercury-injection pressures ranging from 0.014 to 69 MPa (2-10,000 psia). Unconfined mercury porosimetry allows mercury to enter a sample from all sides. To measure percolation threshold or critical saturation it is necessary to test for continuity from one side of a network to another. To determine the non-wetting phase, critical saturation, S_{nwc} , mercury intrusion analysis was performed on 2.54-cm diameter by 5-cm to 7-cm long cores hydrostatically confined. The first 20 analyses were performed at a confining pressure of 33.4 MPa (5,000 psi) greater than the mercury injection pressure, maintaining a net effective stress of 33.4 MPa (5,000 psi). All subsequent samples were measured at a confining pressure of 26.7 MPa (4,000 psi) greater than the mercury injection pressure, maintaining a net effective stress of 26.7 MPa (4,000 psi). Resistance across the core was measured using stainless steel electrodes on each end of the core (Figure 4.2.2).

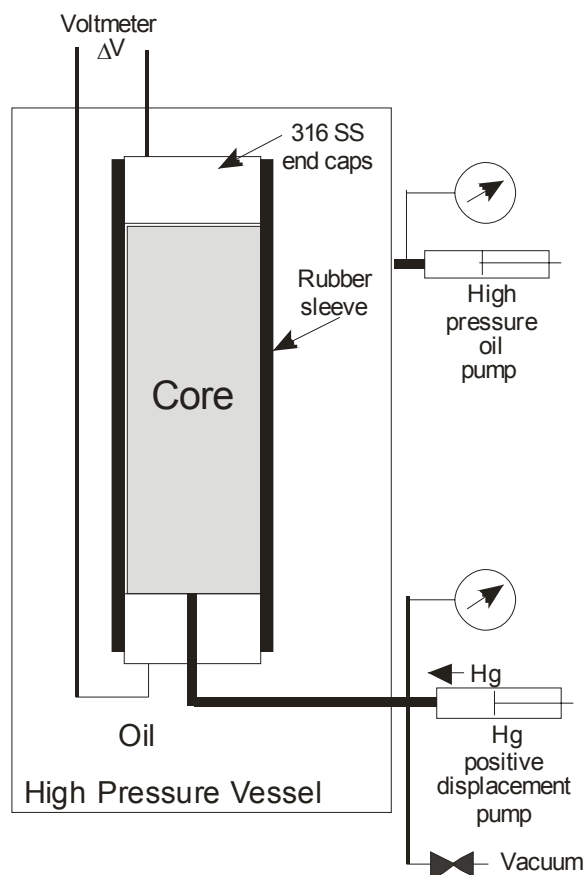


Figure 4.2.2. Schematic of high-pressure, mercury-intrusion and electrical-resistance instrument. Samples were confined at a pressure of 26.7 MPa (4,000 psi) greater than the mercury-injection pressure for all pressures.

Sandstone matrix and evacuated pore space are both highly resistive and the clean, dry, evacuated sandstone samples investigated all exhibited resistance ranging from $0.15\text{-}4 \times 10^6$ ohms. At the critical saturation of the percolation threshold, with formation of a continuous mercury tendril across the sample, resistance across the core decreases abruptly by one to five orders of magnitude. From each sample's capillary pressure curve the saturation associated with the characteristic length, l_c , as defined by Thompson et al. (1987), was measured at the first inflection point. Figure 4.2.3 illustrates the determination of the inflection point saturation for two samples of different permeability. Curvature at wetting phase saturations above the inflection is zero or positive and below the inflection is negative. Uncertainty in the determination of the mercury saturation associated with the inflection point is estimated to be $S_{nvc} \pm 0.01$ to ± 0.005 depending on the injection curve profile.

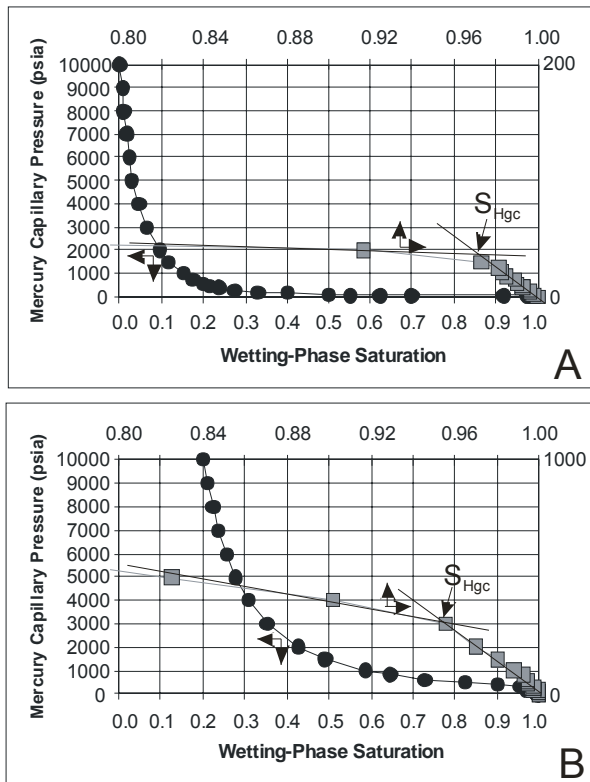


Figure 4.2.3. Illustration of the estimation of the critical-mercury saturation at which mercury forms a sample-spanning cluster using the method of Thompson et al. (1987) for sandstone samples of $k = 1.16$ mD (A) and $k = 0.0035$ mD (B). Prior to forming the sample-spanning cluster, mercury saturation increases approximately linearly or has positive curvature with pressure. Note black curves show entire capillary-pressure curve and grey curves show only low-pressure portion of curve to magnify the region of the critical-saturation inflection.

4.2.2.2 Air-Brine Critical Gas Saturation Measurement

Sample preparation for air-brine critical gas saturation, S_{gc} , measurements involved vacuum/ pressure saturation of the cores with brine as described in Section 4.1.2.2 for compressibility measurements. For most of the samples the critical gas saturation measurement was performed subsequent to electrical properties measurements with the core saturated and in equilibrium with brines of either 80,000 ppmw NaCl or 200,000 ppmw NaCl. Measurement of S_{gc} by gravimetric methods involved the following steps:

1. Place the core in a Hassler cell (Figure 4.2.4) with one end sealed by a solid stainless steel billet
2. hydrostatically confine the sample with a confining stress of $P = 26.7$ MPa (4,000 psi)

3. allow the core to expel water due to pore volume compressibility for a period of 2 days
4. record total brine expelled
5. remove core from Hassler cell and weigh
6. immediately after weighing place the core with excess brine back in a Hassler cell (Figure 4.2.4)
7. hydrostatically confine the sample with a confining stress of $P = 26.7 \text{ MPa}$ (4,000 psi)
8. allow the core to equilibrate with confining pressure for 1 day
9. displace brine from inlet tube by inserting wire in tube
10. attach partially water filled micropipette to effluent tube with water meniscus marked on tube
11. attach high-pressure gas line to inlet tube
12. apply first gas pressure to inlet tube
13. twice a day inspect effluent tube for meniscus movement and/or presence of gas bubbles
14. if no bubbles are observed after a period of 2 days record any meniscus movement and incrementally increase inlet gas pressure and apply new gas pressure to inlet tube
15. repeat steps 13-14 until gas bubble(s) are observed in the effluent micropipette
16. when gas bubble(s) are observed, remove micropipette
17. remove core from Hassler cell and weigh
18. calculate *in situ* porosity, pore volume, and saturated weight from change in weight resulting from steps 1-5 and any meniscus movement in pressure steps prior to breakthrough pressure
19. calculate critical gas saturation from change in weight between steps 17 and 18 correcting for brine density.

It should be noted that gas effective permeability and gas saturation were not estimated from the volume of brine displaced prior to gas bubble breakthrough. Because it was not known at what applied gas pressure breakthrough would occur, the rate of brine expulsion for a given applied gas pressure could only be known if the precise time from gas pressure application to gas bubble breakthrough was known. With 15 cells running simultaneously over a period of

months it was not feasible to make meniscus observations on the time scale required for accurate rate values and many cells exhibited breakthrough during the night.

Steps 1-5 were designed to remove most of the pore volume compression effects but small volumes of brine were expelled in the period prior to the pressure step resulting in breakthrough. The in situ porosity, pore volume, and weight of the core were corrected for this compression in step 18. Correction for the additional compression that occurred during the period associated with the breakthrough pressure step was not done because these values were less than the error in the weight measurement.

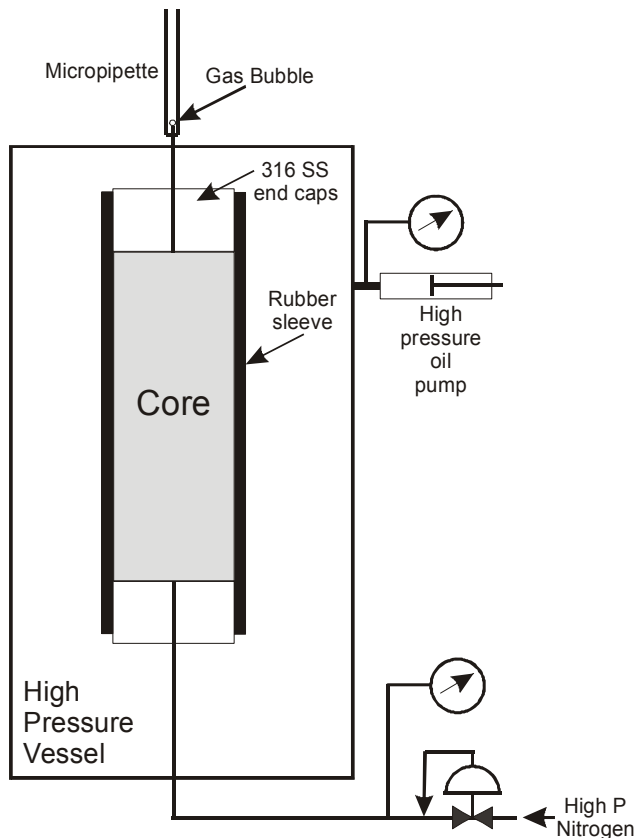


Figure 4.2.4. Schematic of high-pressure, air-brine critical gas saturation measurement apparatus. Samples were confined at a pressure of 26.7 MPa (4,000 psi) greater than the mean gas injection pressure.

The cores were analyzed in sequence sorted from the highest to lowest permeability and beginning analysis with the highest permeability core that required the lowest inlet gas pressure to achieve breakthrough. Fifteen (15) Hassler cells, plumbed in parallel for overburden and inlet pressure, were in operation for this measurement allowing the simultaneous analysis of 15 cores. When a core measurement was complete for a sample, the next core in the series was placed in

the available Hassler cell and the first gas pressure applied was equal to the gas pressure being applied for the other cores. Using this procedure, the first gas pressure for the lowest-permeability cores, analyzed near the end of the series, was significantly greater than the first gas pressure for the early, high-permeability cores. Only 4 cores exhibited breakthrough on the first gas pressure application, indicating breakthrough might have been achieved at a lower pressure and gas saturation might have been less than observed.

4.2.3 Results and Discussion

The following discussion is taken, in part, from Byrnes (2008), and also after Byrnes (2005). Critical gas saturation data are presented in Appendix 3.

4.2.3.1 Executive Summary

A review of gas relative permeability (k_{rg}) studies of low-permeability sandstones indicates they can be modeled using the Corey equation, but scarce data near the critical-gas saturation (S_{gc}) limit k_{rg} modeling at high water saturations. Confined mercury injection capillary pressure and coupled electrical resistance measurements on Mesaverde sandstones of varied lithology were used to measure critical non-wetting saturation. Most of these data support the commonly applied assumption that $S_{gc} < 0.05$. However, a few heterolithic samples exhibiting higher S_{gc} indicate the dependence of S_{gc} on pore network architecture. Concepts from percolation theory and upscaling indicate that S_{gc} varies among four pore network architecture models: 1) percolation (N_p); 2) parallel ($N_{//}$); 3) series (N_{\perp}); and 4) discontinuous series ($N_{\perp d}$). Analysis suggests that S_{gc} is scale- and bedding-architecture dependent in cores and in the field.

The models suggest that S_{gc} is likely to be very low in cores with laminae and laminated reservoirs and low (e.g., $S_{gc} < 0.03$ - 0.07 at core scale and $S_{gc} < 0.02$ at reservoir scale) in massive-bedded sandstones of any permeability. In cross-bedded lithologies exhibiting series network properties, S_{gc} approaches a constant reflecting the capillary pressure property differences and relative pore volumes among the beds in series. For these networks S_{gc} can range widely but can reach high values (e.g., $S_{gc} < 0.6$). Discontinuous series networks, representing lithologies exhibiting series network properties but for which the restrictive beds are not sample-spanning, exhibit S_{gc} intermediate between N_p and N_{\perp} networks.

Consideration of the four network architectures lends insight into the complications of heterogeneous lithologies at differing spatial scales and underscores the difficulty of upscaling laboratory-derived relative permeabilities for reservoir simulation. Analysis also indicates that for some architectures capillary pressure and relative permeability anisotropy may need to be considered.

4.2.3.2 Introduction

Numerous studies have investigated absolute permeability in low-permeability sandstones (Section 2.1.1.1.2). Studies of gas relative permeability (k_{rg}) have appropriately focused first on the gas relative permeability curve at low water saturations but fewer studies have investigated the end-point of the relative permeability curve, the critical-gas saturation (S_{gc}). The critical-gas saturation can be defined as the minimum gas saturation at which the gas phase has sufficient connectivity to form a system-spanning cluster and can consequently flow freely across the system. Experimental complexity makes it difficult to obtain k_{rg} data at high water saturations due to the extremely low gas permeabilities of the rocks and questions of the uniform distribution of saturation. High water saturation rocks are abundant and may predominate in resource plays. Therefore, understanding gas relative permeability at high water saturations is important to defining reservoir performance and the recoverable resource.

Although low-permeability sandstone petrophysical properties exhibit a continuum with higher permeability rocks, their properties can be significantly more sensitive to pressure-volume-temperature-composition-time (PVTXt) conditions and can change with PVTXt changes that for higher permeability rocks might be unimportant. This often requires that petrophysical properties, and the PVTXt conditions under which they apply, be carefully defined and measured. It also often leads to miscommunication where property definitions that are robust for a wide PVTXt range in high-permeability rocks must be modified to account for PVTXt influences in low-permeability rocks. Definitions for petrophysical terms used in this section are presented in Table 4.2.1.

This section examines some, but certainly not all, of the issues concerning gas relative permeability in low-permeability sandstone with a focus on critical-gas saturation that represents the end-point of the gas relative permeability curve. After a brief summary of previous work, it attempts to add to the data on critical-gas

saturation by presenting mercury injection and resistance analyses directed at measuring the critical non-wetting phase saturation, which is analogous to the critical-gas saturation. To understand the observed critical saturations and the theoretical scale-dependence and bedding-architecture dependence of S_{gc} , models of pore architecture and percolation theory analysis are examined and applied.

Abbreviation	Definition
D	Fractal dimension
E	Euclidean dimension
f	Fraction of total network sites where gas nucleation occurs
k	Permeability, mD
kik	<i>In situ</i> Klinkenberg-corrected gas permeability, mD
krg	Relative permeability to gas, fractionl (v/v)
L	Network size
MICP	Mercury injection capillary pressure, MPa
Mpa	Megapascals, 10 ⁶ pascals
Nii	Parallel network
Np	Percolation network, random
Ns	Series network
Ns2	Discontinuous series network
p	Modified Corey equation gas exponent
Pc	Capillary pressure, Pa
Pc Sgc,high	Capillary pressure at Sgc,high
phi	Porosity, fraction (v/v)
psi	Pounds per square inch
PVTXt	Pressure-Volume-Temperature-Composition-time
q	Modified Corey equation gas exponent
Sg,Pc-Sgc-high	Gas saturation at PcSgc,high
Sgc	Critical gas saturation, expressed as a fractional (v/v) hydrocarbon saturation (1-Sw), saturation below which krg = 0
Sgc, low	Lowest critical gas saturation in parallel network, fraction (v/v)
Sgc,high	Highest critical gas saturation in series network, fraction (v/v)
Shg	Mercury (non-wetting phase) saturation, fraction (v/v) Critical non-wetting phase saturation, fraction (v/v), saturation below which non-wetting phase does not form a sample-spanning cluster
Snwc	
Sw	Water saturation, fraction (v/v)
Swc	Critical water saturation, fraction (v/v), saturation below which krw = 0
Swc,g	Critical water saturation, fraction (v/v) with respect to gas drainage, saturation at which krg = 1 and below which krg = 1
V	System volume (v)

Table 4.2.1 List of Abbreviations and Symbols in Critical Gas Analysis

4.2.3.3 Previous Work

4.2.3.3.1 Gas Relative Permeability

Relative gas permeability (k_{rg}) data for low-permeability sandstones have been reported in numerous studies ([Thomas and Ward, 1972](#); [Byrnes et al., 1979](#); [Jones and Owens, 1980](#); [Sampath and Keighin, 1981](#); [Walls, 1981](#); [Walls et al., 1982](#); [Randolph, 1983](#); [Ward and Morrow, 1987](#); [Chowdiah, 1987](#); [Byrnes, 1997](#); [Kamath and Boyer, 1995](#); [Castle and Byrnes, 1998, 2005](#); [Byrnes and Castle, 2000](#); [Byrnes, 2003, 2005](#); [Shanley et al., 2004](#)). Some k_{rg} measurements have been performed at water saturations (S_w) less than the saturation at which water is immobile under a pressure gradient, and by definition, water relative permeability approaches zero. In the laboratory these sub- S_{wc} saturations were usually achieved by evaporation. Such saturations may or may not exist in nature where PVTX changes to the fluids and rock or sufficiently long times are available for ultra-low flow rates that can potentially reduce water saturations below S_{wc} . The k_{rg} data in the $S_w < S_{wc}$ region exhibit continuity with data in the $S_w \geq S_{wc}$ region. To model these data in Corey-type equations, and avoid the apparent contradiction of water saturations below the saturation at which water is immobile, the term $S_{wc,g}$ is used here that defines water saturations specific for gas only. Alternately, Boolean expressions could be used to model these conditions but this approach was considered simpler. Byrnes et al. (1979) utilized a modified-Corey (1954) equation to predict gas relative permeability in low-permeability sandstones:

$$k_{rg} = (1 - (S_w - S_{wc,g}) / (1 - S_{gc} - S_{wc,g}))^p (1 - ((S_w - S_{wc,g}) / (1 - S_{wc,g})))^q \quad [4.2.1]$$

where all terms are defined in Table 4.2.1. Assigning $p = 2$ and $q = 2$ to generally model theoretical and observed data, Corey noted that p and q can change with pore structure. Brooks and Corey (1956) more thoroughly investigated the nature of pore-size distribution influence on relative permeability. They also noted that the Corey- or Brooks-Corey type equations are not defined at water saturations greater than S_{gc} and less than $S_{wc,g}$ even though “minor” flow may exist in these saturation regions. Issues related to operational, experimental and theoretical definitions of critical saturations underlie many debates about these properties.

Byrnes et al. (1979) modeled k_{rg} data of Mesaverde cores using Equation 4.2.1 with $S_{gc} = 0.2-0.3$, $S_{wc,g} = 0$, $p = 1.1-1.3$, and $q = 2$. For Mesaverde cores studied by Sampath and Keighin (1981) and Ward and Morrow (1987), reformatted to Equation 4.2.1, their equations utilized $S_{gc} = 0.3$, $S_{wc,g} = 0$, $p = 1.5$, and $q = 2$. Chowdiah (1987) utilized a Corey-type equation formulated differently than Equation 4.2.1 that included a S_{gc} term in the parenthetic portion of the numerator of the first term in Equation 4.2.1. For this formulation, Chowdiah reported S_{gc} values of 0.096-0.47 and p values of 1.40-4.13 for data where water saturation was obtained by evaporation. The k_{rg} formulation of Chowdiah implicitly assumed $S_{wc,g} = 0$. For the other studies cited above k_{rg} data and curves are reported but model equations are not presented. Byrnes (2003, 2005) compiled published k_{rg} curves for 43 samples from various western low-permeability sandstone formations (Figure 4.2.5) and individual k_{rg} values obtained at single S_w conditions (Figure 4.2.6). These data are shown parametrically with respect to the absolute permeability of the samples. For most of the studies, water saturations were achieved by drainage gas displacement of water (i.e., water saturation decreasing) using centrifuge, porous-plate or evaporation. Chowdiah (1987) hypothesized that saturations obtained by evaporation represented imbibition conditions and that k_{rg} values measured for these conditions are lower than those obtained by drainage displacement. Many of the data in Figure 4.2.6 were obtained using centrifuge, though samples were briefly reversed to remove water retained at the end-face, and some were obtained using porous-plate method. The difference among methods is not immediately evident but needs to be investigated further. For all data shown in Figures 4.2.5 and 4.2.6 the relative permeabilities were measured under a confining pressure generally greater than 10.3 MPa (1,500 psi) and the relative permeability values represent Klinkenberg-corrected values that are referenced to the Klinkenberg absolute-gas permeability measured on a dry sample (k_{ik} at $S_w = 0$) and not to water permeability. Chowdiah (1987) also hypothesizes that stress hysteresis resulting from sample removal from pressure for desaturation might result in a decrease in relative permeability. The reproducibility of k_{rg} curves in studies such as Thomas and Ward (1972) argues that this effect is not universal.

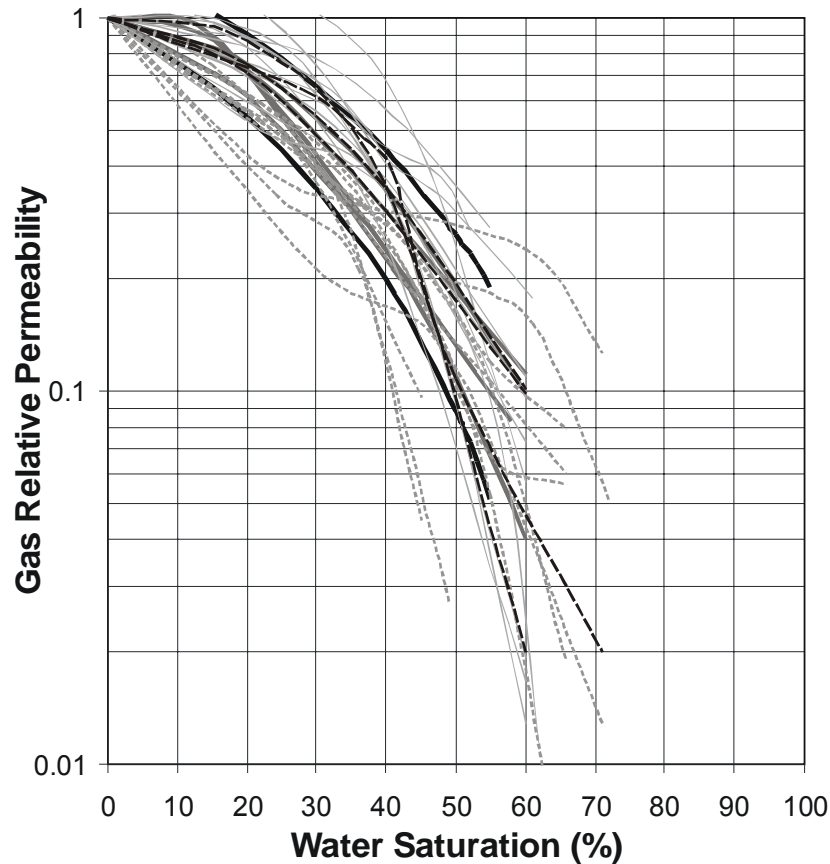


Figure 4.2.5. Relative gas permeability curves for 43 samples shown parametrically with permeability compiled from seven studies. Curves are separated into $k_{ik} < 0.01$ mD (dashed grey), $0.01 < k_{ik} < 0.03$ mD (thin light grey), $0.03 < k_{ik} < 0.1$ mD (heavy dark grey), $0.1 < k_{ik}$ mD (dashed black), Bounding heavy black curves are derived from the Corey equation model using parameters discussed in the text for $k_{ik} = 0.001$ mD (lower curve) and $k_{ik} = 1$ mD (upper curve).

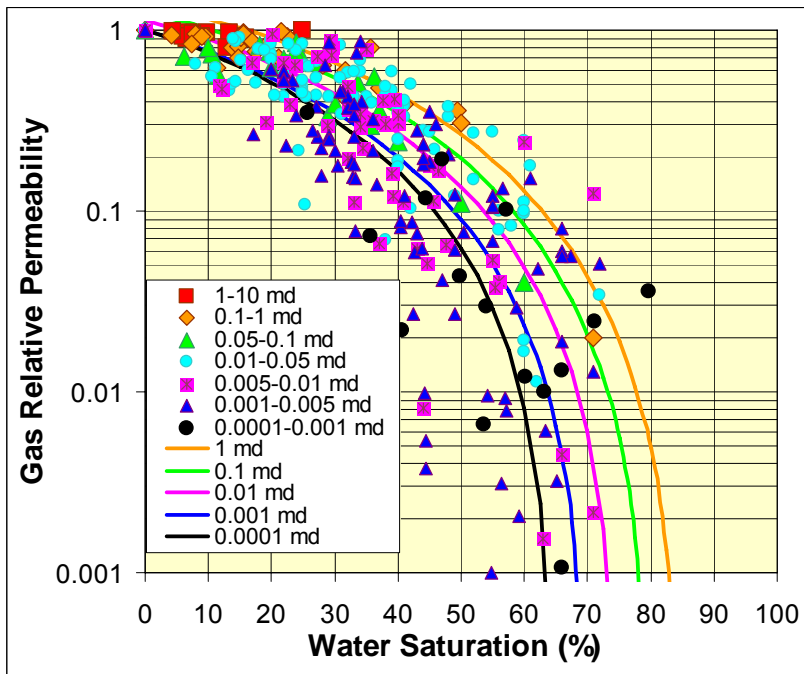
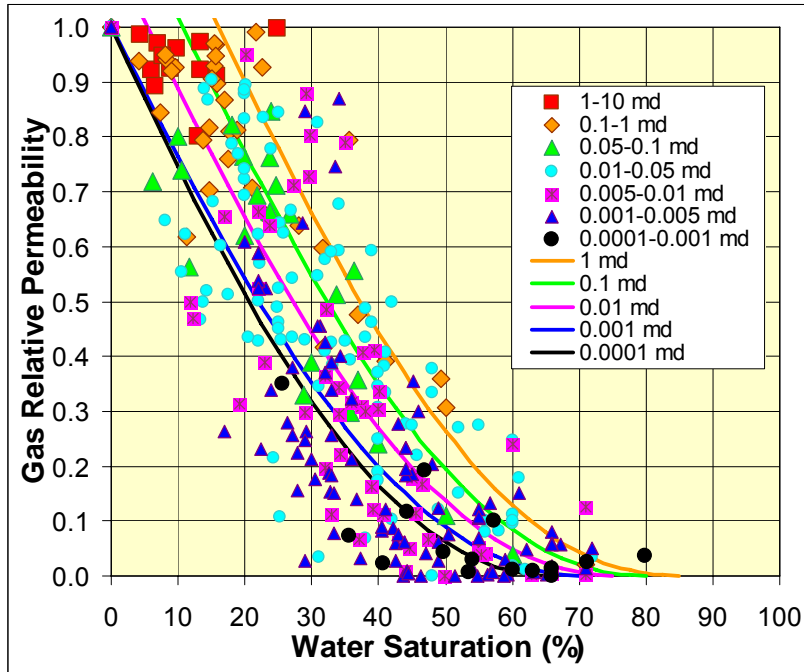


Figure 4.2.6. Gas relative permeabilities measured at single water saturations shown parametrically with sample k_{ik} . Curves show Corey-predicted k_{rg,S_w} values for samples with $k_{ik}=0.0001$ mD to $k_{ik}=1$ mD using Equations 1-6. Linear format (A) illustrates the decrease in critical-water saturation from ~ 0.16 for 1 mD rocks to zero for 0.001 mD rocks. The logarithmic format (B) illustrates the abrupt decrease in relative permeability as water saturations increase above 0.5 and how critical-gas saturation appears to increase with decreasing permeability.

Though there is scatter, interpreted to primarily represent pore architecture variation in rocks of different lithofacies, for both the complete k_{rg} curves and the composite individual k_{rg,S_w} measurements there is a general trend that at any given water saturation the gas relative permeability of lower permeability samples is less than that of higher permeability samples. Byrnes (2003) empirically fit the data in Figures 4.2.5 and 4.2.6 to Equation 4.2.1 using:

$$S_{wc,g} \approx 0.16 + 0.053 \cdot \log_{10} k_{ik} \quad (\text{for } k_{ik} \geq 0.001 \text{ mD}) \quad [4.2.2]$$

$$S_{wc,g} = 0 \quad (\text{for } k_{ik} < 0.001 \text{ mD}) \quad [4.2.3]$$

$$S_{gc} \approx 0.15 - 0.05 \cdot \log_{10} k_{ik} \quad [4.2.4]$$

$$p = 1.7 \quad [4.2.5]$$

$$q = 2 \quad [4.2.6]$$

These empirical equations were interpreted to be consistent with previously published parameters and to bracket existing data and approximately model the parametric relationship with absolute permeability. Figure 4.2.7 shows the same bounding k_{rg} curves as Figures 4.2.5 and 4.2.6 but extended to high S_w and low k_{rg} values. The bounding black curves were constructed using the equations for rocks of 0.001 millidarcies (mD; 1 mD = 0.000987 μm^2) and 1 mD, where $S_{gc} = 0.3$ for $k_{ik} = 0.001$ mD and $S_{gc} = 0.15$ for 1 mD, and $p = 1.7$, $q = 2$. The bounding dark grey curves illustrate a match for the data but with a constant $S_{gc} = 0.01$ and with the exponent p varying with absolute permeability and $q = 2$; e.g., $p = 2.9$ for $k_{ik} = 0.001$ mD and $p = 2$ for $k_{ik} = 1$ mD, respectively. Within the relative permeability range of most of the measured data ($S_w < 0.6$), k_{rg} can be modeled equally well by holding S_{gc} constant and expressing $p(k)$ or setting p constant and expressing $S_{gc}(k)$. However, at $S_w > 0.6$ the variable p /constant low- S_{gc} model ($p(k)$; $S_{gc} < 0.05$) exhibits significantly higher k_{rg} values than the constant p /variable S_{gc} model ($p \approx C$; $S_{gc}(k)$).

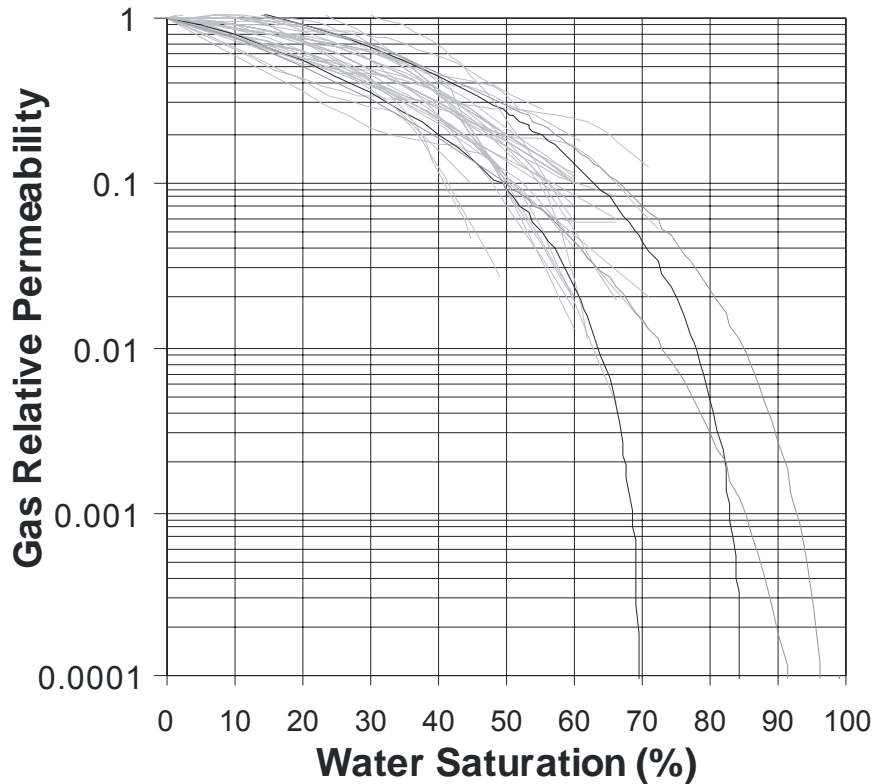


Figure 4.2.7. Relative-, gas-permeability curves (light grey) for 43 samples compiled from seven studies shown in Figure 4.2.5. The bounding black curves are the same as shown in Figure 4.2.5 and were constructed using the Equations 4.2.1-4.2.6 for rocks of 0.001 mD and 1 mD, where $S_{gc} = 0.3$ and 0.15 for $k_{ik} = 0.001$ mD and 1 mD, respectively, and $p = 1.7$, $q = 2$. The bounding dark gray curves illustrate a match for the data but with a constant $S_{gc} = 0.01$ and $p = 2.9$ for $k_{ik} = 0.001$ mD and $p = 2$ for $k_{ik} = 1$ mD, respectively.

4.2.3.3.2 Critical-Gas Saturation

Critical-gas saturation has been defined variously as: the minimum gas saturation at which the gas phase flows freely ([Firoozabadi et al., 1989](#)), the maximum gas saturation before any gas flow occurs ([Moulo and Longeron, 1989](#)); the gas saturation at which gas freely flows to the top of a reservoir ([Kortekaas and Poelgeest, 1989](#)); and the gas saturation at which gas is produced at the outlet of a core ([Li and Yortsos, 1991](#)). Li and Yortsos ([1993](#)) appropriately clarified a robust definition as the gas saturation at which the gas forms a system-spanning cluster (and consequently flows freely). This definition is consistent with the critical percolation threshold at which the gas is connected to all parts of the system and not just flowing in a subset of the system. Using this definition, S_{gc} denotes the critical value of the pore volume fraction occupied by the gas for the formation of a system-spanning cluster.

The majority of critical-gas saturation studies have focused on modeling S_{gc} in solution gas drive oil reservoirs where gas saturation is achieved by gas nucleation resulting from pressure decline and gas bubble growth within a network of variable pore size and connectivity. Solution-gas laboratory-measured S_{gc} values have ranged from 0.006 to 0.38 ([Hunt and Berry, 1956](#); [Handy, 1958](#); [Moulu and Longeron, 1989](#); [Kortekaas and Poelgeest, 1989](#); [Firoozabadi et al., 1989](#); and [Kamath and Boyer, 1993](#)). The majority of studies report that S_{gc} increases with increasing pressure decline rate, interpreted to be due to the formation of a greater number of nucleation sites ([Li and Yortsos, 1993](#)). Sampling the Mesaverde in two closely-spaced Piceance Basin wells, Chowdiah ([1987](#)) performed drainage experiments on eleven Mesaverde cores with $0.0008 \text{ mD} < k_{ik} < 0.031 \text{ mD}$ and reported $0.03 < S_{gc} < 0.11$. For a low-permeability ($k = 0.10 \text{ mD}$) Colton sandstone sample, Kamath and Boyer ([1993](#)) reported $S_{gc}=0.01$ for external gas drive and $S_{gc} = 0.10$ for solution gas drive. In gas injection studies on a long Torpedo sandstone core with $k = 413 \text{ mD}$, Closmann ([1987](#)) found a saturation gradient from the inlet $S_g=0.08$ to the outlet ($S_g=0.02$) of the core. They interpreted the low $S_g = 0.02$ value at the outlet end of the core as representing the critical-gas saturation. Schowalter ([1979](#)) reported results from nitrogen-water and mercury intrusion displacement tests on ten samples of various sandstone and carbonate lithologies, ranging in permeability from $0.01 \text{ mD} < k < 30.09 \text{ mD}$ that exhibited a range of critical saturations ranging from 0.045 to 0.17.

4.2.3.3.3 Percolation Theory

Introduced by Broadbent and Hammersley ([1957](#)), the application of percolation theory has provided significant insight to the problem of critical-gas saturation and relative permeability. Using this approach, the pore system can be considered to comprise a network of pore bodies (sites) connected by pore throats (bonds) with specified size distribution for each, random distribution of the sizes in the network, and with a specified connectivity. The properties of an invading phase can be modeled either by random occupation of bonds or sites (ordinary percolation, OP), or occupation from the boundaries of the network or within the network at one or more nucleation sites by an invading phase that grows while maintaining connectivity following specified rules of occupation for how the invader-defender interface is allowed to move (invasion percolation, IP; first introduced by [Wilkinson and Willemsen, 1983](#)). For any network the probability that a site is occupied must equal or exceed a critical threshold value, the

percolation threshold, before sufficient sites are occupied and connected to form an infinitely-spanning, or system-spanning, cluster. This condition can be considered to correspond to the critical-gas saturation. Occupation fractions less than the percolation threshold do not allow gas flow across the system. It is important to note that percolation theory applies to networks with randomly distributed properties (i.e. no spatial correlation for site or bond sizes). Spatial correlations can modify the percolation threshold and consequently the critical-gas saturation. Possible implications of this are discussed below.

The physics and petroleum literature exploring percolation theory and application to porous media is extensive. Sahimi ([1993](#), [1994](#)) provides a comprehensive review. Berkowitz and Ewing ([1998](#)) review application to soils and Du and Yortsos ([1999](#)) summarize work on gas bubble growth and percolation. Beyond the experimental, critical-gas saturation work cited above, studies have investigated various aspects of two-phase percolation including issues with: mathematics of percolation in networks ([Larson et al., 1977](#); [Larson et al., 1981](#); [Wall and Brown, 1981](#); [Chandler et al., 1982](#); [Koplik and Lasseter, 1982](#); [Lenormand et al., 1983, 1985](#); [Feder, 1988](#)); invasion percolation ([Wilkinsen and Willemsen, 1983](#)); invasion under buoyant force ([Wilkinson, 1984, 1986](#)); invasion with trapping ([Yanuka and Balberg, 1991](#)); surface effects ([Yortsos and Parlar, 1989](#); [Cafiero et al., 1997](#)); gas bubble formation, growth and percolation as a function of fraction of nucleation sites and capillary number ([Li and Yortsos, 1995a, 1995b](#); [Du and Yortsos, 1999](#); [Ferer et al., 2003](#)). Using a variety of methods Lin and Cohenm ([1982](#)), Koplik et al. ([1984](#)) and Yanuka et al. ([1986](#)) estimated that average coordination numbers, Z , for sandstones range between approximately 4 and 8, indicating that a simple cubic lattice with $Z=6$ is appropriate for representing rock pore network topology.

Gas invasion of a reservoir can be envisioned to be sufficiently slow that concentration profiles should be quasi-static similar to the stepwise increase associated with the measurement of a drainage capillary pressure curve. In this process, the invasion of gas into the water-saturated reservoir is represented by growth of a cluster(s) where gas-liquid interfaces in any gas-occupied pore advance one-at-a-time by invading perimeter pore throats in order of increasing capillary resistance (or corresponding decreasing radius). This process has been termed invasion percolation ([Wilkinson and Willemsen, 1983](#); [Feder, 1988](#)) for invasion from one side or point on the perimeter of a network, and is a simpler form of invasion percolation where growth occurs from multiple clusters ([Yortsos and Parler, 1989](#)).

Wilkinson and Willemsen (1983) showed that the volume fraction of the percolation threshold, equivalent to S_{gc} , scales with network dimension, L , as:

$$S_{gc}(L) = A L^{D-E} \quad [4.2.7]$$

where A is a numerical constant, D is the mass fractal dimension of the percolation cluster ($D = 1.89$ for 2-D, $D = 2.52$ for 3-D), E is the Euclidean dimension ($E = 2$ for 2-D and $E = 3$ for 3-D). For a simple 3-D cubic network $A \approx 0.65$. This relation indicates that as $L \rightarrow \infty$ $S_{gc} \rightarrow 0$ (e.g., $S_{gc} = 0.215$ for $L = 10$; $S_{gc} = 0.024$ for $L = 1,000$; $S_{gc} = 0.008$ for $L = 10,000$).

Li and Yortsos (1993, 1995a) and Du and Yortsos (1999) extended the invasion percolation work to include gas nucleation at one or more sites showing that S_{gc} scales with network size, L , and the fraction of total network sites where gas nucleation occurs, f , as:

$$S_{gc}(L; fq) = A L^{D-E} + B f^{1-D/E} \quad [4.2.8]$$

where A and B are numerical constants, D is the mass fractal dimension of the percolation cluster ($D = 1.89$ for 2-D OP, $D = 1.82$ for 2-D IP with trapping, $D = 2.52$ for 3-D OP or IP, with or without trapping), E is the Euclidean dimension ($E = 2$ for 2-D and $E = 3$ for 3-D), and f is the fraction of total network sites where gas nucleation occurs. In the limit of very small f (e.g., one nucleation site only or external drive) the second term is approximately zero and S_{gc} corresponds to the volume fraction of the percolation cluster only, as presented in Equation 4.2.7. When the nucleation fraction increases, the main contribution to S_{gc} results from clusters growing around nucleation sites and not from the percolation cluster (Du and Yortsos, 1999). For large networks the first term in Equation 4.2.8 vanishes and S_{gc} becomes primarily a function of the fraction of nucleation sites.

4.2.3.4 Critical Non-Wetting Phase Saturation

Figure 4.2.8 illustrates the relationship between S_{nwc} and permeability, as measured by the inflection point on the 71 unconfined MICP curves and 54 confined MICP curves. Average unconfined $S_{nwc} = 0.026 \pm 0.028$ for rocks with $k_{ik} > 0.01$ mD and average $S_{nwc} = 0.050 \pm 0.050$ for rocks with $k_{ik} \leq 0.01$ mD (error bars represent two standard deviations). Ignoring the six

confined samples with $S_{nwc} > 0.010$, confined S_{nwc} values range from 4% to 22% less than unconfined with average $S_{nwc} = 0.025 \pm 0.052$ for $k_{ik} \geq 0.01$ mD, and average $S_{nwc} = 0.039 \pm 0.050$ for $k_{ik} < 0.01$ mD. Both the unconfined and confined S_{nwc} data sets exhibit a weak increase in S_{nwc} with decreasing permeability.

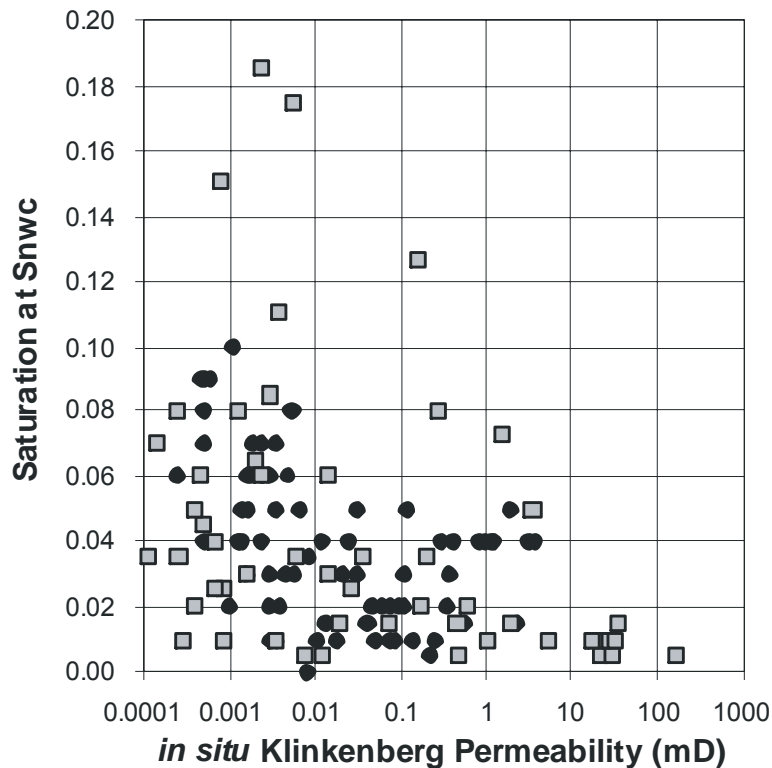


Figure 4.2.8. Critical-, mercury (non-wetting phase) saturation (S_{nwc}) versus *in situ* Klinkenberg permeability, interpreted from the inflection in the capillary-pressure curve shown in Figure 4.2.3, for unconfined (black circles) and confined (grey squares) samples. Average unconfined $S_{nwc} = 0.026 \pm 0.028$ for rocks with $k_{ik} > 0.01$ mD and average $S_{nwc} = 0.050 \pm 0.050$ for rocks with $k_{ik} \leq 0.01$ mD (error bars represent two standard deviations). Ignoring the six confined samples with $S_{nwc} > 0.010$, average confined $S_{nwc} = 0.025 \pm 0.052$ for $k_{ik} \geq 0.01$ mD, and average $S_{nwc} = 0.039 \pm 0.050$ for $k_{ik} < 0.01$ mD).

The majority of the cores that exhibit low S_{nwc} also exhibit massive, laminar, low-angle cross beddings, and ripple-laminated bedding that provides a continuous sandstone path across the core. Six cores exhibit anomalously higher S_{nwc} . Five of these six cores are moderately shaly sandstones with convolute, discontinuous-wavy, or flaser-bedded sedimentary structures. The sixth core exhibited low-angle cross-bedding.

Figure 4.2.9 compares the mercury saturations associated with resistance decreases and the inflection-interpreted S_{nwc} . For 52% of the samples, the inflection-interpreted S_{nwc}

corresponds to the mercury saturation (S_{Hg}) above which electrical resistance across the core exhibits values greater than $0.15-4 \times 10^6$ ohms and below which resistance values are less than 5-50 ohm, a decrease of up to six-orders of magnitude. This is interpreted to result from formation of a highly-conductive continuous path of mercury through the sample. For an additional 19% of the samples the interpreted S_{nwc} corresponded to a decrease in resistance of greater than 20%, interpreted to result from formation of a continuous mercury path of limited volume and high tortuosity. From these results it can be interpreted that for 71% of the samples the inflection and the resistance measurements agree on the interpreted critical saturation. Within this population, average $S_{nwc} = 0.042$ with a maximum value of $S_{nwc} = 0.175$. The remaining 29% of samples did not exhibit a resistance decrease until mercury saturation increased an additional $S_{Hg} = 0.03-0.29$ (average $S_{Hg} = 0.13$), corresponding to mercury saturations of $S_{Hg} = 0.04-0.44$ (average $S_{Hg} = 0.18$). For these 29% of samples the inflection S_{nwc} is interpreted to represent “pretender” clusters in a series network and the resistance-interpreted S_{nwc} provides a measure of the sample-spanning S_{nwc} .

Within a given capillary pressure step increase it is worthwhile to note that for almost 33% of samples the decrease in resistance did not occur at the final equilibrium saturation for a given applied capillary pressure. Rather, the resistance decrease occurred at a lower mercury saturation intermediate between the previous, lower, equilibrium saturation and the final, higher, equilibrium saturation associated with the applied capillary pressure. This implies that a backbone cluster formed at a lower saturation than the final equilibrium saturation for the applied pressure and that subsequent saturation increase was associated with either filling of adjacent sample-spanning clusters or sites peripheral to the backbone cluster. For some samples the saturation increase between resistance decrease and capillary equilibrium was as high as $S_{Hg} = 0.15$. This saturation difference can also result from the application of capillary pressure steps that result in large saturation changes due to a narrow pore size distribution.

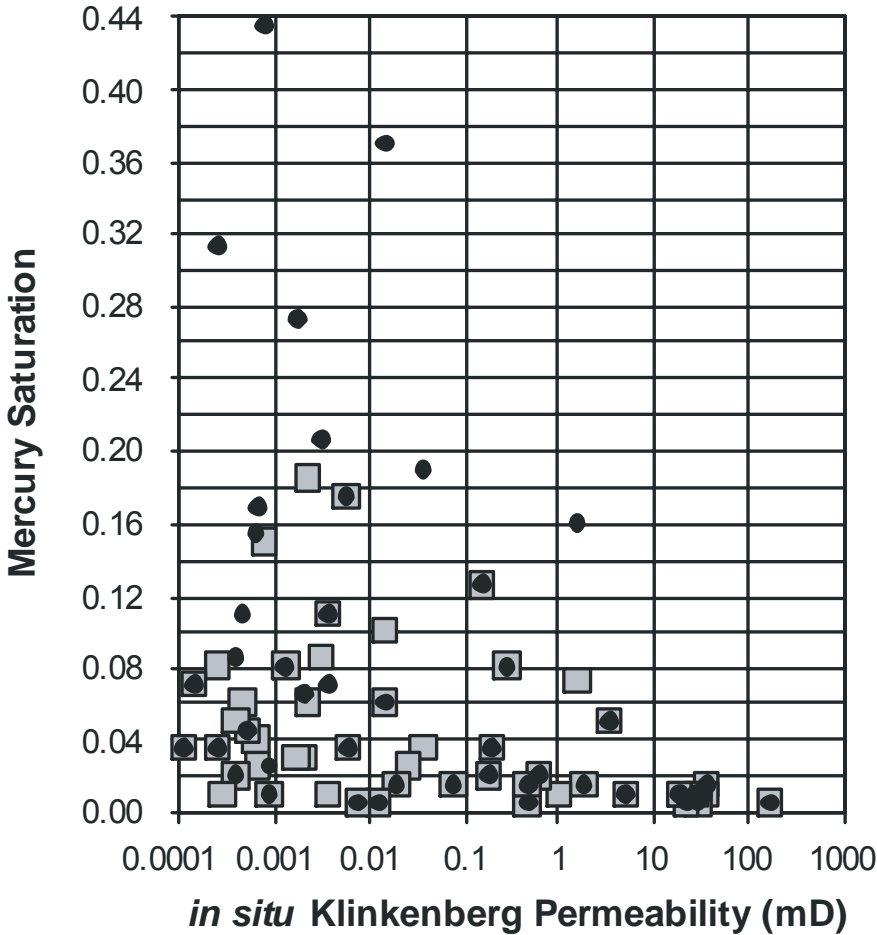


Figure 4.2.9. Cross-plot of confined S_{nwc} , interpreted from the inflection in the capillary-pressure curves (grey squares), and the mercury saturations at which electrical resistance across the sample decreased by greater than 20% and for 52% of samples by more than several orders of magnitude (black circles). Inflection and resistance measures of S_{nwc} agree for 71% of samples. For remaining 29%, the inflection S_{nwc} is interpreted to represent “pretender” clusters in series network and resistance- S_{nwc} provides an accurate measure of the sample-spanning S_{nwc} .

4.2.3.5 Critical Gas Saturation

Appendix 3 summarizes results for air-brine critical gas saturations measurements. Figure 4.2.10 shows the distribution histogram of *in situ* air-brine critical gas saturations (S_{gc}) measured on 150 core plugs from a wide range of lithofacies of varied porosity and permeability.

Approximately 66% of the samples exhibit critical gas saturations less than $S_{gc} < 0.06$ and 84% of the samples exhibit $S_{gc} < 0.10$. These results are similar to the air-mercury critical non-wetting phase saturation values.

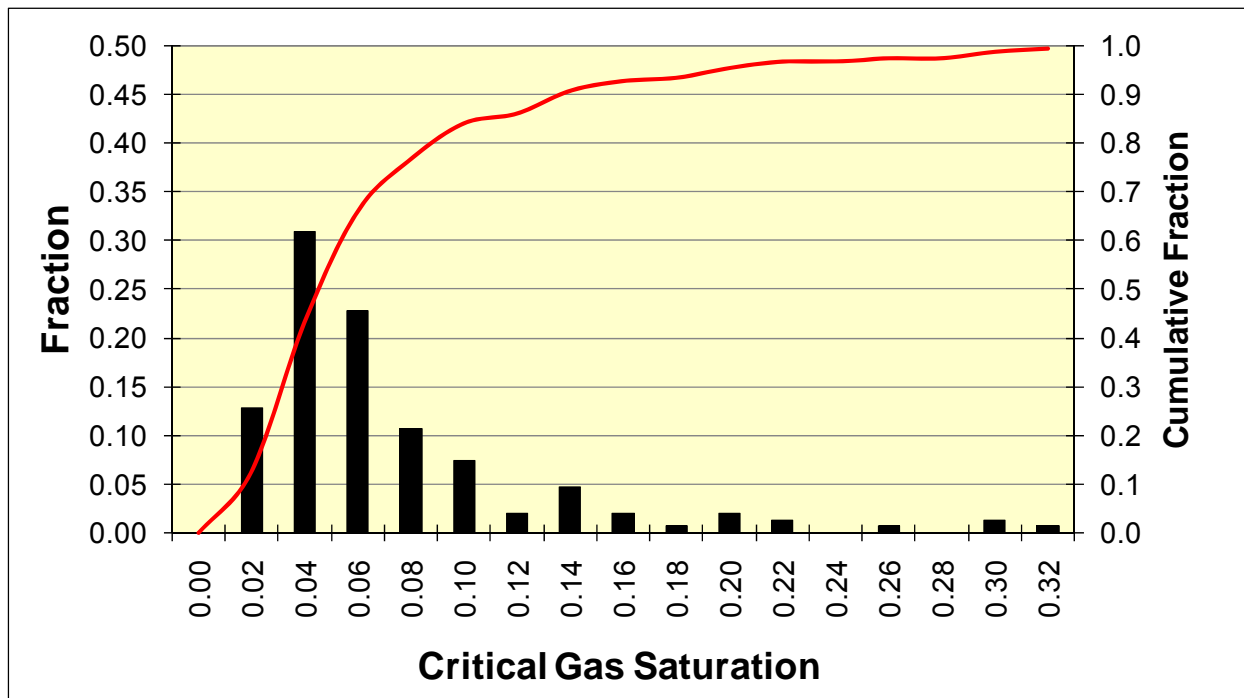


Figure 4.2.10. Distribution histogram of air-brine critical gas saturation for 150 Mesaverde core samples of widely varied lithofacies, porosity, and permeability.

Although the majority of samples exhibit low S_{gc} values, Figure 4.2.11 illustrates the relationship between S_{gc} and both permeability and primary sedimentary structure (PSS, as represented by the lithologic classification digit number 4). This figure shows that the distribution of S_{gc} values is not the same among rocks of different primary sedimentary structure and permeability.

The digital rock classification system used is discussed in more detail in Section 4.6. To represent primary sedimentary structure the cores and plugs were classified using the following values for the fourth digit in the classification scheme:

FOURTH DIGIT: Primary sedimentary structures

- 1xx0x Vertical perm barriers, shale dikes, cemented vert. fractures
- 1xx1x Churned/bioturbated to burrow mottled (small scale)
- 1xx2x Convolute, slumped, large burrow mottled bedding (large scale)
- 1xx3x Lenticular bedded, discontinuous sand/silt lenses
- 1xx4x Wavy bedded, continuous sand/silt and mud layers
- 1xx5x Flaser bedded, discontinuous mud layers
- 1xx6x Small scale (< 4 cm) x-laminated, ripple x-lam, small scale hummocky x-bd
- 1xx7x Large scale (> 4 cm) trough or planar x-bedded
- 1xx8x Planar laminated or very low angle x-beds, large scale hummocky x-bd
- 1xx9x Massive, structureless

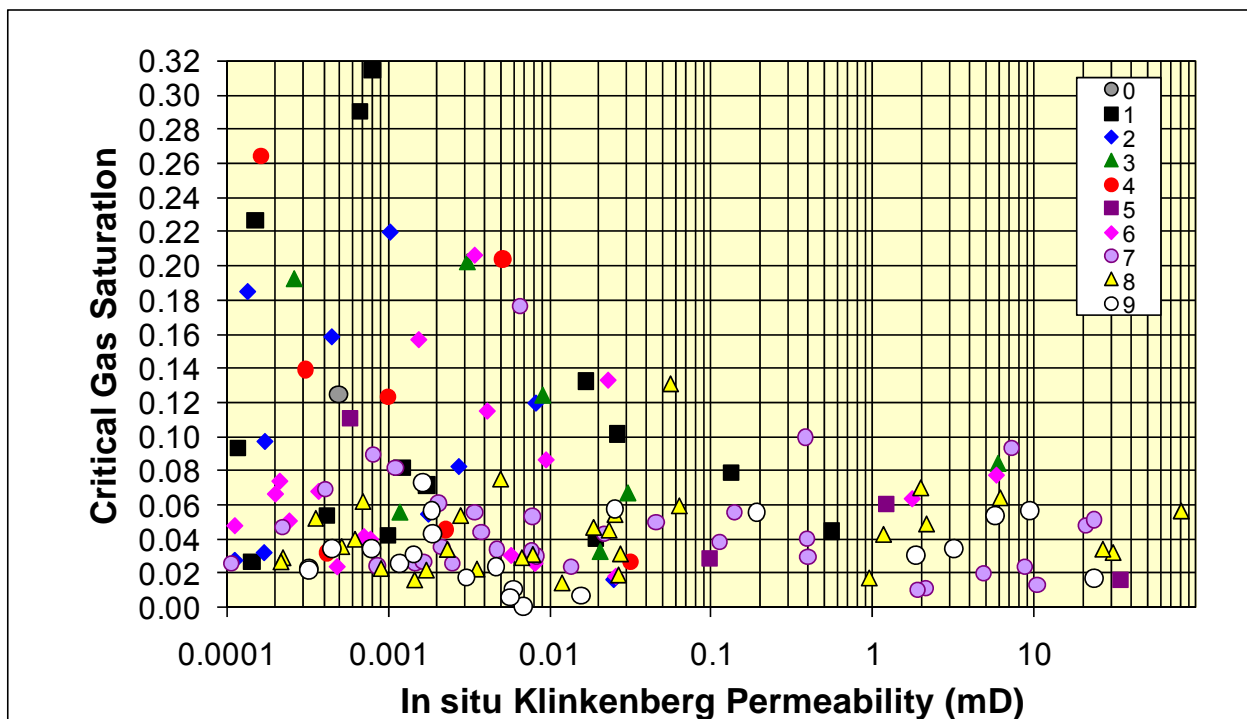


Figure 4.2.11. Cross-plot of air-brine critical gas saturation versus *in situ* Klinkenberg permeability for 150 Mesaverde core samples shown parametrically with primary sedimentary structure.

Figure 4.2.11 shows that S_{gc} is influenced by both primary sedimentary structure and permeability. Because permeability is also dependent on primary sedimentary structure the relative influence of these two variables requires principal component analysis (PCA). However, given the small sample population, PCA would not be quantitatively useful and the analysis here is more semi-quantitative. Although it is highly dependent on the distribution of permeabilities of the samples measured in each PSS class, in general, average S_{gc} increases with decreasing PSS

RC4 value (Table 4.2.2). Over 90% of all large-scale trough and planar cross-bedded, planar laminated, and massive bedded sandstones and siltstones ($1 \times 7 \leq RC4 \leq 1 \times 9$) of any permeability exhibit $S_{gc} < 0.06$. Sandstones with small-scale cross-laminated and ripple-cross-laminated bedding can exhibit low S_{gc} (i.e., $S_{gc} < 0.08$) but exhibit higher S_{gc} ($0.08 < S_{gc} < 0.22$) for rocks with $k_{ik} < 0.01$ mD. With increasing complexity of sedimentary structures that lead to baffles or restriction to flow along the axis of the core (and in the direction of gas movement for breakthrough), rocks with primary sedimentary structure digital classification values less than 5 (i.e., $1 \times 0 \leq RC4 \leq 1 \times 5$) each exhibit a general pattern of increasing S_{gc} with decreasing permeability. Critical gas saturation values for all the rocks with $1 \times 0 \leq RC4 \leq 1 \times 5$ range widely from low to high values. This wide range is interpreted to be the result of the highly variable nature of the exact structure of the bedding perpendicular to flow. Rock with a PSS that is very highly churned and bioturbated can exhibit properties similar to massive-bedded rock or can have convolute but continuous beds that span the sample length. Both of these rock types would exhibit low S_{gc} .

RC4	S_{gc}
0	0.125
1	0.1150
2	0.100
3	0.109
4	0.119
5	0.055
6	0.070
7	0.047
8	0.043
9	0.032

Table 4.2.2. General increase of average S_{gc} with decreasing PSS RC4 values.

4.2.3.6 Discussion

With the exception of the six high S_{nwc} values, the low S_{nwc} values measured for confined and unconfined conditions, and the low S_{gc} values for rocks with $1 \times 7 \times \leq RC4 \leq 1 \times 9 \times$, are consistent with published, low-permeability sandstone, gas S_{gc} values ([Chowdiah, 1987](#); [Kamath and Boyer, 1993](#)). Unconfined S_{nwc} values may be slightly higher than confined because mercury is allowed to enter the sample from all sides, representing a larger surface area and consequently more surface pores, allowing more invasion prior to establishment of the sample-spanning cluster. The effect of sample size and surface area on capillary pressure was investigated by Larson and Morrow ([1981](#)). Thompson et al. ([1987](#)) referred to these invaded paths that do not ultimately lead to a sample-spanning cluster as “pretender” paths. Higher S_{gc} values are also consistent with the larger surface area supporting multiple nucleation sites, which is associated with higher S_{gc} ([Li and Yortsos, 1993, 1995a](#); [Du and Yortsos, 1999](#)).

Given that average grain size for these rocks ranged from 50 to 200 μm (microns), and assuming that pore throats are distributed between each grain, then a 2.5-cm cube of rock (approximately a core plug) contains a network of pores with a lattice size dimension of $L = \sim 500$ to 125 for grain sizes of 50 μm and 200 μm , respectively. Inserting these dimensions into Equation 4.2.7, the theoretical, critical-percolation saturation for the core plug networks, assuming they comprise a random percolating network, is $S_{gc} = 0.033$ ($L = 500$) and $S_{gc} = 0.064$ ($L = 125$). These values are in reasonable agreement with the values measured by mercury intrusion analysis. If scaled up to bed-scale or reservoir-thickness scales that can exceed 1 meter in thickness, Equation 4.2.7 would indicate that S_{gc} approaches < 0.01 - 0.02 .

The above analysis supports the commonly applied assumption that $S_{gc} < 0.05$. However, the six mercury samples exhibiting higher S_{nwc} and complex sedimentary structure, the fourteen samples exhibiting higher S_{Hg} before resistance decreased, and the association of increasing air-brine S_{gc} with decreasing RC4 value, indicate that critical saturation can be greater for certain sedimentary structures, pore architectures, or boundary conditions. Percolation theory and averaging of capillary pressure as it applies to S_{gc} for different bed architectures provide a conceptual framework for understanding S_{gc} and models for predicting limits on S_{gc} .

4.2.3.6.1 Pore Networks and k_{rg} , S_{gc}

Pore networks can be broadly classified as exhibiting three end-member architectures and an important intermediate architecture: 1) Percolation network (N_p)- random orientation of pore sizes within the network; 2) Parallel network ($N_{//}$)- preferential orientation of pore sizes or beds of different N_p networks parallel to the invasion direction; 3) Series network (N_{\perp}) - preferential sample-spanning orientation of pore sizes or beds of different N_p networks perpendicular to the invasion direction; and 4) Discontinuous series network ($N_{\perp d}$) - preferential non-sample-spanning orientation of pore sizes or beds of different N_p networks perpendicular to the invasion direction (Figure 4.2.12). Different sandstone lithologies and the four pore-networks and their relationship to S_{gc} and k_{rg} is discussed. Gas is used as the invading phase for the following discussion.

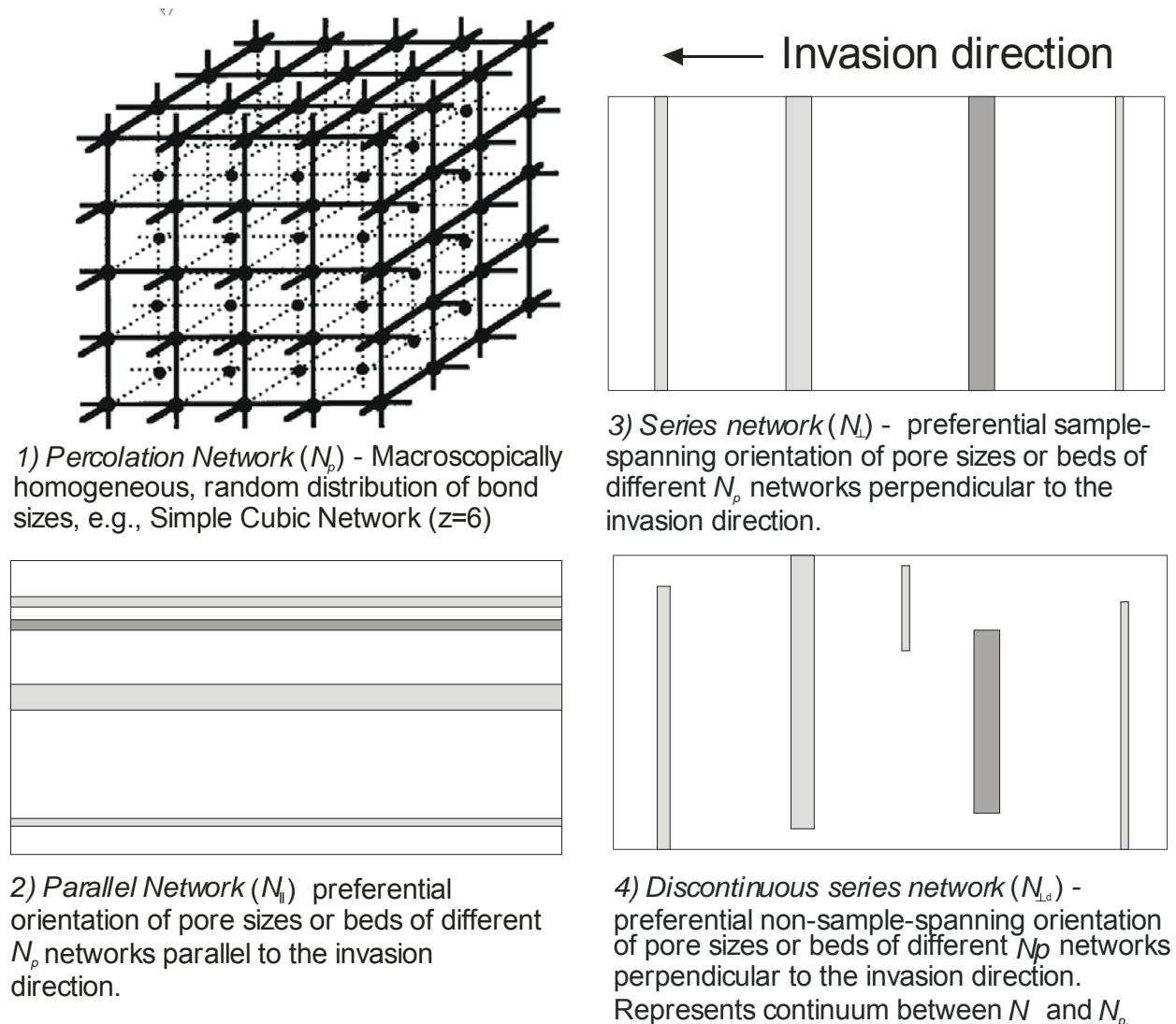


Figure 4.2.12. Conceptual pore network models: 1) percolation (N_p), 2) parallel ($N_{||}$), 3) series (N_{\perp}), and 4) discontinuous series ($N_{\perp d}$).

Percolation Network (N_p)

A massive-bedded or uniformly bioturbated sandstone, siltstone, or shale might exhibit a pore network that can be represented by a percolation network. As discussed above, for this network, formation of the percolation cluster would occur at $S_g < 0.03-0.07$ at the core-plug scale and would approach $S_{gc} < 0.01-0.02$ at large scales following Equation 4.2.7. Massive-bedded sandstone and siltstone is a common lithology in low-permeability sandstones and therefore low S_{gc} is likely to be common in many reservoir systems.

Parallel Network ($N_{//}$)

Planar- and horizontally-laminated bedding is common in many sedimentary environments. In addition, many sedimentary structures that might be Series Networks on a large scale can exhibit $N_{//}$ properties at smaller scales including core scale. Parallel networks perform similarly to percolation networks except that portions of the network are not involved in the invasive flow associated with establishing S_{gc} . The critical-gas saturation of this system is the critical saturation of the lowest threshold-entry pressure layer ($S_{gc,low}$; generally the highest-permeability layer) within the system, volumetrically normalized to the total system volume to express the critical saturation relative to the total system volume (S_{gc}). Because the volume of the layer is less than the volume of the total system, the network dimension is smaller and $S_{gc,low}$, from Equation 4.2.7, is greater than if the entire system exhibited the percolating layer properties. However, renormalization of the layer $S_{gc,low}$ to the total system volume results in a lower S_{gc} . Since S_{gc} approaches $S_{gc} < 0.02$ at large scales in percolating systems, it approaches similar or lower values in parallel systems. It is important to note that many rocks exhibit microscopic to millimeter-scale lamination. The presence of a single, sample-spanning, one-millimeter-thick lamina in a core, even with high $S_{gc,low}$, can result in a very low S_{gc} value for the core (e.g., a lamina with $S_{gc,low} = 0.5$, representing 1% of the total core volume, results in a core $S_{gc} = 0.005$). Frequently, core sampling procedures avoid sampling series flow architecture by orienting plugs parallel to bedding, thereby creating a sample with $N_{//}$ properties. Following establishment of S_{gc} , the total system gas relative permeability represents the vector solution of the various layer relative permeabilities both parallel to flow and between layers (cross-flow).

Series Network (N_{\perp})

Sedimentary bedding structures that represent series networks in one or more dimensions at one or more scales are abundant in nature (e.g., trough cross-bedding, large- and small-scale planar cross-bedding, low-angle planar bedding, hummocky bedding, flaser bedding). Within these structures scales of series networks range from millimeter-scale laminae to decameter scale cross-bedding. If the continuity of the beds is broken such that the beds are not sample-spanning then the series network is discontinuous as discussed below.

In a N_{\perp} network, percolation across the system does not occur until the invading gas pressure equals or exceeds the threshold pressure ($P_{CS_{gc,high}}$) required to achieve critical

saturation in the single barrier-bed with the highest pressure needed to allow percolation through that barrier-bed ($S_{gc,high}$). If invasion occurs under equilibrium-capillary pressure conditions then S_{gc} for the entire system is a function of the capillary-pressure properties of the barrier-beds in the system and is the average of the individual bed saturations at $P_{C_{S_{gc},high}}$ ($S_{g,P_{C-S_{gc},high}}$) normalized for bed pore volumes :

$$S_{gc} = [\Sigma(S_{g,P_{C-S_{gc},high}})_i \phi_i V_i] / [\Sigma \phi_i V_i] \quad [4.2.9]$$

Figure 4.2.13 illustrates a simple cross-bedded system consisting of two lithologies that exhibits very high S_{gc} as a result of the significant difference in the capillary pressure properties of the beds (e.g., siltstone laminae within sandstone). Corey and Rathjens (1956) observed critical-gas saturations of 0.60 in a cross-bedded sandstone with flow perpendicular to bedding.

$S_{gc,high}$ for the most-restrictive barrier-bed can be considered to follow Equation 4.2.7 and approaches zero at infinite size. However, the system S_{gc} does not approach zero but approaches a constant since the adjacent beds are all at the saturations associated with the threshold pressure of the restrictive barrier-bed. Equilibrium capillary-pressure conditions result in the maximum S_{gc} for a system. For systems with a pressure gradient across the system (e.g., flowing core test) S_{gc} is reduced as a result of the lower capillary pressures, and consequent lower gas saturations, in the down-gradient portion of the system. Given the time frames available, reservoirs are likely to be charged under capillary pressure equilibrium conditions.

Average absolute permeability in series flow has been shown to be the harmonic average of the bed permeabilities. Weber (1982) presented equations for calculating directional permeability in common cross-bedding structures. Directional, gas-relative permeability can be calculated using similar methodology. It is important to note that most reservoir, flow-simulation software treat capillary pressure and relative permeability as scalars and do not provide directional components (e.g., $kr_{g,x}$, $kr_{g,y}$, $P_{c,x}$, etc.) as they do for permeability (e.g., k_x , k_y , k_z)

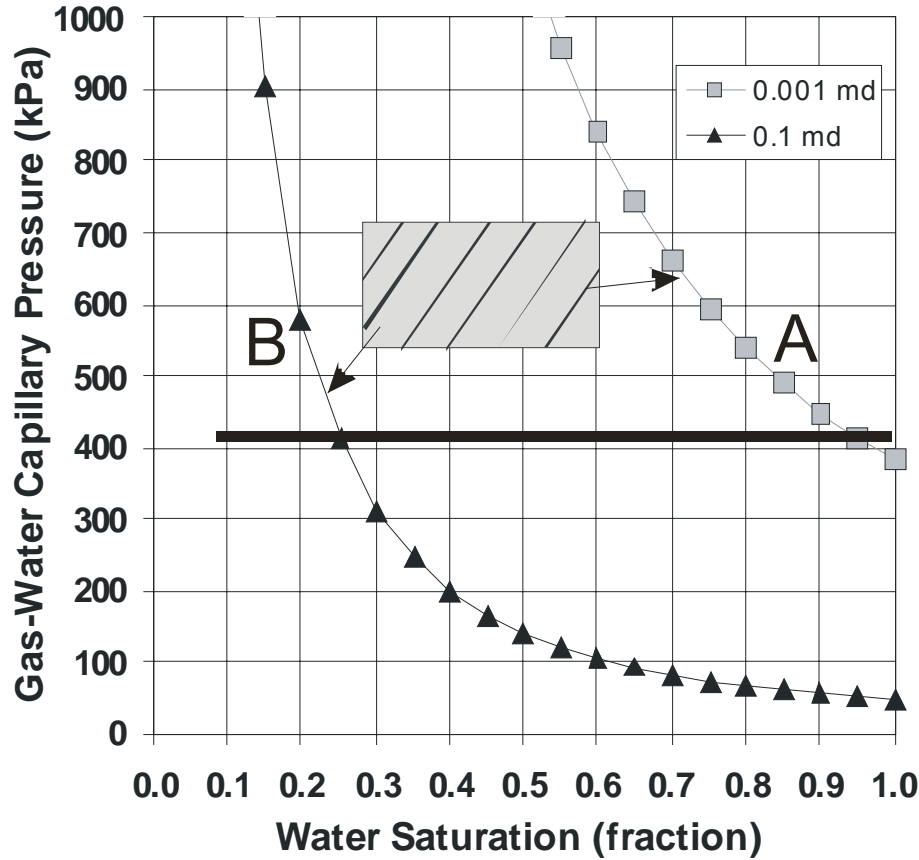


Figure 4.2.13. Example for a cross-bedded sandstone, consisting of higher-permeability/low-capillary-pressure sandstone (B) interbedded with low-permeability/high-capillary-pressure siltstone laminae (A), showing how S_{gc} can reach high values for invasion in a series network. For gas to flow across this system it must exceed the capillary pressure for the S_{gc} of the 0.001 mD fine beds ($P_{cS_{gc},high}$ on curve A). At $P_{cS_{gc},high}$ the 0.1 mD sandstone is desaturated to $S_{g,P_{cS_{gc},high}} = 0.75$. Assuming that the pore volume of the shale is negligible, the volume of this rock is largely the 0.1 mD facies and $S_{gc} = 0.75$.

Discontinuous Series Network ($N_{\perp d}$)

The N_{\perp} network discussed above requires that the barrier-beds be sample-spanning perpendicular to the direction of invasion. Beds may not be sample-spanning or may have holes. These represent discontinuous series networks ($N_{\perp d}$) and represent a continuum between a Percolation, N_p , and a Series, N_{\perp} , network. Critical saturations in a $N_{\perp d}$ network range between N_p and N_{\perp} critical saturations as a function of the network size, and the frequency, length, and property differences among the discontinuous barriers and the “host” sample-spanning network. Fundamentally, since a continuous path across the system exists through the “host” network, S_{gc} in a $N_{\perp d}$ network follows Equation 4.2.7. However, because some potential paths for the sample-

spanning cluster are blocked, at any given network dimension, more “pretender” paths ([Thompson et al., 1987](#)) are formed and S_{gc} is greater than for a N_p network of the same dimension. Though a formal mathematical analysis is not known, it can be estimated that S_{gc} in a $N_{\perp d}$ network follows Equation 4.2.7 but exhibits a decrease in slope as barrier-beds approach sample-spanning dimensions.

4.2.3.7 Conclusions

Mercury intrusion capillary pressure and associated resistance data, and air-brine critical gas saturation measurements presented for low-permeability sandstones exhibiting a wide range in lithology, support the commonly applied assumption that $S_{gc} < 0.05$. However, the association of increasing S_{gc} with decreasing primary sedimentary structure rock classification digit 4, and higher S_{nwc} with rocks exhibiting complex sedimentary structure, indicate the dependence of S_{gc} on pore network architecture. Percolation theory for random networks indicates that S_{gc} asymptotically approaches zero as the network dimension approaches infinity. Analysis of pore-network dimensions appropriate for cores and reservoir beds indicates that S_{gc} approaches $< 0.01-0.02$. Percolation theory and averaging of capillary pressure as it applies to S_{gc} for different primary sedimentary structures and bed architectures provide a conceptual framework for understanding S_{gc} and models for predicting limits on S_{gc} . Three end-member network architectures and an important intermediate architecture are appropriate: 1) Percolation network, N_p ; 2) Parallel network, $N_{//}$; 3) Series network, N_{\perp} ; and 4) Discontinuous series network, $N_{\perp d}$.

Applying these models to sedimentary structures, the models suggest that critical-gas saturation is likely to be low (e.g., $S_{gc} < 0.03-0.07$ at core scale and $S_{gc} < 0.02$ at reservoir scale) in massive-bedded or homogeneous sandstones of any permeability representing N_p networks. In lithologies representing parallel networks, $N_{//}$, such as sandstone cores with laminae and reservoirs with planar- and horizontally bedding, S_{gc} is likely to be lower than massive-bedded sandstones. In lithologies exhibiting series network, N_{\perp} properties, such as sandstones with trough cross-bedding, large- and small-scale planar cross-bedding, low-angle planar bedding, hummocky bedding, and flaser bedding, S_{gc} does not asymptotically approach zero with increasing network dimension but approaches a constant reflecting the capillary pressure property differences and relative pore volumes among the beds in series and the “tightest” bed limiting percolation. For these networks S_{gc} values range widely and have been observed to reach

$S_{gc} = 0.6$. Discontinuous series networks, $N_{\perp d}$, representing lithologies exhibiting series network properties but for which the restrictive beds are not sample-spanning, exhibit S_{gc} values intermediate between N_p and N_{\perp} networks.

The analysis and data presented in this study indicate that gas relative permeability can be effectively modeled in low-permeability gas sandstones using the modified Corey (1954) equation. The limited data support two different Corey-type models: 1) constant k_{rg} exponents ($p = 1.7, q = 2$) with variable S_{gc} ; and 2) near-constant, low S_{gc} with a varied p exponent. Results from this study can be interpreted to indicate that in heterolithic lithologies with complex sedimentary structures the ($p=C; S_{gc}(k)$) model may be more appropriate whereas in massive-bedded and laminated lithologies the ($p(k); S_{gc}<0.05$) may apply.

Consideration of the four network architectures lends insight into the complications of heterogeneous lithologies at differing spatial scales and underscores the difficulty of upscaling laboratory-derived relative permeabilities for reservoir simulation. Though anisotropy is well recognized and dealt with for absolute permeability, the analysis here suggests that consideration of capillary pressure and relative permeability anisotropy may be warranted. Finally, given the limited amount of air-brine S_{gc} data for low-permeability sandstones, further work is needed but this study would indicate that this work should be closely integrated with rock lithology.

Subtask 4.3. Measure *In Situ* and Routine Capillary Pressure

4.3.1 Task Statement

Relationships between “irreducible” water saturation and permeability ([Byrnes, 1997](#); [Byrnes and Castle, 2000](#)) and between threshold entry pressure or principal pore throat diameter and permeability ([Byrnes and Keighin, 1993](#); [Keighin, 1997](#); [Byrnes, 1997](#); [Byrnes, 2003](#)) have been published. The relationship between threshold entry pressure (P_{te}) and permeability and between permeability and lithofacies at any given porosity requires that capillary pressure change with lithofacies at any given porosity. With change in both the threshold entry pressure, the critical or percolating pore throat size capillary pressure (P_{pc}) and pore throat size distribution with decreasing permeability, Byrnes ([2003](#), [2005](#)) illustrated generalized capillary pressure shapes for western tight gas sandstones. Byrnes and Keighin ([1993](#)) and Keighin ([1997](#)) showed that the *in situ* P_{pc} values range from 15-84% of unconfined P_{te} values illustrating the change in capillary pressure with confining stress.

Though general capillary pressure relationships for low-permeability sandstones have been published, very few publications thoroughly characterize the lithologic properties of the samples. In addition, with the exception of Byrnes and Keighin ([1993](#)) and Keighin ([1997](#)), no published studies have investigated the stress dependence of Mesaverde capillary pressure properties. To fully characterize both the basic capillary pressure relationships of Mesaverde rocks ranging widely in lithology, porosity, permeability and basin, capillary pressure analysis was performed on pairs of representative samples. Mercury intrusion analysis from 2 to 9,300 psi (14-64,124 kPa) injection pressure was used. Paired samples, exhibiting similar porosity, permeability, and lithology were used for the unconfined analysis and the confined analysis.

All of the capillary pressure published work cited above investigates drainage capillary pressure properties. These, in fact, represent the principal capillary pressure property of interest for many low-permeability sandstones because they have remained on a primary drainage cycle throughout geologic time. There are, however, regions where reservoirs have leaked and undergone water imbibition and areas where portions of the gas column have undergone cyclic drainage-imbibition in response to burial and resulting pore volume change from compaction and diagenesis and saturation change from pore pressure increases and decrease ([Shanley et al., 2007](#)). For these areas an understanding of the drainage and imbibition capillary pressure

properties is required. To address the need for this information samples were selected for cyclic drainage-imbibition capillary pressure analysis.

4.3.2 Methods

4.3.2.1 Unconfined Capillary Pressure

Subsequent to lithologic description and paired-plugs porosity and permeability analysis core pairs were selected for unconfined, confined, and unconfined imbibition-drainage analysis. Samples were selected to represent each basin, the range in lithofacies, and range in porosity and permeability. The selected cores were transferred to a vacuum desiccator and maintained at vacuum conditions for a period of not less than 8 hours until ready for analysis. Each sample was transferred from the vacuum desiccator to the capillary pressure instrument and evacuated to a pressure of less than 0.01 torr for a period of 15 minutes. The sample was then subjected to increasing incremental mercury injection pressures ranging from 2 to 9,300 psia (14-64,124 kPa)). At each pressure, saturation equilibrium was assumed to have been established when the volume of mercury injected was less than 0.1% of the pore volume for a three minute period. Injected mercury volumes were corrected for system and mercury compressibility effects. Pore volume was corrected for sample compressibility to the threshold entry pressure. Accuracy and precision vary with sample pore volume and outer pore sizes and surface roughness. Pump injection volumes are readable to 0.001cc. Based on pore volumes from 1 to 3 cc, estimated precision for the measurement is 0.5% for pore sizes less than 107 μ m. A simple flow schematic of the unconfined mercury intrusion apparatuses is shown on the right side of Figure 4.3.1.

4.3.2.2 Confined Capillary Pressure

For confined samples each matching plug was transferred from the vacuum desiccator to a Hassler type confining pressure cell and subjected to a hydrostatic confining stress and evacuated to a pressure of less than 0.01 torr for a period of 30 minutes. The first 20 analyses were performed at a hydrostatic confining pressure of 34.5 MPa (5,000 psi) greater than the mercury injection pressure, maintaining a net effective stress of 34.5 MPa (5,000 psi). All subsequent samples were measured at a hydrostatic confining pressure of 27.6 MPa (4,000 psi) greater than the mercury injection pressure, maintaining a net effective stress of 27.6 MPa (4,000 psi). Resistance across

the core was measured using stainless steel electrodes on each end of the core. A schematic of the apparatus is shown on the left side of Figure 4.3.1. Confining pressures ranged from 4,000 psi (27.6 MPa) up to 11,300 psi (77.2 MPa). Because of the small pressure steps taken during the analysis the application of a new, higher, confining stress before increasing mercury pressure did not result in a significant additional stress although issues arise for stress on uninvaded pores as discussed below.

Incremental pore pressure ranged from 2 to 7,200 psi (0.01 – 49.6 MPa). At each pressure, equilibrium was assumed to have been established when the volume of mercury injected was less than 0.1% of the pore volume for a three minute period. Injected mercury volumes were corrected for system and mercury compressibility effects. Pore volume was corrected for sample compressibility. Accuracy and precision vary with sample pore volume, outer pore sizes and surface roughness, and uncertainty in the precise sample pore volume compressibility. Pump injection volumes are readable to 0.001cc. Based on pore volumes from 1 to 3 cc, estimated precision for the measurement is 0.5% for pore sizes less than 107 μ m.

It is important to note that the equilibration times of the confined samples were significantly greater than the unconfined samples. Equilibration times for pressures below the threshold entry pressure were similar to unconfined samples but at injection pressures where mercury was entering the pore space, and particularly at the pressures associated with initial saturation changes, equilibration times for a single pressure step could reach as long as 0.5-3 hours with time dependent on the pore size (and associated permeability). These equilibration times resulted in most of the confined mercury intrusion analyses requiring 2-3 days to perform.

Because the confined analysis required more than a standard work day to complete, analyses were stopped at the end of a work day to be resumed the following day. To test equilibrium criteria for some samples injection at the end of a work day was stopped following achieving equilibrium at a given injection pressure step. The sample was then left overnight with the confining stress held constant and the mercury injection system shut-in at the last equilibrium pressure. If mercury continued to enter the sample during the night as a result of the sample having not been at complete equilibrium, the injection pressure would decrease. For over 80% of the samples tested the volume of mercury required to return the mercury injection pressure to the equilibrium pressure of the previous day, when the analysis was halted, was less than 0.2% of the pore volume. This is greater than the defined equilibrium criteria but was insufficient to significantly change the capillary pressure curve

and was considered acceptable for an 8-12 hour equilibration time period. These results are interpreted to confirm that the equilibrium criteria used met acceptable standards for obtaining equilibrium saturation. For the remaining ~20% of samples that required greater than 0.2% of the pore volume to re-establish the previous day's injection pressure, most of these were very low permeability samples ($k_{ik} < 0.001$ mD); were stopped at a saturation early in the capillary pressure transition interval; and were stopped at a point that met equilibrium criteria but, unlike other samples, exhibited continued injection near the equilibrium criteria.

4.3.2.3 Unconfined, Cyclic Drainage-Imbibition Capillary Pressure

Unconfined, cyclic drainage-imbibition capillary pressure analyses were performed similar to the unconfined (drainage) capillary pressure analyses described above. The sample began on a primary drainage cycle with the goal of trying to achieve a mercury saturation near approximately $S_{Hg} = 33 \pm 10\%$. At any equilibrium saturation of $S_{Hg} < 25\%$ another pressure injection step was performed. If $25\% < S_{Hg} < 33\%$ the primary drainage cycle was terminated. If $S_{Hg} < 25\%$ and the next pressure injection step resulted in $S_{Hg} > 33\%$, the primary drainage cycle was terminated only when saturation reached equilibrium and not at $S_{Hg} = 33\%$. The exact saturation at which a given injection pressure would reach equilibrium was not known and, as such, the saturation at the termination of the primary drainage curve was not known until equilibrium saturation for the pressure applied was achieved.

Once the sample had reached the saturation at which the primary drainage cycle was to be stopped injection pressures were incrementally reduced in the same increments at which they were increased for the primary drainage cycle. Equilibrium on this primary imbibition cycle was assumed to have been established when the volume of mercury injected was less than 0.1% of the pore volume for a three minute period. Pressure was reduced incrementally until the pressure was returned to initial vacuum conditions. The mercury level was dropped below the sample and the sample allowed to equilibrate with the atmosphere. The sample was then removed from the apparatus, weighed to confirm the residual saturation, and immediately returned to the apparatus. In the apparatus the sample was again confined and evacuated to a pressure of less than 0.01 torr for a period of 30 minutes.

To measure the secondary drainage cycle the sample was then subjected to increasing incremental mercury injection pressures the same as the primary drainage pressure steps and then

continuing to incrementally increase injection pressures with the goal of trying to achieve a mercury saturation near approximately $S_{Hg} = 60 \pm 10\%$. At any equilibrium saturation of $S_{Hg} < 50\%$ another pressure injection step was performed. If $S_{Hg} > 50\%$ the secondary drainage cycle was terminated. If $S_{Hg} < 50\%$ and the next pressure injection step resulted in $S_{Hg} > 60\%$, the secondary drainage cycle was terminated only when saturation reached equilibrium and not at $S_{Hg} = 60\%$. The exact saturation at which a given injection pressure would reach equilibrium was not known and, as such, the saturation at the termination of the secondary drainage curve was not known until equilibrium saturation for the pressure applied was achieved.

Following the secondary drainage cycle the sample was subjected to a secondary imbibitions cycle following a procedure similar to the primary imbibitions cycle. A third drainage and imbibitions cycle were also performed. The third drainage cycle was stopped at the maximum injection pressure of 9,300 psi (64.1 MPa).

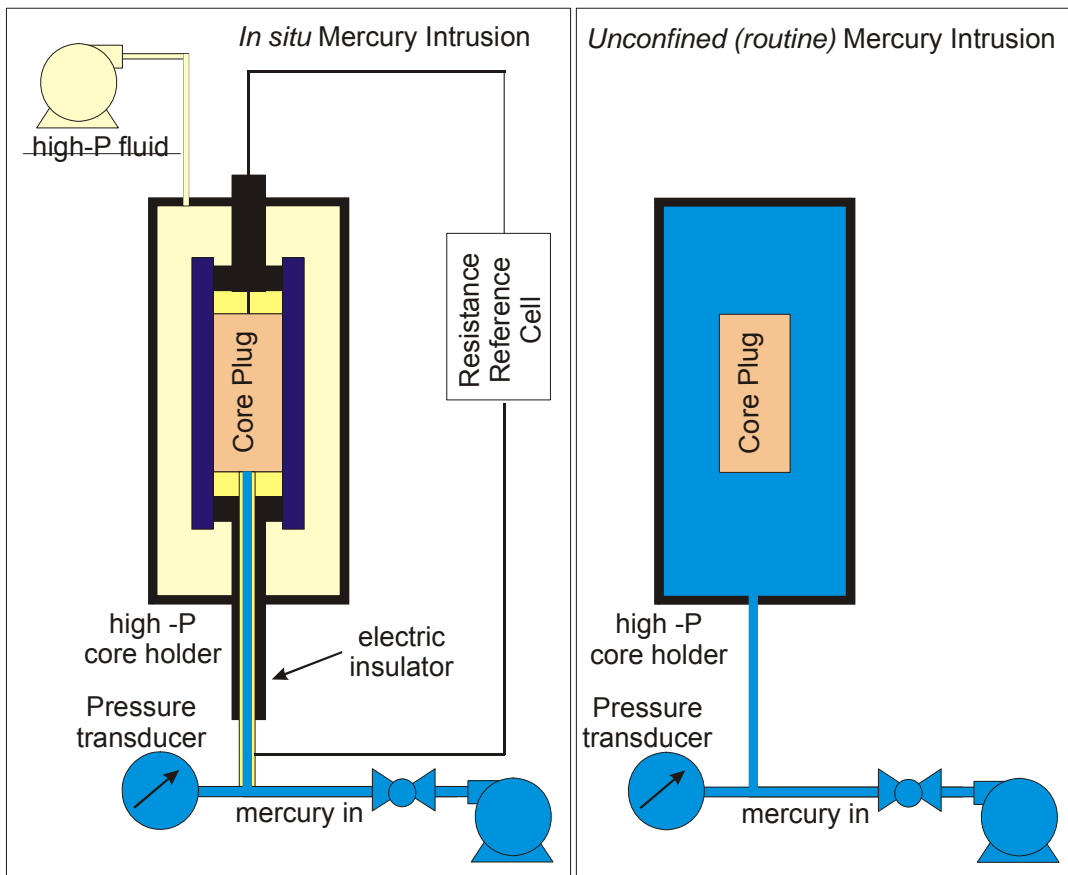


Figure 4.3.1 Flow schematic of unconfined and confined mercury intrusion apparatuses.

4.3.3 Results

Standard unconfined mercury intrusion analysis for injection pressures ranging from 2 to 9,300 psi (14-64,124 kPa) provided drainage capillary pressure curves for 121 advanced properties samples. Confined (at a net effective stress of 4,000 psi (27.6 MPa)) mercury capillary pressure curves were measured on 81 cores. For 33 cores unconfined imbibition-drainage capillary pressure curves were measured for three (3) drainage and three (3) imbibitions cycles, representing a total of 99 capillary pressure curves. Capillary pressure data were obtained for samples from 38 wells in all basins, representing the range of lithofacies, and a range of routine porosity from 1.3% to 23.8% and in situ Klinkenberg permeability from 0.000005 mD to 171 mD. Capillary pressure data are presented in Appendix 4.

Figure 4.3.2 illustrates that capillary pressure ranges widely for all Mesaverde rock samples. Selected representative drainage capillary pressure curves are shown in Figure 4.3.3. These curves exhibit the trend that threshold entry pressure (P_{te} , the minimum pressure at which the non-wetting phase can invade the sample pore space excluding minor surface pores) measured by extrapolation of the P_c curve in the transition zone to $S_w = 100\%$ (avoiding surface pore influence on the P_c curve), increases with decreasing permeability. This trend is the direct result of the association between decreasing pore throat size and permeability. They also show that at any given capillary pressure wetting-phase saturation increases with decreasing permeability.

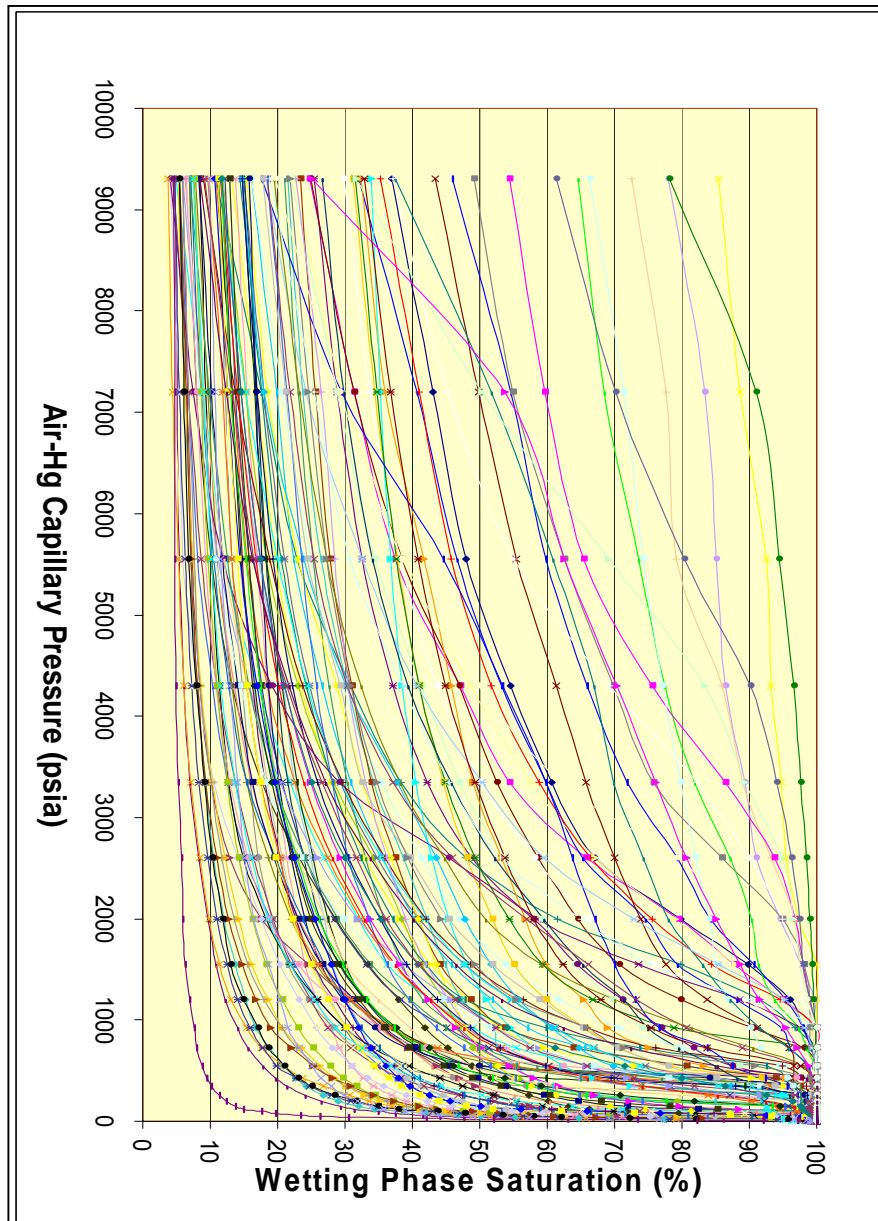


Figure 4.3.2. Air-mercury capillary pressure curves for selected samples ranging in *in situ* Klinkenberg permeability from 0.000005 mD to 171 mD. These curves exhibit increasing threshold entry pressure and increasing “irreducible” water saturation with decreasing permeability.

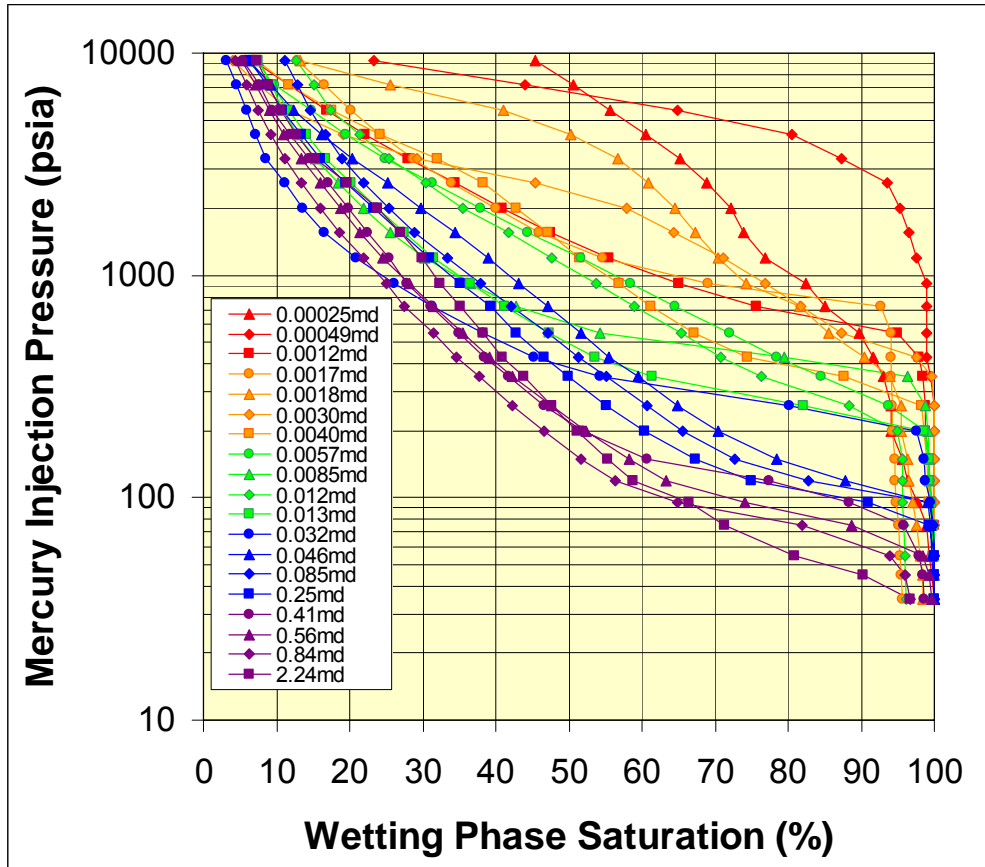


Figure 4.3.3. Air-mercury capillary pressure curves for selected samples ranging in *in situ* Klinkenberg permeability from 0.00025 mD to 2.24 mD. These curves exhibit increasing threshold entry pressure and increasing “irreducible” wetting-phase saturation with decreasing permeability.

4.3.3.1 Capillary Pressure Drainage-Imbibition Hysteresis

Thirty three (33) samples were tested for capillary pressure drainage-imbibition hysteresis involving three drainage-imbibition cycles for each sample (99 capillary pressure curves in total). These three cycles represent drainage saturations reaching successively non-wetting phase saturations (S_{nw}) of $S_{nw} = 0.33 \pm 0.15$, $S_{nw} = 0.57 \pm 0.10$, and $S_{nw} = 0.87 \pm 0.10$. Figure 4.3.4 illustrates the hysteresis curves for a single sample, while Figure 4.3.5 illustrates eight sandstones spanning a range of permeabilities. A significant fraction of the trapped non-wetting phase saturation (S_{nw}) results from the early intrusion at low S_{nw} values.

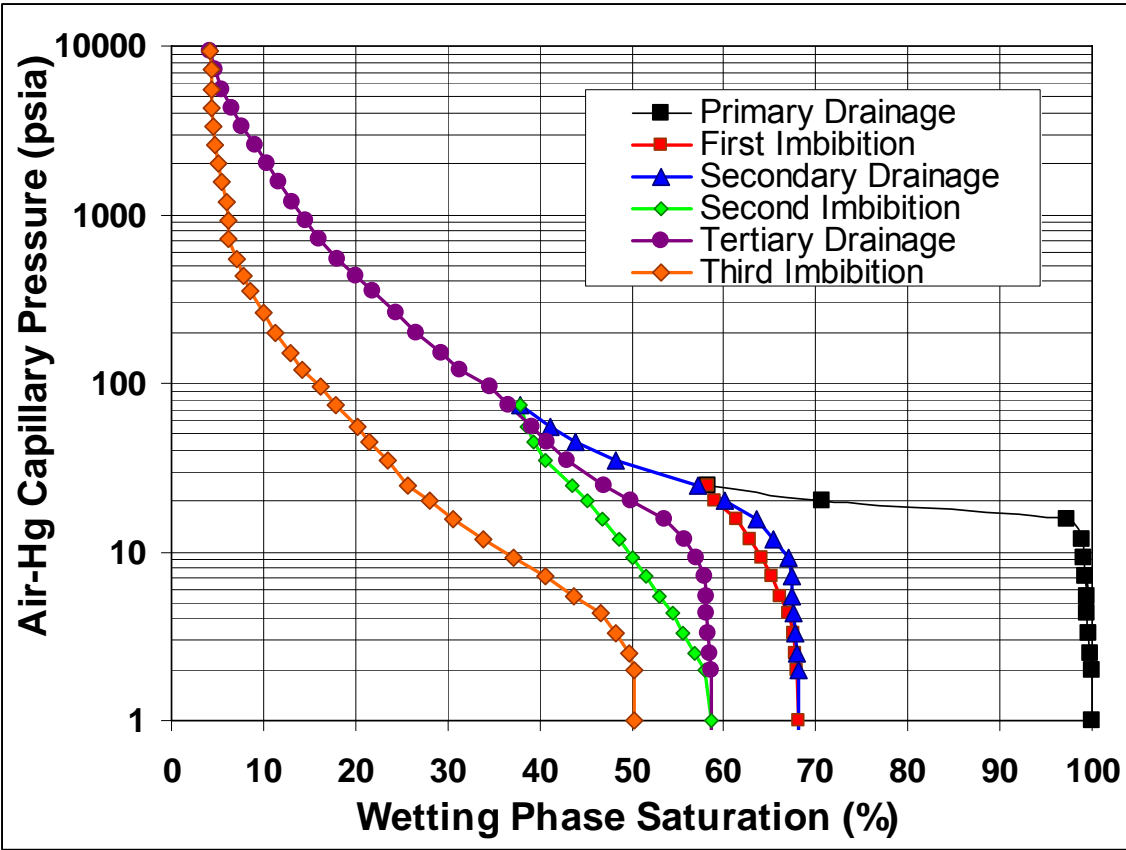


Figure 4.3.4. Air-mercury successive drainage and imbibition capillary pressure curves for one sample exhibiting hysteresis with successively increasing residual non-wetting phase saturation (S_{nwr}) with increasing initial non-wetting phase saturation (S_{nwi}).

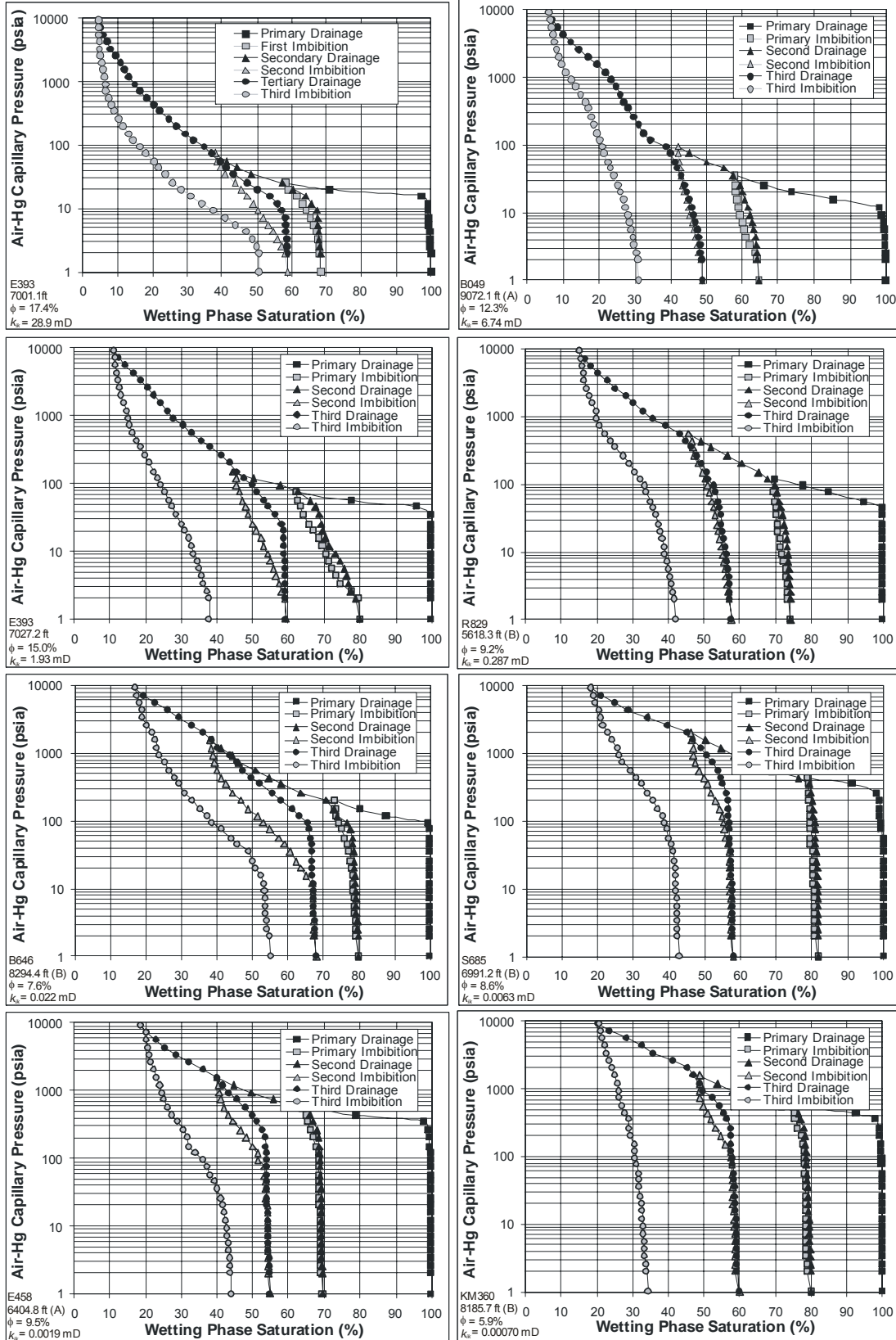


Figure 4.3.5. Example air-mercury successive drainage and imbibition capillary pressure curves

Figure 4.3.6 illustrates the relationship between the residual saturation to imbibition and the initial drainage saturation for each cycle. In addition to residual saturation measurements on the 33 hysteresis samples, all MICP samples were weighed following analysis. Residual mercury trapped in the core was determined gravimetrically and residual non-wetting phase saturation calculated. For these samples the initial mercury (non-wetting phase) saturation represented the mercury saturation achieved at 9,300 psi (64.1 MPa) intrusion pressure. This saturation is near, or represents a wetting phase saturation less than, “irreducible” saturation. Figure 4.3.7 illustrates the relationship between residual non-wetting phase saturation and the initial non-wetting phase saturation for the hysteresis and the single-cycle unconfined MICP samples. The relationship between initial and residual non-wetting phase saturation was characterized by Land (1971) for strongly water wet samples:

$$1/S_{nwr}^* - 1/S_{nwi}^* = C \quad [4.3.1]$$

where $S_{nwr}^* = S_{nwr}/(1-S_{wirr})$ and $S_{nwi}^* = S_{nwi}/(1-S_{wirr})$.

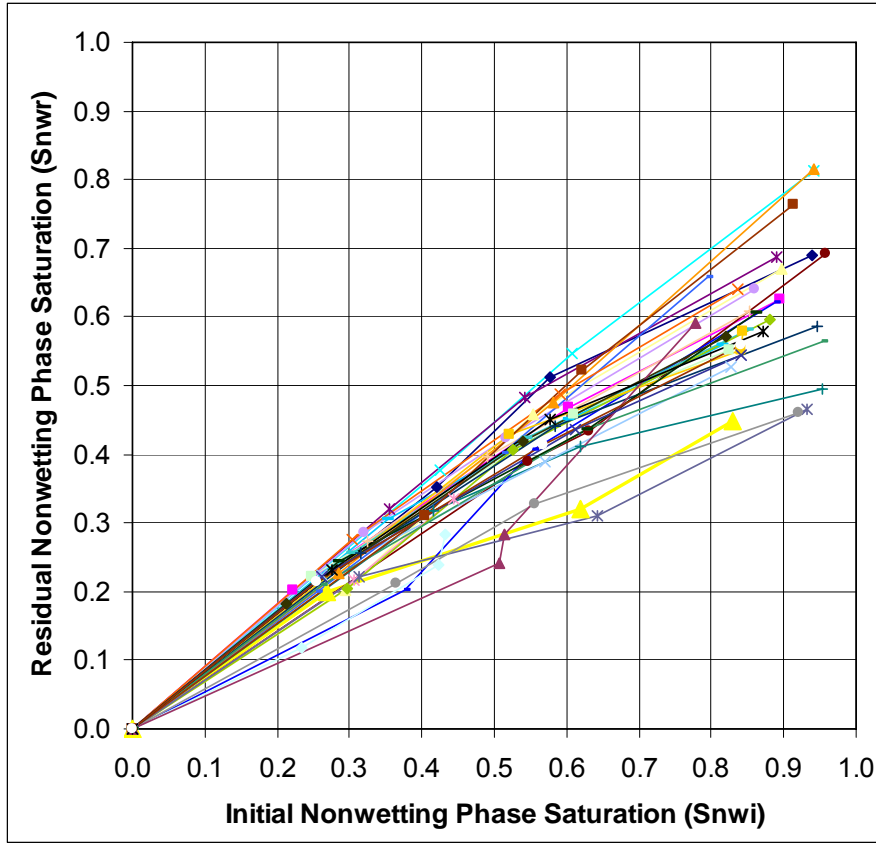


Figure 4.3.6. Cross-plot of residual versus initial mercury (non-wetting) saturation for 33 Mesaverde sandstone samples.

Three different measurement populations are compared; unconfined, unconfined with hysteresis, and confined. Unconfined with hysteresis are separated from the unconfined because the hysteresis samples have data for measurements at $S_w < S_{wirr}$ except for the third and last hysteresis drainage-imbibition cycle. Confined samples are samples for which capillary pressure analysis was performed with the sample under a net confining stress of 4,000 psi (27.6 MPa) as described below. Table 4.3.1 compares Land C values for the different sample populations with S_{wirr} defined as either equal to the minimum saturation achieved in the MICP analysis ($S_{wirr} = 1 - S_{nwmax}$) or S_{wirr} equal to zero ($S_{wirr} = 0$). The average Land C values represent the average of individual C values calculated for each sample using equation 4.3.1. The Land C Minimum Error values represent the C values that provide a minimum error for all samples in a given population using a single C value.

Sample Condition	Swirr definition	Land C Average	C Standard Error	Land C Minimum Error	Snwr Standard Error	Snwr Std Error C=0.55
all	$S_{wirr} = 1 - S_{nwmax}$	0.57	0.329	0.53	0.077	0.077
unconfined	$S_{wirr} = 1 - S_{nwmax}$	0.61	0.294	0.59	0.087	0.088
hysteresis	$S_{wirr} = 1 - S_{nwmax}$	0.61	0.383	0.51	0.056	0.057
confined	$S_{wirr} = 1 - S_{nwmax}$	0.44	0.249	0.45	0.088	0.085
all	$S_{wirr} = 0$	0.73	0.443	0.63	0.073	0.073
unconfined	$S_{wirr} = 0$	0.78	0.360	0.71	0.080	0.081
hysteresis	$S_{wirr} = 0$	0.75	0.562	0.59	0.057	0.057
confined	$S_{wirr} = 0$	0.61	0.316	0.54	0.078	0.078
all	$S_{wirr} = 0, S_{nwi} < 70\%$			0.70	0.054	0.053
unconfined	$S_{wirr} = 0, S_{nwi} < 70\%$			0.83	0.062	0.061
hysteresis	$S_{wirr} = 0, S_{nwi} < 70\%$			0.70	0.052	0.051
confined	$S_{wirr} = 0, S_{nwi} < 70\%$			0.50	0.038	0.039

Table 4.3.1. Comparison of average Land C values for different sample populations calculated from averaging individual sample C values and from solution of the minimum error for each a single C value for each population.

Average C values, calculated from the average of the individual sample C values using equation 4.3.1 (with $S_{wirr} = 1 - S_{wmin}$ and $S_{wirr} = 0$) average 0.07 greater than minimum error C values. Variance of the individually determined C values is significant, averaging 0.37. Land C values that result in the minimum error for a given population average 0.61 ± 0.20 for all populations and 0.65 ± 0.20 for the populations where $S_{wirr} = 0$. Standard error is greater for $S_{wirr} = 1 - S_{nwmax}$ than for $S_{wirr} = 0$ even with input of individual known sample S_{wirr} values. This argues that optimum prediction of S_{nwr} is obtained using $S_{wirr} = 0$.

Although the Land C values appear to vary widely, resulting predicted residual saturation values are not highly sensitive for the range of C values exhibited. Iterative solution indicates that $C = 0.55$ results in the minimum error in residual saturation for all populations with $S_{wirr} = 0$. Using $C = 0.55$ the resulting error in S_{nwr} prediction is only 0.001 ± 0.0015 different from the standard error values obtained using C value that provide the minimum error for each population (Table 4.3.1). Figure 4.3.7 illustrates initial (S_{nwi}) and residual non-wetting phase saturations (S_{nwr}) for the unconfined MICP samples, for which $S_{nwi} = 1 - S_{nwmax}$, and the unconfined hysteresis samples, for which 2 of 3 $S_{nwi} < 1 - S_{nwmax}$. Trapping is slightly greater in the hysteresis samples.

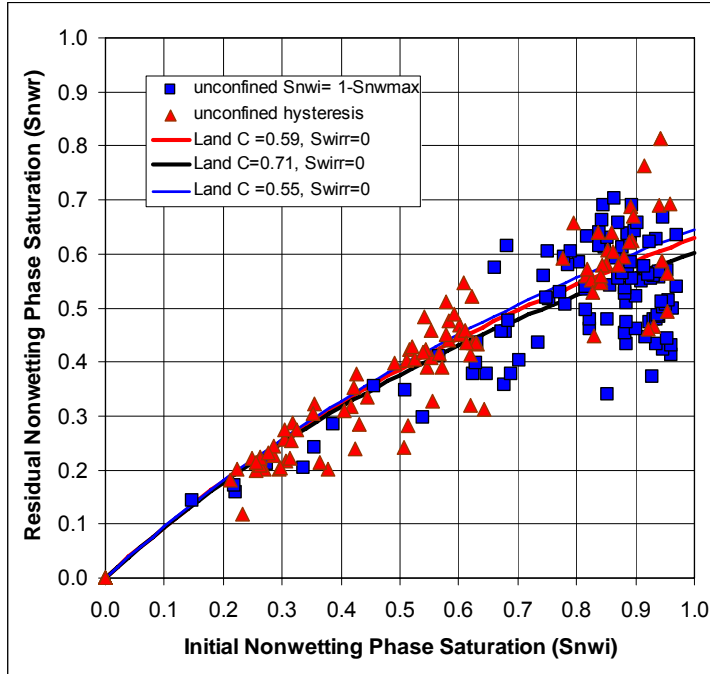


Figure 4.3.7. Cross-plot of residual and initial non-wetting phase saturation for unconfined samples including samples where $S_{nwi} = 1 - S_{nwmax}$ (blue squares) and hysteresis/imbibition samples where 2 of 3 measurements were obtained at $S_{nwi} < 1 - S_{nwmax}$ (red triangle).

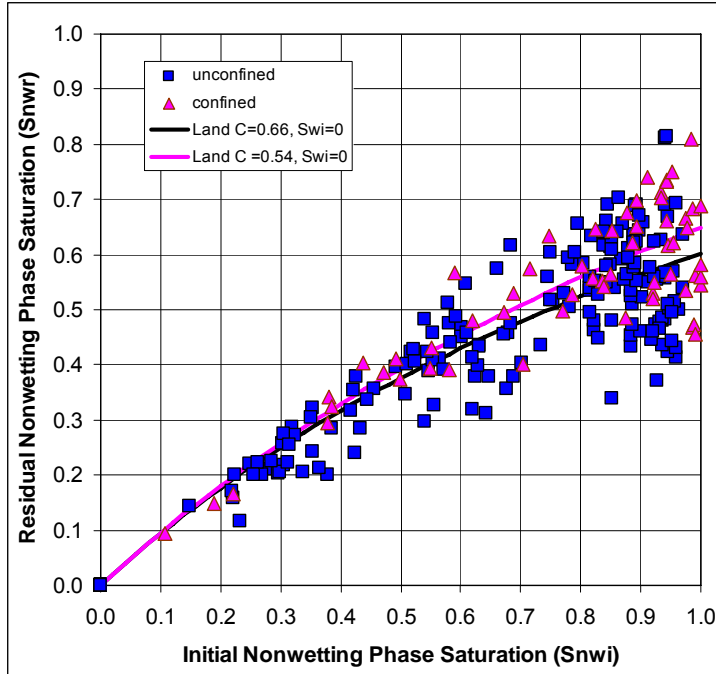


Figure 4.3.8. Cross-plot of residual and initial non-wetting phase saturation for unconfined samples (blue squares) and confined samples (magenta triangles). Higher S_{nwr} values in confined samples result in slightly greater Land C value.

Comparing the residual and initial saturations for unconfined and confined samples (Figure 4.3.8) shows that confined samples exhibit slightly greater residual saturation than unconfined with $C = 0.54$ and $C = 0.66$ for confined and unconfined (including unconfined and unconfined hysteresis samples), respectively. Greater trapping in confined samples may be the result of a change in the pore body – pore throat relationship due to confining stress or it may be the result of the limit placed on exit boundary conditions. Unconfined samples allow mercury to exit the sample from all sides whereas confined samples only allow mercury to exit from one entry face. Assuming a constant number of exit paths in any given direction and the same snap-off conditions, a decrease in the number of exit paths is likely to increase the non-wetting phase volume behind junctions undergoing snap-off in one direction. This change in boundary conditions would likely result in some additional trapping. Whether the increase in residual non-wetting phase saturation is the result of confining stress effects or the difference in boundary conditions is being investigated. Assuming that pore bodies are not strongly affected by confining stress and that confined samples have smaller pore throats than unconfined samples,

then greater pore body: pore throat ratios in confined samples compared with unconfined samples would also result in higher residual non-wetting phase saturations.

Based on analysis of prediction error for the confined and unconfined sample populations, prediction of S_{nwr} using $C = 0.55$ and $S_{wirr} = 0$ appears to provide minimum error for the range of possible measurement condition populations. Utilization of C values specific for a population results in improvement in prediction that is generally less than 2% of S_{nwr} .

4.3.3.2 Unconfined and Confined Capillary Pressure

Unconfined and *in situ* (confined) mercury intrusion capillary pressure (MICP) analyses are compared for 81 pairs of twinned sandstones core plugs. Two matched core plugs were obtained by cutting a single long core plug into two plugs of 3-5 cm in length. On both plugs porosity and permeability were measured. Statistics for the 652 adjacent core plug pairs have been discussed in Section 4.1.3. From the total population of 652 core plug pairs, the 81 pairs were selected to represent the range of basins, lithofacies, porosity and permeability for unconfined and *in situ* (confined) MICP analysis. Pairs represent all basins, 27 wells, and range in porosity from 1.3% to 24.3% and *in situ* Klinkenberg permeability from 0.000036 mD to 171 mD (3.6×10^{-8} to $1.7 \times 10^{-1} \mu\text{m}^2$). Appendix 4 presents capillary pressure data.

Figure 4.3.9 illustrates example unconfined and *in situ* MICP curves for pairs of high- to low-permeability from different wells and basins. Comparison among pairs shows that threshold entry pressures increase with decreasing permeability. Between core plugs in a pair set several trends are evident. *In situ* and unconfined curves for high-permeability cores ($k_{ik} > 1$ mD) are nearly identical. With decreasing permeability the difference between unconfined and *in situ* threshold entry pressure increases. For all pairs this difference is greatest at the threshold entry pressure and decreases with decreasing wetting-phase saturation. At wetting phase saturations of 30-50% the *in situ* MICP curve crosses the unconfined curve and exhibits 0-5% lower wetting phase saturation with increasing capillary pressure. It can be interpreted that confining stress exerts principal influence on the largest pore throats and that pore throats accessed at non-wetting phase saturations below approximately 50% are not significantly affected by confining stress. This is consistent with these smaller pores comprising pore space within pore bodies or in regions of the rocks where stress is not concentrated. Combined with the stress dependence

discussed in section 4.1.3.2.1, this also implies the largest pore throats are probably sheet-like or slots in aspect.

Laboratory air-mercury capillary pressure data were converted to reservoir gas brine capillary pressure data using the standard equation ([Purcell, 1949](#)):

$$P_{C_{res}} = P_{C_{lab}} (\sigma \cos \theta_{res} / \sigma \cos \theta_{lab}) \quad [4.3.2]$$

where $P_{C_{res}}$ is the gas brine capillary pressure (psia) at reservoir conditions, $P_{C_{lab}}$ is the laboratory-measured capillary pressure (psia), $\sigma \cos \theta_{res}$ is the interfacial tension (σ , dyne/cm) times the cosine of the contact angle (θ , degrees) at reservoir conditions, and $\sigma \cos \theta_{lab}$ is the interfacial tension times the cosine of the contact angle at laboratory conditions. For air-mercury capillary pressure measurements an air-mercury interfacial tension of 484 dyne/cm and a contact angle of 140 degrees was assumed.

To determine the water saturation in any given rock as a function of height above the free-water level, it is necessary to convert the capillary pressure data to height above free-water level. This conversion was performed using the standard relation ([Hubbert, 1953](#)):

$$H = P_{C_{res}} / (E(\rho_{brine} - \rho_{gas})) \quad [4.3.3]$$

where H is the height (ft) above free-water level, $P_{C_{res}}$ is the capillary pressure (psia) at reservoir conditions, ρ_{brine} and ρ_{gas} are the density of brine and gas at reservoir conditions and E is a constant (0.433(psia/ft)/(g/cc)) for converting density to pressure gradient.

From the air-mercury capillary pressure data, pore-throat diameter was calculated using the modified Washburn ([1921](#)) relation:

$$D = 4F\sigma \cos \theta / P_c \quad [4.3.4]$$

where P_c = capillary pressure (psia), $F = 0.145$ ((psia·cm· μ m)/dyne), θ = contact angle (140 degrees), σ = interfacial tension (484 dyne/cm), and D = pore-throat diameter (μ m, microns). This relation assumes that the non-wetting phase (i.e., gas) enters the pores through circular pore throats.

Variables in equations 4.3.2 to 4.3.4 that change with reservoir pressure, temperature, gas chemistry, and brine chemistry include σ , ρ_{brine} , and ρ_{gas} . To convert laboratory properties to reservoir properties for use in the equations above the range of Mesaverde reservoir conditions were defined as: 1) reservoir pressures - 2,500-13,000 psia (17.2-89.6 MPa); 2) temperatures- 90-260 °F (32.2-126.7 °C); 3) gas gravity - 0.55-0.70; and 4) brine density -1.00-1.11 grams/cubic centimeter (g/cc). For the range in temperature, methane-water interfacial tension (σ) ranges from 33-58 dyne/cm ([Jennings and Newman, 1971](#)). To provide a common reference frame for all capillary pressure curves the following values were assigned: $\sigma\cos\theta_{\text{res}} = 40$ dyne/cm, $\sigma\cos\theta_{\text{lab}} = 370.8$ dyne/cm, $\rho_{\text{gas}} = 0.216$ g/cc (0.935 psi/ft, 2.115 kPa/m), and $\rho_{\text{brine}} = 1$ g/cc (0.430 psi/ft, 9.727 kPa/m), MICP pressures can be transformed into equivalent height above free water using Equation 4.3.3.

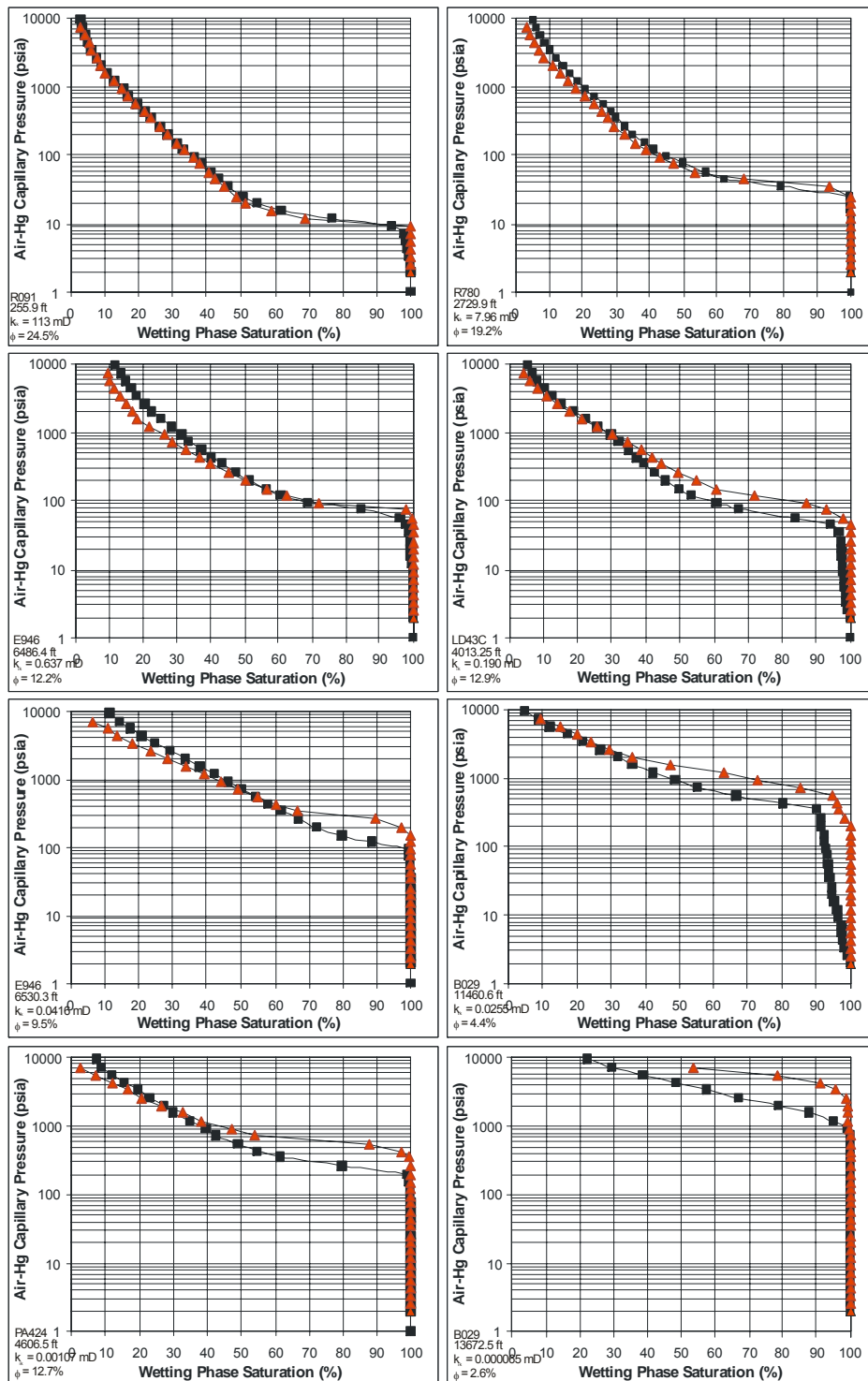


Figure 4.3.9. Examples of *in situ* (red triangles) and unconfined (black squares) air-mercury capillary pressure curves. Threshold entry pressure for samples under *in situ* conditions are greater than for unconfined conditions with the difference in pressure increasing with decreasing permeability. At higher pressures curves frequently cross. Trends are similar to those reported by Byrnes and Keighin (1993).

Figure 4.3.10 illustrates the relationship between MICP-measured threshold entry pressure and the ratio of Klinkenberg permeability/porosity. It also shows the equivalent relationships for threshold entry pore diameter and threshold entry gas column height calculated using equations 4.3.2 through 4.3.4.

Data are presented for both unconfined and *in situ* MICP measurements. Several details concerning the variables plotted are important to note. The abscissa in Figure 4.3.10 represents two different ratios; the unconfined and *in situ* data. For the *in situ* data the abscissa represents k_{ik}/ϕ_i , the ratio of the *in situ* Klinkenberg permeability and the *in situ* porosity (calculated from the routine helium porosity corrected for compression to *in situ* conditions using equations presented in Section 4.1.3. The MICP equipment used does not provide direct measurement of the sample pore volume under confining stress thus empirical correction of unconfined measured pore volume using helium to confined stress conditions is required. This empirical correction introduces uncertainty of approximately $\pm 0-3.5\%$ (1 std. dev.) into the *in situ* pore volume, varying with saturation, that translates to a possible error in wetting phase saturation of up to $\pm 0-3.5\%$ (1 std dev). Error increases with decreasing wetting phase saturation and “irreducible” saturation is the most affected.

The compressible nature and the threshold entry pressure of these rocks also results in uncertainty for standard unconfined MICP. Up to the threshold entry pressure mercury has not entered the sample and mercury both surrounds the sample and compresses the sample hydrostatically. For sandstones with permeability greater than 0.2 mD ($2 \times 10^{-4} \mu\text{m}^2$), the threshold entry pressure of mercury is less than 100 psi (700 kPa) and corresponding pore volume compression is less than 1%. However, with decreasing permeability the threshold entry pressure and resulting confining stress increases (Figure 4.3.10) and pore volume decreases. For low-permeability sandstones with $k_{ik} < 0.001$ mD ($1 \times 10^{-6} \mu\text{m}^2$), confining stress exceeds 1,000 psi (6.9 MPa) and pore volume is correspondingly an average of 3.5% less than unconfined conditions. As mercury enters the sample pore volume it increases the pore pressure of that fraction of the pore volume occupied and decreases the net effective stress for portions of the sample while uninvaded portions of the rock sample remain compressed. With step-wise increase in injection pressure and confining stress for uninvaded rock volume the net effective stress on the uninvaded rock continually changes while invaded portions are decompressed.

For the unconfined data the abscissa represents k_{mk}/ϕ_a , the ratio of the geometric mean of the routine Klinkenberg permeability, measured under “routine” conditions of 600 psi (4.1 MPa) confining stress, and the *in situ* Klinkenberg permeability, measured under 4,000 psi (27.6 MPa) confining stress, divided by the unconfined routine helium porosity, ϕ_a . The mean permeability and not the routine Klinkenberg permeability is used because: 1) the lower-permeability rocks are under confining stress by surrounding mercury at the threshold entry pressure; and 2) for all samples routine and *in situ* permeabilities were measured prior to MICP resulting in permeability hysteresis. *In situ* permeability was measured at 4,000 psi (27.6 MPa) confining stress. When this confining stress was released the permeability of most samples does not return immediately to the routine permeability but instead exhibits permeability hysteresis and time-dependent change of routine permeability. The permeability that most closely corresponds to the stress conditions of the unconfined MICP is a Klinkenberg permeability measured at the threshold entry pressure (P_{te}) measured immediately prior to MICP analysis. This permeability is intermediate between the initially measured routine and *in situ* Klinkenberg permeabilities. Klinkenberg permeability at this precise stress condition was not measured and the mean Klinkenberg permeability represents a value that is closer to this condition than either the routine or *in situ* values. Figure 4.3.11 illustrates the relationship between unconfined P_{te} and routine, *in situ* and mean permeabilities and shows that the mean permeability exhibits the same relationship as the *in situ* MICP for which these stress issues do not exist.

Figure 4.3.10 illustrates the good correlation between the threshold entry pore size (and corresponding pressure or gas column height) and permeability. The slope of this relationship is statistically identical for both unconfined and confined conditions because the abscissa represents each set of conditions. Unconfined samples exhibited higher permeabilities and larger threshold entry pore diameters. With application of confining stress the permeability decreased due to the decrease in pore throat diameter. The slope of the relationship between pore size and permeability, 0.5, is the same as the scaling parameter proposed by Leverett (1941) who proposed normalizing capillary pressure using $(k/\phi)^{0.5}$. Because permeability is well correlated with threshold pore throat size it can be used to correct unconfined capillary pressure curves to *in situ* conditions.

Permeability shows little dependence on confining stress for high-permeability rocks ($k > 1$ mD, $1 \times 10^{-3} \mu\text{m}^2$) because confining stress induces little change in pore throat size. The influence

of confining stress on permeability increases with decreasing permeability. Figures 4.3.9 through 11 show that confining stress has little influence on pore size or capillary pressure in the higher-permeability rocks and the influence increases with decreasing rock permeability. Although permeability is treated as the independent variable because it is a convenient variable to measure, and is the abscissa in Figures 4.3.9-11, permeability is actually the dependent variable and pore throat size, and its change with confining stress, is the independent variable.

The results presented here indicate that capillary pressure measurements on low-permeability sandstones are significantly influenced by confining stress, consistent with observed permeability changes.

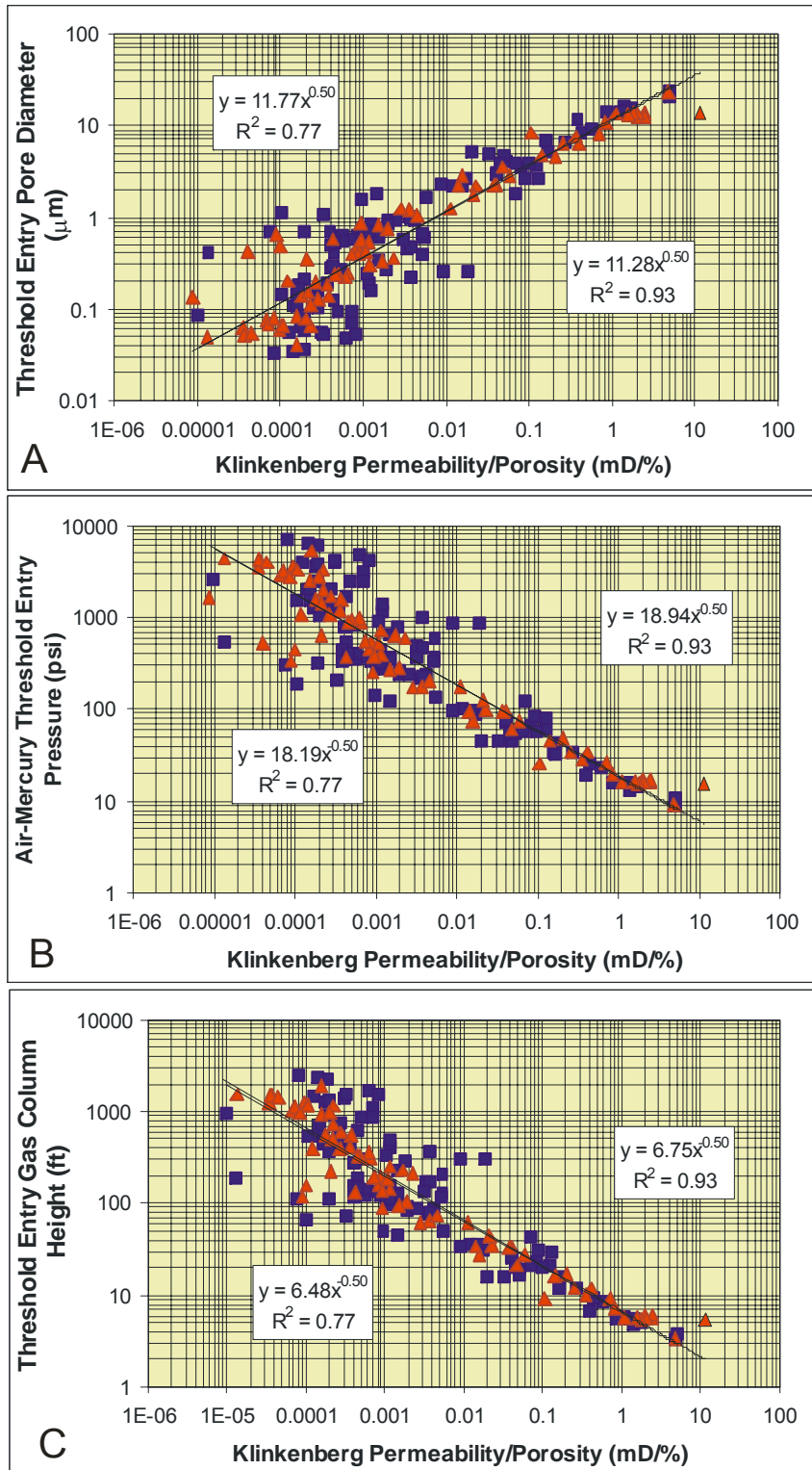


Figure 4.3.10. Cross-plot of threshold entry pore diameter (A), air-Hg pressure (B), and gas column height (C), measured by MICP and calculated using equations 4.3.1-4.3.3 in text, versus the ratio of k_{ik}/ϕ_i for *in situ* data (red triangles), and k_{mk}/ϕ_a for unconfined data (blue squares). Variables and stress conditions are discussed in the text.

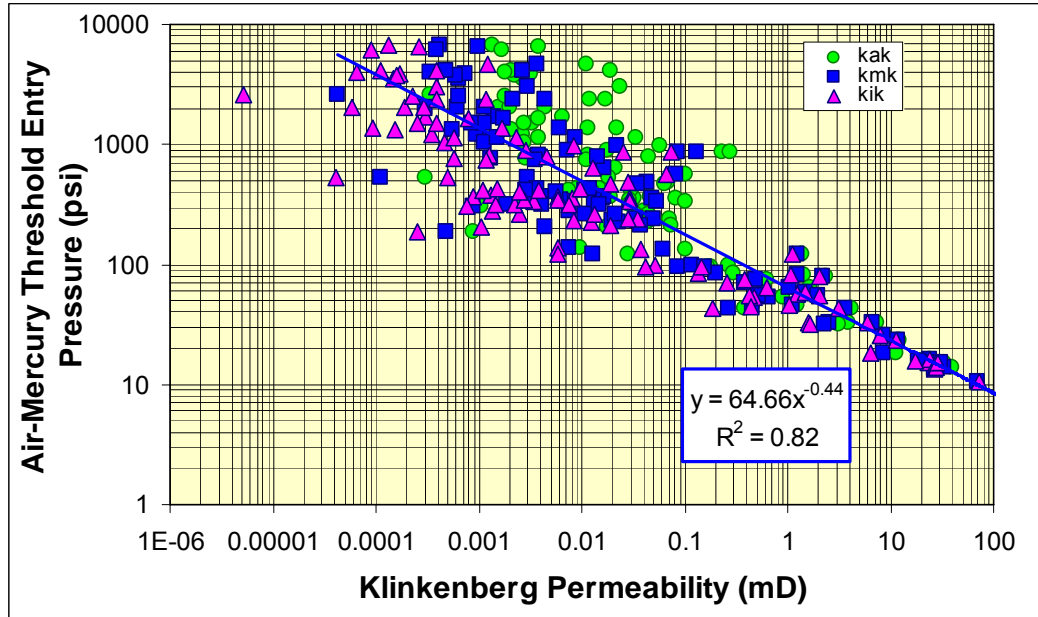


Figure 4.3.11. Cross-plot of air-mercury threshold entry pressure versus the routine Klinkenberg permeability (green circles), measured at 600 psi (4.1 MPa) confining stress, *in situ* Klinkenberg permeability (magenta triangles), measured at 4,000 psi (27.6 MPa) confining stress, and the geometric mean of these permeabilities (blue squares).

Subtask 4.4. Measure Electrical Properties

4.4.1 Task Statement

Wireline log determination of water saturation and identification of pay in tight gas sandstones is complicated by the low porosity, clay content, and, in some rocks, the high cation exchange capacity (CEC) of the clays in the sandstones and the low salinity of the formation brines ([Kukul et al., 1983](#)). The problems of wireline log analysis in shaly sands is well recognized ([Fertl and Frost, 1980](#); [Worthington, 1985](#)) and numerous algorithms have been proposed for calculating water saturations in shaly sands including the empirical Simandoux ([1963](#)) or Indonesia ([Poupon and Leveaux, 1971](#)) equations and the more theoretical Dual Water ([Clavier, Coates, and Dumanoir, 1984](#)) and Waxman-Smits models ([Waxman and Smits, 1968](#); [Waxman and Thomas, 1974](#)). To calculate water saturation, accurate values of water salinity, porosity exponent, saturation exponent, and cation exchange capacity (if present) are needed. Only isolated CEC data are available for Mesaverde ([Volk et al., 1979](#)).

To supplement the published electrical resistivity data and provide data for rocks that are well characterized lithologically the goal of this task was to measure the electrical resistivity of 150 cores at multiple salinities to be able to provide a basis for estimating the Archie porosity exponent at a specified brine salinity. These data would provide a basis on which water saturation can be more accurately calculated from electric wireline log response.

4.4.2 Methods

To measure the Archie exponent from brine-saturated resistivity the cleaned cores were evacuated for a period of eight (8) hours and then saturated with a deaerated sodium chloride brine solution. The brine concentrations used and the sequence of concentrations are discussed below. After vacuum saturation, complete saturation was obtained by applying a pressure of 1,000 psi (7 MPa) for a period of 24 hours to the saturating brine and samples. Complete saturation was confirmed by agreement between helium-measured porosity and gravimetric-saturation porosity values within 0.1 porosity percent. The cores were left immersed in deaerated brine for a period of 2-8 weeks.

After the cores had reached equilibrium with the brine, each was placed in a biaxial Hassler-type core holder and subjected to a hydrostatic confining stress of 200 psi (1.38 MPa) and a

micropipette for effluent fluid set to zero. A schematic of the resistivity apparatus is shown in Figure 4.4.1. The confining stress was then increased to 4,000 psi (27.6 MPa) approximating reservoir stress conditions. Pore volume decrease was determined by measuring the brine displaced from the core by compression using the micropipette, correcting for system compressibility and estimating pore volume change from the sleeve set pressure of 50 psi (0.35 MPa) to 200 psi (1.38 MPa). Pore pressure was at atmospheric pressure. Porosity calculations were performed assuming that the grains of the rock were incompressible and hence the bulk volume decreased by the same amount as the pore volume. Porosity was referenced to an assumed condition that at 50 psi (0.35 MPa) the pore volume equaled the routine helium pore volume.

Electrical resistivity was measured using a two electrode configuration with gold plated end electrodes. Brine-saturated core resistivity at 10 kHz (R_o) was recorded only after the core had achieved equilibrium with the electrical resistivity of the core remaining constant within 0.1% for a three (3) minute period. In general, resistivity equilibrium, including reaching a near constant pore volume compression on the time scale of the resistivity measurement, required 10 ± 5 minutes but for some cores approached one hour. Values were referenced to a temperature of 20 °C (68 °F). Archie porosity exponents, m , representing the ratio of the logarithm of measured formation resistivity factor ($\log(R_o/R_w)$) and the logarithm of porosity ($\log\phi$) are presented in Appendix 5. These porosity exponent values assume an Archie intercept, $a=1$, where $R_o/R_w = 1$ at $\phi = 100\%$.

Electrical resistivity measurements were performed on core plugs selected to range widely in geographic location, lithology, porosity, and permeability. To evaluate possible Waxman-Smiths cation exchange effects, analyses were performed at 20,000 ppm NaCl ($n = 138$), 40,000 ppm NaCl ($n = 310$), 80,000 ppm NaCl ($n = 198$), and 200,000 ppm NaCl ($n = 265$). In comparison to high-permeability rocks, achieving a known salinity in low-permeability rocks is experimentally difficult. Low brine permeability does not easily allow flow-through displacement, especially for large numbers of samples. To change sample pore water salinities, samples were dried at 70 °C for several hours and then immersed in a methyl alcohol bath for 24-48 hours. The samples were then Soxhlet extracted with methyl alcohol for 3 days, dried, and vacuum/pressure saturated with methyl alcohol and again immersed in the methyl alcohol bath for a minimum of 3 days. The samples were then dried at 70 °C in a convection oven for not less than 24 hours and weighed to confirm that sample weights returned to original pre-saturation weights for clean, dry samples. The samples were then vacuum/pressure saturated, as described

above, with the next brine of different salinity and left immersed for 2-8 weeks. For each salinity change this process was repeated.

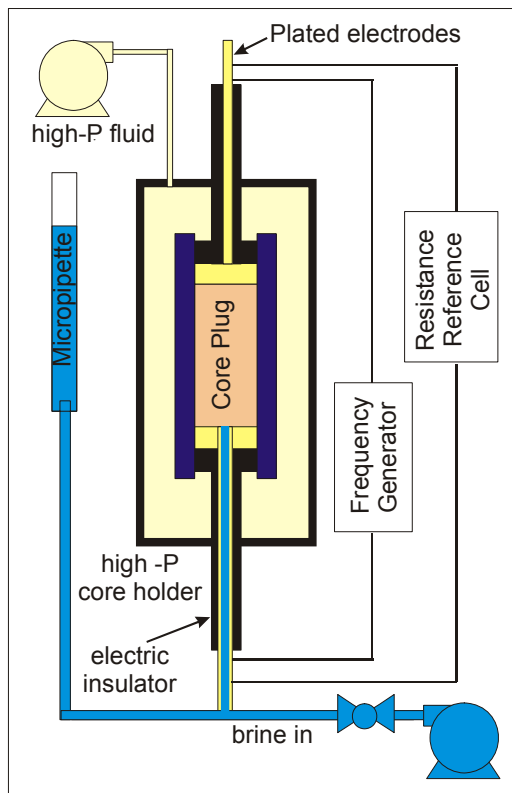


Figure 4.4.1. Schematic of resistivity apparatus.

The sequence of measurements at different salinities varied with each sample due to the long time period over which sample selection and measurements were performed. Early in the program 108 samples were selected and saturated with 200,000 ppmw NaCl to measure a resistivity similar to, though not precisely the same as, a multisalinity-measured, salinity-independent resistivity. A complete suite of 150 samples (as defined by the project design) was not selected because at the time it was known more industry cores would be added to the study. Although equilibrium was established for the 200,000 ppmw NaCl brine, subsequent measurements for two lower-salinity brines did not result in linear core conductivity-brine conductivity relationships indicating that the salinity of the brine in the pores was not as designed or the cores had not reached equilibrium with the lower-salinity brine(s). It was interpreted that removing salt left by high salinity brines was not sufficiently effective for subsequent constant, known, low-salinity resistivity measurements. For these samples, data are

reported for the equilibrium 200,000 ppmw NaCl but subsequent non-equilibrium, low-salinity data are not reported.

To avoid having to remove high concentration of salt for subsequent salinity measurements, new, clean cores were selected and saturated, measured, cleaned, and resaturated, as described above, with brines in the sequence 40,000 ppmw NaCl, 80,000 ppmw NaCl, and 200,000 ppmw NaCl brine. By sequentially increasing in brine salinity, minor remnant salt not removed by the cleaning process would increase the salinity of the subsequent brine but represented a negligible change in salinity of the higher-salinity brine.

Subsequent to the analysis of the cores above, it was decided that measurements should be conducted at lower salinities. A new set of cores were selected and were saturated, measured, cleaned, and resaturated, as described above with brines in the sequence 20,000 ppmw NaCl, 40,000 ppmw NaCl, and 80,000 ppmw NaCl brine.

4.4.3 Results

4.4.3.1 Archie Porosity Exponent versus Porosity

A total of 907 resistivity measurements on 308 core samples were performed at various salinities (Appendix 5). These data provided a basis for examining the relationship between the Archie porosity exponent and porosity and the salinity dependence of the porosity exponent. The estimation of water saturation in sandstones is commonly performed using the empirical relation developed by Archie (1942), known as Archie's Law:

$$S_w = [(a * R_w) / (\phi^m * R_t)]^{1/n} \quad [4.4.1]$$

where; S_w = water saturation (fraction), a = Archie cementation intercept, R_w = water resistivity (ohm-m), R_t = formation resistivity (ohm-m), ϕ = porosity (fraction), m = Archie porosity exponent, and n = Archie saturation exponent.

This relation implicitly assumes that the rock matrix is nonconductive and that the brine with resistivity R_w , is the single electrical conductor within a nonconductive matrix. Guyod (1944) termed m the "cementation exponent" because it often increases with increased cementation. The more general term for m , porosity exponent, is used here due to porosity exponent-porosity relations shown below.

Models exist that account for multiple conducting phases. The generalized model of Glover et al (2000) models two conducting phases of any volume fraction and connection distribution. Waxman and Smits (1968) and others (Waxman and Thomas, 1974; Clavier, Coates, and Dumanoir, 1984) proposed modification of the Archie equation to model conductive solids, and excess conductivity related to elevated salinity near charged clay surfaces along pore walls resulting from the cation exchange capacity of the clay surfaces:

$$S_w = [(F^*R_w)/R_t(1 + R_wBQ_v/S_w)]^{1/n^*} \quad [4.4.2]$$

where F^* = salinity/clay conductivity independent formation factor, Q_v = cation exchange capacity of the core (meq/cc), B = specific counter-ion activity [(equiv/l)/(ohm-m)], and n^* = saturation exponent free of excess conductivity. This equation is similar to the Archie equation but includes an additional term for the conductivity associated with the exchange cations. This can also be written as:

$$S_w = n^* \sqrt[n^*]{\frac{\frac{a^*}{\phi^{m^*}} R_w}{R_t \left(1 + \frac{R_w B Q_v}{S_w} \right)}} \quad [4.4.3]$$

where the F^* term (intrinsic formation factor; free of excess conductivity) has been replaced by a^*/ϕ^{m^*} .

The salinity dependence of m is presented in the following section. The data measured support the interpretation that rock conductivity is influenced by both conductive clays and by pore architecture. The following discussion treats the porosity exponent within a simple modified Archie model. The following section discusses aspects of Waxman-Smits Modeling. It is important to note that these are empirical models and do not present a fundamental physical-chemical relationship (Herrick and Kennedy, 1993).

Figure 4.4.2 shows the individual Archie porosity exponent values for all samples sorted by brine salinity. The data for all salinities exhibit a significant change in the m vs. ϕ relationship for samples with porosity less than approximately 6-8% compared with those with porosity

greater than 6-8%. Archie porosity exponents for rocks with $\phi > 8\%$ range from $1.7 < m < 2.2$, which are values commonly reported for consolidated sandstones. Archie porosity exponents for rocks with $\phi < 8\%$ exhibit a strong correlation with m decreasing with decreasing porosity and approaching a value of $1.0 < m < 1.2$ at $\phi = 0$.

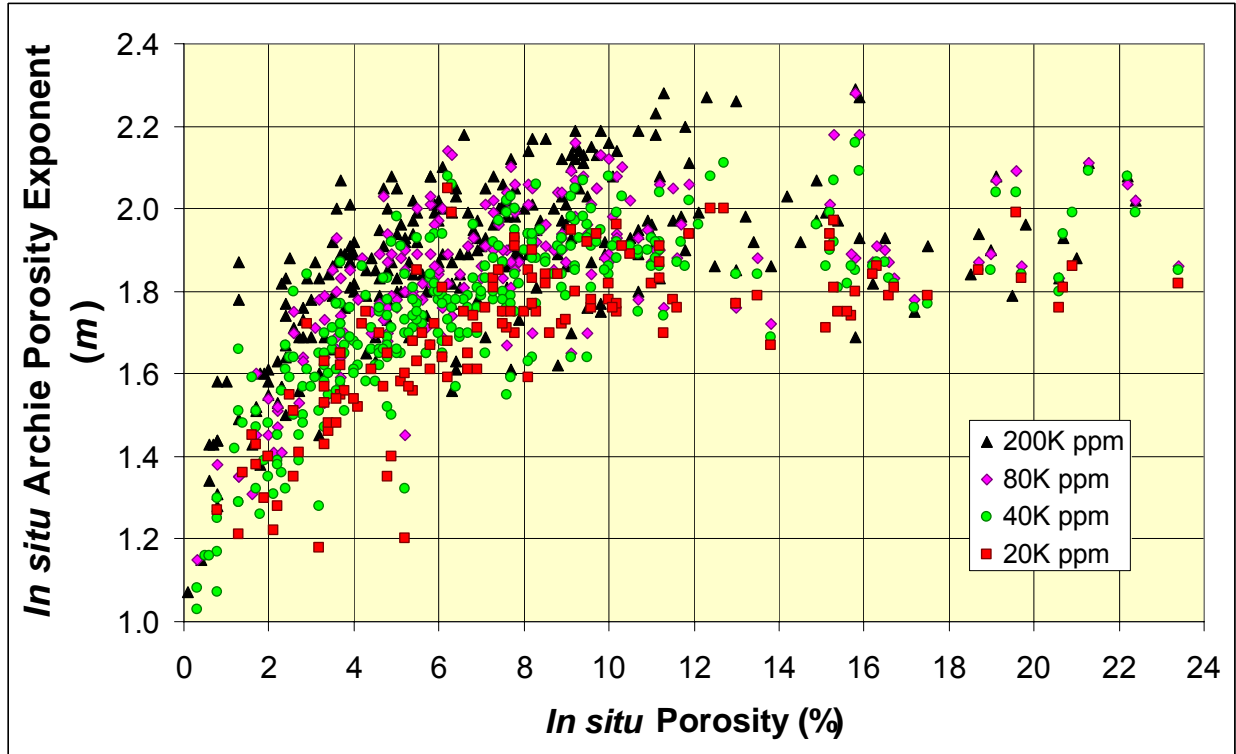


Figure 4.4.2. Archie porosity exponent, m , versus *in situ* porosity for Mesaverde sandstone samples at various salinity. Trends for all salinities indicate m decreases with decreasing porosity.

Utilizing the largest set of data at 40,000 ppm NaCl, which also represents a salinity similar to those commonly found in the Mesaverde, the Archie porosity exponent can be modeled either empirically or with a dual porosity model (Serra, 1984). In Figure 4.4.2 the apparent porosity exponent is the result of both the influence of conductive clays and salinity-independent pore architecture change discussed further in the following section.

The dual porosity model for a fractured reservoir or a reservoir with touching vugs represents the conductivity as two circuits in parallel and can be represented by:

$$m = \log[(\phi - \phi_2)^{m_1} + \phi_2^{m_2}] / \log \phi \quad [4.4.4]$$

where: ϕ = bulk porosity (fraction), ϕ_2 = fracture or touching vug porosity, m_1 = matrix porosity exponent, m_2 = fracture or touching vug porosity exponent

In Figure 4.4.3 the porosity exponent data are bracketed by the following conditions:

High: $m_1 = 2.15, \phi_2 = 0.0015, m_2 = 1$

Intermediate: $m_1 = 2.0, \phi_2 = 0.0035, m_2 = 1$

Low: $m_1 = 1.8, \phi_2 = 0.007, m_2 = 1$

The intermediate solution parameters were estimated by trail-and-error solution for the parameters that provided the minimum average error between the dual-porosity model and the measured data.

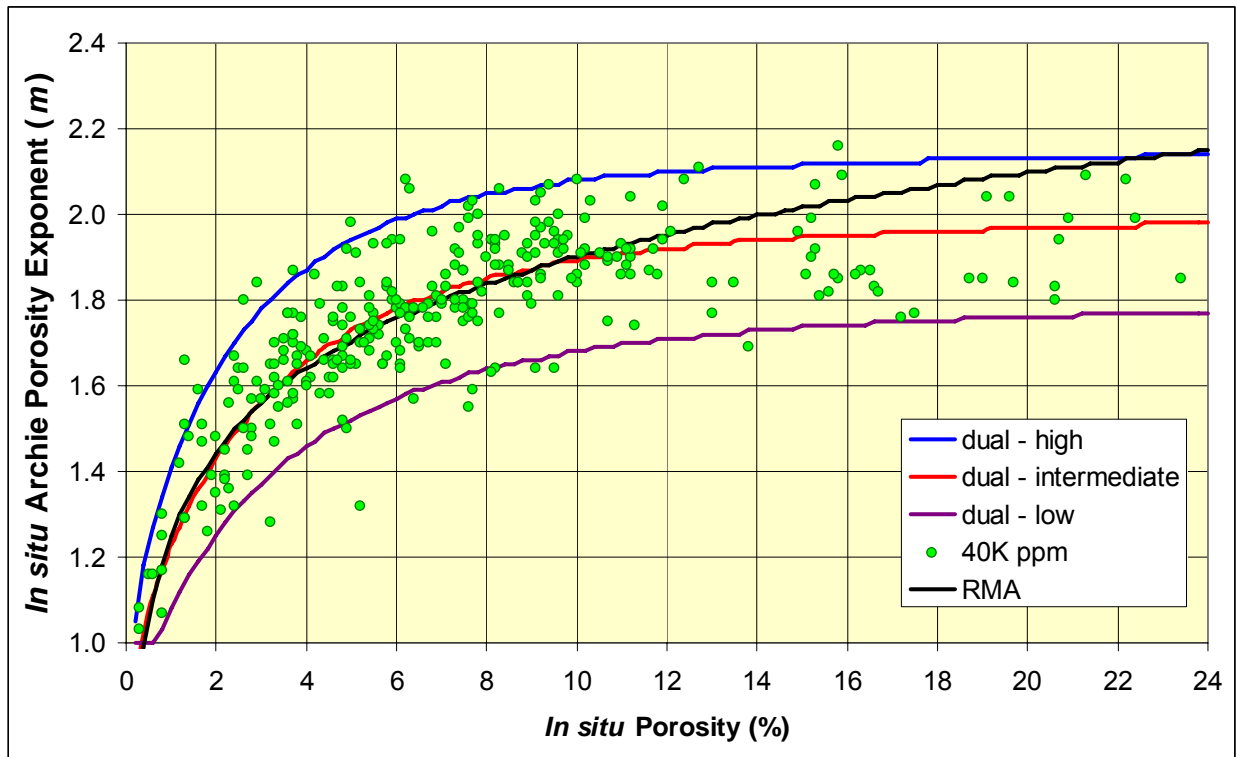


Figure 4.4.3. Cross-plot of *in situ* Archie porosity exponent, m (assuming $a = 1$) at 40K ppm NaCl versus *in situ* porosity showing decreasing m with decreasing porosity and both RMA empirical model (black curve) and high (blue), low (purple), and intermediate (red) dual-porosity models.

Also shown in Figure 4.4.3 is the empirical reduced major axis (RMA) analysis solution of the relationship between $\log_{10}m$ and porosity. This relationship can be expressed:

$$m_{40k} = 0.653 \log\phi + 1.248 \quad [4.4.5]$$

where m_{40k} = Archie porosity exponent at 40,000 ppm NaCl, ϕ = porosity in percent.

The RMA analysis provides a more accurate solution for minimum error at the low and high end porosities and appropriately handles the uncertainty in the porosity variable. A linear regression analysis (LRA) provides an estimation of m using:

$$m_{40k} = 0.530 \log\phi + 1.344 \quad [4.4.6]$$

The contrast between the RMA and linear regression analysis (LRA) solutions are shown in Figure 4.4.4.

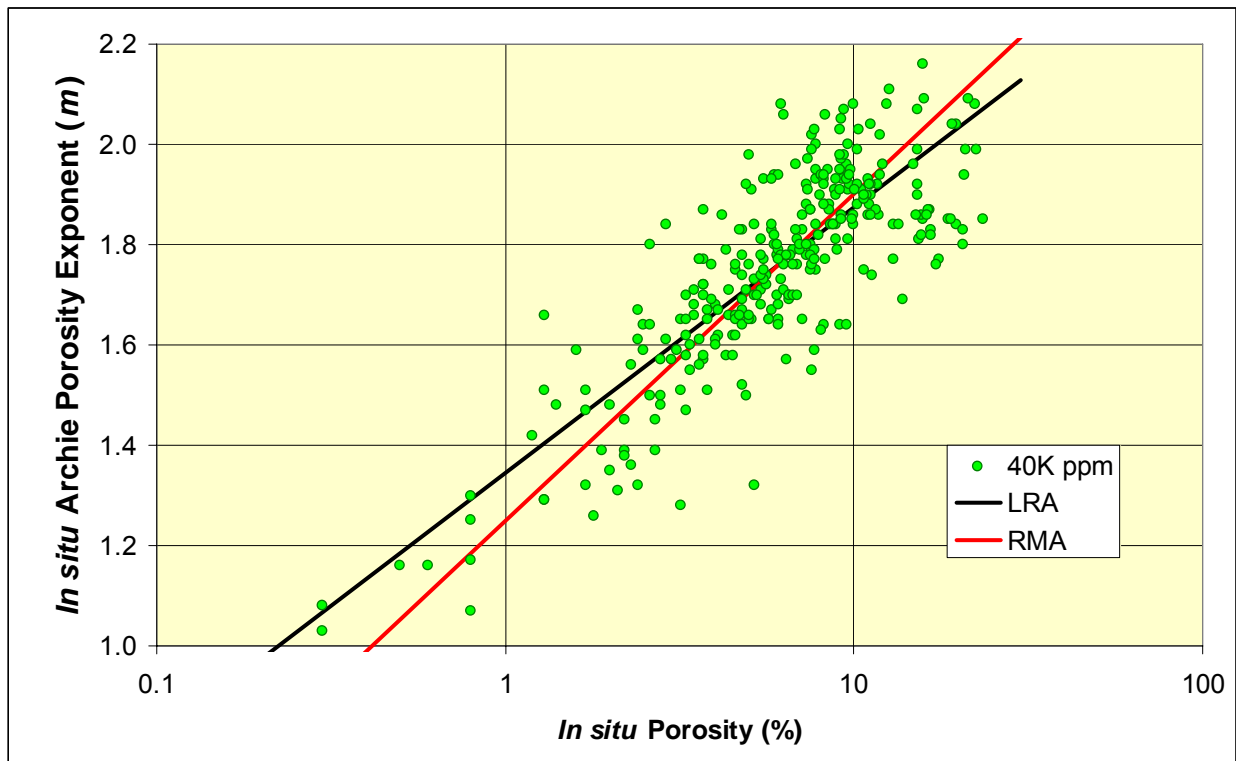


Figure 4.4.4. Cross-plot of *in situ* Archie porosity exponent, m (assuming $A=1$), versus \log_{10} *in situ* porosity. Correlations can be interpreted using either LRA (black line) or RMA (red line).

Although the dual porosity model is capable of matching the pattern of Archie m data in Figure 4.4.3, this alone does not validate the implicit pore architecture of the model for the tight gas sandstones studied. This model assumes that there are one or more microfractures that carry

current parallel to the matrix. This has not been directly observed. Alternate interpretations of the results is that as porosity decreases:

- 1) Electrical efficiency increases ([Herrick and Kennedy, 1993](#));
- 2) Remaining pores may become progressively more sheet-like or fracture-like with diminishing tortuosity (c.f. the [Winsauer et al., 1952](#), concept of porosity exponent as representing the average length of the conductive path through the rock as compared to a straight tube);
- 3) Conductivity of a few larger pores increases disproportionately to their relative volume;
- 4) Remaining pores may exhibit decreased m .

The empirical RMA log-linear equation predicts very similar m values to the dual porosity model up to approximately 14% porosity. At greater porosity each dual-porosity model approaches a constant that remains constant for all greater porosity; however, the RMA model predicts increasing m values with increasing porosity, which is incorrect. Therefore this equation is limited to $\phi < 14\%$. For $\phi > 14\%$ a constant $m = 1.95$ is the average of all values.

These results and models cannot be robustly extrapolated to porosity values greater than 24%. Both modeling approaches predict constant porosity exponent values with increasing porosity which cannot hold true for all higher porosity values.

A porosity exponent approaching $m = 1$ is consistent with a simple model that as porosity approaches zero the pore system must approach a very limited number of sample-spanning pores and ultimately for electrical current to flow at all across a system at very low porosity the remaining pore must have limited tortuosity. The porosity exponent of a straight capillary tube and a sheet-like crack or slot is $m = 1$ irrespective of the cross-sectional shape ([Herrick and Kennedy, 1993](#)). With this simple model it would be predicted that $m \rightarrow 1$ as $\phi \rightarrow 0\%$.

The models for m above all predict increasing or constant m with increasing porosity. However, because $m = 1$ at $\phi = 100\%$ (the system is 100% brine therefore $R_o = R_w$ and $FRF = R_o/R_w = 1$), m must decrease at some high porosity and with increasing porosity $m \rightarrow 1$ as $\phi \rightarrow 100\%$. Mesaverde rocks do not approach these porosity values and the nature of m at the high porosities where this may occur is not an issue for these reservoir rocks.

The trends depicted Figures 4.4.2 and 4.4.3 are contrary to commonly held expectations for porosity exponent behavior in tight rocks. The common interpretation that the Archie porosity exponent being related to the tortuosity or average path length of the electrical path across a rock ([Wyllie and Rose, 1950](#); [Winsauer et al, 1952](#)) has led to a mental construct where with increasing cementation, or decreasing porosity, the tortuosity should increase and therefore m is expected to also increase. The so-called “Shell formula” for cementation exponent in low-porosity carbonates ([Neustaedter, 1968](#)) predicts a constantly increasing m as porosity decreases towards zero:

$$m_{\text{shell}} = 1.87 + 0.019/\phi \quad [4.4.7]$$

where ϕ is in %. Conceptually, this is the model for m behavior held by many practicing petrophysicists.

A trend of decreasing m with decreasing porosity similar to that found in this study has been observed by others in both carbonate and clastic reservoirs. Borai ([1987](#)), and Focke and Munn ([1987](#)) describe trends of decreasing m in Middle East carbonate reservoirs from Abu Dhabi and Qatar, with the falloff beginning at about 10% porosity but most pronounced below 6%. We are currently unaware of published datasets in tight sandstone reservoirs that show similar trends, but at least one large joint industry project dataset and several proprietary single core datasets show similar trends to that found in this project. The following section shows that this trend is evident in the salinity independent data also.

4.4.3.2 Salinity Dependence of Archie Porosity Exponent and Cation Exchange Capacity

Figure 4.4.5 illustrates the basic Waxman-Smiths ([1968](#)) model for excess conductivity and how BQv can be determined from multiple salinity measurements of core and brine conductivity. The relationship can be expressed:

$$C_o = (1/F^*) (C_w + BQ_v) \quad [4.4.8]$$

where C_o = core conductivity at $S_w=100\%$ (mho/m), C_w = water conductivity (mho/m), F^* = salinity/clay conductivity independent formation factor, Q_v = cation exchange capacity of the core (meq/cc), B = specific counter-ion activity [(equiv/l)/(ohm-m)], $F^*/F = (1 + BQ_v/C_w)$.

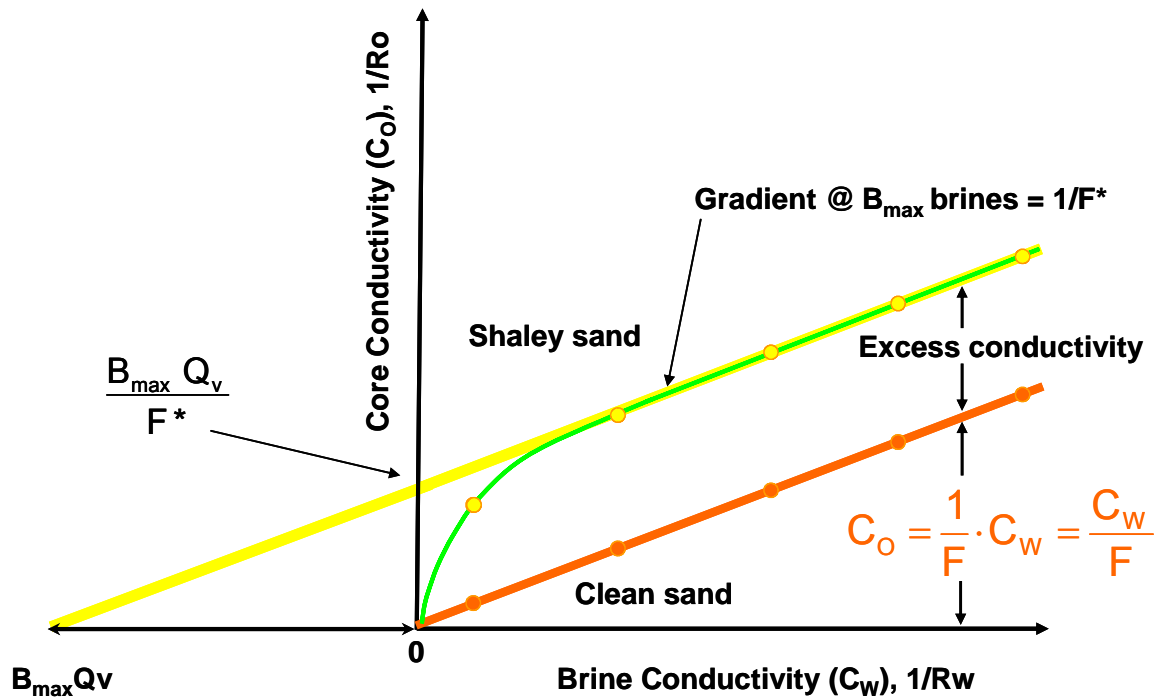


Figure 4.4.5. Relationship of Waxman-Smiths model parameters illustrating their determination from multi-salinity measurements of core and brine conductivity.

Comparing measured core conductivities versus the saturating brine conductivity (Figure 4.4.6), nearly all cores exhibit some salinity dependence and that dependence is highly linear with a mean correlation coefficient $r^2 = 0.97 \pm 0.05$ for 308 samples (Figure 4.4.6). This dependence can be modeled using the Waxman-Smiths equations or using empirical relationships.

Estimating $B_{max}Q_v/F^*$ and F^* from the data in Figure 4.4.6, and assigning a values of $B_{max} = 3.83$ (1/(ohm m) equiv/liter), values for the cation exchange capacity per unit pore volume, Q_v , were calculated for each sample (Appendix 5). Figure 4.4.7 illustrates that Q_v values increase with decreasing permeability and comparison with Rock Digital Classification values supports the conclusion that Q_v is correlated with increasing argillaceousness and decreasing grain size. Using the salinity-independent F^* and solving for the salinity-independent

porosity exponent, m^* , Figure 4.4.8 illustrates that the m^* decreases with decreasing porosity below approximately $\phi = 6\%$.

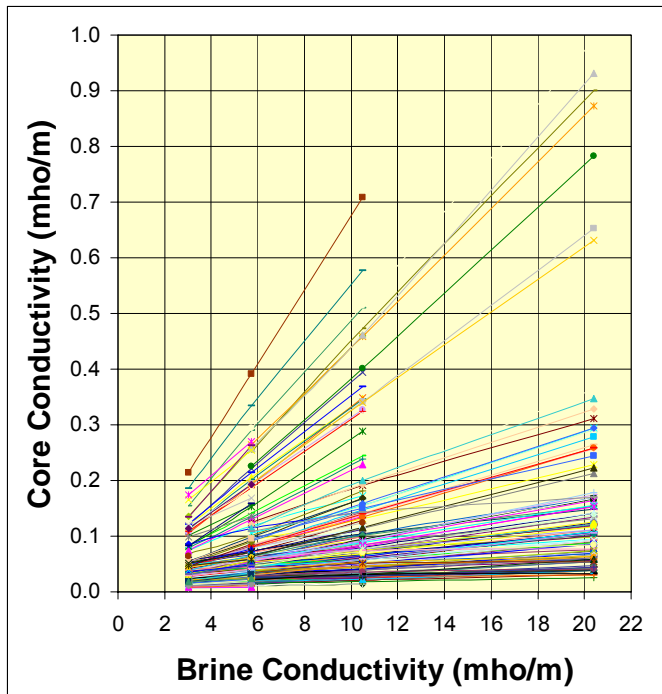


Figure 4.4.6. Core conductivity versus saturating brine conductivity for 308 samples. (Note: conductivity is often expressed as mmho/m, where 1 mho/m = 1000 mmho/m)

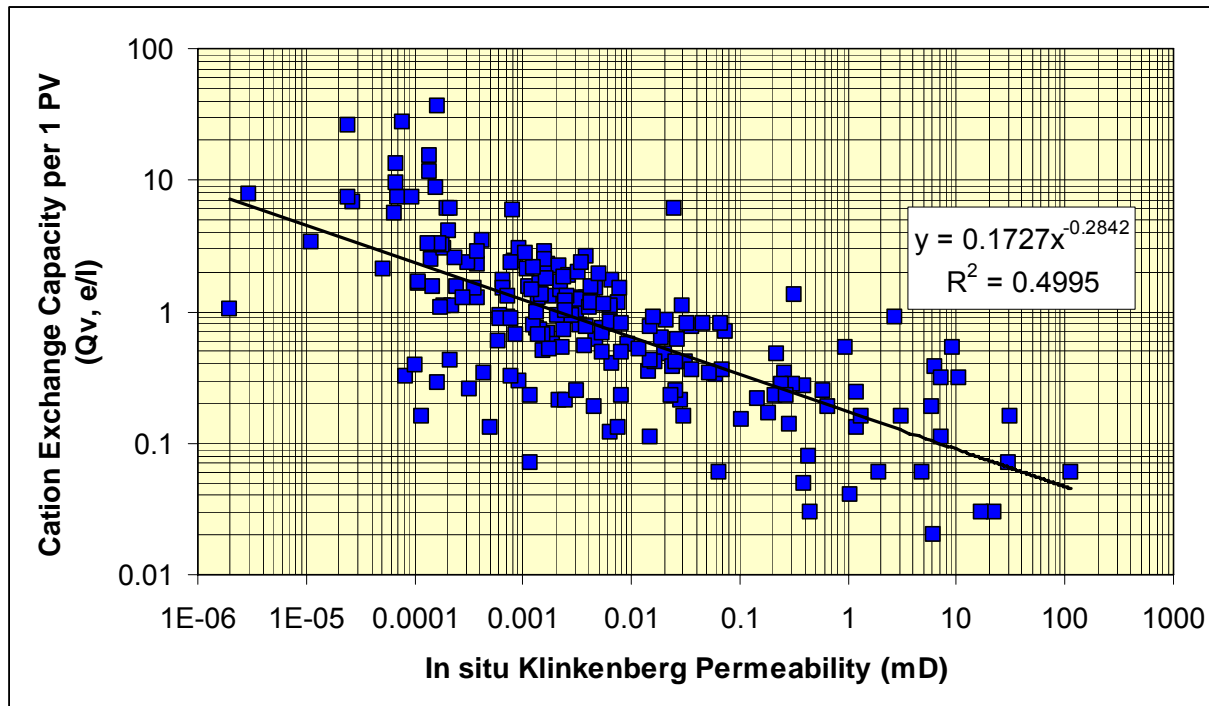


Figure 4.4.7. Crossplot of Cation Exchange Capacity per unit pore volume (equiv/liter) measured from multisalinity measurements versus in situ Klinkenberg permeability (mD) showing increase in Q_v with decreasing permeability.

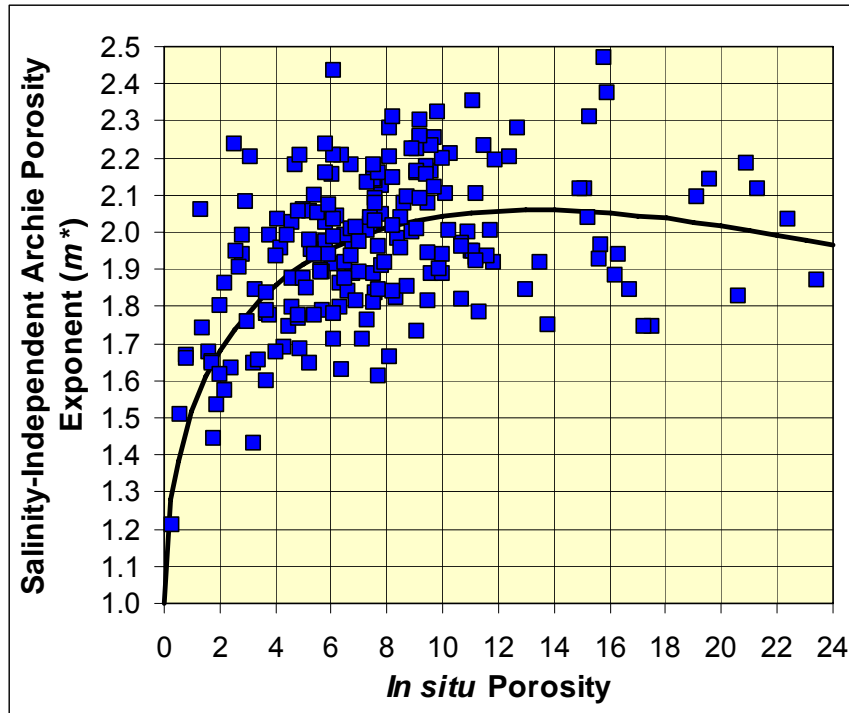


Figure 4.4.8. Salinity-independent porosity exponent versus in situ porosity showing decrease in m^* with decreasing porosity below $\phi = 6\%$. The trendline represents the empirical relationship; $m^* = 1 - 0.0917\phi_i + 0.0003069 \phi_i^2 + 0.61 \phi_i^{0.5}$.

The relationship evident in Figure 4.4.8 is consistent with models discussed in the previous section. Although a Waxman-Smits-type model can be effectively applied in many wireline log analysis applications, this requires knowledge of Q_v and m^* , and iterative solution of equation 4.4.3. Q_v can be estimated using relations similar to that in Figure 4.4.7 and m^* can be estimated using the relation in Figure 4.4.8, but simple direct empirical models provide an easy method to predict the Archie porosity exponents. These methods for apparent m effective incorporate the Q_v and m^* relations into the models. The following discussion provides a simple model for predicting the Archie porosity exponent from empirical equations.

The salinity dependence shown in Figure 4.4.6 can be translated to a relationship between porosity exponent and salinity as shown in Figure 4.4.9. The log-linear relationship between m and logarithm of brine resistivity (R_w) allows the correction of predicted m values obtained using Equation 4.4.5 to any salinity.

Although each core exhibits a highly linear relationship between m and $\log R_w$, the exact slope of each core varies with a mean value for all cores of:

$$\text{Average Slope}_{m-R_w} = -0.27 \pm 0.32 \text{ (2 standard deviations)} \quad [4.4.9]$$

where Slope_{m-R_w} = slope of m_{R_w} versus $\log R_w$.

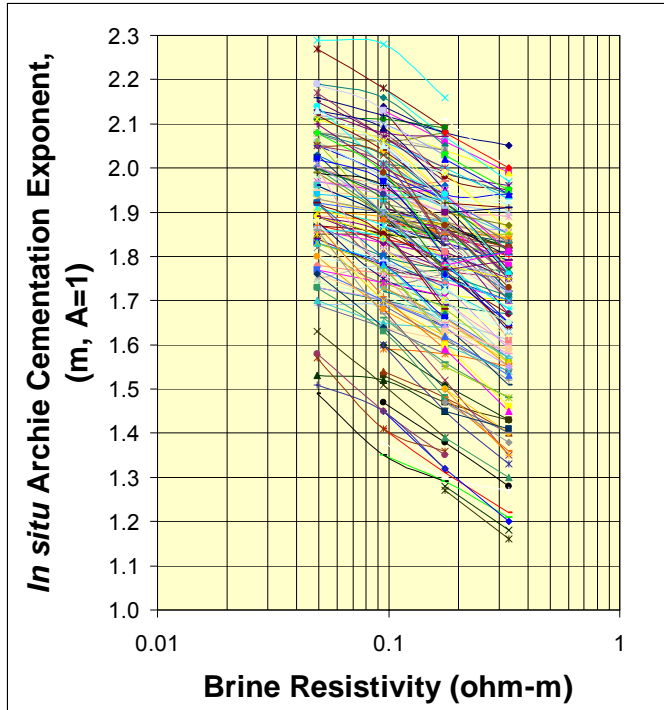


Figure 4.4.9. Cross-plot of Archie porosity exponent versus saturating brine resistivity for 308 samples. All samples exhibit a highly linear relationship.

The slopes exhibit a very weak tendency to increase with increasing porosity. This correlation can be used to improve the prediction of m at any salinity:

$$\text{Slope}_{m-Rw} = 0.00118 \phi (\%) - 0.355 \quad [4.4.10]$$

Combining equations 4.4.5 and 4.4.10, the Archie porosity exponent at any given porosity and reservoir brine salinity can be predicted using:

$$m_x = m_{40} + \text{Slope}_{m-Rw} (\log R_{wX} + \log R_{w40K}) \quad [4.4.11]$$

replacing all terms:

$$m_x = (0.653 \log \phi + 1.248) + (0.0118 \phi - 0.355) \times (\log R_{wX} + 0.758); \quad 0\% \leq \phi < 14\% \quad [4.4.12]$$

$$m_x = 1.95 + (0.0118 \phi - 0.355) \times (\log R_{wX} + 0.758); \quad \phi \geq 14\% \quad [4.4.13]$$

where $m_x = m$ at salinity X, $m_{40} = m$ at 40K ppm NaCl, $\log R_{wX} = \log_{10}$ of resistivity of brine at salinity X, $\log R_{w40K} = \log_{10}$ of resistivity of 40K ppm NaCl = 0.758 (at 20 °C).

Subtask 4.5. Measure Geologic and Petrologic Properties

4.5.1 Task Statement

Most published studies of TGS properties are tied to location but are rarely distinguished by lithofacies. This places potential, and sometimes unknown, limits on application or results. Though non-lithofacies specific petrophysical relationships can be developed, because rock mineralogy and texture exert control on pore architecture, petrophysical properties can be lithofacies dependent. Lithofacies can be estimated from wireline log signatures. This calibration requires that the lithofacies be characterized using a digital system. To address this need all cores were described to provide an understanding of pay and non-pay rock types, their log signatures, lithofacies, stratigraphy, depositional sequences, and flow-unit continuity. The cores were graphically logged with emphasis on lithology, including bedform type, clay content, small-scale (i.e., centimeters to meter-scale) heterogeneities, porosity type and distribution, and macro-scale diagenetic products. Based on the lithofacies present, representative core samples were obtained from all wells sampled and a subset was selected for advanced properties. For these samples thin section point count analysis (300 counts) was performed to assist in characterization of rock composition and rock and pore architecture. Core photos and thin-section photomicrographs illustrating lithofacies and interpretations were obtained.

4.5.2 Methods

Core descriptions were prepared by examining slabbed and un-slabbed core material at various core storage facilities, including the USGS Core Research Center and Triple O Slabbing (both of Denver, Colorado); and Shell Oil Bellaire Technology Center and PTS Laboratories, Inc. (both of Houston, Texas). Core material is permanently stored at these facilities, as well as the facilities of Core Laboratories, Inc., and ExxonMobil (both of Houston, Texas). Table 4.5.1 lists the wells from which cores were described. In all, a total of 6,447 feet of core are included in this study, from seven Rocky Mountain tight gas sand basins.

API STATE CODE	API COUNTY CODE	API WELL #	BASIN	FIELD	WELL	OPERATOR	Twn		Rng		Sec
49	035	20622	GREEN RIVER	WILDCAT	1 OLD ROAD	AMERICAN HUNTER EXPL	27	N	108	W	27
49	013	08024	GREEN RIVER	PINEDALE	5 PINEDALE	EL PASO NATURAL GAS	30	N	108	W	5
49	035	20088	GREEN RIVER	MERNA	A-1 WASP	INEXCO OIL COMPANY	36	N	112	W	28
49	035	06020	GREEN RIVER	BIG PINEY	B-54 BIG PINEY	BELCO PETROLEUM	29	N	113	W	26
49	035	05742	GREEN RIVER	TIP TOP SHALLOW	C-47 TIP TOP SHALLOW	BELCO PETROLEUM	28	N	113	W	22
49	035	06200	GREEN RIVER	MASON	K-2 MASON	BELCO PETROLEUM	31	N	113	W	13
49	035	24198	GREEN RIVER	PINEDALE	VIBLE 1B-11D	SHELL E&P	31	N	109	W	11
05	045		PICEANCE		1 BOOK CLIFFS-DRILL HOLE	USGS-CG	7	S	104	W	17
05	103		PICEANCE	LOWER WHITE RIVER	21011-5 MOON LAKE	WESTERN FUELS ASSOC	2	N	101	W	1
05	103	10391	PICEANCE	WILLOW RIDGE	EM T63X-2G	EXXON-MOBIL	3	S	97	W	2
05	045	11402	PICEANCE	MAMM CREEK	LAST DANCE 43C-3-792	BILL BARRETT CORP.	7	S	92	W	3
05	103	09406	PICEANCE	WHITE RIVER DOME	M-30-2-96W / D-037934	FUEL RESOURCES DEV	2	N	96	W	30
05	045	06578	PICEANCE	GRAND VALLEY	MV 33-34 CHEVRON	BARRETT ENERGY	6	S	96	W	20
05	045	06001	PICEANCE	RULISON	MWX-2 SUPERIOR	CER CORPORATION	6	S	94	W	34
05	045	10927	PICEANCE	PARACHUTE	PUCKETT/TOSCO PA 424-34	WILLIAMS E&P	6	S	95	W	34
49	005	25627	POWDER RIVER	BRIDGE DRAW	1 BARLOW 21-20	LOUISIANA LAND & EXP	48	N	75	W	20
49	009	21513	POWDER RIVER	MIKES DRAW	2 FRED STATE	DAVIS OIL COMPANY	35	N	70	W	36
49	009	06335	POWDER RIVER	FLAT TOP	2 SHAWNEE	BELCO PETROLEUM	33	N	69	W	2
49	009	05481	POWDER RIVER	FLAT TOP	3 SHAWNEE	BELCO PETROLEUM	33	N	69	W	23
05	081	06718	SAND WASH	WEST CRAIG	1-691-0513	COCKRELL OIL CORP	6	N	91	W	5
05	081	06724	SAND WASH	CRAIG DOME	1-791-2613	COCKRELL OIL CORP	7	N	91	W	26
43	047	30584	UINTA	NATURAL BUTTES	11-17F RIVER BEND UNIT	MAPCO INCORPORATED	10	S	20	E	17
43	047	30545	UINTA	BONANZA	2-7 FLAT MESA FEDERAL	ENSERCH EXPLORATION	10	S	23	E	7
43	019		UINTA		3 BOOK CLIFFS	USGS-CG	17	S	24	E	3
43	047	30860	UINTA	WILDCAT	3-24 US LAMCO	CHAMPLIN PETROLEUM	13	S	20	E	24
43	019		UINTA		4 BOOK CLIFFS	USGS-CG	17	S	24	E	31
43	047	30584	UINTA	AGENCY DRAW	4-5 LAMCO	ENSERCH EXPLORATION	13	S	20	E	5
43	047	36565	UINTA	NATURAL BUTTES	NBU 1022-1A	KERR-MCGEE OIL&GAS ONSHORE	10	S	22	E	1
46	047	36401	UINTA	NATURAL BUTTES	NBU 920-360	KERR-MCGEE OIL&GAS ONSHORE	9	S	22	E	36
99	999	99999	WASHAKIE		WILD ROSE 1						
49	037	21053	WASHAKIE	FIVE MILE GULCH	3 UNIT	AMOCO PRODUCTION	21	N	93	W	35
49	037	23956	WASHAKIE	SIBERIA RIDGE	5-2 SIBERIA RIDGE UNIT	AMOCO PRODUCTION	21	N	94	W	5
49	037	05683	WASHAKIE	PATRICK DRAW	65-1-7 ARCH UNIT	FOREST OIL CORP	19	N	99	W	1
49	037	05577	WASHAKIE	ARCH	ARCH UNIT UPRR #102-7-10	ANADARKO E&P CO. LP	19	N	98	W	7
49	037	05349	WASHAKIE		B-2A SPIDER CREEK	HUMBLE OIL & REF	18	N	110	W	27
49	007	21170	WASHAKIE	SAVERY	C-11 / FEE	FUEL RESOURCES DEV	12	N	90	W	11
49	037	22304	WASHAKIE	DRIPPING ROCK	DRIPPING ROCK #3	CELSIUS	14	N	94	W	8
49	037	22355	WASHAKIE	DRIPPING ROCK	DRIPPING ROCK #5	CELSIUS	14	N	94	W	19
49	013	20836	WIND RIVER	MADDEN	1-27 LOOKOUT	MONSANTO OIL	39	N	91	W	27
49	013	20966	WIND RIVER	MADDEN	2-1 CHEVRON	MONSANTO OIL	38	N	91	W	1
49	013	20724	WIND RIVER		31-22 TRIBAL PHILLIPS	BROWN TOM INC	4	N	3	E	31

Table 4.5.1 List of wells for which cores were described.

4.5.2.1 Core and Sample Description

Core and core plug samples were examined using a stereo binocular microscope or hand lens. Grain size and sorting of sediment was determined by using grain size comparators standardized for geologic investigation. In addition, lithology, composition, bed thickness, bedding contacts, sedimentary structures and details of visible porosity, fractures and cementation were recorded. A key feature of this investigation is the use of a rock typing classification system that characterizes lithology, composition, grain size, sorting, sedimentary structure, and cementation in a simple five digit code (Table 4.5.2) previously reported by Cluff, Byrnes and Webb ([1994](#)). This digital classification system has allowed us to closely correlate core analysis data with wire-line log data, allowing direct comparison of measured and calculated petrophysical data. The rock descriptor is objective and independent of any interpretations of depositional environments or stratigraphic position. Digital rock type data and interpreted depositional environments are presented on graphic charts for each core interval that was described. These core charts are available as PDF images on the Project Website. Digital rock type data for all cores examined during this study are also presented in Excel spreadsheets which are included on the Project Website.

FIRST DIGIT: Basic Lithology

- 0xxxx Organic rocks (coals, etc.)
- 1xxxx Siliciclastic rocks

SECOND DIGIT: Grain size, sorting, texture

- 10xxx Shales
- 11xxx Silty shales (60-90% clay)
- 12xxx Siltstones or very shaly sandstones (40-65% clay and silt)
- 13xxx Moderately shaly sandstones (10-40% clay and silt)
- 14xxx Sandstones, very fine
- 15xxx Sandstones, fine
- 16xxx Sandstones, medium
- 17xxx Sandstones, coarse
- 18xxx Sandstones, very coarse to gravely –sandstone
- 19xxx Conglomerate, matrix or clast supported

THIRD DIGIT: Degree of consolidation or cementation

- 1x0xx Totally cemented, dense, hard, unfractured
- 1x1xx Dense, fractured
- 1x2xx Well indurated, mod-low porosity (3-10%), unfractured
- 1x3xx Well indurated, mod-low porosity (3-10%), fractured
- 1x4xx Well indurated, mod-low porosity (3-10%), highly fractured
- 1x5xx Indurated, mod-high porosity (>10%), unfractured
- 1x6xx Indurated, mod-high porosity (>10%), fractured
- 1x7xx Indurated, mod-high porosity (>10%), highly fractured
- 1x8xx Poorly indurated, high-v. high porosity, soft
- 1x9xx Unconsolidated sediment

FOURTH DIGIT: Primary sedimentary structures

- 1xx0x Vertical perm barriers, shale dikes, cemented vert. fractures
- 1xx1x Churned/bioturbated to burrow mottled (small scale)
- 1xx2x Convolute, slumped, large burrow mottled bedding (large scale)
- 1xx3x Lenticular bedded, discontinuous sand/silt lenses
- 1xx4x Wavy bedded, continuous sand/silt and mud layers
- 1xx5x Flaser bedded, discontinuous mud layers
- 1xx6x Small scale (< 4 cm) x-laminated, ripple x-lam, small scale hummocky x-bd
- 1xx7x Large scale (> 4 cm) trough or planar x-bedded
- 1xx8x Planar laminated or very low angle x-beds, large scale hummocky x-bd
- 1xx9x Massive, structureless

FIFTH DIGIT: Dominant cementation or pore filling mineral

- 1xxx0 Sulfide pore filling (RhoG=3.85-5.0)
- 1xxx1 Siderite (RhoG=3.89)
- 1xxx2 Phosphate (RhoG=3.13-3.21)
- 1xxx3 Anhydrite or Gypsum (RhoG=2.98 or 2.35)
- 1xxx4 Dolomite (RhoG=2.89)
- 1xxx5 Calcite (RhoG=2.71)
- 1xxx6 Quartz (RhoG=2.65)
- 1xxx7 Authigenic clay (RhoG=2.12-2.76)
- 1xxx8 Carbonaceous debris (RhoG= 2.0)
- 1xxx9 No pore filling material or detrital clay filled intergranular voids

Table 4.5.2 Digital rock number scheme for siliciclastic core description.

4.5.2.2 Thin Section Petrography

Thin section preparation of low-permeability sandstones has always been hampered by the inability to efficiently impregnate sandstone samples with blue dye epoxy because of the low permeability and the consequent inability to flow epoxy deeply enough into the sample. To maximize impregnations many techniques have been developed, most notably high pressure impregnation. Most commercial epoxies have an approximate viscosity of 100 centipoise (cp) and a pot life (the time for which the epoxy is liquid before viscosity increases by orders of magnitude) of approximately 30 minutes. The depth of penetration is a function of the driving pressure, the pressure in the pores of the sample, the permeability, epoxy viscosity, and capillary forces if epoxy wets the surface. Table 4.5.3 illustrates the theoretical depth of penetration of a 100 cp viscosity epoxy into billets of 12.5 mm thickness with application of standard atmospheric pressure into a sample initially evacuated by vacuum. These calculations indicate that for the standard pot life of 30 minutes (1800 seconds), epoxy penetrates less than 0.27 mm into rocks of less than 0.1 mD. This would indicate that for most low-permeability sandstones the standard impregnation technique does not provide thin sections with blue dye epoxy in the pore space. Even with high-pressure impregnation, where the samples are placed in a gas pressure vessel and exposed to a gas pressure over the epoxy covering the sample of approximately 1,500 psi (10.3 MPa), impregnation is less than 1 mm for samples with permeability less than 0.01 mD (Table 4.5.3).

To improve impregnation efficiency and depth, experiments using long pot-life epoxy and pressure were conducted by Zach Wenz of the University of Kansas, Department of Geology. Experiments on Mesaverde sandstone samples found that good impregnation was achieved using an extended pot-life viscosity with moderate pressure. The optimum methodology involved the following steps: 1) cut sandstone billets not greater than 1 cm in thickness to allow efficient evacuation prior to epoxy immersion; 2) grind billet face flat prior to impregnation; 3) evacuate sample to $< 10^{-3}$ torr vacuum; 4) pour extended pot-life epoxy over sample while still under vacuum insuring that sample is completely immersed under epoxy; 5) release vacuum; 6) place samples in high pressure vessel; 7) pressure vessel to approximately 100-150 psi (700-1000 kPa); and 8) leave samples under pressure until epoxy sets or becomes very viscous (e.g., 8-16 hours). An effective 10-hour pot-life viscosity that worked well for the

Mesaverde sandstones studied is EPO-TEK 301-2FL®, which is similar to EPO-TEK 301 epoxy that is commonly used in thin section preparation. Table 4.5.3 illustrates the approximate depth of penetration for a 100 cp extended pot-life epoxy.

Applied Pressure psi	Capillary force psi	Total pressure psi	Permeability mD	Epoxy Impregnation Depth (mm)								
				time (min) 2	time (min) 4	time (min) 8	time (min) 10	time (min) 20	time (min) 30	time (min) 300	time (min) 600	
				14.7	0.3	15	1000	1.25E+01	1.25E+01	1.25E+01	1.25E+01	1.25E+01
14.7	0.7	15	100	1.01E+01	1.25E+01	1.25E+01	1.25E+01	1.25E+01	1.25E+01	1.25E+01	1.25E+01	1.25E+01
14.7	1.9	17	10	1.08E+00	2.17E+00	4.33E+00	5.41E+00	1.08E+01	1.25E+01	1.25E+01	1.25E+01	1.25E+01
14.7	4.9	20	1	1.28E-01	2.57E-01	5.13E-01	6.41E-01	1.28E+00	1.92E+00	1.25E+01	1.25E+01	1.25E+01
14.7	13.0	28	0.1	1.81E-02	3.62E-02	7.23E-02	9.04E-02	1.81E-01	2.71E-01	2.71E+00	5.43E+00	5.43E+00
14.7	17.4	32	0.05	1.05E-02	2.10E-02	4.19E-02	5.24E-02	1.05E-01	1.57E-01	1.57E+00	3.14E+00	3.14E+00
14.7	34.2	49	0.01	3.19E-03	6.38E-03	1.28E-02	1.60E-02	3.19E-02	4.79E-02	4.79E-01	9.58E-01	9.58E-01
14.7	45.7	60	0.005	1.97E-03	3.95E-03	7.89E-03	9.87E-03	1.97E-02	2.96E-02	2.96E-01	5.92E-01	5.92E-01
14.7	89.9	105	0.001	6.83E-04	1.37E-03	2.73E-03	3.42E-03	6.83E-03	1.02E-02	1.02E-01	2.05E-01	2.05E-01
14.7	120.3	135	0.0005	4.41E-04	8.81E-04	1.76E-03	2.20E-03	4.41E-03	6.61E-03	6.61E-02	1.32E-01	1.32E-01
147	0.3	147	1000	1.25E+01	1.25E+01	1.25E+01	1.25E+01	1.25E+01	1.25E+01	1.25E+01	1.25E+01	1.25E+01
147	0.7	148	100	1.25E+01	1.25E+01	1.25E+01	1.25E+01	1.25E+01	1.25E+01	1.25E+01	1.25E+01	1.25E+01
147	1.9	149	10	9.72E+00	1.25E+01	1.25E+01	1.25E+01	1.25E+01	1.25E+01	1.25E+01	1.25E+01	1.25E+01
147	4.9	152	1	9.92E-01	1.98E+00	3.97E+00	4.96E+00	9.92E+00	1.25E+01	1.25E+01	1.25E+01	1.25E+01
147	13.0	160	0.1	1.04E-01	2.09E-01	4.18E-01	5.22E-01	1.04E+00	1.57E+00	1.25E+01	1.25E+01	1.25E+01
147	17.4	164	0.05	5.37E-02	1.07E-01	2.15E-01	2.68E-01	5.37E-01	8.05E-01	8.05E+00	1.61E+01	1.61E+01
147	34.2	181	0.01	1.18E-02	2.37E-02	4.73E-02	5.92E-02	1.18E-01	1.77E-01	1.77E+00	3.55E+00	3.55E+00
147	45.7	193	0.005	6.29E-03	1.26E-02	2.52E-02	3.15E-02	6.29E-02	9.44E-02	9.44E-01	1.89E+00	1.89E+00
147	89.9	237	0.001	1.55E-03	3.09E-03	6.19E-03	7.74E-03	1.55E-02	2.32E-02	2.32E-01	4.64E-01	4.64E-01
147	120.3	267	0.0005	8.73E-04	1.75E-03	3.49E-03	4.36E-03	8.73E-03	1.31E-02	1.31E-01	2.62E-01	2.62E-01
1470	0.3	1470	1000	1.25E+01	1.25E+01	1.25E+01	1.25E+01	1.25E+01	1.25E+01	1.25E+01	1.25E+01	1.25E+01
1470	0.7	1471	100	1.25E+01	1.25E+01	1.25E+01	1.25E+01	1.25E+01	1.25E+01	1.25E+01	1.25E+01	1.25E+01
1470	1.9	1472	10	1.25E+01	1.25E+01	1.25E+01	1.25E+01	1.25E+01	1.25E+01	1.25E+01	1.25E+01	1.25E+01
1470	4.9	1475	1	9.63E+00	1.25E+01	1.25E+01	1.25E+01	1.25E+01	1.25E+01	1.25E+01	1.25E+01	1.25E+01
1470	13.0	1483	0.1	9.68E-01	1.94E+00	3.87E+00	4.84E+00	9.68E+00	1.25E+01	1.25E+01	1.25E+01	1.25E+01
1470	17.4	1487	0.05	4.86E-01	9.71E-01	1.94E+00	2.43E+00	4.86E+00	7.29E+00	1.25E+01	1.25E+01	1.25E+01
1470	34.2	1504	0.01	9.82E-02	1.96E-01	3.93E-01	4.91E-01	9.82E-01	1.47E+00	1.25E+01	1.25E+01	1.25E+01
1470	45.7	1516	0.005	4.95E-02	9.90E-02	1.98E-01	2.47E-01	4.95E-01	7.42E-01	7.42E+00	1.48E+01	1.48E+01
1470	89.9	1560	0.001	1.02E-02	2.04E-02	4.07E-02	5.09E-02	1.02E-01	1.53E-01	1.53E+00	3.06E+00	3.06E+00
1470	120.3	1590	0.0005	5.19E-03	1.04E-02	2.08E-02	2.60E-02	5.19E-02	7.79E-02	7.79E-01	1.56E+00	1.56E+00
Standard Pot-life											Extended Pot-life	

Table 4.5.3. Epoxy impregnation into 12.5 mm thick sample, $\phi = 10\%$, with 100 cp viscosity epoxy for various impregnation pressures, sample permeabilities, and time of impregnation. Note that standard pot-life epoxies have pot-life of 30 minutes and impregnation effectively stops at this time and corresponding depth. Extended pot-life epoxies remain viscous for periods up to 300-600 minutes and are capable of effective to complete penetration at moderate to high injection pressures. Depth of penetration for a given pressure, permeability and time is color coded for convenience: Orange < 0.1 mm, tan 0.1-1mm, white 1-10mm, blue >10mm.

After curing, the epoxy-impregnated sample is sliced, polished and mounted on a glass slide. The sample is then trimmed with a fine diamond saw, and ground to near 30 microns on a lapidary wheel, with final polishing accomplished by hand on a lapidary wheel. Each thin section is stained with a mixture of Alizarin red-S and potassium ferricyanide for identification of calcite and ferroan carbonates and stained for identification of potassium feldspar by etching over HF acid, and staining in solutions of barium chloride and sodium cobaltinitrate. A cover slip is applied using an easily removable, synthetic, heat sensitive adhesive.

Thin sections were examined using Nikon Optiphot and E. Leitz Orthoplan petrographic microscopes. Photomicrographs of representative textural and diagenetic features were taken with an Olympus E410 Digital camera. Additional photomicrographs for illustration of detailed features of diagenesis and porosity evolution were taken with a trinocular mounted Nikon FM2 data back camera and Nikon AFX auto-exposure unit. Photograph magnifications are calibrated by an E. Leitz micrometer, with a 0.01 mm graduated scale. Photomicrographs for each thin section sample at multiple magnifications are posted on the Project Website.

Point counting of 150 thin sections for composition and porosity distribution (modal analysis) was accomplished using a Swift Instruments Automatic Point Count stage, which is designed to move the sample through a predetermined grid, while the analyst identifies constituents of the sample at each point on the grid. Three hundred points were counted for each sample. Details of grain size, sorting, nature and distribution of cements, porosity and clay distribution are noted during point count analysis. All data are recorded in Microsoft Excel spreadsheets. Percentage and compositional ratios are calculated in Microsoft Excel spreadsheets, graphic plots are generated in Excel and Corel Quattro spreadsheets.

4.5.3 Results

Core descriptions, core slab images, thin section photomicrographs, and graphic presentation of core descriptions are too large for presentation in this report. Both data and images are available on the Project Website (<http://www.kgs.ku.edu/mesaverde/>). It is beyond the scope of this study to provide a comprehensive analysis of the lithologic and petrologic properties of the cores studied. The goal of this task in the study was to provide the needed lithologic characterization of the cores primarily lithology, composition and digital rock type.

Using the digital core description techniques, we were able to correlate the cored intervals to wireline logs, and precisely correlate core analysis data to wireline log response (Figure 4.5.1). The Project Website presents graphic images of all digitally described cores listed in Table 4.5.1. Figures 4.5.2 and 4.5.3 provide examples of representative core descriptions. Digital classification for each 0.5-ft interval are presented both on the core description and in separate Excel files.

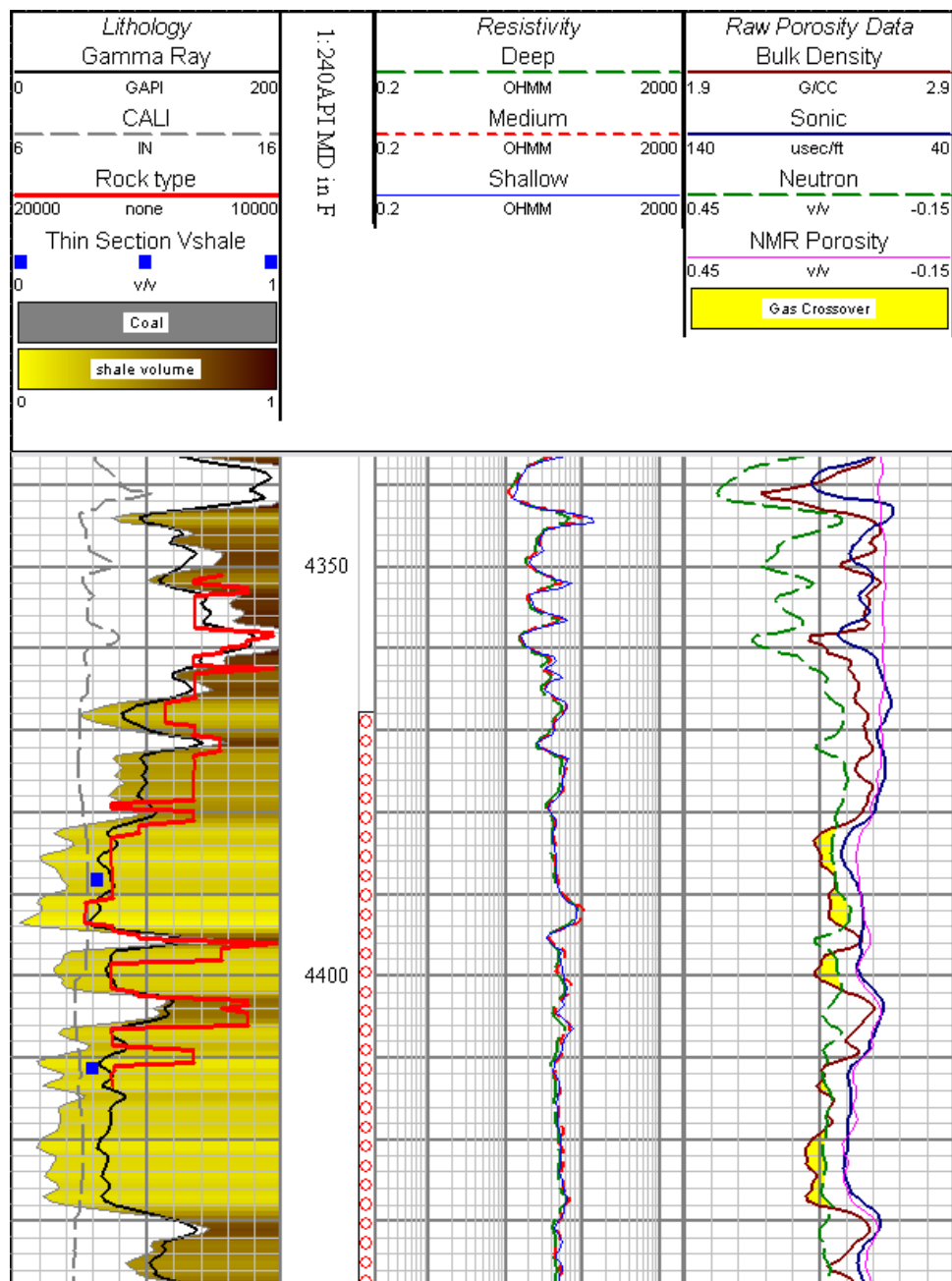


Figure 4.5.1. Correlation of digital rock type with wire-line log response, Williams Fork Formation, Barrett Last Dance 43C-3-792, Piceance basin, Colorado.



**Client: Kansas Geological Survey
DOE Mesaverde Petrophysics Project**

Operator: Bill Barrett Corporation
 Location: NESE sec. 3, T7S-R92W
 Formation: Ohio Creek, Williams Fork and Cameo
 Core depth: 2800-2860' (OC), 3539-6197' (WF), 6197-6352' (C)
 Core storage location/Library no.: Core Laboratories, Houston
 Described by: John C. Webb

Lease: Last Dance 43C-3-792
 County: Garfield State: Colorado
 Basin: Piceance
 Log depth = Core depth +/-
 API: 05-045-11402-0000
 Core diam: 4 inch Slabs: 1/3 Condition: Excellent

2780 to 2860 = Core - 3 ft
 3530 to 3600 = Core - 4 ft
 3950 to 4030 = Core - 3 ft
 4350 to 4420 = Core - 4 ft
 4840 to 4870 = Core - 3 ft
 5320 to 5340 = Core
 5700 to 5770 = Core - 3 ft
 6030 to 6070 = Core - 4 ft
 6280 to 6350 = Core - 10 ft

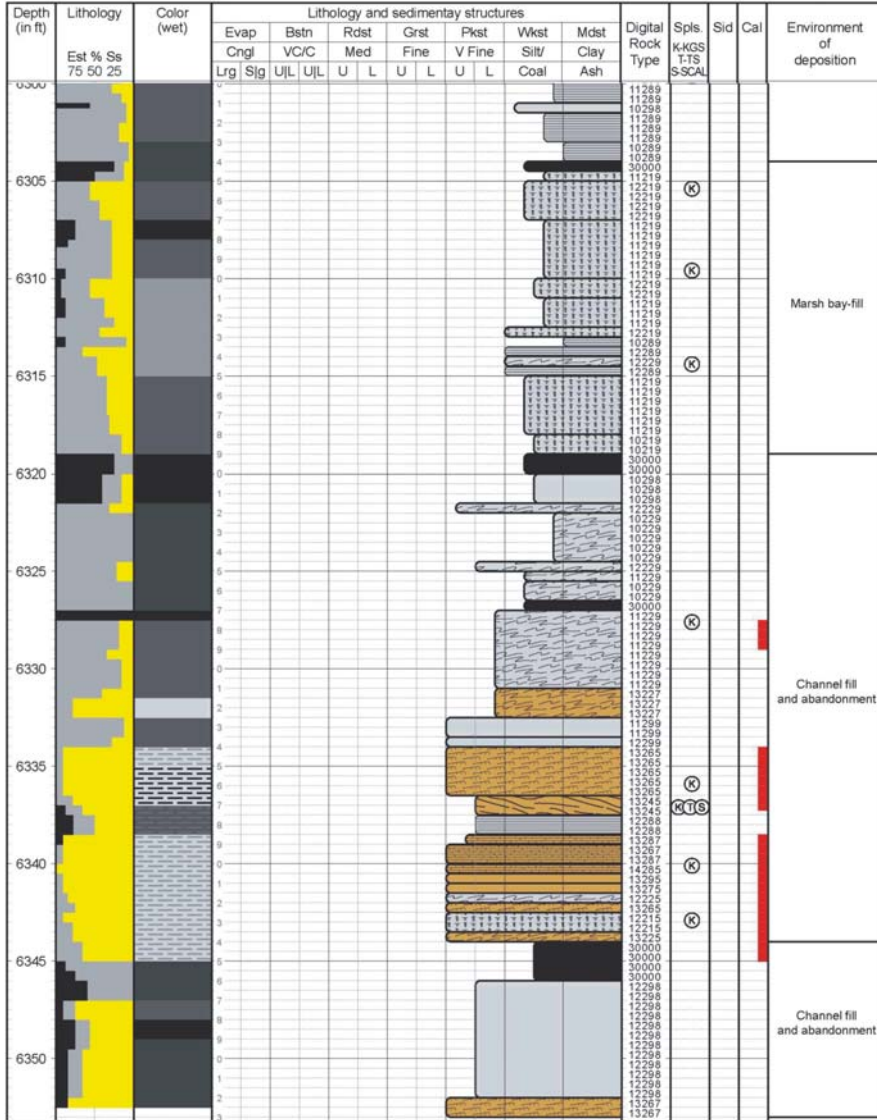


Figure 4.5.2. Example of core description, coastal mudstones of the Williams Fork Formation, Barrett Last Dance 43C-3-792, Piceance basin, Colorado.

The Project Website contains over 550 images of core slabs from which core plugs were obtained. These images represent a comprehensive image library of the lithofacies present in the Mesaverde in the basins studied. Figure 4.5.4 illustrates some of the lithofacies present in the Mesaverde.

The following discussion briefly summarizes some of the lithologic properties exhibited by sandstones and mudstones of the Mesaverde.

4.5.3.1 Lithofacies and Sedimentary Structures

Sedimentary lithofacies in the Mesaverde Group include coal and carbonaceous shale to shale and silty shale, very fine to medium, and locally coarse-grained sandstones as well as sparse lime mudstone and volcanic ash beds (bentonite). Figure 4.5.4 illustrates some of the lithofacies present in the Mesaverde. The fine grained intervals of the Mesaverde Group are dominated by mudstones and silty shales (rock types 10x19 and 11x29), lenticular and wavy bedded very shaly sandstones (12x3x and 12x4x), and wavy bedded to ripple cross-laminated shaly sandstones (13x4x and 13x6x). The sandstone intervals of the Mesaverde Group are dominated by ripple cross-laminated and cross-bedded, very fine to fine grained sandstones (rock types 14x6x, 15x6x, 14x7x, 15x7x), low angle cross-laminated to planar laminated sandstones (14x8x), and massive sandstones (14x9x, 15x9x). Medium grained sandstones are present in sandy portions of the Mesaverde in the Uinta and Piceance basins, in the Williams Fork Formation and in the Upper Almond Formation in the Washakie basin (16x7x and 16x9x). Shale lithoclast supported conglomerates with clast and sandy matrix supported textures are also locally present (13x2x and 19x9x).

4.5.3.2 Depositional Environment

Depositional environments range from near shore marine to continental, and include nearshore marine, shoreface, foreshore, prodeltaic and deltaic, lagoonal and bay-fill, tidal inlet, tidal channel and mudflat, swamp and raised mire, active and abandoned fluvial channel fill, overbank and levee deposits (Figures 4.5.2 and 4.5.3). Rooted and texturally disturbed lithologies indicate the intermittent to prolonged presence of vegetation, subaerial exposure and weathering in some cored intervals ([Pemberton, 1992](#)). Tidal influence is recognized in channel

and bay fill environments by the presence of clay and carbonaceous drapes on ripple, planar and trough cross laminations, inclined heterolithic bedding (typically consisting of thinly bedded, closely alternating, horizontal to low angle beds of shale, mudstone, shaly sandstone or sandstone ([Dalrymple, 1992](#)). In addition, some active channel fill sandstones exhibit cryptobioturbation (a blotchy pattern of highly concentrated, indistinct burrowing commonly attributed to *Macaronichnus*), which may indicate the presence of brackish to saline environments and the possibility of tidal influence ([Pemberton, 1992](#)).

4.5.3.3 Mineralogy

Point count (modal) analysis reveals that sandstones of the Mesaverde Group consist of mixtures of detrital quartz and feldspar (commonly grouped as siliciclastic grains) and lithic (rock) fragments, sparse to trace amounts of glauconite, heavy minerals and carbonaceous material, various mineral cements and pore space (see Point Count data table on project website). Siltstones and mudstones include small to moderate proportions of detrital siliciclastic and lithic grains, as well as small to large proportions of carbonaceous and argillaceous material. Detrital quartz consists of monocrystalline and sparse polycrystalline grains. Feldspar is predominantly plagioclase, much of which has been altered to albite. Potassium feldspar is locally prominent, especially where associated rock fragments indicate a contribution from volcanic or plutonic terrains. Rock fragments include those derived from sedimentary (chert, mudstone, carbonate), metamorphic (phyllite, schist, micaceous and quartzose metamorphic), volcanic (silicified, argillitic, porphyritic, microlitic), and plutonic (quartzose and feldspathic grains) sources. Ternary plots of the relative proportions of each major detrital constituent show that sandstones of the Mesaverde have a wide range in detrital composition. These sandstones fall into the quartzarenite, subarkose and sublitharenite, lithic arkose, feldspathic litharenite, and litharenite compositional clans, as described by Folk ([1974](#)). Figure 4.5.5 is a ternary diagram that illustrates these compositional variations for Mesaverde sandstones from Uinta and Piceance basins. The wide range of composition reflects the variation in source terrains, tectonic history, and depositional environments that characterize the Mesaverde Group ([Dickinson, et al., 1986](#); [Lawton, et al., 2003](#)). Depositional environments influence sandstone detrital composition by a variety of processes, including abrasion and mechanical destruction of grains, sorting of grains during transport, incorporation of shaly rock fragments from erosion of stream banks, clay

laminations, and degree of bioturbation. For most samples, sediment deposited in marine shoreline environments exhibits a more quartzose composition than coeval sediment deposited in fluvial or coastal plain environments ([Winn, et al., 1984](#)). For example, in Mesaverde sandstones of the Uinta and Piceance basins, detrital composition shows significant partitioning by depositional environment and sedimentary basin, with fluvial sandstones of the Piceance basin falling into the lower portions of the litharenite, feldspathic litharenite and lithic arkose fields, compared to sandstones deposited in marine environments (Figure 4.5.6). In addition, a separate population of sandstones having a more quartzose composition (sublitharenite, subarkose and quartzarenite) appears in samples from fluvial environments in the Uinta basin (Quartzose fluvial, Figure 4.5.6). A ternary plot of lithic fragment population indicates that most of the rock fragments (and presumably the associated quartz and feldspar grains) were derived from sedimentary sources, with moderate contributions from volcanic and plutonic sources, and sparse contributions from metamorphic sources (Figure 4.5.7). Additional plots for each well are located on the Project Website.

4.5.3.4 Diagenesis

Diagenetic alterations include compaction, ductile deformation of soft grains, brittle deformation of feldspar and chert grains, precipitation of pore-lining and pore-filling cements, dissolution and replacement of unstable grains such as feldspar and carbonate rock fragments, and the formation and cementation of natural fractures. Cements include siderite, pyrite, chlorite and mixed-layer illite-smectite, nonferroan calcite, quartz overgrowths, albite (particularly as a replacement or mold-filling cement), ferroan calcite, ferroan dolomite, and kaolinite, listed in typical order of occurrence. Of these, clay mineral and quartz overgrowths are the most abundant, followed by ferroan calcite and ferroan dolomite (see Point Count Data on Project Website).

Detrital composition influences the type and degree of diagenesis. Porosity reduction in quartzose sandstones occurs by pervasive cementation by quartz, while feldspathic and lithic-rich sandstones exhibit little cementation by quartz. Instead, these lithologies exhibit strong to severe compaction, and may contain small to moderate amounts of clay mineral cement. Clay cements are also locally present in quartzose sandstones, and where abundant, may inhibit the precipitation of quartz cement. Secondary intergranular and moldic porosity have developed in

some sandstones, where they may comprise the bulk of mesoporosity. Typical dissolution targets include carbonate and chert rock fragments, precursor calcite cements, detrital feldspars and rarely, volcanic rock fragments.

4.5.3.5 Lithologic Influence on Porosity and Permeability

For most lithofacies, average porosity increases with increasing grain size (including decreasing shaliness; example Figure 4.5.8). Permeability at any given porosity increases with increasing grain size and increasing sorting, though this relationship is further influenced by the nature of cementation, and to a much lower degree, sedimentary structure. A visual assessment of the partitioning of porosity (microporosity vs. mesoporosity) and the abundance and distribution of clay mineral cement helps with in a particular sample to explain the variation of permeability within rock types of similar grain size.

4.5.3.6 Porosity in the Mesaverde Group

Both porosity and permeability in samples from the Mesaverde Group are closely tied to grain size and abundance of detrital clay, as represented by digital rock type (Figure 4.5.8). Porosity within the Mesaverde Group consists of a mixture of intergranular, clay-filled intergranular, moldic and intragranular (“dissolution porosity” of some authors, e.g. [Pittman, 1979](#)), and fractures, both macroscopic and microscopic. Intergranular pores are the result of preservation of primary intergranular voids and the dissolution of prior cements (such as calcite), forming secondary intergranular pores ([Schmidt and McDonald, 1979a](#)). Both types of intergranular porosity tend to be moderately to well connected, with pore throat size and permeability decreasing in proportion to decreasing grain size, and pore throat aperture radii greater than 5 microns ([Beard and Weyl, 1973](#); [Pittman, 1979](#); [Nelson, 2009](#)). Moldic pores are formed by dissolution of framework grains, particularly potassium feldspar, carbonate and volcanic rock fragments or replacement cements such as calcite or ferroan calcite ([Pittman, 1979](#); [Schmidt and McDonald, 1979b](#)). Clay-filled porosity is characterized by small pore diameters and extremely small pore throat radii (< 5 micron, [Pittman, 1979](#)). In addition, the high specific surface area of clay mineral cements contributes to elevated irreducible water saturation ([Nesham, 1977](#); [Wilson and Pittman, 1977](#)). Partial dissolution of feldspar grains or volcanic rock fragments results in skeletal or “spongy” grains that have intragranular porosity, composed

of extremely small, poorly connected pore spaces. For the purposes of this report, intergranular, secondary intergranular and moldic pores are classified as mesoporosity. Intragranular pores, clay-filled intergranular pores and pores within clay matrix and carbonaceous material are classified as microporosity. Figure 4.5.9 illustrates the relative proportions of intergranular mesoporosity, moldic mesoporosity, and microporosity from point count data as an example of porosity distribution in sandstones of the Mesaverde Group in the Uinta and Piceance basins. Most samples plot within the field dominated by clay-filled microporosity, with typically only sparse to moderate amounts of intergranular and moldic mesoporosity.

Howard (1992) demonstrated that the distribution of authigenic clay, rather than any measure of clay abundance, was responsible reduction in permeability in reservoir sandstones. In an effort to further characterize the nature and distribution of porosity and the influence of porosity type and clay mineral cements on permeability of sandstones in the Mesaverde Group, we have developed a five-tiered classification of porosity, based on visual examination of thin sections. Table 4.5.4 describes criteria for classification of pore networks into five porosity network types, which characterize the nature and distribution of porosity in sandstones, siltstones and mudstones of the Mesaverde. Each successive pore network type reflects the changes in porosity caused by increasingly severe compaction and diagenetic alteration. Type I pore networks are dominated by well connected, primary and secondary intergranular pores (mesoporosity) that lack significant amounts of clay mineral cements. Moldic porosity is sparse to absent (Figure 4.5.10). Type II pore networks contain both intergranular and moldic mesopores, which are moderately to poorly connected, and lack significant amounts of clay mineral cement (Figure 4.5.11). Type III pore networks contain intergranular and moldic mesopores that have reduced connectivity, primarily due to the presence of moderate to common clay mineral cement (Figure 4.5.12). Type IV pore networks consist entirely of clay-filled intergranular microporosity (Figure 4.5.13). Type V pore networks consist entirely of clay-sized intergranular micropores within detrital shaly matrix or carbonaceous material (Figure 4.5.14). Figure 4.4.15 illustrates the effect of pore network type on porosity and permeability in samples from the Mesaverde Group in the Piceance basin.

Pore network	Description	Intergranular porosity	Moldic porosity	Clay-filled intergranular porosity	Porosity distribution	Typical core analysis data
Type I	Porosity consists of well to moderately connected primary and secondary intergranular mesopores and traces of pore-lining chlorite clay containing microporosity.	Common to moderate	Trace	Trace to Absent	Mesoporosity>> Microporosity	Porosity= 11.4%, Rhob = 2.65 g/cc, Ka=0.8716 mD, Kins=0.4287 mD
Type II	Porosity consists of poorly to moderately connected moldic and secondary intergranular mesopores with traces of pore-lining clay containing microporosity.	Moderate	Sparse to moderate	Trace	Mesoporosity> Microporosity	Porosity= 9.9%, Rhob = 2.66 g/cc, Ka=0.0237 mD, Kins=0.0076 mD
Type III	Porosity consists of clay-lined intergranular pores, pore throats are occluded by clay cement.	Moderate to sparse	Sparse to moderate	Sparse	Microporosity≥ Mesoporosity	Porosity= 12.2%, Rhob = 2.65 g/cc, Ka=0.0178 mD, Kins=0.0019 mD
Type IV	Porosity consists almost entirely of sparse, poorly connected, clay-filled intergranular microporosity.	Extremely sparse to absent	Trace	Moderate to sparse	Microporosity>> Mesoporosity	Porosity= 7.9%, Rhob = 2.65 g/cc, Ka=0.0211 mD, Kins=0.0031 mD
Type V	Porosity consists entirely of sparse, poorly connected microporosity within interparticle voids of mudstone and shale matrix.	Not present	Not present	Sparse	Microporosity only	Porosity= 2.4%, Rhob = 2.70 g/cc, Ka=0.0020 mD, Kins=0.00004 mD

Table 4.5.4 Porosity network types of the Mesaverde Group.

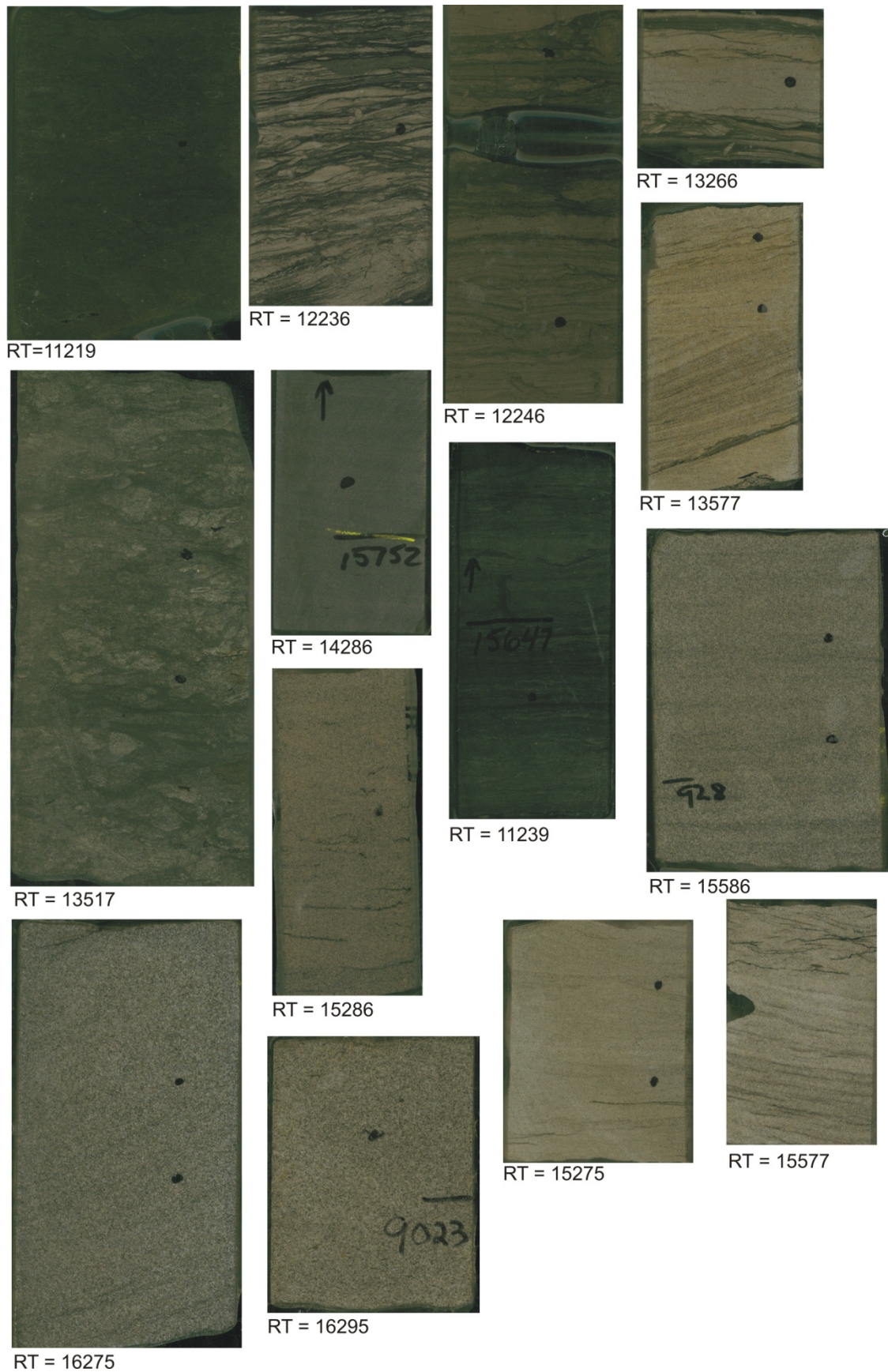


Figure 4.5.4. Example Mesaverde lithofacies with rock type digital classification.

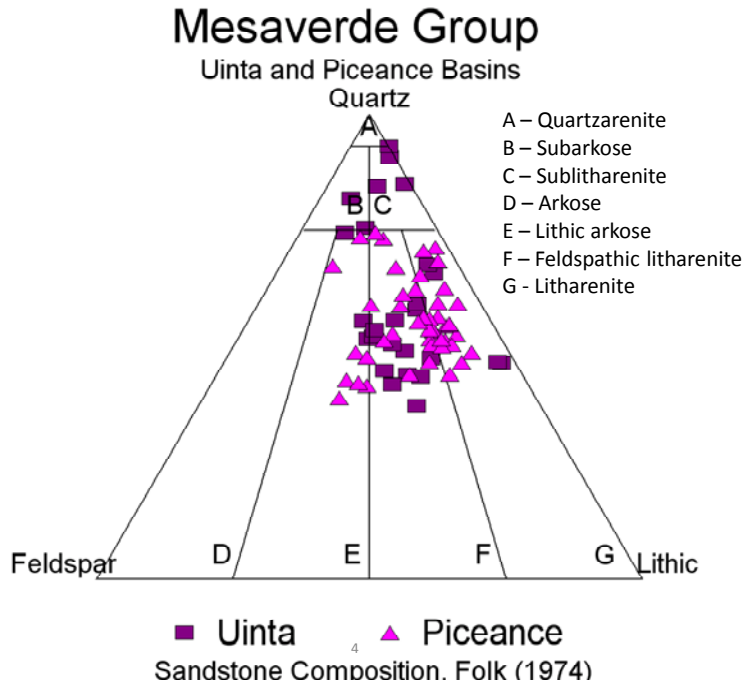


Figure 4.5.5. Example Quartz : Feldspar : Lithic (QFL) ternary plot comparing sandstone composition between the Uinta and Piceance basins. (after [Folk, 1974](#))

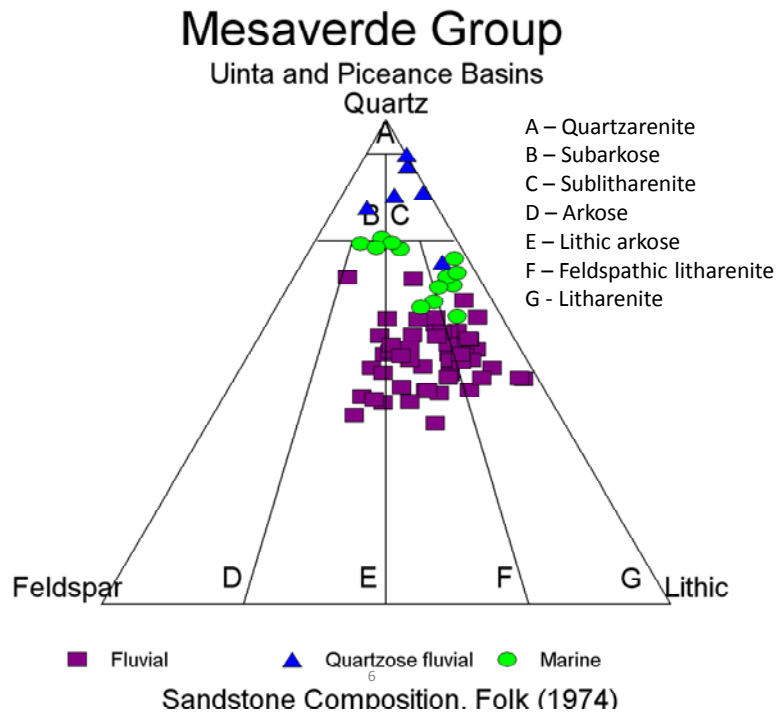


Figure 4.5.6. Example Quartz : Feldspar : Lithic (QFL) ternary plot comparing sandstone composition among different depositional environments in the Uinta and Piceance basins. (after [Folk, 1974](#))

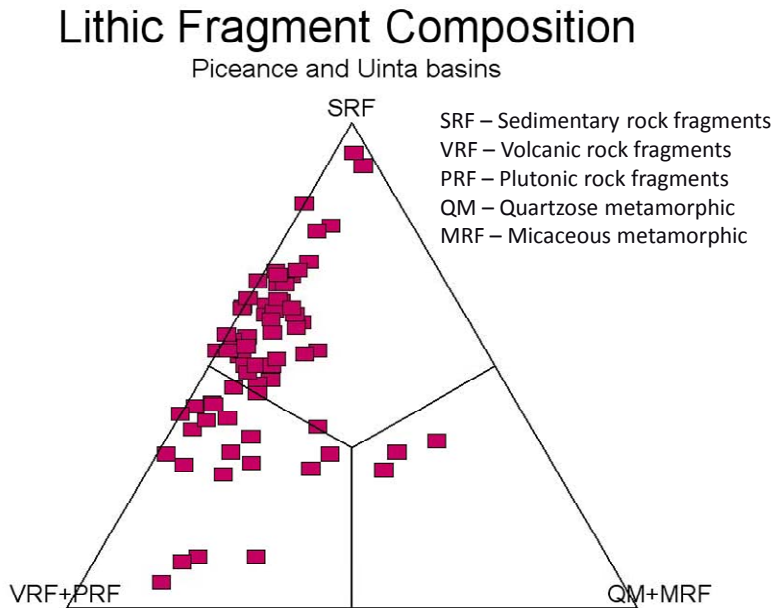


Figure 4.5.7. Ternary plot of lithic fragment provenance for sandstones in the Piceance and Uinta basins.

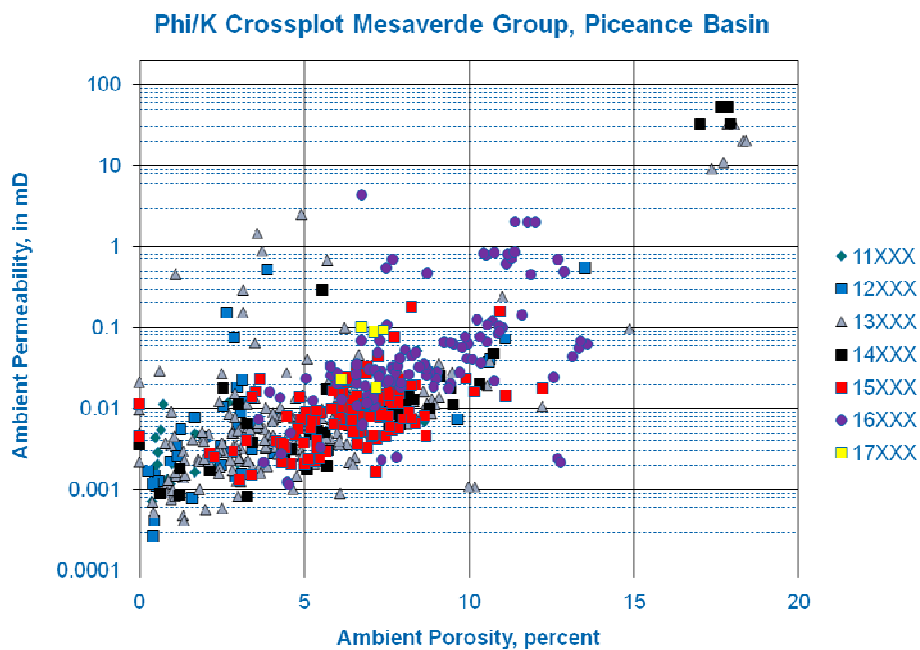


Figure 4.5.8. Example from Piceance Basin illustrating the influence of grain size and sorting, as reflected in digital rock type on permeability and porosity in the Piceance Basin.

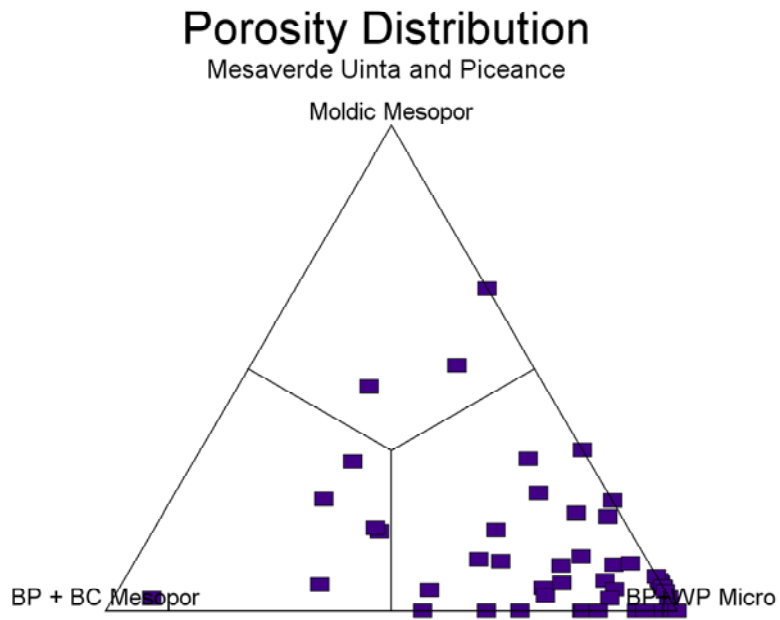


Figure 4.5.9. Ternary plot of porosity distribution for sandstones of the Mesaverde Group, Piceance and Uinta basins, Utah and Colorado.

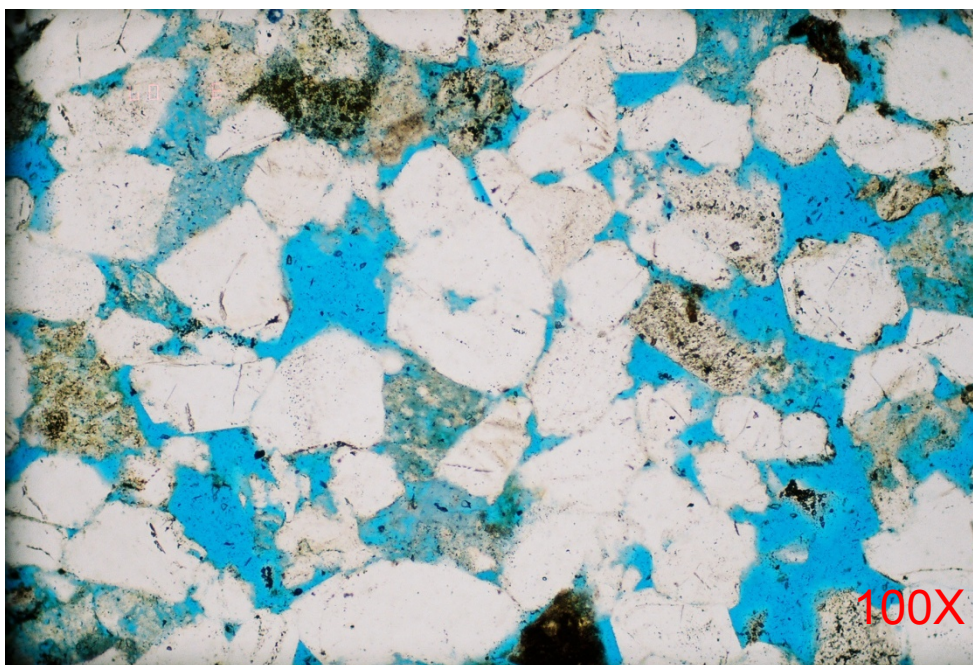
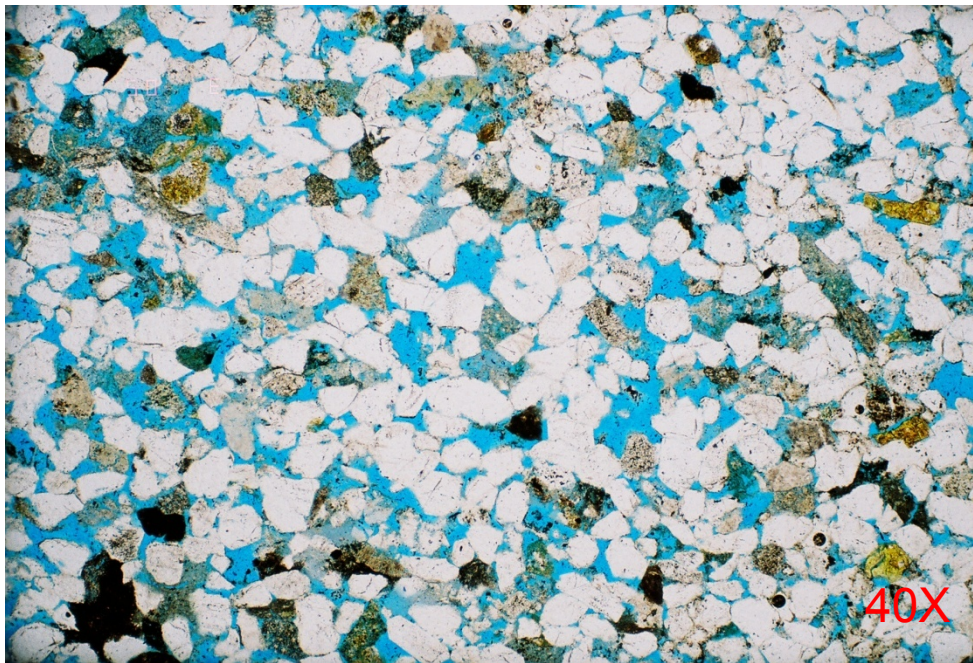


Figure 4.5.10. Example Mesaverde thin section for Type I porosity (shallow burial). Porosity consists of well connected primary and secondary intergranular mesopores, sparse moldic pores, quartz overgrowth cement. Quartz cement is sparse. Lack of pore-lining clay cement reduces S_{wi} and improves relative permeability. USGS CB #1 Book Cliffs, 255.8', Rock type 15567, $\phi = 24.8\%$, $GD = 2.64 \text{ g/cc}$, $K_a = 137.62 \text{ mD}$, $K_{ins} = 112.2 \text{ mD}$.

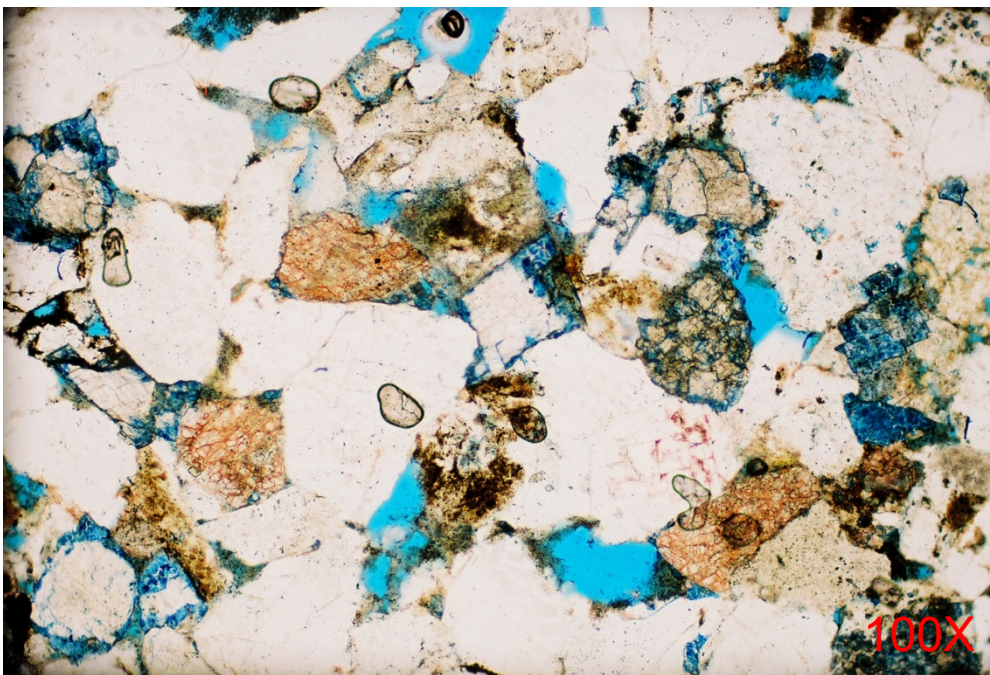


Figure 4.5.11. Example Mesaverde thin section for Type II porosity. Porosity consists of poorly to moderately connected moldic and secondary intergranular mesopores with traces of pore-lining ML/IS(?) clay, containing microporosity. Quartz cement is prominent, ferroan calcite is sparse. Pore-lining clay cement causes elevated S_{wi} and reduced relative permeability. Williams PA 424, 6148.8' , Rock Type 15276, $\phi = 9.9\%$, $GD = 2.66 \text{ g/cc}$, $K_a = 0.0237 \text{ mD}$, $K_{ins} = 0.0076 \text{ mD}$.

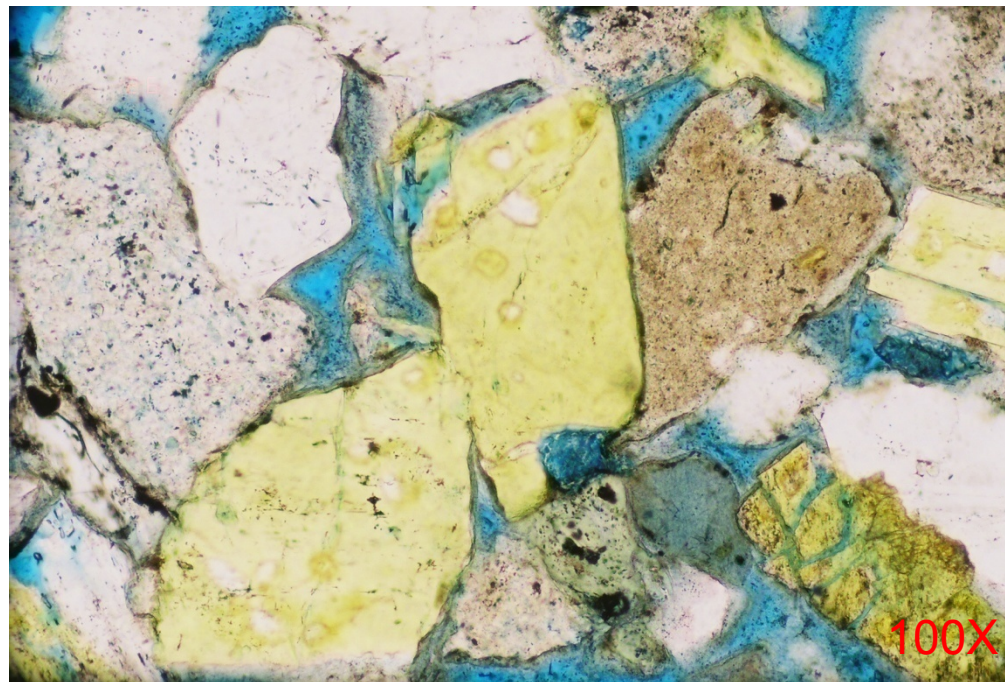


Figure 4.5.12. Example Mesaverde thin section for Type III porosity. Porosity consists of clay-lined intergranular pores, pore throats are occluded by clay cement, which causes elevated S_{wi} , reduced relative permeability and increased P_c entry pressure. Cements include chlorite or ML-IS clay, traces of non-ferroan or ferroan calcite, traces of quartz overgrowths. Inhomogeneous packing and over-sized intergranular pores indicate the development of secondary intergranular porosity. Williams PA424, 4600.3', Rock Type 15297, $\phi=12.2\%$, $GD=2.65g/cc$, $K_a=0.0178$ mD, $K_{ins} = 0.0019$ mD.



Figure 4.5.13. Example Mesaverde thin section for Type IV porosity. Porosity consists almost entirely of sparse, poorly connected, clay-filled intergranular microporosity. Quartz cement is prominent, ferroan calcite is sparse. Pore-filling clay cement causes elevated S_{wi} , reduced relative permeability and increased P_c entry pressure. Williams PA 424, 4686.4', Rock Type 15286, $\phi = 7.9\%$, $GD = 2.65 \text{ g/cc}$, $K_a = 0.211 \text{ mD}$, $K_{ins} = 0.0031 \text{ mD}$.

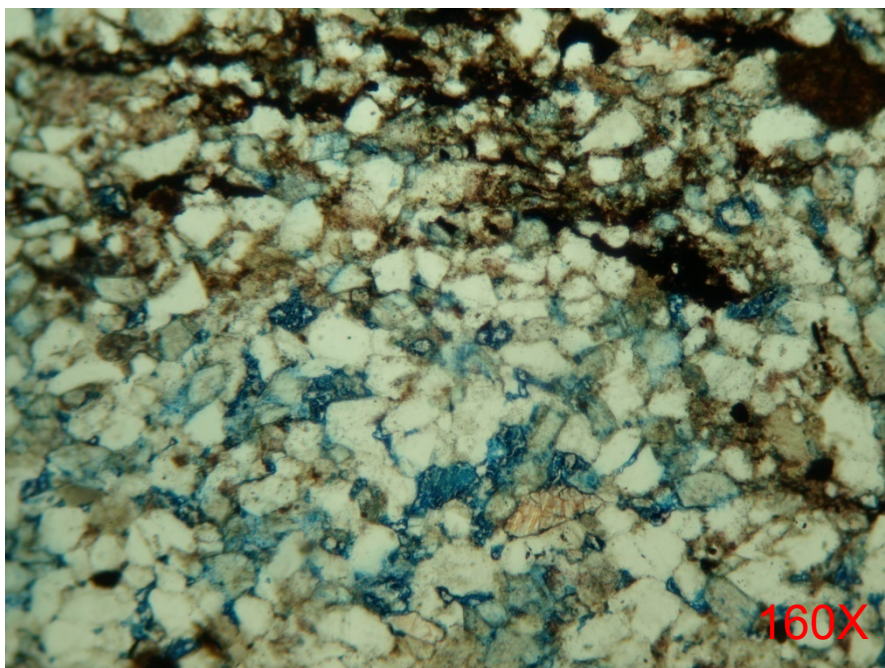


Figure 4.5.14. Example Mesaverde thin section for Type V porosity. Porosity consists entirely of sparse, poorly connected microporosity within interparticle voids of mudstone and shale matrix. Cements include siderite, ferroan calcite and pyrite. Organic matter is locally common. Abundant clay causes highly elevated S_{wi} , severely reduced permeability and elevated P_c entry pressure. CER MWX-2, 7085.5', Rock Type 11299, $\phi = 2.4\%$, $GD = 2.70$ g/cc, $K_a = 0.0020$ mD, $K_{ins} = 0.00004$ mD.

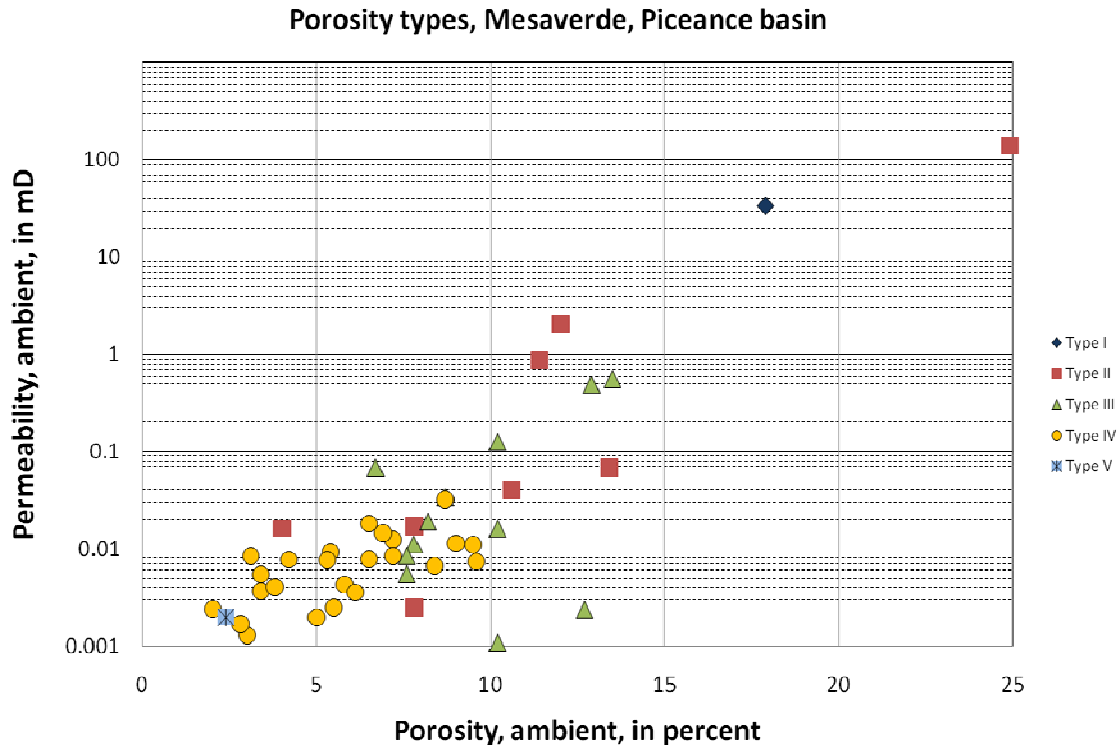


Figure 4.5.15. Example from Piceance basin of the influence of pore type on porosity and permeability in the Piceance Basin.

Subtask 4.6. Perform standard logs analysis

4.6.1 Task Statement

Standard log analysis is the benchmark by which newly developed algorithms are measured. The goal of this subtask is to obtain standard wireline log interpretation of the wells using industry standard practices.

4.6.2 Methods

The basic log model employed in this project is a generic, Rocky Mountain tight gas petrophysical model similar to that used by several large companies and service vendors active in the Mesaverde plays. The model begins with a volume of shale computation based on the gamma ray log, computes total porosity and effective porosity from the neutron and density logs, an Archie water saturation using locally determined formation water resistivity, and a permeability estimate using a Timur equation approach.

4.6.2.1 Basic log analysis parameters

The log analysis parameters were initially set as follows:

- Volume of shale model: linear using GR log
- GR clean and GR shale endpoints: set by zone, individually picked for each well log
- Density matrix: 2.65 g/c³
- Fluid density: 1.0 g/c³
- Neutron matrix: neutron porosity input in limestone units, output in sandstone units
- Porosity used: density-neutron cross-plot porosity corrected for shale effect (“effective” porosity)
- Water saturation model: Archie
- Archie constants: $a = 1$, $m = 1.85$, $n = 2$
- Permeability model: Timur equation with porosity exponent set by zone, BVWirr set by zone, and Swi exponent of 2

4.6.2.2 Shale volume.

Shale volume was estimated from the gamma ray with a linear relationship:

$$V_{sh} = \frac{GR_{log} - GR_{clean}}{GR_{shale} - GR_{clean}} \quad [4.6.1]$$

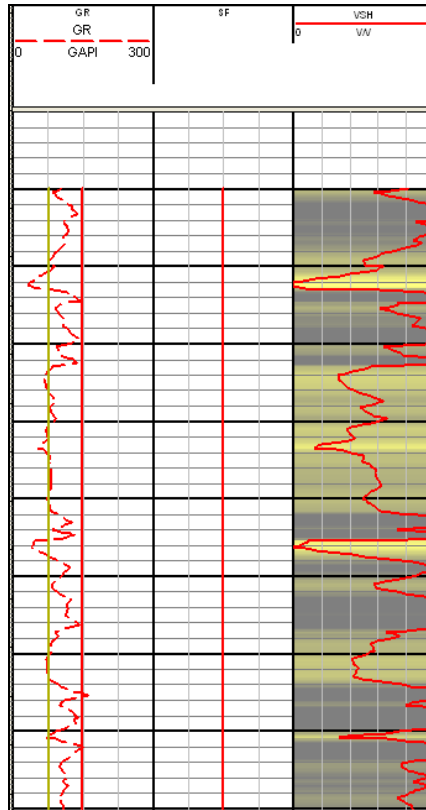


Figure 4.6.1. The clean and shale values of the GR that are needed to calculate the total volume of shale are interactively chosen on this depth plot.

- The clean gamma ray value was set at or near the lowest gamma ray value in the zone. (Figure 4.6.1)
- The shale gamma ray value was set at an average gamma ray value of the shales in the zone, ignoring any organic rich or black shale intervals.

4.6.2.3 Total and cross plot porosity

a. Density porosity calculated by equation 4.6.2, where the output was labeled PHID, in sandstone units with an initial matrix density of 2.65 g/c3.

$$PHID = \frac{RHOMA - RHOB}{RHOMA - RHOFL} \tag{4.6.2}$$

b. Neutron porosity output was labeled PHIN and is also in sandstone units.

c. Sonic porosity was calculated by equation 4.6.3 and the output was labeled PHIS, in sandstone units.

$$PHIS = \frac{\Delta t_{log} - DTMA}{DTF - DTMA} \tag{4.6.3}$$

d. Total cross-plot porosity (PHIDN) was determined by interpolation from a standard neutron-density cross-plot (Figure 4.6.2), where the density input was bulk density (g/cm3) and the neutron porosity was input in limestone units (v/v). A copy of this curve is also labeled PHIX. The neutron conversion from sandstone to limestone units is a software requirement to accomplish the chartbook lookup.

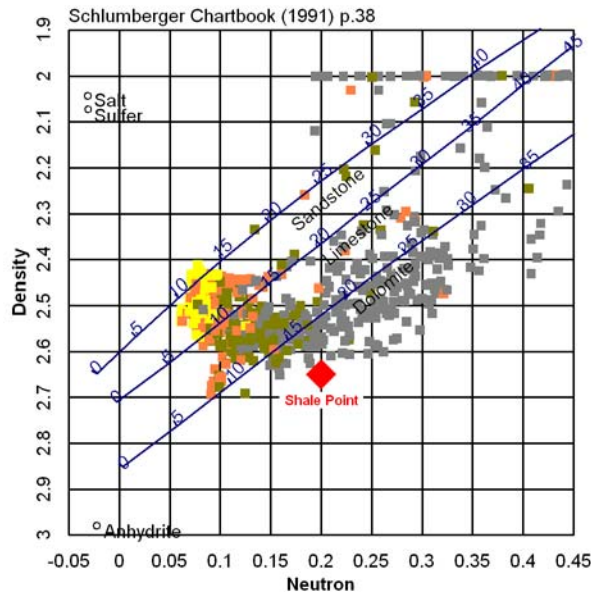


Figure 4.6.2. Neutron-density cross-plot used to calculate a cross-plot porosity PHIDN. Schlumberger Chartbook (1991) p. 38.

4.6.2.4 Effective porosity

We use effective porosity in the sense of a clay bound water corrected porosity. In sandstone reservoirs, this is assumed to be close to the connected pore volume available to store hydrocarbons. It was determined from the neutron and density by the following procedure:

- For each zone in each well, a locally determined shale porosity was determined from a graphic density-neutron cross-plot color coded by V_{shale} as the Z value as shown in Figure 4.6.3. The shale porosity value was set at the center of the high V_{shale} cluster.
- From the selected shale point, three values are determined- the density porosity of shale (PHIDsh), neutron porosity of shale (PHINsh), and the total cross-plot porosity of shale (PHIDNsh).

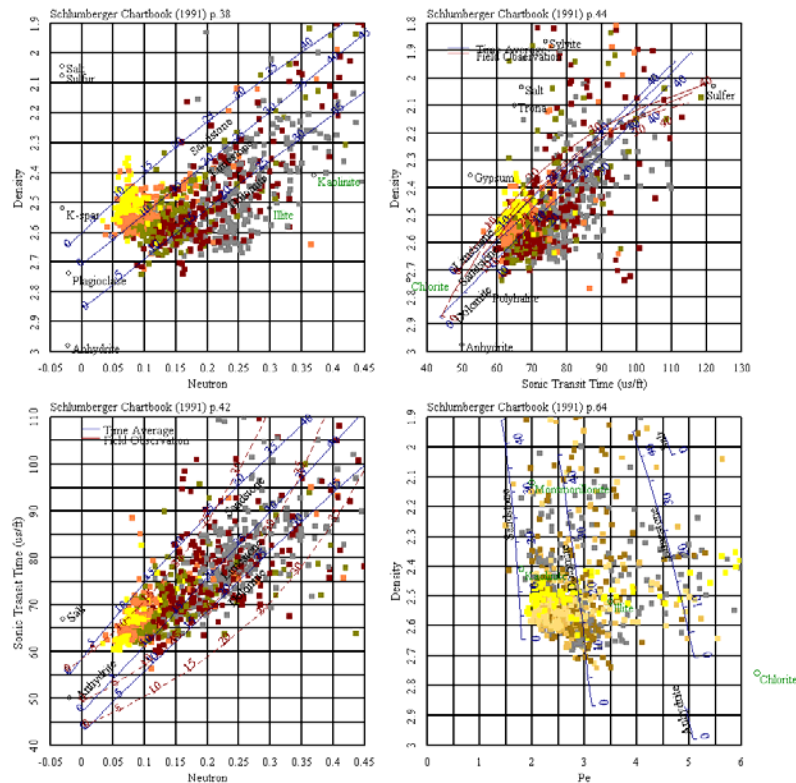


Figure 4.6.3. Multiple cross-plots to visually choose the locally determined shale porosity. Color coded by V_{shale} as the z value

- c. Each of the individual porosity values, PHID, PHIN, and PHIDN are then corrected to effective porosity by the following equation

$$\text{PhiE} = \text{PhiT} - \text{Vsh} * \text{PhiSh} \quad [4.6.4]$$

where PhiE is the shale corrected effective porosity, PhiT is the log determined total porosity (density, neutron, or cross-plot), and PhiSh is the matching shale total porosity. Vsh is the linear estimate of shale volume from the gamma ray (equation 4.6.1).

- d. The effective density-neutron cross-plot porosity (PHIDNE) was used in this study as the main porosity. A copy of this curve is also saved as PHIE.
- e. A porosity comparison plot (Figure 4.6.4) was used as a porosity check. Total porosity included errors introduced by volume of shale, varying grain densities and gas effects. These errors are estimated and subtracted iteratively until the difference of the effective porosity between tools (neutron, density and sonic) is minimized. The effective porosity correction (Eqn 4.6.4) minimizes the volume of shale effect, and the cross-plot porosities eliminates the effect of variable grain densities.
- f. PHIE was compared to the *in situ* corrected core porosities and the input variables for either grain density or the shale point were adjusted in an iterative approach to calibrate the porosity model to core. The final PHID therefore often has a zoned grain density that varied from the starting value of 2.65.

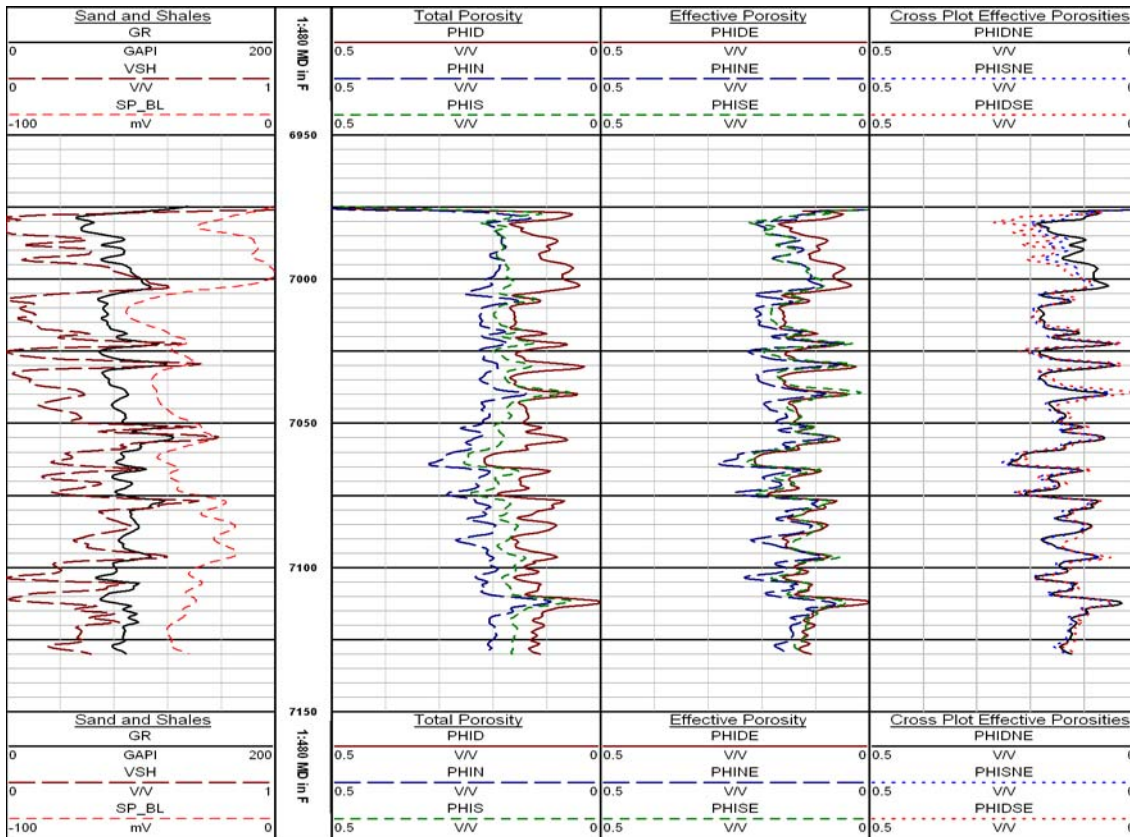


Figure 4.6.4. From left to right the porosities converge as the errors introduced by shale volume, variable grain densities and gas effects are minimized.

4.6.2.5 Water saturation computation

The basic log analysis model used the Archie (1942) saturation equation with constant electrical parameters, variable formation water salinity, and deep resistivity as an approximation of R_t .

- a. The deep resistivity curve was copied to R_t . For most wells with array induction logs the deep curve is a good approximation of R_t . For older wells with induction logs this assumption is not valid, but the tornado chart solutions for formation resistivity rarely changes the answer significantly except in shallow, water bearing intervals of the Mesaverde.
- b. The neutron-density cross-plot porosity (PHIX) was used for the saturation calculation.

- c. The Archie exponents were set to $a = 1$, $m = 1.85$, $n = 2$ based on prior experience and general Rocky Mountain guidelines. R_w was estimated from a Pickett plot for each zone in each well (Figure 4.6.5).

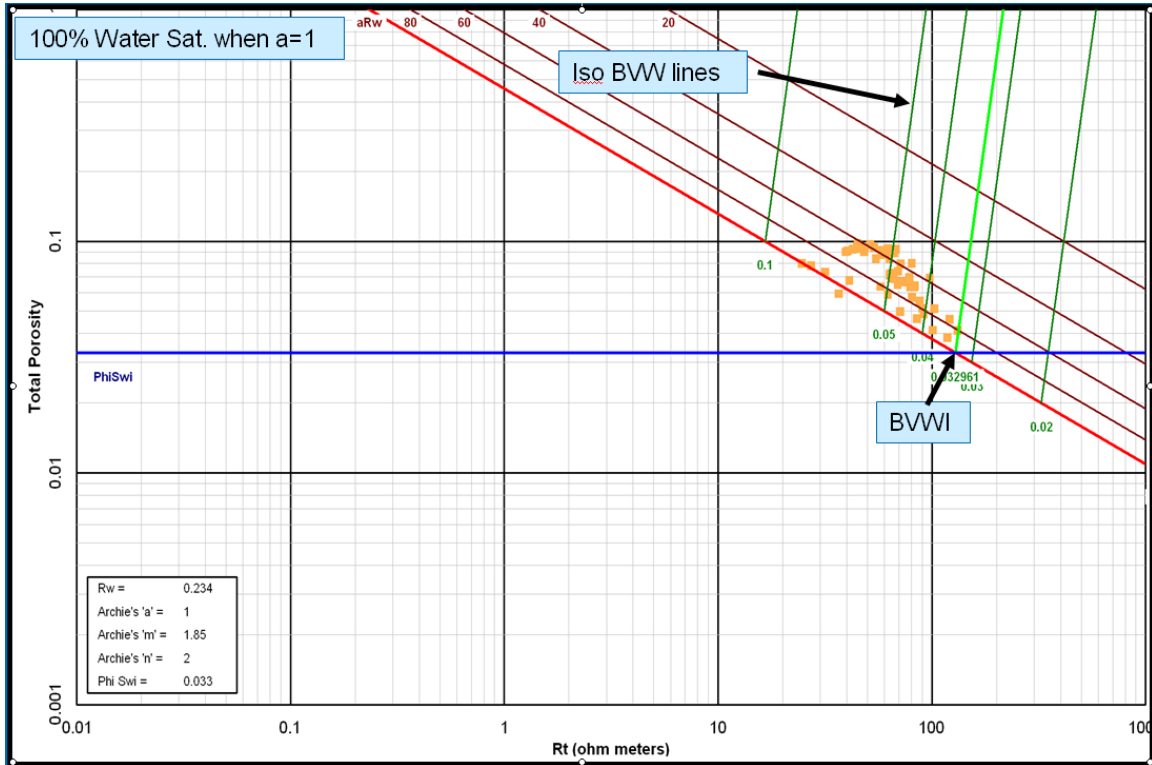


Figure 4.6.5. An interactive Pickett plot was used to calculate R_w . Red line is the assumed R_o (wet) line for this well. The slope of the R_o line is $-m$, and the x intercept at porosity = 1 is R_w (assumes $a=1$).

S_w is therefore:

$$S_w = [(a \cdot R_w) / (\Phi X^m \cdot R_t)]^{1/n} \quad [4.6.5]$$

$$S_w = [R_w / (\Phi X^{1.85} \cdot R_t)]^{0.5} \quad [4.6.6]$$

- d. Bulk Volume Water was computed from the effective porosity:

$$BVW = PHIE \cdot SW \quad [4.6.7]$$

4.6.2.6 Permeability

- a. Bulk volume water irreducible (BVWI) was estimated from one of two methods:
 - i. On a depth plot intervals where the value of BVW is approximately constant over several sandstones was assumed to indicate zones at or near irreducible saturation (Figure 4.6.6, Track 7); or
 - ii. On a Pickett plot, (e.g. Figure 4.6.5) we looked for vertical trends in the data at the right side of the data cloud, which also represent a constant value of BVW irreducible. Generally this is more difficult.

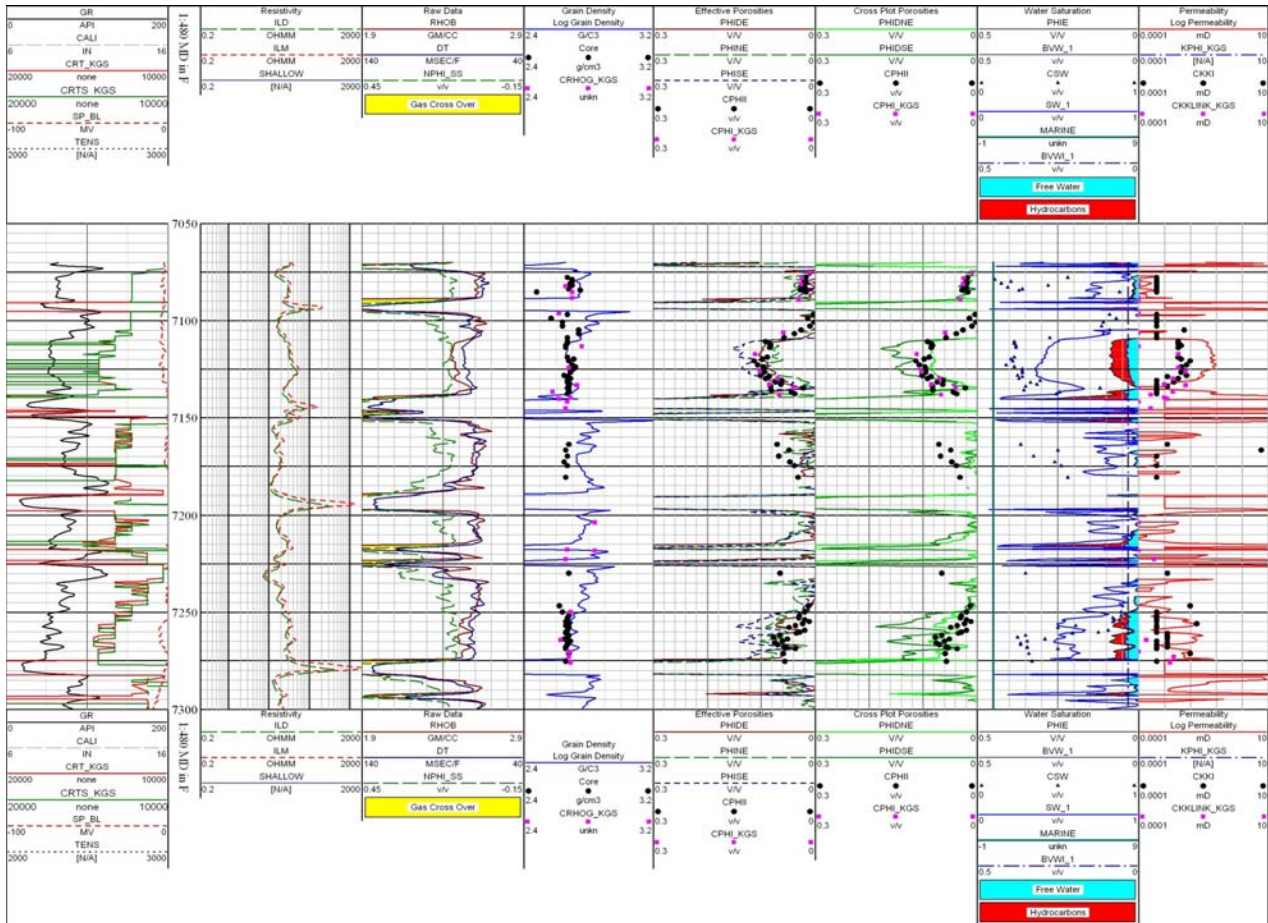


Figure 4.6.6. Depth plot showing the BVWI value that was chosen for this well in the water saturation (i.e. track 7). The value was determined by the average boundary between the “free water” and hydrocarbons.

- b. Swi is calculated from the bulk volume irreducible and total porosity:

$$SWI = BVWI / PHIX \quad [4.6.8]$$

By using total porosity instead of effective the Swi estimate includes clay bound water.

- c. Estimated permeability from the generalized Timur ([1968](#), eq. 8) equation:

$$K \log = KCOEF \frac{PHIX^{KPHIEXP}}{SWI^{KSWIEXP}} \quad [4.6.9]$$

where the permeability exponents KPHIEXP and KSWIEXP were set by zone to best approximate the *in situ* core permeabilities. Nominal values of 6 and 2 were used initially, then iteratively adjusted to match core. KCOEF was set to 62,500 (= 250²). Total porosity was used in this formula instead of effective by convention; consequently the porosity coefficients determined are lower than they would be if PhiE were substituted in the formula.

4.6.2.7 Filter results for coals and bad hole.

Two filters were run to clean up the results for graphical output.

- a. Coals were flagged as clean intervals (Vsh < 0.3) with low bulk density (RHOB < 2.1 g/c3)
- b. Bad hole was flagged by intervals with excessive borehole size (greater than 3” above bit size) or excessive density correction (DRHO > 0.2 g/c3). The calculated porosity and saturations in the bad hole intervals were nulled.

File: GR_AmHunter 1 Old Road.las
 Plot: Single Porosities Comparison Log_KGS.plt
 Gross Interval: 7425 to 12075 by 0.5
 Ranges: 11850-12075
 Time: 06:32 PM

Well Name: Old Road Unit 1
 Plot Name: Single Porosities Comparison Log_KC
 F

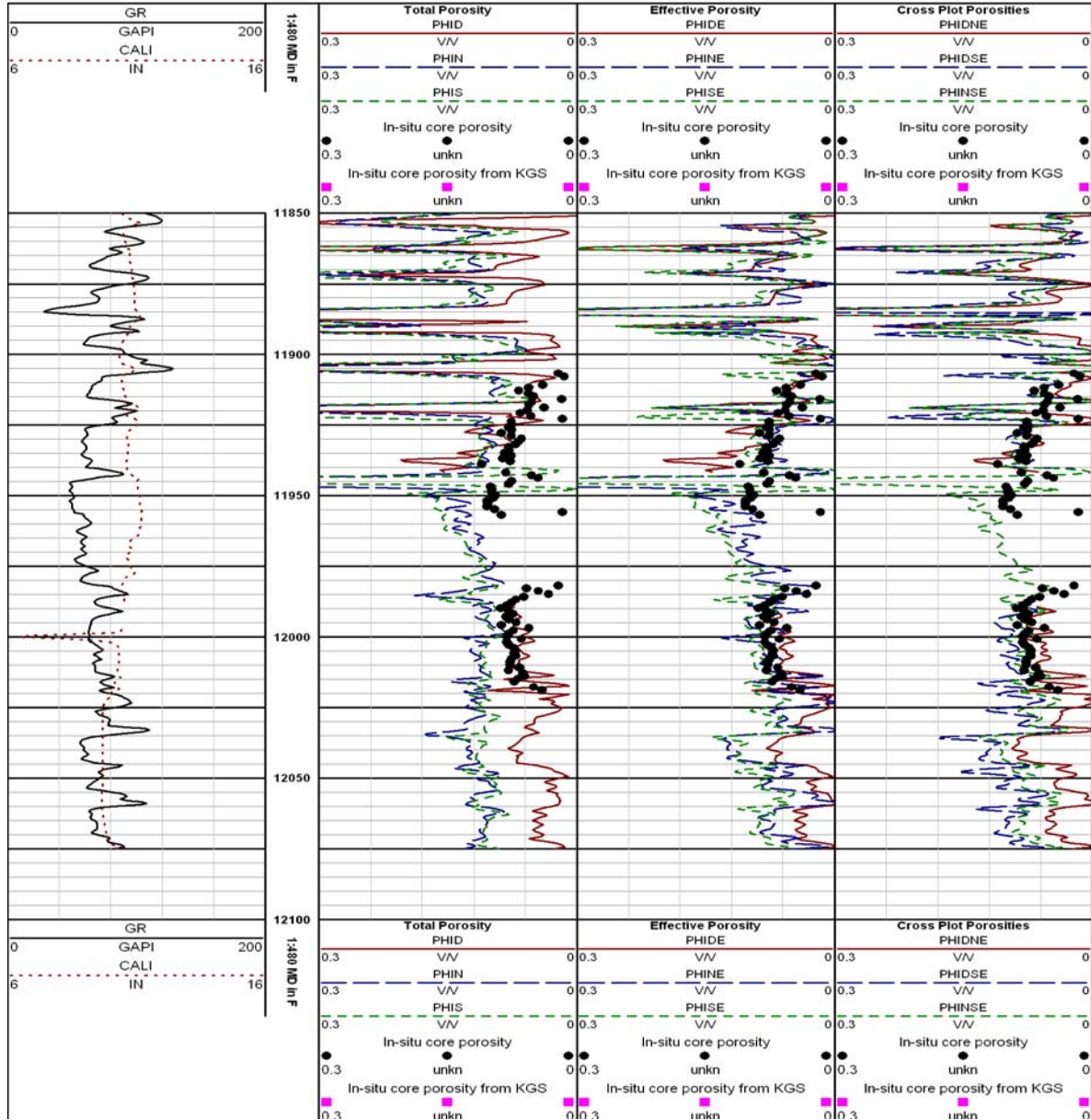


Figure 4.6.8. Example of porosity comparison plot from the standard log analysis interpretation. Track 2 presents Total Porosity comparisons as described above; Track 3 compares the Effective Porosity calculations (shale corrected), and Track 4 the Cross-plot Effective Porosities.

Task 5. Build Database and Web-based Rock Catalog

Subtask 5.1. Compile Published and Measured Data into Database

5.1.1 Task Description

Many prior published studies have reported Mesaverde petrophysical properties but the data are in print form and not digital. To make these previously published data accessible, the data were digitized in Task 3. The goal of this task was to develop code for providing the data on the web. Code was to be written that would provide web-based access to the data and all data were to be available as a complete database.

5.1.2 Methods

Original plans were to present data in a single database format. However, it was found that the nature of publication reporting format and the diverse nature of the data collected was not conducive to the use of a single database. Such a format would have resulted in the data being in what would have been subsections of a master database that would have effectively been individual tables. At two public technical presentations at technical society meetings the audience was polled as to whether they preferred a simple Excel-style workbook format or an Oracle-style database. The response at both surveys was greater than 90% preferred the Excel-style format. An Excel format for data presentation was therefore used.

5.1.3 Results

Over 9 gigabytes of data are available for download from the Project Website (<http://www.kgs.ku.edu/mesaverde/>). In brief these data comprise:

1. Excel workbooks containing tables of data from previous studies;
2. Excel workbooks containing data for all petrophysical measurements performed in this study including:
 - a. 2,102 helium porosity
 - b. 2,075 routine air permeability
 - c. 2,062 *in situ* Klinkenberg permeability
 - d. 2,101 grain density measurements
 - e. 907 electrical resistivity measurements

- f. 301 mercury intrusion capillary pressure analyses
 - g. 150 air-brine critical gas saturation measurements
 - h. 113 pore volume compressibility analyses
 - i. 310 air-brine *in situ* porosity measurements;
3. 550 core slab images representing the range of lithofacies exhibited by the Mesaverde in the six basins studied;
 4. 750 thin-section photomicrographs from 41 wells;
 5. 6,447 feet (2,054 m) of digital core descriptions presented both in Excel workbook format and in graphical core descriptions for 42 wells from 6 basins;
 6. graphical core descriptions of core from 42 wells;
 7. 21 standard wireline log analyses;
 8. 21 advanced wireline log analyses;
 9. pdf files of all technical slide and poster presentations;
 10. pdf files of all technical quarterly reports.

Subtask 5.2. Modify Existing Web-Based Software to Provide Data Access

5.2.1 Task Description

The goal of this task was to provide data in a user-friendly format. It was originally planned that users would be able to investigate relational properties on the Project Website. However, in polling of users at national technical meetings, including two presentation sessions where 50 to 150 people were polled following a technical presentation on the project, users unanimously voted for the site to provide facile download of data and that they preferred to analyze the data on their own computers rather than using a link to the data.

5.2.2 Methods

User friendly web pages were constructed that provide easy selection and downloading of project reports, data, and images. The Project Website was designed to provide what is believed to be the easiest format for data selection and download. The total amount of data exceeds 9 gigabytes precluding a single selection and download option.

5.2.3 Results

A Project Website was constructed that has been in operation since the projection inception. All products of the study are available on the website. Rapid download is provided by packaging of the large datasets in Zip file format. Data are organized by basin, well, and labeled by data type.

Task 6. Analyze Wireline-Log Signature and Log Analysis Algorithms

Subtask 6.1: Compare Log and Core Properties

6.1.1 Task Statement

Wireline log-calculated properties, including porosity, water saturation and lithofacies, will be integrated and compared with core-derived properties including porosity, permeability, lithofacies and capillary pressure-derived water saturation. Possible unique log signatures for lithofacies will be evaluated and differences between standard log-calculated parameters and core properties will be analyzed.

6.1.2 Methods

Comparisons between wireline log-calculated properties and core data were conducted using the basic model calculations described in Subtask 4.6. The log-calculated properties included volume of shale from the gamma ray curve, porosity, absolute permeability, water saturation, and apparent grain density.

The core data used for comparison were the measured *in situ* porosity or permeability for core plug samples collected in this study, as documented in Subtask 4.1, or the calculated *in situ* porosity and permeability based on available routine core analyses after application of the equations given in Subtask 4.1. The 5-digit lithofacies descriptor (Subtask 4.5) was also imported, and correlation between the rock type data curve and the open-hole gamma ray was used to depth shift the core data into alignment with the wireline logs. Depth corrections are all linear shifts, without interpolation of values between core sample depths, and any breaks in the depth shifting were placed at physical gaps in the core coverage. The depth corrections were recorded in the well data spreadsheets posted on the project website. Examples of depth shifted core data are shown in Figures 4.6.7, and 4.6.8.

Cross-plots between various wireline log determined properties and the corresponding core determined properties (e.g. log porosity vs. core porosity) were constructed in Excel using the depth shifted core data and the log properties at those depths. All cross plots are listed in

Table 6.1.1 below, and are included in the Excel files “ConstantM_xplots.xls” posted on the Project Website under each well. These plots were used with the automatic trend fitting functions in Excel to evaluate the strength of correlations between the core determined properties vs. various log derived estimations of the corresponding properties.

Density porosity vs. Core porosity
Effective density porosity vs. Core porosity
Effective density-neutron cross plot porosity vs. Core porosity
Log determined permeability vs. <i>In-situ</i> core permeability
Core porosity vs. Core permeability
Log determined water saturation vs. Log porosity
Log porosity vs. Log permeability

Table 6.1.1 – Core to Log comparison plots included in Excel ConstantM_xplots.xls

6.1.3 Results

Petrophysical log models in Rocky Mountain tight gas sandstone reservoirs generally follow the following four-step sequence:

1. Compute shale volume (V_{shale}) from the gamma ray, neutron-density separation, or spontaneous potential logs. Due to gas suppression of the SP and variable formation water salinities, the SP is rarely used as a V_{shale} indicator in the Mesaverde. Neutron-density separation can be an accurate measure of shaliness, but because proper tool standoff procedures are often not followed the neutron log is often unreliable and this method is not widely used. Most analysts use the gamma ray with some form of a V_{shale} equation. We used a linear model as described in Subtask 4.6; in areas with lithic sandstones and high potassium feldspar contents the sands become radioactive and an alternate model such as the Steiber or Clavier equations may be more appropriate ([Ransom, 1977](#)). Because we do not have a direct quantitative measure of shaliness from cores, the only comparisons between our log V_{shale} computations and cores was comparison to the visual core description rock numbers. For select points with their sections, we were also able to compare the log V_{shale} to total radioactive components as determined by point counting.

2. Compute total and effective porosity from the density, neutron and sonic logs. Total porosity is calculated in the conventional manner with appropriate matrix and fluid assumptions. Our total porosity computations (Subtask 4.6) assumed a constant sandstone matrix, 2.65 g/c³ grain density, 51 μsec/f matrix transit time, and fresh water in the formation. These are typical Rocky Mountain values. Many companies prefer to stop at this point and use the density log determined total porosity for all subsequent calculations.

The main problems with the total porosity computations involve variable matrix properties, especially the matrix density, and the presence of gas in the near wellbore environment. Uncorrected environmental effects on the neutron log plague log evaluations in many areas, particularly when incomplete information was recorded about the tool configuration and corrections applied in the field. Additionally, both the sonic and the neutron logs show a strong shale or clay bound water effect, such that they read porosities that are significantly higher than measured core porosities in shaly intervals. When the total porosity is corrected for clay bound water this is usually called the “effective porosity”, which in sandstone reservoirs is close to the engineering definition of the connected pore volume available for hydrocarbon storage. Both total and effective porosities can be cross-plotted to determine variable matrix property independent porosities, including density-neutron cross-plot porosity and a sonic-neutron cross-plot porosity. The density-sonic cross-plot was also calculated, but was found to be of limited value and usually yields a value similar to the density log alone.

The cross-plots between the various total and effective porosity measures and core porosity were used to evaluate which log measure of porosity is closest to the core determined value, and if the corrections used to calculate effective porosity are appropriate.

3. Compute water saturation by the Archie equation or a shaly sandstone derivative thereof. In this project, we used the Archie method as outlined in Subtask 4.6. Comparisons to routine core analysis water saturations are directionally useful, with the core saturations often validating the magnitude of the changes in the log saturations, but quantitatively are of limited use due to flushing during the coring process. No native state core data were available for comparisons. Some comparisons to theoretical S_{wi} from capillary pressure data were made, but this was not investigated exhaustively due to time limitations.

4. Compute permeability from either porosity or porosity and estimated irreducible water saturation. Our preliminary estimate of permeability from logs used a modified Timur equation as described in Subtask 4.6, which was compared to core data using both depth plots and cross-plots. These plots were useful to evaluate the appropriate coefficients for the Timur equation and the approximate expected range in those coefficients.

6.1.3.1 Log-Core Porosity Comparisons

Log porosity-core porosity comparison plots were created in Excel for all wells with *in situ* core porosity data. Depth plots showing the depth shifted core data and the log calculated porosities were also printed for each well. The log calculated porosities that were compared to the cores included:

- Single porosity comparisons
 - Total density porosity, effective density porosity
 - Total neutron porosity, effective neutron porosity
 - Total sonic porosity, effective sonic porosity
- Cross-plot porosity comparisons
 - Total density-neutron porosity, effective density-neutron porosity
 - Total sonic-neutron porosity, effective sonic-neutron porosity

The total density porosity vs. core and effective density porosity vs. core cross-plots are included in the Excel workbooks for each well described above. Also, the effective density-neutron cross-plot porosity vs. core is included for each well. Examples of these plots are shown below in Figures 6.1.1 through 6.1.3.

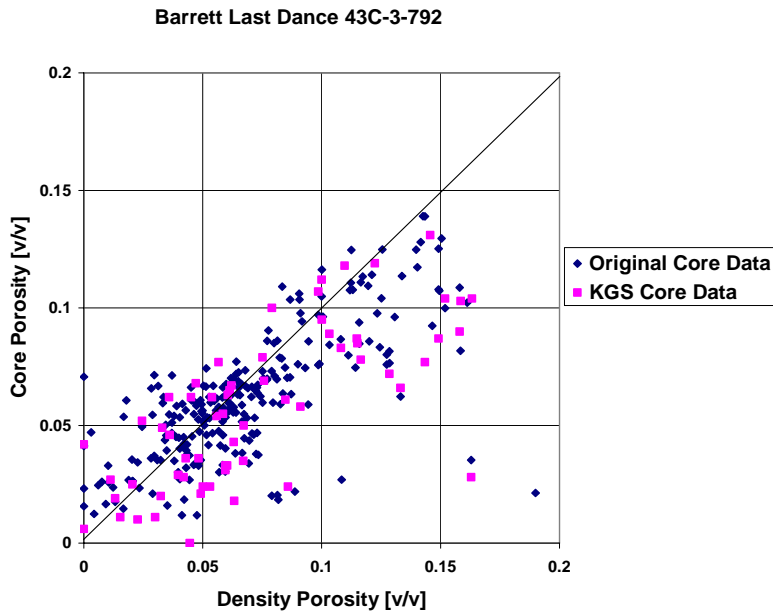


Figure 6.1.1. Total density porosity vs. core porosity, Barrett Last Dance 43C-3-792 well, Piceance basin. 1:1 line shown for reference, not a data regression line.

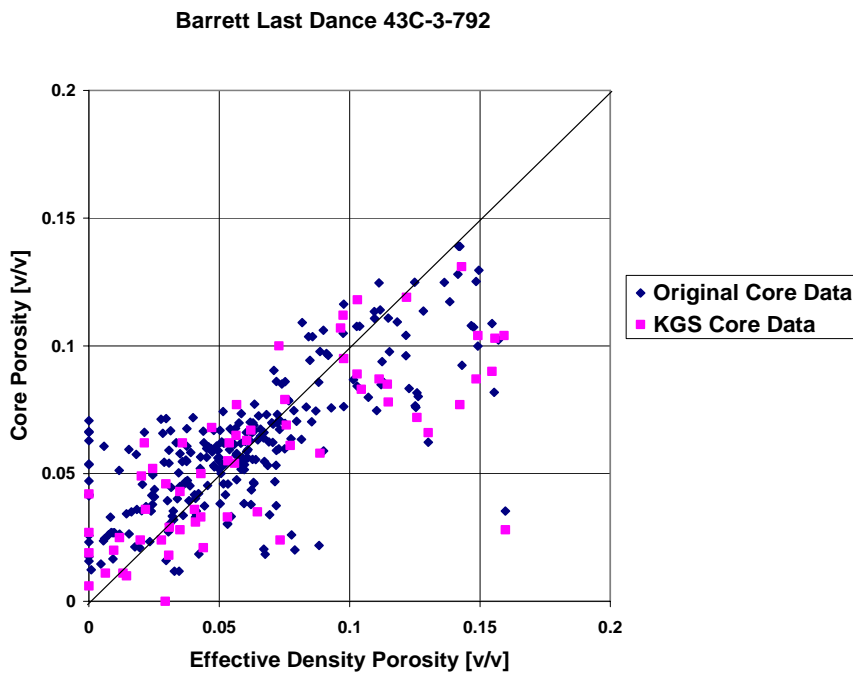


Figure 6.1.2. Effective (shale corrected) density porosity vs. core porosity, Barrett Last Dance 43C-3-792 well, Piceance basin. 1:1 line shown for reference, not a data regression line.

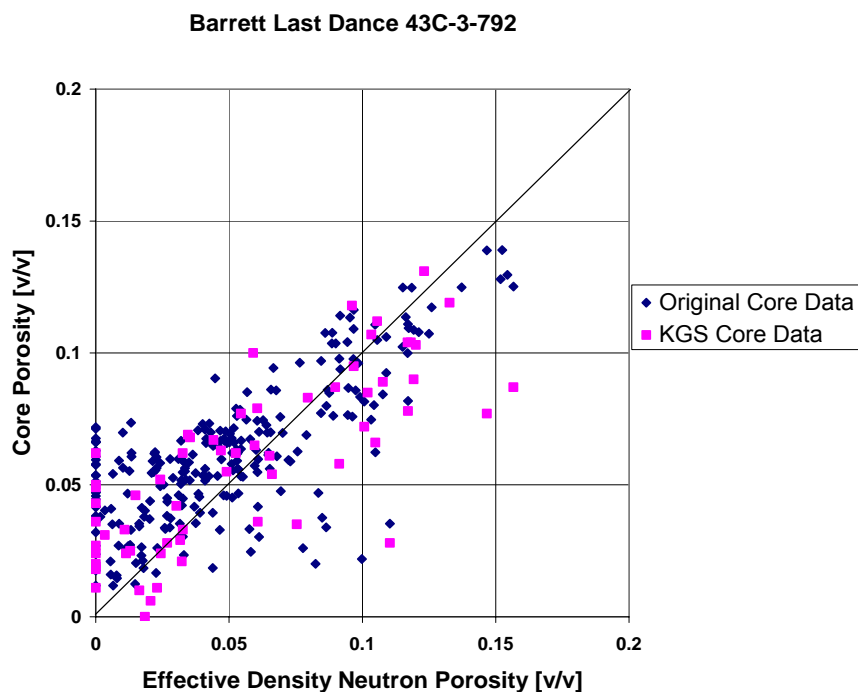


Figure 6.1.3 Effective (shale corrected) density-neutron porosity vs. core porosity, Barrett Last Dance 43C-3-792 well, Piceance basin. 1:1 line shown for reference, not a data regression line.

6.1.3.2 Core Permeability vs. Log Permeability Comparisons

Log derived permeability was calculated using several alternative models and several parameters in each model equation were varied. Comparisons to core permeability were made to validate the approach and assess which methods have the broadest application.

Commonly used permeability estimators from logs are based on the empirical Carman-Kozeny model (c.f. discussion in [Dullien, 1992](#)):

$$K = A * \phi^3 / S^2 \quad [6.1.1]$$

where K is permeability in millidarcies, A is an empirical constant (“the Kozeny constant”), ϕ is porosity, and S is the surface area per unit bulk volume. Because S is not directly measured with any logging device, irreducible or residual water saturation of the formation has been considered a proxy for internal surface area, leading to various empirical equations of the general form:

$$K = A * \phi^B / Swi^C \quad [6.1.2]$$

where A , B , and C are rock type or formation specific variables determined from core data. Timur (1968) summarized the development of these models and proposed a specific model based on 155 sandstone cores we refer to as the “Timur equation”. The particular form of equation 6.1.2 we use in modified form was first published by Schlumberger as a chart in August 1955:

$$K = 250^2 * \phi^6 / Swi^2 = 62,500 * \phi^6 / Swi^2$$

[6.1.3]

This chart was printed in the 1957 through 1979 editions of the Schlumberger chartbooks as Chart E-4 and later as Chart K-2¹. The chart was not cited to any source other than prior general work by Wyllie and Rose (1950), but the specific empirical equation presented has been attributed to Tixier in many texts and secondary references. Chart K-2 was dropped from the 1984 and later chartbooks and replaced by a similar empirical relationship (Chart K-3) with different values for A and B .

We adjusted the values for the exponent B in equation 6.1.2 to achieve the best possible match between the core data and the log estimated permeability. We generally leave the leading constant at 250 and also maintain the value of C as 2 as in equations 6.1.3 and 4.6.9. Swi is calculated at every depth step by comparing the calculated water saturation to the theoretical minimum water saturation determined from an assumed bulk volume irreducible divided by porosity, taking the lesser of the two. The calculated permeability turns out to be relatively insensitive to the choice of bulk volume irreducible, which we set between 0.03 and 0.06 by inspection of each log on a zone by zone basis.

Finding the best value for the exponent B was accomplished visually in a depth plot view (e.g. Figure 6.1.4) without resorting to detailed statistical analysis. For rocks with microdarcy permeability the appropriate value for B was often close to the nominal value of 6 in equation 6.1.3, with higher values driving the calculated permeability towards lower values. Generally

¹ Historical Logging Interpretation Chartbooks from the period 1947-1999, now long out of print, have been compiled in electronic format by the Denver Well Logging Society and are available from the American Association of Petroleum Geologists bookstore and other professional societies.

speaking the log estimates of permeability are within an order of magnitude of the core results, but commonly show greater spread than the core data as illustrated below. The log model is highly sensitive to very small changes in effective porosity which are magnified by the exponent in the model.

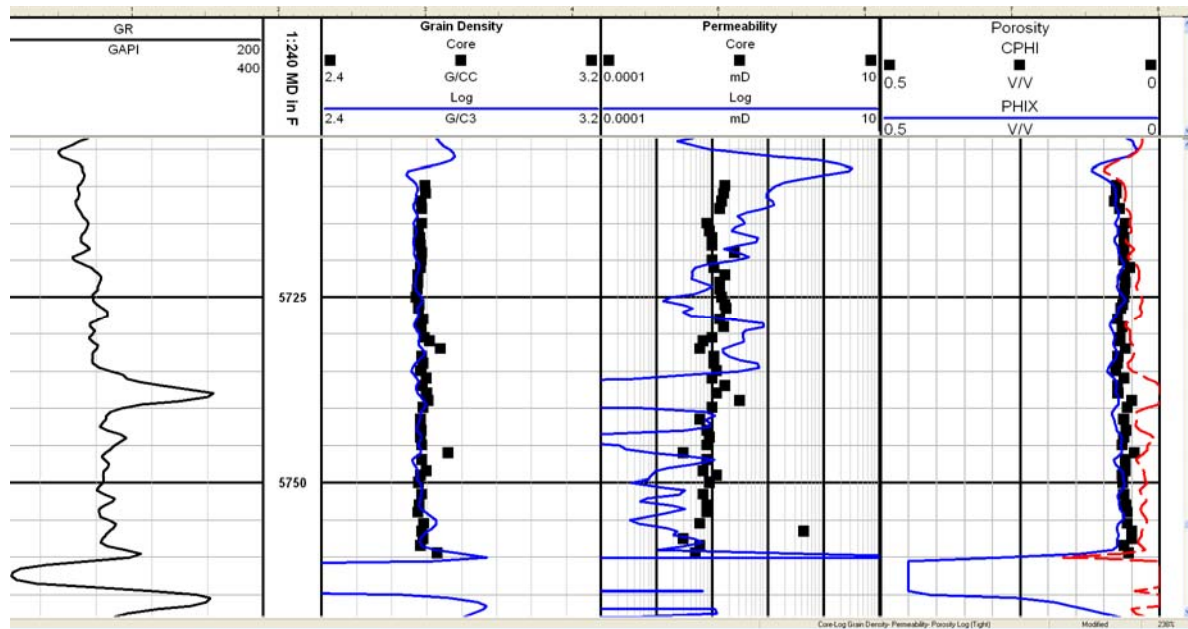


Figure 6.1.4 Depth plot comparison of log determined grain density, permeability, and porosity to core data; Barrett Last Dance 43C-3-792 well, Piceance basin.

Alternative log models, using basin specific porosity-permeability equations derived from the core analyses in this study, are described in Subtask 6.2 below.

6.1.3.3 Permeability from NMR Logs

An alternative approach to determining permeability from conventional porosity and saturation is to use a nuclear magnetic resonance (NMR) log to directly measure total porosity and bulk volume irreducible. To the extent the NMR porosity is lithology independent (it is relatively insensitive to the matrix density and mineralogy as compared to nuclear porosity tools) and the bulk volume irreducible is measured as opposed to estimated, the resulting permeability from a Timur-like equation should be considerably improved.

The two primary equations used to calculate permeability from NMR tools are the Coates equation ([Coates et al, 1991](#)):

$$K_{\text{coates}} = C * (\text{FFI/BVI})^2 \phi^4 \quad [6.1.4]$$

and the SDR (Schlumberger Doll Research) or T2GM equation ([Kenyon et al, 1988](#)):

$$K_{\text{sdr}} = C * T_{2gm}^2 \phi^4 \quad [6.1.5]$$

where the FFI/BVI is based on a T_2 cutoff dividing the NMR spectra into a bound fluid (BVI) and a free fluid (FFI) region, T_{2gm} is the geometric mean of the T_2 spectra, and C is a locally determined constant (not the same between equations). In both cases these are functionally equivalent to the general form proposed by Timur (Eqn. 6.1.2) where FFI/BVI and T_{2gm} serve as the proxy for internal surface area of the rock instead of $1/S_{wi}$. Furthermore, if the porosity exponent is allowed to vary, these equations become sufficiently flexible that they can match a very wide range in rock types and formation permeability.

In this study, only two wells had NMR logs in the public domain. These were the Amoco Siberia Ridge 5-2 in the Washakie basin, and the Williams PA 424-34 in the Piceance basin. NMR logs have not gained wide acceptance in tight gas sandstones, and consequently are infrequently run and the data are not always released to state agencies.

In the case of the Siberia Ridge 5-2, NMR data from a 1998 version Schlumberger CMR tool (CMRT²) and core data were available over one reservoir zone, an Upper Almond marine bar sandstone. These data are shown in Figure 6.1.5. The PA 424-34 was logged with a 2005 Halliburton MRIL³ tool over several thousand feet, with three intervals extensively cored. The middle of these intervals is shown in Figure 6.1.6. In both wells, permeability was calculated by the Coates and SDR models, the vendor calculated permeability is shown, and the conventional log Timur equation permeability is shown. The correspondence between the NMR permeability and core permeability is excellent.

² CMRT is a service mark of Schlumberger.

³ MRIL is a service mark of Halliburton.

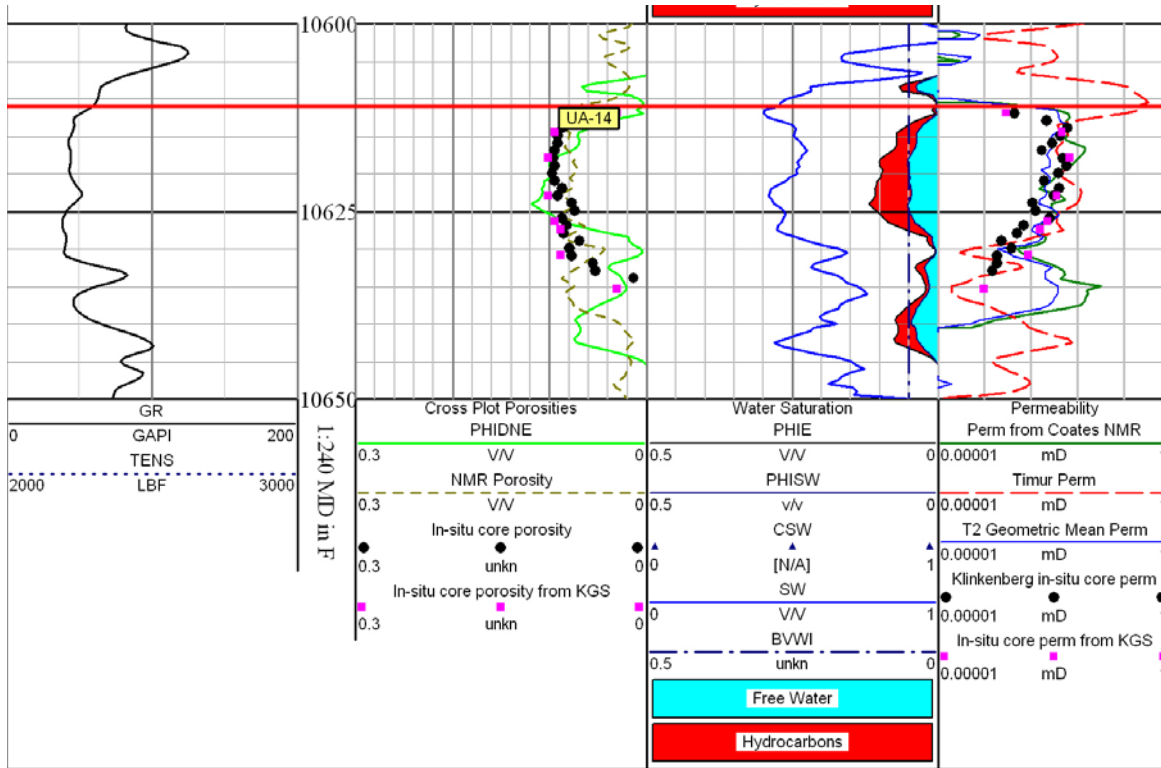


Figure 6.1.5. CMR porosity and permeability comparison to standard density-neutron derived effective porosity (PHIDNE), standard log based permeability (Timur perm), and core data. In this well, all methods compare favorably with all log measures and cores agreeing within less than an order of magnitude of permeability.

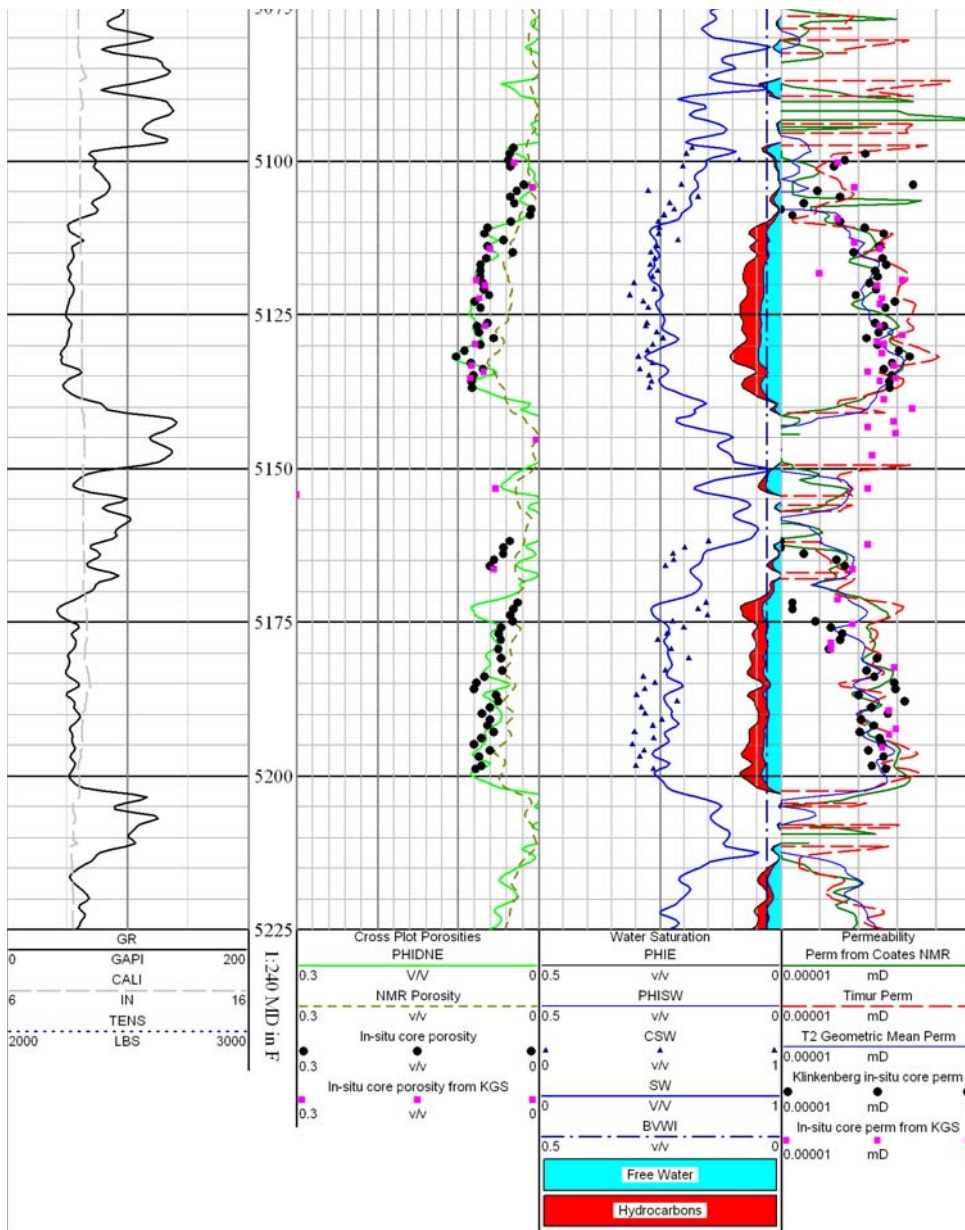


Figure 6.1.6. MRIL porosity and permeability comparison to standard density-neutron derived effective porosity (PHIDNE), standard log based permeability (Timur perm), and core data. Again all methods compare favorably with all log measures and cores agreeing within less than an order of magnitude of permeability, although the Timur equation permeability tends to drift above the core data cloud while the NMR estimates by both the Coates and T2GM (SDR) methods track closely. Note the correspondence in this well between log calculated water saturation and routine core analysis saturation. In this well the NMR porosity undershoots both core and the conventional PHIDNE calculations.

6.1.3.4 Water Saturation

Ground truth data for the log water saturation model was limited. Routine core analysis saturations as reported by operators are of limited value and only provide directional information about saturation trends. The reasons for this include the fact that all of the wells were drilled with water based muds and, although the rocks are very tight and do not invade deeply, they are invaded within the diameter of a standard core. Proprietary special core studies using radioactive tracers at Wamsutter, Jonah, and Pinedale fields have all demonstrated contamination of the cores by mud filtrate. Also, as a high pressured gas reservoir core is slowly retrieved, the gas expansion will try to blow out some of the native fluids which could drive routine water saturations towards lower values. The net result is the as-received saturations are of limited utility for calibrating a log model.

Without special coring procedures, the only other methods for independently verifying log model calculated saturations are: 1) comparison to capillary pressure derived saturations, based on a saturation-height model; or 2) comparison to an independent wireline measurement of saturation such as NMR bulk volume irreducible. Capillary Sw-h models are limited because the hydrocarbon column heights are generally unknown, appear to be greater than appears reasonable when calculated assuming the rocks are in drainage equilibrium, and do not agree with reservoir pressure-elevation plots. Most formation evaluation specialists in the Rockies no longer attempt to fit capillary height models to observed saturation trends, given very limited insight from attempts in the past. One possibility is most of these fields are no longer in primary drainage equilibrium, but instead are on imbibition curves or secondary (or higher) drainage curves as a result of basin uplift, structural tilting, and/or breaching of the original reservoir seals ([Shanley et al, 2007](#)).

Figure 6.1.7 from the deep Piceance basin illustrates the problem very well. On a saturation-porosity cross-plot (“Buckles plot”) most of the points in the well lie along a iso-BVW line close to 0.03. This suggests the entire section is at or near irreducible water saturation, which would imply a very substantial hydrocarbon column height in this well assuming the reservoirs are all connected and in primary drainage equilibrium. Although most, if not all, of these sandstones are gas charged as evidenced by shows and production testing, the pressure data in this basin do not support continuous gas columns thousands of feet thick. If that were the

case, the deviation from a hydrostatic pressure gradient would be greatest at the top of the section and would steadily diminish downwards along a gas density gradient to intersect the hydrostatic line at the free water level, which presumably is close to or below the TD of the well. In fact the observed pressure gradients in this basin, as documented by Nelson (2003a; 2003b; Figure 6.1.8), are generally the opposite, with the deviation increasing downwards and then abruptly returning to hydrostatic if the well was drilled deep enough. If mud weights are taken as an approximate indicator of pore pressure at depth, there are hundreds of well profiles to support this observation.

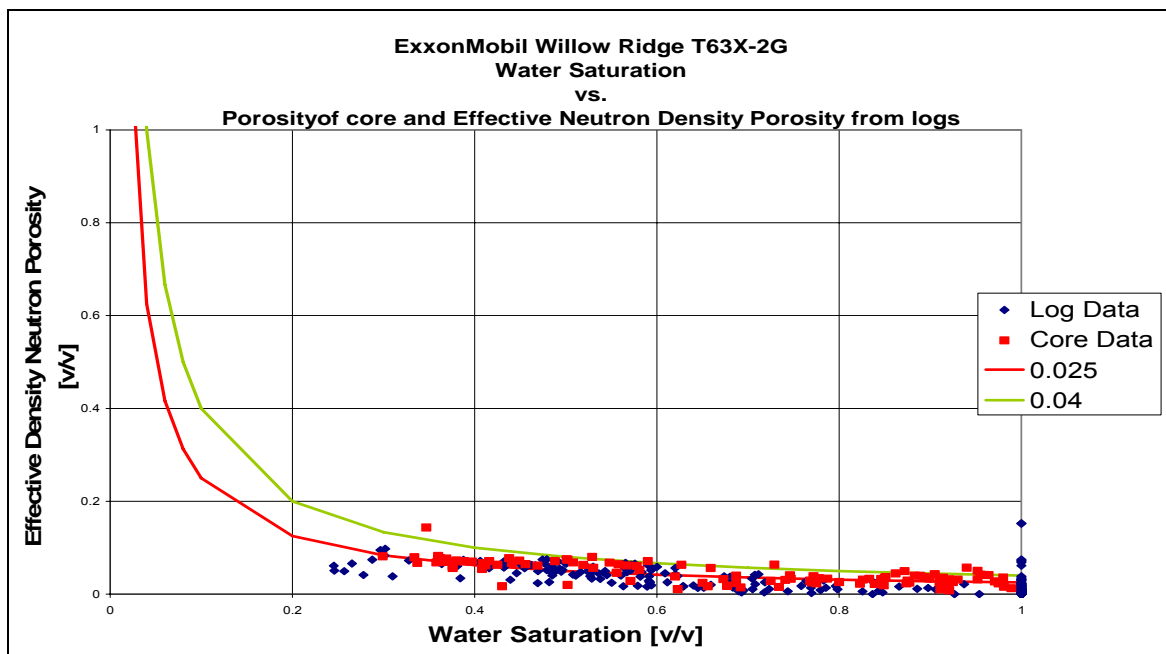


Figure 6.1.7 Water saturation-porosity cross-plot with iso-bulk volume water lines at 2.5% and 4%. Note the close correspondence between log and core data, and both follow a low and roughly constant BVW near bulk volume irreducible.

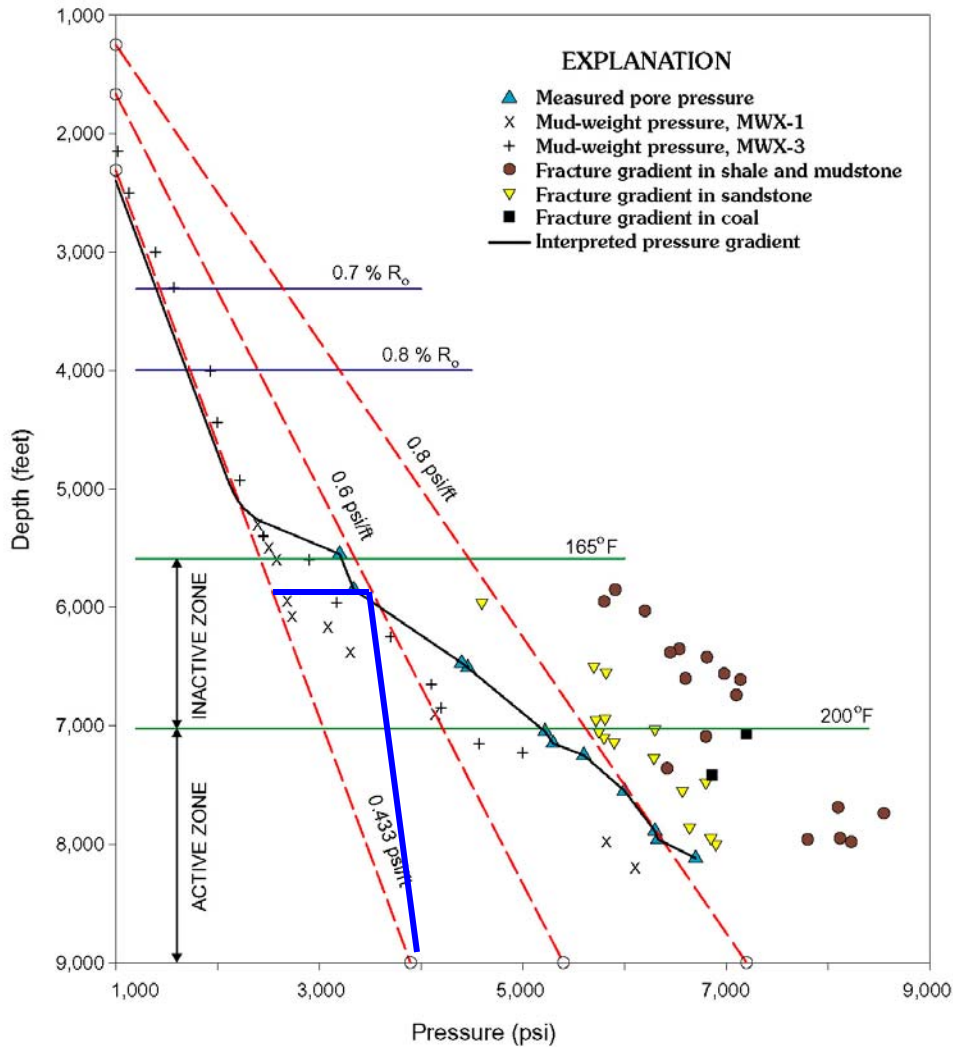


Figure 6.1.8 Pressure-depth plot for the MWX site in Rulison field, Piceance basin, Colorado (from [Nelson, 2003b](#), Fig 8). Assuming top of a single continuous gas column lies at or near 6,000 ft, and a free water level exists near 9,000 ft (~3,000 ft column height), the measured pressure profile should look something like the blue line shown here, with a gas column rising off the water line at the free water level at a slope of 0.1-0.2 psi/ft (depending on exact gas density) and then abruptly returning to the hydrostatic gradient at the top of the gas column. The observed pressure trend in these wells, and many others in the basin, increases downwards towards a value approaching the lithostatic gradient.

6.1.3.5 Rock Type Identification from Log Data

One of the most vexing problems in log analysis of sand-shale sequences is detailed rock type identification given a limited suite of measurements. A broad variety of cross-plots were constructed to investigate relationships between raw and calculated log data and the rock type codes from core descriptions in an attempt to derive algorithms to predict rock types from log data in the absence of core. These included cross-plots of the data against selected digits extracted from the rock type code (e.g. the second digit or the grain-size term) and aggregates of rock types. Based on inspection of the more promising plots, select multivariate plots were constructed to determine if a more detailed multivariate analysis, for example cluster analysis, might improve the predictability. Generally speaking, multivariate methods sometimes work well if broad trends are visible in the single variable comparisons, but if no significant trends are visible in any of the variables considered then combining variables rarely improves the situation.

Due to limited time and the very large size of the database, we were not able to perform a comprehensive data mining that compares all possible combinations of variables. Consequently we used our general knowledge of the system and tool responses to guide the comparisons we investigated. The raw data needed to explore rock typing relationships are available in the individual LAS files on the project website, which include both the depth shifted full 5-digit rock numbers and the individual digits parsed apart as separate curves.

6.1.3.5.1 Gamma Ray and Vshale - Cross-plots of raw gamma ray values and calculated Vshale values, which substitute for rigorously normalized gamma ray logs in this study, were made against the entire rock numbers and against the 2nd digit (grain size term) of the rock number. Depth plots of the rock number in the gamma ray track proved extremely useful for depth shifting the core descriptions and also for general rock type interpretation. However, in a more rigorous quantitative application that attempts to predict the actual rock number or grain size of the sandstones from the gamma ray log, the rock type classes proved to have too much overlap (Figure 6.1.9). Although the gamma ray (Vshale) generally decreases with increasing average grain size, a specific value of the gamma ray is of little use in predicting what the grain size term would be. R2 values of regressions were not significant.

Depth plots illustrating the rock type-gamma ray correlation are included in the well files on the Project Website.

6.1.3.5.2 Deep Resistivity - As with the gamma ray log, plots of deep resistivity against rock number and the 2nd digit of the rock number were made for several wells where by visual inspection we felt correlations were likely. Again a trend of increasing resistivity with increasing grain size is apparent (e.g. Figure 6.1.10), but in all cases the overlap between rock types limits the utility of the relationship.

6.1.3.5.3 Bulk Density, Neutron Porosity, and Photoelectric Factor- The bulk density, neutron porosity, PEF, and combinations thereof were investigated as the most lithology sensitive measurements available in a common logging suite. There were too few sonic logs available in our data set to add this additional curve. Conventional cross-plots of density-neutron, sonic-neutron, sonic-density, and density-PEF proved to be of little value other than to distinguish clean sandstone from shaly sandstone, shale, and carbonate cemented sandstone. Cross-plots were constructed coding for the rock type number, 2nd and 3rd rock type digits, and comparing the density-neutron separation against lithology (Figure 6.1.11). All plots were strongly overlapping and the results were considered inconclusive. No further effort was expended on this task.

File: GR_Five Mile Gulch Unit 3.las
 Plot: KGS_Vshale_vs_CRTnum.plt
 Gross Interval: 2470 to 11020 by 0.5
 Ranges: 10585-10764
 Time:04:01 PM Date: Mon, Apr 13, 2009

Well Name: 5 MILE GULCH UNIT #3
 Plot Name: Vshale
 F

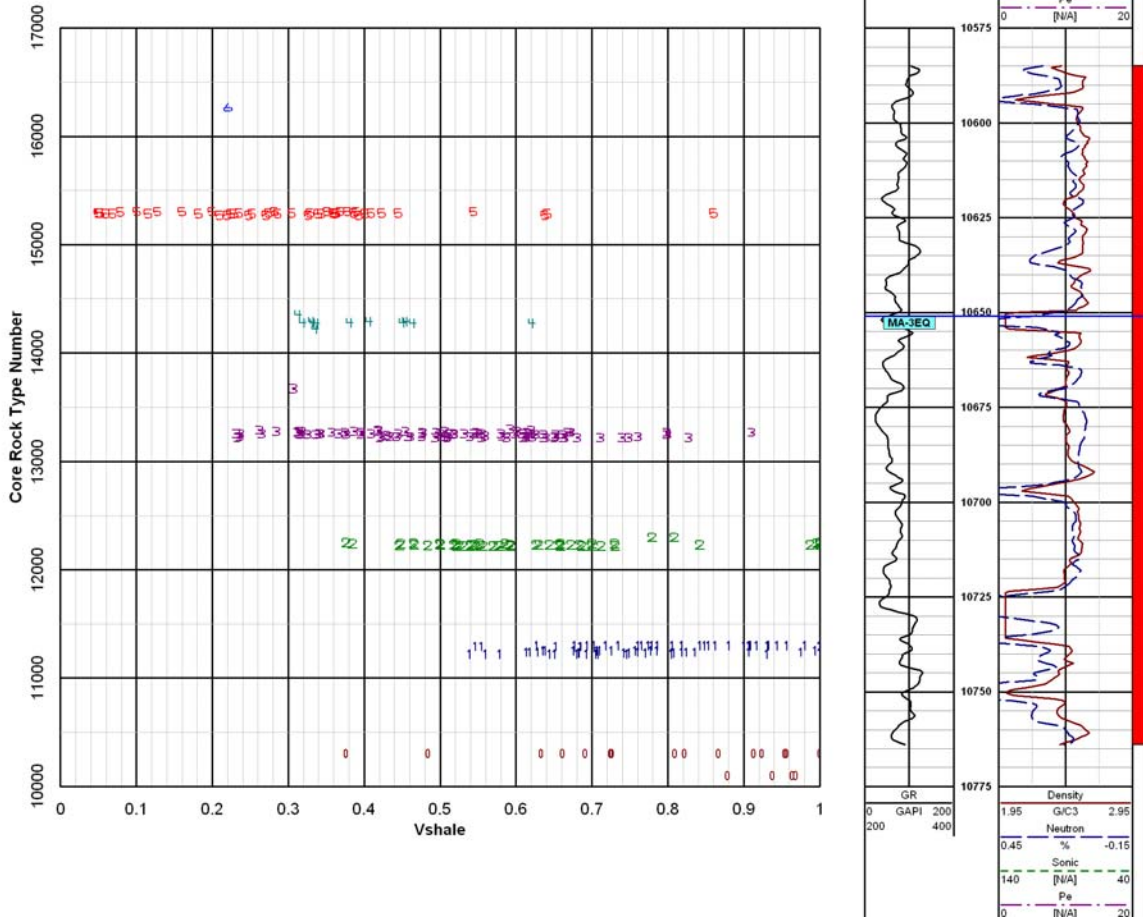


Figure 6.1.9 Volume of shale vs. rock type number. This plot shows the relative progression of rock type number increasing with decreasing Vshale. The trend is largely a function of grain size. The broad overlap between rock type numbers at any given Vshale largely negates the utility of this log indicator for quantitative log analysis (e.g., at Vsh = 0.6 the rock numbers range from 12000 to 15200's).

File: Wind_Monsanto_1-27 Lookout.las Well Name: NO 1 27 LOOKOUT
 Plot: KGS_ILD_vs_CRTnum.plt Plot Name: ILD
 Gross Interval: 30 to 18795 by 0.5 F
 Ranges: 16550-16750
 Time: 03:57 PM Date: Mon, Apr 13, 2009

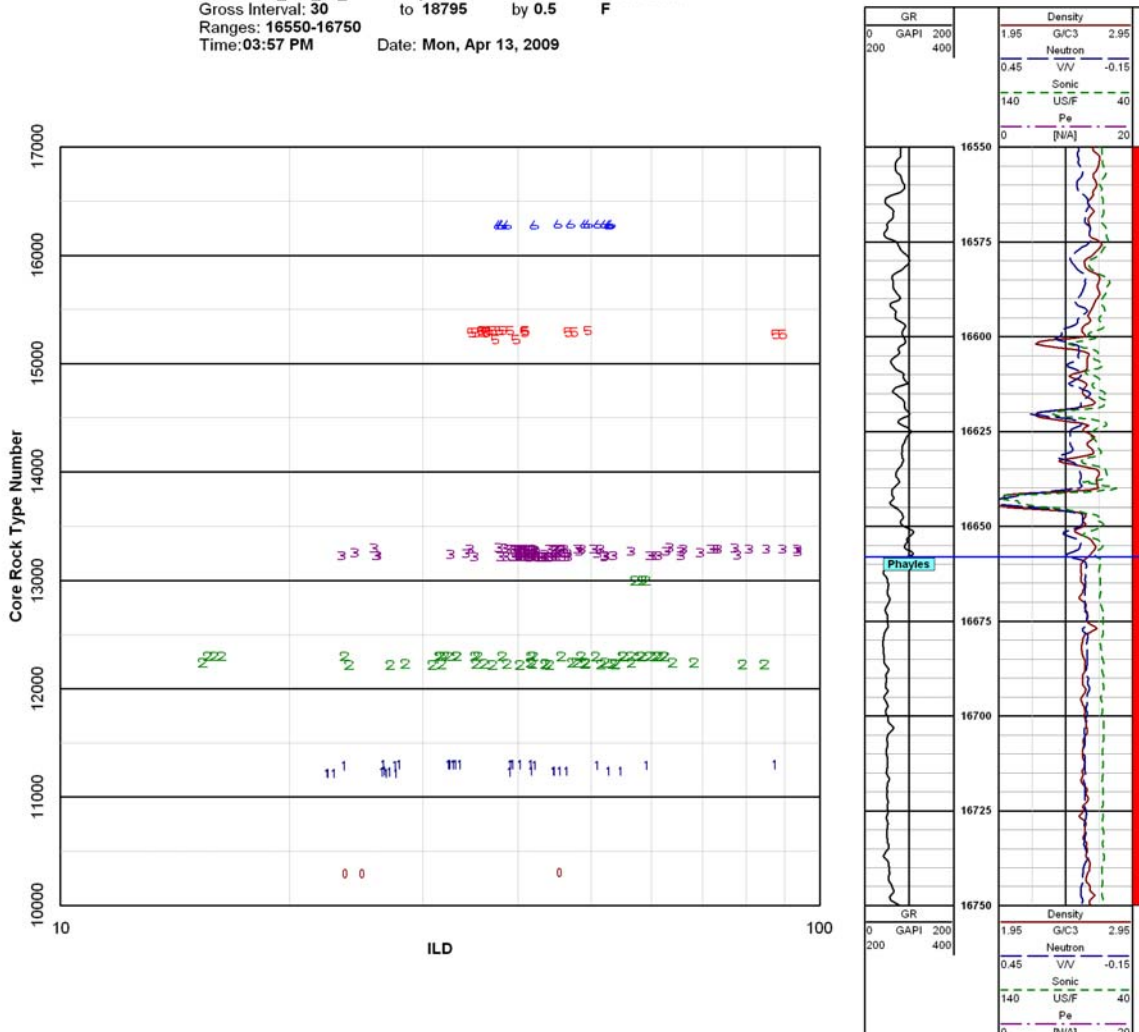


Figure 6.1.10 Log of deep resistivity vs. rock type number. In this case the shalier sands (rock types <13300) dominate the low resistivity (<30 ohmm) sandstones, but over 30 ohmm all rock types are represented at any resistivity.

File: Wind_Monsanto_1-27 Lookout.las
 Plot: KGS_PHI_DN_diff_vs_CRTnum.plt
 Gross Interval: 30 to 18795 by 0.5
 Ranges: 16550-16750
 Time: 03:41 PM Date: Mon, Apr 13, 2009

Well Name: NO 1 27 LOOKOUT
 Plot Name: KGS_PHI_DN_diff_vs_CRTnum
 F

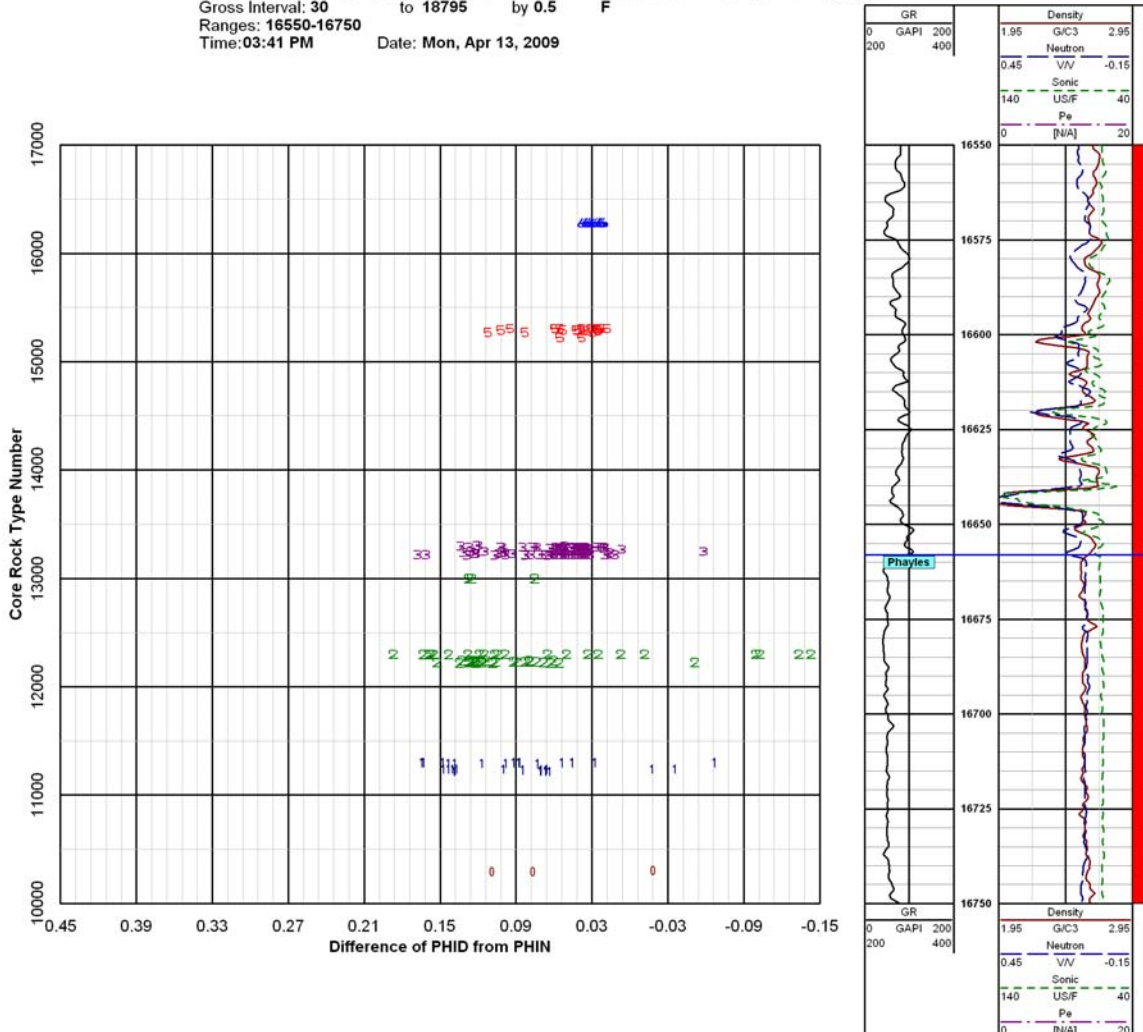


Figure 6.1.11 NPHI - DPHI separation vs. rock type number. Clean sandstones (rock type 14000 and higher) tend to track or show slight gas cross-over effect, but the shalier rock types show a broad range in separation. This is partly due to shale effect on the neutron log, but also to mismatched vertical resolution of the neutron and density tools. Again the utility of this measurement for quantitative rock typing is very limited.

Subtask 6.2: Evaluate Results and Determine Log-Analysis

Algorithm Inputs

6.2.1 Methods

The advanced log analysis procedure builds on the basic analysis methodology outlined under Task 4.6.2, with changes to the saturation and permeability calculations as described below.

6.2.1.1 Porosity Models

We were unable to improve significantly on the porosity models described in Subtasks 4.6 and 6.1. Although a variable grain density vs. rock type model could be a significant improvement over other methods, our inability to find a means to perform detailed rock typing from log data alone precludes this approach. Using a zoned grain density model based on geologic knowledge of the section, tied to core grain densities, offers the best approach for single log porosity determination. For example, in the Washakie basin the upper Almond marine sandstones exhibit grain densities clustered around 2.68 g/c³, while the main Almond fluvial sandstones cluster near 2.65 g/c³. The main problem lies in determining where to draw a boundary between the dominantly fluvial and dominantly marine section, because the uppermost part of the main Almond exhibits transitional characteristics. Most workers in the area draw the break near the top of the uppermost significant coal seam. Similar approaches work in the Mesaverde sections of the Uinta and Piceance basins, separating dominantly marine sandstones with some carbonate cement and higher average grain densities from non-marine sandstone intervals.

Overall, the shale corrected density-neutron cross-plot porosity was the best predictor of *in situ* porosity; however, this method only works with good neutron log data. The sonic-neutron effective porosity was the second best predictor, and it tends to be more robust in areas with poor hole conditions.

6.2.1.2 Permeability Modeling Using Basin-Specific Phi-K Relations

For this analysis each basin was evaluated individually and basin-specific porosity-permeability regression coefficients were determined as described in Subtask 4.1 of this report.

The individual y on x linear regressions are located on the spreadsheet KGS_PermRegression_ByBasin_FINAL.xls on the Project Website and are summarized in the following table:

Table 6.2.1 Porosity-permeability regression parameters determined by basin.

Basin	β_0	β_1
Green River Basin	-4.417	28.102
Piceance Basin	-4.437	26.724
Powder River Basin	-4.515	29.319
Uinta Basin	-4.295	29.905
Wind River Basin	-4.361	17.874
Washakie Basin	-5.027	31.751

Permeability was calculated as a function of effective porosity using the basin specific values for β_0 and β_1 given above:

$$\log_{10}K_{\text{DOE}} = \beta_0 + \beta_1 \cdot \text{PhiE} \quad [6.2.1]$$

where β_1 is the slope of the linear regression, β_0 is the y intercept, and PhiE is porosity in %.

This permutation of the permeability was labeled K_{DOE} in the LAS files.

Alternate methods to estimate permeability from logs include the Timur equation approach that was previously described in Subtask 6.1. This was calculated using two different estimates of water saturation: the first using a basic Archie water saturation equation with constant $m = 1.85$ and $n = 2$; and the second using a variable m in the Archie saturation equation as described below. The change from a constant porosity exponent to a variable exponent based on porosity and water salinity in Archie’s equation changes the resultant water saturation. This in turn changes the computed bulk volume water, but because $BVW = \phi * S_w$ the change tends to be quite small. Therefore the impact on permeability is insignificant.

Comparing the three calculated permeabilities, in the majority of wells the match to core permeability was best using the basin-specific regression equation. Generally speaking the match

is better at high porosities (>9%) than at low porosity. Our estimates of permeability using the Timur equation tend to overshoot the core measured permeability values at porosities <9%. This was true for both the constant m and variable m approaches. Nonetheless, the Timur equation approach is better than using a single equation for the entire Mesaverde such as Eqn. 4.1.4.

6.2.1.3 Advanced Water Saturation Model

Under Subtask 6.1 our basic approach to water saturation calculations was described. We also described the results of our core determined electrical resistivity properties in Subtask 4.4, including the variation in Archie porosity exponent as a function of porosity and water salinity. These observations lead to an improved water saturation methodology that we believe corrects for excess surface conductivity effects that are normally accounted for using some variation of a shaly sand equation, oftentimes requiring estimates of bound water conductivity or cation exchange capacity of the rock that may not be available.

The data described in Subtask 4.4 are broadly summarized as follows:

1. The Archie porosity exponent m decreases with decreasing porosity with a general trend of:

$$m = 0.676 \log \phi + 1.22 \quad [6.2.2]$$

where ϕ is the *in situ* porosity in %. This equation was determined using the 40k ppm salinity dataset, which is the largest single dataset.

2. At any given porosity, the porosity exponent increases with increasing water salinity.
3. At porosity >14% m is capped at a constant value of 1.95. The regression equation above predicts a continuously increasing value for m as porosity increases, but the dataset at high porosities, if analyzed independently, does not support an ever increasing porosity exponent.

Subtask 4.4 discusses several explanations for this behavior, including a dual porosity model where a small fraction of the porosity (<1% porosity) consists of microfractures or sheet like pores that carry current in a parallel circuit to the matrix porosity. The apparent m of this circuit is quite low, approaching 1, whereas the matrix porosity has an m close to the conventional value of 2 for sandstone porosity. An alternative view is there is a small but very electrically efficient surface conductivity effect that is in parallel to the matrix. Because the grain surfaces are extremely highly connected, there is no dead space and electrical efficiency of the surfaces

approach unity. Matrix conductivity, on the other hand, is entirely through brine filled pores and their connecting pore throats and is dominated by the geometry of the pore throats ([Herrick and Kennedy, 1993](#)).

Brine occupying those parts of pore bodies off the shortest conductive paths through the rock carry only small eddy currents or are electrical dead space, reducing the efficiency of the rock in terms of how much of the porosity participates in electrical conduction. The average apparent m of a conventional sandstone reservoir is typically about 2, which is close to the value we observed in higher porosity Mesaverde sandstones. This is equivalent to saying the proportion of the total porosity that participates in electrical conduction is roughly the same as the porosity; for example, if a rock has 10% porosity and an m of 2, 10% of the porosity or 1% porosity conducts the electricity, the rest of the pore space is electrically dead or “inefficient”. The total conductivity of the rock is the sum of the surface conductance and the matrix conductance. Because the surface conductivity effect is ubiquitous and dominates the conductivity at low porosity, but is only a small percentage contributor to conductivity at high porosity, the net effect is the trend of m vs. porosity shown in Figure 4.4.2.

The considerable scatter in Figure 4.4.2 represents natural variability of the pore geometry from one sample to the next, with attendant differences in electrical efficiency. Differences in surface conductivity, because it is a small part of the total conductivity, are secondary. The salinity dependence illustrated by Figures 4.4.6 and 4.4.7 is porosity independent, since the slopes of the log R_w vs. m are highly linear and generally parallel. If Figure 4.4.2 is broken apart by brine salinity range, the entire data cloud is observed to rise as the salinity increases, rather than one end rising faster than the other. These data suggest the impact of the surface conductance on the overall conductance decreases as salinity increases, which is consistent with a roughly constant surface conductance combined with increasing matrix conductivity with increasing brine conductivity.

6.2.1.4 Stepwise Log Analysis Procedure

Fundamentally, this process computes a variable Archie porosity exponent m using the analytical data described in Subtask 4.4, using the 40,000 ppm salinity dataset as the base equation. The procedure begins by computing the formation water resistivity at laboratory conditions, to take it back to the conditions under which the electrical properties were measured.

The Archie porosity exponent is then calculated as a function of porosity and water resistivity. This value of m is substituted into Archie's equation in the usual manner with an $a=1$ to compute water saturation.

No resistivity index data were collected as part of this project and we continue to use $n=2$ for the saturation exponent.

- a. Follow steps in section 4.6.2 up to "Water Saturation Computation".
- b. Correct the formation water resistivity (R_w) at formation conditions, from Pickett plot or produced water analysis, to the equivalent resistivity at laboratory temperature of 75 degF using the Arps equation:

$$R_{w_75} = \frac{R_{WTf}(RESTEMP + 6.77)}{81.77} \quad [6.2.3]$$

R_{WTf} = R_w at formation temperature, in ohmm

$RESTEMP$ = reservoir temperature in degF

- c. Compute the variable Archie porosity exponent m as a function of porosity as follows:

$$\text{ArchieM} = (0.676 * \log \text{PHIX} + 1.22) + (0.0118 * \text{PHIX} - 0.355) * (\log R_{WTf} + 0.758) \quad [6.2.4]$$

This is identical to Eqn 4.4.9. At high porosity (>14%), Eqn 4.4.10 should be substituted.

- d. Compute water saturation by the Archie equation (Subtask 2.6.2.5d) as before (Water Saturation computation in section 4.6.2), except with the variable m , which we labeled as SW_VARM .
- e. Recalculate BVW , $BVWI$, and SWI from the new Sw . (All labeled with $_VARM$ in our dataset)
- f. Using the new Sw and SWI the Timur equation was re-run.

6.2.2 Results

Comparisons of the basic log model and the advanced saturation model are illustrated in Figures 6.2.1 and 6.2.2 below. Depth plots for all wells illustrating both models are included on the Project Website.

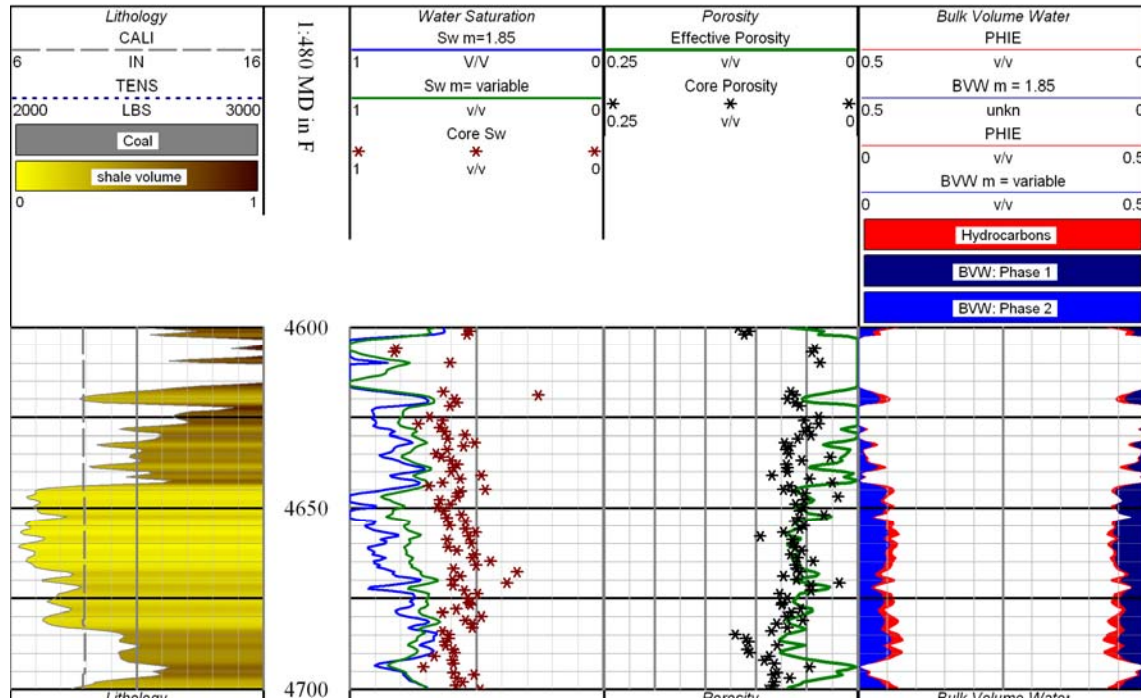


Figure 6.2.1. Example of water saturation computed using the constant $m = 1.85$ model (blue line) and variable m model (green line) in a low porosity, generally wet zone. The separation is greatest in the clean sandstone interval around 4650 ft. The variable m model generally calculates lower water saturations, closer to the routine core Sw's, because the m value is lower than 1.85 at these porosities and formation water salinity.

Overall, the impact of using the variable m model can be summarized as follows:

1. In low porosity rocks, less than 8%, the calculated water saturations are significantly lower and there is more gas in place;
2. The calculated bulk volume water irreducible is reduced slightly;
3. At porosities below bulk volume irreducible, typically 3-5%, there is no difference between the models;

4. At high porosities, over ~9%, the variable m model calculates slightly higher water saturations than the base case model. This is because our base model uses an average m of 1.85, which is centered on 8.5% porosity. Companies that use a conventional value of 2.0 will see an improvement in calculated water saturation at all porosities using our model.
5. This is a simpler approach than most shaly sand models that have been applied to the Mesaverde, and probably yields a more accurate estimate of *in situ* saturations.

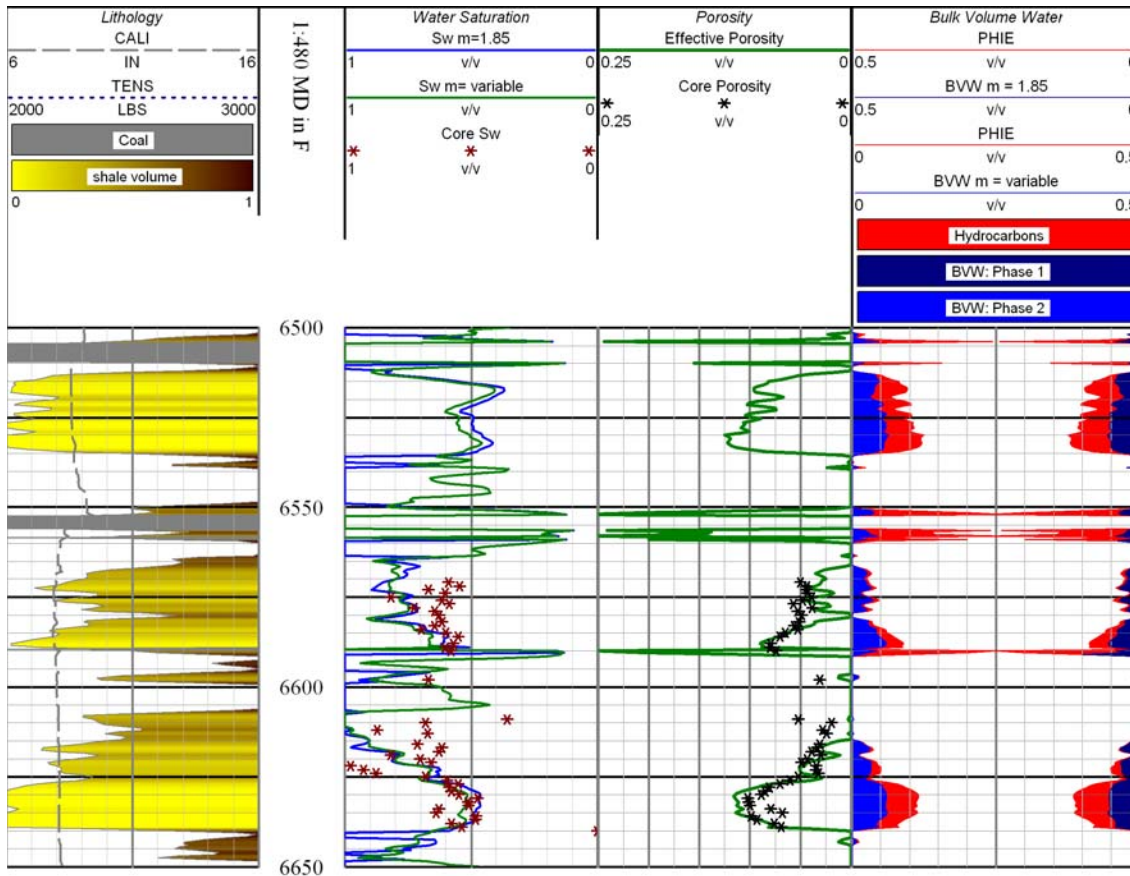


Figure 6.2.2. Example of water saturation computed using the constant $m = 1.85$ model (blue line) and variable m model (green line) in a higher porosity, gas zone. The separation is generally small because at these porosities the calculated m is close to the base case value of 1.85. Where the variable m model computes an $m > 1.85$, the calculated water saturation curves cross and the base case model computes a lower saturation than the variable m model.

Task 7. Simulate Scale-Dependence of Relative Permeability

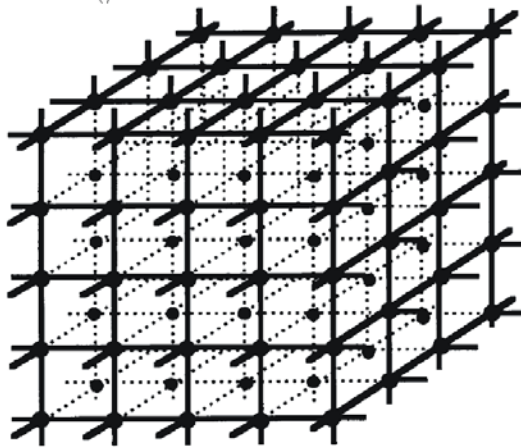
Subtask 7.1. Construct Basic Bedform Architecture Simulation

Models

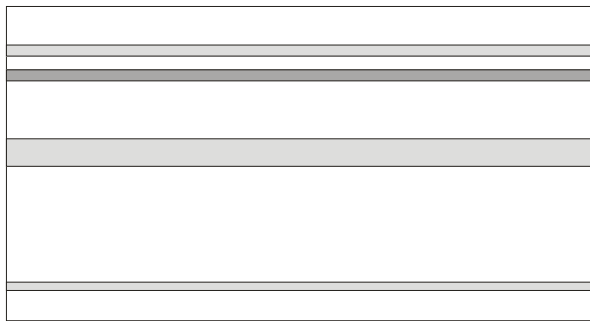
Initial results of critical gas saturation (S_{gc}) measurements and interpretation were presented at the RMAG Gas in Low Permeability Reservoirs Symposium in 2005. This early research led to this study of critical gas saturation. The results of the earlier work and the results found to date in this study were combined and presented in Byrnes (2005) and also Byrnes (2008). A more complete analysis of the critical gas saturation results is presented in Subtask 4.2 of this report.

Most of the S_{gc} data support the commonly applied assumption that $S_{gc} < 0.05$. However, a few heterolithic samples exhibiting higher S_{gc} indicate the dependence of S_{gc} on pore network architecture and scale. Concepts from percolation theory and upscaling indicate that S_{gc} varies among four pore network architecture models: 1) percolation (N_p); 2) parallel ($N_{//}$); 3) series (N_{\perp}); and 4) discontinuous series ($N_{\perp d}$). Analysis suggests that S_{gc} is scale- and bedding-architecture dependent in cores and in the field.

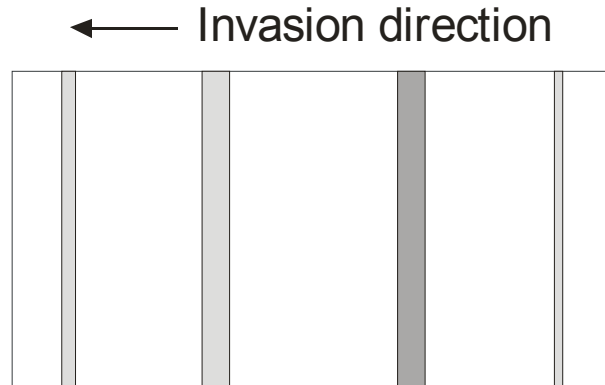
The models suggest that S_{gc} is likely to be very low in cores with laminae and laminated reservoirs and low (e.g., $S_{gc} < 0.03$ - 0.07 at core scale and $S_{gc} < 0.02$ at reservoir scale) in massive-bedded sandstones of any permeability. In cross-bedded lithologies exhibiting series network properties, S_{gc} approaches a constant reflecting the capillary pressure property differences and relative pore volumes among the beds in series. For these networks S_{gc} can range widely but can reach high values (e.g., $S_{gc} < 0.6$). Discontinuous series networks, representing lithologies exhibiting series network properties but for which the restrictive beds are not sample-spanning, exhibit S_{gc} intermediate between N_p and N_{\perp} networks. Figure 7.1.1, presented previously, illustrates the possible bedform models. Equations presented in Section 4.2 provide the basis for predicting critical gas saturation.



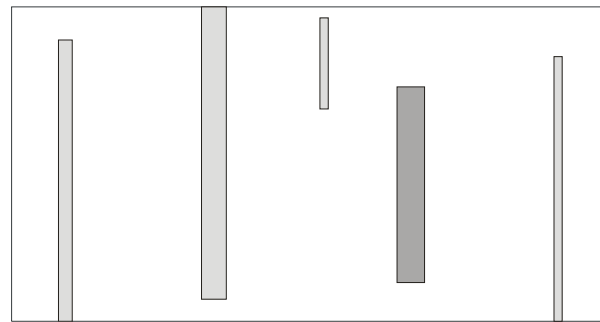
1) *Percolation Network (N_p)* - Macroscopically homogeneous, random distribution of bond sizes, e.g., Simple Cubic Network ($z=6$)



2) *Parallel Network ($N_{||}$)* preferential orientation of pore sizes or beds of different N_p networks parallel to the invasion direction.



3) *Series network (N_{\perp})* - preferential sample-spanning orientation of pore sizes or beds of different N_p networks perpendicular to the invasion direction.



4) *Discontinuous series network ($N_{\perp,d}$)* - preferential non-sample-spanning orientation of pore sizes or beds of different N_p networks perpendicular to the invasion direction. Represents continuum between $N_{||}$ and N_p .

Figure 7.1.1. Conceptual pore network models: 1) percolation (N_p), 2) parallel ($N_{||}$), 3) series (N_{\perp}), and 4) discontinuous series ($N_{\perp,d}$).

Subtask 7.2. Perform Numerical Simulation of Flow for Basic Bedform Architectures

The analysis presented in subtask 4.2 indicates that critical gas saturation can vary widely as a function of bedform architecture. At the well scale the influence of critical gas saturation on relative permeability approaches the simple flow end members (Figure 7.2.1). Massive-bedded sandstones are appropriately represented by the matrix-scale relative permeability with $S_{gc} = 0$ and can be solved numerically. For sandstones with laminae or parallel bedding the numerical solution at the wellbore scale can be represented by the parallel flow solution. Based on the observed vertical change in porosity and permeability in the wells in this study, the relative contribution to flow changes on a vertical scale of as small as 0.5 feet (0.2 m).

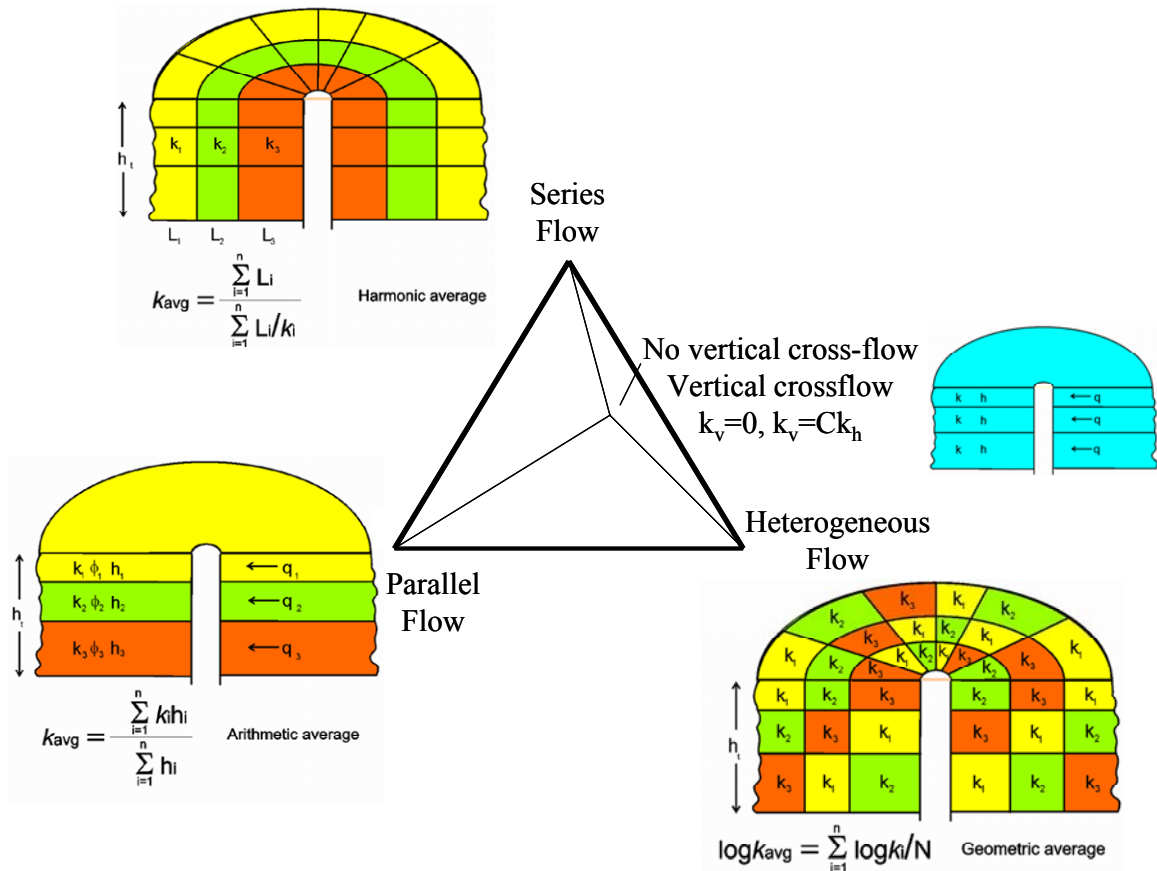


Figure 7.2.1 Flow end members upscaling (averaging) equations.

A key question in assessing low-permeability reservoirs is the distribution of permeability. Assumptions or models of permeability architecture are fundamental to how permeability is modeled and is upscaled from finer-scale measurements. Frequently, in low-permeability rocks, core and log-analysis derived permeabilities are averaged geometrically to obtain an effective average k . Use of the geometric mean k assumes a random distribution of the permeabilities measured. Given that the drainage radius of many low-permeability reservoirs may range from 20 to 40 acres, assumption of a random permeability distribution may not be consistent with the depositional environments. Rather, it is possible these reservoirs exhibit lateral continuity of lithofacies up to hundreds of feet. On this basis, average permeability should be calculated using the arithmetic average equation consistent with a parallel flow model with each bed contributing to total flow as a function of their permeability, saturation, and relative permeability curves. Using this approach, thin, high-permeability beds result in a significant increase in average permeability.

The number of combinations of parallel-bedded permeability architecture is infinite. To provide insight on the relative role of horizontal permeability vertical heterogeneity a series of models were analyzed that parametrically investigate the role of total bed thickness, thin high permeability bed permeability, and vertical permeability. For the parallel flow model the differences in relative permeability result simply in different effective gas permeability values. A simple layer model was constructed using the Computer Modeling Group (CMG) *IMEX* reservoir simulator. The model comprises thirteen layers with total thickness varying from 50 ft to 300 ft (15-91 m) and measured 2 miles (3.2 km) on a side with a single well in the center (Fig. 7.2.2). In all models a single laterally extensive 1-foot (0.3 m) thick bed exists in the vertical center of the model. Average uniform properties of the base model are given in Table 7.2.1.

<i>Parameter</i>	<i>Value</i>
Number of layers	13
Number of cells	1125
Average porosity	8.25%
Avg. in situ Klinkenberg permeability	0.01 mD
Average water saturation	50%
Gas relative permeability at 50% Sw	14%
Horizontal effective gas permeability at 50% Sw	0.0014 mD
Vertical effective gas permeability at 50% Sw	0.00014 mD
Alt model: in situ Klinkenberg permeability	0.001 mD
Alt model: horizontal K_{eg} at 50% Sw	0.00014 mD
Alt model: vertical K_{eg} at 50% Sw	0.000014 mD
Gas gravity	0.55
Reservoir pressure	4000 psi
Bottomhole flowing pressure	1000 psi

Table 7.2.1 Reservoir simulation base model parameters.

Figure 7.2.3 illustrates cumulative recovery from reservoirs with horizontal absolute permeabilities ranging from 0.001mD to 10 mD (1×10^{-6} - $1 \times 10^{-2} \mu\text{m}^2$; corresponding to *in situ* effective gas permeabilities of 0.00014 mD to 1.4 mD; 1.4×10^{-7} – $1.4 \times 10^{-3} \mu\text{m}^2$) and thicknesses ranging from 50 ft to 300 ft (15-91 m). For all models with permeability less than ~ 10 mD ($1 \times 10^{-2} \mu\text{m}^2$) flow is still transient (i.e., pressure transient has not reached the reservoir boundary). Recovery from the 10 mD ($1 \times 10^{-2} \mu\text{m}^2$) reservoir begins to decline after 10 years due to the pressure decline reaching the model boundary (i.e., semi-steady state flow). Reservoirs with permeability equal to 100 mD ($1 \times 10^{-1} \mu\text{m}^2$) begin semi-steady state flow within 2 years.

The influence of a single 1-foot (0.3 m) thick higher permeability bed on cumulative gas production and gas rate from a reservoir with horizontal permeability of 0.01 mD ($1 \times 10^{-5} \mu\text{m}^2$) and vertical permeability of 0.001 mD is shown in Figure 7.2.4. Though the gas produced by the 100 mD ($1 \times 10^{-1} \mu\text{m}^2$), 10 mD ($1 \times 10^{-2} \mu\text{m}^2$) and 1 mD ($1 \times 10^{-3} \mu\text{m}^2$), 1 ft (0.3 m) intervals is significant (720 MMcf (20 MMm³), 640 MMcf (18 MMm³), and 204 MMcf (5.8 MMm³) respectively at 50 yrs; Fig. 7.2.5), the role that a single high-permeability bed plays in draining vertically adjacent low-permeability beds is evident by comparing Figures 7.2.4A and 7.2.4B. Both of these figures show the enhanced recovery due to the presence of a high-permeability thin bed expressed as the ratio of gas produced when a 1-ft thick (0.3 m) high-permeability is present to the gas produced when there is no high-permeability thin bed (shown in 0.01 mD ($1 \times 10^{-5} \mu\text{m}^2$)).

red curves in Fig. 7.2.4). Figure 7.2.4A shows the ratio including the recovery from the thin bed and Figure 7.2.4B shows the ratio of incremental gas excluding the recovery from the thin bed and thus shows only the increased recovery from the vertically adjacent reservoir.

For the case where the thin bed has the same permeability as the adjacent reservoir (0.01 mD), the ratio is 1.0. If the thin bed has a permeability of 0.1 mD ($1 \times 10^{-5} \mu\text{m}^2$), the increased recovery ratio including the thin-bed contribution is 1.16 for a 50-ft thick (15.2 m) reservoir, but the incremental ratio is only 1.01-1.02. Gas recovery progressively increases with increase in the horizontal permeability of the single, 1-ft thick (0.3 m) high-permeability bed when the bed permeability exceeds ~ 1 mD ($1 \times 10^{-3} \mu\text{m}^2$). Increase in recovery increases with increasing permeability of the thin bed and decreasing thickness of the reservoir. Increase with increasing thin-bed permeability is due to an increase in the ability of the bed to drain vertically adjacent reservoir and carry the gas to the wellbore. Comparison of pressures in the upper- and lower-most beds with the central, thin, high-permeability bed shows that pressure differences are generally less than 5 psi (34.52 kPa) and are not greater than 20 psi (138 MPa) at any given time during production for thin-bed permeabilities from 0.01 mD to 100 mD (1×10^{-4} - $1 \times 10^{-1} \mu\text{m}^2$). The relative increase with decreasing reservoir thickness is therefore not due to inability to drain beds that are vertically farther from the thin bed, but rather is due to the limited flow capacity of the bed. Gas flow into the high-permeability bed and the ability of the bed to flow that gas to the wellbore control what the pressure is in the thin bed, which in turn controls total flow. Where the thin bed only has to drain up and down 25 ft (7.6 m) in comparison to 150 ft (45.7 m), gas flow and pressure decrease are greater and the thin bed is able to effectively drain the vertical beds and in so doing decrease in pressure and thereby reach out laterally to a greater distance from the wellbore.

For the vertical permeabilities present in the models shown ($k_v = 0.001$ mD; $1 \times 10^{-6} \mu\text{m}^2$), the primary rate limiting constraint is the thin-bed permeability. But the ability of gas to flow vertically to the high-permeability thin bed is controlled by vertical permeability (k_v). Figure 7.2.5 shows the dependence of incremental cumulative gas (cumulative gas less gas from thin bed) on the vertical permeability for a reservoir with 0.01 mD ($1 \times 10^{-4} \mu\text{m}^2$) and a 1-ft (0.3 m) thick bed of 10 mD ($1 \times 10^{-2} \mu\text{m}^2$). The ratio of incremental cumulative gas decreases with increasing reservoir thickness, however, the ratio for each reservoir thickness is relative to the recovery at that thickness without the thin bed. Ratios are lower for the 300-ft (91 m) thick than

the 50-ft (15.2 m) thick reservoir, but recovery from the 300-ft (91 m)thick reservoir is six times greater. For all reservoir thicknesses, increase in k_v greater than 1×10^{-5} mD ($1 \times 10^{-8} \mu\text{m}^2$) does not significantly increase recovery over that obtained at $k_v = 1 \times 10^{-5}$ mD ($1 \times 10^{-8} \mu\text{m}^2$). With k_v decrease below 1×10^{-5} mD ($1 \times 10^{-8} \mu\text{m}^2$) recovery decreases with decreasing vertical permeability down to 1×10^{-8} mD ($1 \times 10^{-11} \mu\text{m}^2$). For k_v below approximately 1×10^{-8} mD ($1 \times 10^{-11} \mu\text{m}^2$), recovery is similar to recovery for vertical permeability equal to zero, that is, there is no cross-flow and no vertical drainage to the high-permeability thin bed.

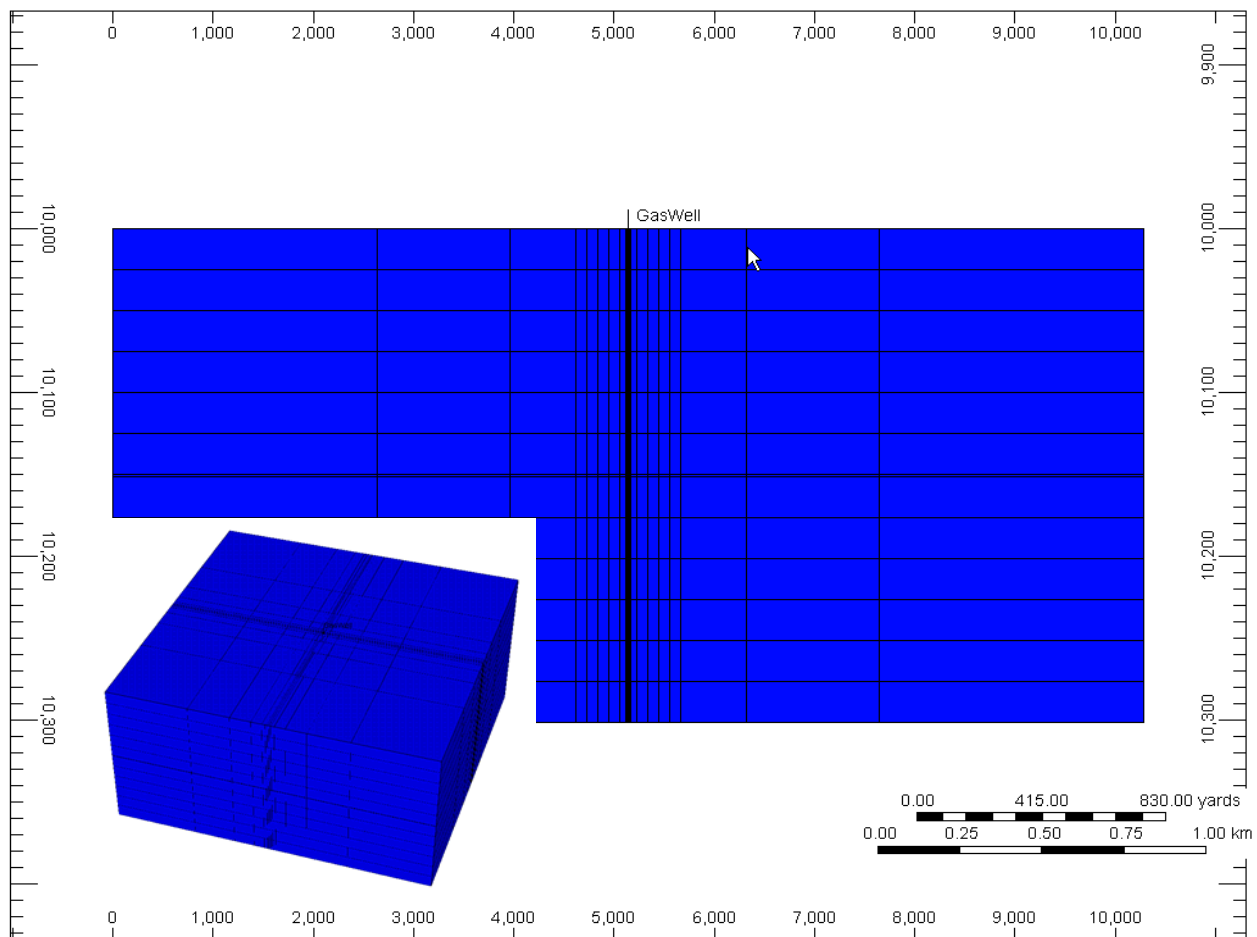


Figure 7.2.2. Computer Modeling Group (CMG) *IMEX* simulation model used to examine influence of reservoir properties. Large cross-section shows cut-away to vertical layer with gas well. Inset 3-D figures shows the central locations of the gas well.

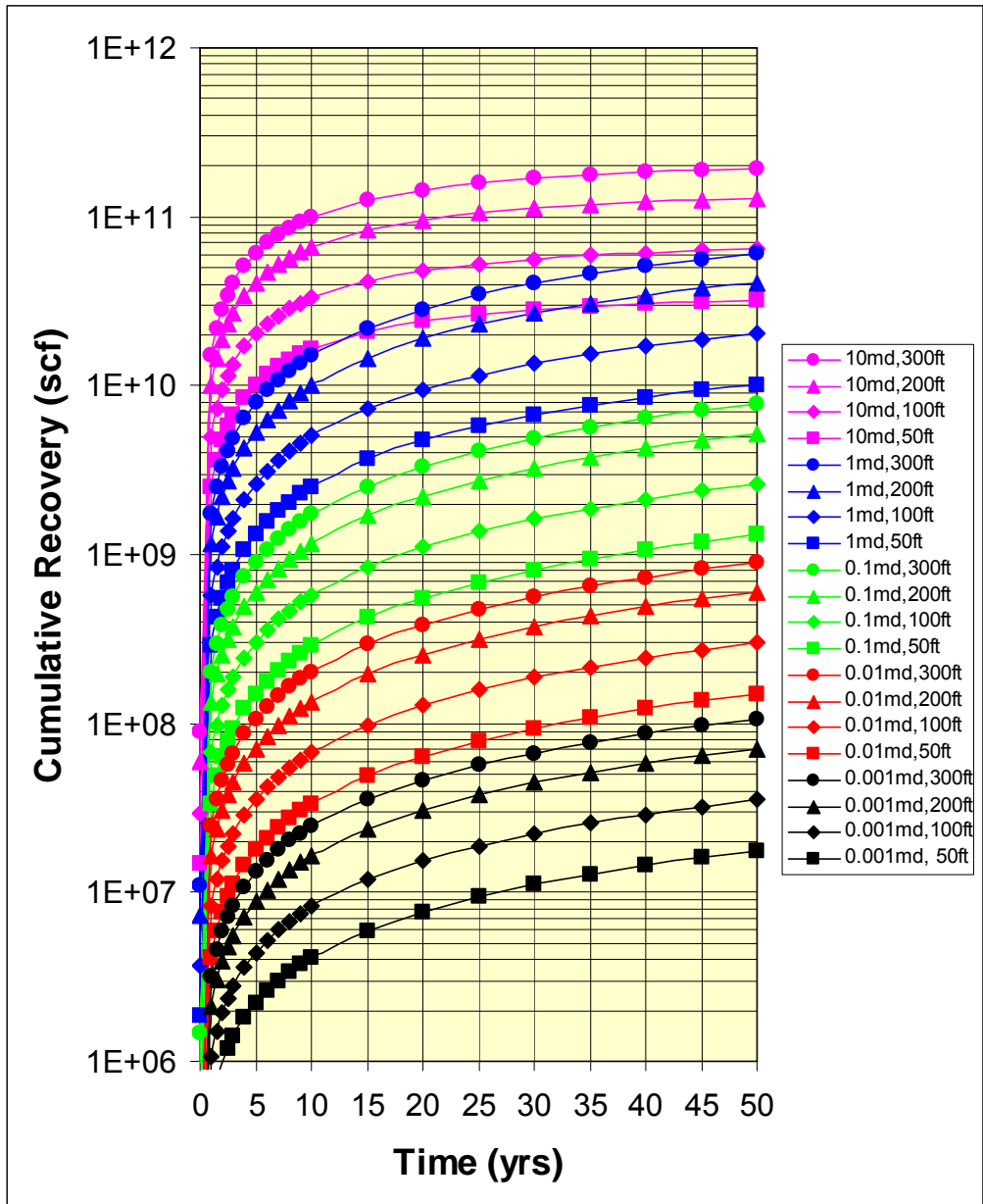


Figure 7.2.3. Cumulative gas recovery versus time for models with varying absolute permeability and thickness. Legend lists absolute permeability values but model results reflect recovery from reservoirs at $S_w = 50\%$ and $k_{rg} = 0.14$. Recovery also reflects assumed initial pressure of 4,000 psi, flowing bottom-hole pressure of 1,000 psi and gas properties consistent with a 0.55 gravity gas. $1E + 06 = 1$ MMCF; $1E + 09 = 1$ BCF; $1E + 12 = 1$ TCF.

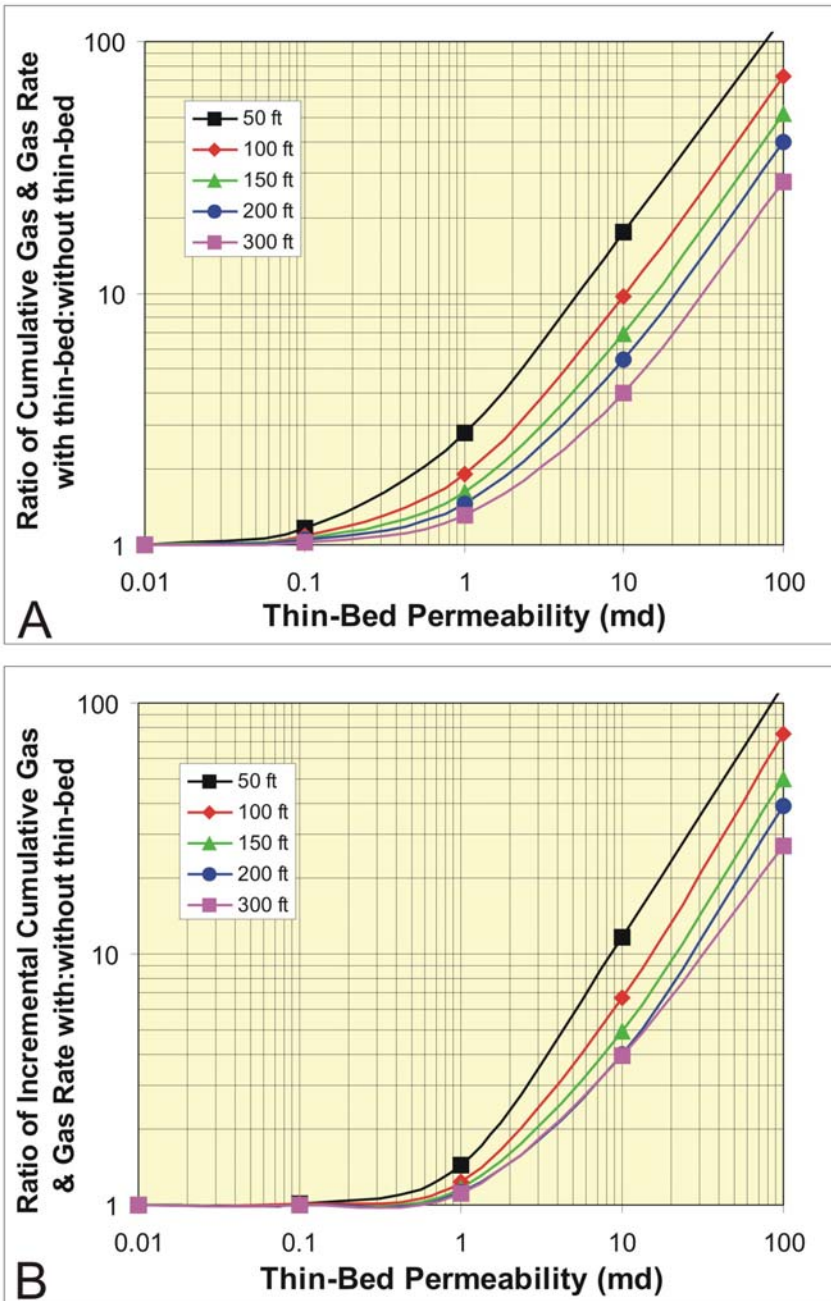


Figure 7.2.4. Cross-plot of the ratio of the cumulative gas and gas production rate with a 10-mD thin bed (1-ft thick) to the cumulative gas or gas rate without the thin-bed including the gas recovered from the thin bed (A) and excluding the gas recovered from the thin bed representing only the additional gas produced from beds vertically adjacent to the high-permeability thin bed (B). Cumulative recovery increases significantly with increasing thin-bed permeability above ~1 mD and with decreasing total reservoir thickness.

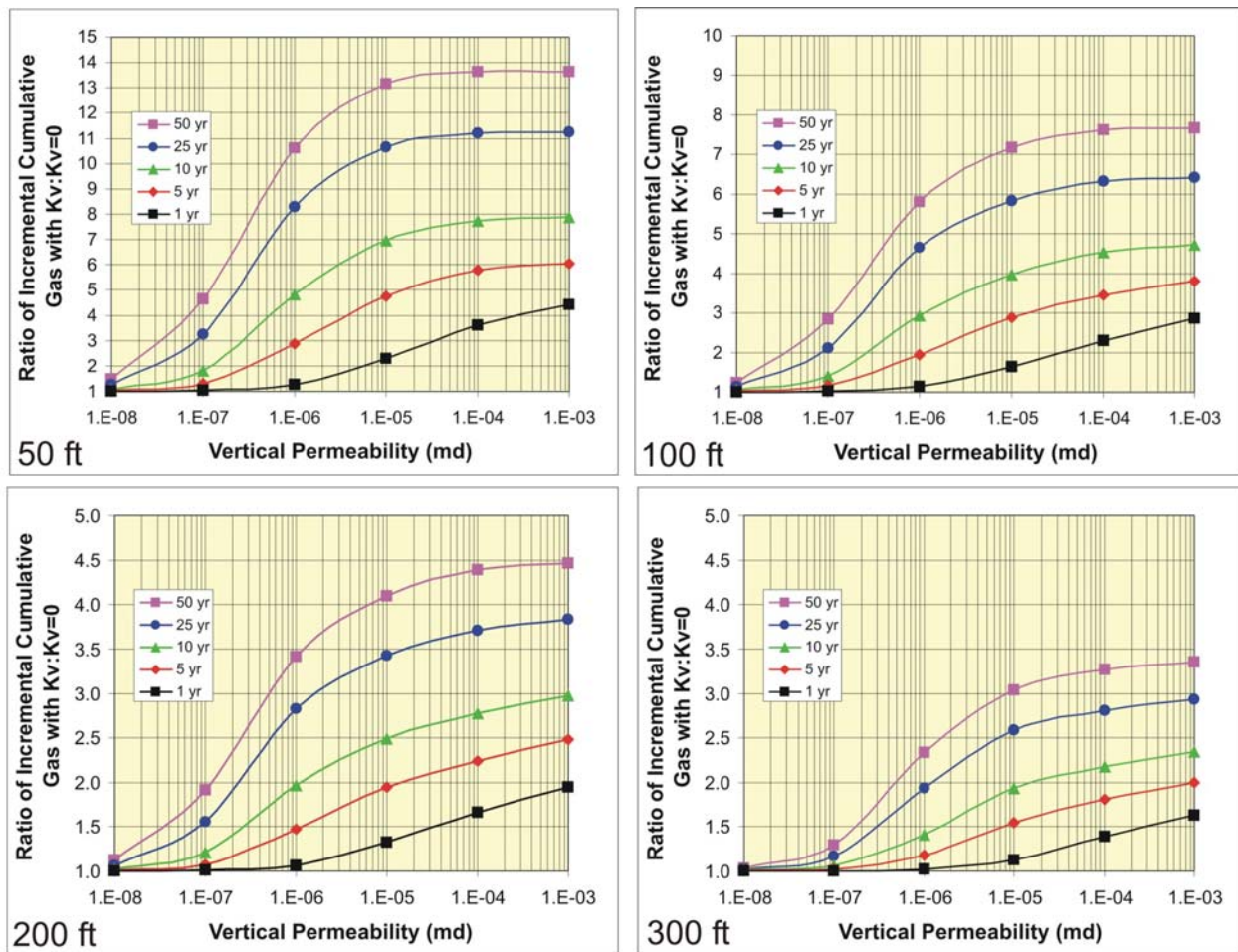


Figure 7.2.5. Cross-plot showing the dependence of incremental cumulative gas (cumulative gas less gas from thin bed) on the vertical permeability (k_v) for a reservoir with 0.01 mD and a 1-ft thick bed of 10 mD. Ratio increases with increasing time with expansion of drainage radius. The ratio decreases with increasing reservoir thickness, however, the ratio for each reservoir thickness is relative to the recovery at that thickness without the thin bed. For all reservoir thicknesses increase in k_v greater than 1×10^{-5} mD does not significantly increase recovery over that obtained at $k_v = 1 \times 10^{-5}$ mD. With k_v decrease below 1×10^{-5} mD recovery decreases with decreasing vertical permeability down to 1×10^{-8} mD. For k_v below approximately 1×10^{-8} mD recovery is similar to recovery for vertical permeability equal to zero, that is, no cross-flow and no vertical drainage to the high-permeability thin bed.

Task 8. Technology Transfer

Subtask 8.1 Technology Transfer

8.1.1 Early Project Presentations

A PowerPoint presentation was created at the start of the project to present to companies to inform them of the project and request participation through contribution of newly-obtained fresh core. Presentations were made to major and independent gas industry companies to solicit participation directly through contribution of core and indirectly through review of activities and methods and results. Presentations were made in both Denver, CO and Houston, TX. Examples of companies for whom presentations were made include: Exxon-Mobil, BP Exploration and Production, Inc., Shell Exploration and Production, EnCana, Williams Gas, Bill Barrett Corp.

Companies that contributed core to the study as a result of these solicitations and in-house presentations included Kerr-McGee, Bill Barrett Corp., Williams Rocky Mountain Production Company, Exxon-Mobil, Shell Exploration and Production, and EnCana. Many other companies expressed interest in the project but were unable to contribute cores due to logistical constraints.

8.1.2 Project Website

The Mesaverde Project Website was initiated at the project inception. All reports, including technical quarterly reports were posted on the website, and available for download, when they were submitted. The Mesaverde Project Website (<http://www.kgs.ku.edu/mesaverde>) includes all project findings, copies of project reports and presentations in PDF format.

8.1.3 Technical Presentations

Technical presentations at professional society meetings were an integral part of the project. The following lists the technical presentations followed by abstracts. Beyond technical society meeting presentations, technical talks were presented at several society lunches but are not reviewed here.

A technical paper was prepared as part of the proceedings of the American Association of Petroleum Geologists Hedberg Conference on Understanding, Exploring and Developing Tight

Gas Sands held in Vail, Colorado. The paper explores models for critical gas saturation. Aspects of the paper are presented in Section 4.2. An abstract of the paper follows. A publication resulting from this presentation is included in the AAPG Hedberg Conference volume #3 published in May 2008.

A combined oral and poster presentation was presented at the Rocky Mountain Section meeting of the American Association of Petroleum Geologists at Snowbird, UT in October 6-9, 2007. The presentations covered results of Mesaverde properties measured as of mid-2007. In addition, residual saturation measurement trends were used to interpret properties of the Ericson and a talk was presented on this subject. The talk and poster are posted on the Project Website.

A technical talk was presented at the American Association of Petroleum Geologists Annual Meeting in San Antonio, TX, April 20-23, 2008. This was the last overview presentation that attempted to cover all aspects of the project.

Three technical presentations were given at the American Association of Petroleum Geologists Rocky Mountain Section/Colorado Oil & Gas Association Regional Meeting in Denver, CO, July 7-10, 2008. Each of these were in-depth analyses of particular tasks that were of special interest to the E&P community. All presentations are on the Project Website and abstracts are presented below.

A one-day workshop was presented at AAPG Annual Meeting in Denver, CO in June, 2009. This workshop completed the technology transfer phase of the project.

Abstracts of technical presentations and posters

Issues with gas relative permeability in low-permeability sandstones

Alan P. Byrnes

Review of gas relative permeability (k_{rg}) studies of low-permeability sandstones indicates they can be modeled using the Corey equation, but scarce data near the critical-gas saturation (S_{gc}) limit k_{rg} modeling at high water saturations. Confined mercury injection capillary pressure and coupled electrical resistance measurements on Mesaverde sandstones of varied lithology were used to measure critical non-wetting saturation. Most of these data support the commonly applied assumption that $S_{gc} < 0.05$. However, a few heterolithic samples exhibiting higher S_{gc} indicate the dependence of S_{gc} on pore network architecture. Concepts from percolation theory and upscaling indicate that S_{gc} varies among four pore network architecture models: 1) percolation (N_p), 2) parallel ($N_{//}$), 3) series (N_{\perp}), and 4) discontinuous series ($N_{\perp d}$). Analysis suggests that S_{gc} is scale- and bedding-architecture dependent in cores and in the field.

The models suggest that S_{gc} is likely to be very low in cores with laminae and laminated reservoirs and low (e.g., $S_{gc} < 0.03$ - 0.07 at core scale and $S_{gc} < 0.02$ at reservoir scale) in massive-bedded sandstones of any permeability. In cross-bedded lithologies exhibiting series network properties, S_{gc} approaches a constant reflecting the capillary pressure property differences and relative pore volumes among the beds in series. For these networks S_{gc} can range widely but can reach high values (e.g., $S_{gc} < 0.6$). Discontinuous series networks, representing lithologies exhibiting series network properties but for which the restrictive beds are not sample-spanning, exhibit S_{gc} intermediate between N_p and N_{\perp} networks.

Consideration of the four network architectures lends insight into the complications of heterogeneous lithologies at differing spatial scales and underscores the difficulty of upscaling laboratory-derived relative permeabilities for reservoir simulation. Analysis also indicates that for some architectures capillary pressure and relative permeability anisotropy may need to be considered.

Reference: A. P. Byrnes, 2008, Issues with gas relative permeability in low-permeability sandstones; in K. Shanley, W. Camp, and S. Cumella (eds.), Understanding, exploring, and developing tight-gas sands – 2005 Vail Hedberg Conference, Chapter 5, p. 1-14.

Regional petrophysical properties of Mesaverde low-permeability sandstones

Alan P. Byrnes, John C. Webb, and Robert M. Cluff

Petrophysical properties of Mesaverde Group tight gas sandstones for the range of lithofacies present in the Washakie, Uinta, Piceance, Upper Greater Green River, Wind River, and Powder River basins exhibit consistent trends among lithofacies. Grain density for 2400 samples averages 2.654 ± 0.033 g/cc (± 1 sd) with grain density distributions differing slightly among basins. The Klinkenberg gas slip proportionality constant, b , can be approximated using the relation: $b(\text{atm}) = 0.851 k_{ik}^{-0.34}$. Regression provides a relation for *in situ* Klinkenberg permeability (k_{ik}): $\log k_{ik} = 0.282 \phi_i + 0.18 \text{RC2} - 5.13$ ($\pm 4.5X, 1$ sd), where ϕ_i = *in situ* porosity, and RC2 = a size-sorting index. Artificial neural network analysis provides prediction within $\pm 3.3X$. Analysis of 700 paired samples indicates 90% of all samples exhibit porosity within 10%-20%. Permeability exhibits up to 40% variance from a mean value for 80% of samples.

Capillary pressure (P_c) exhibits an air-mercury threshold entry pressure (P_{te}) versus k_{ik} trend of $P_{te} = 30.27 k_{ik}^{-0.44}$ and wetting-phase saturation at any given P_c (for $350 < P_c < 3350$ psia air-Hg) and k_{ik} of $S_w = A k_{ik}^{-0.138}$ where $A = -13.1 * \ln(P_{c_{\text{air-Hg}}}) + 117$. Accuracy of the Leverett J function is poorer. Hysteresis P_c analysis indicates that residual nonwetting-phase saturation to imbibition (S_{rnw}) increases with increasing initial nonwetting phase saturation (S_{nwi}) consistent with the Land-type relation: $1/S_{nwr} - 1/S_{nwi} = 0.8 \pm 0.2$. Electrical resistivity measurements show that the Archie cementation exponent (m) decreases with decreasing porosity (ϕ) below approximately 6% and can be generally described by the empirical relationship: $m = 0.95 - 0.092 \phi + 0.635 \phi^{0.5}$. These relationships are still being investigated. The Mesaverde Project website is (<http://www.kgs.ku.edu/mesaverde>).

Presented at AAPG Rocky Mountain section meeting, Snowbird, UT, October 2007

What's the matter with the Ericson?

Robert M. Cluff, Keith W. Shanley, and John W. Robinson

The Cretaceous Ericson Formation is a clean, quartzose, blanket-like sandstone that underlies the prolific gas productive Almond Formation across the entire Washakie basin. The top several tens of feet of the Ericson are penetrated by most wells drilled to the Almond in order to obtain sufficient rathole for logging the entire Almond. Thus there are thousands of Ericson tests, most of which show one or more indications of gas pay in the Ericson. These include 6-11% porosity, resistivity >50 ohm-m, neutron-density gas cross-over, and mud log shows. Archie saturation calculations using appropriate R_w values almost universally indicate "gas pay" comparable to overlying Almond sands. And yet, nearly all attempts at completions in the Ericson result in extremely high water volumes with minor amounts of gas, typically <250 MCFD. Commercial production has only been found over large structural closures, such as Canyon Creek Field, or in very small areas of a few wells on regional dip.

Our interpretation is the Ericson displays all the characteristics of a watered out gas reservoir. Log and mud log gas shows are probably real, and calculated Archie saturations are approximately correct. Completion attempts demonstrate the Ericson is at or near residual gas saturation (S_{gr}), with high relative permeability to water and low relative permeability to gas. Consequently the Ericson appears to have formerly been a widespread gas reservoir, perhaps filled over most of the central Washakie basin in the early Tertiary, but with late Tertiary uplift and structural re-adjustment of the Wamsutter Arch gas spilled laterally to the east and west leaving a residual gas column behind. The stratigraphic continuity of the Ericson and high net: gross offers little in the way of internal trapping opportunities, so producible gas only occurs in local stratigraphic traps and over structural closures. The remaining enigma was the very high S_{gr} , by our calculations 40 to 60% in most wells, which we find to be fully consistent with recently determined imbibition capillary pressure behavior in tight sandstones.

What's the matter with the Ericson is that it has leaked it's gas charge, and what was left behind is not producible. Clearly gas charge is widespread and there is sufficient reservoir quality for the sands to produce, so exploration efforts should focus on structural closures, subtle fault traps, or large stratigraphic pinchouts. Minor producible accumulations will continue to be

found by serendipity, but they will be difficult to recognize because S_{gr} is so high and is close to initial saturation conditions.

Presented at AAPG Rocky Mountain section meeting, Snowbird, UT, October 2007

Lithofacies and petrophysical properties of Mesaverde tight-gas sandstones in Western U.S. basins

Alan P. Byrnes, John C. Webb, Robert M. Cluff, Daniel A. Krygowski, and Stefani D. Whittaker

The relationship between core and log petrophysical properties and lithofacies sedimentary characteristics is examined in Mesaverde Group tight gas sandstones from forty cores in the Washakie, Uinta, Piceance, Upper Greater Green River, Wind River, Sand Wash, and Powder River basins. Fine-grained intervals of the Mesaverde Group are dominated by mudstones and silty shales; burrowed, lenticular and wavy-bedded very shaly sandstones; and wavy-bedded to ripple cross-laminated shaly sandstones. Sandstone intervals are dominated by ripple cross-laminated and cross-bedded, very fine to fine-grained sandstones, low-angle cross-laminated to planar laminated sandstones, and massive sandstones. For all lithofacies undifferentiated in the cores sampled, grain density averages 2.654 ± 0.033 g/cc (error of 1 std dev) with grain density distributions differing slightly among basins. Core porosity ranges from 0-25%, averaging 7.2% (n=2200). *In situ* Klinkenberg permeability ranges from 0.0000001-200 millidarcies, averaging 0.002 millidarcies. Characteristic of most sandstones, permeability at any given porosity increases with increasing grain size and increasing sorting though this relationship is further influenced by sedimentary structure and the nature of cementation. Multivariate and neural network permeability prediction methods exhibit a standard error of 4.5X and 3.3X respectively. Capillary threshold entry pressure and pore characteristic length are well correlated with permeability. Archie cementation exponent, m, can be modeled with a dual porosity matrix-fracture model with m approaching one as porosity approaches zero. Critical gas saturation is generally less than 5% but increases with increasing bedform complexity. Integration of wireline log analysis and core petrophysical relationships provides guidelines and equations for predicting reservoir properties. The Mesaverde Project website is (<http://www.kgs.ku.edu/mesaverde>).

Presented at AAPG Annual meeting, San Antonio, TX, April 2008

Evidence for a Variable Archie Porosity Exponent “m” and Impact on Saturation Calculations for Mesaverde Tight Gas Sandstones; Piceance, Uinta, Green River, Wind River, and Powder River Basins

Robert M. Cluff and Alan P. Byrnes

We have measured formation resistivity factors (FRF = R_o/R_w) on a suite of over 300 Mesaverde core plugs at four brine salinities. The samples range from 0.2 to 23.4% porosity at 4000 psi NCS (ϕ_i); *in situ* permeability from 2 nD to 206 mD; and brine salinities of 20K, 40K, 80K and 200K ppm NaCl. The Archie porosity (cementation) exponent “m” was calculated from the measured FRF assuming $a=1$. Our prior unpublished work in the Washakie basin focused on sample sets with porosity > 6% and found only a weak correlation between m and porosity. Present data show strong curvature where m decreases as a function of porosity below approximately 8% porosity. The relationship can be described by the dual porosity model or equally well by a family of logarithmic equations: $m = a \ln(\phi_i) + b$ (m standard deviation = 0.13). The zero porosity intercept b increases with salinity from 1.25 (20K ppm) to 1.57 (200K ppm). The coefficient “ a ” decreases (0.23 to 0.16) with increasing salinity.

The impact of these relationships is that m decreases with decreasing porosity and salinity. At low porosity (<6%) m is significantly less than the nominal constant value of 1.85 commonly assumed for tight gas sandstones. Above 12% porosity, m is best characterized by a constant value of 1.9 ± 0.05 . Therefore there is more gas in these rocks at low porosities than a constant m model predicts, but there is little impact on saturation calculations at high porosity.

Presented at AAPG Rocky Mountain Section meeting, Denver, Colorado, July 2008

Lithofacies and Petrophysical Properties of Mesaverde Tight-Gas Sandstones in Western U.S. Basins

John C. Webb, Robert M. Cluff, Daniel A. Krygowski, Stefani D. Whittaker, Alan P. Byrnes

The relationship between core and log petrophysical properties and lithofacies are examined in Mesaverde Group tight gas sandstones from forty cores in the Washakie, Uinta, Piceance, Greater Green River, Wind River, and Powder River basins. Fine-grained intervals of the Mesaverde Group include mudstones and silty shales; burrowed, lenticular and wavy-bedded very shaly sandstones; and wavy-bedded to ripple cross-laminated shaly sandstones. Sandstone intervals include ripple cross-laminated and cross-bedded, very fine to fine-grained sandstones, low-angle cross-laminated to planar laminated sandstones, and massive sandstones. Lithofacies were deposited in nonmarine, paludal, marginal marine and marine environments. For all lithofacies undifferentiated in the cores sampled, grain density averages 2.654 ± 0.033 g/cc (error of 1 std dev) with grain density distributions differing slightly among basins. Core porosity ranges from 0-25%, averaging 7.2% (n=2200). In situ Klinkenberg permeability ranges from 0.0000001-200 millidarcies, averaging 0.002 millidarcies. Characteristic of most sandstones, permeability at any given porosity increases with increasing grain size and increasing sorting though this relationship is further influenced by the nature of cementation. Cements include chlorite, ML-IS and illitic clays, quartz, calcite and ferroan calcite. Capillary threshold entry pressure and pore characteristic length are well correlated with permeability. Archie cementation exponent, m , can be modeled with a dual porosity matrix-fracture model with m approaching one as porosity approaches zero. Critical gas saturation is generally less than 5% but increases with increasing bedform complexity. Integration of wireline log analysis and core petrophysical relationships provides guidelines and equations for predicting reservoir properties. The Mesaverde Project website is (<http://www.kgs.ku.edu/mesaverde>).

Presented at AAPG Rocky Mountain Section meeting, Denver, Colorado, July 2008

Capillary Pressure Properties of Mesaverde Group Low-Permeability Sandstones in Six Basins, Western U.S

Alan P. Byrnes, D. Osborn, A. Knoderer, O. Metheny, T. Hommertzheim, J. Byrnes, R. Cluff, J. Webb

Drainage and imbibition air-mercury capillary-pressure properties were measured for over 100 Mesaverde Group low-permeability sandstones from six basins in the Western U.S. For all samples pore-throat diameters associated with the threshold-entry pressure (P_e) decrease with decreasing permeability. Stressed (4,000 psi NCS) and unstressed curve pairs for high-permeability cores ($k > 1$ mD) are nearly identical; however, with decreasing permeability the unstressed and stressed threshold-entry pressures diverge. For all sample pairs this difference is greatest at P_e and the curves converge with decreasing wetting phase saturation (S_w) down to 30-50%, where the stressed curve crosses the unstressed curve and thereafter exhibits 0-5% lower S_w with increasing capillary pressure.

The data imply that confining stress exerts principal influence on the largest pore throats and that pore throats accessed at non-wetting phase saturations below approximately 50% are not significantly affected by confining stress. This is consistent with these smaller pores comprising pore space within pore bodies or in regions of the rocks where stress is not concentrated.

Hysteresis analysis involving three drainage-imbibition cycles for each sample were performed on 32 samples and residual mercury saturation was measured for over 200 samples where initial mercury non-wetting phase saturation (S_{nwi}) corresponds to conditions near “irreducible” wetting-phase saturation (S_{wirr}). The relationship between S_{nwi} and residual non-wetting (S_{nwr}) saturations following imbibition is well characterized by a Land-type relationship: $1/S_{nwr}^* - 1/S_{nwi}^* = C$, where $S_{nwr}^* = S_{nwr}/(1-S_{wirr})$, $S_{nwi}^* = S_{nwi}/(1-S_{wirr})$, and $C = 0.55$ at $S_{wirr} = 0$. Results indicate that residual non-wetting phase saturations (e.g., gas) are high following imbibition.

Presented at AAPG Rocky Mountain Section meeting, Denver, Colorado, July 2008

Subtask 8.2. Reporting Requirements

A project overview including project objectives and improvements to be achieved, project schedule and budget was presented at a project kickoff meeting at the National Energy Technology Laboratory in Morgantown, WV on December 12, 2005.

All project quarterly reports and technical presentations are posted on the Mesaverde Project Website.

REFERENCES

- Aguilera, R., 2002, Incorporating Capillary Pressure, Pore Throat Aperture Radii, Height Above Free-Water Table, and Winland r35 Values on Pickett Plots: American Association of Petroleum Geologists Bulletin, v. 86, n. 4, p. 605-624. DOI: [10.1306/61EEDB5C-173E-11D7-8645000102C1865D](https://doi.org/10.1306/61EEDB5C-173E-11D7-8645000102C1865D).
- Andersen, M.A., and Jones, F.O., 1985, A Comparison Of Hydrostatic-Stress And Uniaxial-Strain Pore-Volume Compressibilities Using Nonlinear Elastic Theory: paper ARMA 85-0403-1, The 26th U.S. Symposium on Rock Mechanics (USRMS), June 26-28, 1985, Rapid City, SD.
- Archie, G., 1942, The Electrical Resistivity Log as an Aid in Determining Some Reservoir Characteristics: paper SPE 942054-G, Transactions of AIME, v. 31, p. 350-386.
- Athy, L.F., 1930, Density, porosity, and compaction of sedimentary rocks: American Association of Petroleum Geologists, Bulletin, v. 14, n. 1, p. 1-24.
- Baldwin, B., and Butler, C.O., 1985, Compaction Curves: American Association of Petroleum Geologists Bulletin, v. 69, n. 4, p. 622-626.
- Beard, D.C., and Weyl, P.K., 1973, Influence of texture on porosity and permeability of unconsolidated sand: American Association of Petroleum Geologists Bulletin, v. 57, no. 2, p. 349-369. DOI: [10.1306/819A4272-16C5-11D7-8645000102C1865D](https://doi.org/10.1306/819A4272-16C5-11D7-8645000102C1865D).
- Berg, R.R., 1975, Capillary Pressures in Stratigraphic Traps: American Association of Petroleum Geologists Bulletin, v. 59, p. 939-956.
- Berkowitz, B., and R.P. Ewing, 1998, Percolation theory and network modeling applications in soil physics: Surveys in Geophysics, v. 19, n. 1, p. 23-72. DOI: [10.1023/A:1006590500229](https://doi.org/10.1023/A:1006590500229).
- Brace, W.F., Walsh, J.B., and Frangos, W.T., 1968, Permeability of granite under high pressure: Journal of Geophysical Research, v. 73, p. 2225-2236.
- Borai, A.M., 1987, A new correlation for the cementation factor in low-porosity carbonates: paper SPE 14401, SPE Formation Evaluation, v. 2 n. 4, p. 495-499.
- Broadbent, S.R., and J.M. Hammersley, 1957, Percolation processes I. Crystals and mazes: Proceedings of the Cambridge Philosophical Society, v. 53, p. 629-641.
- Brooks, R.H., and A.T. Corey, 1966, Properties of porous media affecting fluid flow: Journal Irrigation Drainage Division, v. 6 (June 1966), p. 61-88.
- Brower, K.R., and Morrow, N.R., 1985, Fluid Flow in Cracks as Related to Low-Permeability Gas Sands: paper SPE 11623-PA, Society of Petroleum Engineers Journal, April 1985, p. 12. DOI: [10.2118/11623-PA](https://doi.org/10.2118/11623-PA).

- Bush, D.C., and Jenkins, R.E., 1970, Proper Hydration of Clays for Rock Property Determinations: paper SPE 2589-PA, Journal of Petroleum Technology, July, 1970, p. 800-804. DOI: [10.2118/2589-PA](https://doi.org/10.2118/2589-PA).
- Byrnes, A. P., 1997, Reservoir characteristics of low-permeability sandstones in the Rocky Mountains: *The Mountain Geologist* v. 43, no. 1, p. 37-51.
- Byrnes, A.P., 2003, Aspects of Permeability, Capillary Pressure, and Relative Permeability Properties and Distribution in Low-Permeability Rocks Important to Evaluation, Damage, and Stimulation: Proceedings Rocky Mountain Association of Geologists - Petroleum Systems and Reservoirs of Southwest Wyoming Symposium, Denver, Colorado, September 19, 2003, 12 p.
- Byrnes, A.P., 2005, Permeability, capillary pressure, and relative permeability properties in low-permeability reservoirs and the influence of thin, high-permeability beds on production: *in* M.G. Bishop, S.P. Cumella, J.W. Robinson, and M.R. Silverman (eds.), Gas in Low Permeability Reservoirs of the Rocky Mountain Region, Rocky Mountain Assoc. of Geologists 2005 Guidebook CD, p. 69-108.
- Byrnes, A. P., 2008, Issues with gas relative permeability in low-permeability sandstones: *in* S.P. Cumella, K.W. Shanley, and W. Camp (eds.), Understanding, exploring, and developing tight-gas sands – 2005 Vail Hedberg Conference, American Association of Petroleum Geologists Hedberg Series n. 3, Chapter 5, p. 63-76.
- Byrnes, A.P., and Castle, J.W., 2000, Comparison of core petrophysical properties between low-permeability sandstone reservoirs: Eastern U.S. Medina Group and Western U.S. Mesaverde Group and Frontier Formation: paper SPE 60304, Proceedings of the 2000 SPE Rocky Mountain Regional/Low Permeability Reservoirs Symposium, Denver, CO, March 12-15, 2000, 10 p. DOI: [10.2118/60304-MS](https://doi.org/10.2118/60304-MS).
- Byrnes, A.P., and C.W. Keighin, 1993, Effect of confining stress on pore throats and capillary pressure measurements, selected sandstone reservoir rocks: American Association of Petroleum Geologists Annual Convention Program Abstracts, April 25-28, New Orleans, p. 82.
- Byrnes, A.P., Dubois, and M.K., Magnuson, M., 2001, Western Tight Gas Carbonates: Comparison of Council Grove Group, Panoma Field, Southwest Kansas and Western Low Permeability Sandstones: 2001 AAPG Annual Convention Official Program, Denver, CO, p. A31.
- Byrnes, A. P., K. Sampath, and P.L. Randolph, 1979, Effect of pressure and water saturation on the permeability of western tight sandstones: Proceedings of the 5th Annual U.S. Dept. Energy Symposium on enhanced oil and gas recovery, Tulsa, Oklahoma, August 22-26, 1979, p. 247-263.

- Byrnes, A.P., J.C. Webb, and R.M., Cluff, 2007, Regional petrophysical properties of Mesaverde low-permeability sandstones: American Association of Petroleum Geologists Rocky Mountain Section Meeting Abstracts, October 6-9, 2007, Snowbird, UT.
- Byrnes, A. P., D. Osborn, A. Knoderer, O. Metheny, T. Hommertzhaim, J. P. Byrnes, R. C. Cluff, J. C. and Webb, 2008, Capillary Pressure Properties of Mesaverde Group Low-Permeability Sandstones in Six Basins, Western U.S: American Association of Petroleum Geologists Rocky Mountain Section Meeting Abstracts, July, 2008, Denver, CO.
- Byrnes, A. P., J. C. Webb, R. M. Cluff, D. A. Krygowski, and S. D. Whittaker, 2008, Lithofacies and petrophysical properties of Mesaverde tight-gas sandstones in Western U.S. basins: American Association of Petroleum Geologists Annual Convention Program Abstracts, San Antonio, TX.
- Caffero, R., G. Caldarelli and A. Gabrielli, 1997, Surface effects in invasion percolation: Physical Review E, v. 56, no. 2, p. R1291-R1294. DOI: [10.1103/PhysRevE.56.R1291](https://doi.org/10.1103/PhysRevE.56.R1291).
- Carpenter, C.B., and G.B. Spencer, 1940, Measurements of compressibility of consolidated oil bearing sandstones: Bureau of Mines Report of Investigations #3540, October, 20 p.
- Caruso, G.F., 2008, Outlook for U.S. natural gas markets: presentation given at LNG 2008, April 22, San Antonio, Texas, <http://www.eia.doe.gov/neic/speeches/caruso042208.pdf>
- Castle, J.W., and Byrnes, A.P., 1998, Petrophysics of low-permeability Medina Sandstone, northwestern Pennsylvania, Appalachian Basin: paper SPWLA 1998-v39n4a3, The Log Analyst, v. 39, no. 4, p. 36-46.
- Castle, J.W., and A.P. Byrnes, 2005, Petrophysics of Lower Silurian sandstones and integration with the tectonic-stratigraphic framework, Appalachian basin, United States: American Association of Petroleum Geologists Bulletin, v. 89, no. 1 (January 2005), p. 41-60. DOI: [10.1306/080170404028](https://doi.org/10.1306/080170404028).
- Chandler, R., J. Koplík, K. Lerman, and J.F. Willemsen, 1982, Capillary displacement and percolation in porous media: Journal of Fluid Mechanics, v. 119, p. 249-267. DOI: [10.1017/S0022112082001335](https://doi.org/10.1017/S0022112082001335).
- Chen, J., Petersen, M.E., and Jamison, W., 2004, From the Reservoir to Microscopic Scales: What Do We Learn Through the Characterization of Tight Gas Reservoirs?: American Association of Petroleum Geologists, p. 3.
- Cheng, C.H., and Toksoz, M.N., 1979, Inversion of seismic velocities for the pore aspect ratio spectrum of rock: Journal of Geophysical Research, v. 84, n. B13, p. 7533-7544.
- Chowdiah, P., 1987, Laboratory measurements relevant to two-phase flow in a tight gas sand matrix: paper SPE 16945-MS, Proceedings of the 62nd Annual Technical Conference and

Exhibition of the Society of Petroleum Engineers, Dallas, Texas, September 27-30, 12 p.
DOI: [10.2118/16945-MS](https://doi.org/10.2118/16945-MS).

Clavier, C., G. Coates, and J. Dumanoir, 1984, Theoretical and experimental bases for the Dual-Water model for interpretation of shaly sands: paper SPE 6859-PA, SPE Journal, v. 24, n. 2, p. 153-168. DOI: [10.2118/6859-PA](https://doi.org/10.2118/6859-PA).

Closmann, P.J., 1987, Studies of critical gas saturation during gas injection: paper SPE 12335-PA, SPE Reservoir Engineering, Aug. (1987), p. 387-393. DOI: [10.2118/12335-PA](https://doi.org/10.2118/12335-PA).

Cluff, R.M., Byrnes, A.P., and Webb, J.C., 1994, Rock-petrophysics-log correlation in the Mesaverde group, Washakie basin: American Association of Petroleum Geologists Annual Convention Program Abstracts, June 12-15, Denver, CO, p. 122. DOI: [10.1306/A25FF8CD-171B-11D7-8645000102C1865D](https://doi.org/10.1306/A25FF8CD-171B-11D7-8645000102C1865D).

Cluff, R. M., K.W. Shanley, and J. W. Robinson, 2007, What's the matter with the Ericson?: American Association of Petroleum Geologists Rocky Mountain Section Meeting Abstracts, October 6-9, 2007, Snowbird, UT.

Cluff, R. M., and A. P. Byrnes, 2008, Evidence for a variable Archie porosity exponent “m” and impact on saturation calculations for Mesaverde tight gas sandstones; Piceance, Uinta, Green River, Wind River, and Powder River Basins: American Association of Petroleum Geologists Rocky Mountain Section Meeting Abstracts, July, 2008, Denver, CO.

Coates, G.R., R.C.A. Peveraro, A. Hardwick, and D. Roberts, 1991, The Magnetic Resonance Imaging Log Characterized by Comparison With Petrophysical Properties and Laboratory Core Data: paper SPE 22723-MS, SPE Annual Technical Conference and Exhibition, 6-9 October 1991, Dallas, Texas, p. 9. DOI: [10.2118/22723-MS](https://doi.org/10.2118/22723-MS).

Corey, A.T., 1954, The interrelations between gas and oil relative permeabilities: Producers Monthly, v. 19 (Nov 1954), p 38-41.

Corey, A.T., and C.H. Rathjens, 1956, Effect of stratification on relative permeability: paper SPE 744-G, Journal of Petroleum Technology, v. 8, n. 12 (Dec 1956), p. 69-71. DOI: [10.2118/744-G](https://doi.org/10.2118/744-G).

Cornell, D., and Katz, D.L., 1953, Flow of Gases through Consolidated Porous Media: Industrial and Engineering Chemistry, v. 45, n. 10, p. 2145-2152. DOI: [10.1021/ie50526a021](https://doi.org/10.1021/ie50526a021).

Craft, B.C., and M.F. Hawkins, 1991, Applied Petroleum Reservoir Engineering. Second edition: Prentice Hall PTR, Englewood Cliffs, N.J., p. 424.

Craig, D.P., and Brown, T.D., 1999, Estimating Pore Pressure and Permeability in Massively Stacked Lenticular Reservoirs Using Diagnostic Fracture-Injection Tests: paper SPE 56600-MS, Society of Petroleum Engineers International, p. 1-14. DOI: [10.2118/56600-MS](https://doi.org/10.2118/56600-MS).

- Dalrymple, R.W., 1992, Tidal depositional systems: *in*: Walker, R.G, and James, N.P., Facies Models – Response to Sea Level Change, Geological Association of Canada, p. 195-218.
- David, C., Wong, T.F., Zhu, W., and Zhang, J., 1994, Laboratory measurement of compaction-induced permeability change in porous rocks: implication for the generation and maintenance of pore pressure excess in the crust: *Pageoph (Pure and Applied Geophysics)* v. 143, p. 425-456. DOI: [10.1007/BF00874337](https://doi.org/10.1007/BF00874337).
- Debschutz, W., Kruckel, U., and Schopper, J. R., 1989, Effect of geostatic stress and pore pressure on the Klinkenberg permeability factor and other fluid flow parameter: *in* Maury, V. and Fourmaintraux, D. (eds.). *Proc. Symposium on Rock at Great Depth*, Vol. 1, A.A. Balkema, Rotterdam, p. 79-186.
- Desbarats, A.J., 1987, Numerical simulation of effective permeability in sand-shale formation: *Water Resources Research*, v. 23, no. 2, p. 273-286.
- Dickinson, G., 1953, Geological aspects of abnormal reservoir pressures in Gulf Coast Louisiana: paper WPC 4001, *American Association of Petroleum Geologists Bulletin*, v. 37, p. 410-432.
- Dickinson, W.R., T.F. Lawton, and T.F., K.F. Inman, 1986, Sandstone detrital modes, Central Utah Foreland region: Stratigraphic record of Cretaceous-Paleogene tectonic evolution: *Journal of Sedimentary Petrology*, v. 56, no. 2, p. 276-293. DOI: [10.1306/212F88E6-2B24-11D7-8648000102C1865D](https://doi.org/10.1306/212F88E6-2B24-11D7-8648000102C1865D).
- Dobrynin, V.M., 1962, Effect of Overburden Pressure on Some Properties of Sandstones: paper SPE 461-PA, *Society of Petroleum Engineers Journal*, v. 2, n. 4, p. 360-366. DOI: [10.2118/461-PA](https://doi.org/10.2118/461-PA).
- Donaldson, E.C., Kendall, R.F., and Manning, F.S., 1975, Surface-Area Measurement of Geologic Materials: paper SPE 4987-PA, *Society of Petroleum Engineers Journal*, April, 1975, p. 111-116. DOI: [10.2118/4987-PA](https://doi.org/10.2118/4987-PA).
- Du, C., and Y.C. Yortsos, 1999, A numerical study of the critical gas saturation in a porous medium: *Transport in Porous Media*, v. 35, n. 2, p. 205-225. DOI: [10.1023/A:1006582222356](https://doi.org/10.1023/A:1006582222356).
- Dullien, F.A.L., 1992, *Porous media, fluid transport and pore structure*, 2nd edition: Academic Press, San Diego, CA, p. 574.
- Dutton, S. P., et al, 1993, Major low-permeability sandstone gas reservoirs in the continental United States: Texas Bureau of Economic Geology Report of Investigations no. 211, 221 p.
- Evans, J.P., Forster, C.B., and Goddard, J.V., 1997, Permeability of fault-related rocks, and implications for hydraulic structure of fault: *Journal of Structural Geology*, v. 19, n. 11, p. 1393-1404. DOI: [10.1016/S0191-8141\(97\)00057-6](https://doi.org/10.1016/S0191-8141(97)00057-6).

- Faris, S.R., Woessner, D.E., Melrose, J.C., 1983, Significance of Surface Area Data To Sandstone Petrophysical Analysis: ACS Symposium on Surface Chemistry of Sedimentary Rocks, Seattle, Washington, March 20-25, p. 54.
- Fatt, I., 1958, Pore volume compressibilities of sandstone reservoir rocks: paper SPE 970-G, Journal of Petroleum Technology, v. 10, n. 3, p 64-66. DOI: [10.2118/970-G](https://doi.org/10.2118/970-G).
- Fatt, I., and Davis, D.H., 1952, Reduction in Permeability with Overburden Pressure: paper SPE 952329-G, Petroleum Transactions, AIME, v. 195, p. 329.
- Feder, J.: 1988, Fractals: Plenum Press, New York. 283 pgs.
- Ferer, M., G.S. Bromhal, and D.H. Smith, 2003, Pore-level modeling of drainage: Crossover from invasion percolation fingering to compact flow: Physical Review E, v. 67, n. 5, p. 1-12. DOI: [10.1103/PhysRevE.67.051601](https://doi.org/10.1103/PhysRevE.67.051601).
- Fertl, W. H., and E. Frost Jr, 1980, Evaluation of shaly classic reservoir rocks: paper SPE 8450-PA, Journal of Petroleum Technology, v. 32, p. 1641-1646. DOI: [10.2118/8450-PA](https://doi.org/10.2118/8450-PA).
- Finley R.J., 1984, Geology and engineering characteristics of selected low-permeability gas sandstones, a National Survey: Texas Bureau of Economic Geology, Report of Investigations n. 138, p. 228.
- Firoozabadi, A., B. Ottesen, and M. Mikklesen, 1989, Measurement and modeling of supersaturation and critical gas saturation: Part 1. Measurements: paper SPE 19694, Proceedings of the 1989 Soc. Petroleum Engineers Fall Meeting, San Antonio, Texas, Oct. 8-11.
- Focke, J.W. and D. Munn, 1987, Cementation exponents in Middle Eastern carbonate reservoirs: paper SPE 13735, SPE Formation Evaluation, v. 2 n. 2, p. 155-167.
- Folk, R.L., 1974, Petrology of Sedimentary Rocks: Austin, TX: Hemphill's Drawer M. University Station, 182 p.
- Glover, P.W., M.J. Hole, and J. Pous, 2000, A modified Archie's law for two conducting phases: Earth and Planetary Science Letters, V. 180, no. 3-4, p. 369-383. DOI: [10.1016/S0012-821X\(00\)00168-0](https://doi.org/10.1016/S0012-821X(00)00168-0).
- Greenwald, R.F., 1981, Volumetric Response of Porous Media to Pressure Variations: Dissertations Abstracts International Section B., v. 41, n. 7, 2727-B; p. 184.
- Greenwald, R.F., and Somerton, W.H., 1981a, A Theoretical Model for Determination of Pore Volume Compressibilities of Consolidated Sandstones: paper SPE 10076-MS, Society of Petroleum Engineers, p. 13. DOI: [10.2118/10076-MS](https://doi.org/10.2118/10076-MS).

- Greenwald, R.F., and Somerton, W.H., 1981b, Pore Volume Compressibility Data for Bandera, Berea, and Boise Sandstones: paper SPE 9746-MS, Society of Petroleum Engineers, p. 31.
- Guyod, H, 1944, Fundamental Data for the Interpretation of Electric Logs: The Oil Weekly v. 115, no. 38 (October 30, 1944): p. 21-27.
- Hall, H.N., 1953, Compressibility of reservoir rocks, Trans. Am. Inst. Mining and Mechanical Engineers, vo. 198, 309-311.
- Handy, L. L., 1958, A laboratory study of oil recovery by solution gas drive: paper SPE 797-G, Petroleum Transactions AIME, v. 213, p. 310-315.
- Hartmann, D.J., and MacMillan, L., 1992, Petrophysics of the Wasatch Formation and Mesa Verde Group, Natural Buttes Producing Area, Uinta Basin, Utah: Utah Geological Association Guidebook 20, p. 175-191.
- Harville, D.W., and Hawkins, M.F. Jr., 1969, Rock Compressibility and Failure as Reservoir mechanisms in Geopressed Gas Reservoirs: paper SPE 2500-PA, Journal of Petroleum Technology, December, 1969, p. 1528-1530. DOI: [10.2118/2500-PA](https://doi.org/10.2118/2500-PA).
- Heid, J. G., McMahon, J. J., Nielsen, R.F., and Yuster, S. T., 1950, Study of the permeability of rocks to homogeneous fluids, Am Petroleum Institute Drilling and Production Practices, p. 230-246.
- Herrick, D.C., and W.D. Kennedy, 1993, Electrical efficiency: a pore geometric model for the electrical properties of rocks: paper SPWLA 1993-HH, Trans. SPWLA 34th Ann. Logging Symposium, paper HH, p. 20.
- Hill, H.J., Shirley, O.J., Klein, G.E., Thomas, E.C., and Waxman, M.H., 1979, Bound Water in Shaly Sands - Its Relation to Q and Other Formation Properties: paper SPWLA 1979-vXXn3a1, May-June, p. 3-19.
- Hoholick, J.D., Metarko, T., and Potter, P.E., 1984, Regional variations of porosity and cement: St. Peter and Mount Simon Sandstones in Illinois Basin: American Association Petroleum Geologists Bulletin, v. 68, n. 6, p. 753-764. DOI: [10.1306/AD461381-16F7-11D7-8645000102C1865D](https://doi.org/10.1306/AD461381-16F7-11D7-8645000102C1865D).
- Holditch, S.A., 1979, Factors Affecting Water Blocking and Gas Flow From Hydraulically Fractured Gas Wells: paper SPE 7561-PA, Journal of Petroleum Technology, December, p. 1515-1524. DOI: [10.2118/7561-PA](https://doi.org/10.2118/7561-PA).
- Honarpour, M.M., Cullick, A.S., Saad, N., and Humphreys, N.V., 1995, Effect of rock heterogeneity on relative permeability: implications for scale-up: paper SPE 29311-PA, Journal of Petroleum Technology, Nov., p. 980-986. DOI: [10.2118/29311-PA](https://doi.org/10.2118/29311-PA).

- Howard, J.J., 1992, Influence of authigenic clays minerals on permeability: *in*: Houseknecht, D.W., and Pittman, E.D., Origin, Diagenesis, and Petrophysics of Clay Minerals in Sandstones, SEPM (Society for Sedimentary Geology) Special Publication no. 47, p. 257-264.
- Hubbert, M. K., 1953, Entrapment of petroleum under hydrodynamic conditions: American Association of Petroleum Geologists Bulletin, v. 37, p. 1954-2026.
- Hunt, E. B., Jr. and V.J.Jr. Berry, 1956, Evolution of gas from liquids flowing through porous media: American Institute of Chemical Engineering Journal, v. 2, n. 4, p. 560-567. DOI: [10.1002/aic.690020426](https://doi.org/10.1002/aic.690020426).
- Hyman, L.A., Malek, D.J., Admire, C.A., and Walls, J.D., 1991, The Effects of Microfractures on Directional Permeability in Tight Gas Sands: paper SPE 21878-MS, Society of Petroleum Engineers, Denver, Colorado, April 15-17, 1991, p. 5. DOI: [10.2118/21878-MS](https://doi.org/10.2118/21878-MS).
- Jennings, H.Y. Jr., and Newman, G.H., 1971, The Effect of Temperature and Pressure on the Interfacial Tension of Water Against Methane-Normal Decane Mixtures: paper SPE 3071-PA, Society of Petroleum Engineers Journal, v. 11, n.2, p. 171-175. DOI: [10.2118/3071-PA](https://doi.org/10.2118/3071-PA).
- Jones, F.O. Jr., 1964, Influence of Chemical Composition of Water on Clay Blocking of Permeability: Journal of Petroleum Technology, April, 1964, p. 441-446. DOI: [10.2118/631-PA](https://doi.org/10.2118/631-PA).
- Jones, F. O., and W.W. Owens, 1980, A laboratory study of low-permeability gas sands: paper SPE 7551-PA, Journal of Petroleum Technology, v. 32, no. 9, p.1631-1640. DOI: [10.2118/7551-PA](https://doi.org/10.2118/7551-PA).
- Jones, S.C., 1972, A Rapid Accurate Unsteady-State Klinkenberg Permeameter: paper SPE 3535-PA, Society of Petroleum Engineers Journal, October, 1972, p. 383-397. DOI: [10.2118/3535-PA](https://doi.org/10.2118/3535-PA).
- Juhasz, I., 1979, The Central Role Of Qv and Formation-Water Salinity in the Evaluation of Shaly Formations: paper SPWLA 1979-vXXn4a1, v. XX, n. 4, p. 1-25. (also SPWLA 20th Anniversary Logging Symposium, paper AA).
- Kamath, J. and R.E. Boyer, 1993, Critical gas saturation and supersaturation in low permeability rocks: paper SPE 26663, Presented at the 1993 Society of Petroleum Engineers Fall Meeting, Houston, TX, Oct. p. 3-6.
- Kamath, J. and R. E. Boyer, 1995, Critical Gas Saturation and Supersaturation in Low-Permeability Rocks: SPE 2663-PA, Society of Petroleum Engineers Formation Evaluation, v. 10, n. 4, p. 247-254. DOI: [10.2118/26663-PA](https://doi.org/10.2118/26663-PA).
- Katsube, T.J., B.S. Munford, and M.E. Best, 1991, Petrophysical characteristics of shales from the Scotian shelf: Geophysics, v. 56, p. 1681-1688. <http://dx.doi.org/10.1190/1.1442980>

- Katsube, T.J., Williamson, M., and Best, M.E., 1992, Shale pore structure evolution and its effect on permeability: paper SCA-9214, 1992 SCA Conference paper, http://www.scaweb.org/assets/papers/1992_papers/1-SCA1992-14.pdf, p. 1-22.
- Katsube, T.J., and K. Coyner, 1994, Determination of permeability (k)-compaction relationship from interpretation of k-stress data for shales from eastern and northern Canada: Geological Survey of Canada, Current Research 1994-D, p. 169-177.
- Keelan, D.K., 1986, Automated Core Measurement System for Enhanced Core Data at Overburden Conditions: paper SPE 15185-MS, SPE Rocky Mountain Regional Meeting, 19-21 May 1986, Billings, Montana, 13 p. DOI: [10.2118/15185-MS](https://doi.org/10.2118/15185-MS).
- Keighin, W.C., 1980, Evaluation of Pore Geometry of Some Low-Permeability Sandstones, Uinta Basin, Utah: paper SPE 9251, Society of Petroleum Engineers of AIME, Dallas, Texas, September 21-24, 1980, p. 4.
- Keighin, C.W., 1997, Physical properties of elastic reservoir rocks in the Uinta, Wind River, and Anadarko Basins, as determined by mercury-injection porosimetry: US Geological Survey Bulletin 2146-G, p. 73-83.
- Keighin, W.C., and Sampath, K., 1982, Evaluation of Pore Geometry of Some Low-Permeability Sandstones - Uinta Basin: paper SPE 9251-PA, Journal of Petroleum Technology, v. 34, n. 1, p. 65-70. DOI: [10.2118/9251-PA](https://doi.org/10.2118/9251-PA).
- Kenyon, W.E., P.I. Day, C. Straley, and J.F. Willemsen, 1988, A Three-Part Study of NMR Longitudinal Relaxation Properties of Water-Saturated Sandstones: paper SPE-15643-PA, SPE Formation Evaluation, v. 3, n. 3, p. 622-636. DOI: [10.2118/15643-PA](https://doi.org/10.2118/15643-PA).
- Kern, J.W., Hoyer, W.A., and Spann, M.M., 1977, High Temperature Electrical Conductivity of Shaly Sands: paper SPWLA 1977-U, SPWLA 18th Annual Logging Symposium, June 5-8, 1977, p. 14.
- Klinkenberg, L.J., 1941, The permeability of porous media to liquids and gases: paper API 41-200, Drilling and Production Practice, p.14.
- Knutson, C.F., and Bohor, B.F., 1962, Reservoir Rock Behavior Under Moderate Confining Pressure: Proc. 5th Symposium of Rock Mechanics, Minnesota, p. 627-658.
- Koplik, J., and T.J. Lasseter, 1982, Two-phase flow in random network models of porous media: paper SPE 11014, Proc. Annual Meeting of Society of Petroleum Engineers., New Orleans, LA., 12 pgs. DOI: [10.2118/11014-PA](https://doi.org/10.2118/11014-PA).
- Koplik, J., C. Lin, and M. Vermette, 1984, Conductivity and permeability from microgeometry: Journal Applied Physics, v. 56, n. 11, p. 3127-3131. DOI: [10.1063/1.333872](https://doi.org/10.1063/1.333872).

- Kortekaas, T. F. M., 1985, Water/Oil Displacement Characteristics in Crossbedded Reservoir Zones: paper SPE 12112-PA, Society of Petroleum Engineers Journal, v. 25, n. 6, p. 917-926. DOI: [10.2118/12112-PA](https://doi.org/10.2118/12112-PA).
- Kortekaas, T.F.M., and F.V. Poelgeest, 1989, Liberation of solution gas during pressure depletion of virgin and watered-out reservoirs: paper SPE 19693, Presented at the 1989 Fall Meeting of the Society of Petroleum Engineers, San Antonio, Texas, Oct. 8-11. DOI: [10.2118/19693-PA](https://doi.org/10.2118/19693-PA).
- Kukul, G. C., Biddison, C. L., Hill, R. E., Monson, E. R., and Simons, K. E., 1983, Critical problems hindering accurate log interpretation of tight gas sand reservoirs: paper SPE 11620-MS, Proceedings of the SPE, AIME/U.S. DOE 1983 Symposium on low permeability reservoirs, Denver, CO, March 14-16 (1983) p. 181. DOI: [10.2118/11620-MS](https://doi.org/10.2118/11620-MS).
- Land, C.S., 1971, Comparison of Calculated with Experimental Imbibition Relative Permeability: paper SPE 3360-PA, Society of Petroleum Engineers Journal, v. 11, n. 4, p. 419-425. DOI: [10.2118/3360-PA](https://doi.org/10.2118/3360-PA).
- Larson, R.G., and N.R. Morrow, 1981, Effects of sample size on capillary pressure in porous media: Powder Technology, V. 30, no. 2, pp 123-139.
- Larson, R.G., L.E. Scriven, and H.T. Davis, 1977, Percolation theory of residual phases in porous media: Nature, v. 268, 409-413. DOI: [10.1038/268409a0](https://doi.org/10.1038/268409a0).
- Larson, R.G., L.E. Scriven, and H.T. Davis, 1981, Percolation theory of two phase flow in porous media: Chemical Engineering Science, v. 36, n. 1, 57-73.
- Law, B.E., 2002, Basin-centered gas systems: American Association of Petroleum Geologists Bulletin, v. 86, n. 11, p. 1891-1919. DOI: [10.1306/61EEDDB4-173E-11D7-8645000102C1865D](https://doi.org/10.1306/61EEDDB4-173E-11D7-8645000102C1865D).
- Lawton, T.F., S.L. Pollack and R.A.J. Robinson, 2003, Integrating sandstone petrology and nonmarine sequence Stratigraphy: Application to the Late Cretaceous fluvial systems of southwestern Utah: U.S.A: Journal of Sedimentary Research, v. 73, no. 3, p. 389-406. DOI: [10.1306/100702730389](https://doi.org/10.1306/100702730389).
- Lee, W.J., and Hopkins, C.W., 1994, Characterization of Tight Reservoirs: paper SPE 29091-PA, Journal of Petroleum Technology, v. 46, n. 11, p. 956-964. DOI: [10.2118/29091-PA](https://doi.org/10.2118/29091-PA).
- Lenormand, R., and C. Zarcone, 1985, Invasion percolation in an etched network: measurement of a fractal dimension: Physical Review Letters, v. 54, p. 2226-2229. DOI: [10.1103/PhysRevLett.54.2226](https://doi.org/10.1103/PhysRevLett.54.2226).
- Lenormand, R., C. Zarcone, and A. Sarr, 1983, Mechanisms of the displacement of one fluid by another in a network of capillary ducts: Journal of Fluid Mechanics, v. 135, p. 337-353. DOI: [10.1017/S0022112083003110](https://doi.org/10.1017/S0022112083003110).

- Lerner, D.B., Dacy, J.M., Raible, C.J., Rathmell, J.J., Swanson, G., and Walls, J.D., 1990, SCA Guidelines for Sample Preparation and Porosity Measurement of Electrical Resistivity Samples; Part II - Sample Preparation and Porosity Measurement: paper SPWLA 1990-v31n2a1, *The Log Analyst*, v. 31, n. 2, p. 57-63.
- Leverett, M.C., 1941, Capillary behavior in porous solids: paper SPE 941152-G, *Petroleum Transactions, AIME*, v. 142, p. 152-169.
- Li, X. and Y.C. Yortsos, 1991, Visualization and numerical studies of bubble growth during pressure depletion: paper SPE 22589-MS, Presented at the 64th Annual Technical and Exhibition of the Soc. Petroleum Engineers, Dallas, Texas, Oct. 6-9. DOI: [10.2118/22589-MS](https://doi.org/10.2118/22589-MS).
- Li, X. and Y.C. Yortsos, 1993, Critical gas saturation, modeling and sensitivity studies: paper SPE 26662-MS, Proceedings of the 68th Annual Technical Conference of the Soc. Petroleum Engineers, Houston, Texas, Oct. 3-6, p. 589-604. DOI: [10.2118/26662-MS](https://doi.org/10.2118/26662-MS).
- Li, X., and Y.C. Yortsos, 1995a, Theory of multiple bubble growth in porous media by solute diffusion: *Chem. Engineering Science*, v. 50, n. 8, 1247-1271. DOI: [10.1016/0009-2509\(95\)98839-7](https://doi.org/10.1016/0009-2509(95)98839-7).
- Li, X., and Y.C. Yortsos, 1995b, Visualization and simulation of bubble growth in pore networks: *American Institute Chemical Engineers Journal*, v. 41, n. 2, 214-222. DOI: [10.1002/aic.690410203](https://doi.org/10.1002/aic.690410203).
- Lin, C. and M.H. Cohenm, 1982, Quantitative methods for microgeometric modeling: *Journal of Applied Physics*, v. 53, p. 4152-4165. DOI: [10.1063/1.331238](https://doi.org/10.1063/1.331238).
- Logan, W.D., 1989, Bridging the Gap Between Core Permeability and Log-Derived Permeability: SPWLA 30th Annual Logging Symposium, June 11-14, 1989, p. 23.
- Lomax, J., and Howard, A., 1994, New Logging Tool Identifies Permeability in Shaley Sands: *Oil & Gas Journal*, December, 1994, p. 104-108.
- Luffel, D.L., Howard, W.E., and Hunt, E.R., 1991, Travis Peak core permeability and porosity relationships at reservoir stress: paper SPE 19008-PA, Society of Petroleum Engineers Formation Evaluation, September, 1991, v. 6, n. 3, p. 310-319. DOI: [10.2118/19008-PA](https://doi.org/10.2118/19008-PA).
- Mahadevan, J., and Sharma, M.M., 2003, Clean-up Water Blocks in Low Permeability Formations: SPE 84216-MS, Society of Petroleum Engineers International, p. 1-11. DOI: [10.2118/84216-MS](https://doi.org/10.2118/84216-MS).
- Maloney, D., Doggett, K., and Brinkmeyer, A., 1993, Special Core Analyses and Relative Permeability Measurements on Almond Formation Reservoir Rocks: DE-FC22-83FE60149, NIPER - 648, p. 1-30. DOI: [10.2172/10131819](https://doi.org/10.2172/10131819).

- Mann, R.L., and Fatt, I., 1960, Effect of Pore Fluids on the Elastic Properties of Sandstone: *Geophysics* 25, April 1960, p. 433-444. DOI: [10.1190/1.1438713](https://doi.org/10.1190/1.1438713).
- Mattax, C.C., McKinley, R.M., and Clothier, A.T., 1975, Core Analysis of Unconsolidated and Friable Sands: paper SPE 4986-PA, *Journal of Petroleum Technology*, v. 27, n. 12, p. 1423-1432. DOI: [10.2118/4986-PA](https://doi.org/10.2118/4986-PA).
- McLatchie, A.S., Hemstock, R.A., and Young, J.W., 1958, The Effective compressibility of reservoir rock and its effects on permeability: paper SPE 894-G, *Journal of Petroleum Technology*, v. 10, n. 6, p. 49-51. DOI: [10.2118/894-G](https://doi.org/10.2118/894-G).
- McPeck, L.A., 1981, Eastern Green River Basin: A Developing Giant Gas Supply from Deep, Overpressured Upper Cretaceous Sandstones: American Association of Petroleum Geologists Annual Convention, Denver, Colorado, June 1980, v. 65, n. 6, p. 1078-1098.
- Mian, M.A., and Hilchie, D.W., 1982, Comparison of Results From Three Cation Exchange Capacity (CEC) Analysis Techniques: *The Log Analyst*, September-October, v. XXIII, n. 5, p. 10-16.
- Morrow, N.R., 1971, Small-Scale Packing Heterogeneities in Porous Sedimentary Rocks: *American Association of Petroleum Geologists Bulletin*, v. 55, n. 3, p. 514-522.
- Morrow, C.A., Shi, L, and Byerlee, J.D., 1984, Permeability of fault gouge under confining pressure and shear stress: *Journal of Geophysical Research*, v. 89, p. 3193-3200.
- Morrow, N.R., Cather, M.E., and Buckley, J.S., 1991, The Effects of Drying Absolute and Relative Permeabilities of Low-Permeability Gas Sands: paper SPE 21880-MS, Society of Petroleum Engineers, Low Permeability Reservoirs Symposium, 15-17 April 1991, Denver, Colorado. DOI: [10.2118/21880-MS](https://doi.org/10.2118/21880-MS).
- Moulu, J. C. and D. Longeron, 1989, Solution-gas drive: experiments and simulation: *Journal of Petroleum Science & Engineering*, Paper presented at the Fifth European Symposium on Improved Oil Recovery, Budapest, Hungary, v. 2, n. 4, p. 379-386.
- Neasham, J.W., 1977, The Morphology of Dispersed Clay in Sandstone Reservoirs and its Effect on Sandstone Shaliness, Pore Space and Fluid Flow Properties: paper SPE 6858-MS, Society of Petroleum Engineers of AIME, Denver, Colorado, Oct 9-12, 1977, p. 8. DOI: [10.2118/6858-MS](https://doi.org/10.2118/6858-MS).
- Nelson, P.H., 1994, Permeability-Porosity Relationships in Sedimentary Rocks: paper SPWLA 1994-v35n3a4, *The Log Analyst*, v. 35, n. 3, p. 38-62.
- Nelson, P.H., 2003a, Subsurface pressures from drill-stem tests, Uinta and Piceance Basins, Utah and Colorado: U.S. Geological Survey Digital Data Series DDS-69-B, Chap 14, 35 p.

- Nelson, P.H., 2003b, A review of the Multiwell Experiment, Williams Fork and Iles Formations, Garfield County, Colorado: U.S. Geological Survey Digital Data Series DDS-69-B, Chap 15, 28 p.
- Nelson, P.H., 2009, Pore-throat sizes in sandstones, tight sandstones, and shales: American Association of Petroleum Geologists Bulletin, v. 93, no. 3, p. 329-340. DOI: [10.1306/10240808059](https://doi.org/10.1306/10240808059).
- Nesham, J.W., 1977, The morphology of dispersed clay in sandstone reservoirs and its effect on sandstone shaliness, pore space and fluid flow properties: paper SPE 6858, Society of Petroleum Engineers of AIME, 8 p.
- Neustaedter, R.H., 1968, Log evaluation of deep Ellenburger gas zones: paper SPE 2071, Deep Drilling and Development Symposium-Delaware basin, Monahans, TX, March 28, 1968, 7 p.
- Newman, G.H., 1973, Pore-Volume compressibility of consolidated, friable, and unconsolidated reservoir rocks under hydrostatic loading: paper SPE 3835-PA, Journal of Petroleum Technology, v. 25, n. 2, p. 129-134. DOI: [10.2118/3835-PA](https://doi.org/10.2118/3835-PA).
- Newman, G.H., and Martin, J.C., 1977, Equipment and experimental methods for obtaining laboratory compression characteristics of reservoir rocks under various stress pressure conditions: paper SPE 6855, Society of Petroleum Engineers of AIME, Denver, Colorado, October 9-12, 1977, p. 16. DOI: [10.2118/6855-MS](https://doi.org/10.2118/6855-MS).
- Ohirhian, P.U., 1998, Explicit Form of the Waxman-Smits Equation for Shaly Sands: paper SPWLA 1998-v39n3a3, The Log Analyst, May-June, p. 54-57.
- Ostensen, R. W., 1983, Microcrack permeability in tight gas sandstone: paper SPE 10924-PA, Society of Petroleum Engineering Journal, v. 23, no. 6, p. 919-927. DOI: [10.2118/10924-PA](https://doi.org/10.2118/10924-PA).
- Patchett, J.G., and Coalson, E.B., 1979, The Determination of Porosity in Sandstones and Shaly Sandstones Part One - Quality Control: paper SPWLA 1979-QQ, SPWLA 20th Annual Logging Symposium, June 3-6, 1979, p. 1-17.
- Pemberton, S.G., 1992, Applications of Ichnology to Petroleum Exploration: A Core Workshop: Society for Sedimentary Geology Core Workshop no. 17, 429 p.
- Pittman, E.D., 1979, Porosity, diagenesis and productive capability of sandstone reservoirs: *in*: Scholle, P.A., and Schluger, P.R., Aspects of diagenesis, SEPM (Society for Sedimentary Geology) Special Publication no. 26, p. 159-174.
- Pittman, E.D., 1992, Relationship of Porosity and Permeability to Various Parameters Derived from Mercury Injection-Capillary Pressure Curves for Sandstone: American Association of Petroleum Geologists Bulletin, v. 76, n. 2, p. 191-198.

- Plumb, R.A., 1994, Influence of Composition and Texture on the Failure Properties of Clastic Rocks: paper SPE 28022-MS, Proceedings of 'Eurock 94, Balkema, Rotterdam 1994, p. 13-20. DOI: [10.2118/28022-MS](https://doi.org/10.2118/28022-MS).
- Poupon, A., and J. Leveaux, 1971, Evaluation of water saturations in shaly formations: paper SPWLA 1971-O, Trans. SPWLA 12th Ann. Logging Symposium, Paper O, p. 15. (Indonesia model)
- Purcell, W.R., 1949, Capillary pressures – their measurement using mercury and the calculation of permeability therefrom: paper SPE 949039-G, Trans. AIME, v. 186, p. 39-48.
- Randolph, P.L., 1983, Porosity and permeability of Mesaverde sandstone core from the U.S. DOE Multiwell Experiment, Garfield County, Colorado: paper SPE 11765-MS, Proceedings 1983 SPE/DOE Joint Symposium on low permeability gas reservoirs, March 13-16, 1983, Denver, CO, p. 449-460. DOI: [10.2118/11765-MS](https://doi.org/10.2118/11765-MS).
- Randolph, P.L., Soeder, D.J., and Chowdiah, P., 1984, Porosity and Permeability of Tight Sands: paper SPE 12836-MS, SPE/DOE/GRI Unconventional Gas Recovery Symposium, Pittsburgh, PA May 13-15 1984, p. 10. DOI: [10.2118/12836-MS](https://doi.org/10.2118/12836-MS).
- Ransom, R.C., 1977, Methods Based On Density And Neutron Well-logging Responses to Distinguish Characteristics of Shaly Sandstone Reservoir Rock: paper SPWLA 1977-vXVIIIIn3a5, The Log Analyst, v. 18, n. 3, p. 47.
- Revil, A., and Cathles, L.M. III, 1999, Permeability of shaly sands: Water Resources Research, v. 35, n. 3, p. 651-662.
- Ringrose, P.S., Jensen, J.L., and Sorbie, K.S., 1996, Use of Geology in the Interpretation of Core-Scale Relative Permeability Data: paper SPE 28448-PA, SPE Formation Evaluation, v. 11, n. 3, p. 171-176. DOI: [10.2118/28448-PA](https://doi.org/10.2118/28448-PA).
- Robinson, B.M., Holditch, S.A., and Lee, W.J., 1986, A Case Study of the Wilcox (Lobo) Trend in Webb and Zapata Counties, TX: paper SPE 11600-PA, Journal of Petroleum Technology, v. 38, n. 12, p. 1355-1364. DOI: [10.2118/11600-PA](https://doi.org/10.2118/11600-PA).
- Rose, W., and Sampath, K., 1981, Measurement of Formation Characteristics for Western Tight Sands, Institute of Gas Technology, April, p. 1-15.
- Rosepiler, M.J., 1981, Calculation and Significance of Water Saturations in Low Porosity Shaly Gas Sands: paper SPWLA 1981-OO, SPWLA 22nd Annual Logging Symposium, 1981, p. 23.
- Ruhovets, N., and Fertl, W.H., 1982, Digital Shaly Sand Analysis Based on Waxman-Smits Model and Log-Derived Clay Typing: paper SPWLA 1982-vXXIIIIn3a2, The Log Analyst, May-June, p. 7-22.

- Sahimi, M., 1993, Flow phenomena in rocks: from continuum models to fractals, percolation, cellular automata, and simulated annealing: *Reviews of Modern Physics*, v. 65, no. 4, p. 1393-1534.
- Sahimi, M., 1994, *Applications of Percolation Theory*: Taylor and Francis, London, 258 pgs.
- Sampath, K., 1982, A New Method To Measure Pore Volume Compressibility of Sandstones: paper SPE 10545-PA, *Journal of Petroleum Technology*, June, p. 1360-1362. DOI: [10.2118/10545-PA](https://doi.org/10.2118/10545-PA).
- Sampath, K., and C.W. Keighin, 1981, Factors affecting gas slippage in tight sandstones: paper SPE 9872, *Proceedings of the 1981 SPE/DOE Symposium on Low Permeability Gas Reservoirs*, Denver, CO, May 27-29 (1981) p. 409-416.
- Sattler, A.R., 1991, Multiwell Experiment Core Analyses - An Overview of the Core Analysis of a Low-Permeability Sandstone Reservoir: *The Log Analyst*, September-October, p. 498-510.
- Schmidt and McDonald, 1979a, The role of secondary porosity in the course of sandstone diagenesis: *in*: Scholle, P.A., and Schluger, P.R., *Aspects of diagenesis*, SEPM (Society for Sedimentary Geology) Special Publication no. 26, p. 175-208.
- Schmidt and McDonald, 1979b, Texture and recognition of secondary porosity in sandstones: *in*: Scholle, P.A., and Schluger, P.R., *Aspects of diagenesis*, SEPM (Society for Sedimentary Geology) Special Publication no. 26, p. 209-226.
- Schmoker, J.W., and Halley, R.B., 1982, Carbonate porosity versus depth: A predictable relation for south Florida: *American Association Petroleum Geologists Bulletin*, v. 66, p. 2561-2570.
- Schowalter, T.T., 1979, Mechanics of secondary hydrocarbon migration and entrapment: *American Association of Petroleum Geologists Bulletin*, v. 63, no. 5, p. 723-760.
- Serra, O., 1984, *Fundamentals of Well-log Interpretation*, Elsevier (Amsterdam).
- Shanley, K.W., R.M. Cluff, and J.W. Robinson, 2004, Factors controlling prolific gas production from low-permeability sandstone reservoirs: Implications for resource assessment, prospect development, and risk analysis, *American Association of Petroleum Geologists Bulletin*, v. 88, no. 8, p. 1083-1121. DOI: [10.1306/03250403051](https://doi.org/10.1306/03250403051).
- Shanley, K.W., R.M. Cluff, and J.W. Robinson, 2007, Prolific gas production from low-permeability sandstone reservoirs - Part II: Reconciling basin history, fluid saturations, gas shows, and capillary pressure: AAPG 2007 Annual Convention, Long Beach, CA, Search and Discovery Article #110042.
- Shi, T., and Wang, C.Y., 1986, Pore pressure generation in sedimentary basins: overloading versus aquathermal: *Journal of Geophysical Research*, v. 91(B2), p. 2153-2162.

- Simandoux, P., 1963, Dielectric measurements in porous media and application to shaly formations (*in French*): Revue de L'institut Francais du Petrole, p. 193-215. English translation by L. Moinard, 1982, *in* SPWLA Reprint Volume Shaly Sand, v. IV, p. 97-124.
- Simon, D.E., McDaniel, B.W., and Coon, R.M., 1976, Evaluation of Fluid pH Effects on Low Permeability Sandstones: paper SPE 6010-MS, Society of Petroleum Engineers of AIME, New Orleans, LA, Oct 3-6, 1976, p. 12. DOI: [10.2118/6010-MS](https://doi.org/10.2118/6010-MS).
- Sloat, B., and Brown, M., 1968, How to Flood a Tight Sand: paper SPE 2129-PA, Journal of Petroleum Technology, v. 20, n. 10, p. 1119-1128. DOI: [10.2118/2129-PA](https://doi.org/10.2118/2129-PA).
- Soeder, D.J., and Chowdiah, P., 1988, Comparison of Pore Geometry in High- and Low-Permeability Sandstones, Travis Peak Formation, East Texas: paper SPE 17729, Society of Petroleum Engineers, p. B-3 - B-43.
- Soeder, D.J., 1986, Laboratory Drying Procedures and the Permeability of Tight Sandstone Core: paper SPE 11622-PA, SPE Formation Evaluation, v. 1, n. 1, p. 16-22. DOI: [10.2118/11622-PA](https://doi.org/10.2118/11622-PA).
- Somerton, W.H., and A.K. Mathur, 1978, Effects of temperature and stress on fluid flow and storage capacity of porous rocks: 17th Symposium on Rock Mechanics, p. 2A2-1 - 2A2-8.
- Spencer, C.W., 1989, Review of Characteristics of Low-Permeability gas reservoirs in Western United States: Bulletin of the American Association of Petroleum Geologists, v. 73, p. 613.
- Strickland, F.G., and Feves, M.L., Sorrells, D., 1979, Microstructural Damage in Cotton Valley Formation Cores; paper SPE 8303-MS, Society of Petroleum Engineers of AIME, p. 8. DOI: [10.2118/8303-MS](https://doi.org/10.2118/8303-MS).
- Thomas, R. D., and D.C. Ward, 1972, Effect of overburden pressure and water saturation on gas permeability of tight sandstone cores: paper SPE 3634-PA, Journal of Petroleum Technology, v. 25, no. 2, p.120-124. DOI: [10.2118/3634-PA](https://doi.org/10.2118/3634-PA).
- Thompson, A.H., A.J. Katz, and R.A. Raschke, 1987, Mercury injection in porous media: a resistance Devil's staircase with percolation geometry: Physical Review Letters, v. 58, no. 1, p. 29-32.
- Timur, A., 1968, An investigation of permeability, porosity and residual water saturation relationships for sandstone reservoirs: The Log Analyst, v. 9, n. 4, p. 8-17.
- Toksoz, M.N., Cheng, C.H., and Timur, A., 1976, Velocities of Seismic Waves in Porous Rocks: Geophysics, v. 41, p. 621. DOI: [10.1190/1.1440639](https://doi.org/10.1190/1.1440639).
- USEIA, 2005, Annual Energy Outlook 2005: Energy Information Administration, DOE/EIA-0383(2005), <http://www.eia.doe.gov/oiaf/archive/aeo05/>, 249 p.

- Vairogs, J., Hearn, C. L., Dareing, D. W., and Rhoades, V. W., 1971, Effect of rock stress on gas production for low-permeability rocks: *Journal of Petroleum Technology*, v. 24, no. 9, p. 1161-1167. DOI: [10.2118/3001-PA](https://doi.org/10.2118/3001-PA).
- Volk, L.J., Carroll, H.B., and Raible, C.J., 1979, Influence of Shale Conductivities on Electric Conductivity of Low Permeability Rocks: paper SPE 7918-MS, Society of Petroleum Engineers of AIME, Denver, Colorado May 20-22 1979, p. 8. DOI: [10.2118/7918-MS](https://doi.org/10.2118/7918-MS).
- Volk, L.J., Raible, C.J., and Carroll, H.B., 1980, Influence of Shale Conductivities on the Electrical Conductivity of Low-Permeability Rocks: *Journal of Petroleum Technology*, May 1980, p. 865-867.
- Wall, G. C., and R.J.C. Brown, 1981, The determination of pore-size distributions from sorption isotherms and mercury penetration in interconnected pores: the application of percolation theory: *Journal Colloid Interface Science*, v. 82:141-49
- Walls, J.D., 1981, Tight gas sands: permeability, pore structure and clay: paper SPE 9871-PA, Proceedings of the 1981 SPE/DOE Symposium on Low Permeability Gas Reservoirs, Denver, CO, May 27-29 (1981) p. 399-409. DOI: [10.2118/9871-PA](https://doi.org/10.2118/9871-PA).
- Walls, J.D., Nur, A.M., and Bourbie, T., 1982, Effects of pressure and partial water saturation on gas permeability in tight sands: experimental results: paper SPE 9378-PA, *Journal of Petroleum Technology*, v. 34, n. 4, p. 930-936. DOI: [10.2118/9378-PA](https://doi.org/10.2118/9378-PA).
- Walsh, J.B., and Grosenbaugh, M. A., 1979, A new model for analyzing the effect of fractures on compressibility: *Journal of Geophysical Research*, v. 84, B7, p. 3532-3536. DOI: [10.1029/JB084iB07p03532](https://doi.org/10.1029/JB084iB07p03532).
- Ward, J.S., and N.R. Morrow, 1987, Capillary pressure and gas relative permeabilities of low permeability sandstone: paper SPE 13882-PA, Society of Petroleum Engineers Formation Evaluation, Sept. 1987, p. 345-356. DOI: [10.2118/13882-PA](https://doi.org/10.2118/13882-PA).
- Warren, C.A., and H.S. Price, 1961, Flow in heterogeneous porous media: paper SPE 1579-G, *SPE Journal*, v. 1, n. 3, p. 153-169. DOI: [10.2118/1579-G](https://doi.org/10.2118/1579-G).
- Washburn, E.W., 1921, Note on a method of determining the distribution of pore sizes in a porous material: *Proceedings of the National Academy of Science*, v. 7, n. 4, p. 115-116.
- Waxman, M.H., and Smits, L.J.M., 1968, Electrical conductivities in oil-bearing shaly sands: paper SPE 1863-A, *SPE Journal*, v. 8, n. 2, p. 107-122. DOI: [10.2118/1863-A](https://doi.org/10.2118/1863-A).
- Waxman, M.H., and Thomas, E.C., 1974, Electrical conductivities in shaly sands - I. The relation between hydrocarbon saturation and resistivity index. II. The temperature coefficient of electrical conductivity: paper SPE 4094-PA, *Journal Petroleum Technology*, v. 26, n. 2, p. 213-225. DOI: [10.2118/4094-PA](https://doi.org/10.2118/4094-PA).

- Webb, J. C., R. M. Cluff, D. A. Krygowski, S. D. Whittaker, and A. P. Byrnes, 2008, Lithofacies and Petrophysical Properties of Mesaverde Tight-Gas Sandstones in Western U.S. Basins: American Association of Petroleum Geologists Rocky Mountain Section Meeting Abstracts, July, 2008, Denver, CO.
- Webb, J.C., Cluff, S.G., Murphy, C.M., and Byrnes, A.P., 2004, Petrology and Petrophysics of the Lance Formation (Upper Cretaceous), American Hunter Old Road Unit No. 1, Sublette County, Wyoming: American Association of Petroleum Geologists Studies in Geology, v. 52, Chapter 11, p. 183-214.
- Weber, K.J., 1982, Influence of common sedimentary structures on fluid flow in reservoir models: paper SPE 9247-PA, Journal of Petroleum Technology, v. 34, n. 3, p. 665-672. DOI: [10.2118/9247-PA](https://doi.org/10.2118/9247-PA).
- Wei, K.K., Morrow, N.R., and Brower, K.R., 1986, Effect of fluid, confining pressure, and temperature on absolute permeabilities of low permeability sandstones: paper SPE 13093-PA, SPE Formation Evaluation, v. 1, n. 4, p. 413-423. DOI: [10.2118/13093-PA](https://doi.org/10.2118/13093-PA).
- White, E.J., Baptist, C.C., and Land, C.S., 1960, Susceptibility of Petroleum Reservoir Sands To Water Damage, Powder River Basin, Wyoming: paper SPE 1514-G, Society of Petroleum Engineers of AIME, p. 10. DOI: [10.2118/1514-G](https://doi.org/10.2118/1514-G).
- Wilkinson, D., 1984, Percolation model of immiscible displacement in the presence of buoyancy forces: Physical Review A, v. 30, p. 520-531. DOI: [10.1103/PhysRevA.30.520](https://doi.org/10.1103/PhysRevA.30.520).
- Wilkinson, D., 1986, Percolation effects in immiscible displacement: Physical Review A, v. 34, p. 1380-1391. DOI: [10.1103/PhysRevA.34.1380](https://doi.org/10.1103/PhysRevA.34.1380).
- Wilkinson, D., and J.F. Willemsen, 1983, Invasion percolation: a new form of percolation theory: Journal Physics A: Mathematical General, v. 16, p. 3365-3376. DOI: [10.1088/0305-4470/16/14/028](https://doi.org/10.1088/0305-4470/16/14/028).
- Wilson, M.D., 1981, Origins of Clays Controlling Permeability in Tight Gas Sands: paper SPE 9843-PA, Proceedings of the 1981 SPE/DOE Symposium on Low Permeability Gas reservoirs, Denver, Colorado, May 27-29, 1981, p. 8. DOI: [10.2118/9843-PA](https://doi.org/10.2118/9843-PA).
- Wilson, M.D., and Pittman, E.D., 1977, Authigenic Clays in Sandstones: Recognition and Influence on Reservoir Properties and Paleoenvironmental Analysis: Journal of Sedimentary Petrology, v. 47, n. 1, p. 3-31.
- Winn, R.D., Stonecipher, S.A., and Bishop, M.G., 1984, Sorting and wave abrasion: Controls on composition and diagenesis in Lower Frontier sandstones, Southwestern Wyoming: American Association of Petroleum Geologists Bulletin, v. 68, no. 3, p. 268-284. DOI: [10.1306/AD460A0D-16F7-11D7-8645000102C1865D](https://doi.org/10.1306/AD460A0D-16F7-11D7-8645000102C1865D).

- Winsauer, W.O., Shearin, H.M. Jr., Masson, P.H., and Williams, M., 1952, Resistivity of Brine-Saturated Sands in Relation to Pore Geometry: American Association of Petroleum Geologists Bulletin, v. 36, n. 2, p. 253-277.
- Worthington, Paul F., 1985, The evolution of shaly-sand concepts in reservoir evaluation: paper SPWLA 1985-vXXVIn1a2, The Log Analyst, v. 25, n.1, p 23-40.
- Worthington, P.F., Daines, J.M., Bratli, R.K., and Nicolaysen, R., 1997, Comparative Evaluation of Core Compaction Corrections for Clastic Reservoirs: paper SPWLA 1996-NN, SPWLA 37th Annual Logging Symposium, September-October, p. 19-29.
- Wu, T., and Berg, R.R., 2003, Relationship of Reservoir Properties for Shaly Sandstones Based on Effective Porosity: paper SPWLA 2003-v44n5a3, Petrophysics, v. 44, n. 5, p. 328-341.
- Wyllie, M.R.J., and W.D. Rose, 1950, Some theoretical considerations related to the quantitative evaluation of the physical characteristics of reservoir rock from electric log data: paper SPE 950105-G, Trans. AIME, v. 189, p. 105-118.
- Yale, D.P., and Nabor, G.W., Russell, J.A., Pham, H.D., Yousef, M., 1993, Application of Variable Formation Compressibility for Improved Reservoir Analysis: paper SPE 26647-MS, SPE Annual Technical Conference and Exhibition, 3-6 October 1993, Houston, Texas. DOI: [10.2118/26647-MS](https://doi.org/10.2118/26647-MS).
- Yanuka, M., and I. Balberg, 1991, Invasion percolation in a continuum model: Journal Physics A: Mathematical and General, v. 24, p. 2565-2568.
- Yanuka, M., F. Dullien, and D. Elrick, 1986, Percolation processes and porous media: I. geometrical and topological model of porous media using a three dimensional joint pore size distribution: Journal of Colloid and Interface Science, v. 112, n. 1, p. 24-36.
- Yortsos, Y. C. and M. Parlar, 1989, Phase change in binary systems in porous media: Application to solution gas drive: paper SPE 19697-MS, Presented at the 1989 Society of Petroleum Engineers Fall Meeting, San Antonio, Texas, Oct. 8-9. DOI: [10.2118/19697-MS](https://doi.org/10.2118/19697-MS).

APPENDICES

Porosity, Permeability and Grain Density Data.....	A1-1
Pore Volume Compressibility Data.....	A2-1
Critical Gas Saturation Data.....	A3-1
Capillary Pressure Data.....	A4-1
Electrical Resistivity Data.....	A5-1

Appendix A1

Summary of Porosity, Permeability and Grain Density

Analysis of Critical Permeability, Capillary Pressure and Electrical Properties for Mesaverde Tight Gas Sandstones from Western U.S. Basins

US DOE # DE-FC26-05NT42660 Final Scientific/Technical Report

Alan P. Byrnes, Robert M. Cluff, John C. Webb

website: <http://www.kgs.ku.edu/mesaverde>

USGS Library Number	Basin	API Number	Well Name	Operator	State	Township	Range	Section	Quarter Section	Plug Depth	Plug Letter	Ambient Porosity	Grain Density	Routine Gas Permeability	in situ		Rock Type	Formations
															Klinkenberg Gas Permeability	Klinkenberg constant b (psia)		
											ft	A/B/C	%	g/cc	mD	mD		
B029	Green River	4903520088	A-1 WASP	INEXCO OIL COMPANY	WY	36N	112W	28	NWNE	10441.1	B	1.6	2.62	0.00427	0.000167	311	13216	MVRD
B029	Green River	4903520088	A-1 WASP	INEXCO OIL COMPANY	WY	36N	112W	28	NWNE	10441.1	A	1.6	2.63	0.00234	0.000061	363	13216	MVRD
B029	Green River	4903520088	A-1 WASP	INEXCO OIL COMPANY	WY	36N	112W	28	NWNE	10441.1	B	1.6	2.62	0.00226	0.000123	240	13216	MVRD
B029	Green River	4903520088	A-1 WASP	INEXCO OIL COMPANY	WY	36N	112W	28	NWNE	10450.5	B	1.8	2.63	0.00629	0.000219	486	14276	MVRD
B029	Green River	4903520088	A-1 WASP	INEXCO OIL COMPANY	WY	36N	112W	28	NWNE	10450.5	A	1.7	2.63	0.00172	0.000014	353	14276	MVRD
B029	Green River	4903520088	A-1 WASP	INEXCO OIL COMPANY	WY	36N	112W	28	NWNE	10450.5	C	1.7	2.63	0.000362	0.000001	2918	14276	MVRD
B029	Green River	4903520088	A-1 WASP	INEXCO OIL COMPANY	WY	36N	112W	28	NWNE	10455.1	B	2.2	2.62	0.0102	0.000010	737	13217	MVRD
B029	Green River	4903520088	A-1 WASP	INEXCO OIL COMPANY	WY	36N	112W	28	NWNE	10455.1	C	1.9	2.61	0.00541	0.000131	238	13217	MVRD
B029	Green River	4903520088	A-1 WASP	INEXCO OIL COMPANY	WY	36N	112W	28	NWNE	10455.1	A	2.2	2.63	0.00539	0.000176	283	13217	MVRD
B029	Green River	4903520088	A-1 WASP	INEXCO OIL COMPANY	WY	36N	112W	28	NWNE	10458.8	C	2.8	2.63	0.00601	0.000019	384	13256	MVRD
B029	Green River	4903520088	A-1 WASP	INEXCO OIL COMPANY	WY	36N	112W	28	NWNE	10458.8	A	3.7	2.64	0.00513	0.000354	169	13256	MVRD
B029	Green River	4903520088	A-1 WASP	INEXCO OIL COMPANY	WY	36N	112W	28	NWNE	10458.8	B	3.5	2.62	0.00286	0.000169	289	13256	MVRD
B029	Green River	4903520088	A-1 WASP	INEXCO OIL COMPANY	WY	36N	112W	28	NWNE	10462.0	B	3.5	2.64	0.00489	0.000291	263	13256	MVRD
B029	Green River	4903520088	A-1 WASP	INEXCO OIL COMPANY	WY	36N	112W	28	NWNE	10462.0	A	3.5	2.64	0.00334	0.000223	471	15286	MVRD
B029	Green River	4903520088	A-1 WASP	INEXCO OIL COMPANY	WY	36N	112W	28	NWNE	10462.0	C	3.1	2.63	0.00239	0.000118	242	15286	MVRD
B029	Green River	4903520088	A-1 WASP	INEXCO OIL COMPANY	WY	36N	112W	28	NWNE	10481.9	C	1.9	2.62	0.00761	0.000021	407	14296	MVRD
B029	Green River	4903520088	A-1 WASP	INEXCO OIL COMPANY	WY	36N	112W	28	NWNE	10481.9	B	1.8	2.62	0.00484	0.000290	109	14296	MVRD
B029	Green River	4903520088	A-1 WASP	INEXCO OIL COMPANY	WY	36N	112W	28	NWNE	10481.9	A	2.1	2.62	0.00356	0.000045	867	14296	MVRD
B029	Green River	4903520088	A-1 WASP	INEXCO OIL COMPANY	WY	36N	112W	28	NWNE	10493.2	C	1.0	2.63	0.0131	0.000033	189	14296	MVRD
B029	Green River	4903520088	A-1 WASP	INEXCO OIL COMPANY	WY	36N	112W	28	NWNE	10493.2	A	1.1	2.63	0.00272	0.000022	690	14296	MVRD
B029	Green River	4903520088	A-1 WASP	INEXCO OIL COMPANY	WY	36N	112W	28	NWNE	10493.2	B	0.8	2.63	0.0162	0.000152	14296		MVRD
B029	Green River	4903520088	A-1 WASP	INEXCO OIL COMPANY	WY	36N	112W	28	NWNE	10500.8	C	1.1	2.63	0.00846	0.000013	732	13266	MVRD
B029	Green River	4903520088	A-1 WASP	INEXCO OIL COMPANY	WY	36N	112W	28	NWNE	10500.8	B	1.2	2.63	0.00791	0.000059	340	13266	MVRD
B029	Green River	4903520088	A-1 WASP	INEXCO OIL COMPANY	WY	36N	112W	28	NWNE	10500.8	A	1.6	2.64	0.00160	0.000039	535	13266	MVRD
B029	Green River	4903520088	A-1 WASP	INEXCO OIL COMPANY	WY	36N	112W	28	NWNE	10504.5	B	0.9	2.65	0.00932	0.000026	379	13266	MVRD
B029	Green River	4903520088	A-1 WASP	INEXCO OIL COMPANY	WY	36N	112W	28	NWNE	10504.5	C	0.9	2.65	0.00470	0.000131	228	13266	MVRD
B029	Green River	4903520088	A-1 WASP	INEXCO OIL COMPANY	WY	36N	112W	28	NWNE	10504.5	C	0.9	2.66			13266		MVRD
B029	Green River	4903520088	A-1 WASP	INEXCO OIL COMPANY	WY	36N	112W	28	NWNE	10514.8	C	1.9	2.61	1.54	0.0642	47.6	13216	MVRD
B029	Green River	4903520088	A-1 WASP	INEXCO OIL COMPANY	WY	36N	112W	28	NWNE	10514.8	A	1.0	2.59	0.243	0.000558	179	13216	MVRD
B029	Green River	4903520088	A-1 WASP	INEXCO OIL COMPANY	WY	36N	112W	28	NWNE	10514.8	B	4.6	2.60	0.0336	0.000155	150	13216	MVRD
B029	Green River	4903520088	A-1 WASP	INEXCO OIL COMPANY	WY	36N	112W	28	NWNE	10529.9	B	2.4	2.60	0.0193	0.000029	385	13256	MVRD
B029	Green River	4903520088	A-1 WASP	INEXCO OIL COMPANY	WY	36N	112W	28	NWNE	10529.9	C	2.3	2.60	0.00344	0.000101	389	13256	MVRD
B029	Green River	4903520088	A-1 WASP	INEXCO OIL COMPANY	WY	36N	112W	28	NWNE	10529.9	A	2.3	2.59	0.00315	0.000048	1240	13256	MVRD
B029	Green River	4903520088	A-1 WASP	INEXCO OIL COMPANY	WY	36N	112W	28	NWNE	10537.2	A	3.5	2.65	0.0118	0.000190	195	13256	MVRD
B029	Green River	4903520088	A-1 WASP	INEXCO OIL COMPANY	WY	36N	112W	28	NWNE	10537.2	B	3.3	2.64	0.00640	0.000337	271	13256	MVRD
B029	Green River	4903520088	A-1 WASP	INEXCO OIL COMPANY	WY	36N	112W	28	NWNE	10537.2	C	3.4	2.63	0.00330	0.000287	121	13256	MVRD
B029	Green River	4903520088	A-1 WASP	INEXCO OIL COMPANY	WY	36N	112W	28	NWNE	10540.5	C	1.7	2.62	0.00375	0.000120	211	13285	MVRD
B029	Green River	4903520088	A-1 WASP	INEXCO OIL COMPANY	WY	36N	112W	28	NWNE	10540.5	B	1.6	2.62	0.00241	0.000054	391	13285	MVRD
B029	Green River	4903520088	A-1 WASP	INEXCO OIL COMPANY	WY	36N	112W	28	NWNE	10540.5	A	1.7	2.63	0.00712	0.000066	455	13285	MVRD
B029	Green River	4903520088	A-1 WASP	INEXCO OIL COMPANY	WY	36N	112W	28	NWNE	10544.5	B	1.0	2.67	0.00252	0.000012	263	13216	MVRD
B029	Green River	4903520088	A-1 WASP	INEXCO OIL COMPANY	WY	36N	112W	28	NWNE	10544.5	C	0.6	2.66	0.000826	0.000006	426	16286	MVRD
B029	Green River	4903520088	A-1 WASP	INEXCO OIL COMPANY	WY	36N	112W	28	NWNE	10547.9	A	0.9	2.65	0.00299	0.000024	120	15286	MVRD
B029	Green River	4903520088	A-1 WASP	INEXCO OIL COMPANY	WY	36N	112W	28	NWNE	10547.9	A	1.2	2.65	0.000684	0.000014	464	15286	MVRD
B029	Green River	4903520088	A-1 WASP	INEXCO OIL COMPANY	WY	36N	112W	28	NWNE	10547.9	B	0.8	2.65	0.000628	0.000024	287	15286	MVRD
B029	Green River	4903520088	A-1 WASP	INEXCO OIL COMPANY	WY	36N	112W	28	NWNE	10557.5	C	1.1	2.63	0.00473	0.000132	214	13216	MVRD
B029	Green River	4903520088	A-1 WASP	INEXCO OIL COMPANY	WY	36N	112W	28	NWNE	10557.5	A	0.6	2.63	0.00399	0.000185	214	13216	MVRD
B029	Green River	4903520088	A-1 WASP	INEXCO OIL COMPANY	WY	36N	112W	28	NWNE	10557.5	B	0.8	2.63	0.00353	0.000083	247	13216	MVRD
B029	Green River	4903520088	A-1 WASP	INEXCO OIL COMPANY	WY	36N	112W	28	NWNE	10565.3	B	0.11	2.60	0.0112	0.000020	454	13216	MVRD
B029	Green River	4903520088	A-1 WASP	INEXCO OIL COMPANY	WY	36N	112W	28	NWNE	10565.3	A	1.1	2.60	0.00386	0.000063	454	13216	MVRD
B029	Green River	4903520088	A-1 WASP	INEXCO OIL COMPANY	WY	36N	112W	28	NWNE	10565.3	C	0.9	2.60	0.00303	0.000047	343	13216	MVRD
B029	Green River	4903520088	A-1 WASP	INEXCO OIL COMPANY	WY	36N	112W	28	NWNE	10573.1	B	3.1	2.66	0.00350	0.000201	152	13266	MVRD
B029	Green River	4903520088	A-1 WASP	INEXCO OIL COMPANY	WY	36N	112W	28	NWNE	10573.1	C	3.0	2.66	0.00307	0.000160	312	13266	MVRD
B029	Green River	4903520088	A-1 WASP	INEXCO OIL COMPANY	WY	36N	112W	28	NWNE	10573.1	A	3.3	2.67	0.00289	0.000155	465	13266	MVRD
B029	Green River	4903520088	A-1 WASP	INEXCO OIL COMPANY	WY	36N	112W	28	NWNE	11332.9	C	3.6	2.64	0.00491	0.000832	151	16286	MVRD
B029	Green River	4903520088	A-1 WASP	INEXCO OIL COMPANY	WY	36N	112W	28	NWNE	11332.9	A	3.5	2.64	0.00300	0.000728	136	16286	MVRD
B029	Green River	4903520088	A-1 WASP	INEXCO OIL COMPANY	WY	36N	112W	28	NWNE	11332.9	B	7.6	2.75	0.0298	0.000669	216	16286	MVRD
B029	Green River	4903520088	A-1 WASP	INEXCO OIL COMPANY	WY	36N	112W	28	NWNE	11332.9	A	3.7	2.64	0.0309	0.000484	135	16276	MVRD
B029	Green River	4903520088	A-1 WASP	INEXCO OIL COMPANY	WY	36N	112W	28	NWNE	11338.2	A	3.5	2.64	0.00436	0.000402	350	16276	MVRD
B029	Green River	4903520088	A-1 WASP	INEXCO OIL COMPANY	WY	36N	112W	28	NWNE	11338.2	C	3.6	2.66	0.00256	0.000398	178	16276	MVRD
B029	Green River	4903520088	A-1 WASP	INEXCO OIL COMPANY	WY	36N	112W	28	NWNE	11374.9	A	0.9	2.65	0.00353	0.000098	276	14296	MVRD
B029	Green River	4903520088	A-1 WASP	INEXCO OIL COMPANY	WY	36N	112W	28	NWNE	11374.9	A	0.9	2.65	0.00322	0.000083	228	14296	MVRD
B029	Green River	4903520088	A-1 WASP	INEXCO OIL COMPANY	WY	36N	112W	28	NWNE	11374.9	B	0.5	2.64	0.00112	0.000018	552	14296	MVRD
B029	Green River	4903520088	A-1 WASP	INEXCO OIL COMPANY	WY	36N	112W	28	NWNE	11388.3	C	1.4	2.62	0.00935	0.000222	176	12217	MVRD
B029	Green River	4903520088	A-1 WASP	INEXCO OIL COMPANY	WY	36N	112W	28	NWNE	11388.3	B	1.7	2.62	0.00632	0.000096	489	12217	MVRD
B029	Green River	4903520088	A-1 WASP	INEXCO OIL COMPANY	WY	36N	112W	28	NWNE	11388.3	A	1.1	2.61	0.00460	0.000101	743	12217	MVRD
B029	Green River	4903520088	A-1 WASP	INEXCO OIL COMPANY	WY	36N	112W	28	NWNE	11395.5	B	4.2	2.63	0.00445	0.000105	350	13267	MVRD
B029	Green River	4903520088	A-1 WASP	INEX														

Appendix A1

Summary of Porosity, Permeability and Grain Density

Analysis of Critical Permeability, Capillary Pressure and Electrical Properties for Mesaverde Tight Gas Sandstones from Western U.S. Basins

US DOE # DE-FC26-05NT42660 Final Scientific/Technical Report

Alan P. Byrnes, Robert M. Cluff, John C. Webb

website: <http://www.kgs.ku.edu/mesaverde>

USGS Library Number	Basin	API Number	Well Name	Operator	State	Township	Range	Section	Quarter Section	Plug Depth	Plug Letter	Ambient Porosity	Grain Density	Routine Gas Permeability	in situ		Rock Type Code	Formations
															Klinkenberg Gas Permeability	Klinkenberg constant b (psia)		
											ft	A/B/C	%	g/cc	mD	mD		
B029	Green River	4903520088	A-1 WASP	INEXCO OIL COMPANY	WY	36N	112W	28	NWNE	11460.5	B	5.1	2.65	0.0544	0.00177	104	15286	MVRD
B029	Green River	4903520088	A-1 WASP	INEXCO OIL COMPANY	WY	36N	112W	28	NWNE	11460.6	B	4.4	2.64	0.384	0.0255	37.1	15286	MVRD
B029	Green River	4903520088	A-1 WASP	INEXCO OIL COMPANY	WY	36N	112W	28	NWNE	11460.6	A	4.3	2.64	0.300	0.0155	83.8	15286	MVRD
B029	Green River	4903520088	A-1 WASP	INEXCO OIL COMPANY	WY	36N	112W	28	NWNE	11460.6	C	4.7	2.65	0.144	0.00744	78.0	15286	MVRD
B029	Green River	4903520088	A-1 WASP	INEXCO OIL COMPANY	WY	36N	112W	28	NWNE	11461.3	A	3.5	2.64	0.0105	0.000218	368	15296	MVRD
B029	Green River	4903520088	A-1 WASP	INEXCO OIL COMPANY	WY	36N	112W	28	NWNE	11461.3	B	3.6	2.65	0.00629		15296		MVRD
B029	Green River	4903520088	A-1 WASP	INEXCO OIL COMPANY	WY	36N	112W	28	NWNE	11461.3	C	3.4	2.66	0.000428	0.000256	155	15296	MVRD
B029	Green River	4903520088	A-1 WASP	INEXCO OIL COMPANY	WY	36N	112W	28	NWNE	11471.5	A	3.0	2.59	49.1	1.55	21.4	13296	MVRD
B029	Green River	4903520088	A-1 WASP	INEXCO OIL COMPANY	WY	36N	112W	28	NWNE	11471.5	B	0.7	2.59	0.0285	0.00170	147	13296	MVRD
B029	Green River	4903520088	A-1 WASP	INEXCO OIL COMPANY	WY	36N	112W	28	NWNE	11471.5	C	1.0	2.59	0.0103	0.000026	438	13296	MVRD
B029	Green River	4903520088	A-1 WASP	INEXCO OIL COMPANY	WY	36N	112W	28	NWNE	11474.5	A	2.8	2.64	0.0375	0.00146	43.8	13276	MVRD
B029	Green River	4903520088	A-1 WASP	INEXCO OIL COMPANY	WY	36N	112W	28	NWNE	11474.5	A	3.2	2.64	0.0353	0.00341	133	13276	MVRD
B029	Green River	4903520088	A-1 WASP	INEXCO OIL COMPANY	WY	36N	112W	28	NWNE	11474.5	B	2.6	2.63	0.0144	0.000407	242	13276	MVRD
B029	Green River	4903520088	A-1 WASP	INEXCO OIL COMPANY	WY	36N	112W	28	NWNE	11477.8	B	1.0	2.66	0.00382	0.000239	224	15276	MVRD
B029	Green River	4903520088	A-1 WASP	INEXCO OIL COMPANY	WY	36N	112W	28	NWNE	11477.8	C	1.3	2.66	0.00365	0.000121	337	15276	MVRD
B029	Green River	4903520088	A-1 WASP	INEXCO OIL COMPANY	WY	36N	112W	28	NWNE	11477.8	A	1.2	2.66	0.00233	0.000078	370	15276	MVRD
B029	Green River	4903520088	A-1 WASP	INEXCO OIL COMPANY	WY	36N	112W	28	NWNE	11478.1	B	0.4	2.61	0.00554	0.000105	377	13296	MVRD
B029	Green River	4903520088	A-1 WASP	INEXCO OIL COMPANY	WY	36N	112W	28	NWNE	11478.1	A	1.3	2.63	0.00293	0.000037	675	13296	MVRD
B029	Green River	4903520088	A-1 WASP	INEXCO OIL COMPANY	WY	36N	112W	28	NWNE	11478.1	c	1.4	2.66			13296		MVRD
B029	Green River	4903520088	A-1 WASP	INEXCO OIL COMPANY	WY	36N	112W	28	NWNE	11487.5	B	1.2	2.63	0.00459	0.000074	485	12296	MVRD
B029	Green River	4903520088	A-1 WASP	INEXCO OIL COMPANY	WY	36N	112W	28	NWNE	11487.5	A	1.2	2.62	0.00152	0.000010	1211	12296	MVRD
B029	Green River	4903520088	A-1 WASP	INEXCO OIL COMPANY	WY	36N	112W	28	NWNE	11487.5	C	0.8	2.61	0.00116	0.000015	1520	12296	MVRD
B029	Green River	4903520088	A-1 WASP	INEXCO OIL COMPANY	WY	36N	112W	28	NWNE	11488.8	A	1.0	2.62	0.00407	0.000071	496	12296	MVRD
B029	Green River	4903520088	A-1 WASP	INEXCO OIL COMPANY	WY	36N	112W	28	NWNE	11488.8	B	0.9	2.62	0.00396	0.000052	540	12296	MVRD
B029	Green River	4903520088	A-1 WASP	INEXCO OIL COMPANY	WY	36N	112W	28	NWNE	11488.8	C	0.9	2.60	0.00209	0.000018	262	12296	MVRD
B029	Green River	4903520088	A-1 WASP	INEXCO OIL COMPANY	WY	36N	112W	28	NWNE	11495.5	C	0.9	2.64	0.00377	0.000107	357	15276	MVRD
B029	Green River	4903520088	A-1 WASP	INEXCO OIL COMPANY	WY	36N	112W	28	NWNE	11495.5	A	0.7	2.63	0.00175	0.000023	409	15276	MVRD
B029	Green River	4903520088	A-1 WASP	INEXCO OIL COMPANY	WY	36N	112W	28	NWNE	11495.5	B	1.0	2.64	0.000669	0.000013	443	15276	MVRD
B029	Green River	4903520088	A-1 WASP	INEXCO OIL COMPANY	WY	36N	112W	28	NWNE	11504.0	B	3.5	2.64	0.0207	0.000416	190	16296	MVRD
B029	Green River	4903520088	A-1 WASP	INEXCO OIL COMPANY	WY	36N	112W	28	NWNE	11504.0	A	3.0	2.62	0.0120	0.000194	207	16296	MVRD
B029	Green River	4903520088	A-1 WASP	INEXCO OIL COMPANY	WY	36N	112W	28	NWNE	11504.0	A2	3.3	2.63	0.00607	0.000340	187	16296	MVRD
B029	Green River	4903520088	A-1 WASP	INEXCO OIL COMPANY	WY	36N	112W	28	NWNE	11504.0	B2	3.2	2.63	0.00542	0.000330	187	16296	MVRD
B029	Green River	4903520088	A-1 WASP	INEXCO OIL COMPANY	WY	36N	112W	28	NWNE	11504.0	C	3.0	2.63	0.00250	0.000235	90.6	16296	MVRD
B029	Green River	4903520088	A-1 WASP	INEXCO OIL COMPANY	WY	36N	112W	28	NWNE	11504.0	C2	3.4	2.63	0.00240	0.000105	350	16296	MVRD
B029	Green River	4903520088	A-1 WASP	INEXCO OIL COMPANY	WY	36N	112W	28	NWNE	11504.1	A	3.4	2.63	0.00425	0.000226	247	16296	MVRD
B029	Green River	4903520088	A-1 WASP	INEXCO OIL COMPANY	WY	36N	112W	28	NWNE	11504.1	B	3.0	2.62	0.00422	0.000519	83.8	16296	MVRD
B029	Green River	4903520088	A-1 WASP	INEXCO OIL COMPANY	WY	36N	112W	28	NWNE	11504.1	C	3.3	2.63	0.00230	0.000152	619	16296	MVRD
B029	Green River	4903520088	A-1 WASP	INEXCO OIL COMPANY	WY	36N	112W	28	NWNE	11505.3	A	2.6	2.6	0.00400	0.000152	84.2	15276	MVRD
B029	Green River	4903520088	A-1 WASP	INEXCO OIL COMPANY	WY	36N	112W	28	NWNE	11505.3	C	3.0	2.65	0.00289	0.000207	140	15276	MVRD
B029	Green River	4903520088	A-1 WASP	INEXCO OIL COMPANY	WY	36N	112W	28	NWNE	11505.3	B	2.9	2.65	0.00275	0.000098	521	15276	MVRD
B029	Green River	4903520088	A-1 WASP	INEXCO OIL COMPANY	WY	36N	112W	28	NWNE	11515.1	C	8.8	2.64	0.00412	0.000101	255	14296	MVRD
B029	Green River	4903520088	A-1 WASP	INEXCO OIL COMPANY	WY	36N	112W	28	NWNE	11515.1	B1	0.5	2.64	0.00408	0.000173	250	14296	MVRD
B029	Green River	4903520088	A-1 WASP	INEXCO OIL COMPANY	WY	36N	112W	28	NWNE	11515.1	A	0.6	2.64	0.00492		14296		MVRD
B029	Green River	4903520088	A-1 WASP	INEXCO OIL COMPANY	WY	36N	112W	28	NWNE	11522.5	B	0.3	2.63	0.00466	0.000114	620	13266	MVRD
B029	Green River	4903520088	A-1 WASP	INEXCO OIL COMPANY	WY	36N	112W	28	NWNE	11522.5	A	0.9	2.65	0.00199	0.000039	686	13266	MVRD
B029	Green River	4903520088	A-1 WASP	INEXCO OIL COMPANY	WY	36N	112W	28	NWNE	11522.5	C	0.7	2.64	0.000618	0.000008	765	13266	MVRD
B029	Green River	4903520088	A-1 WASP	INEXCO OIL COMPANY	WY	36N	112W	28	NWNE	11530.7	B	0.5	2.64	0.00423	0.000077	1169	12296	MVRD
B029	Green River	4903520088	A-1 WASP	INEXCO OIL COMPANY	WY	36N	112W	28	NWNE	11530.7	A	0.6	2.64	0.00201	0.000023	488	12296	MVRD
B029	Green River	4903520088	A-1 WASP	INEXCO OIL COMPANY	WY	36N	112W	28	NWNE	11530.7	C	0.7	2.65	0.00194	0.000003	241	12296	MVRD
B029	Green River	4903520088	A-1 WASP	INEXCO OIL COMPANY	WY	36N	112W	28	NWNE	11534.0	B	1.5	2.64	0.00631	0.000137	236	14296	MVRD
B029	Green River	4903520088	A-1 WASP	INEXCO OIL COMPANY	WY	36N	112W	28	NWNE	11534.0	C	0.8	2.64	0.00115	0.000021	493	14296	MVRD
B029	Green River	4903520088	A-1 WASP	INEXCO OIL COMPANY	WY	36N	112W	28	NWNE	11534.0	A	1.9	2.65	0.000901	0.000008	583	14296	MVRD
B029	Green River	4903520088	A-1 WASP	INEXCO OIL COMPANY	WY	36N	112W	28	NWNE	11534.1	B	1.6	2.65	0.00227	0.000014	545	14296	MVRD
B029	Green River	4903520088	A-1 WASP	INEXCO OIL COMPANY	WY	36N	112W	28	NWNE	11534.1	C	1.4	2.64	0.00151	0.000024	513	14296	MVRD
B029	Green River	4903520088	A-1 WASP	INEXCO OIL COMPANY	WY	36N	112W	28	NWNE	11534.1	A	1.4	2.64	0.00148	0.000002	921	14296	MVRD
B029	Green River	4903520088	A-1 WASP	INEXCO OIL COMPANY	WY	36N	112W	28	NWNE	11534.2	B	1.5	2.64	0.00603	0.000119	420	14296	MVRD
B029	Green River	4903520088	A-1 WASP	INEXCO OIL COMPANY	WY	36N	112W	28	NWNE	11534.2	C	1.3	2.64	0.00432	0.000121	261	14296	MVRD
B029	Green River	4903520088	A-1 WASP	INEXCO OIL COMPANY	WY	36N	112W	28	NWNE	11534.2	A	1.7	2.64	0.00263	0.000043	741	14296	MVRD
B029	Green River	4903520088	A-1 WASP	INEXCO OIL COMPANY	WY	36N	112W	28	NWNE	11535.0	C	5.0	2.75	0.00403		14266		MVRD
B029	Green River	4903520088	A-1 WASP	INEXCO OIL COMPANY	WY	36N	112W	28	NWNE	11535.0	B	1.1	2.64	0.00147	0.000010	368	14266	MVRD
B029	Green River	4903520088	A-1 WASP	INEXCO OIL COMPANY	WY	36N	112W	28	NWNE	11535.0	A	1.2	2.64	0.000779	0.000037	183	14266	MVRD
B029	Green River	4903520088	A-1 WASP	INEXCO OIL COMPANY	WY	36N	112W	28	NWNE	11539.0	A	2.1	2.64	0.00828	0.000108	126	14266	MVRD
B029	Green River	4903520088	A-1 WASP	INEXCO OIL COMPANY	WY	36N	112W	28	NWNE	11539.0	B	2.6	2.63	0.00137	0.000029	335	14266	MVRD
B029	Green River	4903520088	A-1 WASP	INEXCO OIL COMPANY	WY	36N	112W	28	NWNE	11539.0	C	3.3	2.65	0.00171	0.000171	283	14266	MVRD
B029	Green River	4903520088	A-1 WASP	INEXCO OIL COMPANY	WY	36N	112W	28	NWNE	11540.9	B	2.3	2.63	0.00674	0.000226	253	13266	MVRD
B029	Green River	4903520088	A-1 WASP	INEXCO OIL COMPANY	WY	36N	112W	28	NWNE	11540.9	C	2.3	2.63	0.00608	0.000118	306	13266	MVRD
B029	Green River	4903520088	A-1 WASP	INEXCO OIL COMPANY	WY	36N	112W	28										

Appendix A1

Summary of Porosity, Permeability and Grain Density

Analysis of Critical Permeability, Capillary Pressure and Electrical Properties for Mesaverde Tight Gas Sandstones from Western U.S. Basins

US DOE # DE-FC26-05NT42660 Final Scientific/Technical Report

Alan P. Byrnes, Robert M. Cluff, John C. Webb

website: <http://www.kgs.ku.edu/mesaverde>

USGS Library Number	Basin	API Number	Well Name	Operator	State	Township	Range	Section	Quarter Section	Plug Depth	Plug Letter	Ambient Porosity	Grain Density	Routine Gas Permeability	in situ		Rock Type Code	Formations
															Klinkenberg Gas Permeability	Klinkenberg constant b		
											ft	A/B/C	%	g/cc	mD	mD		
B029	Green River	4903520088	A-1 WASP	INEXCO OIL COMPANY	WY	36N	112W	28	NWNE	11578.2	A	1.2	2.64	0.00276	0.00042	758	13266	MVRD
B029	Green River	4903520088	A-1 WASP	INEXCO OIL COMPANY	WY	36N	112W	28	NWNE	11578.2	B	0.9	2.64	0.00165	0.00025	435	13266	MVRD
B029	Green River	4903520088	A-1 WASP	INEXCO OIL COMPANY	WY	36N	112W	28	NWNE	11578.2	C	0.2	2.64	0.000682	0.00002	1450	13266	MVRD
B029	Green River	4903520088	A-1 WASP	INEXCO OIL COMPANY	WY	36N	112W	28	NWNE	11584.0	C	1.8	2.64	0.00377	0.000120	405	14297	MVRD
B029	Green River	4903520088	A-1 WASP	INEXCO OIL COMPANY	WY	36N	112W	28	NWNE	11584.0	B	1.7	2.63	0.00346	0.000111	311	14297	MVRD
B029	Green River	4903520088	A-1 WASP	INEXCO OIL COMPANY	WY	36N	112W	28	NWNE	11584.0	A	2.2	2.64	0.00231	0.000071	329	14297	MVRD
B029	Green River	4903520088	A-1 WASP	INEXCO OIL COMPANY	WY	36N	112W	28	NWNE	11587.2	B	4.2	2.63	0.0412	0.000394	192	13267	MVRD
B029	Green River	4903520088	A-1 WASP	INEXCO OIL COMPANY	WY	36N	112W	28	NWNE	11587.2	A	3.5	2.63	0.0324	0.000902	457	13267	MVRD
B029	Green River	4903520088	A-1 WASP	INEXCO OIL COMPANY	WY	36N	112W	28	NWNE	11587.2	C	4.4	2.64	0.0282	0.000432	101	13267	MVRD
B029	Green River	4903520088	A-1 WASP	INEXCO OIL COMPANY	WY	36N	112W	28	NWNE	11592.7	A	4.6	2.62	0.00552	0.000233	448	13257	MVRD
B029	Green River	4903520088	A-1 WASP	INEXCO OIL COMPANY	WY	36N	112W	28	NWNE	11592.7	C	5.4	2.65	0.00512	0.000157	834	13257	MVRD
B029	Green River	4903520088	A-1 WASP	INEXCO OIL COMPANY	WY	36N	112W	28	NWNE	11592.7	B	4.6	2.62	0.00393	0.000227	114	13257	MVRD
B029	Green River	4903520088	A-1 WASP	INEXCO OIL COMPANY	WY	36N	112W	28	NWNE	11605.1	C	4.9	2.63	0.0355	0.000971	99	15276	MVRD
B029	Green River	4903520088	A-1 WASP	INEXCO OIL COMPANY	WY	36N	112W	28	NWNE	11605.1	B	3.2	2.65	0.00255	0.000228	247	15296	MVRD
B029	Green River	4903520088	A-1 WASP	INEXCO OIL COMPANY	WY	36N	112W	28	NWNE	11605.1	A	2.9	2.64	0.00169	0.000138	368	15296	MVRD
B029	Green River	4903520088	A-1 WASP	INEXCO OIL COMPANY	WY	36N	112W	28	NWNE	11609.1	C	5.9	2.64	0.0907	0.00772	59.4	15276	MVRD
B029	Green River	4903520088	A-1 WASP	INEXCO OIL COMPANY	WY	36N	112W	28	NWNE	11609.2	C	6.0	2.63	0.113	0.00663	37.8	15276	MVRD
B029	Green River	4903520088	A-1 WASP	INEXCO OIL COMPANY	WY	36N	112W	28	NWNE	11609.2	B	5.8	2.63	0.0931	0.00833	87.9	15276	MVRD
B029	Green River	4903520088	A-1 WASP	INEXCO OIL COMPANY	WY	36N	112W	28	NWNE	11609.2	A	5.2	2.63	0.0760	0.00475	72.2	15276	MVRD
B029	Green River	4903520088	A-1 WASP	INEXCO OIL COMPANY	WY	36N	112W	28	NWNE	11615.1	A	4.6	2.63	0.0506	0.00192	63.5	15276	MVRD
B029	Green River	4903520088	A-1 WASP	INEXCO OIL COMPANY	WY	36N	112W	28	NWNE	11615.1	B	5.0	2.64	0.0398	0.00169	70.8	15276	MVRD
B029	Green River	4903520088	A-1 WASP	INEXCO OIL COMPANY	WY	36N	112W	28	NWNE	11615.1	C	4.9	2.63	0.0355	0.000971	99	15276	MVRD
B029	Green River	4903520088	A-1 WASP	INEXCO OIL COMPANY	WY	36N	112W	28	NWNE	11621.5	C	1.2	2.62	0.0105	0.000016	514	12286	MVRD
B029	Green River	4903520088	A-1 WASP	INEXCO OIL COMPANY	WY	36N	112W	28	NWNE	11621.5	B	1.4	2.63	0.00393	0.000113	207	12286	MVRD
B029	Green River	4903520088	A-1 WASP	INEXCO OIL COMPANY	WY	36N	112W	28	NWNE	11621.5	A	1.8	2.63	0.00331	0.000072	294	12286	MVRD
B029	Green River	4903520088	A-1 WASP	INEXCO OIL COMPANY	WY	36N	112W	28	NWNE	11626.5	C	0.8	2.64	0.00483	0.000078	477	13286	MVRD
B029	Green River	4903520088	A-1 WASP	INEXCO OIL COMPANY	WY	36N	112W	28	NWNE	11626.5	B	0.3	2.63	0.00355	0.000093	275	13286	MVRD
B029	Green River	4903520088	A-1 WASP	INEXCO OIL COMPANY	WY	36N	112W	28	NWNE	11626.5	A	0.4	2.63	0.00195	0.000062	250	13286	MVRD
B029	Green River	4903520088	A-1 WASP	INEXCO OIL COMPANY	WY	36N	112W	28	NWNE	11660.0	C	1.6	2.63	0.00443	0.000104	164	12216	MVRD
B029	Green River	4903520088	A-1 WASP	INEXCO OIL COMPANY	WY	36N	112W	28	NWNE	11660.0	A	1.2	2.61	0.00289	0.000045	555	12216	MVRD
B029	Green River	4903520088	A-1 WASP	INEXCO OIL COMPANY	WY	36N	112W	28	NWNE	11660.0	B	2.4	2.62	0.00147	0.00006	637	12216	MVRD
B029	Green River	4903520088	A-1 WASP	INEXCO OIL COMPANY	WY	36N	112W	28	NWNE	11888.0	C	2.5	2.65	0.0201	0.000269	35.0	15296	MVRD
B029	Green River	4903520088	A-1 WASP	INEXCO OIL COMPANY	WY	36N	112W	28	NWNE	11888.0	A	2.6	2.65	0.00461	0.000285	199	15296	MVRD
B029	Green River	4903520088	A-1 WASP	INEXCO OIL COMPANY	WY	36N	112W	28	NWNE	11888.0	B	2.8	2.65	0.00343	0.000017	417	15296	MVRD
B029	Green River	4903520088	A-1 WASP	INEXCO OIL COMPANY	WY	36N	112W	28	NWNE	11695.1	A	3.7	2.63	0.00378	0.000078	112	15276	MVRD
B029	Green River	4903520088	A-1 WASP	INEXCO OIL COMPANY	WY	36N	112W	28	NWNE	11695.1	C	3.6	2.63	0.00317	0.000202	174	15276	MVRD
B029	Green River	4903520088	A-1 WASP	INEXCO OIL COMPANY	WY	36N	112W	28	NWNE	11695.1	B	3.6	2.63	0.00228	0.000207	153	15276	MVRD
B029	Green River	4903520088	A-1 WASP	INEXCO OIL COMPANY	WY	36N	112W	28	NWNE	11700.0	C	2.5	2.62	0.00427	0.000237	234	13286	MVRD
B029	Green River	4903520088	A-1 WASP	INEXCO OIL COMPANY	WY	36N	112W	28	NWNE	11700.0	A	2.8	2.62	0.00339	0.000142	239	13286	MVRD
B029	Green River	4903520088	A-1 WASP	INEXCO OIL COMPANY	WY	36N	112W	28	NWNE	11700.0	B	2.4	2.62	0.00202	0.00007	260	13286	MVRD
B029	Green River	4903520088	A-1 WASP	INEXCO OIL COMPANY	WY	36N	112W	28	NWNE	11705.5	A	3.2	2.64	0.0350	0.000520	107	15276	MVRD
B029	Green River	4903520088	A-1 WASP	INEXCO OIL COMPANY	WY	36N	112W	28	NWNE	11705.5	C	3.6	2.64	0.0332	0.000551	149	15276	MVRD
B029	Green River	4903520088	A-1 WASP	INEXCO OIL COMPANY	WY	36N	112W	28	NWNE	11705.5	B	3.6	2.64	0.0195	0.000568	109	15276	MVRD
B029	Green River	4903520088	A-1 WASP	INEXCO OIL COMPANY	WY	36N	112W	28	NWNE	11706.7	A	4.0	2.63	0.0329	0.000524	154	16276	MVRD
B029	Green River	4903520088	A-1 WASP	INEXCO OIL COMPANY	WY	36N	112W	28	NWNE	11706.7	C	5.1	2.63	0.0250	0.000690	155	16276	MVRD
B029	Green River	4903520088	A-1 WASP	INEXCO OIL COMPANY	WY	36N	112W	28	NWNE	11706.8	B	3.9	2.64	0.0344	0.000810	55.4	16276	MVRD
B029	Green River	4903520088	A-1 WASP	INEXCO OIL COMPANY	WY	36N	112W	28	NWNE	11706.8	A	3.3	2.64	0.0330	0.000572	142	16276	MVRD
B029	Green River	4903520088	A-1 WASP	INEXCO OIL COMPANY	WY	36N	112W	28	NWNE	11706.8	C	3.7	2.64	0.0226	0.000374	116	16276	MVRD
B029	Green River	4903520088	A-1 WASP	INEXCO OIL COMPANY	WY	36N	112W	28	NWNE	11706.9	B	3.0	2.63	0.0445	0.00093	91.1	16276	MVRD
B029	Green River	4903520088	A-1 WASP	INEXCO OIL COMPANY	WY	36N	112W	28	NWNE	11706.9	A	4.0	2.64	0.0372	0.00110	75.7	16276	MVRD
B029	Green River	4903520088	A-1 WASP	INEXCO OIL COMPANY	WY	36N	112W	28	NWNE	11706.9	C	3.8	2.64	0.0339	0.000405	227	16276	MVRD
B029	Green River	4903520088	A-1 WASP	INEXCO OIL COMPANY	WY	36N	112W	28	NWNE	11716.1	C	3.4	2.63	0.0495	0.000460	200	16276	MVRD
B029	Green River	4903520088	A-1 WASP	INEXCO OIL COMPANY	WY	36N	112W	28	NWNE	11716.1	B	4.1	2.65	0.0376	0.000431	288	16276	MVRD
B029	Green River	4903520088	A-1 WASP	INEXCO OIL COMPANY	WY	36N	112W	28	NWNE	11716.1	A	3.8	2.65	0.0270	0.000562	155	16276	MVRD
B029	Green River	4903520088	A-1 WASP	INEXCO OIL COMPANY	WY	36N	112W	28	NWNE	11717.9	C	3.0	2.62	0.00500	0.000112	435	13286	MVRD
B029	Green River	4903520088	A-1 WASP	INEXCO OIL COMPANY	WY	36N	112W	28	NWNE	11717.9	B	3.3	2.63	0.00386	0.000129	440	13286	MVRD
B029	Green River	4903520088	A-1 WASP	INEXCO OIL COMPANY	WY	36N	112W	28	NWNE	11717.9	A	3.0	2.62	0.00364	0.000233	238	13286	MVRD
B029	Green River	4903520088	A-1 WASP	INEXCO OIL COMPANY	WY	36N	112W	28	NWNE	11721.9	C	4.5	2.64	0.0337	0.000874	104	16296	MVRD
B029	Green River	4903520088	A-1 WASP	INEXCO OIL COMPANY	WY	36N	112W	28	NWNE	11721.9	B	4.3	2.64	0.0219	0.000320	132	16296	MVRD
B029	Green River	4903520088	A-1 WASP	INEXCO OIL COMPANY	WY	36N	112W	28	NWNE	11721.9	A	4.5	2.64	0.00469	0.000176	343	16296	MVRD
B029	Green River	4903520088	A-1 WASP	INEXCO OIL COMPANY	WY	36N	112W	28	NWNE	11722.0	C	4.4	2.64	0.0375	0.000503	222	16296	MVRD
B029	Green River	4903520088	A-1 WASP	INEXCO OIL COMPANY	WY	36N	112W	28	NWNE	11722.0	B	4.3	2.65	0.0288	0.000757	64.2	16296	MVRD
B029	Green River	4903520088	A-1 WASP	INEXCO OIL COMPANY	WY	36N	112W	28	NWNE	11722.0	A	4.3	2.64	0.0206	0.000447	236	16296	MVRD
B029	Green River	4903520088	A-1 WASP	INEXCO OIL COMPANY	WY	36N	112W	28	NWNE	11724.2	A	3.7	2.64	0.0227	0.000863	128	16296	MVRD
B029	Green River	4903520088	A-1 WASP	INEXCO OIL COMPANY	WY	36N	112W	28	NWNE	11724.2	B	4.1	2.64	0.00466	0.000545	128	16296	MVRD
B029	Green River	4903520088	A-1 WASP	INEXCO OIL COMPANY	WY	36N	112W	28	NWNE	11724.3	A	3.5	2.64	0.00647	0.000841	42.8	16296	MVRD
B029	Green River	4903520088	A-1 WASP	INEXCO OIL COMPANY														

Appendix A1

Summary of Porosity, Permeability and Grain Density

Analysis of Critical Permeability, Capillary Pressure and Electrical Properties for Mesaverde Tight Gas Sandstones from Western U.S. Basins

US DOE # DE-FC26-05NT42660 Final Scientific/Technical Report

Alan P. Byrnes, Robert M. Cluff, John C. Webb

website: <http://www.kgs.ku.edu/mesaverde>

USGS Library Number	Basin	API Number	Well Name	Operator	State	Township	Range	Section	Quarter Section	Plug Depth	Plug Letter	Ambient Porosity	Grain Density	Routine Gas Permeability	in situ		Rock Type Code	Formations
															Klinkenberg Gas Permeability	Klinkenberg constant b (psia)		
											ft	A/B/C	%	g/cc	mD	mD		
E712	Green River	4903506020	B-54 BIG PINEY	BELCO PETROLEUM	WY	29N	113W	26	SESENE	3433.9	B	17.5	2.65	32.6	25.1	3.0	15585	MVRD
E712	Green River	4903506020	B-54 BIG PINEY	BELCO PETROLEUM	WY	29N	113W	26	SESENE	3433.9	B	17.2	2.65	32.5	24.5	3.2	15585	MVRD
E712	Green River	4903506020	B-54 BIG PINEY	BELCO PETROLEUM	WY	29N	113W	26	SESENE	3451.8	B	18.0	2.65	30.9	12.3	24.2	15585	MVRD
E712	Green River	4903506020	B-54 BIG PINEY	BELCO PETROLEUM	WY	29N	113W	26	SESENE	3451.8	A	17.3	2.64	5.31	0.289	11.1	15585	MVRD
E712	Green River	4903506020	B-54 BIG PINEY	BELCO PETROLEUM	WY	29N	113W	26	SESENE	3461.5	B	18.7	2.65	50.0	28.1	11.2	15585	MVRD
E712	Green River	4903506020	B-54 BIG PINEY	BELCO PETROLEUM	WY	29N	113W	26	SESENE	3461.5	A	18.2	2.63	44.1	17.1	3.5	15585	MVRD
E712	Green River	4903506020	B-54 BIG PINEY	BELCO PETROLEUM	WY	29N	113W	26	SESENE	3461.6	B	18.7	2.65	47.5	29.5	8.1	15585	MVRD
E712	Green River	4903506020	B-54 BIG PINEY	BELCO PETROLEUM	WY	29N	113W	26	SESENE	3461.6	A	18.3	2.64	41.1	30.5	3.5	15585	MVRD
E712	Green River	4903506020	B-54 BIG PINEY	BELCO PETROLEUM	WY	29N	113W	26	SESENE	3461.6	A	18.3	2.64	41.1	27.5	6.2	15585	MVRD
E712	Green River	4903506020	B-54 BIG PINEY	BELCO PETROLEUM	WY	29N	113W	26	SESENE	3461.7	A	17.9	2.65	38.5	2.42	8.7	15585	MVRD
E712	Green River	4903506020	B-54 BIG PINEY	BELCO PETROLEUM	WY	29N	113W	26	SESENE	3461.9	A	18.1	2.65	41.4	27.9	6.9	15585	MVRD
E712	Green River	4903506020	B-54 BIG PINEY	BELCO PETROLEUM	WY	29N	113W	26	SESENE	3461.9	B	18.5	2.65	39.7	29.7	4.0	15585	MVRD
E712	Green River	4903506020	B-54 BIG PINEY	BELCO PETROLEUM	WY	29N	113W	26	SESENE	3462.0	A	18.8	2.65	43.7	26.8	9.3	15585	MVRD
E712	Green River	4903506020	B-54 BIG PINEY	BELCO PETROLEUM	WY	29N	113W	26	SESENE	3462.0	B	18.8	2.65	41.9	27.7	7.5	15585	MVRD
E712	Green River	4903506020	B-54 BIG PINEY	BELCO PETROLEUM	WY	29N	113W	26	SESENE	3471.8	A	17.9	2.63	38.2	26.1	6.5	15585	MVRD
E712	Green River	4903506020	B-54 BIG PINEY	BELCO PETROLEUM	WY	29N	113W	26	SESENE	3471.8	B	18.1	2.65	34.6	24.1	5.4	15585	MVRD
E712	Green River	4903506020	B-54 BIG PINEY	BELCO PETROLEUM	WY	29N	113W	26	SESENE	3477.8	A	16.6	2.66	15.3	10.6	8.3	15585	MVRD
E712	Green River	4903506020	B-54 BIG PINEY	BELCO PETROLEUM	WY	29N	113W	26	SESENE	3477.8	B	15.9	2.66	14.7	10.1	7.0	15585	MVRD
E712	Green River	4903506020	B-54 BIG PINEY	BELCO PETROLEUM	WY	29N	113W	26	SESENE	3477.9	A	16.0	2.65	14.5	9.77	6.5	15585	MVRD
E712	Green River	4903506020	B-54 BIG PINEY	BELCO PETROLEUM	WY	29N	113W	26	SESENE	3480.8	A	8.8	2.68	0.0613	0.00580	111	13265	MVRD
E712	Green River	4903506020	B-54 BIG PINEY	BELCO PETROLEUM	WY	29N	113W	26	SESENE	3480.8	B	8.9	2.69	0.0594	0.00579	99.5	13265	MVRD
E712	Green River	4903506020	B-54 BIG PINEY	BELCO PETROLEUM	WY	29N	113W	26	SESENE	3487.9	B	16.1	2.63	9.34	6.35	4.2	15577	MVRD
E712	Green River	4903506020	B-54 BIG PINEY	BELCO PETROLEUM	WY	29N	113W	26	SESENE	3487.9	A	15.8	2.64	3.39	1.63	15.6	16577	MVRD
E712	Green River	4903506020	B-54 BIG PINEY	BELCO PETROLEUM	WY	29N	113W	26	SESENE	3489.1	B	16.5	2.66	10.2	6.49	6.4	15585	MVRD
E712	Green River	4903506020	B-54 BIG PINEY	BELCO PETROLEUM	WY	29N	113W	26	SESENE	3489.1	A	16.5	2.66	9.45	6.42	9.3	15585	MVRD
E712	Green River	4903506020	B-54 BIG PINEY	BELCO PETROLEUM	WY	29N	113W	26	SESENE	3489.3	B	16.5	2.66	9.13	5.02	12.6	15585	MVRD
E712	Green River	4903506020	B-54 BIG PINEY	BELCO PETROLEUM	WY	29N	113W	26	SESENE	3489.3	A	16.2	2.66	8.20	5.33	10.3	15585	MVRD
E712	Green River	4903506020	B-54 BIG PINEY	BELCO PETROLEUM	WY	29N	113W	26	SESENE	3497.9	A	18.4	2.65	18.5	13.9	4.3	15587	MVRD
E712	Green River	4903506020	B-54 BIG PINEY	BELCO PETROLEUM	WY	29N	113W	26	SESENE	3497.9	B	18.9	2.67	18.1	13.9	4.3	15587	MVRD
E712	Green River	4903506020	B-54 BIG PINEY	BELCO PETROLEUM	WY	29N	113W	26	SESENE	3498.1	B	18.9	2.67	18.3	11.8	8.2	15587	MVRD
E712	Green River	4903506020	B-54 BIG PINEY	BELCO PETROLEUM	WY	29N	113W	26	SESENE	3498.1	A	18.5	2.66	14.8	10.3	4.4	15587	MVRD
E712	Green River	4903506020	B-54 BIG PINEY	BELCO PETROLEUM	WY	29N	113W	26	SESENE	3503.7	A	8.8	2.66	0.0207	0.000792	130	12219	MVRD
E712	Green River	4903506020	B-54 BIG PINEY	BELCO PETROLEUM	WY	29N	113W	26	SESENE	3503.7	A	7.8	2.63	0.0201	0.000893	86.8	12219	MVRD
E712	Green River	4903506020	B-54 BIG PINEY	BELCO PETROLEUM	WY	29N	113W	26	SESENE	3503.8	B	8.4	2.65	0.160	0.0532	37.5	12219	MVRD
E712	Green River	4903506020	B-54 BIG PINEY	BELCO PETROLEUM	WY	29N	113W	26	SESENE	3503.8	A	8.4	2.66	0.0178	0.000753	108	12219	MVRD
E712	Green River	4903506020	B-54 BIG PINEY	BELCO PETROLEUM	WY	29N	113W	26	SESENE	3508.2	A	7.9	2.67	0.111	0.00371	95.2	12245	MVRD
E712	Green River	4903506020	B-54 BIG PINEY	BELCO PETROLEUM	WY	29N	113W	26	SESENE	3511.8	B	13.5	2.68	2.32	0.777	40.9	15575	MVRD
E712	Green River	4903506020	B-54 BIG PINEY	BELCO PETROLEUM	WY	29N	113W	26	SESENE	3511.8	A	13.1	2.68	1.22	0.706	20.5	15575	MVRD
E712	Green River	4903506020	B-54 BIG PINEY	BELCO PETROLEUM	WY	29N	113W	26	SESENE	3514.2	A	15.7	2.69	8.23	5.19	13.5	15575	MVRD
E712	Green River	4903506020	B-54 BIG PINEY	BELCO PETROLEUM	WY	29N	113W	26	SESENE	3514.2	B	15.5	2.69	7.86	8.45	10.5	15575	MVRD
E712	Green River	4903506020	B-54 BIG PINEY	BELCO PETROLEUM	WY	29N	113W	26	SESENE	3515.8	A	11.6	2.70	0.150	0.0205	89.5	15275	MVRD
E712	Green River	4903506020	B-54 BIG PINEY	BELCO PETROLEUM	WY	29N	113W	26	SESENE	3515.8	B	12.0	2.71	0.142	0.0199	106	15275	MVRD
E712	Green River	4903506020	B-54 BIG PINEY	BELCO PETROLEUM	WY	29N	113W	26	SESENE	3519.3	B	16.1	2.70	8.42	6.02	13.2	13235	MVRD
E712	Green River	4903506020	B-54 BIG PINEY	BELCO PETROLEUM	WY	29N	113W	26	SESENE	3519.3	A	16.3	2.70	8.29	6.81	7.3	13235	MVRD
E894	Green River	4903520622	1 OLD ROAD	AMERICAN HUNTER EXPL	WY	27N	108W	27	SENWSE	11892.8	B	7.0	2.71	0.0239	0.00431	50.8	13255	LNCE
E894	Green River	4903520622	1 OLD ROAD	AMERICAN HUNTER EXPL	WY	27N	108W	27	SENWSE	11892.8	A	7.0	2.72	0.0158	0.00283	80.7	13255	LNCE
E894	Green River	4903520622	1 OLD ROAD	AMERICAN HUNTER EXPL	WY	27N	108W	27	SENWSE	11894.1	B	6.1	2.70	0.00634	0.000648	187	15265	LNCE
E894	Green River	4903520622	1 OLD ROAD	AMERICAN HUNTER EXPL	WY	27N	108W	27	SENWSE	11894.1	A	6.3	2.70	0.00581	0.000611	158	15265	LNCE
E894	Green River	4903520622	1 OLD ROAD	AMERICAN HUNTER EXPL	WY	27N	108W	27	SENWSE	11894.2	B	7.9	2.68	0.0251	0.00354	148	15265	LNCE
E894	Green River	4903520622	1 OLD ROAD	AMERICAN HUNTER EXPL	WY	27N	108W	27	SENWSE	11894.2	B	8.1	2.68	0.0164	0.00231	164	15265	LNCE
E894	Green River	4903520622	1 OLD ROAD	AMERICAN HUNTER EXPL	WY	27N	108W	27	SENWSE	11897.3	A	5.2	2.72	0.0107	0.000995	146	12245	LNCE
E894	Green River	4903520622	1 OLD ROAD	AMERICAN HUNTER EXPL	WY	27N	108W	27	SENWSE	11897.3	B	4.6	2.72	0.00722	0.000493	223	12245	LNCE
E894	Green River	4903520622	1 OLD ROAD	AMERICAN HUNTER EXPL	WY	27N	108W	27	SENWSE	11915.2	B	8.4	2.67	0.0137	0.00372	52.6	15295	LNCE
E894	Green River	4903520622	1 OLD ROAD	AMERICAN HUNTER EXPL	WY	27N	108W	27	SENWSE	11915.2	A	9.2	2.70	0.0135	0.00256	219	15295	LNCE
E894	Green River	4903520622	1 OLD ROAD	AMERICAN HUNTER EXPL	WY	27N	108W	27	SENWSE	11921.8	A	5.0	2.67	0.00607	0.000271	188	12218	LNCE
E894	Green River	4903520622	1 OLD ROAD	AMERICAN HUNTER EXPL	WY	27N	108W	27	SENWSE	11921.8	B	5.0	2.67	0.00345	0.000232	110	12218	LNCE
E894	Green River	4903520622	1 OLD ROAD	AMERICAN HUNTER EXPL	WY	27N	108W	27	SENWSE	11923.3	A	4.1	2.58	0.0415	0.00644	151	13218	LNCE
E894	Green River	4903520622	1 OLD ROAD	AMERICAN HUNTER EXPL	WY	27N	108W	27	SENWSE	11923.3	B	3.8	2.58	0.00768	0.00169	409	13218	LNCE
E894	Green River	4903520622	1 OLD ROAD	AMERICAN HUNTER EXPL	WY	27N	108W	27	SENWSE	11927.7	B	11.5	2.66	0.0352	0.00749	43.0	15596	LNCE
E894	Green River	4903520622	1 OLD ROAD	AMERICAN HUNTER EXPL	WY	27N	108W	27	SENWSE	11927.7	A	11.4	2.66	0.0271	0.00441	234	15596	LNCE
E894	Green River	4903520622	1 OLD ROAD	AMERICAN HUNTER EXPL	WY	27N	108W	27	SENWSE	11927.8	A	11.3	2.66	0.0406	0.00925	19.1	15596	LNCE
E894	Green River	4903520622	1 OLD ROAD	AMERICAN HUNTER EXPL	WY	27N	108W	27	SENWSE	11927.8	B	11.5	2.66	0.0328	0.00686	92.1	15596	LNCE
E894	Green River	4903520622	1 OLD ROAD	AMERICAN HUNTER EXPL	WY	27N	108W	27	SENWSE	11935.2	A	10.7	2.67	0.0160	0.00296	32.2	15586	LNCE
E894	Green River	4903520622	1 OLD ROAD	AMERICAN HUNTER EXPL	WY	27N	108W	27	SENWSE	11935.2	B	10.5	2.67	0.0147	0.00148	133	15586	LNCE
E894	Green River	4903520622	1 OLD ROAD	AMERICAN HUNTER EXPL	WY	27N	108W	27	SENWSE	11936.3	B	10.3	2.66	0.0175	0.00287	122	15576	LNCE
E894	Green River	4903520622	1 OLD ROAD	AMERICAN HUNTER EXPL	WY	27N	108W	27	SENWSE	11936.3	A	9.8	2.66	0.0157	0.00238	148	15576	LNCE
E894	Green River	4903520622	1 OLD ROAD	AMERICAN HUNTER EXPL	WY	27N	108W	27	SENWSE	11936.3	B	9.9	2.70	0				

Appendix A1

Summary of Porosity, Permeability and Grain Density

Analysis of Critical Permeability, Capillary Pressure and Electrical Properties for Mesaverde Tight Gas Sandstones from Western U.S. Basins

US DOE # DE-FC26-05NT42660 Final Scientific/Technical Report

Alan P. Byrnes, Robert M. Cluff, John C. Webb

website: <http://www.kgs.ku.edu/mesaverde>

USGS Library Number	Basin	API Number	Well Name	Operator	State	Township	Range	Section	Quarter Section	Plug Depth	Plug Letter	Ambient Porosity	Grain Density	Routine Gas Permeability	in situ		Rock Type Code	Formations
															Klinkenberg Gas Permeability	Klinkenberg constant b		
											ft	A/B/C	%	g/cc	mD	mD		
R780	Green River	4903505742	C-47 TIP TOP SHALLOW	BELCO PETROLEUM	WY	28N	113W	22	SWNE	2754.9	A	20.6	2.62	2.18	1.15	25.1	16575	MVRD
R780	Green River	4903505742	C-47 TIP TOP SHALLOW	BELCO PETROLEUM	WY	28N	113W	22	SWNE	2759.9	A	9.1	2.68	0.0126	0.000708	120	15275	MVRD
R780	Green River	4903505742	C-47 TIP TOP SHALLOW	BELCO PETROLEUM	WY	28N	113W	22	SWNE	2759.9	B	7.2	2.66	0.00692	0.000614	106	15275	MVRD
R780	Green River	4903505742	C-47 TIP TOP SHALLOW	BELCO PETROLEUM	WY	28N	113W	22	SWNE	2771.6	B	21.3	2.63	27.4	18.5	5.3	15595	MVRD
R780	Green River	4903505742	C-47 TIP TOP SHALLOW	BELCO PETROLEUM	WY	28N	113W	22	SWNE	2771.6	A	21.4	2.64	17.5	12.2	5.2	15595	MVRD
R780	Green River	4903505742	C-47 TIP TOP SHALLOW	BELCO PETROLEUM	WY	28N	113W	22	SWNE	2771.7	A	22.4	2.65	43.5	30.4	5.0	15595	MVRD
R780	Green River	4903505742	C-47 TIP TOP SHALLOW	BELCO PETROLEUM	WY	28N	113W	22	SWNE	2771.7	B	21.4	2.64	1.99	0.498	18.4	15595	MVRD
R780	Green River	4903505742	C-47 TIP TOP SHALLOW	BELCO PETROLEUM	WY	28N	113W	22	SWNE	2783.3	B	22.1	2.64	31.3	24.0	2.8	15595	MVRD
R780	Green River	4903505742	C-47 TIP TOP SHALLOW	BELCO PETROLEUM	WY	28N	113W	22	SWNE	2783.3	A	22.3	2.64	28.9	23.3	2.7	15595	MVRD
R780	Green River	4903505742	C-47 TIP TOP SHALLOW	BELCO PETROLEUM	WY	28N	113W	22	SWNE	2783.4	A	21.9	2.63	29.6	21.7	4.3	15595	MVRD
R780	Green River	4903505742	C-47 TIP TOP SHALLOW	BELCO PETROLEUM	WY	28N	113W	22	SWNE	2783.4	B	22.3	2.65	26.0	21.5	3.9	15595	MVRD
R780	Green River	4903505742	C-47 TIP TOP SHALLOW	BELCO PETROLEUM	WY	28N	113W	22	SWNE	2800.7	A	19.9	2.63	9.85	7.13	5.8	15575	MVRD
R780	Green River	4903505742	C-47 TIP TOP SHALLOW	BELCO PETROLEUM	WY	28N	113W	22	SWNE	2800.7	B	15.6	2.67	1.42	0.810	21.7	15575	MVRD
R780	Green River	4903505742	C-47 TIP TOP SHALLOW	BELCO PETROLEUM	WY	28N	113W	22	SWNE	2800.8	B	19.7	2.65	8.18	4.17	16.1	15575	MVRD
R780	Green River	4903505742	C-47 TIP TOP SHALLOW	BELCO PETROLEUM	WY	28N	113W	22	SWNE	2800.8	A	19.9	2.65	7.74	4.24	16.1	15575	MVRD
R780	Green River	4903505742	C-47 TIP TOP SHALLOW	BELCO PETROLEUM	WY	28N	113W	22	SWNE	2811.7	B	20.0	2.66	4.09	2.04	11.7	15575	MVRD
R780	Green River	4903505742	C-47 TIP TOP SHALLOW	BELCO PETROLEUM	WY	28N	113W	22	SWNE	2811.7	A	19.1	2.63	4.50	3.08	10.4	15575	MVRD
R780	Green River	4903505742	C-47 TIP TOP SHALLOW	BELCO PETROLEUM	WY	28N	113W	22	SWNE	2811.8	A	18.9	2.63	3.81	2.51	11.1	15575	MVRD
R780	Green River	4903505742	C-47 TIP TOP SHALLOW	BELCO PETROLEUM	WY	28N	113W	22	SWNE	2811.8	B	19.7	2.66	3.01	1.88	13.1	15575	MVRD
R780	Green River	4903505742	C-47 TIP TOP SHALLOW	BELCO PETROLEUM	WY	28N	113W	22	SWNE	2817.7	A	20.1	2.69	2.46	2.12	8.9	15575	MVRD
R780	Green River	4903505742	C-47 TIP TOP SHALLOW	BELCO PETROLEUM	WY	28N	113W	22	SWNE	2817.7	B	19.8	2.69	2.90	2.07	8.2	15575	MVRD
R780	Green River	4903505742	C-47 TIP TOP SHALLOW	BELCO PETROLEUM	WY	28N	113W	22	SWNE	2817.8	B	19.6	2.69	2.36	1.19	42.4	15575	MVRD
R780	Green River	4903505742	C-47 TIP TOP SHALLOW	BELCO PETROLEUM	WY	28N	113W	22	SWNE	2817.8	A	20.1	2.69	2.81	1.61	18.7	15575	MVRD
R780	Green River	4903505742	C-47 TIP TOP SHALLOW	BELCO PETROLEUM	WY	28N	113W	22	SWNE	2829.7	A	12.2	2.69	0.0405	0.0131	130	15285	MVRD
R780	Green River	4903505742	C-47 TIP TOP SHALLOW	BELCO PETROLEUM	WY	28N	113W	22	SWNE	2829.7	B	8.4	2.68	0.0160	0.00225	124	15285	MVRD
R780	Green River	4903505742	C-47 TIP TOP SHALLOW	BELCO PETROLEUM	WY	28N	113W	22	SWNE	2829.8	A	8.6	2.70	0.0105	0.0142	111	15285	MVRD
R780	Green River	4903505742	C-47 TIP TOP SHALLOW	BELCO PETROLEUM	WY	28N	113W	22	SWNE	2829.8	B	6.1	2.69	0.00433	0.000397	169	15285	MVRD
R780	Green River	4903505742	C-47 TIP TOP SHALLOW	BELCO PETROLEUM	WY	28N	113W	22	SWNE	2829.9	A	6.6	2.67	0.00551	0.000610	185	15285	MVRD
R780	Green River	4903505742	C-47 TIP TOP SHALLOW	BELCO PETROLEUM	WY	28N	113W	22	SWNE	2829.9	B	5.3	2.70	0.00550	0.000478	201	15285	MVRD
R780	Green River	4903505742	C-47 TIP TOP SHALLOW	BELCO PETROLEUM	WY	28N	113W	22	SWNE	2831.8	A	20.9	2.68	5.38	3.18	15.2	15285	MVRD
R780	Green River	4903505742	C-47 TIP TOP SHALLOW	BELCO PETROLEUM	WY	28N	113W	22	SWNE	2831.8	B	23.6	2.68	4.68	2.73	20.3	15285	MVRD
R780	Green River	4903505742	C-47 TIP TOP SHALLOW	BELCO PETROLEUM	WY	28N	113W	22	SWNE	2831.9	A	20.4	2.68	3.93	3.22	6.8	15285	MVRD
R780	Green River	4903505742	C-47 TIP TOP SHALLOW	BELCO PETROLEUM	WY	28N	113W	22	SWNE	2831.9	A	19.2	2.67	2.90	1.86	12.1	15285	MVRD
R780	Green River	4903505742	C-47 TIP TOP SHALLOW	BELCO PETROLEUM	WY	28N	113W	22	SWNE	2845.5	B	22.0	2.67	12.6	6.34	18.2	15277	MVRD
R780	Green River	4903505742	C-47 TIP TOP SHALLOW	BELCO PETROLEUM	WY	28N	113W	22	SWNE	2845.5	A	22.6	2.67	11.8	8.69	6.2	15277	MVRD
R780	Green River	4903505742	C-47 TIP TOP SHALLOW	BELCO PETROLEUM	WY	28N	113W	22	SWNE	2850.9	A	21.1	2.69	8.50	4.51	18.1	15287	MVRD
R780	Green River	4903505742	C-47 TIP TOP SHALLOW	BELCO PETROLEUM	WY	28N	113W	22	SWNE	2850.9	B	21.0	2.69	6.91	4.93	8.5	15287	MVRD
S873	Green River	4903506200	K-2 MASON	BELCO PETROLEUM	WY	31N	113W	13	SESE	6988.1	A	10.0	2.69	0.142	0.0526	190	15275	MVRD
S873	Green River	4903506200	K-2 MASON	BELCO PETROLEUM	WY	31N	113W	13	SESE	6988.8	A	10.7	2.69	0.288	0.138	55.2	15275	MVRD
S873	Green River	4903506200	K-2 MASON	BELCO PETROLEUM	WY	31N	113W	13	SESE	6989.9	A	10.4	2.69	0.156	0.0823	44.5	15275	MVRD
S873	Green River	4903506200	K-2 MASON	BELCO PETROLEUM	WY	31N	113W	13	SESE	7703.7	A	11.9	2.69	0.393	0.228	22.6	16295	MVRD
S873	Green River	4903506200	K-2 MASON	BELCO PETROLEUM	WY	31N	113W	13	SESE	7703.7	A2	11.5	2.68	0.0210	0.0127	102	16295	MVRD
S873	Green River	4903506200	K-2 MASON	BELCO PETROLEUM	WY	31N	113W	13	SESE	7703.7	A1	11.4	2.67	0.0207	0.0115	82.0	16295	MVRD
S873	Green River	4903506200	K-2 MASON	BELCO PETROLEUM	WY	31N	113W	13	SESE	7703.8	A	12.1	2.69	0.433	0.239	25.4	16295	MVRD
S873	Green River	4903506200	K-2 MASON	BELCO PETROLEUM	WY	31N	113W	13	SESE	9370.1	A	2.9	2.67	0.00164	0.000663	352	13216	MVRD
S873	Green River	4903506200	K-2 MASON	BELCO PETROLEUM	WY	31N	113W	13	SESE	9370.2	A	2.6	2.66	0.00388	0.000143	273	13216	MVRD
S873	Green River	4903506200	K-2 MASON	BELCO PETROLEUM	WY	31N	113W	13	SESE	9370.9	A	2.7	2.70	0.000942	0.000006	2675	13215	MVRD
S873	Green River	4903506200	K-2 MASON	BELCO PETROLEUM	WY	31N	113W	13	SESE	9393.3	A	3.4	2.70	0.000745	0.000024	426	12235	MVRD
S873	Green River	4903506200	K-2 MASON	BELCO PETROLEUM	WY	31N	113W	13	SESE	9393.5	A	2.7	2.68	0.00177	0.000544	263	13265	MVRD
S873	Green River	4903506200	K-2 MASON	BELCO PETROLEUM	WY	31N	113W	13	SESE	9397.2	A	8.2	2.67	0.00594	0.000450	200	15286	MVRD
S873	Green River	4903506200	K-2 MASON	BELCO PETROLEUM	WY	31N	113W	13	SESE	9397.2	A1	8.3	2.67	0.000482	0.000041	763	15286	MVRD
S873	Green River	4903506200	K-2 MASON	BELCO PETROLEUM	WY	31N	113W	13	SESE	9397.2	A2	8.2	2.67	0.000413	0.000064	462	15286	MVRD
S873	Green River	4903506200	K-2 MASON	BELCO PETROLEUM	WY	31N	113W	13	SESE	9397.3	A	8.4	2.67	0.00476	0.000358	223	15286	MVRD
SHV	Green River	4903523799	VIBLÉ 10-11D	SHELL E&P	WY	31N	109W	11	SENE	12505.7		4.7	2.69	0.00101	0.000170	197	13287	MVRD
SHV	Green River	4903523799	VIBLÉ 10-11D	SHELL E&P	WY	31N	109W	11	SENE	12507.1		5.1	2.68	0.00244	0.000627	150	15287	MVRD
SHV	Green River	4903523799	VIBLÉ 10-11D	SHELL E&P	WY	31N	109W	11	SENE	12508.7		3.0	2.67	0.00132	0.000219	190	15275	MVRD
SHV	Green River	4903523799	VIBLÉ 10-11D	SHELL E&P	WY	31N	109W	11	SENE	12510.1		7.3	2.60	0.0694	0.0250	105	16277	MVRD
SHV	Green River	4903523799	VIBLÉ 10-11D	SHELL E&P	WY	31N	109W	11	SENE	12513.0		7.4	2.65	0.0148	0.00665	150	15277	MVRD
SHV	Green River	4903523799	VIBLÉ 10-11D	SHELL E&P	WY	31N	109W	11	SENE	12516.5		2.9	2.65	0.00649	0.00172	189	15217	MVRD
SHV	Green River	4903523799	VIBLÉ 10-11D	SHELL E&P	WY	31N	109W	11	SENE	12520.3		4.3	2.67	0.00277	0.000212	553	16275	MVRD
SHV	Green River	4903523799	VIBLÉ 10-11D	SHELL E&P	WY	31N	109W	11	SENE	12520.9		3.4	2.67	0.00389	0.000188	167	14265	MVRD
SHV	Green River	4903523799	VIBLÉ 10-11D	SHELL E&P	WY	31N	109W	11	SENE	12529.0		1.4	2.67	0.000416	0.000025	372	13266	MVRD
SHV	Green River	4903523799	VIBLÉ 10-11D	SHELL E&P	WY	31N	109W	11	SENE	12553.7		1.3	2.67	0.000478	0.000037	213	13265	MVRD
T195	Green River	4903508024	5 PINEDALE	EL PASO NATURAL GAS	WY	30N	108W	5	C SE	12158.5	A	11.0	2.65	0.0325	0.0167	97.2	13276	MVRD
T195	Green River	4903508024	5 PINEDALE	EL PASO NATURAL GAS	WY	30N	108W	5	C SE	12158.5	B	10.6	2.66	0.0255	0.0127	89.7	13276	MVRD
T195	Green River	4903508024	5 PINEDALE	EL PASO NATURAL GAS	WY	30N	108W	5	C SE	12159.5	B	8.9	2.66	0.0251	0.0130	75.7	16295	MVRD
T195	Green River	4903508024	5 PINEDALE	EL PASO NATURAL GAS	WY	30N	108W	5	C SE	12159.5	A	9.3	2.66	0.000295	0.000003	898	16295	

Appendix A1

Summary of Porosity, Permeability and Grain Density

Analysis of Critical Permeability, Capillary Pressure and Electrical Properties for Mesaverde Tight Gas Sandstones from Western U.S. Basins

US DOE # DE-FC26-05NT42660 Final Scientific/Technical Report

Alan P. Byrnes, Robert M. Cluff, John C. Webb

website: <http://www.kgs.ku.edu/mesaverde>

USGS Library Number	Basin	API Number	Well Name	Operator	State	Township	Range	Section	Quarter Section	Plug Depth	Plug Letter	Ambient Porosity	Grain Density	Routine Gas Permeability	in situ Permeability	in situ Permeability constant b (psia)	Rock Type Code	Formations	
																			ft
B43C	Piceance	0504511402	LAST DANCE 43C-3-792	BILL BARRETT CORP.	CO	7S	92W	3	NESE	3573.2	C	4.2	2.66	0.00275	0.000095	411	13297	RLNS/WMFRK	
B43C	Piceance	0504511402	LAST DANCE 43C-3-792	BILL BARRETT CORP.	CO	7S	92W	3	NESE	3573.2	A	4.3	2.66	0.00271	0.000111	323	13297	RLNS/WMFRK	
B43C	Piceance	0504511402	LAST DANCE 43C-3-792	BILL BARRETT CORP.	CO	7S	92W	3	NESE	3573.3	C	4.4	2.66	0.00295	0.000083	249	13297	RLNS/WMFRK	
B43C	Piceance	0504511402	LAST DANCE 43C-3-792	BILL BARRETT CORP.	CO	7S	92W	3	NESE	3573.3	B	4.0	2.67	0.00241	0.000119	308	13297	RLNS/WMFRK	
B43C	Piceance	0504511402	LAST DANCE 43C-3-792	BILL BARRETT CORP.	CO	7S	92W	3	NESE	3573.3	B	4.8	2.66	0.00148	0.000092	290	13297	RLNS/WMFRK	
B43C	Piceance	0504511402	LAST DANCE 43C-3-792	BILL BARRETT CORP.	CO	7S	92W	3	NESE	3577.6	C	2.0	2.69	0.00240	0.000088	152	13297	RLNS/WMFRK	
B43C	Piceance	0504511402	LAST DANCE 43C-3-792	BILL BARRETT CORP.	CO	7S	92W	3	NESE	3577.6	B	2.1	2.68	0.00228	0.000059	275	13297	RLNS/WMFRK	
B43C	Piceance	0504511402	LAST DANCE 43C-3-792	BILL BARRETT CORP.	CO	7S	92W	3	NESE	3577.6	A	1.8	2.69	0.00223	0.000062	419	13297	RLNS/WMFRK	
B43C	Piceance	0504511402	LAST DANCE 43C-3-792	BILL BARRETT CORP.	CO	7S	92W	3	NESE	3581.5	A	3.6	2.63	1.47	0.0304	33.0	13217	RLNS/WMFRK	
B43C	Piceance	0504511402	LAST DANCE 43C-3-792	BILL BARRETT CORP.	CO	7S	92W	3	NESE	3586.7	A	2.7	2.61	0.154	0.00232	106	12247	RLNS/WMFRK	
B43C	Piceance	0504511402	LAST DANCE 43C-3-792	BILL BARRETT CORP.	CO	7S	92W	3	NESE	3586.7	C	2.9	2.63	0.0758	0.00241	154	12247	RLNS/WMFRK	
B43C	Piceance	0504511402	LAST DANCE 43C-3-792	BILL BARRETT CORP.	CO	7S	92W	3	NESE	3586.7	B	3.1	2.64	0.0228	0.00105	85.3	12247	RLNS/WMFRK	
B43C	Piceance	0504511402	LAST DANCE 43C-3-792	BILL BARRETT CORP.	CO	7S	92W	3	NESE	3591.1	B	5.0	2.67	0.00049	0.000049	232	13267	RLNS/WMFRK	
B43C	Piceance	0504511402	LAST DANCE 43C-3-792	BILL BARRETT CORP.	CO	7S	92W	3	NESE	3591.5	B	2.9	2.67	0.00313	0.000131	270	13267	RLNS/WMFRK	
B43C	Piceance	0504511402	LAST DANCE 43C-3-792	BILL BARRETT CORP.	CO	7S	92W	3	NESE	3591.5	A	2.4	2.66	0.00292	0.000045	467	13267	RLNS/WMFRK	
B43C	Piceance	0504511402	LAST DANCE 43C-3-792	BILL BARRETT CORP.	CO	7S	92W	3	NESE	3593.6	A	3.3	2.63	0.0115	0.000342	410	13267	RLNS/WMFRK	
B43C	Piceance	0504511402	LAST DANCE 43C-3-792	BILL BARRETT CORP.	CO	7S	92W	3	NESE	3593.6	B	3.3	2.63	0.00586	0.000262	477	13267	RLNS/WMFRK	
B43C	Piceance	0504511402	LAST DANCE 43C-3-792	BILL BARRETT CORP.	CO	7S	92W	3	NESE	3593.6	C	3.4	2.63	0.00480	0.000174	290	13267	RLNS/WMFRK	
B43C	Piceance	0504511402	LAST DANCE 43C-3-792	BILL BARRETT CORP.	CO	7S	92W	3	NESE	3593.8	A	3.1	2.62	0.155	0.00577	379	13267	RLNS/WMFRK	
B43C	Piceance	0504511402	LAST DANCE 43C-3-792	BILL BARRETT CORP.	CO	7S	92W	3	NESE	3593.8	B	2.9	2.60	0.0154	0.00122	166	13267	RLNS/WMFRK	
B43C	Piceance	0504511402	LAST DANCE 43C-3-792	BILL BARRETT CORP.	CO	7S	92W	3	NESE	3598.1	A	2.0	2.66	0.00443	0.000064	404	12215	RLNS/WMFRK	
B43C	Piceance	0504511402	LAST DANCE 43C-3-792	BILL BARRETT CORP.	CO	7S	92W	3	NESE	3598.1	B	2.5	2.67	0.00340	0.000038	893	12215	RLNS/WMFRK	
B43C	Piceance	0504511402	LAST DANCE 43C-3-792	BILL BARRETT CORP.	CO	7S	92W	3	NESE	3970.0	A	1.1	2.87	0.00344	0.000097	167	12215	RLNS/WMFRK	
B43C	Piceance	0504511402	LAST DANCE 43C-3-792	BILL BARRETT CORP.	CO	7S	92W	3	NESE	3970.0	C	1.2	2.89	0.00258	0.000054	387	12215	RLNS/WMFRK	
B43C	Piceance	0504511402	LAST DANCE 43C-3-792	BILL BARRETT CORP.	CO	7S	92W	3	NESE	3970.0	B	0.9	2.69	0.00224	0.000088	172	12215	RLNS/WMFRK	
B43C	Piceance	0504511402	LAST DANCE 43C-3-792	BILL BARRETT CORP.	CO	7S	92W	3	NESE	3974.4	A	1.9	2.65	0.00445	0.000085	187	13267	RLNS/WMFRK	
B43C	Piceance	0504511402	LAST DANCE 43C-3-792	BILL BARRETT CORP.	CO	7S	92W	3	NESE	3974.4	C	1.9	2.64	0.00394	0.000038	446	13267	RLNS/WMFRK	
B43C	Piceance	0504511402	LAST DANCE 43C-3-792	BILL BARRETT CORP.	CO	7S	92W	3	NESE	3974.4	B	1.8	2.64	0.00237	0.000031	429	13267	RLNS/WMFRK	
B43C	Piceance	0504511402	LAST DANCE 43C-3-792	BILL BARRETT CORP.	CO	7S	92W	3	NESE	3992.4	A	2.8	2.64	0.00528	0.000419	254	13257	RLNS/WMFRK	
B43C	Piceance	0504511402	LAST DANCE 43C-3-792	BILL BARRETT CORP.	CO	7S	92W	3	NESE	3992.4	B	2.8	2.63	0.00493	0.000360	225	13257	RLNS/WMFRK	
B43C	Piceance	0504511402	LAST DANCE 43C-3-792	BILL BARRETT CORP.	CO	7S	92W	3	NESE	3992.4	C	2.9	2.63	0.00493	0.000387	301	13257	RLNS/WMFRK	
B43C	Piceance	0504511402	LAST DANCE 43C-3-792	BILL BARRETT CORP.	CO	7S	92W	3	NESE	3992.5	B	2.2	2.61	0.291	0.00798	62.3	13257	RLNS/WMFRK	
B43C	Piceance	0504511402	LAST DANCE 43C-3-792	BILL BARRETT CORP.	CO	7S	92W	3	NESE	3992.5	A	3.5	2.60	0.0170	0.000830	139	13257	RLNS/WMFRK	
B43C	Piceance	0504511402	LAST DANCE 43C-3-792	BILL BARRETT CORP.	CO	7S	92W	3	NESE	3992.5	C	2.9	2.62	0.0125	0.000576	334	13257	RLNS/WMFRK	
B43C	Piceance	0504511402	LAST DANCE 43C-3-792	BILL BARRETT CORP.	CO	7S	92W	3	NESE	3997.1	A	1.0	2.62	0.000979	0.000025	755	13297	RLNS/WMFRK	
B43C	Piceance	0504511402	LAST DANCE 43C-3-792	BILL BARRETT CORP.	CO	7S	92W	3	NESE	4001.2	A	3.6	2.62	0.00739	0.00106	110	16287	RLNS/WMFRK	
B43C	Piceance	0504511402	LAST DANCE 43C-3-792	BILL BARRETT CORP.	CO	7S	92W	3	NESE	4004.2	C	8.8	2.67					16287	RLNS/WMFRK
B43C	Piceance	0504511402	LAST DANCE 43C-3-792	BILL BARRETT CORP.	CO	7S	92W	3	NESE	4004.3	B	10.2	2.63	0.127	0.0288	51.2	16287	RLNS/WMFRK	
B43C	Piceance	0504511402	LAST DANCE 43C-3-792	BILL BARRETT CORP.	CO	7S	92W	3	NESE	4004.3	A	10.7	2.63	0.122	0.0341	42.1	16287	RLNS/WMFRK	
B43C	Piceance	0504511402	LAST DANCE 43C-3-792	BILL BARRETT CORP.	CO	7S	92W	3	NESE	4004.3	C	10.1	2.63	0.136	0.0392	35.0	16287	RLNS/WMFRK	
B43C	Piceance	0504511402	LAST DANCE 43C-3-792	BILL BARRETT CORP.	CO	7S	92W	3	NESE	4006.2	A	5.8	2.64	0.0259	0.00782	37.8	16227	RLNS/WMFRK	
B43C	Piceance	0504511402	LAST DANCE 43C-3-792	BILL BARRETT CORP.	CO	7S	92W	3	NESE	4009.2	A	7.7	2.54	0.474	0.136	30.7	16227	RLNS/WMFRK	
B43C	Piceance	0504511402	LAST DANCE 43C-3-792	BILL BARRETT CORP.	CO	7S	92W	3	NESE	4012.2	A	8.7	2.54	0.474	0.239	30.7	16227	RLNS/WMFRK	
B43C	Piceance	0504511402	LAST DANCE 43C-3-792	BILL BARRETT CORP.	CO	7S	92W	3	NESE	4013.2	C	6.7	2.53	4.43	0.220	40.3	16297	RLNS/WMFRK	
B43C	Piceance	0504511402	LAST DANCE 43C-3-792	BILL BARRETT CORP.	CO	7S	92W	3	NESE	4013.3	B	12.7	2.64	0.702	0.320	9.6	16297	RLNS/WMFRK	
B43C	Piceance	0504511402	LAST DANCE 43C-3-792	BILL BARRETT CORP.	CO	7S	92W	3	NESE	4013.3	A	12.9	2.64	0.491	0.190	19.5	16297	RLNS/WMFRK	
B43C	Piceance	0504511402	LAST DANCE 43C-3-792	BILL BARRETT CORP.	CO	7S	92W	3	NESE	4013.3	A	11.9	2.62	0.460	0.163	15.8	16297	RLNS/WMFRK	
B43C	Piceance	0504511402	LAST DANCE 43C-3-792	BILL BARRETT CORP.	CO	7S	92W	3	NESE	4015.2	A	7.8	2.62	0.0338	0.00568	317	16287	RLNS/WMFRK	
B43C	Piceance	0504511402	LAST DANCE 43C-3-792	BILL BARRETT CORP.	CO	7S	92W	3	NESE	4017.2	A	8.9	2.64	0.0186	0.00699	118	16287	RLNS/WMFRK	
B43C	Piceance	0504511402	LAST DANCE 43C-3-792	BILL BARRETT CORP.	CO	7S	92W	3	NESE	4019.2	A	9.5	2.67					16287	RLNS/WMFRK
B43C	Piceance	0504511402	LAST DANCE 43C-3-792	BILL BARRETT CORP.	CO	7S	92W	3	NESE	4019.3	A	10.0	2.63	0.0636	0.0132	76.1	16287	RLNS/WMFRK	
B43C	Piceance	0504511402	LAST DANCE 43C-3-792	BILL BARRETT CORP.	CO	7S	92W	3	NESE	4019.3	B	9.8	2.64	0.0574	0.00872	164	16287	RLNS/WMFRK	
B43C	Piceance	0504511402	LAST DANCE 43C-3-792	BILL BARRETT CORP.	CO	7S	92W	3	NESE	4019.3	C	8.2	2.64	0.0267	0.00506	225	16287	RLNS/WMFRK	
B43C	Piceance	0504511402	LAST DANCE 43C-3-792	BILL BARRETT CORP.	CO	7S	92W	3	NESE	4021.5	A	4.9	2.66	0.00693	0.000214	161	13297	RLNS/WMFRK	
B43C	Piceance	0504511402	LAST DANCE 43C-3-792	BILL BARRETT CORP.	CO	7S	92W	3	NESE	4021.5	C	5.2	2.60	0.00403	0.000137	282	13297	RLNS/WMFRK	
B43C	Piceance	0504511402	LAST DANCE 43C-3-792	BILL BARRETT CORP.	CO	7S	92W	3	NESE	4021.5	A	4.9	2.66	0.00256	0.000120	418	13297	RLNS/WMFRK	
B43C	Piceance	0504511402	LAST DANCE 43C-3-792	BILL BARRETT CORP.	CO	7S	92W	3	NESE	4356.3	A	1.1	2.65	0.462	0.0348	27.8	13227	RLNS/WMFRK	
B43C	Piceance	0504511402	LAST DANCE 43C-3-792	BILL BARRETT CORP.	CO	7S	92W	3	NESE	4356.3	B	2.1	2.58	0.00965	0.00191	114	13227	RLNS/WMFRK	
B43C	Piceance	0504511402	LAST DANCE 43C-3-792	BILL BARRETT CORP.	CO	7S	92W	3	NESE	4356.3	C	0.8	2.65	0.00079	0.000079	216	13227	RLNS/WMFRK	
B43C	Piceance	0504511402	LAST DANCE 43C-3-792	BILL BARRETT CORP.	CO	7S	92W	3	NESE	4358.6	A	0.012	0.0175	0.0212	0.00175	142	13217	RLNS/WMFRK	
B43C	Piceance	0504511402	LAST DANCE 43C-3-792	BILL BARRETT CORP.	CO	7S	92W	3	NESE	4358.6	B	1.6	2.64	0.00417	0.000073	318	13217	RLNS/WMFRK	
B43C	Piceance	0504511402	LAST DANCE 43C-3-792	BILL BARRETT CORP.	CO	7S	92W	3	NESE	4367.3	A	2.4	2.67	0.00191	0.000516	77.8	13217	RLNS/WMFRK	
B43C	Piceance	0504511402	LAST DANCE 43C-3-792	BILL BARRETT CORP.	CO	7S	92W	3	NESE	4372.0	B	2.5	2.63	0.0183	0.000604	192	14297	RLNS/WMFRK	
B43C	Piceance	0504511402	LAST DANCE 43C-3-792	BILL BARRETT CORP.	CO	7S	92W	3	NESE	4372.0	C	3.0	2.64	0.0116	0.000708	148			

Appendix A1

Summary of Porosity, Permeability and Grain Density

Analysis of Critical Permeability, Capillary Pressure and Electrical Properties for Mesaverde Tight Gas Sandstones from Western U.S. Basins

US DOE # DE-FC26-05NT42660 Final Scientific/Technical Report

Alan P. Byrnes, Robert M. Cluff, John C. Webb

website: <http://www.kgs.ku.edu/mesaverde>

USGS Library Number	Basin	API Number	Well Name	Operator	State	Township	Range	Section	Quarter Section	Plug Depth	Plug Letter	Ambient Porosity	Grain Density	Routine Gas Permeability	in situ		Rock Type Code	Formations	
															Klinkenberg Gas Permeability	Klinkenberg constant b			
											ft	A/B/C	%	g/cc	mD	mD	(psia)		
B43C	Piceance	0504511402	LAST DANCE 43C-3-792	BILL BARRETT CORP.	CO	7S	92W	3	NESE	5715.4	B	7.8	2.67	0.0170	0.00340	24.9	15297	RLNS/WMFRK	
B43C	Piceance	0504511402	LAST DANCE 43C-3-792	BILL BARRETT CORP.	CO	7S	92W	3	NESE	5715.4	B	7.6	2.71	0.0169	0.00334	53.5	15297	RLNS/WMFRK	
B43C	Piceance	0504511402	LAST DANCE 43C-3-792	BILL BARRETT CORP.	CO	7S	92W	3	NESE	5720.1	C	6.2	2.68	0.00622	0.000834	355	15277	RLNS/WMFRK	
B43C	Piceance	0504511402	LAST DANCE 43C-3-792	BILL BARRETT CORP.	CO	7S	92W	3	NESE	5720.3	C	6.6	2.67	0.0142	0.00182	95.1	15277	RLNS/WMFRK	
B43C	Piceance	0504511402	LAST DANCE 43C-3-792	BILL BARRETT CORP.	CO	7S	92W	3	NESE	5720.3	A	6.4	2.67	0.0128	0.00189	95.6	15277	RLNS/WMFRK	
B43C	Piceance	0504511402	LAST DANCE 43C-3-792	BILL BARRETT CORP.	CO	7S	92W	3	NESE	5720.3	B	6.2	2.67	0.0116	0.00165	151	15277	RLNS/WMFRK	
B43C	Piceance	0504511402	LAST DANCE 43C-3-792	BILL BARRETT CORP.	CO	7S	92W	3	NESE	5720.4	B	7.0	2.64	0.0103	0.00140	130	15277	RLNS/WMFRK	
B43C	Piceance	0504511402	LAST DANCE 43C-3-792	BILL BARRETT CORP.	CO	7S	92W	3	NESE	5720.4	C	6.9	2.68	0.00959	0.000935	98.8	15277	RLNS/WMFRK	
B43C	Piceance	0504511402	LAST DANCE 43C-3-792	BILL BARRETT CORP.	CO	7S	92W	3	NESE	5720.4	A	6.3	2.67	0.00894	0.00124	151	15277	RLNS/WMFRK	
B43C	Piceance	0504511402	LAST DANCE 43C-3-792	BILL BARRETT CORP.	CO	7S	92W	3	NESE	5723.3	C	4.7	2.68	0.00471	0.000573	128	15277	RLNS/WMFRK	
B43C	Piceance	0504511402	LAST DANCE 43C-3-792	BILL BARRETT CORP.	CO	7S	92W	3	NESE	5726.1	C	4.8	2.65	0.00561	0.000668	284	15287	RLNS/WMFRK	
B43C	Piceance	0504511402	LAST DANCE 43C-3-792	BILL BARRETT CORP.	CO	7S	92W	3	NESE	5727.1	C	5.9	2.65	0.0167	0.00246	117	15277	RLNS/WMFRK	
B43C	Piceance	0504511402	LAST DANCE 43C-3-792	BILL BARRETT CORP.	CO	7S	92W	3	NESE	5727.1	A	6.2	2.66	0.0154	0.00182	240	15277	RLNS/WMFRK	
B43C	Piceance	0504511402	LAST DANCE 43C-3-792	BILL BARRETT CORP.	CO	7S	92W	3	NESE	5727.1	B	6.1	2.66	0.0153	0.00255	75.8	15277	RLNS/WMFRK	
B43C	Piceance	0504511402	LAST DANCE 43C-3-792	BILL BARRETT CORP.	CO	7S	92W	3	NESE	5727.2	A	5.5	2.66	0.00900	0.00104	135	15277	RLNS/WMFRK	
B43C	Piceance	0504511402	LAST DANCE 43C-3-792	BILL BARRETT CORP.	CO	7S	92W	3	NESE	5727.2	B	5.5	2.66	0.00884	0.00120	128	15277	RLNS/WMFRK	
B43C	Piceance	0504511402	LAST DANCE 43C-3-792	BILL BARRETT CORP.	CO	7S	92W	3	NESE	5727.2	C	5.2	2.66	0.00821	0.000743	240	15277	RLNS/WMFRK	
B43C	Piceance	0504511402	LAST DANCE 43C-3-792	BILL BARRETT CORP.	CO	7S	92W	3	NESE	5730.1	C	5.4	2.68	0.00408	0.000635	201	15397	RLNS/WMFRK	
B43C	Piceance	0504511402	LAST DANCE 43C-3-792	BILL BARRETT CORP.	CO	7S	92W	3	NESE	5730.4	A	7.9	2.67	0.0154	0.00218	223	15397	RLNS/WMFRK	
B43C	Piceance	0504511402	LAST DANCE 43C-3-792	BILL BARRETT CORP.	CO	7S	92W	3	NESE	5730.4	C	7.6	2.67	0.0146	0.00151	246	15397	RLNS/WMFRK	
B43C	Piceance	0504511402	LAST DANCE 43C-3-792	BILL BARRETT CORP.	CO	7S	92W	3	NESE	5730.4	B	7.9	2.67	0.0125	0.00201	103	15397	RLNS/WMFRK	
B43C	Piceance	0504511402	LAST DANCE 43C-3-792	BILL BARRETT CORP.	CO	7S	92W	3	NESE	5734.4	C	6.5	2.67	0.00524	0.000118	173	15387	RLNS/WMFRK	
B43C	Piceance	0504511402	LAST DANCE 43C-3-792	BILL BARRETT CORP.	CO	7S	92W	3	NESE	5737.1	C	6.0	2.68	0.00810	0.00178	107	13317	RLNS/WMFRK	
B43C	Piceance	0504511402	LAST DANCE 43C-3-792	BILL BARRETT CORP.	CO	7S	92W	3	NESE	5737.3	C	6.3	2.67	0.0143	0.00143	251	13317	RLNS/WMFRK	
B43C	Piceance	0504511402	LAST DANCE 43C-3-792	BILL BARRETT CORP.	CO	7S	92W	3	NESE	5737.3	A	6.9	2.65	0.0124	0.00157	238	13317	RLNS/WMFRK	
B43C	Piceance	0504511402	LAST DANCE 43C-3-792	BILL BARRETT CORP.	CO	7S	92W	3	NESE	5737.3	B	6.6	2.67	0.00999	0.00123	159	13317	RLNS/WMFRK	
B43C	Piceance	0504511402	LAST DANCE 43C-3-792	BILL BARRETT CORP.	CO	7S	92W	3	NESE	5740.1	C	4.4	2.68	0.00265	0.000492	186	13317	RLNS/WMFRK	
B43C	Piceance	0504511402	LAST DANCE 43C-3-792	BILL BARRETT CORP.	CO	7S	92W	3	NESE	5743.0	A	6.7	2.67	0.0101	0.000731	141	13397	RLNS/WMFRK	
B43C	Piceance	0504511402	LAST DANCE 43C-3-792	BILL BARRETT CORP.	CO	7S	92W	3	NESE	5743.0	C	5.8	2.67	0.00738	0.000523	196	13397	RLNS/WMFRK	
B43C	Piceance	0504511402	LAST DANCE 43C-3-792	BILL BARRETT CORP.	CO	7S	92W	3	NESE	5743.0	B	6.6	2.68	0.00651	0.000591	201	13397	RLNS/WMFRK	
B43C	Piceance	0504511402	LAST DANCE 43C-3-792	BILL BARRETT CORP.	CO	7S	92W	3	NESE	5743.6	C	6.2	2.68	0.00296	0.000055	170	13397	RLNS/WMFRK	
B43C	Piceance	0504511402	LAST DANCE 43C-3-792	BILL BARRETT CORP.	CO	7S	92W	3	NESE	5747.3	C	5.0	2.67	0.00381	0.000610	223	15287	RLNS/WMFRK	
B43C	Piceance	0504511402	LAST DANCE 43C-3-792	BILL BARRETT CORP.	CO	7S	92W	3	NESE	5750.6	C	7.1	2.73	0.00471	0.000746	182	15397	RLNS/WMFRK	
B43C	Piceance	0504511402	LAST DANCE 43C-3-792	BILL BARRETT CORP.	CO	7S	92W	3	NESE	5753.5	C	4.4	2.65	0.00359	0.000671	215	15387	RLNS/WMFRK	
B43C	Piceance	0504511402	LAST DANCE 43C-3-792	BILL BARRETT CORP.	CO	7S	92W	3	NESE	5755.6	B	6.1	2.67	0.0104	0.000736	567	15277	RLNS/WMFRK	
B43C	Piceance	0504511402	LAST DANCE 43C-3-792	BILL BARRETT CORP.	CO	7S	92W	3	NESE	5755.6	C	6.1	2.67	0.00890	0.00130	146	15277	RLNS/WMFRK	
B43C	Piceance	0504511402	LAST DANCE 43C-3-792	BILL BARRETT CORP.	CO	7S	92W	3	NESE	5755.6	A	6.8	2.67	0.00820	0.00105	175	15277	RLNS/WMFRK	
B43C	Piceance	0504511402	LAST DANCE 43C-3-792	BILL BARRETT CORP.	CO	7S	92W	3	NESE	5757.3	B	5.1	2.67	0.00749	0.000866	134	15277	RLNS/WMFRK	
B43C	Piceance	0504511402	LAST DANCE 43C-3-792	BILL BARRETT CORP.	CO	7S	92W	3	NESE	5757.3	C	5.3	2.68	0.00724	0.000573	218	15277	RLNS/WMFRK	
B43C	Piceance	0504511402	LAST DANCE 43C-3-792	BILL BARRETT CORP.	CO	7S	92W	3	NESE	5757.3	A	6.2	2.68	0.00582	0.000560	142	15287	RLNS/WMFRK	
B43C	Piceance	0504511402	LAST DANCE 43C-3-792	BILL BARRETT CORP.	CO	7S	92W	3	NESE	5757.7	C	5.0	2.72	0.00209	0.000287	219	15277	RLNS/WMFRK	
B43C	Piceance	0504511402	LAST DANCE 43C-3-792	BILL BARRETT CORP.	CO	7S	92W	3	NESE	5760.5	C	3.6	2.64	0.00579	0.00113	143	13228	RLNS/WMFRK	
B43C	Piceance	0504511402	LAST DANCE 43C-3-792	BILL BARRETT CORP.	CO	7S	92W	3	NESE	6042.2	C	4.1	2.64					15387	RLNS/WMFRK
B43C	Piceance	0504511402	LAST DANCE 43C-3-792	BILL BARRETT CORP.	CO	7S	92W	3	NESE	6042.4	B	6.1	2.66	0.0106	0.000677	403	15387	RLNS/WMFRK	
B43C	Piceance	0504511402	LAST DANCE 43C-3-792	BILL BARRETT CORP.	CO	7S	92W	3	NESE	6042.4	C	5.8	2.66	0.00991	0.00129	93.9	15387	RLNS/WMFRK	
B43C	Piceance	0504511402	LAST DANCE 43C-3-792	BILL BARRETT CORP.	CO	7S	92W	3	NESE	6042.4	A	5.4	2.65	0.00945	0.000854	279	15387	RLNS/WMFRK	
B43C	Piceance	0504511402	LAST DANCE 43C-3-792	BILL BARRETT CORP.	CO	7S	92W	3	NESE	6053.1	C	6.1	2.72	0.00403	0.000540	428	13287	RLNS/WMFRK	
B43C	Piceance	0504511402	LAST DANCE 43C-3-792	BILL BARRETT CORP.	CO	7S	92W	3	NESE	6056.0	C	7.0	2.69	0.00826	0.000945	178	13287	RLNS/WMFRK	
B43C	Piceance	0504511402	LAST DANCE 43C-3-792	BILL BARRETT CORP.	CO	7S	92W	3	NESE	6056.8	B	6.1	2.68	0.0172	0.00238	142	13287	RLNS/WMFRK	
B43C	Piceance	0504511402	LAST DANCE 43C-3-792	BILL BARRETT CORP.	CO	7S	92W	3	NESE	6058.5	C	6.9	2.69	0.0157	0.00207	156	13287	RLNS/WMFRK	
B43C	Piceance	0504511402	LAST DANCE 43C-3-792	BILL BARRETT CORP.	CO	7S	92W	3	NESE	6058.5	A	6.2	2.70	0.0149	0.00243	81.3	13287	RLNS/WMFRK	
B43C	Piceance	0504511402	LAST DANCE 43C-3-792	BILL BARRETT CORP.	CO	7S	92W	3	NESE	6058.6	B	4.9	2.70	2.53	0.109	22.9	13287	RLNS/WMFRK	
B43C	Piceance	0504511402	LAST DANCE 43C-3-792	BILL BARRETT CORP.	CO	7S	92W	3	NESE	6058.6	B	5.1	2.69	0.0411	0.00333	131	13287	RLNS/WMFRK	
B43C	Piceance	0504511402	LAST DANCE 43C-3-792	BILL BARRETT CORP.	CO	7S	92W	3	NESE	6058.6	C	6.0	2.69	0.0139	0.00176	132	13287	RLNS/WMFRK	
B43C	Piceance	0504511402	LAST DANCE 43C-3-792	BILL BARRETT CORP.	CO	7S	92W	3	NESE	6060.7	C	6.3	2.75	0.00733	0.00235	205	13218	RLNS/WMFRK	
B43C	Piceance	0504511402	LAST DANCE 43C-3-792	BILL BARRETT CORP.	CO	7S	92W	3	NESE	6291.9	A	1.0	2.75	0.000756	0.000024	60.0	13266	RLNS/WMFRK	
B43C	Piceance	0504511402	LAST DANCE 43C-3-792	BILL BARRETT CORP.	CO	7S	92W	3	NESE	6297.9	A	0.5	2.69	0.00110	0.000017	299	12219	RLNS/WMFRK	
B43C	Piceance	0504511402	LAST DANCE 43C-3-792	BILL BARRETT CORP.	CO	7S	92W	3	NESE	6298.4	A	0.4	2.64	0.00169	0.000049	843	11289	RLNS/WMFRK	
B43C	Piceance	0504511402	LAST DANCE 43C-3-792	BILL BARRETT CORP.	CO	7S	92W	3	NESE	6305.5	A	0.5	2.66	0.00148	0.000449	238	12219	RLNS/WMFRK	
B43C	Piceance	0504511402	LAST DANCE 43C-3-792	BILL BARRETT CORP.	CO	7S	92W	3	NESE	6305.9	A	0.4	2.70	0.000406	0.000100	775	12219	RLNS/WMFRK	
B43C	Piceance	0504511402	LAST DANCE 43C-3-792	BILL BARRETT CORP.	CO	7S	92W	3	NESE	6309.1	A	0.8	2.63	0.00132	0.000037	261	11219	RLNS/WMFRK	
B43C	Piceance	0504511402	LAST DANCE 43C-3-792	BILL BARRETT CORP.	CO	7S	92W	3	NESE	6314.8	A	0.4	2.70	0.000261	0.000012	530	12289	RLNS/WMFRK	
B43C	Piceance	0504511402	LAST DANCE 43C-3-792	BILL BARRETT CORP.	CO	7S	92W	3	NESE	6327.8	B	0.5	2.71	0.00434	0.000094	214	11229	RLNS/WMFRK	
B43C	Piceance	0504511402	LAST DANCE 43C-3-792	BILL BARRETT CORP.	CO	7S	92W	3	NESE	63									

Appendix A1

Summary of Porosity, Permeability and Grain Density

Analysis of Critical Permeability, Capillary Pressure and Electrical Properties for Mesaverde Tight Gas Sandstones from Western U.S. Basins

US DOE # DE-FC26-05NT42660 Final Scientific/Technical Report

Alan P. Byrnes, Robert M. Cluff, John C. Webb

website: <http://www.kgs.ku.edu/mesaverde>

USGS Library Number	Basin	API Number	Well Name	Operator	State	Township	Range	Section	Quarter Section	Plug Depth	Plug Letter	Ambient Porosity	Grain Density	Routine Gas Permeability	in situ		Rock Type Code	Formations			
															Permeability	Permeability					
														ft	A/B/C	%	g/cc	mD	mD		
E458	Piceance	0510309406	M-30-2-96W /D-037934	FUEL RESOURCES DEV	CO	2N	96W	30	SWSW	6374.4	A	5.3	2.64	0.00230	0.000176	412	13216	WMFK			
E458	Piceance	0510309406	M-30-2-96W /D-037934	FUEL RESOURCES DEV	CO	2N	96W	30	SWSW	6375.4	A	3.4	2.64	0.00189	0.000080	348	13226	WMFK			
E458	Piceance	0510309406	M-30-2-96W /D-037934	FUEL RESOURCES DEV	CO	2N	96W	30	SWSW	6375.6	A	3.3	2.63	0.00228	0.000101	237	13226	WMFK			
E458	Piceance	0510309406	M-30-2-96W /D-037934	FUEL RESOURCES DEV	CO	2N	96W	30	SWSW	6379.2	A	4.1	2.61	0.00769	0.000250	221	12246	WMFK			
E458	Piceance	0510309406	M-30-2-96W /D-037934	FUEL RESOURCES DEV	CO	2N	96W	30	SWSW	6379.5	A	3.8	2.63	0.00328	0.000303	115	13246	WMFK			
E458	Piceance	0510309406	M-30-2-96W /D-037934	FUEL RESOURCES DEV	CO	2N	96W	30	SWSW	6379.9	A	3.1	2.68	0.00155	0.000036	652	12226	WMFK			
E458	Piceance	0510309406	M-30-2-96W /D-037934	FUEL RESOURCES DEV	CO	2N	96W	30	SWSW	6380.5	A	4.9	2.72		0.000055	107	11236	WMFK			
E458	Piceance	0510309406	M-30-2-96W /D-037934	FUEL RESOURCES DEV	CO	2N	96W	30	SWSW	6380.6	A	13.5	2.70	0.559	0.436	57	12246	WMFK			
E458	Piceance	0510309406	M-30-2-96W /D-037934	FUEL RESOURCES DEV	CO	2N	96W	30	SWSW	6402.2	A	0.5	2.51	0.00203	0.000021	599	11229	WMFK			
E458	Piceance	0510309406	M-30-2-96W /D-037934	FUEL RESOURCES DEV	CO	2N	96W	30	SWSW	6404.7	A	9.1	2.65	0.0254	0.00309	142	14296	WMFK			
E458	Piceance	0510309406	M-30-2-96W /D-037934	FUEL RESOURCES DEV	CO	2N	96W	30	SWSW	6404.8	A	9.5	2.66	0.0112	0.00186	157	14296	WMFK			
E458	Piceance	0510309406	M-30-2-96W /D-037934	FUEL RESOURCES DEV	CO	2N	96W	30	SWSW	6407.1	A	6.7	2.70	0.00529	0.000641	180	15276	WMFK			
E458	Piceance	0510309406	M-30-2-96W /D-037934	FUEL RESOURCES DEV	CO	2N	96W	30	SWSW	6407.3	A	5.4	2.71	0.00317	0.000284	360	15276	WMFK			
E458	Piceance	0510309406	M-30-2-96W /D-037934	FUEL RESOURCES DEV	CO	2N	96W	30	SWSW	6508.1	A	10.6	2.65	0.0393	0.0189	151	13286	WMFK			
E458	Piceance	0510309406	M-30-2-96W /D-037934	FUEL RESOURCES DEV	CO	2N	96W	30	SWSW	6508.3	A	9.1	2.66	0.0365	0.0180	146	13286	WMFK			
E458	Piceance	0510309406	M-30-2-96W /D-037934	FUEL RESOURCES DEV	CO	2N	96W	30	SWSW	6509.4	A	10.7	2.66	0.0484	0.0269	46.6	14286	WMFK			
PA424	Piceance	0504510927	Williams PA-424-34	WILLIAMS E&P	CO	6S	95W	34	NWSWSE	4569.5	A	3.1	2.68	0.00323	0.000505	176	13217	WMFK			
PA424	Piceance	0504510927	Williams PA-424-34	WILLIAMS E&P	CO	6S	95W	34	NWSWSE	4572.2	A	6.3	2.64	0.00747	0.00468	191	15277	WMFK			
PA424	Piceance	0504510927	Williams PA-424-34	WILLIAMS E&P	CO	6S	95W	34	NWSWSE	4574.6	A	4.7	2.66	0.0136	0.00279	144	13277	WMFK			
PA424	Piceance	0504510927	Williams PA-424-34	WILLIAMS E&P	CO	6S	95W	34	NWSWSE	4578.8	A	3.9	2.65	0.0162	0.00216	158	16225	WMFK			
PA424	Piceance	0504510927	Williams PA-424-34	WILLIAMS E&P	CO	6S	95W	34	NWSWSE	4578.8	A1	4.5	2.65	0.00124	0.000252	133	16225	WMFK			
PA424	Piceance	0504510927	Williams PA-424-34	WILLIAMS E&P	CO	6S	95W	34	NWSWSE	4579.8	A2	4.5	2.65	0.00116	0.000173	413	16225	WMFK			
PA424	Piceance	0504510927	Williams PA-424-34	WILLIAMS E&P	CO	6S	95W	34	NWSWSE	4582.5	A	6.1	2.66	0.0232	0.00649	40.3	13226	WMFK			
PA424	Piceance	0504510927	Williams PA-424-34	WILLIAMS E&P	CO	6S	95W	34	NWSWSE	4585.2	A	7.5	2.65	0.0109	0.0170	259	16296	WMFK			
PA424	Piceance	0504510927	Williams PA-424-34	WILLIAMS E&P	CO	6S	95W	34	NWSWSE	4587.3	A	7.5	2.66	0.551	0.0996	66.4	16296	WMFK			
PA424	Piceance	0504510927	Williams PA-424-34	WILLIAMS E&P	CO	6S	95W	34	NWSWSE	4592.3	A	2.5	2.67	0.00288	0.000325	142	13246	WMFK			
PA424	Piceance	0504510927	Williams PA-424-34	WILLIAMS E&P	CO	6S	95W	34	NWSWSE	4593.4	A	4.9	2.64	0.00577	0.000847	113	13226	WMFK			
PA424	Piceance	0504510927	Williams PA-424-34	WILLIAMS E&P	CO	6S	95W	34	NWSWSE	4596.5	A	5.2	2.64	0.00711	0.000583	209	15286	WMFK			
PA424	Piceance	0504510927	Williams PA-424-34	WILLIAMS E&P	CO	6S	95W	34	NWSWSE	4598.2	A	6.8	2.65	0.0100	0.000531	177	15226	WMFK			
PA424	Piceance	0504510927	Williams PA-424-34	WILLIAMS E&P	CO	6S	95W	34	NWSWSE	4600.3	A	12.2	2.65	0.0178	0.00188	50	15297	WMFK			
PA424	Piceance	0504510927	Williams PA-424-34	WILLIAMS E&P	CO	6S	95W	34	NWSWSE	4602.2	A	4.5	2.65	0.00809	0.000721	101	15277	WMFK			
PA424	Piceance	0504510927	Williams PA-424-34	WILLIAMS E&P	CO	6S	95W	34	NWSWSE	4604.8	A	3.3	2.66	0.0122	0.00119	113	13227	WMFK			
PA424	Piceance	0504510927	Williams PA-424-34	WILLIAMS E&P	CO	6S	95W	34	NWSWSE	4606.5	A	12.6	2.66	0.0244	0.00313	348	16227	WMFK			
PA424	Piceance	0504510927	Williams PA-424-34	WILLIAMS E&P	CO	6S	95W	34	NWSWSE	4606.5	A1	12.7	2.65	0.00243	0.000431	190	16227	WMFK			
PA424	Piceance	0504510927	Williams PA-424-34	WILLIAMS E&P	CO	6S	95W	34	NWSWSE	4606.5	A2	12.8	2.65	0.00217	0.000473	203	16227	WMFK			
PA424	Piceance	0504510927	Williams PA-424-34	WILLIAMS E&P	CO	6S	95W	34	NWSWSE	4609.2	A	4.3	2.66	0.0138	0.00146	94.8	16277	WMFK			
PA424	Piceance	0504510927	Williams PA-424-34	WILLIAMS E&P	CO	6S	95W	34	NWSWSE	4615.6	A	2.1	2.69	0.00486	0.000638	184	13266	WMFK			
PA424	Piceance	0504510927	Williams PA-424-34	WILLIAMS E&P	CO	6S	95W	34	NWSWSE	4623.3	A	5.3	2.69	0.00209	0.000501	738	13246	WMFK			
PA424	Piceance	0504510927	Williams PA-424-34	WILLIAMS E&P	CO	6S	95W	34	NWSWSE	4626.5	A	6.9	2.66	0.00985	0.000889	156	15276	WMFK			
PA424	Piceance	0504510927	Williams PA-424-34	WILLIAMS E&P	CO	6S	95W	34	NWSWSE	4630.4	A	5.0	2.65	0.0146	0.00140	104	13228	WMFK			
PA424	Piceance	0504510927	Williams PA-424-34	WILLIAMS E&P	CO	6S	95W	34	NWSWSE	4635.4	A	2.4	2.65	0.0123	0.000771	245	13226	WMFK			
PA424	Piceance	0504510927	Williams PA-424-34	WILLIAMS E&P	CO	6S	95W	34	NWSWSE	4637.5	A	6.7	2.65	0.00856	0.000812	148	15226	WMFK			
PA424	Piceance	0504510927	Williams PA-424-34	WILLIAMS E&P	CO	6S	95W	34	NWSWSE	4638.8	A	5.5	2.65	0.00992	0.000698	200	13276	WMFK			
PA424	Piceance	0504510927	Williams PA-424-34	WILLIAMS E&P	CO	6S	95W	34	NWSWSE	4640.7	A	6.1	2.65	0.0130	0.00144	97.7	16276	WMFK			
PA424	Piceance	0504510927	Williams PA-424-34	WILLIAMS E&P	CO	6S	95W	34	NWSWSE	4645.8	A	7.2	2.64	0.0230	0.00318	108	13276	WMFK			
PA424	Piceance	0504510927	Williams PA-424-34	WILLIAMS E&P	CO	6S	95W	34	NWSWSE	4651.6	A	6.7	2.64	0.104	0.0134	61.8	17276	WMFK			
PA424	Piceance	0504510927	Williams PA-424-34	WILLIAMS E&P	CO	6S	95W	34	NWSWSE	4654.5	A	4.5	2.64	0.0275	0.00247	114	13276	WMFK			
PA424	Piceance	0504510927	Williams PA-424-34	WILLIAMS E&P	CO	6S	95W	34	NWSWSE	4656.7	A	5.8	2.64	0.0330	0.00182	471	16296	WMFK			
PA424	Piceance	0504510927	Williams PA-424-34	WILLIAMS E&P	CO	6S	95W	34	NWSWSE	4660.4	A	6.0	2.65	0.0307	0.00357	83.9	16296	WMFK			
PA424	Piceance	0504510927	Williams PA-424-34	WILLIAMS E&P	CO	6S	95W	34	NWSWSE	4666.2	A	5.1	2.65	0.0238	0.00242	87.6	16226	WMFK			
PA424	Piceance	0504510927	Williams PA-424-34	WILLIAMS E&P	CO	6S	95W	34	NWSWSE	4671.5	A	5.8	2.64	0.0347	0.00280	333	16276	WMFK			
PA424	Piceance	0504510927	Williams PA-424-34	WILLIAMS E&P	CO	6S	95W	34	NWSWSE	4674.7	A	5.7	2.65	0.685	0.0527	65.6	13276	WMFK			
PA424	Piceance	0504510927	Williams PA-424-34	WILLIAMS E&P	CO	6S	95W	34	NWSWSE	4677.7	A	4.6	2.66	0.0168	0.000814	312	19296	WMFK			
PA424	Piceance	0504510927	Williams PA-424-34	WILLIAMS E&P	CO	6S	95W	34	NWSWSE	4679.4	A	7.1	2.65	0.0164	0.00162	129	15296	WMFK			
PA424	Piceance	0504510927	Williams PA-424-34	WILLIAMS E&P	CO	6S	95W	34	NWSWSE	4681.5	A	7.1	2.64	0.0146	0.00102	169	15286	WMFK			
PA424	Piceance	0504510927	Williams PA-424-34	WILLIAMS E&P	CO	6S	95W	34	NWSWSE	4683.5	A	6.9	2.64	0.0270	0.00254	143	15285	WMFK			
PA424	Piceance	0504510927	Williams PA-424-34	WILLIAMS E&P	CO	6S	95W	34	NWSWSE	4686.4	A	7.9	2.65	0.0211	0.00311	85.9	15286	WMFK			
PA424	Piceance	0504510927	Williams PA-424-34	WILLIAMS E&P	CO	6S	95W	34	NWSWSE	4691.5	A	13.3	2.65	0.0595	0.00987	234	16296	WMFK			
PA424	Piceance	0504510927	Williams PA-424-34	WILLIAMS E&P	CO	6S	95W	34	NWSWSE	4695.5	A	10.8	2.65	0.0223	0.00306	94.3	16296	WMFK			
PA424	Piceance	0504510927	Williams PA-424-34	WILLIAMS E&P	CO	6S	95W	34	NWSWSE	4698.5	A	7.3	2.64	0.0288	0.00385	29.8	16276	WMFK			
PA424	Piceance	0504510927	Williams PA-424-34	WILLIAMS E&P	CO	6S	95W	34	NWSWSE	4699.4	A	4.9	2.64	0.0140	0.00102	171	15276	WMFK			
PA424	Piceance	0504510927	Williams PA-424-34	WILLIAMS E&P	CO	6S	95W	34	NWSWSE	4704.2	A	7.9	2.64	0.0266	0.00168	137	13226	WMFK			
PA424	Piceance	0504510927	Williams PA-424-34	WILLIAMS E&P	CO	6S	95W	34	NWSWSE	4707.8	A	7.7	2.64	0.0330	0.00509	148	16276	WMFK			
PA424	Piceance	0504510927	Williams PA-424-34	WILLIAMS E&P	CO	6S	95W	34	NWSWSE	4712.5	A	5.2	2.66	0.00468	0.000530	183	13246	WMFK			
PA424	Piceance	0504510927	Williams PA-424-34	WILLIAMS E&P	CO	6S	9														

Appendix A1

Summary of Porosity, Permeability and Grain Density

Analysis of Critical Permeability, Capillary Pressure and Electrical Properties for Mesaverde Tight Gas Sandstones from Western U.S. Basins

US DOE # DE-FC26-05NT42660 Final Scientific/Technical Report

Alan P. Byrnes, Robert M. Cluff, John C. Webb

website: <http://www.kgs.ku.edu/mesaverde>

USGS Library Number	Basin	API Number	Well Name	Operator	State	Township	Range	Section	Quarter Section	Plug Depth	Plug Letter	Ambient Porosity	Grain Density	Routine Gas Permeability	in situ		Rock Type Code	Formations
															Klinkenberg Gas Permeability	Klinkenberg constant b (psia)		
											ft	A/B/C	%	g/cc	mD	mD		
PA424	Piceance	0504510927	Williams PA-424-34	WILLIAMS E&P	CO	6S	95W	34	NWSWSE	6085.5	A	6.0	2.70	0.00496	0.000570	191	13265	WMFK
PA424	Piceance	0504510927	Williams PA-424-34	WILLIAMS E&P	CO	6S	95W	34	NWSWSE	6085.6	A	6.1	2.71	0.0233	0.00263	84.8	13265	WMFK
PA424	Piceance	0504510927	Williams PA-424-34	WILLIAMS E&P	CO	6S	95W	34	NWSWSE	6090.7	A	7.1	2.66	0.0134	0.00229	138	16276	WMFK
PA424	Piceance	0504510927	Williams PA-424-34	WILLIAMS E&P	CO	6S	95W	34	NWSWSE	6098.5	A	0.6	2.41	0.00542	0.000319	309	11229	WMFK
PA424	Piceance	0504510927	Williams PA-424-34	WILLIAMS E&P	CO	6S	95W	34	NWSWSE	6102.3	A	1.2	2.89	0.00183	0.00061	418	14295	WMFK
PA424	Piceance	0504510927	Williams PA-424-34	WILLIAMS E&P	CO	6S	95W	34	NWSWSE	6115.5	A	1.7	2.74	0.00776	0.000761	123	12221	WMFK
PA424	Piceance	0504510927	Williams PA-424-34	WILLIAMS E&P	CO	6S	95W	34	NWSWSE	6130.3	A	6.0	2.68	0.00745			13255	WMFK
PA424	Piceance	0504510927	Williams PA-424-34	WILLIAMS E&P	CO	6S	95W	34	NWSWSE	6135.5	A	8.1	2.69	0.00660	0.000876	242	13256	WMFK
PA424	Piceance	0504510927	Williams PA-424-34	WILLIAMS E&P	CO	6S	95W	34	NWSWSE	6138.8	A	8.4	2.67	0.0196	0.00442	113	15271	WMFK
PA424	Piceance	0504510927	Williams PA-424-34	WILLIAMS E&P	CO	6S	95W	34	NWSWSE	6140.1	A	6.3	2.66	0.00365	0.000502	182	13226	WMFK
PA424	Piceance	0504510927	Williams PA-424-34	WILLIAMS E&P	CO	6S	95W	34	NWSWSE	6144.5	A	7.9	2.66	0.0228	0.00674	166	15286	WMFK
PA424	Piceance	0504510927	Williams PA-424-34	WILLIAMS E&P	CO	6S	95W	34	NWSWSE	6146.5	A	9.4	2.66	0.0204	0.00580	55.8	16276	WMFK
PA424	Piceance	0504510927	Williams PA-424-34	WILLIAMS E&P	CO	6S	95W	34	NWSWSE	6148.6	A	9.9	2.66	0.0237	0.00761	82.3	15276	WMFK
PA424	Piceance	0504510927	Williams PA-424-34	WILLIAMS E&P	CO	6S	95W	34	NWSWSE	6152.5	A	9.5	2.65	0.0281	0.00567	59.1	13278	WMFK
PA424	Piceance	0504510927	Williams PA-424-34	WILLIAMS E&P	CO	6S	95W	34	NWSWSE	6155.5	A	6.6	2.73	0.00519	0.000693	247	15276	WMFK
PA424	Piceance	0504510927	Williams PA-424-34	WILLIAMS E&P	CO	6S	95W	34	NWSWSE	6584.5	A	1.7	2.65	0.00163	0.000031	551	11219	WMFK
PA424	Piceance	0504510927	Williams PA-424-34	WILLIAMS E&P	CO	6S	95W	34	NWSWSE	6586.8	A	4.5	2.70	0.00480	0.000537	138	13265	WMFK
PA424	Piceance	0504510927	Williams PA-424-34	WILLIAMS E&P	CO	6S	95W	34	NWSWSE	6590.4	A	1.7	2.65	0.00488	0.000325	259	11249	WMFK
PA424	Piceance	0504510927	Williams PA-424-34	WILLIAMS E&P	CO	6S	95W	34	NWSWSE	6593.8	A	4.4	2.68	0.00275	0.000294	314	14265	WMFK
PA424	Piceance	0504510927	Williams PA-424-34	WILLIAMS E&P	CO	6S	95W	34	NWSWSE	6597.3	A	6.9	2.65	0.0154	0.00109	128	13266	WMFK
PA424	Piceance	0504510927	Williams PA-424-34	WILLIAMS E&P	CO	6S	95W	34	NWSWSE	6599.5	A	7.8	2.68	0.0113	0.00155	231	13266	WMFK
PA424	Piceance	0504510927	Williams PA-424-34	WILLIAMS E&P	CO	6S	95W	34	NWSWSE	6603.8	A	0.4	2.64				11229	WMFK
PA424	Piceance	0504510927	Williams PA-424-34	WILLIAMS E&P	CO	6S	95W	34	NWSWSE	6604.0	A	5.9	2.82				11229	WMFK
PA424	Piceance	0504510927	Williams PA-424-34	WILLIAMS E&P	CO	6S	95W	34	NWSWSE	6620.2	A	0.4	2.67	0.00118	0.000035	300	12295	WMFK
PA424	Piceance	0504510927	Williams PA-424-34	WILLIAMS E&P	CO	6S	95W	34	NWSWSE	6626.5	A	1.0	2.65	0.00918	0.00163	131	13225	WMFK
PA424	Piceance	0504510927	Williams PA-424-34	WILLIAMS E&P	CO	6S	95W	34	NWSWSE	6632.8	A	3.5	2.68	0.00654	0.00507	88.0	13245	WMFK
PA424	Piceance	0504510927	Williams PA-424-34	WILLIAMS E&P	CO	6S	95W	34	NWSWSE	6635.1	A	3.8	2.67	0.00339	0.000362	191	13265	WMFK
PA424	Piceance	0504510927	Williams PA-424-34	WILLIAMS E&P	CO	6S	95W	34	NWSWSE	6639.4	A	3.3	2.66	0.0131	0.00231	150	14295	WMFK
PA424	Piceance	0504510927	Williams PA-424-34	WILLIAMS E&P	CO	6S	95W	34	NWSWSE	6640.5	A	8.9	2.67	0.0132	0.00374	39.8	13248	WMFK
PA424	Piceance	0504510927	Williams PA-424-34	WILLIAMS E&P	CO	6S	95W	34	NWSWSE	6641.5	A	10.3	2.67	0.0204	0.00265	227	14295	WMFK
PA424	Piceance	0504510927	Williams PA-424-34	WILLIAMS E&P	CO	6S	95W	34	NWSWSE	6643.5	A	9.4	2.66	0.0182	0.00463	55.0	14295	WMFK
PA424	Piceance	0504510927	Williams PA-424-34	WILLIAMS E&P	CO	6S	95W	34	NWSWSE	6645.5	A	9.1	2.66	0.0139	0.00344	60.4	13225	WMFK
PA424	Piceance	0504510927	Williams PA-424-34	WILLIAMS E&P	CO	6S	95W	34	NWSWSE	6645.5	A2	10.0	2.67	0.00108	0.000261	321	13225	WMFK
PA424	Piceance	0504510927	Williams PA-424-34	WILLIAMS E&P	CO	6S	95W	34	NWSWSE	6645.5	A1	10.2	2.67	0.00108	0.000359	122	13225	WMFK
PA424	Piceance	0504510927	Williams PA-424-34	WILLIAMS E&P	CO	6S	95W	34	NWSWSE	6647.1	A	8.8	2.70	0.00998	0.00276	95.3	14295	WMFK
PA424	Piceance	0504510927	Williams PA-424-34	WILLIAMS E&P	CO	6S	95W	34	NWSWSE	6649.5	A	6.1	2.72	0.00358	0.000644	175	13265	WMFK
R091	Piceance	05045XXXX4	BOOK CLIFFS 1	USGS-CG	CO	7S	104W	17	NESW	213.0	A	6.4	2.64	0.00617	0.000225	156	12295	MVRD
R091	Piceance	05045XXXX4	BOOK CLIFFS 1	USGS-CG	CO	7S	104W	17	NESW	242.4	A	6.7	2.56	0.00626	0.000164	163	13219	MVRD
R091	Piceance	05045XXXX4	BOOK CLIFFS 1	USGS-CG	CO	7S	104W	17	NESW	247.0	A	14.9	2.66	0.0973	0.00542	51.7	13217	MVRD
R091	Piceance	05045XXXX4	BOOK CLIFFS 1	USGS-CG	CO	7S	104W	17	NESW	255.8	A	24.2	2.64	1.41	0.12	4.5	15567	MVRD
R091	Piceance	05045XXXX4	BOOK CLIFFS 1	USGS-CG	CO	7S	104W	17	NESW	255.9	A1	24.8	2.64	1.38	0.59	9.9	15567	MVRD
R091	Piceance	05045XXXX4	BOOK CLIFFS 1	USGS-CG	CO	7S	104W	17	NESW	255.9	A1	24.5	2.63	28.5	12.9	23.4	15567	MVRD
R091	Piceance	05045XXXX4	BOOK CLIFFS 1	USGS-CG	CO	7S	104W	17	NESW	255.9	A2	24.3	2.63	26.3	19.6	6.5	15567	MVRD
R091	Piceance	05045XXXX4	BOOK CLIFFS 1	USGS-CG	CO	7S	104W	17	NESW	256.5	A	11.0	2.69	0.242	0.000802	322	13258	MVRD
R091	Piceance	05045XXXX4	BOOK CLIFFS 1	USGS-CG	CO	7S	104W	17	NESW	257.3	A	6.9	2.63	0.00460	0.000167	336	11219	MVRD
R091	Piceance	05045XXXX4	BOOK CLIFFS 1	USGS-CG	CO	7S	104W	17	NESW	264.0	A	23.4	2.59				13247	MVRD
R091	Piceance	05045XXXX4	BOOK CLIFFS 1	USGS-CG	CO	7S	104W	17	NESW	296.9	A	4.9	2.71	0.00258	0.000168	272	13226	MVRD
R091	Piceance	05045XXXX4	BOOK CLIFFS 1	USGS-CG	CO	7S	104W	17	NESW	387.3	A	9.6	2.59	0.00742	0.000985	163	13219	MVRD
R091	Piceance	05045XXXX4	BOOK CLIFFS 1	USGS-CG	CO	7S	104W	17	NESW	512.2	A	10.0	2.61	0.00376	0.000376	72.7	13236	MVRD
R091	Piceance	05045XXXX4	BOOK CLIFFS 1	USGS-CG	CO	7S	104W	17	NESW	523.5	A	12.2	2.64	0.0107	0.00321	145	13227	MVRD
S905	Piceance	05103XXXX3	21011-5 MOON LAKE	WESTERN FUELS ASSOC	CO	2N	101W	1	NESW	788.0	A	1.9	2.82	0.00222	0.000067	213	12226	MVRD
S905	Piceance	05103XXXX3	21011-5 MOON LAKE	WESTERN FUELS ASSOC	CO	2N	101W	1	NESW	790.3	A	5.0	2.85	0.00775	0.000209	263	12339	MVRD
S905	Piceance	05103XXXX3	21011-5 MOON LAKE	WESTERN FUELS ASSOC	CO	2N	101W	1	NESW	790.3	B	5.0	2.64	0.00198	0.000132	76.5	12239	MVRD
S905	Piceance	05103XXXX3	21011-5 MOON LAKE	WESTERN FUELS ASSOC	CO	2N	101W	1	NESW	812.2	B	17.7	2.64	11.1	6.80	13.6	13216	MVRD
S905	Piceance	05103XXXX3	21011-5 MOON LAKE	WESTERN FUELS ASSOC	CO	2N	101W	1	NESW	812.2	A	17.4	2.63	9.24	5.89	10.5	13216	MVRD
S905	Piceance	05103XXXX3	21011-5 MOON LAKE	WESTERN FUELS ASSOC	CO	2N	101W	1	NESW	812.3	B	17.9	2.65	54.1	42.1	3.7	14296	MVRD
S905	Piceance	05103XXXX3	21011-5 MOON LAKE	WESTERN FUELS ASSOC	CO	2N	101W	1	NESW	812.3	A	17.6	2.64	54.1	37.9	5.3	14296	MVRD
S905	Piceance	05103XXXX3	21011-5 MOON LAKE	WESTERN FUELS ASSOC	CO	2N	101W	1	NESW	812.6	B	18.4	2.63	20.4	17.2	1.6	13296	MVRD
S905	Piceance	05103XXXX3	21011-5 MOON LAKE	WESTERN FUELS ASSOC	CO	2N	101W	1	NESW	812.6	A	18.3	2.63	20.3	16.2	2.5	13296	MVRD
S905	Piceance	05103XXXX3	21011-5 MOON LAKE	WESTERN FUELS ASSOC	CO	2N	101W	1	NESW	812.7	B	18.7	2.65	33.3	26.3	3.7	13276	MVRD
S905	Piceance	05103XXXX3	21011-5 MOON LAKE	WESTERN FUELS ASSOC	CO	2N	101W	1	NESW	812.7	A	18.1	2.65	32.6	22.0	6.9	13276	MVRD
S905	Piceance	05103XXXX3	21011-5 MOON LAKE	WESTERN FUELS ASSOC	CO	2N	101W	1	NESW	812.9	B	17.9	2.65	33.8	24.6	4.7	14577	MVRD
S905	Piceance	05103XXXX3	21011-5 MOON LAKE	WESTERN FUELS ASSOC	CO	2N	101W	1	NESW	812.9	A	17.0	2.64	32.5	20.9	7.7	14577	MVRD
S905	Piceance	05103XXXX3	21011-5 MOON LAKE	WESTERN FUELS ASSOC	CO	2N	101W	1	NESW	815.5	B	16.7	2.61				13256	MVRD
S905	Piceance	05103XXXX3	21011-5 MOON LAKE	WESTERN FUELS ASSOC	CO	2N	101W	1	NESW	815.5	A	7.4	2.35				13256	MVRD
S905	Piceance	05103XXXX3	21011-5 MOON LAKE	WESTERN FUELS ASSOC	CO	2N	101W	1	NESW	816.5	B	11.1	2.66	0.0730	0.0241	29.4	12239	MVRD
S905	Piceance	05103XXXX3	21011-5 MOON LAKE	WESTERN FUELS ASSOC	CO	2N	101W	1	NESW	816.5	A	10.6	2.63	0.0408	0.0			

Appendix A1
Summary of Porosity, Permeability and Grain Density
Analysis of Critical Permeability, Capillary Pressure and Electrical Properties for Mesaverde Tight Gas Sandstones from Western U.S. Basins
US DOE # DE-FC26-05NT42660 Final Scientific/Technical Report
Alan P. Byrnes, Robert M. Cluff, John C. Webb
website: <http://www.kgs.ku.edu/mesaverde>

USGS Library Number	Basin	API Number	Well Name	Operator	State	Township	Range	Section	Quarter Section	Plug Depth	Plug Letter	Ambient Porosity	Grain Density	Routine Gas Permeability	in situ		Rock Type Code	Formations
															Klinkenberg Gas Permeability	Klinkenberg constant b		
											ft	A/B/C	%	g/cc	mD	mD		
T63X-2G	Piceance	0510310391	T63X-2G	EXXON-MOBIL	CO	3S	97W	2	NESWNE	10623.6	B	7.0	2.66	0.00463	0.000535	323	15265	MVRD
T63X-2G	Piceance	0510310391	T63X-2G	EXXON-MOBIL	CO	3S	97W	2	NESWNE	10623.6	A	6.9	2.67	0.00332	0.000839	101	15265	MVRD
T63X-2G	Piceance	0510310391	T63X-2G	EXXON-MOBIL	CO	3S	97W	2	NESWNE	10625.0	B	7.7	2.65	0.00546	0.00129	218	15276	MVRD
T63X-2G	Piceance	0510310391	T63X-2G	EXXON-MOBIL	CO	3S	97W	2	NESWNE	10625.0	A	7.1	2.65	0.00478	0.00162	93.8	15276	MVRD
T63X-2G	Piceance	0510310391	T63X-2G	EXXON-MOBIL	CO	3S	97W	2	NESWNE	10633.6	B	3.0	2.66	0.00127	0.000088	317	13265	MVRD
T63X-2G	Piceance	0510310391	T63X-2G	EXXON-MOBIL	CO	3S	97W	2	NESWNE	10633.6	A	3.0	2.68	0.000829	0.000084	316	13265	MVRD
T63X-2G	Piceance	0510310391	T63X-2G	EXXON-MOBIL	CO	3S	97W	2	NESWNE	10636.3	B	2.5	2.68	0.00272	0.000074	145	13265	MVRD
T63X-2G	Piceance	0510310391	T63X-2G	EXXON-MOBIL	CO	3S	97W	2	NESWNE	10636.3	A	2.5	2.69	0.000584	0.000084	602	13265	MVRD
T63X-2G	Piceance	0510310391	T63X-2G	EXXON-MOBIL	CO	3S	97W	2	NESWNE	10643.9	A	0.4	2.68	0.000703	0.000014	516	13267	MVRD
T63X-2G	Piceance	0510310391	T63X-2G	EXXON-MOBIL	CO	3S	97W	2	NESWNE	10643.9	B	0.4	2.68	0.000525	0.000006	920	13267	MVRD
T63X-2G	Piceance	0510310391	T63X-2G	EXXON-MOBIL	CO	3S	97W	2	NESWNE	10653.8	A	1.1	2.65	0.00149	0.000050	412	13265	MVRD
T63X-2G	Piceance	0510310391	T63X-2G	EXXON-MOBIL	CO	3S	97W	2	NESWNE	10653.8	B	1.1	2.65	0.000834	0.000020	835	13265	MVRD
T649	Piceance	0504560011	MWX-2	CER CORPORATION	CO	6S	94W	34	SESWNW	4885.4	A	4.1	2.65	0.00400	0.000372	285	15215	MVRD
T649	Piceance	0504560011	MWX-2	CER CORPORATION	CO	6S	94W	34	SESWNW	4885.4	B	4.3	2.65	0.00382	0.000427	251	15215	MVRD
T649	Piceance	0504560011	MWX-2	CER CORPORATION	CO	6S	94W	34	SESWNW	4905.1	B	3.2	2.64	0.00405	0.000517	159	15276	MVRD
T649	Piceance	0504560011	MWX-2	CER CORPORATION	CO	6S	94W	34	SESWNW	4905.1	A	2.8	2.64	0.00301	0.000377	258	15276	MVRD
T649	Piceance	0504560011	MWX-2	CER CORPORATION	CO	6S	94W	34	SESWNW	4909.1	A	7.7	2.64	0.0220	0.00485	44.5	16276	MVRD
T649	Piceance	0504560011	MWX-2	CER CORPORATION	CO	6S	94W	34	SESWNW	4909.1	B	7.5	2.64	0.0211	0.00330	180	16276	MVRD
T649	Piceance	0504560011	MWX-2	CER CORPORATION	CO	6S	94W	34	SESWNW	4918.2	A	7.4	2.63	0.00939	0.0108	87.4	17276	MVRD
T649	Piceance	0504560011	MWX-2	CER CORPORATION	CO	6S	94W	34	SESWNW	4918.2	B	7.1	2.64	0.0890	0.0141	113	17276	MVRD
T649	Piceance	0504560011	MWX-2	CER CORPORATION	CO	6S	94W	34	SESWNW	4930.4	A	3.5	2.65	0.0163	0.00193	104	15266	MVRD
T649	Piceance	0504560011	MWX-2	CER CORPORATION	CO	6S	94W	34	SESWNW	4930.4	B	3.4	2.65	0.0139	0.00231	36.7	15266	MVRD
T649	Piceance	0504560011	MWX-2	CER CORPORATION	CO	6S	94W	34	SESWNW	4935.5	A	6.7	2.63	0.0485	0.00646	91.0	13276	MVRD
T649	Piceance	0504560011	MWX-2	CER CORPORATION	CO	6S	94W	34	SESWNW	4935.5	B	6.4	2.63	0.0210	0.00331	72.9	13276	MVRD
T649	Piceance	0504560011	MWX-2	CER CORPORATION	CO	6S	94W	34	SESWNW	4939.8	B	9.0	2.63	0.0283	0.00340	105	16275	MVRD
T649	Piceance	0504560011	MWX-2	CER CORPORATION	CO	6S	94W	34	SESWNW	4939.8	A	9.0	2.63	0.0260	0.00426	86.9	16275	MVRD
T649	Piceance	0504560011	MWX-2	CER CORPORATION	CO	6S	94W	34	SESWNW	4945.1	A	9.9	2.63	0.0415	0.00627	128	16275	MVRD
T649	Piceance	0504560011	MWX-2	CER CORPORATION	CO	6S	94W	34	SESWNW	4945.1	B	10.1	2.63	0.0409	0.00750	86.6	16275	MVRD
T649	Piceance	0504560011	MWX-2	CER CORPORATION	CO	6S	94W	34	SESWNW	5174.8	B	1.3	2.63	0.00298	0.00056	200	13215	MVRD
T649	Piceance	0504560011	MWX-2	CER CORPORATION	CO	6S	94W	34	SESWNW	5174.8	A	3.1	2.71	0.00232	0.00040	588	13215	MVRD
T649	Piceance	0504560011	MWX-2	CER CORPORATION	CO	6S	94W	34	SESWNW	5174.8	A	3.1	2.68	0.00125	0.000035	526	13265	MVRD
T649	Piceance	0504560011	MWX-2	CER CORPORATION	CO	6S	94W	34	SESWNW	5174.8	B	0.7	2.68	0.00000	0.00000	19	13365	MVRD
T649	Piceance	0504560011	MWX-2	CER CORPORATION	CO	6S	94W	34	SESWNW	5207.0	A	4.7	2.69	0.00765	0.000058	250	13226	MVRD
T649	Piceance	0504560011	MWX-2	CER CORPORATION	CO	6S	94W	34	SESWNW	5207.0	B	0.3	2.68	0.00000	0.00000	19	13226	MVRD
T649	Piceance	0504560011	MWX-2	CER CORPORATION	CO	6S	94W	34	SESWNW	5225.0	A	3.8	2.66	0.00217	0.000117	279	16295	MVRD
T649	Piceance	0504560011	MWX-2	CER CORPORATION	CO	6S	94W	34	SESWNW	5227.7	B	8.8	2.65	0.0284	0.00356	133	16276	MVRD
T649	Piceance	0504560011	MWX-2	CER CORPORATION	CO	6S	94W	34	SESWNW	5227.7	A	9.0	2.65	0.0235	0.00181	423	16276	MVRD
T649	Piceance	0504560011	MWX-2	CER CORPORATION	CO	6S	94W	34	SESWNW	5234.1	B	8.7	2.66	0.0324	0.00514	91.1	16276	MVRD
T649	Piceance	0504560011	MWX-2	CER CORPORATION	CO	6S	94W	34	SESWNW	5234.1	A	8.7	2.66	0.0259	0.00471	64.1	16276	MVRD
T649	Piceance	0504560011	MWX-2	CER CORPORATION	CO	6S	94W	34	SESWNW	5237.3	B	9.7	2.66	0.0329	0.00419	39.2	16276	MVRD
T649	Piceance	0504560011	MWX-2	CER CORPORATION	CO	6S	94W	34	SESWNW	5237.3	A	9.4	2.66	0.0180	0.00220	112	16276	MVRD
T649	Piceance	0504560011	MWX-2	CER CORPORATION	CO	6S	94W	34	SESWNW	5244.2	B	5.3	2.67	0.00579	0.00107	490	12226	MVRD
T649	Piceance	0504560011	MWX-2	CER CORPORATION	CO	6S	94W	34	SESWNW	5244.2	A	4.3	2.67	0.00278	0.000042	549	12226	MVRD
T649	Piceance	0504560011	MWX-2	CER CORPORATION	CO	6S	94W	34	SESWNW	5245.5	A	5.7	2.65	0.0210	0.00294	72.0	13265	MVRD
T649	Piceance	0504560011	MWX-2	CER CORPORATION	CO	6S	94W	34	SESWNW	5246.6	B	4.4	2.69	0.00834	0.000315	242	13286	MVRD
T649	Piceance	0504560011	MWX-2	CER CORPORATION	CO	6S	94W	34	SESWNW	5246.6	A	4.1	2.69	0.00338	0.000169	320	13286	MVRD
T649	Piceance	0504560011	MWX-2	CER CORPORATION	CO	6S	94W	34	SESWNW	5257.0	B	1.0	2.80	0.00355	0.000103	554	13225	MVRD
T649	Piceance	0504560011	MWX-2	CER CORPORATION	CO	6S	94W	34	SESWNW	5257.0	A	0.8	2.71	0.000922	0.000014	674	13225	MVRD
T649	Piceance	0504560011	MWX-2	CER CORPORATION	CO	6S	94W	34	SESWNW	5260.4	B	5.3	2.68	0.00568	0.00288	207	14285	MVRD
T649	Piceance	0504560011	MWX-2	CER CORPORATION	CO	6S	94W	34	SESWNW	5260.4	A	5.1	2.69	0.00175	0.000223	224	14285	MVRD
T649	Piceance	0504560011	MWX-2	CER CORPORATION	CO	6S	94W	34	SESWNW	5271.2	A	1.3	2.61	0.00552	0.000027	283	12229	MVRD
T649	Piceance	0504560011	MWX-2	CER CORPORATION	CO	6S	94W	34	SESWNW	5271.2	B	2.4	2.62	0.00000	0.00000	13	12229	MVRD
T649	Piceance	0504560011	MWX-2	CER CORPORATION	CO	6S	94W	34	SESWNW	5272.9	B	0.6	2.67	0.000902	0.000022	525	14216	MVRD
T649	Piceance	0504560011	MWX-2	CER CORPORATION	CO	6S	94W	34	SESWNW	5272.9	A	1.2	2.67	0.000853	0.000024	398	14216	MVRD
T649	Piceance	0504560011	MWX-2	CER CORPORATION	CO	6S	94W	34	SESWNW	5276.1	A	1.2	2.68	0.00182	0.000052	295	13255	MVRD
T649	Piceance	0504560011	MWX-2	CER CORPORATION	CO	6S	94W	34	SESWNW	5276.1	B	1.3	2.68	0.00140	0.000015	555	13255	MVRD
T649	Piceance	0504560011	MWX-2	CER CORPORATION	CO	6S	94W	34	SESWNW	5278.4	B	5.2	2.69	0.00476	0.000176	567	14295	MVRD
T649	Piceance	0504560011	MWX-2	CER CORPORATION	CO	6S	94W	34	SESWNW	5278.4	A	5.7	2.69	0.00309	0.00109	225	14295	MVRD
T649	Piceance	0504560011	MWX-2	CER CORPORATION	CO	6S	94W	34	SESWNW	5285.3	B	6.4	2.68	0.00541	0.000252	192	14295	MVRD
T649	Piceance	0504560011	MWX-2	CER CORPORATION	CO	6S	94W	34	SESWNW	5285.3	A	5.7	2.68	0.00196	0.000120	158	14295	MVRD
T649	Piceance	0504560011	MWX-2	CER CORPORATION	CO	6S	94W	34	SESWNW	5286.7	B	5.6	2.68	0.00509	0.000443	69.1	14295	MVRD
T649	Piceance	0504560011	MWX-2	CER CORPORATION	CO	6S	94W	34	SESWNW	5286.7	A	0.0368	0.000167	305	14295			

Appendix A1

Summary of Porosity, Permeability and Grain Density

Analysis of Critical Permeability, Capillary Pressure and Electrical Properties for Mesaverde Tight Gas Sandstones from Western U.S. Basins

US DOE # DE-FC26-05NT42660 Final Scientific/Technical Report

Alan P. Byrnes, Robert M. Cluff, John C. Webb

website: <http://www.kgs.ku.edu/mesaverde>

USGS Library Number	Basin	API Number	Well Name	Operator	State	Township	Range	Section	Quarter Section	Plug Depth	Plug Letter	Ambient Porosity	Grain Density	Routine Gas Permeability	in situ		Rock Type Code	Formations
															Permeability	Permeability		
											ft	A/B/C	%	g/cc	mD	mD		
T649	Piceance	0504560011	MWX-2	CER CORPORATION	CO	6S	94W	34	SESWNW	7124.7	B	10.9	2.68	0.160	0.0496	66.2	15266	MVRD
T649	Piceance	0504560011	MWX-2	CER CORPORATION	CO	6S	94W	34	SESWNW	7124.7	A	11.1	2.68	0.0145	0.00345	237	15266	MVRD
T649	Piceance	0504560011	MWX-2	CER CORPORATION	CO	6S	94W	34	SESWNW	7133.5	A	10.2	2.73	0.0163	0.00670	91.3	15266	MVRD
T649	Piceance	0504560011	MWX-2	CER CORPORATION	CO	6S	94W	34	SESWNW	7136.8	B	10.6	2.66	0.0192	0.00342	104	13266	MVRD
T649	Piceance	0504560011	MWX-2	CER CORPORATION	CO	6S	94W	34	SESWNW	7136.8	A	6.9	2.58	0.0104	0.00219	182	13266	MVRD
T649	Piceance	0504560011	MWX-2	CER CORPORATION	CO	6S	94W	34	SESWNW	7140.2	B	7.6	2.68	0.0117	0.000709	195	13216	MVRD
T649	Piceance	0504560011	MWX-2	CER CORPORATION	CO	6S	94W	34	SESWNW	7140.2	A	8.4	2.69	0.00768	0.00101	87.3	13216	MVRD
T649	Piceance	0504560011	MWX-2	CER CORPORATION	CO	6S	94W	34	SESWNW	7140.7	B	8.6	2.68	0.0163	0.00129	157	13226	MVRD
T649	Piceance	0504560011	MWX-2	CER CORPORATION	CO	6S	94W	34	SESWNW	7140.7	A	6.5	2.62	0.00936	0.00127	87.3	13226	MVRD
T649	Piceance	0504560011	MWX-2	CER CORPORATION	CO	6S	94W	34	SESWNW	7141.9	A	3.9	2.67	0.00459	0.00065	562	13246	MVRD
T649	Piceance	0504560011	MWX-2	CER CORPORATION	CO	6S	94W	34	SESWNW	7145.5	B	8.0	2.68	0.00754	0.000502	182	15296	MVRD
T649	Piceance	0504560011	MWX-2	CER CORPORATION	CO	6S	94W	34	SESWNW	7145.5	A	6.6	2.66	0.00368	0.000258	115	15296	MVRD
T649	Piceance	0504560011	MWX-2	CER CORPORATION	CO	6S	94W	34	SESWNW	7204.0	B	2.2	2.66	0.00422	0.000180	357	30000	MVRD
T649	Piceance	0504560011	MWX-2	CER CORPORATION	CO	6S	94W	34	SESWNW	7204.0	A	7.1	2.84	0.00292	0.000078	396	30000	MVRD
T649	Piceance	0504560011	MWX-2	CER CORPORATION	CO	6S	94W	34	SESWNW	7217.8	B	2.7	2.66	0.00858	0.000085	506	13229	MVRD
T649	Piceance	0504560011	MWX-2	CER CORPORATION	CO	6S	94W	34	SESWNW	7217.8	A	3.1	2.67				13229	MVRD
T649	Piceance	0504560011	MWX-2	CER CORPORATION	CO	6S	94W	34	SESWNW	7218.7	B	3.6	2.75	0.00587	0.000385	96.8	13266	MVRD
T649	Piceance	0504560011	MWX-2	CER CORPORATION	CO	6S	94W	34	SESWNW	7218.7	A	6.1	2.84	0.000898	0.000056	402	13266	MVRD
T649	Piceance	0504560011	MWX-2	CER CORPORATION	CO	6S	94W	34	SESWNW	7223.0	B	6.7	2.69	0.00870	0.000547	125	15266	MVRD
T649	Piceance	0504560011	MWX-2	CER CORPORATION	CO	6S	94W	34	SESWNW	7223.0	A	5.7	2.66	0.00299	0.000439	180	15266	MVRD
T649	Piceance	0504560011	MWX-2	CER CORPORATION	CO	6S	94W	34	SESWNW	7249.7	B	2.9	2.68	0.00145	0.000019	569	12219	MVRD
T649	Piceance	0504560011	MWX-2	CER CORPORATION	CO	6S	94W	34	SESWNW	7249.9	A	8.4	2.69	0.00319	0.000047	310	12219	MVRD
T649	Piceance	0504560011	MWX-2	CER CORPORATION	CO	6S	94W	34	SESWNW	7264.4	A	4.1	2.59	0.00744	0.000346	240	13265	MVRD
T649	Piceance	0504560011	MWX-2	CER CORPORATION	CO	6S	94W	34	SESWNW	7264.4	B	6.3	2.64	0.00729	0.000255	159	13265	MVRD
T649	Piceance	0504560011	MWX-2	CER CORPORATION	CO	6S	94W	34	SESWNW	7264.5	A	6.1	2.63	0.00360	0.000221	277	13265	MVRD
T649	Piceance	0504560011	MWX-2	CER CORPORATION	CO	6S	94W	34	SESWNW	7270.7	B	4.1	2.67	0.00474	0.000097	339	13256	MVRD
T649	Piceance	0504560011	MWX-2	CER CORPORATION	CO	6S	94W	34	SESWNW	7270.7	A	4.7	2.68	0.00382	0.000123	147	13256	MVRD
T649	Piceance	0504560011	MWX-2	CER CORPORATION	CO	6S	94W	34	SESWNW	7272.8	B	9.0	2.68	0.0115	0.00148	154	13285	MVRD
T649	Piceance	0504560011	MWX-2	CER CORPORATION	CO	6S	94W	34	SESWNW	7272.8	A	8.9	2.68	0.00873	0.00234	38.9	13285	MVRD
T649	Piceance	0504560011	MWX-2	CER CORPORATION	CO	6S	94W	34	SESWNW	7276.2	B	8.2	2.68	0.00898	0.00202	159	15295	MVRD
T649	Piceance	0504560011	MWX-2	CER CORPORATION	CO	6S	94W	34	SESWNW	7276.2	A	8.4	2.69	0.00669	0.000173	134	13285	MVRD
T649	Piceance	0504560011	MWX-2	CER CORPORATION	CO	6S	94W	34	SESWNW	7319.7	B	6.0	2.67	0.00553	0.000550	120	13257	MVRD
T649	Piceance	0504560011	MWX-2	CER CORPORATION	CO	6S	94W	34	SESWNW	7319.7	A	5.6	2.68	0.00448	0.000183	394	13257	MVRD
T649	Piceance	0504560011	MWX-2	CER CORPORATION	CO	6S	94W	34	SESWNW	7331.6	B	8.3		0.180	0.0115	51.0	15276	MVRD
T649	Piceance	0504560011	MWX-2	CER CORPORATION	CO	6S	94W	34	SESWNW	7331.6	A	7.9	2.72	0.00573	0.000836	235	15276	MVRD
T649	Piceance	0504560011	MWX-2	CER CORPORATION	CO	6S	94W	34	SESWNW	7334.8	B	8.6		0.00818	0.00134	118	15276	MVRD
T649	Piceance	0504560011	MWX-2	CER CORPORATION	CO	6S	94W	34	SESWNW	7334.8	A	8.7	2.69	0.00460	0.000911	240	15276	MVRD
T649	Piceance	0504560011	MWX-2	CER CORPORATION	CO	6S	94W	34	SESWNW	7337.3	B	6.6	2.71	0.00605	0.000434	179	13265	MVRD
T649	Piceance	0504560011	MWX-2	CER CORPORATION	CO	6S	94W	34	SESWNW	7337.3	A	6.4	2.70	0.00217	0.000212	444	13265	MVRD
T649	Piceance	0504560011	MWX-2	CER CORPORATION	CO	6S	94W	34	SESWNW	7340.4	B	2.1	2.76	0.00279	0.000166	665	15275	MVRD
T649	Piceance	0504560011	MWX-2	CER CORPORATION	CO	6S	94W	34	SESWNW	7340.4	A	2.3	2.78	0.00254	0.000160	388	15275	MVRD
T649	Piceance	0504560011	MWX-2	CER CORPORATION	CO	6S	94W	34	SESWNW	7347.8	B	3.1		0.00905	0.000344	66.1	12235	MVRD
T649	Piceance	0504560011	MWX-2	CER CORPORATION	CO	6S	94W	34	SESWNW	7347.8	A	4.1	2.71	0.00279	0.000058	260	12235	MVRD
T649	Piceance	0504560011	MWX-2	CER CORPORATION	CO	6S	94W	34	SESWNW	7350.4	B			0.00455	0.000386	146	15265	MVRD
T649	Piceance	0504560011	MWX-2	CER CORPORATION	CO	6S	94W	34	SESWNW	7350.4	A	4.5	2.71	0.00331	0.000372	67.7	15265	MVRD
T649	Piceance	0504560011	MWX-2	CER CORPORATION	CO	6S	94W	34	SESWNW	7832.9	B	3.5	2.65	0.0135	0.000308	289	13266	MVRD
T649	Piceance	0504560011	MWX-2	CER CORPORATION	CO	6S	94W	34	SESWNW	7832.9	A	4.1	2.66	0.00892	0.000437	192	13266	MVRD
T649	Piceance	0504560011	MWX-2	CER CORPORATION	CO	6S	94W	34	SESWNW	7832.9	B	3.9	2.65				13266	MVRD
T649	Piceance	0504560011	MWX-2	CER CORPORATION	CO	6S	94W	34	SESWNW	7841.4	A	2.9	2.66	0.00349	0.000074	533	13316	MVRD
T649	Piceance	0504560011	MWX-2	CER CORPORATION	CO	6S	94W	34	SESWNW	7841.4	B	2.4	2.64				13316	MVRD
T649	Piceance	0504560011	MWX-2	CER CORPORATION	CO	6S	94W	34	SESWNW	7841.5	B	3.7	2.66	0.893	0.0101	7.8	13316	MVRD
T649	Piceance	0504560011	MWX-2	CER CORPORATION	CO	6S	94W	34	SESWNW	7841.5	A	4.0	2.67	0.00704	0.000171	180	13316	MVRD
T649	Piceance	0504560011	MWX-2	CER CORPORATION	CO	6S	94W	34	SESWNW	7851.3	A	3.8	2.66	0.00412	0.000244	291	13276	MVRD
T649	Piceance	0504560011	MWX-2	CER CORPORATION	CO	6S	94W	34	SESWNW	7857.6	B	7.4	2.67	0.0100	0.000628	159	14286	MVRD
T649	Piceance	0504560011	MWX-2	CER CORPORATION	CO	6S	94W	34	SESWNW	7857.6	A	7.7	2.68	0.00853	0.000538	278	14286	MVRD
T649	Piceance	0504560011	MWX-2	CER CORPORATION	CO	6S	94W	34	SESWNW	7865.5	B	7.7	2.66	0.0117	0.000929	180	15286	MVRD
T649	Piceance	0504560011	MWX-2	CER CORPORATION	CO	6S	94W	34	SESWNW	7865.5	A	7.6	2.66	0.00598	0.000721	167	15286	MVRD
T649	Piceance	0504560011	MWX-2	CER CORPORATION	CO	6S	94W	34	SESWNW	7865.6	B	7.6	2.67	0.0124	0.000505	91.4	15286	MVRD
T649	Piceance	0504560011	MWX-2	CER CORPORATION	CO	6S	94W	34	SESWNW	7877.3	B	8.1	2.68	0.0113	0.00152	214	14286	MVRD
T649	Piceance	0504560011	MWX-2	CER CORPORATION	CO	6S	94W	34	SESWNW	7877.3	A	8.9	2.68	0.00760	0.00137	114	14286	MVRD
T649	Piceance	0504560011	MWX-2	CER CORPORATION	CO	6S	94W	34	SESWNW	7877.4	B	7.8	2.68	0.0112	0.00185	146	14286	MVRD
T649	Piceance	0504560011	MWX-2	CER CORPORATION	CO	6S	94W	34	SESWNW	7877.4	A	7.9	2.68	0.00627	0.00143	124	14286	MVRD
T649	Piceance	0504560011	MWX-2	CER CORPORATION	CO	6S	94W	34	SESWNW	7877.5	A	7.6	2.67	0.00564	0.000910	264	14286	MVRD
T649	Piceance	0504560011	MWX-2	CER CORPORATION	CO	6S	94W	34	SESWNW	7877.6	B	7.7	2.68	0.0100	0.00165	139	14286	MVRD
T649	Piceance	0504560011	MWX-2	CER CORPORATION	CO	6S	94W	34	SESWNW	7877.6	A	7.6	2.68	0.00860	0.00152	74.7	14286	MVRD
T649	Piceance	0504560011	MWX-2	CER CORPORATION	CO	6S	94W	34	SESWNW	7880.1	A	7.6	2.68	0.00859	0.00179	145	14286	MVRD
T649	Piceance	0504560011	MWX-2	CER CORPORATION	CO	6S	94W	34	SESWNW	7880.2	B	6.2	2.69	0.0141	0.00376	91.4	14286	MVRD
T649	Piceance	0504560011	MWX-2	CER CORPORATION	CO	6S	94W	34	SESWNW	7880.2	A	7.9	2.69	0.00904	0.00237	214	14286	MVRD
T649	Piceance	0504560011	MWX-2	CER CORPORATION	CO	6S	94W	34	SESWNW	7891.1	B	7.5	2.68	0.0144	0.00261	244	14286	MVRD
T649	Piceance	0504560011	MWX-2	CER CORPORATION	CO	6S	94W	34	SESWNW	7891.1	A	7.4	2.68	0.0113	0.00254	176	14286	M

Appendix A1

Summary of Porosity, Permeability and Grain Density

Analysis of Critical Permeability, Capillary Pressure and Electrical Properties for Mesaverde Tight Gas Sandstones from Western U.S. Basins

US DOE # DE-FC26-05NT42660 Final Scientific/Technical Report

Alan P. Byrnes, Robert M. Cluff, John C. Webb

website: <http://www.kgs.ku.edu/mesaverde>

USGS Library Number	Basin	API Number	Well Name	Operator	State	Township	Range	Section	Quarter Section	Plug Depth	Plug Letter	Ambient Porosity	Grain Density	Routine Gas Permeability	in situ		Rock Type Code	Formations
															Klinkenberg Permeability	Klinkenberg constant b (psia)		
											ft	A/B/C	%	g/cc	mD	mD		
E393	Powder River	4900252627	1 BARLOW 21-20	LOUISIANA LAND & EXP	WY	48N	75W	20	NENW	6995.8	A	5.1	2.69	0.0131	0.00115	50.2	15295	PRKM
E393	Powder River	4900252627	1 BARLOW 21-20	LOUISIANA LAND & EXP	WY	48N	75W	20	NENW	6995.8	B	5.4	2.70	0.00934	0.00111	170	15295	PRKM
E393	Powder River	4900252627	1 BARLOW 21-20	LOUISIANA LAND & EXP	WY	48N	75W	20	NENW	6996.0	A	5.9	2.69	0.0121	0.00143	172	15295	PRKM
E393	Powder River	4900252627	1 BARLOW 21-20	LOUISIANA LAND & EXP	WY	48N	75W	20	NENW	6996.0	B	6.2	2.70	0.00963	0.00108	176	15295	PRKM
E393	Powder River	4900252627	1 BARLOW 21-20	LOUISIANA LAND & EXP	WY	48N	75W	20	NENW	6996.2	A	7.1	2.69	0.0245	0.00473	211	15295	PRKM
E393	Powder River	4900252627	1 BARLOW 21-20	LOUISIANA LAND & EXP	WY	48N	75W	20	NENW	6996.2	B	6.3	2.69	0.0156	0.00207	123	15295	PRKM
E393	Powder River	4900252627	1 BARLOW 21-20	LOUISIANA LAND & EXP	WY	48N	75W	20	NENW	7000.9	A	17.3	2.67	46.0	31.0	5.9	15587	PRKM
E393	Powder River	4900252627	1 BARLOW 21-20	LOUISIANA LAND & EXP	WY	48N	75W	20	NENW	7000.9	A	17.1	2.66	44.5	29.1	7.4	15587	PRKM
E393	Powder River	4900252627	1 BARLOW 21-20	LOUISIANA LAND & EXP	WY	48N	75W	20	NENW	7001.1	A	17.0	2.67	41.9	34.6	1.7	15587	PRKM
E393	Powder River	4900252627	1 BARLOW 21-20	LOUISIANA LAND & EXP	WY	48N	75W	20	NENW	7001.1	B	17.4	2.68	41.6	28.9	5.3	15587	PRKM
E393	Powder River	4900252627	1 BARLOW 21-20	LOUISIANA LAND & EXP	WY	48N	75W	20	NENW	7008.1	A	16.6	2.66	32.5	23.6	5.8	15577	PRKM
E393	Powder River	4900252627	1 BARLOW 21-20	LOUISIANA LAND & EXP	WY	48N	75W	20	NENW	7008.1	B	16.6	2.65	30.5	21.0	4.8	15577	PRKM
E393	Powder River	4900252627	1 BARLOW 21-20	LOUISIANA LAND & EXP	WY	48N	75W	20	NENW	7012.0	B	6.2	2.72	0.00155			14276	PRKM
E393	Powder River	4900252627	1 BARLOW 21-20	LOUISIANA LAND & EXP	WY	48N	75W	20	NENW	7012.0	A	6.1	2.66	0.00140	0.000068	291	14276	PRKM
E393	Powder River	4900252627	1 BARLOW 21-20	LOUISIANA LAND & EXP	WY	48N	75W	20	NENW	7012.2	B	6.2	2.66	0.00256	0.000090	75.9	14276	PRKM
E393	Powder River	4900252627	1 BARLOW 21-20	LOUISIANA LAND & EXP	WY	48N	75W	20	NENW	7012.2	A	5.9	2.71	0.000959	0.000019	481	14276	PRKM
E393	Powder River	4900252627	1 BARLOW 21-20	LOUISIANA LAND & EXP	WY	48N	75W	20	NENW	7013.9	A	16.6	2.65	25.4	20.2	2.7	15587	PRKM
E393	Powder River	4900252627	1 BARLOW 21-20	LOUISIANA LAND & EXP	WY	48N	75W	20	NENW	7013.9	B	17.0	2.66	23.2	16.3	5.9	15587	PRKM
E393	Powder River	4900252627	1 BARLOW 21-20	LOUISIANA LAND & EXP	WY	48N	75W	20	NENW	7014.1	A	17.2	2.66	21.8	16.8	3.3	15587	PRKM
E393	Powder River	4900252627	1 BARLOW 21-20	LOUISIANA LAND & EXP	WY	48N	75W	20	NENW	7014.1	B	17.3	2.66	20.6	12.9	9.3	15587	PRKM
E393	Powder River	4900252627	1 BARLOW 21-20	LOUISIANA LAND & EXP	WY	48N	75W	20	NENW	7019.9	B	9.9	2.69	0.149	0.0745	26.9	15285	PRKM
E393	Powder River	4900252627	1 BARLOW 21-20	LOUISIANA LAND & EXP	WY	48N	75W	20	NENW	7019.9	A	9.0	2.68	0.127	0.0577	65.1	15285	PRKM
E393	Powder River	4900252627	1 BARLOW 21-20	LOUISIANA LAND & EXP	WY	48N	75W	20	NENW	7027.0	B	15.0	2.68	4.00	2.65	11.4	14286	PRKM
E393	Powder River	4900252627	1 BARLOW 21-20	LOUISIANA LAND & EXP	WY	48N	75W	20	NENW	7027.0	A	15.3	2.69	3.95	2.45	10.2	14286	PRKM
E393	Powder River	4900252627	1 BARLOW 21-20	LOUISIANA LAND & EXP	WY	48N	75W	20	NENW	7027.2	B	14.7	2.68	4.07	2.53	11.8	14286	PRKM
E393	Powder River	4900252627	1 BARLOW 21-20	LOUISIANA LAND & EXP	WY	48N	75W	20	NENW	7027.2	B	15.0	2.70	3.24	1.93	17.1	14286	PRKM
E393	Powder River	4900252627	1 BARLOW 21-20	LOUISIANA LAND & EXP	WY	48N	75W	20	NENW	7039.2	B	17.1	2.70	8.59	6.21	5.6	14286	PRKM
E393	Powder River	4900252627	1 BARLOW 21-20	LOUISIANA LAND & EXP	WY	48N	75W	20	NENW	7039.2	A	16.6	2.68	8.32	6.28	6.3	14286	PRKM
E393	Powder River	4900252627	1 BARLOW 21-20	LOUISIANA LAND & EXP	WY	48N	75W	20	NENW	7039.4	B	16.6	2.69	9.03	6.29	8.2	14286	PRKM
E393	Powder River	4900252627	1 BARLOW 21-20	LOUISIANA LAND & EXP	WY	48N	75W	20	NENW	7039.4	A	16.6	2.69	8.92	7.57	1.7	14286	PRKM
E393	Powder River	4900252627	1 BARLOW 21-20	LOUISIANA LAND & EXP	WY	48N	75W	20	NENW	7052.9	B	23.8	2.71	11.1	11.1	51.8	14286	PRKM
E393	Powder River	4900252627	1 BARLOW 21-20	LOUISIANA LAND & EXP	WY	48N	75W	20	NENW	7052.9	A	23.6	2.70	9.88	6.90	6.3	14597	PRKM
E393	Powder River	4900252627	1 BARLOW 21-20	LOUISIANA LAND & EXP	WY	48N	75W	20	NENW	7053.0	A	23.7	2.70	9.72	7.37	3.5	14597	PRKM
E393	Powder River	4900252627	1 BARLOW 21-20	LOUISIANA LAND & EXP	WY	48N	75W	20	NENW	7053.0	B	23.8	2.70	9.71	5.98	9.6	14597	PRKM
E393	Powder River	4900252627	1 BARLOW 21-20	LOUISIANA LAND & EXP	WY	48N	75W	20	NENW	7060.1	A	6.4	2.67	0.00430	0.000281	489	12285	PRKM
E393	Powder River	4900252627	1 BARLOW 21-20	LOUISIANA LAND & EXP	WY	48N	75W	20	NENW	7060.1	B	7.0	2.68	0.00255	0.000230	201	12285	PRKM
E393	Powder River	4900252627	1 BARLOW 21-20	LOUISIANA LAND & EXP	WY	48N	75W	20	NENW	7060.4	B	15.4	2.68	0.128	0.0669	16.2	13285	PRKM
E393	Powder River	4900252627	1 BARLOW 21-20	LOUISIANA LAND & EXP	WY	48N	75W	20	NENW	7060.4	A	14.5	2.66	0.110	0.0564	30.0	13285	PRKM
E393	Powder River	4900252627	1 BARLOW 21-20	LOUISIANA LAND & EXP	WY	48N	75W	20	NENW	7060.6	A	16.1	2.67	4.19	2.74	9.4	13285	PRKM
E393	Powder River	4900252627	1 BARLOW 21-20	LOUISIANA LAND & EXP	WY	48N	75W	20	NENW	7060.6	B	15.9	2.67	0.263	0.12	51.8	13285	PRKM
E393	Powder River	4900252627	1 BARLOW 21-20	LOUISIANA LAND & EXP	WY	48N	75W	20	NENW	7076.6	B	15.0	2.69	2.77	1.88	9.5	14297	PRKM
E393	Powder River	4900252627	1 BARLOW 21-20	LOUISIANA LAND & EXP	WY	48N	75W	20	NENW	7076.6	A	22.4	2.69	1.50	1.03	16.8	14297	PRKM
E393	Powder River	4900252627	1 BARLOW 21-20	LOUISIANA LAND & EXP	WY	48N	75W	20	NENW	7076.7	B	21.8	2.70	2.85	1.77	15.3	14297	PRKM
E393	Powder River	4900252627	1 BARLOW 21-20	LOUISIANA LAND & EXP	WY	48N	75W	20	NENW	7076.7	A	22.6	2.70	1.88	1.28	6.1	14297	PRKM
E932	Powder River	4900921513	2 FRED STATE	DAVIS OIL COMPANY	WY	35N	70W	36	NESESW	7538.0	B	16.7	2.65	3.15	2.02	10.8	13517	TPOT
E932	Powder River	4900921513	2 FRED STATE	DAVIS OIL COMPANY	WY	35N	70W	36	NESESW	7538.0	A	15.9	2.66	1.64	0.940	15.9	13517	TPOT
E932	Powder River	4900921513	2 FRED STATE	DAVIS OIL COMPANY	WY	35N	70W	36	NESESW	7544.1	A	16.6	2.67	5.30	3.53	9.2	15597	TPOT
E932	Powder River	4900921513	2 FRED STATE	DAVIS OIL COMPANY	WY	35N	70W	36	NESESW	7544.1	B	16.7	2.67	4.93	3.35	9.7	15597	TPOT
E932	Powder River	4900921513	2 FRED STATE	DAVIS OIL COMPANY	WY	35N	70W	36	NESESW	7544.3	A	16.2	2.66	4.80	3.13	11.5	15597	TPOT
E932	Powder River	4900921513	2 FRED STATE	DAVIS OIL COMPANY	WY	35N	70W	36	NESESW	7544.3	B	16.6	2.68	4.36	2.98	6.2	15597	TPOT
E932	Powder River	4900921513	2 FRED STATE	DAVIS OIL COMPANY	WY	35N	70W	36	NESESW	7546.7	B	13.4	2.69	0.118	0.0559	33.0	13217	TPOT
E932	Powder River	4900921513	2 FRED STATE	DAVIS OIL COMPANY	WY	35N	70W	36	NESESW	7546.7	A	13.1	2.67	0.0944	0.0407	53.9	13217	TPOT
E932	Powder River	4900921513	2 FRED STATE	DAVIS OIL COMPANY	WY	35N	70W	36	NESESW	7546.9	A	10.5	2.69	0.0583	0.0192	26.4	13217	TPOT
E932	Powder River	4900921513	2 FRED STATE	DAVIS OIL COMPANY	WY	35N	70W	36	NESESW	7546.9	B	10.3	2.75	0.0256	0.00809	72.2	13217	TPOT
E932	Powder River	4900921513	2 FRED STATE	DAVIS OIL COMPANY	WY	35N	70W	36	NESESW	7549.9	B	3.3	2.71	0.00213	0.000051	78.4	15295	TPOT
E932	Powder River	4900921513	2 FRED STATE	DAVIS OIL COMPANY	WY	35N	70W	36	NESESW	7549.9	A	2.6	2.70	0.00192	0.000152	285	15295	TPOT
E932	Powder River	4900921513	2 FRED STATE	DAVIS OIL COMPANY	WY	35N	70W	36	NESESW	7550.1	B	4.0	2.71	0.00287	0.000191	206	15295	TPOT
E932	Powder River	4900921513	2 FRED STATE	DAVIS OIL COMPANY	WY	35N	70W	36	NESESW	7550.1	A	3.4	2.71	0.00194	0.000146	185	15295	TPOT
E932	Powder River	4900921513	2 FRED STATE	DAVIS OIL COMPANY	WY	35N	70W	36	NESESW	7557.1	A	12.4	2.67	0.0185	0.00259	213	13217	TPOT
E932	Powder River	4900921513	2 FRED STATE	DAVIS OIL COMPANY	WY	35N	70W	36	NESESW	7557.1	B	13.2	2.70	0.0131	0.00217	139	13217	TPOT
E932	Powder River	4900921513	2 FRED STATE	DAVIS OIL COMPANY	WY	35N	70W	36	NESESW	7557.4	B	12.8	2.68	0.0280	0.00647	103	13217	TPOT
E932	Powder River	4900921513	2 FRED STATE	DAVIS OIL COMPANY	WY	35N	70W	36	NESESW	7557.4	A	12.0	2.67	0.0143	0.00217	182	13217	TPOT
E932	Powder River	4900921513	2 FRED STATE	DAVIS OIL COMPANY	WY	35N	70W	36	NESESW	7560.0	A	16.0	2.67	0.0205	0.00416	79.1	15297	TPOT
E932	Powder River	4900921513	2 FRED STATE	DAVIS OIL COMPANY	WY	35N	70W	36	NESESW	7560.0	B	16.3	2.68	0.0201	0.00251	116	15297	TPOT
E932	Powder River	4900921513	2 FRED STATE	DAVIS OIL COMPANY	WY	35N	70W	36	NESESW	7568.1	B	16.7	2.66	0.0478	0.00635	76.4	15587	TPOT
E932	Powder River	4900921513	2 FRED STATE	DAVIS OIL COMPANY	WY	35N	70W	36	NESESW	7568.1	A	16.2	2.66	0.0244	0.00609	58.6	15587	TPOT

Appendix A1

Summary of Porosity, Permeability and Grain Density

Analysis of Critical Permeability, Capillary Pressure and Electrical Properties for Mesaverde Tight Gas Sandstones from Western U.S. Basins

US DOE # DE-FC26-05NT42660 Final Scientific/Technical Report

Alan P. Byrnes, Robert M. Cluff, John C. Webb

website: <http://www.kgs.ku.edu/mesaverde>

USGS Library Number	Basin	API Number	Well Name	Operator	State	Township	Range	Section	Quarter Section	Plug Depth	Plug Letter	Ambient Porosity	Grain Density	Routine Gas Permeability	in situ		Rock Type Code	Formations	
															Kninberg Gas Permeability	Kninberg constant b			
										ft	A/B/C	%	g/cc	mD	mD				
S838	Powder River	4900905481	3 SHAWNEE	BELCO PETROLEUM	WY	33N	69W	23	C SENE	6977.9	B	4.3	2.72	0.00116	0.000131	250	15275	TPOT	
S838	Powder River	4900905481	3 SHAWNEE	BELCO PETROLEUM	WY	33N	69W	23	C SENE	6979.9	B	15.7	2.77	0.0598	0.0170	45.8	13216	TPOT	
S838	Powder River	4900905481	3 SHAWNEE	BELCO PETROLEUM	WY	33N	69W	23	C SENE	6979.9	A	11.2	2.65	0.0461	0.0153	134	13216	TPOT	
S838	Powder River	4900905481	3 SHAWNEE	BELCO PETROLEUM	WY	33N	69W	23	C SENE	6982.1	A	7.1	2.67	0.0200	0.00451	275	15285	TPOT	
S838	Powder River	4900905481	3 SHAWNEE	BELCO PETROLEUM	WY	33N	69W	23	C SENE	6982.1	B	7.6	2.68	0.0150	0.00406	293	15285	TPOT	
S838	Powder River	4900905481	3 SHAWNEE	BELCO PETROLEUM	WY	33N	69W	23	C SENE	6985.7	A	7.8	2.67	0.0103	0.000798	243	13286	TPOT	
S838	Powder River	4900905481	3 SHAWNEE	BELCO PETROLEUM	WY	33N	69W	23	C SENE	6985.7	B	8.0	2.67	0.00882	0.00123	51.9	13286	TPOT	
S838	Powder River	4900905481	3 SHAWNEE	BELCO PETROLEUM	WY	33N	69W	23	C SENE	6985.8	B	6.5	2.68	0.00743	0.000925	168	13286	TPOT	
S838	Powder River	4900905481	3 SHAWNEE	BELCO PETROLEUM	WY	33N	69W	23	C SENE	6985.8	A	5.5	2.68	0.00735	0.000378	223	13286	TPOT	
S838	Powder River	4900905481	3 SHAWNEE	BELCO PETROLEUM	WY	33N	69W	23	C SENE	6988.0	B	18.3	2.66	0.0916	5.61	15.8	15296	TPOT	
S838	Powder River	4900905481	3 SHAWNEE	BELCO PETROLEUM	WY	33N	69W	23	C SENE	6988.0	A	17.3	2.65	8.24	5.15	16.1	15296	TPOT	
S838	Powder River	4900905481	3 SHAWNEE	BELCO PETROLEUM	WY	33N	69W	23	C SENE	6985.9	A	11.8	2.64	0.0739	0.0377	50.7	13216	TPOT	
S838	Powder River	4900905481	3 SHAWNEE	BELCO PETROLEUM	WY	33N	69W	23	C SENE	6985.9	B	13.5	2.66	0.0693	0.0340	61.0	13216	TPOT	
S838	Powder River	4900905481	3 SHAWNEE	BELCO PETROLEUM	WY	33N	69W	23	C SENE	6996.0	A	12.8	2.65	0.091	0.639	17.7	15216	TPOT	
S838	Powder River	4900905481	3 SHAWNEE	BELCO PETROLEUM	WY	33N	69W	23	C SENE	6996.0	B	13.7	2.66	0.452	0.295	17.8	15216	TPOT	
S838	Powder River	4900905481	3 SHAWNEE	BELCO PETROLEUM	WY	33N	69W	23	C SENE	6996.9	A	11.1	2.64	0.0220	0.00584	40.3	13216	TPOT	
S838	Powder River	4900905481	3 SHAWNEE	BELCO PETROLEUM	WY	33N	69W	23	C SENE	6996.9	B	11.7	2.66	0.0141	0.00315	136	13216	TPOT	
S838	Powder River	4900905481	3 SHAWNEE	BELCO PETROLEUM	WY	33N	69W	23	C SENE	6998.5	B	6.3	2.64	0.0200	0.00159	48.3	12216	TPOT	
S838	Powder River	4900905481	3 SHAWNEE	BELCO PETROLEUM	WY	33N	69W	23	C SENE	6998.5	A	5.8	2.63	0.0138	0.00121	207	12216	TPOT	
1715	Sand Wash	0508106724	1-791-2613 Craig Dome	COCKRELL OIL CORP	CO	7N	91W	26	NESWSW	3465.9	B	16.9	2.64	22.4	9.67	10.5	13286	WMFK	
1715	Sand Wash	0508106724	1-791-2613 Craig Dome	COCKRELL OIL CORP	CO	7N	91W	26	NESWSW	3465.9	A	16.7	2.64	17.4	12.1	8.5	13286	WMFK	
1715	Sand Wash	0508106724	1-791-2613 Craig Dome	COCKRELL OIL CORP	CO	7N	91W	26	NESWSW	3467.1	A	17.3	2.64	15.3	8.04	28.3	15557	WMFK	
1715	Sand Wash	0508106724	1-791-2613 Craig Dome	COCKRELL OIL CORP	CO	7N	91W	26	NESWSW	3467.2	A	17.1	2.64			6.4	15557	WMFK	
1715	Sand Wash	0508106724	1-791-2613 Craig Dome	COCKRELL OIL CORP	CO	7N	91W	26	NESWSW	3467.3	A	17.0	2.64	18.8	12.7	6.4	15557	WMFK	
1715	Sand Wash	0508106724	1-791-2613 Craig Dome	COCKRELL OIL CORP	CO	7N	91W	26	NESWSW	3467.4	A	17.5	2.64	30.4	23.4	5.0	15577	WMFK	
1715	Sand Wash	0508106724	1-791-2613 Craig Dome	COCKRELL OIL CORP	CO	7N	91W	26	NESWSW	3467.6	A	17.3	2.64	39.4	30.1	5.5	15577	WMFK	
1715	Sand Wash	0508106724	1-791-2613 Craig Dome	COCKRELL OIL CORP	CO	7N	91W	26	NESWSW	3467.8	A	16.4	2.64	4.40	2.89	5.3	13277	WMFK	
1715	Sand Wash	0508106724	1-791-2613 Craig Dome	COCKRELL OIL CORP	CO	7N	91W	26	NESWSW	3467.9	A	16.4	2.64	4.62	2.97	7.4	13277	WMFK	
1715	Sand Wash	0508106724	1-791-2613 Craig Dome	COCKRELL OIL CORP	CO	7N	91W	26	NESWSW	3469.2	A	17.8	2.64	37.2	30.2	1.8	15577	WMFK	
1715	Sand Wash	0508106724	1-791-2613 Craig Dome	COCKRELL OIL CORP	CO	7N	91W	26	NESWSW	3469.2	B	17.9	2.64	32.6	27.2	2.6	15577	WMFK	
1715	Sand Wash	0508106724	1-791-2613 Craig Dome	COCKRELL OIL CORP	CO	7N	91W	26	NESWSW	3470.8	A	16.5	2.66	21.3	6.5	16.7	6.5	13577	WMFK
1715	Sand Wash	0508106724	1-791-2613 Craig Dome	COCKRELL OIL CORP	CO	7N	91W	26	NESWSW	3470.9	A	17.1	2.67	26.9	17.7	13.1	13577	WMFK	
1717	Sand Wash	0508106718	1-691-0513 West Craig	COCKRELL OIL CORP	CO	6N	91W	5	SESWSW	1732.9	A	3.5	2.59	0.0861	0.00390	55.4	11219	WMFK	
1717	Sand Wash	0508106718	1-691-0513 West Craig	COCKRELL OIL CORP	CO	6N	91W	5	SESWSW	1732.9	B	4.1	2.59	0.0137	0.000304	299	11219	WMFK	
1717	Sand Wash	0508106718	1-691-0513 West Craig	COCKRELL OIL CORP	CO	6N	91W	5	SESWSW	1733.0	A	5.8	2.65	0.0693	0.0247	4.28	12226	WMFK	
1717	Sand Wash	0508106718	1-691-0513 West Craig	COCKRELL OIL CORP	CO	6N	91W	5	SESWSW	1733.0	B	17.9	2.63	0.00591	0.00102	269	12226	WMFK	
1717	Sand Wash	0508106718	1-691-0513 West Craig	COCKRELL OIL CORP	CO	6N	91W	5	SESWSW	1733.8	A	3.9	2.61	0.00617	0.000172	281	12216	WMFK	
1717	Sand Wash	0508106718	1-691-0513 West Craig	COCKRELL OIL CORP	CO	6N	91W	5	SESWSW	1733.8	B	4.7	2.62	0.00415	0.000303	214	12216	WMFK	
1717	Sand Wash	0508106718	1-691-0513 West Craig	COCKRELL OIL CORP	CO	6N	91W	5	SESWSW	1734.0	A	4.2	2.62	0.00490	0.000277	283	12216	WMFK	
1717	Sand Wash	0508106718	1-691-0513 West Craig	COCKRELL OIL CORP	CO	6N	91W	5	SESWSW	1734.0	B	4.8	2.63	0.00338	0.000390	249	12216	WMFK	
1717	Sand Wash	0508106718	1-691-0513 West Craig	COCKRELL OIL CORP	CO	6N	91W	5	SESWSW	1747.9	A	5.1	2.65	0.0124	0.00126	171	13225	WMFK	
1717	Sand Wash	0508106718	1-691-0513 West Craig	COCKRELL OIL CORP	CO	6N	91W	5	SESWSW	1747.9	B	5.1	2.65	0.00317	0.000168	527	13225	WMFK	
1717	Sand Wash	0508106718	1-691-0513 West Craig	COCKRELL OIL CORP	CO	6N	91W	5	SESWSW	1749.9	A	5.8	2.61			12229	WMFK		
1717	Sand Wash	0508106718	1-691-0513 West Craig	COCKRELL OIL CORP	CO	6N	91W	5	SESWSW	1750.1	A	6.3	2.63	0.00777	0.00131	133	13226	WMFK	
1717	Sand Wash	0508106718	1-691-0513 West Craig	COCKRELL OIL CORP	CO	6N	91W	5	SESWSW	1750.1	B	6.9	2.65	0.00592	0.00118	114	13226	WMFK	
1717	Sand Wash	0508106718	1-691-0513 West Craig	COCKRELL OIL CORP	CO	6N	91W	5	SESWSW	1750.7	A	4.6	2.62	0.365	0.0121	113	13226	WMFK	
6646	Uinta	4304730584	11-17F RIVER BEND UNIT	MAPCO INCORPORATED	UT	10S	20E	17	SENENW	8287.7	A	6.5	2.65	0.114	0.0148	68.1	17286	MVRD	
6646	Uinta	4304730584	11-17F RIVER BEND UNIT	MAPCO INCORPORATED	UT	10S	20E	17	SENENW	8287.7	B	4.7	2.61	0.0859	0.0151	87.7	17286	MVRD	
6646	Uinta	4304730584	11-17F RIVER BEND UNIT	MAPCO INCORPORATED	UT	10S	20E	17	SENENW	8229.7	B	7.9	2.65	0.0422	0.00629	124	16286	MVRD	
6646	Uinta	4304730584	11-17F RIVER BEND UNIT	MAPCO INCORPORATED	UT	10S	20E	17	SENENW	8229.7	A	7.4	2.64	0.0390	0.0046	32.5	16286	MVRD	
6646	Uinta	4304730584	11-17F RIVER BEND UNIT	MAPCO INCORPORATED	UT	10S	20E	17	SENENW	8233.0	A	5.7	2.65	0.0425	0.00466	92.1	16296	MVRD	
6646	Uinta	4304730584	11-17F RIVER BEND UNIT	MAPCO INCORPORATED	UT	10S	20E	17	SENENW	8233.0	B	5.8	2.65	0.0344	0.00464	125	16296	MVRD	
6646	Uinta	4304730584	11-17F RIVER BEND UNIT	MAPCO INCORPORATED	UT	10S	20E	17	SENENW	8233.7	A	5.6	2.65	0.0416	0.00399	112	16296	MVRD	
6646	Uinta	4304730584	11-17F RIVER BEND UNIT	MAPCO INCORPORATED	UT	10S	20E	17	SENENW	8233.7	B	5.5	2.65	0.0365	0.00464	131	16296	MVRD	
6646	Uinta	4304730584	11-17F RIVER BEND UNIT	MAPCO INCORPORATED	UT	10S	20E	17	SENENW	8236.9	B	5.5	2.67	0.0246	0.00163	237	15276	MVRD	
6646	Uinta	4304730584	11-17F RIVER BEND UNIT	MAPCO INCORPORATED	UT	10S	20E	17	SENENW	8236.9	A	5.3	2.66	0.0197	0.00170	385	15276	MVRD	
6646	Uinta	4304730584	11-17F RIVER BEND UNIT	MAPCO INCORPORATED	UT	10S	20E	17	SENENW	8245.1	A	2.6	2.68	0.00786	0.000781	109	13296	MVRD	
6646	Uinta	4304730584	11-17F RIVER BEND UNIT	MAPCO INCORPORATED	UT	10S	20E	17	SENENW	8245.1	B	3.0	2.69	0.00676	0.000580	490	13296	MVRD	
6646	Uinta	4304730584	11-17F RIVER BEND UNIT	MAPCO INCORPORATED	UT	10S	20E	17	SENENW	8282.8	B	2.5	2.67	0.00682	0.00165	264	12219	MVRD	
6646	Uinta	4304730584	11-17F RIVER BEND UNIT	MAPCO INCORPORATED	UT	10S	20E	17	SENENW	8282.8	A	1.7	2.65	0.00534	0.000091	205	12219	MVRD	
6646	Uinta	4304730584	11-17F RIVER BEND UNIT	MAPCO INCORPORATED	UT	10S	20E	17	SENENW	8287.4	A	8.2	2.66	0.134	0.0187	83.7	16277	MVRD	
6646	Uinta	4304730584	11-17F RIVER BEND UNIT	MAPCO INCORPORATED	UT	10S	20E	17	SENENW	8287.4	B	7.5	2.64	0.131	0.0217	74.8	16277	MVRD	
6646	Uinta	4304730584	11-17F RIVER BEND UNIT	MAPCO INCORPORATED	UT	10S	20E	17	SENENW	8287.8	A	6.4	2.65	0.0943	0.0112	143	16276	MVRD	
6646	Uinta	4304730584	11-17F RIVER BEND UNIT	MAPCO INCORPORATED	UT	10S	20E	17	SENENW	8287.8	B	6.3	2.65	0.0702	0.0124	85.0	16276	MVRD	
6646	Uinta	4304730584	11-17F RIVER BEND UNIT	MAPCO INCORPORATED	UT	10S	20E	17	SENENW	8294.2	A	7.6	2.65	0.288	0.0344	73.9	16277	MVRD	
6646	Uinta																		

Appendix A1

Summary of Porosity, Permeability and Grain Density

Analysis of Critical Permeability, Capillary Pressure and Electrical Properties for Mesaverde Tight Gas Sandstones from Western U.S. Basins

US DOE # DE-FC26-05NT42660 Final Scientific/Technical Report

Alan P. Byrnes, Robert M. Cluff, John C. Webb

website: <http://www.kgs.ku.edu/mesaverde>

USGS Library Number	Basin	API Number	Well Name	Operator	State	Township	Range	Section	Quarter Section	Plug Depth	Plug Letter	Ambient Porosity	Grain Density	Routine Gas Permeability	in situ		Rock Type Code	Formations
															Klinkenberg Gas Permeability	Klinkenberg constant b (psia)		
										ft	A/B/C	%	g/cc	mD	mD			
E946	Uinta	4304730545	2-7 FLAT MESA	ENSERCH EXPLORATION	UT	10S	23E	7	NESENN	6468.5	A	11.9	2.63	0.911	0.382	14.7	16576	MVRD
E946	Uinta	4304730545	2-7 FLAT MESA	ENSERCH EXPLORATION	UT	10S	23E	7	NESENN	6468.5	C	12.2	2.63	0.877	0.431	12.3	16576	MVRD
E946	Uinta	4304730545	2-7 FLAT MESA	ENSERCH EXPLORATION	UT	10S	23E	7	NESENN	6468.6	A	12.1	2.64	0.838	0.257	39.1	16576	MVRD
E946	Uinta	4304730545	2-7 FLAT MESA	ENSERCH EXPLORATION	UT	10S	23E	7	NESENN	6468.6	C	12.1	2.63	0.740	0.297	20.8	16576	MVRD
E946	Uinta	4304730545	2-7 FLAT MESA	ENSERCH EXPLORATION	UT	10S	23E	7	NESENN	6468.6	B	12.3	2.63	0.715	0.319	6.5	16576	MVRD
E946	Uinta	4304730545	2-7 FLAT MESA	ENSERCH EXPLORATION	UT	10S	23E	7	NESENN	6472.7	A	9.0	2.64	0.303	0.0454	26.9	16276	MVRD
E946	Uinta	4304730545	2-7 FLAT MESA	ENSERCH EXPLORATION	UT	10S	23E	7	NESENN	6472.7	B	8.5	2.64	0.163	0.0262	60.5	16276	MVRD
E946	Uinta	4304730545	2-7 FLAT MESA	ENSERCH EXPLORATION	UT	10S	23E	7	NESENN	6475.2	C	12.5	2.63	1.21	0.532	16.6	16576	MVRD
E946	Uinta	4304730545	2-7 FLAT MESA	ENSERCH EXPLORATION	UT	10S	23E	7	NESENN	6475.2	A	13.0	2.64	1.13	0.390	30.7	16576	MVRD
E946	Uinta	4304730545	2-7 FLAT MESA	ENSERCH EXPLORATION	UT	10S	23E	7	NESENN	6475.2	B	11.1	2.63	1.11	0.444	18.5	16576	MVRD
E946	Uinta	4304730545	2-7 FLAT MESA	ENSERCH EXPLORATION	UT	10S	23E	7	NESENN	6475.3	A	12.4	2.63	1.29	0.583	10.3	16576	MVRD
E946	Uinta	4304730545	2-7 FLAT MESA	ENSERCH EXPLORATION	UT	10S	23E	7	NESENN	6475.3	B	12.1	2.63	1.14	0.479	17.7	16576	MVRD
E946	Uinta	4304730545	2-7 FLAT MESA	ENSERCH EXPLORATION	UT	10S	23E	7	NESENN	6475.3	C	12.5	2.63	0.922	0.266	22.5	16576	MVRD
E946	Uinta	4304730545	2-7 FLAT MESA	ENSERCH EXPLORATION	UT	10S	23E	7	NESENN	6475.4	C	11.9	2.63	0.884	0.293	18.6	16576	MVRD
E946	Uinta	4304730545	2-7 FLAT MESA	ENSERCH EXPLORATION	UT	10S	23E	7	NESENN	6475.4	B	11.8	2.63	0.779	0.313	16.6	16576	MVRD
E946	Uinta	4304730545	2-7 FLAT MESA	ENSERCH EXPLORATION	UT	10S	23E	7	NESENN	6475.4	A	11.9	2.64	0.736	0.307	15.5	16576	MVRD
E946	Uinta	4304730545	2-7 FLAT MESA	ENSERCH EXPLORATION	UT	10S	23E	7	NESENN	6482.0	B	3.7	2.67	0.0224	0.000092	210	16286	MVRD
E946	Uinta	4304730545	2-7 FLAT MESA	ENSERCH EXPLORATION	UT	10S	23E	7	NESENN	6482.0	A	2.6	2.65	0.0181	0.000095	272	16286	MVRD
E946	Uinta	4304730545	2-7 FLAT MESA	ENSERCH EXPLORATION	UT	10S	23E	7	NESENN	6482.0	C	2.9	2.66	0.0149	0.000027	782	16286	MVRD
E946	Uinta	4304730545	2-7 FLAT MESA	ENSERCH EXPLORATION	UT	10S	23E	7	NESENN	6486.4	A	12.5	2.64	2.26	0.658	20.1	16576	MVRD
E946	Uinta	4304730545	2-7 FLAT MESA	ENSERCH EXPLORATION	UT	10S	23E	7	NESENN	6486.4	C	12.1	2.64	2.28	0.633	27.8	16576	MVRD
E946	Uinta	4304730545	2-7 FLAT MESA	ENSERCH EXPLORATION	UT	10S	23E	7	NESENN	6486.4	B	12.2	2.64	2.26	0.637	23.7	16576	MVRD
E946	Uinta	4304730545	2-7 FLAT MESA	ENSERCH EXPLORATION	UT	10S	23E	7	NESENN	6486.5	B	11.3	2.63	1.44	0.286	36.7	16576	MVRD
E946	Uinta	4304730545	2-7 FLAT MESA	ENSERCH EXPLORATION	UT	10S	23E	7	NESENN	6486.5	C	11.3	2.63	1.29	0.391	24.7	16576	MVRD
E946	Uinta	4304730545	2-7 FLAT MESA	ENSERCH EXPLORATION	UT	10S	23E	7	NESENN	6486.5	A	10.9	2.63	1.05	0.246	17.9	16576	MVRD
E946	Uinta	4304730545	2-7 FLAT MESA	ENSERCH EXPLORATION	UT	10S	23E	7	NESENN	6486.6	C	9.3	2.63	0.467	0.0724	37.9	16576	MVRD
E946	Uinta	4304730545	2-7 FLAT MESA	ENSERCH EXPLORATION	UT	10S	23E	7	NESENN	6486.6	B	9.3	2.63	0.365	0.0476	26.9	16576	MVRD
E946	Uinta	4304730545	2-7 FLAT MESA	ENSERCH EXPLORATION	UT	10S	23E	7	NESENN	6486.6	A	8.7	2.63	0.344	0.0532	50.5	16576	MVRD
E946	Uinta	4304730545	2-7 FLAT MESA	ENSERCH EXPLORATION	UT	10S	23E	7	NESENN	6486.7	C	9.6	2.63	0.780	0.254	10.2	16576	MVRD
E946	Uinta	4304730545	2-7 FLAT MESA	ENSERCH EXPLORATION	UT	10S	23E	7	NESENN	6486.7	B	9.6	2.63	0.686	0.182	32.3	16576	MVRD
E946	Uinta	4304730545	2-7 FLAT MESA	ENSERCH EXPLORATION	UT	10S	23E	7	NESENN	6486.7	A	9.9	2.63	0.629	0.146	45.8	16576	MVRD
E946	Uinta	4304730545	2-7 FLAT MESA	ENSERCH EXPLORATION	UT	10S	23E	7	NESENN	6489.6	A	11.3	2.63	0.792	0.186	54.9	16576	MVRD
E946	Uinta	4304730545	2-7 FLAT MESA	ENSERCH EXPLORATION	UT	10S	23E	7	NESENN	6489.6	C	11.2	2.63	0.756	0.216	21.9	16576	MVRD
E946	Uinta	4304730545	2-7 FLAT MESA	ENSERCH EXPLORATION	UT	10S	23E	7	NESENN	6489.6	B	11.3	2.64	0.700	0.172	35.9	16576	MVRD
E946	Uinta	4304730545	2-7 FLAT MESA	ENSERCH EXPLORATION	UT	10S	23E	7	NESENN	6489.7	A	11.8	2.63	0.827	0.269	18.1	16576	MVRD
E946	Uinta	4304730545	2-7 FLAT MESA	ENSERCH EXPLORATION	UT	10S	23E	7	NESENN	6489.7	B	11.4	2.63	0.533	0.139	58.4	16576	MVRD
E946	Uinta	4304730545	2-7 FLAT MESA	ENSERCH EXPLORATION	UT	10S	23E	7	NESENN	6489.7	C	11.1	2.63	0.512	0.178	25.0	16576	MVRD
E946	Uinta	4304730545	2-7 FLAT MESA	ENSERCH EXPLORATION	UT	10S	23E	7	NESENN	6492.5	A	9.9	2.66	0.260	0.0629	26.8	15286	MVRD
E946	Uinta	4304730545	2-7 FLAT MESA	ENSERCH EXPLORATION	UT	10S	23E	7	NESENN	6492.5	B	9.8	2.66	0.166	0.0314	36.3	15286	MVRD
E946	Uinta	4304730545	2-7 FLAT MESA	ENSERCH EXPLORATION	UT	10S	23E	7	NESENN	6492.5	C	9.9	2.66	0.0956	0.026	47.6	15286	MVRD
E946	Uinta	4304730545	2-7 FLAT MESA	ENSERCH EXPLORATION	UT	10S	23E	7	NESENN	6492.6	A	10.8	2.66	0.190	0.0193	86.8	15286	MVRD
E946	Uinta	4304730545	2-7 FLAT MESA	ENSERCH EXPLORATION	UT	10S	23E	7	NESENN	6492.6	B	10.2	2.66	0.182	0.0166	122	15286	MVRD
E946	Uinta	4304730545	2-7 FLAT MESA	ENSERCH EXPLORATION	UT	10S	23E	7	NESENN	6492.6	C	9.9	2.66	0.156	0.0282	44.1	15286	MVRD
E946	Uinta	4304730545	2-7 FLAT MESA	ENSERCH EXPLORATION	UT	10S	23E	7	NESENN	6507.5	B	2.5	2.65	0.00479	0.000308	293	13266	MVRD
E946	Uinta	4304730545	2-7 FLAT MESA	ENSERCH EXPLORATION	UT	10S	23E	7	NESENN	6507.5	A	3.0	2.66	0.00385	0.000339	237	13266	MVRD
E946	Uinta	4304730545	2-7 FLAT MESA	ENSERCH EXPLORATION	UT	10S	23E	7	NESENN	6507.5	C	2.5	2.65	0.00312	0.000200	820	13266	MVRD
E946	Uinta	4304730545	2-7 FLAT MESA	ENSERCH EXPLORATION	UT	10S	23E	7	NESENN	6508.2	C	3.1	2.65	0.0319	0.000484	125	13266	MVRD
E946	Uinta	4304730545	2-7 FLAT MESA	ENSERCH EXPLORATION	UT	10S	23E	7	NESENN	6508.3	C	2.9	2.63	0.520	0.0736	67.3	13266	MVRD
E946	Uinta	4304730545	2-7 FLAT MESA	ENSERCH EXPLORATION	UT	10S	23E	7	NESENN	6509.3	B	3.4	2.64	0.324	0.0545	125	13266	MVRD
E946	Uinta	4304730545	2-7 FLAT MESA	ENSERCH EXPLORATION	UT	10S	23E	7	NESENN	6511.4	C	9.3	2.65	0.264	0.0369	38.5	15276	MVRD
E946	Uinta	4304730545	2-7 FLAT MESA	ENSERCH EXPLORATION	UT	10S	23E	7	NESENN	6511.4	C	9.2	2.65	0.162	0.0314	47.6	15276	MVRD
E946	Uinta	4304730545	2-7 FLAT MESA	ENSERCH EXPLORATION	UT	10S	23E	7	NESENN	6511.4	A	8.4	2.65	0.125	0.0244	58.8	15276	MVRD
E946	Uinta	4304730545	2-7 FLAT MESA	ENSERCH EXPLORATION	UT	10S	23E	7	NESENN	6511.5	A	8.7	2.65	0.181	0.0367	29.2	15276	MVRD
E946	Uinta	4304730545	2-7 FLAT MESA	ENSERCH EXPLORATION	UT	10S	23E	7	NESENN	6511.5	C	9.5	2.65	0.148	0.0290	51.5	15276	MVRD
E946	Uinta	4304730545	2-7 FLAT MESA	ENSERCH EXPLORATION	UT	10S	23E	7	NESENN	6511.5	B	9.0	2.65	0.119	0.0198	41.5	15276	MVRD
E946	Uinta	4304730545	2-7 FLAT MESA	ENSERCH EXPLORATION	UT	10S	23E	7	NESENN	6515.5	B	14.5	2.64	4.35	1.86	14.6	16586	MVRD
E946	Uinta	4304730545	2-7 FLAT MESA	ENSERCH EXPLORATION	UT	10S	23E	7	NESENN	6515.5	A	16.3	2.64	4.27	2.00	13.9	16586	MVRD
E946	Uinta	4304730545	2-7 FLAT MESA	ENSERCH EXPLORATION	UT	10S	23E	7	NESENN	6515.5	C	13.3	2.63	4.06	1.31	21.1	16586	MVRD
E946	Uinta	4304730545	2-7 FLAT MESA	ENSERCH EXPLORATION	UT	10S	23E	7	NESENN	6515.6	A	15.1	2.63	4.79	1.94	14.5	16586	MVRD
E946	Uinta	4304730545	2-7 FLAT MESA	ENSERCH EXPLORATION	UT	10S	23E	7	NESENN	6515.6	B	15.4	2.64	4.70	1.61	26.3	16586	MVRD
E946	Uinta	4304730545	2-7 FLAT MESA	ENSERCH EXPLORATION	UT	10S	23E	7	NESENN	6515.6	C	13.8	2.63	3.79	1.67	9.9	16586	MVRD
E946	Uinta	4304730545	2-7 FLAT MESA	ENSERCH EXPLORATION	UT	10S	23E	7	NESENN	6518.1	A	5.2	2.63	0.0459	0.00125	155	13266	MVRD
E946	Uinta	4304730545	2-7 FLAT MESA	ENSERCH EXPLORATION	UT	10S	23E	7	NESENN	6518.1	C	4.8	2.63	0.0292	0.00117	42.5	13266	MVRD
E946	Uinta	4304730545	2-7 FLAT MESA	ENSERCH EXPLORATION	UT	10S	23E	7	NESENN	6518.1	B	5.1	2.63	0.0284	0.00125	75.2	13266	MVRD
E946	Uinta	4304730545	2-7 FLAT MESA	ENSERCH EXPLORATION	UT	10S	23E	7	NESENN	6527.6	B	9.8	2.64	0.378	0.0512	34.8	16596	MVRD
E946	Uinta	4304730545	2-7 FLAT MESA	ENSERCH EXPLORATION	UT	10S	23E	7	NESENN	6527.6	A	10.4	2.64	0.361	0.0643	34.2	16596	MVRD
E946	Uinta	4304730545	2-7 FLAT MESA	ENSERCH EXPLORATION	UT	10S	23E	7	NESENN	6527.6								

Appendix A1

Summary of Porosity, Permeability and Grain Density

Analysis of Critical Permeability, Capillary Pressure and Electrical Properties for Mesaverde Tight Gas Sandstones from Western U.S. Basins

US DOE # DE-FC26-05NT42660 Final Scientific/Technical Report

Alan P. Byrnes, Robert M. Cluff, John C. Webb

website: <http://www.kgs.ku.edu/mesaverde>

USGS Library Number	Basin	API Number	Well Name	Operator	State	Township	Range	Section	Quarter Section	Plug Depth	Plug Letter	Ambient Porosity	Grain Density	Routine Gas Permeability	in situ		Rock Type Code	Formations
															Klinkenberg Gas Permeability	Klinkenberg constant b (psia)		
										ft	A/B/C	%	g/cc	mD	mD			
E946	Uinta	4304730545	2-7 FLAT MESA	ENSERCH EXPLORATION	UT	10S	23E	7	NESENN	6698.0	A	2.0	2.63	0.00133	0.00034	436	12266	MVRD
E946	Uinta	4304730545	2-7 FLAT MESA	ENSERCH EXPLORATION	UT	10S	23E	7	NESENN	6700.1	B	2.2	2.62	0.00329	0.000072	483	12216	MVRD
E946	Uinta	4304730545	2-7 FLAT MESA	ENSERCH EXPLORATION	UT	10S	23E	7	NESENN	6700.1	A	2.1	2.63	0.00275	0.000068	370	12216	MVRD
E946	Uinta	4304730545	2-7 FLAT MESA	ENSERCH EXPLORATION	UT	10S	23E	7	NESENN	6700.1	C	1.7	2.65	0.00284	0.000055	314	12216	MVRD
E946	Uinta	4304730545	2-7 FLAT MESA	ENSERCH EXPLORATION	UT	10S	23E	7	NESENN	6702.8	C	8.2	2.67	0.0615	0.00355	56.0	13266	MVRD
E946	Uinta	4304730545	2-7 FLAT MESA	ENSERCH EXPLORATION	UT	10S	23E	7	NESENN	6702.8	A	7.8	2.68	0.0532	0.00250	90.6	13266	MVRD
E946	Uinta	4304730545	2-7 FLAT MESA	ENSERCH EXPLORATION	UT	10S	23E	7	NESENN	6702.8	B	8.4	2.68	0.0385	0.00280	83.3	13266	MVRD
E946	Uinta	4304730545	2-7 FLAT MESA	ENSERCH EXPLORATION	UT	10S	23E	7	NESENN	6709.8	B	1.7	2.67	0.00364	0.000170	299	13216	MVRD
E946	Uinta	4304730545	2-7 FLAT MESA	ENSERCH EXPLORATION	UT	10S	23E	7	NESENN	6709.8	C	1.8	2.67	0.00347	0.000154	378	13216	MVRD
E946	Uinta	4304730545	2-7 FLAT MESA	ENSERCH EXPLORATION	UT	10S	23E	7	NESENN	6709.8	A	2.2	2.68	0.00179	0.000117	231	13216	MVRD
E946	Uinta	4304730545	2-7 FLAT MESA	ENSERCH EXPLORATION	UT	10S	23E	7	NESENN	7272.3	C	8.9	2.65	0.128	0.00751	57.8	13276	MVRD
E946	Uinta	4304730545	2-7 FLAT MESA	ENSERCH EXPLORATION	UT	10S	23E	7	NESENN	7272.3	A	9.0	2.66	0.125	0.00638	94.7	13276	MVRD
E946	Uinta	4304730545	2-7 FLAT MESA	ENSERCH EXPLORATION	UT	10S	23E	7	NESENN	7272.3	B	9.4	2.66	0.0836	0.00442	90.0	13276	MVRD
E946	Uinta	4304730545	2-7 FLAT MESA	ENSERCH EXPLORATION	UT	10S	23E	7	NESENN	7272.2	B	7.3	2.67	0.0600	0.00653	60.5	14266	MVRD
E946	Uinta	4304730545	2-7 FLAT MESA	ENSERCH EXPLORATION	UT	10S	23E	7	NESENN	7272.2	B	7.3	2.68	0.0563	0.00230	84.9	14266	MVRD
E946	Uinta	4304730545	2-7 FLAT MESA	ENSERCH EXPLORATION	UT	10S	23E	7	NESENN	7272.2	C	8.1	2.68	0.0467	0.00189	81.2	14266	MVRD
E946	Uinta	4304730545	2-7 FLAT MESA	ENSERCH EXPLORATION	UT	10S	23E	7	NESENN	7278.8	A	7.0	2.66	0.0592	0.00133	75.3	13266	MVRD
E946	Uinta	4304730545	2-7 FLAT MESA	ENSERCH EXPLORATION	UT	10S	23E	7	NESENN	7278.8	C	7.8	2.66	0.0413	0.000556	172	13266	MVRD
E946	Uinta	4304730545	2-7 FLAT MESA	ENSERCH EXPLORATION	UT	10S	23E	7	NESENN	7278.8	B	7.5	2.65	0.0404	0.00133	62.8	13266	MVRD
E946	Uinta	4304730545	2-7 FLAT MESA	ENSERCH EXPLORATION	UT	10S	23E	7	NESENN	7279.2	C	6.1	2.64	0.0515	0.00168	41.0	13286	MVRD
E946	Uinta	4304730545	2-7 FLAT MESA	ENSERCH EXPLORATION	UT	10S	23E	7	NESENN	7279.2	A	6.1	2.64	0.0284	0.000356	142	13286	MVRD
E946	Uinta	4304730545	2-7 FLAT MESA	ENSERCH EXPLORATION	UT	10S	23E	7	NESENN	7279.2	B	6.6	2.64	0.0246	0.000781	86.0	13286	MVRD
E946	Uinta	4304730545	2-7 FLAT MESA	ENSERCH EXPLORATION	UT	10S	23E	7	NESENN	7279.4	C	7.0	2.65	0.0489	0.00146	89.8	13286	MVRD
E946	Uinta	4304730545	2-7 FLAT MESA	ENSERCH EXPLORATION	UT	10S	23E	7	NESENN	7279.4	C	7.3	2.65	0.0393	0.00105	116	13286	MVRD
E946	Uinta	4304730545	2-7 FLAT MESA	ENSERCH EXPLORATION	UT	10S	23E	7	NESENN	7279.4	B	7.4	2.65	0.0340	0.00120	112	13286	MVRD
E946	Uinta	4304730545	2-7 FLAT MESA	ENSERCH EXPLORATION	UT	10S	23E	7	NESENN	7279.9	B	6.6	2.63	0.0332	0.000490	293	13296	MVRD
E946	Uinta	4304730545	2-7 FLAT MESA	ENSERCH EXPLORATION	UT	10S	23E	7	NESENN	7279.9	A	6.3	2.63	0.0318	0.000735	110	13296	MVRD
E946	Uinta	4304730545	2-7 FLAT MESA	ENSERCH EXPLORATION	UT	10S	23E	7	NESENN	7279.9	C	6.9	2.64	0.0241	0.00235	43.2	13296	MVRD
E946	Uinta	4304730545	2-7 FLAT MESA	ENSERCH EXPLORATION	UT	10S	23E	7	NESENN	7284.3	C	7.8	2.65	0.0627	0.00310	63.9	14296	MVRD
E946	Uinta	4304730545	2-7 FLAT MESA	ENSERCH EXPLORATION	UT	10S	23E	7	NESENN	7284.3	A	7.7	2.65	0.0499	0.00323	56.7	14296	MVRD
E946	Uinta	4304730545	2-7 FLAT MESA	ENSERCH EXPLORATION	UT	10S	23E	7	NESENN	7284.3	C	7.9	2.65	0.0281	0.00100	139	14296	MVRD
E946	Uinta	4304730545	2-7 FLAT MESA	ENSERCH EXPLORATION	UT	10S	23E	7	NESENN	7284.4	C	8.0	2.65	0.0451	0.00266	96.7	14296	MVRD
E946	Uinta	4304730545	2-7 FLAT MESA	ENSERCH EXPLORATION	UT	10S	23E	7	NESENN	7284.4	B	8.0	2.65	0.0373	0.00248	66.5	14296	MVRD
E946	Uinta	4304730545	2-7 FLAT MESA	ENSERCH EXPLORATION	UT	10S	23E	7	NESENN	7284.4	C	8.2	2.66	0.0303	0.00191	103	14296	MVRD
E946	Uinta	4304730545	2-7 FLAT MESA	ENSERCH EXPLORATION	UT	10S	23E	7	NESENN	7284.5	C	7.9	2.65	0.0491	0.00261	94.6	14296	MVRD
E946	Uinta	4304730545	2-7 FLAT MESA	ENSERCH EXPLORATION	UT	10S	23E	7	NESENN	7284.5	B	8.2	2.65	0.0404	0.00115	239	14296	MVRD
E946	Uinta	4304730545	2-7 FLAT MESA	ENSERCH EXPLORATION	UT	10S	23E	7	NESENN	7284.5	A	7.8	2.65	0.0359	0.00505	61.0	14296	MVRD
E946	Uinta	4304730545	2-7 FLAT MESA	ENSERCH EXPLORATION	UT	10S	23E	7	NESENN	7287.1	C	5.6	2.64	0.0498	0.00115	90.0	13286	MVRD
E946	Uinta	4304730545	2-7 FLAT MESA	ENSERCH EXPLORATION	UT	10S	23E	7	NESENN	7287.1	A	5.6	2.64	0.0426	0.00147	25.7	13286	MVRD
E946	Uinta	4304730545	2-7 FLAT MESA	ENSERCH EXPLORATION	UT	10S	23E	7	NESENN	7287.1	B	5.7	2.64	0.0311	0.000610	139	13286	MVRD
E946	Uinta	4304730545	2-7 FLAT MESA	ENSERCH EXPLORATION	UT	10S	23E	7	NESENN	7289.9	A	9.5	2.65	0.0503	0.00139	129	13266	MVRD
E946	Uinta	4304730545	2-7 FLAT MESA	ENSERCH EXPLORATION	UT	10S	23E	7	NESENN	7289.9	B	5.1	2.65	0.0351	0.000616	189	13266	MVRD
E946	Uinta	4304730545	2-7 FLAT MESA	ENSERCH EXPLORATION	UT	10S	23E	7	NESENN	7289.9	C	5.5	2.66	0.0298	0.00150	68.1	13266	MVRD
E946	Uinta	4304730545	2-7 FLAT MESA	ENSERCH EXPLORATION	UT	10S	23E	7	NESENN	7290.9	C	2.3	2.63	0.00591	0.000308	227	12266	MVRD
E946	Uinta	4304730545	2-7 FLAT MESA	ENSERCH EXPLORATION	UT	10S	23E	7	NESENN	7290.9	B	1.8	2.62	0.00445	0.000334	180	12266	MVRD
E946	Uinta	4304730545	2-7 FLAT MESA	ENSERCH EXPLORATION	UT	10S	23E	7	NESENN	7290.9	A	3.2	2.66	0.00422	0.000124	400	12266	MVRD
E946	Uinta	4304730545	2-7 FLAT MESA	ENSERCH EXPLORATION	UT	10S	23E	7	NESENN	7293.4	C	3.7	2.67	0.00270	0.000584	78.1	13206	MVRD
E946	Uinta	4304730545	2-7 FLAT MESA	ENSERCH EXPLORATION	UT	10S	23E	7	NESENN	7293.4	B	3.1	2.66	0.00455	0.000435	180	13206	MVRD
E946	Uinta	4304730545	2-7 FLAT MESA	ENSERCH EXPLORATION	UT	10S	23E	7	NESENN	7293.4	A	3.5	2.68	0.000372	0.000053	900	13206	MVRD
E946	Uinta	4304730545	2-7 FLAT MESA	ENSERCH EXPLORATION	UT	10S	23E	7	NESENN	7293.5	C	3.3	2.66	0.0304	0.000487	94.8	13206	MVRD
E946	Uinta	4304730545	2-7 FLAT MESA	ENSERCH EXPLORATION	UT	10S	23E	7	NESENN	7293.5	A	3.8	2.68	0.0294	0.000490	145	13206	MVRD
E946	Uinta	4304730545	2-7 FLAT MESA	ENSERCH EXPLORATION	UT	10S	23E	7	NESENN	7293.5	B	3.1	2.66	0.0401	0.000579	194	13206	MVRD
E946	Uinta	4304730545	2-7 FLAT MESA	ENSERCH EXPLORATION	UT	10S	23E	7	NESENN	7294.4	A	4.0	2.64	0.0434	0.000216	92.3	13206	MVRD
E946	Uinta	4304730545	2-7 FLAT MESA	ENSERCH EXPLORATION	UT	10S	23E	7	NESENN	7297.1	C	1.1	2.61	0.00800	0.000344	167	13216	MVRD
E946	Uinta	4304730545	2-7 FLAT MESA	ENSERCH EXPLORATION	UT	10S	23E	7	NESENN	7297.1	B	1.9	2.63	0.00411	0.000144	232	13216	MVRD
E946	Uinta	4304730545	2-7 FLAT MESA	ENSERCH EXPLORATION	UT	10S	23E	7	NESENN	7297.1	A	1.9	2.62	0.00358	0.000137	226	13216	MVRD
E946	Uinta	4304730545	2-7 FLAT MESA	ENSERCH EXPLORATION	UT	10S	23E	7	NESENN	7299.3	A	6.9	2.68	0.0704	0.00170	172	13256	MVRD
E946	Uinta	4304730545	2-7 FLAT MESA	ENSERCH EXPLORATION	UT	10S	23E	7	NESENN	7299.3	B	6.4	2.68	0.0691	0.00251	86.6	13256	MVRD
E946	Uinta	4304730545	2-7 FLAT MESA	ENSERCH EXPLORATION	UT	10S	23E	7	NESENN	7299.3	C	8.8	2.68	0.0536	0.00186	70.0	13256	MVRD
E946	Uinta	4304730545	2-7 FLAT MESA	ENSERCH EXPLORATION	UT	10S	23E	7	NESENN	7300.1	C	5.5	2.67	0.0646	0.00268	71.5	13256	MVRD
E946	Uinta	4304730545	2-7 FLAT MESA	ENSERCH EXPLORATION	UT	10S	23E	7	NESENN	7300.1	A	5.5	2.68	0.0643	0.00244	90.5	13256	MVRD
E946	Uinta	4304730545	2-7 FLAT MESA	ENSERCH EXPLORATION	UT	10S	23E	7	NESENN	7300.1	B	5.7	2.68	0.0585	0.00231	90.0	13256	MVRD
E946	Uinta	4304730545	2-7 FLAT MESA	ENSERCH EXPLORATION	UT	10S	23E	7	NESENN	7300.6	B	5.8	2.68	0.0922	0.00202	100	13256	MVRD
E946	Uinta	4304730545	2-7 FLAT MESA	ENSERCH EXPLORATION	UT	10S	23E	7	NESENN	7300.6	A	5.9	2.68	0.0524	0.00156	82.5	13256	MVRD
E946	Uinta	4304730545	2-7 FLAT MESA	ENSERCH EXPLORATION	UT	10S	23E	7	NESENN	7300.6	C	5.9	2.68	0.0431	0.00163	73.2	13256	MVRD
E946	Uinta	4304730545	2-7 FLAT MESA	ENSERCH EXPLORATION	UT	10S	23E	7	NESENN	7301.4	C	2.5	2.60	0.0				

Appendix A1

Summary of Porosity, Permeability and Grain Density

Analysis of Critical Permeability, Capillary Pressure and Electrical Properties for Mesaverde Tight Gas Sandstones from Western U.S. Basins

US DOE # DE-FC26-05NT42660 Final Scientific/Technical Report

Alan P. Byrnes, Robert M. Cluff, John C. Webb

website: <http://www.kgs.ku.edu/mesaverde>

USGS Library Number	Basin	API Number	Well Name	Operator	State	Township	Range	Section	Quarter Section	Plug Depth	Plug Letter	Ambient Porosity	Grain Density	Routine Gas Permeability	in situ		Rock Type Code	Formations
															Kninckenberg Gas Permeability	Kninckenberg constant b		
											ft	A/B/C	%	g/cc	mD	mD		
E946	Uinta	4304730545	2-7 FLAT MESA	ENSERCH EXPLORATION	UT	10S	23E	7	NESENN	7701.1	A	0.9	2.61	0.00263	0.000097	172	13216	MVRD
E946	Uinta	4304730545	2-7 FLAT MESA	ENSERCH EXPLORATION	UT	10S	23E	7	NESENN	7704.4	A	3.5	2.62	0.00991	0.000414	58.8	12226	MVRD
E946	Uinta	4304730545	2-7 FLAT MESA	ENSERCH EXPLORATION	UT	10S	23E	7	NESENN	7704.4	C	2.6	2.61	0.00527	0.000213	152	12226	MVRD
E946	Uinta	4304730545	2-7 FLAT MESA	ENSERCH EXPLORATION	UT	10S	23E	7	NESENN	7704.4	B	3.2	2.62				12225	MVRD
E946	Uinta	4304730545	2-7 FLAT MESA	ENSERCH EXPLORATION	UT	10S	23E	7	NESENN	7707.5	A	2.9	2.66	0.216	0.0364	32.6	13256	MVRD
E946	Uinta	4304730545	2-7 FLAT MESA	ENSERCH EXPLORATION	UT	10S	23E	7	NESENN	7707.5	B	3.4	2.67	0.0630	0.00364	58.7	13256	MVRD
E946	Uinta	4304730545	2-7 FLAT MESA	ENSERCH EXPLORATION	UT	10S	23E	7	NESENN	7707.5	C	3.0	2.65	0.0629	0.00335	83.4	13256	MVRD
E946	Uinta	4304730545	2-7 FLAT MESA	ENSERCH EXPLORATION	UT	10S	23E	7	NESENN	7712.7	B	3.2	2.69	0.0343	0.000383	134	13266	MVRD
E946	Uinta	4304730545	2-7 FLAT MESA	ENSERCH EXPLORATION	UT	10S	23E	7	NESENN	7712.7	C	3.5	2.71	0.0222	0.000449	91.9	13266	MVRD
E946	Uinta	4304730545	2-7 FLAT MESA	ENSERCH EXPLORATION	UT	10S	23E	7	NESENN	7712.7	A	3.0	2.69	0.1000	0.000528	234	13266	MVRD
E946	Uinta	4304730545	2-7 FLAT MESA	ENSERCH EXPLORATION	UT	10S	23E	7	NESENN	7856.3	A	2.0	2.57	0.00895	0.000065	714	12296	MVRD
E946	Uinta	4304730545	2-7 FLAT MESA	ENSERCH EXPLORATION	UT	10S	23E	7	NESENN	7856.3	B	1.2	2.56	0.00338	0.000129	221	12296	MVRD
E946	Uinta	4304730545	2-7 FLAT MESA	ENSERCH EXPLORATION	UT	10S	23E	7	NESENN	7856.3	C	0.6	2.54	0.00303	0.000066	325	12296	MVRD
E946	Uinta	4304730545	2-7 FLAT MESA	ENSERCH EXPLORATION	UT	10S	23E	7	NESENN	7885.4	C	10.2	2.65	0.121	0.0222	61.6	14266	MVRD
E946	Uinta	4304730545	2-7 FLAT MESA	ENSERCH EXPLORATION	UT	10S	23E	7	NESENN	7885.4	A	9.8	2.65	0.117	0.0258	44.2	14266	MVRD
E946	Uinta	4304730545	2-7 FLAT MESA	ENSERCH EXPLORATION	UT	10S	23E	7	NESENN	7885.4	B	10.2	2.65	0.115	0.0189	89.9	14266	MVRD
E946	Uinta	4304730545	2-7 FLAT MESA	ENSERCH EXPLORATION	UT	10S	23E	7	NESENN	7887.1	A	11.9	2.65	0.130	0.0284	45.9	14266	MVRD
E946	Uinta	4304730545	2-7 FLAT MESA	ENSERCH EXPLORATION	UT	10S	23E	7	NESENN	7887.8	C	7.0	2.61	0.133	0.00462	99.4	13266	MVRD
E946	Uinta	4304730545	2-7 FLAT MESA	ENSERCH EXPLORATION	UT	10S	23E	7	NESENN	7887.8	A	6.9	2.61	0.0972	0.00423	44.7	13266	MVRD
E946	Uinta	4304730545	2-7 FLAT MESA	ENSERCH EXPLORATION	UT	10S	23E	7	NESENN	7887.8	B	7.0	2.61				13266	MVRD
E946	Uinta	4304730545	2-7 FLAT MESA	ENSERCH EXPLORATION	UT	10S	23E	7	NESENN	7889.1	B	1.1	2.53	0.00378	0.000079	255	12296	MVRD
E946	Uinta	4304730545	2-7 FLAT MESA	ENSERCH EXPLORATION	UT	10S	23E	7	NESENN	7891.1	C	1.9	2.55	0.00246	0.000040	424	12296	MVRD
E946	Uinta	4304730545	2-7 FLAT MESA	ENSERCH EXPLORATION	UT	10S	23E	7	NESENN	7891.1	A	1.8	2.54	0.00166	0.000030	362	12296	MVRD
E946	Uinta	4304730545	2-7 FLAT MESA	ENSERCH EXPLORATION	UT	10S	23E	7	NESENN	7892.7	C	0.8	2.68	0.00145	0.000014	1349	12216	MVRD
E946	Uinta	4304730545	2-7 FLAT MESA	ENSERCH EXPLORATION	UT	10S	23E	7	NESENN	7892.7	A	1.0	2.68	0.00134	0.000042	443	12216	MVRD
E946	Uinta	4304730545	2-7 FLAT MESA	ENSERCH EXPLORATION	UT	10S	23E	7	NESENN	7892.7	B	0.7	2.67	0.00130	0.000032	442	12216	MVRD
E946	Uinta	4304730545	2-7 FLAT MESA	ENSERCH EXPLORATION	UT	10S	23E	7	NESENN	7896.2	A	1.3	2.53	0.00517	0.000107	274	12296	MVRD
E946	Uinta	4304730545	2-7 FLAT MESA	ENSERCH EXPLORATION	UT	10S	23E	7	NESENN	7896.2	C	0.8	2.54	0.00328	0.000090	206	12296	MVRD
E946	Uinta	4304730545	2-7 FLAT MESA	ENSERCH EXPLORATION	UT	10S	23E	7	NESENN	7896.2	B	1.8	2.53	0.00247	0.000056	175	12296	MVRD
E946	Uinta	4304730545	2-7 FLAT MESA	ENSERCH EXPLORATION	UT	10S	23E	7	NESENN	7896.5	B	2.7	2.60	0.0112	0.00107	139	13226	MVRD
E946	Uinta	4304730545	2-7 FLAT MESA	ENSERCH EXPLORATION	UT	10S	23E	7	NESENN	7896.5	A	2.6	2.61	0.00938	0.000631	100	13226	MVRD
E946	Uinta	4304730545	2-7 FLAT MESA	ENSERCH EXPLORATION	UT	10S	23E	7	NESENN	7898.5	C	2.2	2.60	0.00717	0.000557	88.3	13226	MVRD
KM1022	Uinta	4304736565	NBU 1022-1A Natural Butte	KERR-MCGEE OILGAS ONSHORE	UT	10S	22E	1	SWSE	7803.5	A	2.0	2.61	0.00469	0.000077	196	13290	MVRD
KM1022	Uinta	4304736565	NBU 1022-1A Natural Butte	KERR-MCGEE OILGAS ONSHORE	UT	10S	22E	1	SWSE	7803.5	B			0.00135	0.000020	363	12290	MVRD
KM1022	Uinta	4304736565	NBU 1022-1A Natural Butte	KERR-MCGEE OILGAS ONSHORE	UT	10S	22E	1	SWSE	7803.8	A	2.1	2.60	0.00256	0.000039	193	12290	MVRD
KM1022	Uinta	4304736565	NBU 1022-1A Natural Butte	KERR-MCGEE OILGAS ONSHORE	UT	10S	22E	1	SWSE	7806.5	B	8.1	2.66	0.0412	0.00175	160	13260	MVRD
KM1022	Uinta	4304736565	NBU 1022-1A Natural Butte	KERR-MCGEE OILGAS ONSHORE	UT	10S	22E	1	SWSE	7806.5	A	8.1	2.66	0.00795	0.00110	193	13260	MVRD
KM1022	Uinta	4304736565	NBU 1022-1A Natural Butte	KERR-MCGEE OILGAS ONSHORE	UT	10S	22E	1	SWSE	7808.7	A	9.8	2.65	0.0382	0.00573	56.0	13260	MVRD
KM1022	Uinta	4304736565	NBU 1022-1A Natural Butte	KERR-MCGEE OILGAS ONSHORE	UT	10S	22E	1	SWSE	7808.7	B	10.0	2.65	0.0358	0.00380	173	13260	MVRD
KM1022	Uinta	4304736565	NBU 1022-1A Natural Butte	KERR-MCGEE OILGAS ONSHORE	UT	10S	22E	1	SWSE	7810.4	B	9.1	2.68	0.0419	0.00147	226	13260	MVRD
KM1022	Uinta	4304736565	NBU 1022-1A Natural Butte	KERR-MCGEE OILGAS ONSHORE	UT	10S	22E	1	SWSE	7810.4	A	8.8	2.69	0.0114	0.00178	139	13260	MVRD
KM1022	Uinta	4304736565	NBU 1022-1A Natural Butte	KERR-MCGEE OILGAS ONSHORE	UT	10S	22E	1	SWSE	7815.8	B	1.2	2.32	0.00340	0.000145	338	13220	MVRD
KM1022	Uinta	4304736565	NBU 1022-1A Natural Butte	KERR-MCGEE OILGAS ONSHORE	UT	10S	22E	1	SWSE	7815.8	A	1.5	2.34	0.0174	0.000507	90.9	13260	MVRD
KM1022	Uinta	4304736565	NBU 1022-1A Natural Butte	KERR-MCGEE OILGAS ONSHORE	UT	10S	22E	1	SWSE	7818.4	B	1.7	2.65	0.0230	0.000326	283	13220	MVRD
KM1022	Uinta	4304736565	NBU 1022-1A Natural Butte	KERR-MCGEE OILGAS ONSHORE	UT	10S	22E	1	SWSE	7818.4	A	1.8	2.65	0.00480	0.000057	422	13260	MVRD
KM1022	Uinta	4304736565	NBU 1022-1A Natural Butte	KERR-MCGEE OILGAS ONSHORE	UT	10S	22E	1	SWSE	7823.5	A	2.0	2.60	0.00445	0.000037	601	12220	MVRD
KM1022	Uinta	4304736565	NBU 1022-1A Natural Butte	KERR-MCGEE OILGAS ONSHORE	UT	10S	22E	1	SWSE	7823.5	B	1.3	2.59	0.00301	0.000012	1587	13240	MVRD
KM1022	Uinta	4304736565	NBU 1022-1A Natural Butte	KERR-MCGEE OILGAS ONSHORE	UT	10S	22E	1	SWSE	7825.5	B	4.7	2.73	0.00536	0.000299	363	13260	MVRD
KM1022	Uinta	4304736565	NBU 1022-1A Natural Butte	KERR-MCGEE OILGAS ONSHORE	UT	10S	22E	1	SWSE	7825.5	A	0.7	2.49	0.00517	0.000514	161	13260	MVRD
KM1022	Uinta	4304736565	NBU 1022-1A Natural Butte	KERR-MCGEE OILGAS ONSHORE	UT	10S	22E	1	SWSE	7825.5	A	5.8	2.75	0.00242	0.000225	378	13260	MVRD
KM1022	Uinta	4304736565	NBU 1022-1A Natural Butte	KERR-MCGEE OILGAS ONSHORE	UT	10S	22E	1	SWSE	7827.7	A	0.8	2.51	0.0243	0.000195	262	13260	MVRD
KM1022	Uinta	4304736565	NBU 1022-1A Natural Butte	KERR-MCGEE OILGAS ONSHORE	UT	10S	22E	1	SWSE	7830.7	B	1.2	2.49	0.141	0.00462	60.7	13240	MVRD
KM1022	Uinta	4304736565	NBU 1022-1A Natural Butte	KERR-MCGEE OILGAS ONSHORE	UT	10S	22E	1	SWSE	7830.7	A	9.9	2.73	0.00292	0.000208	673	13240	MVRD
KM1022	Uinta	4304736565	NBU 1022-1A Natural Butte	KERR-MCGEE OILGAS ONSHORE	UT	10S	22E	1	SWSE	7836.5	A	1.1	2.44	0.0323	0.000187	86.4	13240	MVRD
KM1022	Uinta	4304736565	NBU 1022-1A Natural Butte	KERR-MCGEE OILGAS ONSHORE	UT	10S	22E	1	SWSE	7836.5	A	1.1	2.47	0.00818	0.000137	234	13240	MVRD
KM1022	Uinta	4304736565	NBU 1022-1A Natural Butte	KERR-MCGEE OILGAS ONSHORE	UT	10S	22E	1	SWSE	7840.5	B	1.0	2.48	0.0517	0.000390	88.2	13260	MVRD
KM1022	Uinta	4304736565	NBU 1022-1A Natural Butte	KERR-MCGEE OILGAS ONSHORE	UT	10S	22E	1	SWSE	7840.5	A	1.6	2.51	0.00113	0.000013	699	13260	MVRD
KM1022	Uinta	4304736565	NBU 1022-1A Natural Butte	KERR-MCGEE OILGAS ONSHORE	UT	10S	22E	1	SWSE	7840.5	A	0.7	2.49	0.00164	0.000055	161	13260	MVRD
KM1022	Uinta	4304736565	NBU 1022-1A Natural Butte	KERR-MCGEE OILGAS ONSHORE	UT	10S	22E	1	SWSE	7841.5	B	0.9	2.80	0.00896	0.000085	513	13260	MVRD
KM1022	Uinta	4304736565	NBU 1022-1A Natural Butte	KERR-MCGEE OILGAS ONSHORE	UT	10S	22E	1	SWSE	7841.5	A	0.6	2.65	0.00251	0.000040	416	13260	MVRD
KM1022	Uinta	4304736565	NBU 1022-1A Natural Butte	KERR-MCGEE OILGAS ONSHORE	UT	10S	22E	1	SWSE	7848.8	B	2.2	2.30	0.0210	0.000750	127	12390	MVRD
KM1022	Uinta	4304736565	NBU 1022-1A Natural Butte	KERR-MCGEE OILGAS ONSHORE	UT	10S	22E	1	SWSE	7848.8	A	1.3	2.36	0.00255	0.000061	152	12290	MVRD
KM1022	Uinta	4304736565	NBU 1022-1A Natural Butte	KERR-MCGEE OILGAS ONSHORE	UT	10S	22E	1	SWSE	7849.4	A	1.5	2.60	0.00351	0.000015	488	13260	MVRD
KM1022	Uinta	4304736565	NBU 1022-1A Natural Butte	KERR-MCGEE OILGAS ONSHORE	UT	10S	22E	1	SWSE	7849.4	B	1.1	2.59	0.00132	0.000041	133	13290	MVRD
KM1022	Uinta	430473656																

Appendix A1

Summary of Porosity, Permeability and Grain Density

Analysis of Critical Permeability, Capillary Pressure and Electrical Properties for Mesaverde Tight Gas Sandstones from Western U.S. Basins

US DOE # DE-FC26-05NT42660 Final Scientific/Technical Report

Alan P. Byrnes, Robert M. Cluff, John C. Webb

website: <http://www.kgs.ku.edu/mesaverde>

USGS Library Number	Basin	API Number	Well Name	Operator	State	Township	Range	Section	Quarter Section	Plug Depth	Plug Letter	Ambient Porosity	Grain Density	Routine Gas Permeability	in situ		Rock Type Code	Formations
															Permeability	Permeability		
											ft	A/B/C	%	g/cc	mD	mD		
KM1022	Uinta	4304736565	NBU 1022-1A Natural Butte	KERR-MCGEE OILGAS ONSHORE	UT	10S	22E	1	SWSE	7934.5	B2	1.1	2.64	0.00750	0.000045	424	13290	MVRD
KM1022	Uinta	4304736565	NBU 1022-1A Natural Butte	KERR-MCGEE OILGAS ONSHORE	UT	10S	22E	1	SWSE	7934.5	B	1.1	2.52	0.00393	0.000049	282	13290	MVRD
KM1022	Uinta	4304736565	NBU 1022-1A Natural Butte	KERR-MCGEE OILGAS ONSHORE	UT	10S	22E	1	SWSE	7934.5	A2	1.0	2.56	0.00127	0.000011	921	13260	MVRD
KM1022	Uinta	4304736565	NBU 1022-1A Natural Butte	KERR-MCGEE OILGAS ONSHORE	UT	10S	22E	1	SWSE	7945.5	A	1.4	2.60	0.00811	0.000257	254	13290	MVRD
KM1022	Uinta	4304736565	NBU 1022-1A Natural Butte	KERR-MCGEE OILGAS ONSHORE	UT	10S	22E	1	SWSE	7945.5	B	1.9	2.32	0.0528	0.000934	82.4	13220	MVRD
KM1022	Uinta	4304736565	NBU 1022-1A Natural Butte	KERR-MCGEE OILGAS ONSHORE	UT	10S	22E	1	SWSE	7952.5	A	1.0	2.64	0.0319	0.00138	277	12290	MVRD
KM1022	Uinta	4304736565	NBU 1022-1A Natural Butte	KERR-MCGEE OILGAS ONSHORE	UT	10S	22E	1	SWSE	7955.5	A	6.2	2.66	0.00486	0.000054	198	13260	MVRD
KM1022	Uinta	4304736565	NBU 1022-1A Natural Butte	KERR-MCGEE OILGAS ONSHORE	UT	10S	22E	1	SWSE	7955.5	B	6.2	2.65	0.00474	0.000067	605	13240	MVRD
KM1022	Uinta	4304736565	NBU 1022-1A Natural Butte	KERR-MCGEE OILGAS ONSHORE	UT	10S	22E	1	SWSE	7957.5	A	2.5	2.61	0.00547	0.000044	496	13260	MVRD
KM1022	Uinta	4304736565	NBU 1022-1A Natural Butte	KERR-MCGEE OILGAS ONSHORE	UT	10S	22E	1	SWSE	7957.5	B	1.1	2.56	0.00348	0.000060	235	13260	MVRD
KM1022	Uinta	4304736565	NBU 1022-1A Natural Butte	KERR-MCGEE OILGAS ONSHORE	UT	10S	22E	1	SWSE	7961.5	A	1.4	2.66	0.00258	0.000054	428	13260	MVRD
KM360	Uinta	4304735788	NBU 9-20-360 State	KERR-MCGEE OILGAS ONSHORE	UT	9S	20E	36	SESE	8175.5	B	6.6	2.64	0.0320	0.00134	89.8	15225	MVRD
KM360	Uinta	4304735788	NBU 9-20-360 State	KERR-MCGEE OILGAS ONSHORE	UT	9S	20E	36	SESE	8175.5	A	6.9	2.66	0.0293	0.00129	87.4	15225	MVRD
KM360	Uinta	4304735788	NBU 9-20-360 State	KERR-MCGEE OILGAS ONSHORE	UT	9S	20E	36	SESE	8178.5	B	7.7	2.66	0.0233	0.00295	81.1	15295	MVRD
KM360	Uinta	4304735788	NBU 9-20-360 State	KERR-MCGEE OILGAS ONSHORE	UT	9S	20E	36	SESE	8181.8	B	1.6	2.66	0.00972	0.000322	411	15285	MVRD
KM360	Uinta	4304735788	NBU 9-20-360 State	KERR-MCGEE OILGAS ONSHORE	UT	9S	20E	36	SESE	8181.8	A	1.5	2.66	0.00583	0.000284	232	15285	MVRD
KM360	Uinta	4304735788	NBU 9-20-360 State	KERR-MCGEE OILGAS ONSHORE	UT	9S	20E	36	SESE	8184.5	A	7.0	2.65	0.0520	0.00228	79.1	13286	MVRD
KM360	Uinta	4304735788	NBU 9-20-360 State	KERR-MCGEE OILGAS ONSHORE	UT	9S	20E	36	SESE	8184.5	B	7.1	2.65	0.0233	0.00240	159	13286	MVRD
KM360	Uinta	4304735788	NBU 9-20-360 State	KERR-MCGEE OILGAS ONSHORE	UT	9S	20E	36	SESE	8184.6	A	6.9	2.66	0.0589	0.00170	71.5	13286	MVRD
KM360	Uinta	4304735788	NBU 9-20-360 State	KERR-MCGEE OILGAS ONSHORE	UT	9S	20E	36	SESE	8184.6	B	6.7	2.65	0.0128	0.00231	39.6	13286	MVRD
KM360	Uinta	4304735788	NBU 9-20-360 State	KERR-MCGEE OILGAS ONSHORE	UT	9S	20E	36	SESE	8185.7	A	5.7	2.65	0.0551	0.000809	131	13286	MVRD
KM360	Uinta	4304735788	NBU 9-20-360 State	KERR-MCGEE OILGAS ONSHORE	UT	9S	20E	36	SESE	8185.7	B	5.9	2.65	0.0145	0.000696	153	13286	MVRD
KM360	Uinta	4304735788	NBU 9-20-360 State	KERR-MCGEE OILGAS ONSHORE	UT	9S	20E	36	SESE	8187.2	B	4.5	2.67	0.0519	0.00136	97.5	15296	MVRD
KM360	Uinta	4304735788	NBU 9-20-360 State	KERR-MCGEE OILGAS ONSHORE	UT	9S	20E	36	SESE	8187.2	B	4.7	2.68	0.0149	0.000530	394	15296	MVRD
KM360	Uinta	4304735788	NBU 9-20-360 State	KERR-MCGEE OILGAS ONSHORE	UT	9S	20E	36	SESE	8193.6	B	2.1	2.64	0.00619	0.000205	195	13226	MVRD
KM360	Uinta	4304735788	NBU 9-20-360 State	KERR-MCGEE OILGAS ONSHORE	UT	9S	20E	36	SESE	8193.6	A	2.2	2.64	0.00368	0.000051	357	13226	MVRD
KM360	Uinta	4304735788	NBU 9-20-360 State	KERR-MCGEE OILGAS ONSHORE	UT	9S	20E	36	SESE	8195.6	B	3.0	2.67	0.00558	0.000133	405	14275	MVRD
KM360	Uinta	4304735788	NBU 9-20-360 State	KERR-MCGEE OILGAS ONSHORE	UT	9S	20E	36	SESE	8195.6	A	3.0	2.68	0.00265	0.000075	496	14275	MVRD
KM360	Uinta	4304735788	NBU 9-20-360 State	KERR-MCGEE OILGAS ONSHORE	UT	9S	20E	36	SESE	8198.1	A	8.8	2.67	0.0554	0.000855	100	12219	MVRD
KM360	Uinta	4304735788	NBU 9-20-360 State	KERR-MCGEE OILGAS ONSHORE	UT	9S	20E	36	SESE	8198.1	B	7.3	2.67	0.00406	0.000361	238	12219	MVRD
KM360	Uinta	4304735788	NBU 9-20-360 State	KERR-MCGEE OILGAS ONSHORE	UT	9S	20E	36	SESE	8209.2	B	1.2	2.69	0.00686	0.000253	163	15295	MVRD
KM360	Uinta	4304735788	NBU 9-20-360 State	KERR-MCGEE OILGAS ONSHORE	UT	9S	20E	36	SESE	8209.5	A	5.5	2.69	0.00315	0.000074	403	13255	MVRD
KM360	Uinta	4304735788	NBU 9-20-360 State	KERR-MCGEE OILGAS ONSHORE	UT	9S	20E	36	SESE	8209.5	A	0.8	2.69	0.00275	0.000053	466	13255	MVRD
KM360	Uinta	4304735788	NBU 9-20-360 State	KERR-MCGEE OILGAS ONSHORE	UT	9S	20E	36	SESE	8216.5	A	2.1	2.65	0.0150	0.000415	114	11219	MVRD
KM360	Uinta	4304735788	NBU 9-20-360 State	KERR-MCGEE OILGAS ONSHORE	UT	9S	20E	36	SESE	8218.5	A	5.8	2.66	0.0436	0.00117	109	15795	MVRD
KM360	Uinta	4304735788	NBU 9-20-360 State	KERR-MCGEE OILGAS ONSHORE	UT	9S	20E	36	SESE	8218.6	B	6.0	2.66	0.0111	0.00111	132	15795	MVRD
KM360	Uinta	4304735788	NBU 9-20-360 State	KERR-MCGEE OILGAS ONSHORE	UT	9S	20E	36	SESE	8218.6	A	5.9	2.66	0.0111	0.000638	262	15795	MVRD
KM360	Uinta	4304735788	NBU 9-20-360 State	KERR-MCGEE OILGAS ONSHORE	UT	9S	20E	36	SESE	8223.5	B	6.7	2.65	0.0178	0.00148	162	15395	MVRD
KM360	Uinta	4304735788	NBU 9-20-360 State	KERR-MCGEE OILGAS ONSHORE	UT	9S	20E	36	SESE	8223.5	A	6.3	2.65	0.0159	0.000936	192	15395	MVRD
KM360	Uinta	4304735788	NBU 9-20-360 State	KERR-MCGEE OILGAS ONSHORE	UT	9S	20E	36	SESE	8225.6	B	1.6	2.67	0.00686	0.000133	400	16295	MVRD
KM360	Uinta	4304735788	NBU 9-20-360 State	KERR-MCGEE OILGAS ONSHORE	UT	9S	20E	36	SESE	8225.6	A	1.4	2.67	0.00312	0.000100	400	16295	MVRD
KM360	Uinta	4304735788	NBU 9-20-360 State	KERR-MCGEE OILGAS ONSHORE	UT	9S	20E	36	SESE	8227.3	A	2.54	2.64	0.00337	0.000081	1185	16295	MVRD
KM360	Uinta	4304735788	NBU 9-20-360 State	KERR-MCGEE OILGAS ONSHORE	UT	9S	20E	36	SESE	8228.3	A	4.9	2.65	0.0504	0.000887	312	16295	MVRD
KM360	Uinta	4304735788	NBU 9-20-360 State	KERR-MCGEE OILGAS ONSHORE	UT	9S	20E	36	SESE	8228.3	B	5.2	2.64	0.0371	0.00151	197	16295	MVRD
KM360	Uinta	4304735788	NBU 9-20-360 State	KERR-MCGEE OILGAS ONSHORE	UT	9S	20E	36	SESE	8229.5	A	5.4	2.66	0.0489	0.000695	93.6	13225	MVRD
KM360	Uinta	4304735788	NBU 9-20-360 State	KERR-MCGEE OILGAS ONSHORE	UT	9S	20E	36	SESE	8229.5	B	4.4	2.66	0.0134	0.000623	94.2	13225	MVRD
KM360	Uinta	4304735788	NBU 9-20-360 State	KERR-MCGEE OILGAS ONSHORE	UT	9S	20E	36	SESE	8230.6	A	6.0	2.65	0.0441	0.00115	145	15225	MVRD
KM360	Uinta	4304735788	NBU 9-20-360 State	KERR-MCGEE OILGAS ONSHORE	UT	9S	20E	36	SESE	8230.6	B	5.8	2.64	0.0188	0.00112	144	15225	MVRD
KM360	Uinta	4304735788	NBU 9-20-360 State	KERR-MCGEE OILGAS ONSHORE	UT	9S	20E	36	SESE	8233.5	B	9.2	2.64	0.0774	0.00212	116	13255	MVRD
KM360	Uinta	4304735788	NBU 9-20-360 State	KERR-MCGEE OILGAS ONSHORE	UT	9S	20E	36	SESE	8233.5	A	8.8	2.65	0.0612	0.00474	79.3	17225	MVRD
KM360	Uinta	4304735788	NBU 9-20-360 State	KERR-MCGEE OILGAS ONSHORE	UT	9S	20E	36	SESE	8234.4	A	8.7	2.64	0.0740	0.00400	106	16275	MVRD
KM360	Uinta	4304735788	NBU 9-20-360 State	KERR-MCGEE OILGAS ONSHORE	UT	9S	20E	36	SESE	8234.6	B	9.1	2.65	0.0947	0.00688	103	16275	MVRD
KM360	Uinta	4304735788	NBU 9-20-360 State	KERR-MCGEE OILGAS ONSHORE	UT	9S	20E	36	SESE	8234.6	A	9.1	2.64	0.0880	0.00825	91.6	16275	MVRD
KM360	Uinta	4304735788	NBU 9-20-360 State	KERR-MCGEE OILGAS ONSHORE	UT	9S	20E	36	SESE	8237.5	B	7.7	2.65	0.0621	0.00411	92.8	16295	MVRD
KM360	Uinta	4304735788	NBU 9-20-360 State	KERR-MCGEE OILGAS ONSHORE	UT	9S	20E	36	SESE	8237.5	A	8.0	2.64	0.0302	0.00455	57.2	16295	MVRD
KM360	Uinta	4304735788	NBU 9-20-360 State	KERR-MCGEE OILGAS ONSHORE	UT	9S	20E	36	SESE	8251.4	B	2.8	2.64	0.0866	0.00407	110	12219	MVRD
KM360	Uinta	4304735788	NBU 9-20-360 State	KERR-MCGEE OILGAS ONSHORE</														

Appendix A1

Summary of Porosity, Permeability and Grain Density

Analysis of Critical Permeability, Capillary Pressure and Electrical Properties for Mesaverde Tight Gas Sandstones from Western U.S. Basins

US DOE # DE-FC26-05NT42660 Final Scientific/Technical Report

Alan P. Byrnes, Robert M. Cluff, John C. Webb

website: <http://www.kgs.ku.edu/mesaverde>

USGS Library Number	Basin	API Number	Well Name	Operator	State	Township	Range	Section	Quarter Section	Plug Depth	Plug Letter	Ambient Porosity	Grain Density	Routine Gas Permeability	in situ		Rock Type Code	Formations				
															Permeability	Permeability						
														Permeability	Permeability							
														ft	A/B/C	%	g/cc	mD	mD	(psia)		
R829	Uinta	4304730852	4-5 US LAMCO	ENSERCH EXPLORATION	UT	13S	20E	5	C SW	5702.2	A	2.3	2.67	0.00185	0.00035	231	12245	MVRD				
R829	Uinta	4304730852	4-5 US LAMCO	ENSERCH EXPLORATION	UT	13S	20E	5	C SW	5702.2	B	0.9	2.63	0.00179	0.00024	303	12245	MVRD				
R829	Uinta	4304730852	4-5 US LAMCO	ENSERCH EXPLORATION	UT	13S	20E	5	C SW	5792.9	B	8.3	2.67	0.00429	0.000538	45.4	13266	MVRD				
R829	Uinta	4304730852	4-5 US LAMCO	ENSERCH EXPLORATION	UT	13S	20E	5	C SW	5792.9	A	8.1	2.67	0.00155	0.000275	272	13266	MVRD				
R829	Uinta	4304730852	4-5 US LAMCO	ENSERCH EXPLORATION	UT	13S	20E	5	C SW	5802.9	B	4.6	2.67	0.00405	0.000191	213	13256	MVRD				
R829	Uinta	4304730852	4-5 US LAMCO	ENSERCH EXPLORATION	UT	13S	20E	5	C SW	5802.9	A	4.6	2.67	0.00387	0.000145	279	13256	MVRD				
R829	Uinta	4304730852	4-5 US LAMCO	ENSERCH EXPLORATION	UT	13S	20E	5	C SW	5812.1	B	3.8	2.71	0.00212	0.000101	202	13266	MVRD				
R829	Uinta	4304730852	4-5 US LAMCO	ENSERCH EXPLORATION	UT	13S	20E	5	C SW	5812.1	A	3.1	2.69	0.000904	0.000038	669	13266	MVRD				
R829	Uinta	4304730852	4-5 US LAMCO	ENSERCH EXPLORATION	UT	13S	20E	5	C SW	5818.0	B	13.2	2.66	0.124	0.0543	301	15276	MVRD				
R829	Uinta	4304730852	4-5 US LAMCO	ENSERCH EXPLORATION	UT	13S	20E	5	C SW	5818.0	A	10.6	2.65	0.0323	0.0134	103	15276	MVRD				
R999	Uinta	4304730860	3-24 US LAMCO	CHAMPLIN PETROLEUM	UT	13S	20E	24	NESE	6809.8	B	3.7	2.64	0.00688	0.000159	333	13216	CSLG				
R999	Uinta	4304730860	3-24 US LAMCO	CHAMPLIN PETROLEUM	UT	13S	20E	24	NESE	6809.8	A	3.3	2.64	0.00287	0.000133	124	13216	CSLG				
R999	Uinta	4304730860	3-24 US LAMCO	CHAMPLIN PETROLEUM	UT	13S	20E	24	NESE	6812.2	B	6.0	2.65	0.0503	0.0122	70.9	14266	CSLG				
R999	Uinta	4304730860	3-24 US LAMCO	CHAMPLIN PETROLEUM	UT	13S	20E	24	NESE	6812.2	A	5.1	2.65	0.0175	0.00513	60.6	14266	CSLG				
R999	Uinta	4304730860	3-24 US LAMCO	CHAMPLIN PETROLEUM	UT	13S	20E	24	NESE	7137.1	A	0.6	2.63	0.00368	0.000064	246	12219	CSLG				
R999	Uinta	4304730860	3-24 US LAMCO	CHAMPLIN PETROLEUM	UT	13S	20E	24	NESE	7148.1	A	0.8	2.63	0.00277	0.000045	512	11219	CSLG				
R999	Uinta	4304730860	3-24 US LAMCO	CHAMPLIN PETROLEUM	UT	13S	20E	24	NESE	7148.1	B	0.7	2.63	0.00133	0.000025	164	11219	CSLG				
R999	Uinta	4304730860	3-24 US LAMCO	CHAMPLIN PETROLEUM	UT	13S	20E	24	NESE	7156.0	A	2.7	2.65	0.00493	0.000105	176	11219	CSLG				
R999	Uinta	4304730860	3-24 US LAMCO	CHAMPLIN PETROLEUM	UT	13S	20E	24	NESE	7156.0	B	2.8	2.65	0.00317	0.000119	11219	CSLG					
R999	Uinta	4304730860	3-24 US LAMCO	CHAMPLIN PETROLEUM	UT	13S	20E	24	NESE	7158.9	B	2.7	2.68	0.00491	0.000149	145	13215	CSLG				
R999	Uinta	4304730860	3-24 US LAMCO	CHAMPLIN PETROLEUM	UT	13S	20E	24	NESE	7158.9	A	2.3	2.67	0.00444	0.000171	109	13215	CSLG				
R999	Uinta	4304730860	3-24 US LAMCO	CHAMPLIN PETROLEUM	UT	13S	20E	24	NESE	7169.6	A	1.9	2.68	0.00459	0.000110	370	14295	CSLG				
R999	Uinta	4304730860	3-24 US LAMCO	CHAMPLIN PETROLEUM	UT	13S	20E	24	NESE	7169.6	B	2.0	2.69	0.00409	0.000082	287	14295	CSLG				
S172	Uinta	43019XXXX1	3 BOOK CLIFFS	USGS-CG	UT	17S	24E	3	SE	124.1	A	15.2	2.83	0.144	0.103	16.4	13219	NSLN				
S172	Uinta	43019XXXX1	3 BOOK CLIFFS	USGS-CG	UT	17S	24E	3	SE	124.3	A	11.1	2.63	0.0393	0.00460	149	13219	NSLN				
S172	Uinta	43019XXXX1	3 BOOK CLIFFS	USGS-CG	UT	17S	24E	3	SE	124.7	A	18.9	2.64	0.725	0.496	11.0	13217	NSLN				
S172	Uinta	43019XXXX1	3 BOOK CLIFFS	USGS-CG	UT	17S	24E	3	SE	174.0	A	7.0	2.61	0.00594	0.000416	177	12217	NSLN				
S172	Uinta	43019XXXX1	3 BOOK CLIFFS	USGS-CG	UT	17S	24E	3	SE	175.2	A	3.5	19.9	2.62	15.8	34.0	5.3	13257	NSLN			
S172	Uinta	43019XXXX1	3 BOOK CLIFFS	USGS-CG	UT	17S	24E	3	SE	175.3	A	21.5	2.64	41.2	29.7	6.2	13257	NSLN				
S172	Uinta	43019XXXX1	3 BOOK CLIFFS	USGS-CG	UT	17S	24E	3	SE	175.3	A2	21.5	2.64	24.6	18.6	6.8	13257	NSLN				
S172	Uinta	43019XXXX1	3 BOOK CLIFFS	USGS-CG	UT	17S	24E	3	SE	175.3	A1	21.2	2.64	23.6	17.7	6.8	13257	NSLN				
S172	Uinta	43019XXXX1	3 BOOK CLIFFS	USGS-CG	UT	17S	24E	3	SE	205.0	A	10.6	2.56	0.0294	0.00486	102	11219	NSLN				
S172	Uinta	43019XXXX1	3 BOOK CLIFFS	USGS-CG	UT	17S	24E	3	SE	252.0	A	14.2	2.61	0.154	0.0922	40.8	12217	NSLN				
S172	Uinta	43019XXXX1	3 BOOK CLIFFS	USGS-CG	UT	17S	24E	3	SE	252.1	A	14.9	2.61	0.175	0.133	31.8	12217	NSLN				
S172	Uinta	43019XXXX1	3 BOOK CLIFFS	USGS-CG	UT	17S	24E	3	SE	334.5	A	3.6	2.54	0.00579	0.000142	236	11219	NSLN				
S172	Uinta	43019XXXX1	3 BOOK CLIFFS	USGS-CG	UT	17S	24E	3	SE	384.0	A	7.8	2.59	0.00550	0.000289	263	11219	NSLN				
S172	Uinta	43019XXXX1	3 BOOK CLIFFS	USGS-CG	UT	17S	24E	3	SE	389.8	A	9.9	2.65	0.0133	0.00545	93.1	12219	NSLN				
S172	Uinta	43019XXXX1	3 BOOK CLIFFS	USGS-CG	UT	17S	24E	3	SE	389.9	A	11.5	2.66	0.0290	0.0145	54.1	12219	NSLN				
S172	Uinta	43019XXXX1	3 BOOK CLIFFS	USGS-CG	UT	17S	24E	3	SE	392.5	A	11.0	2.64	0.0134	0.00569	122	12239	NSLN				
S172	Uinta	43019XXXX1	3 BOOK CLIFFS	USGS-CG	UT	17S	24E	3	SE	392.5	A2	11.7	2.66	0.00155	0.000220	142	12239	NSLN				
S172	Uinta	43019XXXX1	3 BOOK CLIFFS	USGS-CG	UT	17S	24E	3	SE	392.5	A1	11.6	2.65	0.00142	0.000769	148	12239	NSLN				
S172	Uinta	43019XXXX1	3 BOOK CLIFFS	USGS-CG	UT	17S	24E	3	SE	392.7	A	9.3	2.63	0.0167	0.00465	53.0	12239	NSLN				
S172	Uinta	43019XXXX1	3 BOOK CLIFFS	USGS-CG	UT	17S	24E	3	SE	398.8	A	10.9	2.65	0.0737	0.0463	29.5	12239	NSLN				
S174	Uinta	43019XXXX2	4 BOOK CLIFFS	USGS-CG	UT	17S	24E	31	NWSW	161.7	B	11.6	2.69	0.110	0.0348	13.5	13249	NSLN				
S174	Uinta	43019XXXX2	4 BOOK CLIFFS	USGS-CG	UT	17S	24E	31	NWSW	161.7	A	12.1	2.66	0.107	0.0313	32.7	13249	NSLN				
S174	Uinta	43019XXXX2	4 BOOK CLIFFS	USGS-CG	UT	17S	24E	31	NWSW	183.2	B	8.8	2.73	0.128	0.0287	83.3	15276	NSLN				
S174	Uinta	43019XXXX2	4 BOOK CLIFFS	USGS-CG	UT	17S	24E	31	NWSW	183.2	A	8.7	2.73	0.105	0.0453	38.9	15276	NSLN				
S174	Uinta	43019XXXX2	4 BOOK CLIFFS	USGS-CG	UT	17S	24E	31	NWSW	183.4	B	10.1	2.72	0.146	0.206	152.76	NSLN					
S174	Uinta	43019XXXX2	4 BOOK CLIFFS	USGS-CG	UT	17S	24E	31	NWSW	183.4	A	9.8	2.72	0.238	0.112	36.6	15276	NSLN				
S174	Uinta	43019XXXX2	4 BOOK CLIFFS	USGS-CG	UT	17S	24E	31	NWSW	184.5	A	14.2	2.70	0.371	0.210	22.4	15526	NSLN				
S174	Uinta	43019XXXX2	4 BOOK CLIFFS	USGS-CG	UT	17S	24E	31	NWSW	184.5	B	14.6	2.69	0.272	0.149	24.3	15526	NSLN				
S174	Uinta	43019XXXX2	4 BOOK CLIFFS	USGS-CG	UT	17S	24E	31	NWSW	189.2	A	21.0	2.67	19.7	5.65	8.1	15596	NSLN				
S174	Uinta	43019XXXX2	4 BOOK CLIFFS	USGS-CG	UT	17S	24E	31	NWSW	189.2	B	22.2	2.67	15.2	9.31	11.3	15596	NSLN				
S174	Uinta	43019XXXX2	4 BOOK CLIFFS	USGS-CG	UT	17S	24E	31	NWSW	189.3	A	21.9	2.67	17.2	6.12	29.3	15596	NSLN				
S174	Uinta	43019XXXX2	4 BOOK CLIFFS	USGS-CG	UT	17S	24E	31	NWSW	189.3	B	21.5	2.67	13.9	6.50	7.9	15596	NSLN				
DR3	Washakie	4903722304	3 DRIPPING ROCK	CELSIUS	WY	14N	94W	8	SESWNW	12415.1	A	14.1	2.68	0.0468	0.0276	70.8	15586	MVRD				
DR3	Washakie	4903722304	3 DRIPPING ROCK	CELSIUS	WY	14N	94W	8	SESWNW	12416.8	A	13.7	2.68	0.0464	0.0271	87.5	15516	MVRD				
DR3	Washakie	4903722304	3 DRIPPING ROCK	CELSIUS	WY	14N	94W	8	SESWNW	12416.9	A	13.2	2.68	0.0486	0.0284	81.0	15516	MVRD				
DR3	Washakie	4903722304	3 DRIPPING ROCK	CELSIUS	WY	14N	94W	8	SESWNW	12419.3	A	12.9	2.70	0.0294	0.0144	124	15596	MVRD				
DR3	Washakie	4903722304	3 DRIPPING ROCK	CELSIUS	WY	14N	94W	8	SESWNW	12420.2	A	7.5	2.69	0.00427	0.000418	212	13546	MVRD				
DR3	Washakie	4903722304	3 DRIPPING ROCK	CELSIUS	WY	14N	94W	8	SESWNW	12422.8	A	11.6	2.69	0.0112	0.00281	116	10					

Appendix A1

Summary of Porosity, Permeability and Grain Density

Analysis of Critical Permeability, Capillary Pressure and Electrical Properties for Mesaverde Tight Gas Sandstones from Western U.S. Basins

US DOE # DE-FC26-05NT42660 Final Scientific/Technical Report

Alan P. Byrnes, Robert M. Cluff, John C. Webb

website: <http://www.kgs.ku.edu/mesaverde>

USGS Library Number	Basin	API Number	Well Name	Operator	State	Township	Range	Section	Quarter Section	Plug Depth	Plug Letter	Ambient Porosity	Grain Density	Routine Gas Permeability	in situ		Rock Type Code	Formations	
															Klinkenberg Gas Permeability	Klinkenberg constant b (psia)			
DR5	Washakie	4903722355	5 DRIPPING ROCK	CELSIUS	WY	14N	94W	19	SESWNE	12703.0	A	11.4	2.67	0.0234	0.00601	113	15576	MVRD	
DR5	Washakie	4903722355	5 DRIPPING ROCK	CELSIUS	WY	14N	94W	19	SESWNE	12703.2	A	11.6	2.67	0.0195	0.00644	53.5	15576	MVRD	
DR5	Washakie	4903722355	5 DRIPPING ROCK	CELSIUS	WY	14N	94W	19	SESWNE	12703.2	B	15.4	2.47	0.0185	0.00648	46.5	15576	MVRD	
DR5	Washakie	4903722355	5 DRIPPING ROCK	CELSIUS	WY	14N	94W	19	SESWNE	12704.2	A	11.4	2.68	0.0190	0.00348	109	15586	MVRD	
DR5	Washakie	4903722355	5 DRIPPING ROCK	CELSIUS	WY	14N	94W	19	SESWNE	12704.2	B	10.6	2.67	0.0141	0.00282	156	15586	MVRD	
DR5	Washakie	4903722355	5 DRIPPING ROCK	CELSIUS	WY	14N	94W	19	SESWNE	12704.3	B	11.4	2.67	0.0115	0.00175	123	15586	MVRD	
DR5	Washakie	4903722355	5 DRIPPING ROCK	CELSIUS	WY	14N	94W	19	SESWNE	12704.3	A	10.8	2.67	0.0113	0.00220	209	15586	MVRD	
DR5	Washakie	4903722355	5 DRIPPING ROCK	CELSIUS	WY	14N	94W	19	SESWNE	12709.8	B	9.9	2.67	0.0186	0.00283	147	15285	MVRD	
DR5	Washakie	4903722355	5 DRIPPING ROCK	CELSIUS	WY	14N	94W	19	SESWNE	12709.8	A	16.0	2.77	0.0140	0.00353	100	15276	MVRD	
DR5	Washakie	4903722355	5 DRIPPING ROCK	CELSIUS	WY	14N	94W	19	SESWNE	12713.7	B	17.3	2.70	0.00814	0.00180	129	15295	MVRD	
DR5	Washakie	4903722355	5 DRIPPING ROCK	CELSIUS	WY	14N	94W	19	SESWNE	12713.7	A	8.6	2.68	0.00766	0.00191	95.6	15295	MVRD	
DR5	Washakie	4903722355	5 DRIPPING ROCK	CELSIUS	WY	14N	94W	19	SESWNE	12718.3	A	3.6	2.69	0.00206	0.000136	169	15285	MVRD	
DR5	Washakie	4903722355	5 DRIPPING ROCK	CELSIUS	WY	14N	94W	19	SESWNE	12718.3	B	3.5	2.69	0.00189	0.000008	449	15285	MVRD	
DR5	Washakie	4903722355	5 DRIPPING ROCK	CELSIUS	WY	14N	94W	19	SESWNE	12721.2	A	1.9	2.69	0.00164	0.000044	212	13225	MVRD	
DR5	Washakie	4903722355	5 DRIPPING ROCK	CELSIUS	WY	14N	94W	19	SESWNE	12721.2	B	2.3	2.71	0.000652	0.000003	1851	13225	MVRD	
DR5	Washakie	4903722355	5 DRIPPING ROCK	CELSIUS	WY	14N	94W	19	SESWNE	12723.0	A	4.8	2.78	0.00172	0.000046	356	13265	MVRD	
DR5	Washakie	4903722355	5 DRIPPING ROCK	CELSIUS	WY	14N	94W	19	SESWNE	12723.0	B	1.7	2.69	0.00133	0.000007	512	13265	MVRD	
E489	Washakie	4903721053	3 UNIT FIVE MILE GULCH	AMOCO PRODUCTION	WY	21N	93W	35	C SW	10608.7	B	4.1	2.67	0.00108			11239	ALMD	
E489	Washakie	4903721053	3 UNIT FIVE MILE GULCH	AMOCO PRODUCTION	WY	21N	93W	35	C SW	10608.7	A	4.3	2.67		0.000079		107	11239	ALMD
E489	Washakie	4903721053	3 UNIT FIVE MILE GULCH	AMOCO PRODUCTION	WY	21N	93W	35	C SW	10612.0	B	6.2	2.67	0.00786			182	14286	ALMD
E489	Washakie	4903721053	3 UNIT FIVE MILE GULCH	AMOCO PRODUCTION	WY	21N	93W	35	C SW	10612.0	A	6.5	2.68	0.00226			14286	ALMD	
E489	Washakie	4903721053	3 UNIT FIVE MILE GULCH	AMOCO PRODUCTION	WY	21N	93W	35	C SW	10612.1	A	6.2	2.68	0.00453	0.000382		267	14286	ALMD
E489	Washakie	4903721053	3 UNIT FIVE MILE GULCH	AMOCO PRODUCTION	WY	21N	93W	35	C SW	10612.3	B	6.6	2.67	0.00437			13236	ALMD	
E489	Washakie	4903721053	3 UNIT FIVE MILE GULCH	AMOCO PRODUCTION	WY	21N	93W	35	C SW	10612.3	B	5.8	2.68	0.00299	0.000185		264	13236	ALMD
E489	Washakie	4903721053	3 UNIT FIVE MILE GULCH	AMOCO PRODUCTION	WY	21N	93W	35	C SW	10613.8	B	9.1	2.68	0.0112	0.00284		126	13256	ALMD
E489	Washakie	4903721053	3 UNIT FIVE MILE GULCH	AMOCO PRODUCTION	WY	21N	93W	35	C SW	10613.8	A	9.5	2.68	0.00607	0.00140		107	13256	ALMD
E489	Washakie	4903721053	3 UNIT FIVE MILE GULCH	AMOCO PRODUCTION	WY	21N	93W	35	C SW	10615.6	A	11.0	2.65	0.0532	0.00814		108	13226	ALMD
E489	Washakie	4903721053	3 UNIT FIVE MILE GULCH	AMOCO PRODUCTION	WY	21N	93W	35	C SW	10615.6	B	10.1	2.65	0.0375	0.0117		152	13226	ALMD
E489	Washakie	4903721053	3 UNIT FIVE MILE GULCH	AMOCO PRODUCTION	WY	21N	93W	35	C SW	10615.8	B	10.6	2.65	0.0560	0.0134		40.5	14216	ALMD
E489	Washakie	4903721053	3 UNIT FIVE MILE GULCH	AMOCO PRODUCTION	WY	21N	93W	35	C SW	10615.8	A	10.4	2.65	0.0512	0.0159		21.0	14216	ALMD
E489	Washakie	4903721053	3 UNIT FIVE MILE GULCH	AMOCO PRODUCTION	WY	21N	93W	35	C SW	10618.1	A	5.8	2.67	0.0125	0.000545		133	13286	ALMD
E489	Washakie	4903721053	3 UNIT FIVE MILE GULCH	AMOCO PRODUCTION	WY	21N	93W	35	C SW	10619.0	B	8.8	2.67	0.0234	0.00132		102	13286	ALMD
E489	Washakie	4903721053	3 UNIT FIVE MILE GULCH	AMOCO PRODUCTION	WY	21N	93W	35	C SW	10619.0	A	7.9	2.66	0.00994	0.00205		81.7	13266	ALMD
E489	Washakie	4903721053	3 UNIT FIVE MILE GULCH	AMOCO PRODUCTION	WY	21N	93W	35	C SW	10623.0	A	2.8	2.64	0.00357	0.000106		205	12246	ALMD
E489	Washakie	4903721053	3 UNIT FIVE MILE GULCH	AMOCO PRODUCTION	WY	21N	93W	35	C SW	10627.0	A	2.3	2.65	0.00463			11289	ALMD	
E489	Washakie	4903721053	3 UNIT FIVE MILE GULCH	AMOCO PRODUCTION	WY	21N	93W	35	C SW	10627.0	B	8.4	2.66	0.00282	0.000083		155	11289	ALMD
E489	Washakie	4903721053	3 UNIT FIVE MILE GULCH	AMOCO PRODUCTION	WY	21N	93W	35	C SW	10629.0	A	5.8	2.65		0.000826		67.5	13296	ALMD
E489	Washakie	4903721053	3 UNIT FIVE MILE GULCH	AMOCO PRODUCTION	WY	21N	93W	35	C SW	10634.0	A	3.3	2.65	0.00501	0.000139		89.7	11229	ALMD
E489	Washakie	4903721053	3 UNIT FIVE MILE GULCH	AMOCO PRODUCTION	WY	21N	93W	35	C SW	10634.0	B	2.2	2.64	0.00417	0.000184		276	11229	ALMD
E489	Washakie	4903721053	3 UNIT FIVE MILE GULCH	AMOCO PRODUCTION	WY	21N	93W	35	C SW	10636.2	A	5.4	2.65	0.0125	0.00145		122	13289	ALMD
E489	Washakie	4903721053	3 UNIT FIVE MILE GULCH	AMOCO PRODUCTION	WY	21N	93W	35	C SW	10636.2	B	3.3	2.66	0.00636	0.000836		78.0	11239	ALMD
E489	Washakie	4903721053	3 UNIT FIVE MILE GULCH	AMOCO PRODUCTION	WY	21N	93W	35	C SW	10641.2	A	1.6	2.71	0.000291			13216	ALMD	
E489	Washakie	4903721053	3 UNIT FIVE MILE GULCH	AMOCO PRODUCTION	WY	21N	93W	35	C SW	10641.2	B	1.7	2.71	0.000090	0.000144		227	13216	ALMD
E489	Washakie	4903721053	3 UNIT FIVE MILE GULCH	AMOCO PRODUCTION	WY	21N	93W	35	C SW	10645.0	B	4.0	2.65	0.00933	0.000293		171	30000	ALMD
E489	Washakie	4903721053	3 UNIT FIVE MILE GULCH	AMOCO PRODUCTION	WY	21N	93W	35	C SW	10645.0	A	4.3	2.64	0.00493	0.000349		180	30000	ALMD
E489	Washakie	4903721053	3 UNIT FIVE MILE GULCH	AMOCO PRODUCTION	WY	21N	93W	35	C SW	10650.0	B	5.8	2.76	0.00693	0.000512		248	13216	ALMD
E489	Washakie	4903721053	3 UNIT FIVE MILE GULCH	AMOCO PRODUCTION	WY	21N	93W	35	C SW	10650.0	A	6.2	2.76	0.00238	0.000309		120	13216	ALMD
E489	Washakie	4903721053	3 UNIT FIVE MILE GULCH	AMOCO PRODUCTION	WY	21N	93W	35	C SW	10651.0	A	4.3	2.65	0.0103			13216	ALMD	
E489	Washakie	4903721053	3 UNIT FIVE MILE GULCH	AMOCO PRODUCTION	WY	21N	93W	35	C SW	10651.0	B	2.1	2.64	0.00754	0.000190		870	15216	ALMD
E489	Washakie	4903721053	3 UNIT FIVE MILE GULCH	AMOCO PRODUCTION	WY	21N	93W	35	C SW	10654.5	B	9.3	2.66	0.0132	0.00236		87.8	30000	ALMD
E489	Washakie	4903721053	3 UNIT FIVE MILE GULCH	AMOCO PRODUCTION	WY	21N	93W	35	C SW	10654.5	A	9.1	2.63	0.00943	0.00197		56.6	30000	ALMD
E489	Washakie	4903721053	3 UNIT FIVE MILE GULCH	AMOCO PRODUCTION	WY	21N	93W	35	C SW	10658.1	A	8.4	2.64	0.0367	0.00541		43.5	14256	ALMD
E489	Washakie	4903721053	3 UNIT FIVE MILE GULCH	AMOCO PRODUCTION	WY	21N	93W	35	C SW	10658.1	B	8.1	2.65	0.0187	0.00519		99.1	14256	ALMD
E489	Washakie	4903721053	3 UNIT FIVE MILE GULCH	AMOCO PRODUCTION	WY	21N	93W	35	C SW	10662.1	A	6.2	2.65	0.0169	0.00147		37.3	13256	ALMD
E489	Washakie	4903721053	3 UNIT FIVE MILE GULCH	AMOCO PRODUCTION	WY	21N	93W	35	C SW	10662.1	B	5.4	2.65	0.00790	0.000940		322	13256	ALMD
E489	Washakie	4903721053	3 UNIT FIVE MILE GULCH	AMOCO PRODUCTION	WY	21N	93W	35	C SW	10662.5	A	4.7	2.60	0.0137	0.000234		90.2	13236	ALMD
E489	Washakie	4903721053	3 UNIT FIVE MILE GULCH	AMOCO PRODUCTION	WY	21N	93W	35	C SW	10662.5	B	4.0	2.59	0.00449	0.000107		386	13236	ALMD
E489	Washakie	4903721053	3 UNIT FIVE MILE GULCH	AMOCO PRODUCTION	WY	21N	93W	35	C SW	10666.3	A	8.4	2.65	0.0210	0.00117		60.2	13256	ALMD
E489	Washakie	4903721053	3 UNIT FIVE MILE GULCH	AMOCO PRODUCTION	WY	21N	93W	35	C SW	10666.3									

Appendix A1

Summary of Porosity, Permeability and Grain Density

Analysis of Critical Permeability, Capillary Pressure and Electrical Properties for Mesaverde Tight Gas Sandstones from Western U.S. Basins

US DOE # DE-FC26-05NT42660 Final Scientific/Technical Report

Alan P. Byrnes, Robert M. Cluff, John C. Webb

website: <http://www.kgs.ku.edu/mesaverde>

USGS Library Number	Basin	API Number	Well Name	Operator	State	Township	Range	Section	Quarter Section	Plug Depth	Plug Letter	Ambient Porosity	Grain Density	Routine Gas Permeability	in situ		Rock Type Code	Formations		
															Permeability	Permeability				
											ft	A/B/C	%	g/cc	mD	mD	(psia)			
E489	Washakie	4903721053	3 UNIT FIVE MILE GULCH	AMOCO PRODUCTION	WY	21N	93W	35	C SW	10717.0	A	11.9	2.63							
E489	Washakie	4903721053	3 UNIT FIVE MILE GULCH	AMOCO PRODUCTION	WY	21N	93W	35	C SW	10723.7	B	0.8	2.62	0.00212		0.000081		13246	ALMD	
E489	Washakie	4903721053	3 UNIT FIVE MILE GULCH	AMOCO PRODUCTION	WY	21N	93W	35	C SW	10723.7	A	1.6	2.63				266	12219	ALMD	
N/A	Washakie	9999999999	WILD ROSE 1	N/A	WY	N/A	N/A	N/A	N/A	9762.5	A	14.4	2.58	0.0761		0.0320		63.1	15597	MVRD
N/A	Washakie	9999999999	WILD ROSE 1	N/A	WY	N/A	N/A	N/A	N/A	9837.7	A	6.7	2.64					12219	MVRD	
N/A	Washakie	9999999999	WILD ROSE 1	N/A	WY	N/A	N/A	N/A	N/A	9839.4	A	6.4	2.69	0.00278	0.000445	0.000445		68.6	12219	MVRD
N/A	Washakie	9999999999	WILD ROSE 1	N/A	WY	N/A	N/A	N/A	N/A	10015.6	A	5.3	2.66	0.00516	0.000779	0.000779		47.9	14267	MVRD
N/A	Washakie	9999999999	WILD ROSE 1	N/A	WY	N/A	N/A	N/A	N/A	10132.7	A	7.2	2.68	0.0105	0.00287	0.00287		11.2	14266	MVRD
N/A	Washakie	9999999999	WILD ROSE 1	N/A	WY	N/A	N/A	N/A	N/A	10133.5	A	6.1	2.68	0.00889	0.00243	0.00243		101	14267	MVRD
N/A	Washakie	9999999999	WILD ROSE 1	N/A	WY	N/A	N/A	N/A	N/A	10204.8	A	8.8	2.68	0.0401	0.0231	0.0231		28.2	14266	MVRD
N/A	Washakie	9999999999	WILD ROSE 1	N/A	WY	N/A	N/A	N/A	N/A	10207.8	A	11.1	2.67	0.254	0.192	0.192		25.8	14326	MVRD
S265	Washakie	4903720033	102-7-10 ARCH UNIT	ANADARKO E&P CO. LP	WY	19N	98W	7	SWSW	4868.0	A	18.9	2.62	1.19	44.2	4.2	4.6	16696	ALMD	
S265	Washakie	4903720033	102-7-10 ARCH UNIT	ANADARKO E&P CO. LP	WY	19N	98W	7	SWSW	4870.0	A	18.9	2.62	34.2	26.3	2.3	16576	ALMD		
S265	Washakie	4903720033	102-7-10 ARCH UNIT	ANADARKO E&P CO. LP	WY	19N	98W	7	SWSW	4875.0	B	18.7	2.61	32.7	23.2	2.9	16576	ALMD		
S265	Washakie	4903720033	102-7-10 ARCH UNIT	ANADARKO E&P CO. LP	WY	19N	98W	7	SWSW	4885.0	B	19.8	2.65	35.6	24.2	4.3	16576	ALMD		
S265	Washakie	4903720033	102-7-10 ARCH UNIT	ANADARKO E&P CO. LP	WY	19N	98W	7	SWSW	4885.0	A	19.3	2.63	34.8	23.7	3.6	16576	ALMD		
S265	Washakie	4903720033	102-7-10 ARCH UNIT	ANADARKO E&P CO. LP	WY	19N	98W	7	SWSW	4889.0	A	17.9	2.62	29.5	19.6	3.5	16576	ALMD		
S265	Washakie	4903720033	102-7-10 ARCH UNIT	ANADARKO E&P CO. LP	WY	19N	98W	7	SWSW	4889.0	C	17.6	2.63	17.6	10.4	6.6	16576	ALMD		
S265	Washakie	4903720033	102-7-10 ARCH UNIT	ANADARKO E&P CO. LP	WY	19N	98W	7	SWSW	4889.0	B	17.5	2.63	16.6	10.2	7.1	16576	ALMD		
S265	Washakie	4903720033	102-7-10 ARCH UNIT	ANADARKO E&P CO. LP	WY	19N	98W	7	SWSW	4890.0	A	8.4	2.67	0.356	0.00949	0.00949		85.4	13265	ALMD
S265	Washakie	4903720033	102-7-10 ARCH UNIT	ANADARKO E&P CO. LP	WY	19N	98W	7	SWSW	4890.0	B	8.9	2.69	0.0236	0.00814	0.00814		60.9	13265	ALMD
S265	Washakie	4903720033	102-7-10 ARCH UNIT	ANADARKO E&P CO. LP	WY	19N	98W	7	SWSW	4891.0	A	21.1	2.63	138	84.7	7.3	16576	ALMD		
S265	Washakie	4903720033	102-7-10 ARCH UNIT	ANADARKO E&P CO. LP	WY	19N	98W	7	SWSW	4895.0	A	20.6	2.63	96.8	75.2	1.9	16576	ALMD		
S265	Washakie	4903720033	102-7-10 ARCH UNIT	ANADARKO E&P CO. LP	WY	19N	98W	7	SWSW	4898.0	B	11.7	2.66	0.136	0.0156	0.0156		41.1	13245	ALMD
S265	Washakie	4903720033	102-7-10 ARCH UNIT	ANADARKO E&P CO. LP	WY	19N	98W	7	SWSW	4898.0	A	10.1	2.65	0.147	0.0422	0.0422		177	13245	ALMD
S265	Washakie	4903720033	102-7-10 ARCH UNIT	ANADARKO E&P CO. LP	WY	19N	98W	7	SWSW	4899.0	C	22.4	2.65	161	121	28	13245	ALMD		
S265	Washakie	4903720033	102-7-10 ARCH UNIT	ANADARKO E&P CO. LP	WY	19N	98W	7	SWSW	4899.0	D	21.6	2.65	140	57.3	17.4	13245	ALMD		
S265	Washakie	4903720033	102-7-10 ARCH UNIT	ANADARKO E&P CO. LP	WY	19N	98W	7	SWSW	4899.0	B	18.1	2.57	56.8	32.1	8.6	13245	ALMD		
S265	Washakie	4903720033	102-7-10 ARCH UNIT	ANADARKO E&P CO. LP	WY	19N	98W	7	SWSW	4899.0	A	20.1	2.62	41.2	28.5	3.8	13245	ALMD		
S276	Washakie	4903705683	65-1-7 ARCH UNIT	FOREST OIL CORP	WY	19N	99W	1	NWSE	4728.0	A	7.4	2.62	0.0639	0.000322	0.000322		241	12219	ALMD
S276	Washakie	4903705683	65-1-7 ARCH UNIT	FOREST OIL CORP	WY	19N	99W	1	NWSE	4728.0	B	6.8	2.62	0.0510	0.00262	0.00262		409	12219	ALMD
S276	Washakie	4903705683	65-1-7 ARCH UNIT	FOREST OIL CORP	WY	19N	99W	1	NWSE	4729.0	B	13.0	2.64	0.0829	0.0278	0.0278		36.3	12219	ALMD
S276	Washakie	4903705683	65-1-7 ARCH UNIT	FOREST OIL CORP	WY	19N	99W	1	NWSE	4729.0	A	12.2	2.62	0.0691	0.0261	0.0261		81.8	12219	ALMD
S276	Washakie	4903705683	65-1-7 ARCH UNIT	FOREST OIL CORP	WY	19N	99W	1	NWSE	4731.0	A	9.4	2.60	0.0681	0.00691	0.00691		76.9	12236	ALMD
S276	Washakie	4903705683	65-1-7 ARCH UNIT	FOREST OIL CORP	WY	19N	99W	1	NWSE	4731.0	B	10.0	2.61	0.1043	0.0406	0.0406		98.2	12236	ALMD
S276	Washakie	4903705683	65-1-7 ARCH UNIT	FOREST OIL CORP	WY	19N	99W	1	NWSE	4733.0	A	16.1	2.64	1.15	0.644	0.644		22.1	13215	ALMD
S276	Washakie	4903705683	65-1-7 ARCH UNIT	FOREST OIL CORP	WY	19N	99W	1	NWSE	4733.0	B	15.2	2.64	0.734	0.437	0.437		14.8	13215	ALMD
S276	Washakie	4903705683	65-1-7 ARCH UNIT	FOREST OIL CORP	WY	19N	99W	1	NWSE	4736.1	A	17.6	2.65	17.2	11.3	6.2	15275	ALMD		
S276	Washakie	4903705683	65-1-7 ARCH UNIT	FOREST OIL CORP	WY	19N	99W	1	NWSE	4736.1	B	17.7	2.65	14.9	8.81	11.7	15275	ALMD		
S276	Washakie	4903705683	65-1-7 ARCH UNIT	FOREST OIL CORP	WY	19N	99W	1	NWSE	4736.2	B	18.0	2.66	14.1	8.84	9.1	15275	ALMD		
S276	Washakie	4903705683	65-1-7 ARCH UNIT	FOREST OIL CORP	WY	19N	99W	1	NWSE	4736.2	A	17.3	2.65	8.84	4.87	16.6	15275	ALMD		
S276	Washakie	4903705683	65-1-7 ARCH UNIT	FOREST OIL CORP	WY	19N	99W	1	NWSE	4738.0	A	17.4	2.64	2.83	1.91	11.5	13275	ALMD		
S276	Washakie	4903705683	65-1-7 ARCH UNIT	FOREST OIL CORP	WY	19N	99W	1	NWSE	4738.0	B	15.5	2.64	0.401	0.250	0.250		16.2	13275	ALMD
S276	Washakie	4903705683	65-1-7 ARCH UNIT	FOREST OIL CORP	WY	19N	99W	1	NWSE	4743.0	B	14.7	2.66	0.821	0.585	0.585		5.2	13255	ALMD
S276	Washakie	4903705683	65-1-7 ARCH UNIT	FOREST OIL CORP	WY	19N	99W	1	NWSE	4743.0	A	14.1	2.66	0.733	0.487	18.8	13255	ALMD		
S276	Washakie	4903705683	65-1-7 ARCH UNIT	FOREST OIL CORP	WY	19N	99W	1	NWSE	4745.0	B	14.6	2.64	0.669	0.393	0.393		17.2	13255	ALMD
S276	Washakie	4903705683	65-1-7 ARCH UNIT	FOREST OIL CORP	WY	19N	99W	1	NWSE	4745.0	A	14.8	2.66	0.454	0.288	13.3	13255	ALMD		
S276	Washakie	4903705683	65-1-7 ARCH UNIT	FOREST OIL CORP	WY	19N	99W	1	NWSE	4746.0	A	8.1	2.63	0.0526	0.000611	0.000611		193	12235	ALMD
S276	Washakie	4903705683	65-1-7 ARCH UNIT	FOREST OIL CORP	WY	19N	99W	1	NWSE	4746.0	B	8.3	2.65	0.0389	0.004651	0.004651		228	12235	ALMD
S276	Washakie	4903705683	65-1-7 ARCH UNIT	FOREST OIL CORP	WY	19N	99W	1	NWSE	4746.2	A	10.1	2.66	0.0118	0.00092	0.00092		156	12235	ALMD
S276	Washakie	4903705683	65-1-7 ARCH UNIT	FOREST OIL CORP	WY	19N	99W	1	NWSE	4746.2	B	9.8	2.66	0.0858	0.0145	0.0145		210	12235	ALMD
S276	Washakie	4903705683	65-1-7 ARCH UNIT	FOREST OIL CORP	WY	19N	99W	1	NWSE	4747.0	A	8.4	2.62	0.00728	0.00209	0.00209		73.6	12235	ALMD
S276	Washakie	4903705683	65-1-7 ARCH UNIT	FOREST OIL CORP	WY	19N	99W	1	NWSE	4747.0	B	8.0	2.62	0.00513	0.0106	0.0106		160	12235	ALMD
S276	Washakie	4903705683	65-1-7 ARCH UNIT	FOREST OIL CORP	WY	19N	99W	1	NWSE	4756.9	A	8.5	2.60	0.0629	0.00308	0.00308		111	12239	ALMD
S276	Washakie	4903705683	65-1-7 ARCH UNIT	FOREST OIL CORP	WY	19N	99W	1	NWSE	4756.9	B	8.7	2.60					12239	ALMD	
S276	Washakie	4903705683	65-1-7 ARCH UNIT	FOREST OIL CORP	WY	19N	99W	1	NWSE	4757.9	B	11.1	2.67	0.145	0.0368	0.0368		49.6	12235	ALMD
S276	Washakie	4903705683	65-1-7 ARCH UNIT	FOREST OIL CORP	WY	19N	99W	1	NWSE	4757.9	A	10.6</								

Appendix A1

Summary of Porosity, Permeability and Grain Density

Analysis of Critical Permeability, Capillary Pressure and Electrical Properties for Mesaverde Tight Gas Sandstones from Western U.S. Basins

US DOE # DE-FC26-05NT42660 Final Scientific/Technical Report

Alan P. Byrnes, Robert M. Cluff, John C. Webb

website: <http://www.kgs.ku.edu/mesaverde>

USGS Library Number	Basin	API Number	Well Name	Operator	State	Township	Range	Section	Quarter Section	Plug Depth	Plug Letter	Ambient	Grain	Routine Gas	<i>in situ</i>		Rock	Formations
												Porosity			Density	Permeability		
											%	g/cc	mD	mD	b (psia)	Code		
D031	Wind River	4901320966	CHEVRON 2-1	MONSANTO OIL	WY	38N	91W	1	SWNENW	15716.9	A	1.8	2.68	0.00138	0.000008	1310	12239	MVRD
D031	Wind River	4901320966	CHEVRON 2-1	MONSANTO OIL	WY	38N	91W	1	SWNENW	15726.9	A	8.4	2.69	0.0115	0.00145	86.0	15266	MVRD
D031	Wind River	4901320966	CHEVRON 2-1	MONSANTO OIL	WY	38N	91W	1	SWNENW	15736.0	A	5.5	2.70	0.00463	0.000197	959	15286	MVRD
D031	Wind River	4901320966	CHEVRON 2-1	MONSANTO OIL	WY	38N	91W	1	SWNENW	15750.1	A	4.1	2.71	0.00691	0.000218	245	14286	MVRD
D031	Wind River	4901320966	CHEVRON 2-1	MONSANTO OIL	WY	38N	91W	1	SWNENW	15751.9	A	0.9	2.73	0.00568	0.000114	286	14286	MVRD
D031	Wind River	4901320966	CHEVRON 2-1	MONSANTO OIL	WY	38N	91W	1	SWNENW	15754.1	A	3.6	2.71	0.00674	0.000215	184	14286	MVRD

Appendix 2
Summary of Core Volume Compressibility Results

Analysis of Critical Permeability, Capillary Pressure and Electrical Properties for Mesaverde Tight Gas Sandstones from Western U.S. Basins

UD DE # DE-FC26-05NT42660 Final Scientific/Technical Report

Alan P. Byrnes, Robert M. Cluff, John C. Webb

website: <http://www.kgs.ku.edu/mesaverde>

USGS Library Number	Basin	API Number	Well Name	Operator	State	Township	Range	Section	Quarter Section	Plug Depth ft	Plug Letter A/B/C	Ambient Porosity %	In situ Permeability mD	Ratio (In situ Pore Volume)/(Ambient Pore Volume) at Stress			PVI/Pore Volume at Stress	PVI/Pore Volume at 1,950 psi	PVI/Pore Volume at 3,950 psi	Correlation Coefficient vs log Pe r ²			
														Approx. Net Effective Confining 10 psi	Approx. Net Effective Confining 150 psi	Approx. Net Effective Confining 950 psi							
B029	Green River	4903520088	A-1 WASP	INEXCO OIL COMPANY	WY	36N	112W	28	NWNESE	11443.8	A	3.1	0.000691	1.000	0.857	0.811	0.763	0.723	0.683	1.1213	-0.1213	0.9999	
B029	Green River	4903520088	A-1 WASP	INEXCO OIL COMPANY	WY	36N	112W	28	NWNESE	11457.9	A	5.5	0.000110	1.000	0.884	0.846	0.805	0.775	0.742	0.690	1.0990	-0.0990	0.9999
B029	Green River	4903520088	A-1 WASP	INEXCO OIL COMPANY	WY	36N	112W	28	NWNESE	11459.1	A	5.4	0.000827	1.000	0.914	0.886	0.855	0.834	0.808	0.734	1.0734	-0.0734	0.9998
B029	Green River	4903520088	A-1 WASP	INEXCO OIL COMPANY	WY	36N	112W	28	NWNESE	11460.6	A	4.3	0.0155	1.000	0.872	0.838	0.778	0.750	0.722	1.1085	-0.1085	0.9979	
B029	Green River	4903520088	A-1 WASP	INEXCO OIL COMPANY	WY	36N	112W	28	NWNESE	11466.1	A	4.0	0.000524	1.000	0.881	0.845	0.796	0.769	0.737	1.1016	-0.1016	0.9987	
B029	Green River	4903520088	A-1 WASP	INEXCO OIL COMPANY	WY	36N	112W	28	NWNESE	11609.1	A	5.9	0.00772	1.000	0.916	0.888	0.860	0.836	0.812	1.0718	-0.0718	0.9997	
B029	Green River	4903520088	A-1 WASP	INEXCO OIL COMPANY	WY	36N	112W	28	NWNESE	11609.2	A	5.2	0.00475	1.000	0.903	0.872	0.839	0.809	0.787	1.0824	-0.0824	0.9996	
B029	Green River	4903520088	A-1 WASP	INEXCO OIL COMPANY	WY	36N	112W	28	NWNESE	11615.1	A	4.6	0.00192	1.000	0.898	0.871	0.825	0.791	0.763	1.0868	-0.0868	0.9939	
B029	Green River	4903520088	A-1 WASP	INEXCO OIL COMPANY	WY	36N	112W	28	NWNESE	11706.1	A	4.0	0.000524	1.000	0.881	0.845	0.796	0.769	0.737	1.1016	-0.1016	0.9987	
B029	Green River	4903520088	A-1 WASP	INEXCO OIL COMPANY	WY	36N	112W	28	NWNESE	11706.9	A	3.8	0.000405	1.000	0.942	0.923	0.904	0.888	0.871	1.0492	-0.0492	0.9997	
B029	Green River	4903520088	A-1 WASP	INEXCO OIL COMPANY	WY	36N	112W	28	NWNESE	11721.9	A	4.3	0.000320	1.000	0.877	0.831	0.804	0.766	0.720	1.1045	-0.1045	0.9941	
B029	Green River	4903520088	A-1 WASP	INEXCO OIL COMPANY	WY	36N	112W	28	NWNESE	11758.3	A	4.7	0.000470	1.000	0.840	0.790	0.731	0.690	0.646	1.1359	-0.1359	1.0000	
B029	Green River	4903520088	A-1 WASP	INEXCO OIL COMPANY	WY	36N	112W	28	NWNESE	11758.4	A	4.6	0.00110	1.000	0.869	0.879	0.847	0.822	0.797	1.0779	-0.0779	0.9999	
E712	Green River	4903506020	B-54 BIG PINEY	BELCO PETROLEUM	WY	29N	113W	26	SESENE	3461.7	A	17.9	2.42	1.000	0.937	0.918	0.894	0.876	0.862	1.0533	-0.0533	1.0000	
E712	Green River	4903506020	B-54 BIG PINEY	BELCO PETROLEUM	WY	29N	113W	26	SESENE	3462.0	A	18.8	26.8	1.000	0.942	0.925	0.900	0.886	0.873	1.0494	-0.0494	0.9992	
E712	Green River	4903506020	B-54 BIG PINEY	BELCO PETROLEUM	WY	29N	113W	26	SESENE	3503.7	B	8.8	0.000792	1.000	0.903	0.871	0.839	0.814	0.784	1.0823	-0.0823	0.9994	
E712	Green River	4903506020	B-54 BIG PINEY	BELCO PETROLEUM	WY	29N	113W	26	SESENE	3519.3	B	16.1	6.02	1.000	0.944	0.928	0.905	0.891	0.878	1.0474	-0.0474	0.9997	
E894	Green River	4903520622	1 OLD ROAD	AMERICAN HUNTER EXPL	WY	27N	108W	27	SENWSE	11921.8	A	5.0	0.000271	1.000	0.960	0.934	0.918	0.904	0.889	1.0422	-0.0422	0.9995	
E894	Green River	4903520622	1 OLD ROAD	AMERICAN HUNTER EXPL	WY	27N	108W	27	SENWSE	11923.3	A	4.1	0.00644	1.000	0.940	0.920	0.901	0.886	0.865	1.0509	-0.0509	0.9984	
E894	Green River	4903520622	1 OLD ROAD	AMERICAN HUNTER EXPL	WY	27N	108W	27	SENWSE	11956.1	A	8.5	0.00792	1.000	0.967	0.955	0.946	0.936	0.926	1.0282	-0.0282	0.9982	
R780	Green River	4903505742	C-47 TIP TOP SHALLOW	BELCO PETROLEUM	WY	28N	113W	22	SWNE	2754.7	A	21.3	1.90	1.000	0.946	0.929	0.909	0.894	0.881	1.0461	-0.0461	0.9999	
R780	Green River	4903505742	C-47 TIP TOP SHALLOW	BELCO PETROLEUM	WY	28N	113W	22	SWNE	2753.2	A	23.9	0.000442	1.000	0.946	0.929	0.910	0.894	0.881	1.0461	-0.0461	0.9999	
R780	Green River	4903505742	C-47 TIP TOP SHALLOW	BELCO PETROLEUM	WY	28N	113W	22	SWNE	2817.7	A	20.1	2.12	1.000	0.954	0.940	0.923	0.907	0.900	1.0393	-0.0393	0.9981	
R780	Green River	4903505742	C-47 TIP TOP SHALLOW	BELCO PETROLEUM	WY	28N	113W	22	SWNE	2831.8	A	23.6	2.73	1.000	0.958	0.945	0.928	0.918	0.906	1.0361	-0.0361	0.9998	
R780	Green River	4903505742	C-47 TIP TOP SHALLOW	BELCO PETROLEUM	WY	28N	113W	22	SWNE	2831.9	B	20.4	3.22	1.000	0.952	0.937	0.920	0.906	0.894	1.0406	-0.0406	0.9999	
R780	Green River	4903505742	C-47 TIP TOP SHALLOW	BELCO PETROLEUM	WY	28N	113W	22	SWNE	2831.9	B	20.4	3.22	1.000	0.952	0.937	0.920	0.906	0.894	1.0406	-0.0406	0.9999	
S873	Green River	4903506200	K2 MASSON	BELCO PETROLEUM	WY	31N	113W	13	SESE	8933.3	A	3.4	0.000224	1.000	0.973	0.962	0.958	0.949	0.937	1.0231	-0.0231	0.9874	
T195	Green River	4903508024	5 PINEDALE	EL PASO NATURAL GAS	WY	30N	108W	5	CSE	12168.5	A	11.0	0.0167	1.000	0.962	0.950	0.937	0.927	0.917	1.0320	-0.0320	0.9999	
T195	Green River	4903508024	5 PINEDALE	EL PASO NATURAL GAS	WY	30N	108W	5	CSE	12169.5	A	9.3	0.000003	1.000	0.929	0.907	0.882	0.859	0.845	1.0602	-0.0602	0.9990	
T195	Green River	4903508024	5 PINEDALE	EL PASO NATURAL GAS	WY	30N	108W	5	CSE	12162.0	A	7.2	0.000796	1.000	0.938	0.918	0.896	0.879	0.862	1.0530	-0.0530	0.9999	
T203	Green River	4903506025	1 MOUNTAIN FUEL SUPPLY	MOUNTAIN FUEL SUPPLY	WY	18N	110W	27	SESW	9041.1	A	11.6	1.82	1.000	0.920	0.894	0.864	0.846	0.821	1.0684	-0.0684	0.9997	
T204	Green River	4903507549	B-2A SPIDER CREEK	HUMBLE OIL & REF	WY	18N	110W	27	SESW	9116.6	A	2.3	0.000138	1.000	0.960	0.944	0.942	0.943	0.940	1.2892	-0.2892	0.9989	
R091	Piceance	05045XXXX4	BOOK CLIFFS 1	USGS-CG	CO	7S	104W	17	SESW	242.4	A	6.7	0.000164	1.000	0.914	0.885	0.857	0.833	0.808	1.0734	-0.0734	0.9996	
R091	Piceance	05045XXXX4	BOOK CLIFFS 1	USGS-CG	CO	7S	104W	17	SESW	242.4	A	6.7	0.000164	1.000	0.914	0.885	0.857	0.833	0.808	1.0734	-0.0734	0.9996	
R091	Piceance	05045XXXX4	BOOK CLIFFS 1	USGS-CG	CO	7S	104W	17	SESW	296.9	A	4.9	0.000168	1.000	0.955	0.939	0.928	0.911	0.900	1.0383	-0.0383	0.9962	
R091	Piceance	05045XXXX4	BOOK CLIFFS 1	USGS-CG	CO	7S	104W	17	SESW	387.3	A	9.6	0.000985	1.000	0.903	0.873	0.839	0.811	0.787	1.0821	-0.0821	0.9999	
S905	Piceance	05103XXXX3	21011-5 MOON LAKE	WESTERN FUELS ASSOC	CO	2N	101W	1	SESW	790.3	A	5.0	0.000209	1.000	0.949	0.932	0.915	0.900	0.886	1.0436	-0.0436	0.9998	
S905	Piceance	05103XXXX3	21011-5 MOON LAKE	WESTERN FUELS ASSOC	CO	2N	101W	1	SESW	812.7	A	18.1	22.0	1.000	0.999	0.996	0.990	0.919	0.899	1.0352	-0.0352	1.0000	
S905	Piceance	05103XXXX3	21011-5 MOON LAKE	WESTERN FUELS ASSOC	CO	2N	101W	1	SESW	817.7	A	19.1	0.00017	1.000	0.963	0.950	0.927	0.910	0.897	1.0397	-0.0397	0.9999	
S905	Piceance	05103XXXX3	21011-5 MOON LAKE	WESTERN FUELS ASSOC	CO	2N	101W	1	SESW	816.5	A	10.6	0.0205	1.000	0.915	0.892	0.862	0.833	0.816	1.0721	-0.0721	0.9973	
S905	Piceance	05103XXXX3	21011-5 MOON LAKE	WESTERN FUELS ASSOC	CO	2N	101W	1	SESW	817.8	A	8.7	0.00118	1.000	0.847	0.794	0.750	0.704	0.658	1.1300	-0.1300	0.9986	
T649	Piceance	0504560011	MMW-2	CER CORPORATION	CO	6S	94W	34	SESWNW	5737.3	A	9.4	0.00220	1.000	0.952	0.936	0.919	0.908	0.892	1.0411	-0.0411	0.9992	
T649	Piceance	0504560011	MMW-2	CER CORPORATION	CO	6S	94W	34	SESWNW	5742.2	A	4.3	0.000442	1.000	0.946	0.929	0.910	0.894	0.881	1.0461	-0.0461	0.9999	
T649	Piceance	0504560011	MMW-2	CER CORPORATION	CO	6S	94W	34	SESWNW	5837.8	A	6.6	0.00146	1.000	0.954	0.938	0.925	0.911	0.897	1.0392	-0.0392	0.9985	
T649	Piceance	0504560011	MMW-2	CER CORPORATION	CO	6S	94W	34	SESWNW	5852.3	A	2.8	0.000447	1.000	0.943	0.921	0.908	0.894	0.869	1.0484	-0.0484	0.9921	
T649	Piceance	0504560011	MMW-2	CER CORPORATION	CO	6S	94W	34	SESWNW	5842.3	B	5.8	0.000249	1.000	0.969	0.960	0.948	0.939	0.933	1.0262	-0.0262	0.9994	
T649	Piceance	0504560011	MMW-2	CER CORPORATION	CO	6S	94W	34	SESWNW	7136.8	A	6.9	0.00218	1.000	0.948	0.932	0.917	0.906	0.895	1.0441	-0.0441	0.9988	
T649	Piceance	0504560011	MMW-2</																				

Appendix 3

Summary of Critical Gas Saturation Results

Analysis of Critical Permeability, Capillary Pressure and Electrical Properties for Mesaverde Tight Gas Sandstones from Western U.S. Basins

US DOE # DE-FC26-05NT42660 Final Scientific/Technical Report

Alan P. Byrnes, Robert M. Cluff, John C. Webb

website: <http://www.kgs.ku.edu/mesaverde>

USGS Library Number	Basin	API Number	Well Name	Operator	State	Township	Range	Sec	Quarter Section	Plug Depth ft	A/B/C	Routine Porosity %	<i>in situ</i> Klinkenberg Gas Permeability mD	<i>in situ</i> Porosity %	<i>in situ</i> Critical Gas Saturation %	Threshold pressure at Sgc (psig)
B029	Green River	4903520088	A-1 WASP	INEXCO OIL COMPANY	WY	36N	112W	28	NW NESW	10573.1	B	3.1	0.000201	2.6	6.7	550
B029	Green River	4903520088	A-1 WASP	INEXCO OIL COMPANY	WY	36N	112W	28	NW NESW	11443.7	A	2.8	0.000322	2.4	2.3	380
B029	Green River	4903520088	A-1 WASP	INEXCO OIL COMPANY	WY	36N	112W	28	NW NESW	11447.8	A	4.8	0.00163	4.2	7.3	200
B029	Green River	4903520088	A-1 WASP	INEXCO OIL COMPANY	WY	36N	112W	28	NW NESW	11457.8	A	4.4	0.00271	3.7	8.3	220
B029	Green River	4903520088	A-1 WASP	INEXCO OIL COMPANY	WY	36N	112W	28	NW NESW	11457.9	A	5.5	0.000110	4.8	2.8	600
B029	Green River	4903520088	A-1 WASP	INEXCO OIL COMPANY	WY	36N	112W	28	NW NESW	11459.2	A	4.5	0.00184	3.8	5.7	150
B029	Green River	4903520088	A-1 WASP	INEXCO OIL COMPANY	WY	36N	112W	28	NW NESW	11460.6	A	4.3	0.0155	3.6	0.7	70
B029	Green River	4903520088	A-1 WASP	INEXCO OIL COMPANY	WY	36N	112W	28	NW NESW	11609.1	A	5.9	0.00772	5.2	5.3	140
B029	Green River	4903520088	A-1 WASP	INEXCO OIL COMPANY	WY	36N	112W	28	NW NESW	11706.9	A	3.8	0.000405	3.2	6.9	340
B029	Green River	4903520088	A-1 WASP	INEXCO OIL COMPANY	WY	36N	112W	28	NW NESW	11721.9	A	4.3	0.000320	3.7	2.3	340
B029	Green River	4903520088	A-1 WASP	INEXCO OIL COMPANY	WY	36N	112W	28	NW NESW	11722.0	A	4.3	0.000447	3.7	3.5	340
E712	Green River	4903506020	B-54 BIG PINEY	BELCO PETROLEUM	WY	29N	113W	26	SESENE	3403.9	A	16.7	1.20	15.9	6.1	40
E712	Green River	4903506020	B-54 BIG PINEY	BELCO PETROLEUM	WY	29N	113W	26	SESENE	3462.0	A	18.8	26.8	18.1	3.4	4
E712	Green River	4903506020	B-54 BIG PINEY	BELCO PETROLEUM	WY	29N	113W	26	SESENE	3480.8	A	8.8	0.00580	8.0	3.1	110
E712	Green River	4903506020	B-54 BIG PINEY	BELCO PETROLEUM	WY	29N	113W	26	SESENE	3503.7	B	8.8	0.000792	8.0	31.5	220
E712	Green River	4903506020	B-54 BIG PINEY	BELCO PETROLEUM	WY	29N	113W	26	SESENE	3519.3	B	16.1	6.02	15.2	8.5	10
E894	Green River	4903520622	1 OLD ROAD	AMERICAN HUNTER EXPL	WY	27N	108W	27	SENWSE	11897.3	A	5.2	0.000995	4.4	12.3	260
E894	Green River	4903520622	1 OLD ROAD	AMERICAN HUNTER EXPL	WY	27N	108W	27	SENWSE	11956.1	A	8.5	0.00792	7.7	3.1	80
R780	Green River	4903505742	C-47 TIP TOP SHALLOW	BELCO PETROLEUM	WY	28N	113W	22	SWNE	2754.7	A	21.3	1.90	20.5	1.0	15
R780	Green River	4903505742	C-47 TIP TOP SHALLOW	BELCO PETROLEUM	WY	28N	113W	22	SWNE	2783.3	A	22.3	23.3	21.5	1.8	4
R780	Green River	4903505742	C-47 TIP TOP SHALLOW	BELCO PETROLEUM	WY	28N	113W	22	SWNE	2817.7	A	20.1	2.12	19.3	1.1	10
R780	Green River	4903505742	C-47 TIP TOP SHALLOW	BELCO PETROLEUM	WY	28N	113W	22	SWNE	2845.5	A	22.6	8.69	22.0	2.4	10
S873	Green River	4903506200	K-2 MASON	BELCO PETROLEUM	WY	31N	113W	13	SESE	6989.8	A	10.7	0.138	9.8	5.6	30
S873	Green River	4903506200	K-2 MASON	BELCO PETROLEUM	WY	31N	113W	13	SESE	9397.3	A	8.4	0.000358	7.6	5.2	340
SHV	Green River	4903523799	VIBLE 1D-11D	SHELL E&P	WY	31N	109W	11	SENE	12507.1	A	5.1	0.000627	4.4	4.0	300
SHV	Green River	4903523799	VIBLE 1D-11D	SHELL E&P	WY	31N	109W	11	SENE	12508.7	A	3.0	0.000219	2.5	4.7	460
SHV	Green River	4903523799	VIBLE 1D-11D	SHELL E&P	WY	31N	109W	11	SENE	12518.5	A	5.9	0.00172	5.2	7.2	280
T195	Green River	4903508024	5 PINEDALE	EL PASO NATURAL GAS	WY	30N	108W	5		12158.5	A	11.0	0.0167	10.2	13.3	60
T195	Green River	4903508024	5 PINEDALE	EL PASO NATURAL GAS	WY	30N	108W	5		12162.0	A	7.2	0.000796	6.4	8.9	260
T203	Green River	4903705405	1 CHIMNEY ROCK	MOUNTAIN FUEL SUPPLY	WY	18N	102W	12	SESW	6741.0	A	14.3	81.9	13.5	5.7	4
T204	Green River	4903705349	B-2A SPIDER CREEK	HUMBLE OIL & REF	WY	18N	110W	27	NESW	9041.1	A	11.6	1.82	10.7	3.1	10
T204	Green River	4903705349	B-2A SPIDER CREEK	HUMBLE OIL & REF	WY	18N	110W	27	NESW	9063.0	A	15.2	206	14.3	1.9	2
T204	Green River	4903705349	B-2A SPIDER CREEK	HUMBLE OIL & REF	WY	18N	110W	27	NESW	9098.0	A	6.6	0.0188	5.9	4.7	60
E437	Piceance	0504506578	MV 24-20 CHEVRON	BARRETT ENERGY	CO	6S	96W	20	SENW	6579.5	A	7.5	0.000441	6.7	15.9	440
E437	Piceance	0504506578	MV 24-20 CHEVRON	BARRETT ENERGY	CO	6S	96W	20	SENW	6591.9	A	2.4	0.000711	2.0	4.2	380
E437	Piceance	0504506578	MV 24-20 CHEVRON	BARRETT ENERGY	CO	6S	96W	20	SENW	6592.5	A	2.6	0.000163	2.0	26.4	340
B43C	Piceance	0504511402	LAST DANCE 43C-3-792	BILL BARRETT CORP.	CO	7S	92W	3	NESE	3544.8	C	10.5	0.392	9.6	4.0	24
B43C	Piceance	0504511402	LAST DANCE 43C-3-792	BILL BARRETT CORP.	CO	7S	92W	3	NESE	3992.5	C	2.9	0.000576	2.4	11.1	320
B43C	Piceance	0504511402	LAST DANCE 43C-3-792	BILL BARRETT CORP.	CO	7S	92W	3	NESE	4013.3	B	12.9	0.190	12.0	5.6	18
B43C	Piceance	0504511402	LAST DANCE 43C-3-792	BILL BARRETT CORP.	CO	7S	92W	3	NESE	4393.6	A	8.7	0.00652	7.9	17.6	120
E458	Piceance	0510309406	M-30-2-96W /D-037934	FUEL RESOURCES DEV	CO	2N	96W	30	SWSW	6379.5	A	3.8	0.000303	3.3	13.9	420
E458	Piceance	0510309406	M-30-2-96W /D-037934	FUEL RESOURCES DEV	CO	2N	96W	30	SWSW	6509.4	A	10.7	0.0269	9.9	1.9	70
PA424	Piceance	0504510927	Williams PA-424-34	WILLIAMS E&P	CO	6S	95W	34	NWSWSE	4600.3	A	12.2	0.00188	11.3	4.3	200
PA424	Piceance	0504510927	Williams PA-424-34	WILLIAMS E&P	CO	6S	95W	34	NWSWSE	4651.6	A	6.7	0.0134	6.0	2.4	80
PA424	Piceance	0504510927	Williams PA-424-34	WILLIAMS E&P	CO	6S	95W	34	NWSWSE	4660.4	A	7.0	0.00357	6.1	2.3	150
PA424	Piceance	0504510927	Williams PA-424-34	WILLIAMS E&P	CO	6S	95W	34	NWSWSE	4691.5	A	13.3	0.00687	12.5	0.1	100
PA424	Piceance	0504510927	Williams PA-424-34	WILLIAMS E&P	CO	6S	95W	34	NWSWSE	5140.5	A	11.6	0.0251	10.8	5.8	60
PA424	Piceance	0504510927	Williams PA-424-34	WILLIAMS E&P	CO	6S	95W	34	NWSWSE	6148.6	A	9.9	0.00761	9.1	3.3	110
PA424	Piceance	0504510927	Williams PA-424-34	WILLIAMS E&P	CO	6S	95W	34	NWSWSE	6599.5	A	7.8	0.00155	7.0	15.7	300
PA424	Piceance	0504510927	Williams PA-424-34	WILLIAMS E&P	CO	6S	95W	34	NWSWSE	6632.8	A	3.5	0.00507	2.9	20.4	220
R091	Piceance	05045XXXX4	BOOK CLIFFS 1	USGS-CG	CO	7S	104W	17	NESW	255.8	A	24.9	112	24.3	0.9	2
R091	Piceance	05045XXXX4	BOOK CLIFFS 1	USGS-CG	CO	7S	104W	17	NESW	296.9	A	4.9	0.000168	4.2	3.3	340
R091	Piceance	05045XXXX4	BOOK CLIFFS 1	USGS-CG	CO	7S	104W	17	NESW	387.3	A	9.6	0.000985	8.8	4.3	300
R091	Piceance	05045XXXX4	BOOK CLIFFS 1	USGS-CG	CO	7S	104W	17	NESW	512.2	A	10.6	0.00904	9.7	12.4	90
S905	Piceance	05103XXXX3	21011-5 MOON LAKE	WESTERN FUELS ASSOC	CO	2N	101W	1	NESW	812.9	A	17.0	20.9	16.2	4.8	6
S905	Piceance	05103XXXX3	21011-5 MOON LAKE	WESTERN FUELS ASSOC	CO	2N	101W	1	NESW	816.5	A	10.6	0.0205	9.8	3.3	50
S905	Piceance	05103XXXX3	21011-5 MOON LAKE	WESTERN FUELS ASSOC	CO	2N	101W	1	NESW	817.8	A	8.7	0.00118	7.9	5.6	200
T63X-2G	Piceance	0510310391	T63X-2G	EXXON-MOBIL	CO	3S	97W	2	NESWNE	10572.9	B	4.3	0.000214	3.7	7.4	480
T63X-2G	Piceance	0510310391	T63X-2G	EXXON-MOBIL	CO	3S	97W	2	NESWNE	10615.6	A	6.1	0.00175	5.3	5.5	340
T63X-2G	Piceance	0510310391	T63X-2G	EXXON-MOBIL	CO	3S	97W	2	NESWNE	10619.7	A	7.3	0.00247	6.5	2.6	180
T649	Piceance	0504560011	MWX-2	CER CORPORATION	CO	6S	94W	34	SESWNW	5734.1	A	8.7	0.00471	7.9	3.4	130
T649	Piceance	0504560011	MWX-2	CER CORPORATION	CO	6S	94W	34	SESWNW	5838.7	A	6.6	0.00146	5.8	2.6	260
T649	Piceance	0504560011	MWX-2	CER CORPORATION	CO	6S	94W	34	SESWNW	7124.7	A	11.1	0.00345	10.2	20.6	130
T649	Piceance	0504560011	MWX-2	CER CORPORATION	CO	6S	94W	34	SESWNW	7272.8	A	8.9	0.00234	8.1	3.4	150
T649	Piceance	0504560011	MWX-2	CER CORPORATION	CO	6S	94W	34	SESWNW	7276.2	A	8.4	0.00173	7.5	2.2	130
T649	Piceance	0504560011	MWX-2	CER CORPORATION	CO	6S	94W	34	SESWNW	7340.4	A	2.1	0.000106	1.7	2.6	600
T649	Piceance	0504560011	MWX-2	CER CORPORATION	CO	6S	94W	34	SESWNW	7350.4	A	4.5	0.000372	3.8	6.8	420
T649	Piceance	0504560011	MWX-2	CER CORPORATION	CO	6S	94W	34	SESWNW	7877.5	A	7.6	0.000910	6.9	2.3	200
T649	Piceance	0504560011	MWX-2	CER CORPORATION	CO	6S	94W	34	SESWNW	8117.9	A	6.5	0.00227	5.8	4.6	160
E393	Powder River	4900525627	1 BARLOW 21-20	LOUISIANA LAND & EXP	WY	48N	75W	20	NENW	6969.7	B	20.7	1.18	20.0	4.3	15
E393	Powder River	4900525627	1 BARLOW 21-20	LOUISIANA LAND & EXP	WY	48N	75W	20	NENW	6996.0	A	5.9	0.00143	5.3	3.2	220
E393	Powder River	4900525627	1 BARLOW 21-20	LOUISIANA LAND & EXP	WY	48N	75W	20	NENW	7000.9	B	17.3	31.0	16.6	3.2	3
E393	Powder River	4900525627	1 BARLOW 21-20	LOUISIANA LAND & EXP	WY	48N	75W	20	NENW	7039.2	B	17.1	6.21	16.2	6.4	10
E393	Powder River	4900525627	1 BARLOW 21-20	LOUISIANA LAND & EXP	WY	48N	75W	20	NENW	7060.4	A	14.5	0.0564	13.7	13.1	40
E932	Powder River	4900921513	2 FRED STATE	DAVIS OIL COMPANY	WY	35N	70W	36	NESESW	7544.3	A	16.4	3.13	15.6	3.5	8
E932	Powder River	4900921513	2 FRED STATE	DAVIS OIL COMPANY	WY	35N	70W	36	NESESW	7546.9	A	10.5	0.0192	9.7	4.1	140
E932	Powder River	4900921513	2 FRED STATE	DAVIS OIL COMPANY	WY	35N	7									

Appendix 3

Summary of Critical Gas Saturation Results

Analysis of Critical Permeability, Capillary Pressure and Electrical Properties for Mesaverde Tight Gas Sandstones from Western U.S. Basins

US DOE # DE-FC26-05NT42660 Final Scientific/Technical Report

Alan P. Byrnes, Robert M. Cluff, John C. Webb

website: <http://www.kgs.ku.edu/mesaverde>

USGS Library Number	Basin	API Number	Well Name	Operator	State	Township	Range	Sec	Quarter Section	Plug Depth ft	A/B/C	Routine Porosity %	<i>in situ</i> Klinenberg Gas Permeability mD	<i>in situ</i> Porosity %	<i>in situ</i> Critical Gas Saturation %	Threshold pressure at Sgc (psig)
B646	Uinta	4304730584	11-17F RIVER BEND UNIT	MAPCO INCOPORATED	UT	10S	20E	17	SENEW	8233.0	B	5.8	0.00464	5.1	2.4	150
B646	Uinta	4304730584	11-17F RIVER BEND UNIT	MAPCO INCOPORATED	UT	10S	20E	17	SENEW	8245.1	A	2.6	0.000781	2.1	3.5	280
B646	Uinta	4304730584	11-17F RIVER BEND UNIT	MAPCO INCOPORATED	UT	10S	20E	17	SENEW	8287.4	B	7.5	0.0217	6.8	4.3	50
B646	Uinta	4304730584	11-17F RIVER BEND UNIT	MAPCO INCOPORATED	UT	10S	20E	17	SENEW	8302.5	A	1.0	0.000112	0.6	4.8	600
E946	Uinta	4304730545	2-7 FLAT MESA	ENSERCH EXPLORATION	UT	10S	23E	7	NESEW	6352.1	A	7.3	0.00110	6.5	8.2	240
E946	Uinta	4304730545	2-7 FLAT MESA	ENSERCH EXPLORATION	UT	10S	23E	7	NESEW	6468.5	A	11.9	0.382	11.1	10.0	20
E946	Uinta	4304730545	2-7 FLAT MESA	ENSERCH EXPLORATION	UT	10S	23E	7	NESEW	6472.7	A	9.0	0.0454	8.2	5.0	50
E946	Uinta	4304730545	2-7 FLAT MESA	ENSERCH EXPLORATION	UT	10S	23E	7	NESEW	6508.2	A	3.1	0.000484	2.6	2.4	340
E946	Uinta	4304730545	2-7 FLAT MESA	ENSERCH EXPLORATION	UT	10S	23E	7	NESEW	6515.5	A	16.3	2.00	15.5	7.0	10
E946	Uinta	4304730545	2-7 FLAT MESA	ENSERCH EXPLORATION	UT	10S	23E	7	NESEW	6530.2	A	9.8	0.0235	8.9	4.5	50
E946	Uinta	4304730545	2-7 FLAT MESA	ENSERCH EXPLORATION	UT	10S	23E	7	NESEW	6530.4	A	9.9	0.0639	9.1	6.0	40
E946	Uinta	4304730545	2-7 FLAT MESA	ENSERCH EXPLORATION	UT	10S	23E	7	NESEW	6709.8	A	2.2	0.000117	1.7	9.4	600
E946	Uinta	4304730545	2-7 FLAT MESA	ENSERCH EXPLORATION	UT	10S	23E	7	NESEW	7287.1	A	5.6	0.00147	4.9	1.6	240
E946	Uinta	4304730545	2-7 FLAT MESA	ENSERCH EXPLORATION	UT	10S	23E	7	NESEW	7293.5	A	3.8	0.000490	3.3	12.5	500
E946	Uinta	4304730545	2-7 FLAT MESA	ENSERCH EXPLORATION	UT	10S	23E	7	NESEW	7312.7	A	7.8	0.00303	7.0	1.8	150
E946	Uinta	4304730545	2-7 FLAT MESA	ENSERCH EXPLORATION	UT	10S	23E	7	NESEW	7314.3	A	5.8	0.00412	5.0	11.5	140
E946	Uinta	4304730545	2-7 FLAT MESA	ENSERCH EXPLORATION	UT	10S	23E	7	NESEW	7671.1	A	4.8	0.0973	4.2	2.9	24
E946	Uinta	4304730545	2-7 FLAT MESA	ENSERCH EXPLORATION	UT	10S	23E	7	NESEW	7689.7	A	7.4	0.00374	6.5	4.4	120
E946	Uinta	4304730545	2-7 FLAT MESA	ENSERCH EXPLORATION	UT	10S	23E	7	NESEW	7885.4	A	9.8	0.0258	9.0	1.9	60
KM360	Uinta	4304735788	NBU 9-20-360 State	KERR-MCGEE OIL&GAS ONSHORE	UT	9S	20E	36	SESE	8218.5	A	5.8	0.00117	5.0	2.6	320
KM360	Uinta	4304735788	NBU 9-20-360 State	KERR-MCGEE OIL&GAS ONSHORE	UT	9S	20E	36	SESE	8234.4	A	8.7	0.00340	7.9	5.6	150
KM360	Uinta	4304735788	NBU 9-20-360 State	KERR-MCGEE OIL&GAS ONSHORE	UT	9S	20E	36	SESE	8234.6	B	9.1	0.00825	8.4	3.0	90
R829	Uinta	4304730852	4-5 US LAMCO	ENSERCH EXPLORATION	UT	13S	20E	5	C SW	5621.2	A	10.4	0.394	9.5	2.9	24
R829	Uinta	4304730852	4-5 US LAMCO	ENSERCH EXPLORATION	UT	13S	20E	5	C SW	5626.2	A	12.5	7.19	11.7	9.3	8
R999	Uinta	4304730860	3-24 US LAMCO	CHAMPLIN PETROLEUM	UT	13S	20E	24	NESE	7158.9	B	2.7	0.000149	2.2	22.7	480
S172	Uinta	43019XXXX1	3 BOOK CLIFFS	USGS-CG	UT	17S	24E	3	SE	174.0	A	7.0	0.000416	6.3	5.4	380
S172	Uinta	43019XXXX1	3 BOOK CLIFFS	USGS-CG	UT	17S	24E	3	SE	175.2	A	19.9	34.0	19.2	1.7	5
S172	Uinta	43019XXXX1	3 BOOK CLIFFS	USGS-CG	UT	17S	24E	3	SE	252.1	A	14.9	0.133	14.1	7.9	40
S172	Uinta	43019XXXX1	3 BOOK CLIFFS	USGS-CG	UT	17S	24E	3	SE	334.5	A	3.6	0.000142	3.1	2.8	550
S174	Uinta	43019XXXX2	4 BOOK CLIFFS	USGS-CG	UT	17S	24E	31	NWSW	161.7	A	12.1	0.0313	11.3	2.7	24
S174	Uinta	43019XXXX2	4 BOOK CLIFFS	USGS-CG	UT	17S	24E	31	NWSW	183.4	A	9.8	0.112	9.0	3.8	30
S174	Uinta	43019XXXX2	4 BOOK CLIFFS	USGS-CG	UT	17S	24E	31	NWSW	189.2	A	21.0	5.65	20.3	5.4	6
S174	Uinta	43019XXXX2	4 BOOK CLIFFS	USGS-CG	UT	17S	24E	31	NWSW	189.2	B	22.2	9.31	21.5	5.7	6
DR3	Washakie	4903722304	3 DRIPPING ROCK	CELSIUS	WY	14N	94W	8	SESWNW	12415.1	A	14.1	0.0276	13.3	3.2	60
DR3	Washakie	4903722304	3 DRIPPING ROCK	CELSIUS	WY	14N	94W	8	SESWNW	12420.2	A	7.5	0.000418	6.8	3.2	300
DR3	Washakie	4903722304	3 DRIPPING ROCK	CELSIUS	WY	14N	94W	8	SESWNW	12428.1	A	12.0	0.00500	11.2	7.5	80
DR5	Washakie	4903722355	5 DRIPPING ROCK	CELSIUS	WY	14N	94W	19	SESWNE	12686.7	A	12.8	0.0120	11.9	1.4	70
DR5	Washakie	4903722355	5 DRIPPING ROCK	CELSIUS	WY	14N	94W	19	SESWNE	12704.2	B	10.6	0.00283	9.8	5.4	160
E489	Washakie	4903721053	3 UNIT FIVE MILE GULCH	AMOCO PRODUCTION	WY	21N	93W	35	C SW	10615.6	A	11.0	0.00814	10.2	12.0	140
E489	Washakie	4903721053	3 UNIT FIVE MILE GULCH	AMOCO PRODUCTION	WY	21N	93W	35	C SW	10668.9	A	6.7	0.00203	6.0	6.1	180
E489	Washakie	4903721053	3 UNIT FIVE MILE GULCH	AMOCO PRODUCTION	WY	21N	93W	35	C SW	10675.8	A	10.1	0.0255	9.2	5.5	70
S231	Washakie	4903721075	1 CHAMPLIN 237 AMOCO C	AMOCO PRODUCTION	WY	17N	94W	5	SWNESW	11110.1	A	4.3	0.000170	3.6	9.8	360
S231	Washakie	4903721075	1 CHAMPLIN 237 AMOCO C	AMOCO PRODUCTION	WY	17N	94W	5	SWNESW	11202.6	B	4.0	0.000846	3.4	2.4	260
S265	Washakie	4903720033	102-7-10 ARCH UNIT	ANADARKO E&P CO. LP	WY	19N	98W	7	SWSW	4889.0	c	17.7	10.5	16.9	1.3	6
S265	Washakie	4903720033	102-7-10 ARCH UNIT	ANADARKO E&P CO. LP	WY	19N	98W	7	SWSW	4890.0	B	8.9	0.00814	8.0	2.6	90
S276	Washakie	4903705683	65-1-7 ARCH UNIT	FOREST OIL CORP	WY	19N	99W	1	NWSE	4729.0	A	12.2	0.0261	11.3	10.2	70
S276	Washakie	4903705683	65-1-7 ARCH UNIT	FOREST OIL CORP	WY	19N	99W	1	NWSE	4736.2	A	17.3	4.87	16.5	2.0	15
S276	Washakie	4903705683	65-1-7 ARCH UNIT	FOREST OIL CORP	WY	19N	99W	1	NWSE	4756.9	A	8.5	0.00308	7.8	20.2	240
S276	Washakie	4903705683	65-1-7 ARCH UNIT	FOREST OIL CORP	WY	19N	99W	1	NWSE	4761.0	A	7.6	0.000260	6.8	19.2	460
T592	Washakie	4900721170	C-11/FEE	FUEL RESOURCES DEV	WY	12N	90W	11	NENW	2340.7	A	13.5	0.0305	12.7	6.7	80
T695	Washakie	4903723956	5-2 SIBERIA RIDGE	AMOCO PRODUCTION	WY	21N	94W	5	SW	10651.9	A	10.1	0.00677	9.2	2.9	110
WLDR	Washakie	9999999999	WILD ROSE 1	N/A	WY	N/A	N/A	N/A	N/A	10015.6	A	5.3	0.000779	4.7	4.0	340
WLDR	Washakie	9999999999	WILD ROSE 1	N/A	WY	N/A	N/A	N/A	N/A	10204.8	A	8.8	0.0231	8.0	13.3	50
B049	Wind River	4901320724	31-22 TRIBAL PHILLIPS	BROWN TOM INC	WY	4N	3E	31	NWSENW	9072.2	A	12.4	5.89	11.5	7.8	8
B049	Wind River	4901320724	31-22 TRIBAL PHILLIPS	BROWN TOM INC	WY	4N	3E	31	NWSENW	9081.0	A	11.4	1.77	10.6	6.4	8
B049	Wind River	4901320724	31-22 TRIBAL PHILLIPS	BROWN TOM INC	WY	4N	3E	31	NWSENW	11698.9	A	1.0	0.000133	0.7	18.5	600
C233	Wind River	4901320786	1-9 LYSITE	MICH WISC PIPELINE	WY	38N	91W	9	SWNE	8163.5	B	5.1	0.000245	4.4	5.1	460
C233	Wind River	4901320786	1-9 LYSITE	MICH WISC PIPELINE	WY	38N	91W	9	SWNE	8616.1	A	12.9	0.00954	12.1	8.7	90
C233	Wind River	4901320786	1-9 LYSITE	MICH WISC PIPELINE	WY	38N	91W	9	SWNE	8619.2	A	6.9	0.00164	6.1	2.7	160
C233	Wind River	4901320786	1-9 LYSITE	MICH WISC PIPELINE	WY	38N	91W	9	SWNE	11927.2	A	9.9	0.00594	9.1	1.1	100
C899	Wind River	4901320836	1-27 LOOKOUT	MONSANTO OIL	WY	39N	91W	27	CSWNE	16565.1	A	2.8	0.000224	2.2	2.9	420
C899	Wind River	4901320836	1-27 LOOKOUT	MONSANTO OIL	WY	39N	91W	27	CSWNE	16706.8	A	5.6	0.000518	4.8	3.6	260
C899	Wind River	4901320836	1-27 LOOKOUT	MONSANTO OIL	WY	39N	91W	27	CSWNE	16723.9	A	5.2	0.000702	4.5	6.2	260
D031	Wind River	4901320966	CHEVRON 2-1	MONSANTO OIL	WY	38N	91W	1	SWNENW	15681.1	A	9.9	0.00212	9.1	3.5	200
D031	Wind River	4901320966	CHEVRON 2-1	MONSANTO OIL	WY	38N	91W	1	SWNENW	15702.1	A	6.9	0.000669	6.1	29.0	320
D031	Wind River	4901320966	CHEVRON 2-1	MONSANTO OIL	WY	38N	91W	1	SWNENW	15750.1	A	4.1	0.000218	3.6	2.7	380

Appendix 4

Index of Mercury Injection Capillary Pressure Analyses by Well and Analysis

Analysis of Critical Permeability, Capillary Pressure and Electrical Properties for Mesaverde

Tight Gas Sandstones from Western U.S. Basins

US DOE # DE-FC26-05NT42660 Final Scientific/Technical Report

Alan P. Byrnes, Robert M. Cluff, John C. Webb

	Basin, API #, Well Name	Sample Depths
#01	Green River 4903505742 C-47 Tip Top Shallow	Ambient Capillary Pressure at 2699.7 Ambient Capillary Pressure at 2717.1 Ambient Capillary Pressure at 2729.9 Ambient Capillary Pressure at 2783.3 Ambient Capillary Pressure at 2817.7 Ambient Capillary Pressure at 2831.8
#02	Green River 4903506020 B-54 Big Piney	Ambient Capillary Pressure at 3433.8 Ambient Capillary Pressure at 3461.5
#03	Green River 4903506200 K-2 Mason	Ambient Capillary Pressure at 7703.7 Ambient Capillary Pressure at 9397.2
#04	Green River 4903508024 5 Pinedale	Ambient Capillary Pressure at 12158.5 Ambient Capillary Pressure at 12162
#05	Green River 4903520088 A-1 Wasp	Ambient Capillary Pressure at 10573.1 Ambient Capillary Pressure at 10573.1b Ambient Capillary Pressure at 11457.8 Ambient Capillary Pressure at 11460.6 Ambient Capillary Pressure at 11548 Ambient Capillary Pressure at 11552.3 Ambient Capillary Pressure at 11587.2 Ambient Capillary Pressure at 11605.1 Ambient Capillary Pressure at 11609.2 Ambient Capillary Pressure at 11615.1 Ambient Capillary Pressure at 11724.3 Ambient Capillary Pressure at 13672.5
#06	Green River 4903520622 1 Old Road	Ambient Capillary Pressure at 11956.1
#07	Green River 4903523799 Shell Vible 1D-11D	Ambient Capillary Pressure at 12510.1 Ambient Capillary Pressure at 12520.3 Ambient Capillary Pressure at 12520.9 Ambient Capillary Pressure at 12553.7
#08	Piceance 0504506571 MV 33-34	Ambient Capillary Pressure at 6580.1 Ambient Capillary Pressure at 6582.3 Ambient Capillary Pressure at 6591.7 Ambient Capillary Pressure at 6591.9
#09	Piceance 0504510927 PA 424-34	Ambient Capillary Pressure at 4578.8 Ambient Capillary Pressure at 4606.5 Ambient Capillary Pressure at 5193.5 Ambient Capillary Pressure at 6645.5
#10	Piceance 0504511402 Last Dance 43C-3-792	Ambient Capillary Pressure at 3544.85 Ambient Capillary Pressure at 3555.4 Ambient Capillary Pressure at 3577.55 Ambient Capillary Pressure at 3577.55b Ambient Capillary Pressure at 4004.3 Ambient Capillary Pressure at 4013.25 Ambient Capillary Pressure at 4393.6b Ambient Capillary Pressure at 4393.6c Ambient Capillary Pressure at 5715.4 Ambient Capillary Pressure at 6042.4

Appendix 4

Index of Mercury Injection Capillary Pressure Analyses by Well and Analysis

Analysis of Critical Permeability, Capillary Pressure and Electrical Properties for Mesaverde

Tight Gas Sandstones from Western U.S. Basins

US DOE # DE-FC26-05NT42660 Final Scientific/Technical Report

Alan P. Byrnes, Robert M. Cluff, John C. Webb

	Basin, API #, Well Name	Sample Depths
#11	Piceance 0504560011 MWX-2	Ambient Capillary Pressure at 5838.7 Ambient Capillary Pressure at 7272.8
#12	Piceance 05045xxxxx 1 Book Cliffs	Ambient Capillary Pressure at 255.9
#13	Piceance 0510309406 M-30-2-96W/D-037934	Ambient Capillary Pressure at 6380.6
#14	Piceance 0510310391 Willow Ridge T63X-2G	Ambient Capillary Pressure at 10547.5 Ambient Capillary Pressure at 10555.7 Ambient Capillary Pressure at 10574.5 Ambient Capillary Pressure at 10633.6
#15	Piceance 051063xxxx 21011-5 Moon Lake	Ambient Capillary Pressure at 790.3
#16	Powder River 4900525627 1 Barlow 21-20	Ambient Capillary Pressure at 6969.9 Ambient Capillary Pressure at 6996 Ambient Capillary Pressure at 7053 Ambient Capillary Pressure at 7060.4 Ambient Capillary Pressure at 7076.6
#17	Powder River 4900905481 3 Shawnee	Ambient Capillary Pressure at 6998.5
#18	Powder River 4900906335 2 Shawnee	Ambient Capillary Pressure at 6946.2 Ambient Capillary Pressure at 6979
#19	Powder River 4900921513 2 Fred State	Ambient Capillary Pressure at 7538 Ambient Capillary Pressure at 7550.1
#21	Sand Wash 0508106724 1-791-2613 Craig Dome	Ambient Capillary Pressure at 3469.2
#22	Uinta 4304730545 2-7 Flat Mesa	Ambient Capillary Pressure at 6351.5 Ambient Capillary Pressure at 6468.4 Ambient Capillary Pressure at 6475.3 Ambient Capillary Pressure at 6482 Ambient Capillary Pressure at 6486.4 Ambient Capillary Pressure at 6486.7 Ambient Capillary Pressure at 6515.6b Ambient Capillary Pressure at 6515.6c Ambient Capillary Pressure at 6527.6 Ambient Capillary Pressure at 6530.3 Ambient Capillary Pressure at 6550.5 Ambient Capillary Pressure at 6688.2 Ambient Capillary Pressure at 7276.2 Ambient Capillary Pressure at 7279.9 Ambient Capillary Pressure at 7293.5 Ambient Capillary Pressure at 7311.9 Ambient Capillary Pressure at 7312.7 Ambient Capillary Pressure at 7689.7 Ambient Capillary Pressure at 7712.7 Ambient Capillary Pressure at 7885.4 Ambient Capillary Pressure at 7885.4c
#24	Uinta 4304730852 4-5 US Lamco	Ambient Capillary Pressure 5638.8
#25	Uinta 4304730860 3-24 US Lamco	Ambient Capillary Pressure at 6812.2 Ambient Capillary Pressure at 7158.9
#26	Uinta 4304735788 NBU 9-20-360 State	Ambient Capillary Pressure at 8279.5
#27	Uinta 4304736565 NBU 1022-1A Natural Butte	Ambient Capillary Pressure at 7808.7
#28	Uinta 43019xxxx1 3 Book Cliffs	Ambient Capillary Pressure at 175.3 Ambient Capillary Pressure at 392.5

Appendix 4

Index of Mercury Injection Capillary Pressure Analyses by Well and Analysis

Analysis of Critical Permeability, Capillary Pressure and Electrical Properties for Mesaverde

Tight Gas Sandstones from Western U.S. Basins

US DOE # DE-FC26-05NT42660 Final Scientific/Technical Report

Alan P. Byrnes, Robert M. Cluff, John C. Webb

	Basin, API #, Well Name	Sample Depths
#29	Uinta 43019xxxx2 4 Book Cliffs	Ambient Capillary Pressure at 161.7 Ambient Capillary Pressure at 183.2 Ambient Capillary Pressure at 183.4 Ambient Capillary Pressure at 189.3
#30	Washakie 4900721170 C-11 Fee	Ambient Capillary Pressure at 2340.7
#31	Washakie 4903705683 65-1-7 Arch Unit	Ambient Capillary Pressure at 4728 Ambient Capillary Pressure at 4729 Ambient Capillary Pressure at 4736.1 Ambient Capillary Pressure at 4757.9
#32	Washakie 4903720033 102-7-10 Arch Unit	Ambient Capillary Pressure at 4878 Ambient Capillary Pressure at 4899
#33	Washakie 4903721053 Unit 3 Five Mile Gulch	Ambient Capillary Pressure at 10608.7 Ambient Capillary Pressure at 10615.8 Ambient Capillary Pressure at 10645 Ambient Capillary Pressure at 10666.3 Ambient Capillary Pressure at 10669 Ambient Capillary Pressure at 10681.2
#34	Washakie 4903722304 3 Dripping Rock	Ambient Capillary Pressure at 12416.9 Ambient Capillary Pressure at 12441.9
#35	Washakie 4903722355 5 Dripping Rock	Ambient Capillary Pressure at 12671.9 Ambient Capillary Pressure at 12673.6
#36	Washakie 9999999999 Wild Rose 1	Ambient Capillary Pressure at 9837.65 Ambient Capillary Pressure at 9839.35
#38	Wind River 4901320966 2-1 Chevron	Ambient Capillary Pressure at 15682.8
#39	Wind River 4901320836 1-27 Lookout	Ambient Capillary Pressure at 16678.9
#01	Green River 4903505742 C-47 Tip Top Shallow	Confining Stress Capillary Pressure at 2699.7 Confining Stress Capillary Pressure at 2717.1 Confining Stress Capillary Pressure at 2729.9
#02	Green River 4903506020 B-54 Big Piney	Confining Stress Capillary Pressure at 3403.9 Confining Stress Capillary Pressure at 3433.8 Confining Stress Capillary Pressure at 3461.5 Confining Stress Capillary Pressure at 3480.8 Confining Stress Capillary Pressure at 3515.8
#03	Green River 4903506200 K-2 Mason	Confining Stress Capillary Pressure at 7703.7 Confining Stress Capillary Pressure at 9397.2
#05	Green River 4903520088 A-1 Wasp	Confining Stress Capillary Pressure at 11457.8 Confining Stress Capillary Pressure at 11460.6 Confining Stress Capillary Pressure at 11552.3 Confining Stress Capillary Pressure at 11587.2 Confining Stress Capillary Pressure at 11609.2 Confining Stress Capillary Pressure at 11615.1 Confining Stress Capillary Pressure at 11706.8 Confining Stress Capillary Pressure at 13672.5
#06	Green River 4903520622 1 Old Road	Confining Stress Capillary Pressure at 11936.3

Appendix 4

Index of Mercury Injection Capillary Pressure Analyses by Well and Analysis

Analysis of Critical Permeability, Capillary Pressure and Electrical Properties for Mesaverde

Tight Gas Sandstones from Western U.S. Basins

US DOE # DE-FC26-05NT42660 Final Scientific/Technical Report

Alan P. Byrnes, Robert M. Cluff, John C. Webb

	Basin, API #, Well Name	Sample Depths
#09	Piceance 0504510927 PA 424-34	Confining Stress Capillary Pressure at 4578.8 Confining Stress Capillary Pressure at 4606.5 Confining Stress Capillary Pressure at 5193.5 Confining Stress Capillary Pressure at 6645.5
#10	Piceance 0504511402 Last Dance 43C-3-792	Confining Stress Capillary Pressure at 3544.85 Confining Stress Capillary Pressure at 3555.4 Confining Stress Capillary Pressure at 4004.3 Confining Stress Capillary Pressure at 4013.25 Confining Stress Capillary Pressure at 4416.6 Confining Stress Capillary Pressure at 5715.4 Confining Stress Capillary Pressure at 6042.4
#12	Piceance 05045xxxxx 1 Book Cliffs	Confining Stress Capillary Pressure at 255.9
#16	Powder River 4900525627 1 Barlow 21-20	Confining Stress Capillary Pressure at 6994.1 Confining Stress Capillary Pressure at 7001.1 Confining Stress Capillary Pressure at 7027.2
#17	Powder River 4900905481 3 Shawnee	Confining Stress Capillary Pressure at 6988
#18	Powder River 4900906335 2 Shawnee	Confining Stress Capillary Pressure at 6991.2
#19	Powder River 4900921513 2 Fred State	Confining Stress Capillary Pressure at 7544.1 Confining Stress Capillary Pressure at 7546.7 Confining Stress Capillary Pressure at 7550.1
#20	Sand Wash 0508106718 1-691-0513 West Craig	Confining Stress Capillary Pressure at 1747.9a Confining Stress Capillary Pressure at 1747.9b Confining Stress Capillary Pressure at 1750.1
#21	Sand Wash 0508106724 1-791-2613 Craig Dome	Confining Stress Capillary Pressure at 3469.2 Confining Stress Capillary Pressure at 6468.4 Confining Stress Capillary Pressure at 6486.4 Confining Stress Capillary Pressure at 6486.7 Confining Stress Capillary Pressure at 6527.6 Confining Stress Capillary Pressure at 6530.3 Confining Stress Capillary Pressure at 6550.5 Confining Stress Capillary Pressure at 7279.9 Confining Stress Capillary Pressure at 7293.5 Confining Stress Capillary Pressure at 7311.9 Confining Stress Capillary Pressure at 7312.7 Confining Stress Capillary Pressure at 7689.7
#24	Uinta 4304730852 4-5 US Lamco	Confining Stress Capillary Pressure at 5618.3 Confining Stress Capillary Pressure at 5633.1
#25	Uinta 4304730860 3-24 US Lamco	Confining Stress Capillary Pressure at 6812.2
#26	Uinta 4304735788 NBU 9-20-360 State	Confining Stress Capillary Pressure at 8184.5 Confining Stress Capillary Pressure at 8184.6 Confining Stress Capillary Pressure at 8185.7 Confining Stress Capillary Pressure at 8279.5

Appendix 4

Index of Mercury Injection Capillary Pressure Analyses by Well and Analysis

Analysis of Critical Permeability, Capillary Pressure and Electrical Properties for Mesaverde

Tight Gas Sandstones from Western U.S. Basins

US DOE # DE-FC26-05NT42660 Final Scientific/Technical Report

Alan P. Byrnes, Robert M. Cluff, John C. Webb

	Basin, API #, Well Name	Sample Depths
#27	Uinta 4304736565 NBU 1022-1A Natural Butte	Confining Stress Capillary Pressure at 7808.7 Confining Stress Capillary Pressure at 7825.5 Confining Stress Capillary Pressure at 7825.5b Confining Stress Capillary Pressure at 7853.5
#28	Uinta 43019xxxx1 3 Book Cliffs	Confining Stress Capillary Pressure at 175.3 Confining Stress Capillary Pressure at 389.8 Confining Stress Capillary Pressure at 392.5
#31	Washakie 4903705683 65-1-7 Arch Unit	Confining Stress Capillary Pressure at 4743 Confining Stress Capillary Pressure at 4745
#32	Washakie 4903720033 102-7-10 Arch Unit	Confining Stress Capillary Pressure at 4899
#33	Washakie 4903721053 Unit 3 Five Mile Gulch	Confining Stress Capillary Pressure at 10650 Confining Stress Capillary Pressure at 10669
#35	Washakie 4903722355 5 Dripping Rock	Confining Stress Capillary Pressure at 12671.9 Confining Stress Capillary Pressure at 12673.6 Confining Stress Capillary Pressure at 12686.5
#36	Washakie 9999999999 Wild Rose 1	Confining Stress Capillary Pressure at 10133.5 Confining Stress Capillary Pressure at 10207.8
#06	Green River 4903520622 1 Old Road	Drainage Imbibition at 11921.8
#06	Green River 4903520622 1 Old Road	Drainage Imbibition at 11936.3
#10	Piceance 0504511402 Last Dance 43C-3-792	Drainage Imbibition at 4416.6
#11	Piceance 0504560011 MWX-2	Drainage Imbibition at 5734.1
#11	Piceance 0504560011 MWX-2	Drainage Imbibition at 6554.3
#11	Piceance 0504560011 MWX-2	Drainage Imbibition at 7877.6
#13	Piceance 0510309406 M-30-2-96W/D-037934	Drainage Imbibition at 6404.8
#15	Piceance 051063xxxx 21011-5 Moon Lake	Drainage Imbibition at 812.9
#16	Powder River 4900525627 1 Barlow 21-20	Drainage Imbibition at 6994.1
#16	Powder River 4900525627 1 Barlow 21-20	Drainage Imbibition at 7001.1
#16	Powder River 4900525627 1 Barlow 21-20	Drainage Imbibition at 7027.2
#17	Powder River 4900905481 3 Shawnee	Drainage Imbibition at 6988
#18	Powder River 4900906335 2 Shawnee	Drainage Imbibition at 6991.2
#19	Powder River 4900921513 2 Fred State	Drainage Imbibition at 7544.1
#19	Powder River 4900921513 2 Fred State	Drainage Imbibition at 7546.7
#23	Uinta 4304730584 11-7F River Bend Unit	Drainage Imbibition at 8294.4
#24	Uinta 4304730852 4-5 US Lamco	Drainage Imbibition at 5618.3
#24	Uinta 4304730852 4-5 US Lamco	Drainage Imbibition at 5633.1
#24	Uinta 4304730852 4-5 US Lamco	Drainage Imbibition at 5638.8
#26	Uinta 4304735788 NBU 9-20-360 State	Drainage Imbibition at 8184.5
#26	Uinta 4304735788 NBU 9-20-360 State	Drainage Imbibition at 8184.6
#26	Uinta 4304735788 NBU 9-20-360 State	Drainage Imbibition at 8185.7
#27	Uinta 4304736565 NBU 1022-1A Natural Butte	Drainage Imbibition at 7853.5
#28	Uinta 43019xxxx1 3 Book Cliffs	Drainage Imbibition at 124.7
#31	Washakie 4903705683 65-1-7 Arch Unit	Drainage Imbibition at 4743
#31	Washakie 4903705683 65-1-7 Arch Unit	Drainage Imbibition at 4745
#31	Washakie 4903705683 65-1-7 Arch Unit	Drainage Imbibition at 4757.9
#32	Washakie 4903720033 102-7-10 Arch Unit	Drainage Imbibition at 4899
#35	Washakie 4903722355 5 Dripping Rock	Drainage Imbibition at 12686.5
#37	Wind River 4901320724 31-22 Tribal Phillips	Drainage Imbibition at 9072.1

Appendix 4

Mercury Injection Capillary Pressure Analysis (Ambient Analyses)

US DOE #De-FC26-05NT42660 Final Scientific/Technical Report

Alan P. Byrnes, Robert M. Cluff, John C. Webb

					Green River 4903505742 C-47 Tip Top Shallow R780 - 2699.7 ft (B)	Green River 4903505742 C-47 Tip Top Shallow R780 - 2717.1 ft (B)	Green River 4903505742 C-47 Tip Top Shallow R780 - 2729.9 ft (B)	Green River 4903505742 C-47 Tip Top Shallow R780 - 2783.3 ft (B)	Green River 4903505742 C-47 Tip Top Shallow R780 - 2817.7 ft (B)	Green River 4903505742 C-47 Tip Top Shallow R780 - 2831.8 ft (B)	Green River 4903506020 B-54 Big Piney E712 - 3433.8 ft (B)	Green River 4903506020 B-54 Big Piney E712 - 3461.5 ft (B)
					2.86E-02	1.13E-02	7.86E-03	2.37E-02	2.04E-03	3.14E-03	2.58E-02	2.77E-02
					29.0	11.5	7.96	24.0	2.07	3.18	26.1	28.1
					21.7	19.9	19.2	22.1	19.8	20.9	17.7	18.7
Mercury Injection Capillary Pressure (psia)	Mercury Injection Capillary Pressure (kPa)	Approx. Pore Entry Diameter (μ m)	Approx. Gas-Water Height Above Free Water Level (ft)	Approx. Gas-Water Height Above Free Water Level (m)	Ambient Cumulative Wetting Phase Saturation (% pore vol)	Ambient Cumulative Wetting Phase Saturation (% pore vol)	Ambient Cumulative Wetting Phase Saturation (% pore vol)					
2.0	13.8	107	0.10	0.03	100.0	100.0	100.0	100.0	100.0	100.0	100.0	100.0
2.5	17.2	86	0.64	0.20	100.0	100.0	100.0	100.0	100.0	100.0	100.0	100.0
3.3	22.8	65	0.80	0.24	99.8	100.0	100.0	100.0	100.0	100.0	99.8	99.8
4.3	29.6	50	1.06	0.32	99.7	100.0	100.0	100.0	100.0	100.0	99.6	99.7
5.5	37.9	39	1.38	0.42	99.6	100.0	100.0	100.0	100.0	100.0	99.5	99.5
7.2	49.6	30	1.76	0.54	99.4	100.0	100.0	100.0	100.0	100.0	99.3	99.3
9.3	64.1	23	2.31	0.70	99.3	100.0	100.0	99.9	100.0	100.0	99.1	99.2
12.0	82.7	18	2.98	0.91	99.0	100.0	100.0	99.7	100.0	100.0	98.9	98.8
15.5	106.9	14	3.85	1.17	98.8	99.9	100.0	99.6	100.0	100.0	98.6	98.3
20	137.9	11	4.97	1.51	98.3	99.8	99.8	99.2	99.8	99.9	97.9	98.1
25	172.4	8.6	6.41	2.0	77.4	99.6	99.7	79.1	99.8	99.8	76.8	63.0
35	241.3	6.1	8.01	2.4	64.7	99.3	99.6	65.6	99.8	99.7	64.0	55.0
45	310.3	4.8	11.2	3.4	55.2	69.2	79.3	56.0	99.6	99.4	54.7	47.6
55	379.2	3.9	14.4	4.4	50.2	61.2	62.6	51.4	99.5	95.4	50.0	44.0
75	517.1	2.9	17.6	5.4	46.8	56.7	56.9	48.8	99.2	75.6	46.8	41.5
95	655.0	2.3	24.0	7.3	42.1	51.3	50.1	45.4	75.9	63.6	42.8	37.4
120	827.4	1.8	30.5	9.3	38.7	47.5	45.0	42.7	65.8	57.6	39.8	34.9
150	1,034	1.4	38.5	11.7	34.4	43.2	41.2	38.1	68.1	51.1	36.5	31.4
200	1,379	1.1	48.1	14.7	32.0	40.6	38.6	36.8	53.6	47.8	34.3	29.4
260	1,793	0.82	64.1	19.5	29.0	37.1	35.2	33.4	46.8	43.1	31.4	26.5
350	2,413	0.61	83.4	25.4	26.7	34.4	32.8	30.4	43.7	38.9	28.8	24.1
430	2,965	0.50	112	34.1	24.3	31.7	30.2	26.5	39.5	33.5	25.7	21.3
550	3,792	0.39	138	42.1	22.7	29.7	28.4	23.6	36.0	30.7	23.7	19.7
725	4,999	0.30	176	53.6	20.9	27.8	26.2	20.7	32.8	26.9	21.5	17.8
925	6,378	0.23	232	70.7	18.8	25.3	18.8	17.4	29.7	23.0	18.9	15.6
1,200	8,274	0.18	297	90.5	16.7	23.0	20.7	15.3	27.1	20.3	17.8	14.1
1,550	10,687	0.14	385	117.3	15.3	20.6	18.7	12.8	24.7	17.8	15.9	12.2
2,000	13,790	0.11	497	151.5	13.8	18.3	16.1	11.2	22.6	15.5	14.4	10.9
2,600	17,926	0.08	641	195.4	12.0	16.3	14.3	9.6	20.7	13.6	13.0	9.7
3,350	23,097	0.06	834	254.2	10.5	14.3	12.2	8.3	19.2	11.8	11.5	8.3
4,300	29,647	0.05	1074	327.4	9.3	12.5	10.3	6.9	17.4	10.3	10.1	6.9
5,550	38,266	0.04	1378	420.0	8.0	11.0	8.7	5.8	15.7	9.2	9.0	6.1
7,200	49,642	0.03	1779	542.2	7.1	9.6	7.4	5.1	14.1	8.1	7.8	5.5
9,300	64,121	0.02	2308	703.5	6.2	8.6	6.2	4.2	12.6	7.3	7.2	5.1
			2981	908.6	5.4	7.6	5.2	3.6	11.6	6.4	6.4	4.8

All Hg calculations assume air-mercury $s=484$ dyne/cm, contact angle=140deg.

Gas-Brine Pc assumes insitu gas-brine $s_{osq}=40$ dyne/cm

Gas-Brine height assumes gas density gradient = 0.0935 psi/ft; 2.115 kPa/m

Gas-Brine height assumes brine density gradient 0.430 psi/ft; 9.727 kPa/m

Analysis of Critical Permeability, Capillary Pressure

and Electrical Properties for Mesaverde

Tight Gas Sandstones from Western U.S. Basins

US DOE # DE-FC26-05NT42660 Final Scientific Report

Alan P. Byrnes, Robert M. Cluff, John C. Webb

Appendix 4
Mercury Injection Capillary Pressure Analysis (Ambient Analyses)
US DOE #De-FC26-05NT42660 Final Scientific/Technical Report
Alan P. Byrnes, Robert M. Cluff, John C. Webb

					Green River 4903506200 K-2 Mason S873 - 7703.7 ft (A1)	Green River 4903506200 K-2 Mason S873 - 9397.2 ft (A1)	Green River 4903508024 5 Pinedale T195 - 12158.5 ft (B)	Green River 4903508024 5 Pinedale T195 - 12162 ft (B)	Green River 4903520088 A-1 Wasp B029- 10573.1 ft (A)	Green River 4903520088 A-1 Wasp B029- 10573.1 ft (C)	Green River 4903520088 A-1 Wasp B029 - 11457.8 ft (B)	Green River 4903520088 A-1 Wasp B029 - 11460.6 ft (B)
					1.35E-04	4.05E-08	1.25E-05	7.80E-07	1.58E-07	1.58E-07	1.58E-07	2.52E-05
					0.137	0.000041	0.0127	0.00079	0.00016	0.00016	0.00016	0.0255
					11.4	8.3	10.6	6.6	3.3	3.0	3.3	4.4
Mercury Injection Capillary Pressure (psia)	Mercury Injection Capillary Pressure (kPa)	Approx. Pore Entry Diameter (μ m)	Approx. Gas-Water Height Above Free Water Level (ft)	Approx. Gas-Water Height Above Free Water Level (m)	Ambient Cumulative Wetting Phase Saturation (% pore vol)							
2.0	13.8	107	0.10	0.03	100.0	100.0	100.0	100.0	100.0	100.0	100.0	100.0
2.5	17.2	86	0.64	0.20	100.0	100.0	100.0	100.0	100.0	100.0	100.0	100.0
3.3	22.8	65	0.80	0.24	100.0	100.0	100.0	100.0	100.0	100.0	100.0	99.3
4.3	29.6	50	1.06	0.32	100.0	100.0	100.0	100.0	100.0	100.0	100.0	98.5
5.5	37.9	39	1.38	0.42	100.0	100.0	100.0	100.0	100.0	100.0	100.0	97.8
7.2	49.6	30	1.76	0.54	100.0	100.0	100.0	100.0	100.0	100.0	100.0	97.7
9.3	64.1	23	2.31	0.70	100.0	100.0	100.0	100.0	100.0	100.0	100.0	97.7
12.0	82.7	18	2.98	0.91	100.0	100.0	100.0	100.0	100.0	100.0	100.0	96.6
15.5	106.9	14	3.85	1.17	100.0	100.0	100.0	100.0	100.0	100.0	100.0	96.2
20	137.9	11	4.97	1.51	100.0	100.0	100.0	100.0	100.0	100.0	100.0	95.4
25	172.4	8.6	6.41	2.0	99.9	100.0	100.0	100.0	100.0	100.0	100.0	94.7
35	241.3	6.1	8.01	2.4	99.7	100.0	100.0	100.0	100.0	100.0	100.0	94.7
45	310.3	4.8	11.2	3.4	99.6	100.0	100.0	100.0	100.0	100.0	100.0	94.2
55	379.2	3.9	14.4	4.4	99.5	100.0	100.0	100.0	100.0	100.0	99.7	93.8
75	517.1	2.9	17.6	5.4	99.3	100.0	100.0	100.0	100.0	100.0	100.0	93.6
95	655.0	2.3	24.0	7.3	99.2	100.0	100.0	100.0	100.0	100.0	99.1	93.3
120	827.4	1.8	30.5	9.3	98.5	100.0	100.0	100.0	100.0	100.0	98.8	93.1
150	1,034	1.4	38.5	11.7	71.2	100.0	100.0	100.0	100.0	100.0	97.6	92.6
200	1,379	1.1	48.1	14.7	63.8	100.0	99.9	100.0	100.0	100.0	97.6	92.6
260	1,793	0.82	64.1	19.5	55.5	99.7	99.6	100.0	100.0	100.0	97.0	91.8
350	2,413	0.61	83.4	25.4	50.3	99.6	98.7	100.0	100.0	100.0	97.0	91.8
430	2,965	0.50	112	34.1	44.2	99.5	88.0	99.7	100.0	100.0	95.1	90.4
550	3,792	0.39	138	42.1	40.6	99.2	69.5	98.9	100.0	100.0	90.0	80.4
725	4,999	0.30	176	53.6	36.7	97.6	59.9	98.2	100.0	100.0	71.9	66.6
925	6,378	0.23	232	70.7	32.6	83.7	53.0	90.5	99.6	100.0	57.6	55.4
1,200	8,274	0.18	297	90.5	28.7	75.4	48.7	81.4	98.0	100.0	50.9	48.9
1,550	10,687	0.14	385	117.3	25.4	67.9	43.8	70.0	96.1	95.1	46.0	42.5
2,000	13,790	0.11	497	151.5	21.8	62.4	39.1	59.1	89.9	87.8	40.1	36.3
2,600	17,926	0.08	641	195.4	18.6	58.0	35.3	50.8	79.8	79.5	35.3	32.0
3,350	23,097	0.06	834	254.2	16.1	53.8	30.5	44.8	67.2	65.7	30.1	27.0
4,300	29,647	0.05	1074	327.4	13.7	49.3	25.9	38.1	60.6	54.4	25.0	21.9
5,550	38,266	0.04	1378	420.0	11.6	44.9	22.2	32.4	54.5	47.2	19.9	17.2
7,200	49,642	0.03	1779	542.2	10.1	40.9	19.4	27.3	47.9	37.5	16.0	12.1
9,300	64,121	0.02	2308	703.5	8.9	36.7	16.9	23.3	43.0	31.4	13.2	8.9
			2981	908.6	7.4	32.8	14.7	19.5	36.9	24.7	9.4	4.9

All Hg calculations assume air-mercury $s=484$ dyne/cm, contact angle=140deg.

Gas-Brine Pc assumes insitu gas-brine $\sigma\cos\theta=40$ dyne/cm

Gas-Brine height assumes gas density gradient = 0.0935 psi/ft; 2.115 kPa/m

Gas-Brine height assumes brine density gradient 0.430 psi/ft; 9.727 kPa/m

Analysis of Critical Permeability, Capillary Pressure

and Electrical Properties for Mesaverde

Tight Gas Sandstones from Western U.S. Basins

US DOE # DE-FC26-05NT42660 Final Scientific Report

Alan P. Byrnes, Robert M. Cluff, John C. Webb

Appendix 4

Mercury Injection Capillary Pressure Analysis (Ambient Analyses)

US DOE #De-FC26-05NT42660 Final Scientific/Technical Report

Alan P. Byrnes, Robert M. Cluff, John C. Webb

					Green River 4903520088 A-1 Wasp B029 -11548 ft (B)	Green River 4903520088 A-1 Wasp B029 -11552.3ft (B)	Green River 4903520088 A-1 Wasp B029 -11587.2 ft (B)	Green River 4903520088 A-1 Wasp B029 -11605.1 ft (B)	Green River 4903520088 A-1 Wasp B029 -11609.2 ft (B)	Green River 4903520088 A-1 Wasp B029 -11615.1 ft (B)	Green River 4903520088 A-1 Wasp B029 -11724.3 ft (B)	Green River 4903520088 A-1 Wasp B029 -13672.5 ft	
					1.18E-06	3.75E-07	3.85E-07	2.27E-07	8.19E-06	1.67E-06	5.92E-07	6.41E-08	
					0.0012	0.00038	0.00039	0.00023	0.00830	0.00169	0.00060	0.000065	
					6.2	4.2	4.2	3.2	5.8	5.0	4.1	2.6	
					Ambient Cumulative Wetting Phase Saturation (% pore vol)								
Mercury Injection Capillary Pressure (psia)	Mercury Injection Capillary Pressure (kPa)	Approx. Pore Entry Diameter (μ m)	Approx. Gas-Water Height Above Free Water Level (ft)	Approx. Gas-Water Height Above Free Water Level (m)	100.0	100.0	100.0	100.0	100.0	100.0	100.0	100.0	
2.0	13.8	107	0.10	0.03	100.0	100.0	100.0	100.0	100.0	100.0	100.0	100.0	
2.5	17.2	86	0.64	0.20	100.0	100.0	100.0	100.0	100.0	100.0	100.0	100.0	
3.3	22.8	65	0.80	0.24	100.0	100.0	100.0	100.0	100.0	100.0	100.0	100.0	
4.3	29.6	50	1.06	0.32	100.0	100.0	100.0	100.0	100.0	100.0	100.0	100.0	
5.5	37.9	39	1.38	0.42	100.0	100.0	100.0	100.0	100.0	100.0	100.0	100.0	
7.2	49.6	30	1.76	0.54	100.0	100.0	100.0	100.0	100.0	100.0	100.0	100.0	
9.3	64.1	23	2.31	0.70	100.0	100.0	100.0	100.0	100.0	100.0	100.0	100.0	
12.0	82.7	18	2.98	0.91	100.0	100.0	100.0	100.0	100.0	100.0	100.0	100.0	
15.5	106.9	14	3.85	1.17	100.0	100.0	100.0	100.0	100.0	100.0	100.0	100.0	
20	137.9	11	4.97	1.51	100.0	100.0	100.0	100.0	100.0	100.0	100.0	100.0	
25	172.4	8.6	6.41	2.0	100.0	100.0	100.0	100.0	100.0	100.0	100.0	100.0	
35	241.3	6.1	8.01	2.4	100.0	100.0	100.0	100.0	100.0	100.0	100.0	100.0	
45	310.3	4.8	11.2	3.4	100.0	100.0	100.0	100.0	100.0	100.0	100.0	100.0	
55	379.2	3.9	14.4	4.4	100.0	100.0	100.0	100.0	100.0	100.0	100.0	100.0	
75	517.1	2.9	17.6	5.4	100.0	100.0	100.0	100.0	100.0	100.0	100.0	100.0	
95	655.0	2.3	24.0	7.3	100.0	100.0	100.0	100.0	100.0	100.0	100.0	100.0	
120	827.4	1.8	30.5	9.3	100.0	100.0	100.0	100.0	100.0	100.0	99.2	100.0	
150	1,034	1.4	38.5	11.7	100.0	100.0	100.0	100.0	100.0	100.0	98.5	100.0	
200	1,379	1.1	48.1	14.7	100.0	100.0	100.0	100.0	100.0	100.0	98.4	100.0	
260	1,793	0.82	64.1	19.5	100.0	100.0	100.0	100.0	99.3	99.4	97.2	100.0	
350	2,413	0.61	83.4	25.4	100.0	100.0	100.0	100.0	99.2	99.4	97.2	100.0	
430	2,965	0.50	112	34.1	100.0	100.0	100.0	100.0	98.2	99.2	96.9	100.0	
550	3,792	0.39	138	42.1	100.0	100.0	100.0	99.2	95.2	98.2	95.5	100.0	
725	4,999	0.30	176	53.6	100.0	100.0	100.0	100.0	80.3	95.3	88.5	100.0	
925	6,378	0.23	232	70.7	99.4	99.9	99.9	96.1	65.6	80.1	79.2	100.0	
1,200	8,274	0.18	297	90.5	97.4	90.5	96.7	94.7	57.2	70.7	74.0	99.2	
1,550	10,687	0.14	385	117.3	88.7	79.8	91.6	88.1	51.8	61.7	69.6	95.1	
2,000	13,790	0.11	497	151.5	73.5	70.7	79.9	79.3	45.8	53.9	64.1	87.9	
2,600	17,926	0.08	641	195.4	58.5	64.5	61.6	74.6	40.3	47.0	59.1	78.9	
3,350	23,097	0.06	834	254.2	48.8	58.7	48.0	65.2	35.6	41.3	53.6	67.2	
4,300	29,647	0.05	1074	327.4	42.2	52.5	38.3	59.8	30.8	35.5	46.9	57.7	
5,550	38,266	0.04	1378	420.0	37.2	46.9	30.8	53.3	26.6	29.7	41.3	48.7	
7,200	49,642	0.03	1779	542.2	32.5	38.4	22.9	46.6	22.4	25.0	34.4	38.9	
9,300	64,121	0.02	2308	703.5	28.8	31.3	17.6	40.6	19.9	20.7	28.8	29.6	
			2981	908.6	25.5	25.0	10.9	32.1	16.1	16.1	22.1	22.4	

All Hg calculations assume air-mercury $s=484$ dyne/cm, contact angle=140deg.

Gas-Brine Pc assumes insitu gas-brine $s_{osq}=40$ dyne/cm

Gas-Brine height assumes gas density gradient = 0.0935 psi/ft; 2.115 kPa/m

Gas-Brine height assumes brine density gradient 0.430 psi/ft; 9.727 kPa/m

Analysis of Critical Permeability, Capillary Pressure

and Electrical Properties for Mesaverde

Tight Gas Sandstones from Western U.S. Basins

US DOE # DE-FC26-05NT42660 Final Scientific Report

Alan P. Byrnes, Robert M. Cluff, John C. Webb

Appendix 4
Mercury Injection Capillary Pressure Analysis (Ambient Analyses)
US DOE #DE-FC26-05NT42660 Final Scientific/Technical Report
Alan P. Byrnes, Robert M. Cluff, John C. Webb

					Green River 4903520622 1 Old Road E894 - 11956.1 ft (B)	Green River 4903523799 Shell Vible 1D-11D VBL- 12510.1 ft (A)	Green River 4903523799 Shell Vible 1D-11D VBL- 12520.3 ft (A)	Green River 4903523799 Shell Vible 1D-11D VBL- 12520.9 ft (A)	Green River 4903523799 Shell Vible 1D-11D VBL- 12553.7 ft (A)	Piceance 504506571 MV 33-34 E436 -6580.1 ft (B)	Piceance 504506571 MV 33-34 E436 - 6582.3 ft (B)	Piceance 504506571 MV 33-34 E436 - 6591.7 ft (B)
<i>In situ</i> Klinkenberg Permeability (μm^2)=					1.90E-05	2.47E-05	2.07E-07	1.88E-07	3.65E-08	4.64E-07	3.39E-07	2.96E-07
<i>In situ</i> Klinkenberg Permeability (mD) =					0.0193	0.0250	0.00021	0.00019	0.000037	0.00047	0.000344	0.00030
Routine Porosity (%) =					9.1	7.3	4.3	3.4	1.3	5.6	5.7	3.1
Mercury Injection Capillary Pressure (psia)	Mercury Injection Capillary Pressure (kPa)	Approx. Pore Entry Diameter (μm)	Approx. Gas-Water Height Above Free Water Level (ft)	Approx. Gas-Water Height Above Free Water Level (m)	Ambient Cumulative Wetting Phase Saturation (% pore vol)	Ambient Cumulative Wetting Phase Saturation (% pore vol)	Ambient Cumulative Wetting Phase Saturation (% pore vol)	Ambient Cumulative Wetting Phase Saturation (% pore vol)	Ambient Cumulative Wetting Phase Saturation (% pore vol)	Ambient Cumulative Wetting Phase Saturation (% pore vol)	Ambient Cumulative Wetting Phase Saturation (% pore vol)	Ambient Cumulative Wetting Phase Saturation (% pore vol)
2.0	13.8	107	0.10	0.03	100.0	100.0	100.0	100.0	100.0	100.0	100.0	100.0
2.5	17.2	86	0.64	0.20	100.0	100.0	100.0	100.0	100.0	100.0	100.0	100.0
3.3	22.8	65	0.80	0.24	100.0	100.0	100.0	100.0	100.0	100.0	100.0	100.0
4.3	29.6	50	1.06	0.32	100.0	100.0	100.0	100.0	100.0	100.0	100.0	100.0
5.5	37.9	39	1.38	0.42	100.0	100.0	100.0	100.0	100.0	100.0	100.0	100.0
7.2	49.6	30	1.76	0.54	100.0	100.0	100.0	100.0	100.0	100.0	100.0	100.0
9.3	64.1	23	2.31	0.70	100.0	100.0	100.0	100.0	100.0	100.0	100.0	100.0
12.0	82.7	18	2.98	0.91	100.0	100.0	100.0	100.0	100.0	100.0	100.0	100.0
15.5	106.9	14	3.85	1.17	100.0	100.0	100.0	100.0	100.0	100.0	100.0	100.0
20	137.9	11	4.97	1.51	100.0	100.0	100.0	100.0	100.0	100.0	100.0	100.0
25	172.4	8.6	6.41	2.0	100.0	100.0	100.0	100.0	100.0	100.0	100.0	100.0
35	241.3	6.1	8.01	2.4	99.9	100.0	100.0	100.0	100.0	100.0	100.0	100.0
45	310.3	4.8	11.2	3.4	99.6	99.8	100.0	100.0	100.0	99.8	100.0	100.0
55	379.2	3.9	14.4	4.4	99.3	99.6	100.0	100.0	100.0	99.6	100.0	100.0
75	517.1	2.9	17.6	5.4	99.2	99.2	100.0	100.0	100.0	99.5	100.0	100.0
95	655.0	2.3	24.0	7.3	99.1	98.8	100.0	100.0	100.0	99.3	100.0	100.0
120	827.4	1.8	30.5	9.3	98.9	98.4	100.0	100.0	100.0	99.0	100.0	100.0
150	1,034	1.4	38.5	11.7	98.2	97.1	100.0	100.0	100.0	98.7	100.0	100.0
200	1,379	1.1	48.1	14.7	98.1	92.8	100.0	100.0	100.0	98.5	100.0	100.0
260	1,793	0.82	64.1	19.5	97.8	76.9	100.0	100.0	100.0	98.4	100.0	100.0
350	2,413	0.61	83.4	25.4	97.5	66.3	99.9	100.0	100.0	98.4	100.0	100.0
430	2,965	0.50	112	34.1	96.8	54.3	99.3	100.0	100.0	98.4	100.0	100.0
550	3,792	0.39	138	42.1	95.7	48.0	98.9	100.0	100.0	97.3	100.0	99.8
725	4,999	0.30	176	53.6	92.5	41.5	91.6	99.8	100.0	97.3	100.0	99.6
925	6,378	0.23	232	70.7	73.7	34.4	78.2	99.3	100.0	96.4	100.0	98.4
1,200	8,274	0.18	297	90.5	59.9	29.1	70.0	99.3	100.0	95.1	100.0	97.3
1,550	10,687	0.14	385	117.3	47.8	23.1	61.1	97.8	100.0	89.4	94.5	93.8
2,000	13,790	0.11	497	151.5	42.1	17.8	56.0	97.1	99.4	76.0	84.4	91.3
2,600	17,926	0.08	641	195.4	37.2	13.0	51.4	96.7	99.1	66.3	75.6	90.4
3,350	23,097	0.06	834	254.2	32.4	8.0	46.1	95.6	97.3	58.2	66.5	87.1
4,300	29,647	0.05	1074	327.4	28.1	3.9	41.1	93.6	94.1	50.1	58.8	81.8
5,550	38,266	0.04	1378	420.0	24.3	1.5	35.8	91.4	89.4	43.8	51.7	77.5
7,200	49,642	0.03	1779	542.2	20.5	1.0	26.5	85.1	81.4	38.2	45.8	73.5
9,300	64,121	0.02	2308	703.5	17.6	0.9	20.3	67.1	72.5	33.7	41.0	68.4
			2981	908.6	14.4	0.5	15.6	46.5	63.6	29.8	35.2	64.6

All Hg calculations assume air-mercury $s=484$ dyne/cm, contact angle=140deg.

Gas-Brine Pc assumes insitu gas-brine $\sigma\cos\theta=40$ dyne/cm

Gas-Brine height assumes gas density gradient = 0.0935 psi/ft; 2.115 kPa/m

Gas-Brine height assumes brine density gradient 0.430 psi/ft; 9.727 kPa/m

Analysis of Critical Permeability, Capillary Pressure
 and Electrical Properties for Mesaverde

Tight Gas Sandstones from Western U.S. Basins

US DOE # DE-FC26-05NT42660 Final Scientific Report

Alan P. Byrnes, Robert M. Cluff, John C. Webb

Appendix 4
Mercury Injection Capillary Pressure Analysis (Ambient Analyses)
US DOE #De-FC26-05NT42660 Final Scientific/Technical Report
Alan P. Byrnes, Robert M. Cluff, John C. Webb

					Piceance 504506571 MV 33-34 E436 - 6591.9 ft (B)	Piceance 504510927 PA 424-34 PA424 - 4578.8 ft (A1)	Piceance 504510927 PA 424-34 PA424 - 4606.5 ft (A1)	Piceance 504510927 PA 424-34 PA424 - 5193.5 ft (A1)	Piceance 504510927 PA 424-34 PA424 - 6645.5 ft (A1)	Piceance 504511402 Last Dance 43C-3-792 B43C - 3544.85 ft (B)	Piceance 504511402 Last Dance 43C-3-792 B43C - 3555.4 ft (C)	Piceance 504511402 Last Dance 43C-3-792 B43C - 3577.55 ft (B)
<i>In situ</i> Klinkenberg Permeability (μm^2)=					1.48E-07	2.47E-07	1.06E-06	5.87E-06	2.24E-06	4.23E-04	1.44E-03	5.82E-08
<i>In situ</i> Klinkenberg Permeability (mD) =					0.000150	0.00025	0.00107	0.00595	0.00227	0.429	1.46	0.000059
Routine Porosity (%) =					3.4	4.5	12.7	7.8	10.2	11.4	12.0	2.1
Mercury Injection Capillary Pressure (psia)	Mercury Injection Capillary Pressure (kPa)	Approx. Pore Entry Diameter (μm)	Approx. Gas-Water Height Above Free Water Level (ft)	Approx. Gas-Water Height Above Free Water Level (m)	Ambient Cumulative Wetting Phase Saturation (% pore vol)	Ambient Cumulative Wetting Phase Saturation (% pore vol)	Ambient Cumulative Wetting Phase Saturation (% pore vol)	Ambient Cumulative Wetting Phase Saturation (% pore vol)	Ambient Cumulative Wetting Phase Saturation (% pore vol)	Ambient Cumulative Wetting Phase Saturation (% pore vol)	Ambient Cumulative Wetting Phase Saturation (% pore vol)	Ambient Cumulative Wetting Phase Saturation (% pore vol)
2.0	13.8	107	0.10	0.03	100.0	100.0	100.0	100.0	100.0	100.0	100.0	100.0
2.5	17.2	86	0.64	0.20	100.0	100.0	100.0	100.0	100.0	100.0	100.0	100.0
3.3	22.8	65	0.80	0.24	100.0	100.0	100.0	100.0	100.0	100.0	100.0	100.0
4.3	29.6	50	1.06	0.32	100.0	100.0	100.0	100.0	100.0	100.0	100.0	100.0
5.5	37.9	39	1.38	0.42	100.0	100.0	100.0	100.0	100.0	100.0	100.0	100.0
7.2	49.6	30	1.76	0.54	100.0	100.0	100.0	100.0	100.0	100.0	100.0	100.0
9.3	64.1	23	2.31	0.70	100.0	100.0	100.0	100.0	100.0	100.0	100.0	100.0
12.0	82.7	18	2.98	0.91	100.0	100.0	100.0	100.0	100.0	100.0	100.0	100.0
15.5	106.9	14	3.85	1.17	100.0	100.0	100.0	100.0	100.0	100.0	100.0	100.0
20	137.9	11	4.97	1.51	100.0	100.0	100.0	100.0	100.0	100.0	100.0	100.0
25	172.4	8.6	6.41	2.0	100.0	100.0	100.0	100.0	100.0	100.0	100.0	100.0
35	241.3	6.1	8.01	2.4	100.0	100.0	100.0	100.0	100.0	99.8	98.4	94.3
45	310.3	4.8	11.2	3.4	100.0	100.0	100.0	100.0	100.0	99.3	93.3	83.3
55	379.2	3.9	14.4	4.4	100.0	100.0	100.0	100.0	100.0	98.5	71.2	100.0
75	517.1	2.9	17.6	5.4	100.0	100.0	100.0	100.0	100.0	97.3	64.1	100.0
95	655.0	2.3	24.0	7.3	100.0	100.0	99.9	99.4	99.8	70.1	56.4	100.0
120	827.4	1.8	30.5	9.3	100.0	99.3	99.8	98.9	99.6	59.4	51.2	100.0
150	1,034	1.4	38.5	11.7	100.0	98.8	99.6	98.1	99.2	52.2	45.6	100.0
200	1,379	1.1	48.1	14.7	100.0	98.7	99.3	95.3	99.2	49.6	42.9	100.0
260	1,793	0.82	64.1	19.5	100.0	97.3	99.0	74.1	98.8	46.5	39.2	100.0
350	2,413	0.61	83.4	25.4	100.0	87.8	79.6	64.7	98.8	44.0	37.0	100.0
430	2,965	0.50	112	34.1	100.0	72.9	61.3	58.6	98.3	41.2	34.2	100.0
550	3,792	0.39	138	42.1	100.0	64.8	54.7	55.3	84.6	39.4	32.7	100.0
725	4,999	0.30	176	53.6	100.0	60.0	49.1	51.6	69.2	37.0	31.0	100.0
925	6,378	0.23	232	70.7	99.2	53.9	42.7	47.6	59.6	34.0	29.1	100.0
1,200	8,274	0.18	297	90.5	97.9	48.3	39.6	43.5	54.3	32.2	28.0	100.0
1,550	10,687	0.14	385	117.3	95.5	45.4	34.9	39.5	48.4	30.3	25.8	99.6
2,000	13,790	0.11	497	151.5	90.6	42.1	30.1	36.2	44.4	28.1	24.1	97.6
2,600	17,926	0.08	641	195.4	84.3	39.0	27.2	33.5	39.9	26.9	22.8	94.5
3,350	23,097	0.06	834	254.2	79.3	36.3	23.0	30.5	35.5	24.9	21.4	91.0
4,300	29,647	0.05	1074	327.4	71.9	33.1	19.7	28.2	31.3	22.5	19.7	89.4
5,550	38,266	0.04	1378	420.0	65.9	30.5	15.6	25.7	27.2	20.8	18.5	86.4
7,200	49,642	0.03	1779	542.2	59.9	28.5	12.0	23.5	24.1	17.2	16.9	85.1
9,300	64,121	0.02	2308	703.5	54.6	26.4	9.0	21.3	21.2	14.2	15.5	83.4
			2981	908.6	46.0	22.7	7.7	18.5	18.5	12.9	13.7	77.9

All Hg calculations assume air-mercury $s=484$ dyne/cm, contact angle=140deg.
 Gas-Brine Pc assumes insitu gas-brine $\sigma\cos\theta=40$ dyne/cm
 Gas-Brine height assumes gas density gradient = 0.0935 psi/ft; 2.115 kPa/m
 Gas-Brine height assumes brine density gradient 0.430 psi/ft; 9.727 kPa/m
 Analysis of Critical Permeability, Capillary Pressure
 and Electrical Properties for Mesaverde
 Tight Gas Sandstones from Western U.S. Basins
 US DOE # DE-FC26-05NT42660 Final Scientific Report
 Alan P. Byrnes, Robert M. Cluff, John C. Webb

Appendix 4
Mercury Injection Capillary Pressure Analysis (Ambient Analyses)
US DOE #DE-FC26-05NT42660 Final Scientific/Technical Report
Alan P. Byrnes, Robert M. Cluff, John C. Webb

					Piceance 504511402 Last Dance 43C-3-792 B43C - 3577.55 ft (C)	Piceance 504511402 Last Dance 43C-3-792 B43C - 4004.3 ft (B)	Piceance 504511402 Last Dance 43C-3-792 B43C - 4013.25 ft (B)	Piceance 504511402 Last Dance 43C-3-792 B43C - 4393.6 ft (B)	Piceance 504511402 Last Dance 43C-3-792 B43C -4393.6 ft (C)	Piceance 504511402 Last Dance 43C-3-792 B43C - 5715.4 ft (A)	Piceance 504511402 Last Dance 43C-3-792 B43C - 6042.4 ft (C)
<i>In situ</i> Klinkenberg Permeability (μm^2)=					8.68E-08	2.84E-05	1.88E-04	5.75E-06	5.74E-06	3.15E-06	1.28E-06
<i>In situ</i> Klinkenberg Permeability (mD) =					0.000088	0.0288	0.190	0.00583	0.00582	0.00319	0.00130
Routine Porosity (%) =					2.0	10.2	12.9	8.7	8.6	7.7	5.8
Mercury Injection Capillary Pressure (psia)	Mercury Injection Capillary Pressure (kPa)	Approx. Pore Entry Diameter (μm)	Approx. Gas-Water Height Above Free Water Level (ft)	Approx. Gas-Water Height Above Free Water Level (m)	Ambient Cumulative Wetting Phase Saturation (% pore vol)	Ambient Cumulative Wetting Phase Saturation (% pore vol)	Ambient Cumulative Wetting Phase Saturation (% pore vol)	Ambient Cumulative Wetting Phase Saturation (% pore vol)	Ambient Cumulative Wetting Phase Saturation (% pore vol)	Ambient Cumulative Wetting Phase Saturation (% pore vol)	Ambient Cumulative Wetting Phase Saturation (% pore vol)
2.0	13.8	107	0.10	0.03	100.0	100.0	100.0	100.0	100.0	100.0	100.0
2.5	17.2	86	0.64	0.20	100.0	100.0	100.0	100.0	100.0	100.0	100.0
3.3	22.8	65	0.80	0.24	100.0	100.0	99.5	100.0	100.0	100.0	100.0
4.3	29.6	50	1.06	0.32	100.0	100.0	99.0	100.0	100.0	100.0	100.0
5.5	37.9	39	1.38	0.42	100.0	100.0	98.6	100.0	100.0	100.0	100.0
7.2	49.6	30	1.76	0.54	100.0	100.0	98.5	100.0	100.0	100.0	100.0
9.3	64.1	23	2.31	0.70	100.0	100.0	98.4	100.0	100.0	100.0	100.0
12.0	82.7	18	2.98	0.91	100.0	100.0	98.0	100.0	100.0	100.0	100.0
15.5	106.9	14	3.85	1.17	100.0	100.0	97.9	100.0	100.0	100.0	100.0
20	137.9	11	4.97	1.51	100.0	100.0	97.7	100.0	100.0	100.0	100.0
25	172.4	8.6	6.41	2.0	100.0	100.0	97.6	100.0	100.0	100.0	100.0
35	241.3	6.1	8.01	2.4	100.0	100.0	97.3	100.0	100.0	100.0	100.0
45	310.3	4.8	11.2	3.4	100.0	100.0	96.9	100.0	100.0	100.0	100.0
55	379.2	3.9	14.4	4.4	100.0	100.0	94.4	100.0	100.0	100.0	100.0
75	517.1	2.9	17.6	5.4	100.0	100.0	83.7	100.0	100.0	100.0	99.9
95	655.0	2.3	24.0	7.3	100.0	99.9	67.3	100.0	99.8	100.0	99.6
120	827.4	1.8	30.5	9.3	100.0	99.6	60.9	99.7	99.6	100.0	99.4
150	1,034	1.4	38.5	11.7	100.0	90.8	53.3	98.9	98.9	100.0	99.2
200	1,379	1.1	48.1	14.7	100.0	82.4	49.8	98.3	97.8	100.0	99.0
260	1,793	0.82	64.1	19.5	100.0	73.3	45.7	84.9	79.4	100.0	98.9
350	2,413	0.61	83.4	25.4	100.0	67.8	42.7	67.6	65.0	100.0	98.7
430	2,965	0.50	112	34.1	100.0	61.1	39.5	60.9	59.0	99.9	98.3
550	3,792	0.39	138	42.1	100.0	56.4	37.4	57.8	55.8	99.7	95.4
725	4,999	0.30	176	53.6	100.0	49.9	35.1	55.3	52.3	98.7	83.2
925	6,378	0.23	232	70.7	99.6	42.6	32.0	52.5	49.0	94.7	75.1
1,200	8,274	0.18	297	90.5	99.3	38.0	29.8	52.1	46.8	91.3	68.9
1,550	10,687	0.14	385	117.3	98.9	33.2	25.9	47.3	44.5	79.5	65.5
2,000	13,790	0.11	497	151.5	97.4	29.4	22.5	45.0	41.3	60.9	59.9
2,600	17,926	0.08	641	195.4	96.7	26.5	19.0	42.2	38.4	51.5	56.7
3,350	23,097	0.06	834	254.2	93.3	22.9	15.2	38.7	34.2	47.8	53.2
4,300	29,647	0.05	1074	327.4	88.9	20.1	12.5	34.2	28.3	43.6	48.9
5,550	38,266	0.04	1378	420.0	85.9	17.1	10.3	30.3	23.0	40.2	45.8
7,200	49,642	0.03	1779	542.2	79.2	14.7	8.2	26.5	18.3	37.0	41.7
9,300	64,121	0.02	2308	703.5	77.7	12.5	6.7	23.7	15.2	32.2	36.0
			2981	908.6	72.5	10.2	5.4	21.6	11.8		32.3

All Hg calculations assume air-mercury $s=484$ dyne/cm, contact angle=140deg.

Gas-Brine Pc assumes insitu gas-brine $s_{\text{cosq}}=40$ dyne/cm

Gas-Brine height assumes gas density gradient = 0.0935 psi/ft; 2.115 kPa/m

Gas-Brine height assumes brine density gradient 0.430 psi/ft; 9.727 kPa/m

Analysis of Critical Permeability, Capillary Pressure
 and Electrical Properties for Mesaverde

Tight Gas Sandstones from Western U.S. Basins

US DOE # DE-FC26-05NT42660 Final Scientific Report

Alan P. Byrnes, Robert M. Cluff, John C. Webb

Appendix 4
Mercury Injection Capillary Pressure Analysis (Ambient Analyses)
US DOE #De-FC26-05NT42660 Final Scientific/Technical Report
Alan P. Byrnes, Robert M. Cluff, John C. Webb

				Piceance 504560011 MWX-2 T649 - 5838.7 ft (B)	Piceance 504560011 MWX-2 T649 - 7272.8 ft (B)	Piceance 05045xxxxx 1 Book Cliffs R091 - 255.9 ft (A1)	Piceance 510309406 M-30-2-96W/D-037934 E458 - 6380.6 ft	Piceance 510310391 Willow Ridge T63X-2G T63X-2G - 10547.5 ft (B)	Piceance 510310391 Willow Ridge T63X-2G T63X-2G - 10555.7 ft (B)	Piceance 510310391 Willow Ridge T63X-2G T63X-2G - 10574.5 ft (B)	
				<i>In situ</i> Klinkenberg Permeability (μm^2)=	1.25E-06	1.47E-06	1.12E-01	4.30E-04	3.39E-07	2.10E-06	1.33E-06
				<i>In situ</i> Klinkenberg Permeability (mD) =	0.00127	0.00149	113	0.436	0.000343	0.00213	0.00135
				Routine Porosity (%) =	6.9	9.0	24.5	13.5	5.5	7.2	6.2
Mercury Injection Capillary Pressure (psia)	Mercury Injection Capillary Pressure (kPa)	Approx. Pore Entry Diameter (μm)	Approx. Gas-Water Height Above Free Water Level (ft)	Approx. Gas-Water Height Above Free Water Level (m)	Ambient Cumulative Wetting Phase Saturation (% pore vol)	Ambient Cumulative Wetting Phase Saturation (% pore vol)	Ambient Cumulative Wetting Phase Saturation (% pore vol)	Ambient Cumulative Wetting Phase Saturation (% pore vol)	Ambient Cumulative Wetting Phase Saturation (% pore vol)	Ambient Cumulative Wetting Phase Saturation (% pore vol)	Ambient Cumulative Wetting Phase Saturation (% pore vol)
2.0	13.8	107	0.10	0.03	100.0	100.0	100.0	100.0	100.0	100.0	100.0
2.5	17.2	86	0.64	0.20	100.0	100.0	100.0	100.0	100.0	100.0	100.0
3.3	22.8	65	0.80	0.24	100.0	100.0	99.7	100.0	100.0	100.0	100.0
4.3	29.6	50	1.06	0.32	100.0	100.0	99.3	100.0	100.0	100.0	100.0
5.5	37.9	39	1.38	0.42	100.0	100.0	99.0	100.0	100.0	100.0	100.0
7.2	49.6	30	1.76	0.54	100.0	100.0	98.7	100.0	100.0	100.0	100.0
9.3	64.1	23	2.31	0.70	100.0	100.0	97.8	100.0	100.0	100.0	100.0
12.0	82.7	18	2.98	0.91	100.0	100.0	94.3	99.8	100.0	100.0	100.0
15.5	106.9	14	3.85	1.17	100.0	100.0	76.9	99.7	100.0	100.0	100.0
20	137.9	11	4.97	1.51	100.0	100.0	61.7	99.5	100.0	100.0	100.0
25	172.4	8.6	6.41	2.0	100.0	100.0	54.6	99.5	100.0	100.0	100.0
35	241.3	6.1	8.01	2.4	100.0	100.0	50.7	99.3	100.0	100.0	100.0
45	310.3	4.8	11.2	3.4	100.0	100.0	46.4	98.9	100.0	99.7	100.0
55	379.2	3.9	14.4	4.4	100.0	100.0	43.7	96.4	100.0	99.7	100.0
75	517.1	2.9	17.6	5.4	100.0	100.0	41.6	93.6	100.0	99.6	100.0
95	655.0	2.3	24.0	7.3	100.0	100.0	38.6	87.1	100.0	99.6	100.0
120	827.4	1.8	30.5	9.3	100.0	100.0	36.4	81.4	100.0	99.2	100.0
150	1,034	1.4	38.5	11.7	100.0	100.0	33.1	74.6	100.0	98.9	100.0
200	1,379	1.1	48.1	14.7	100.0	100.0	31.4	69.3	100.0	98.7	100.0
260	1,793	0.82	64.1	19.5	99.7	100.0	28.6	64.8	100.0	98.7	100.0
350	2,413	0.61	83.4	25.4	99.3	99.9	26.5	61.4	100.0	96.7	100.0
430	2,965	0.50	112	34.1	93.8	99.7	23.6	57.7	100.0	81.7	100.0
550	3,792	0.39	138	42.1	85.0	99.1	21.8	55.3	100.0	72.7	98.4
725	4,999	0.30	176	53.6	78.0	90.9	19.7	52.7	100.0	65.6	85.4
925	6,378	0.23	232	70.7	70.5	71.4	17.0	50.0	100.0	57.3	72.3
1,200	8,274	0.18	297	90.5	65.3	65.9	15.5	47.9	100.0	52.1	62.4
1,550	10,687	0.14	385	117.3	58.8	55.4	13.0	45.9	90.2	46.1	53.3
2,000	13,790	0.11	497	151.5	51.8	49.4	10.9	43.5	75.3	40.8	46.4
2,600	17,926	0.08	641	195.4	45.5	44.3	9.1	40.8	65.1	35.9	40.1
3,350	23,097	0.06	834	254.2	39.6	39.4	7.7	36.7	53.1	31.4	33.8
4,300	29,647	0.05	1074	327.4	32.6	34.8	6.3	32.6	45.4	26.4	27.1
5,550	38,266	0.04	1378	420.0	29.4	30.9	5.1	28.8	38.6	21.3	21.7
7,200	49,642	0.03	1779	542.2	24.4	27.3	4.3	23.0	30.7	16.3	16.3
9,300	64,121	0.02	2308	703.5	21.2	24.5	3.6	18.5	25.5	13.1	12.4
			2981	908.6	17.8	21.8	2.9	15.5	18.8	9.0	8.4

All Hg calculations assume air-mercury $s=484$ dyne/cm, contact angle=140deg.

Gas-Brine Pc assumes insitu gas-brine $s_{\text{osq}}=40$ dyne/cm

Gas-Brine height assumes gas density gradient = 0.0935 psi/ft; 2.115 kPa/m

Gas-Brine height assumes brine density gradient 0.430 psi/ft; 9.727 kPa/m

Analysis of Critical Permeability, Capillary Pressure
 and Electrical Properties for Mesaverde

Tight Gas Sandstones from Western U.S. Basins

US DOE # DE-FC26-05NT42660 Final Scientific Report

Alan P. Byrnes, Robert M. Cluff, John C. Webb

Appendix 4

Mercury Injection Capillary Pressure Analysis (Ambient Analyses)

US DOE #De-FC26-05NT42660 Final Scientific/Technical Report

Alan P. Byrnes, Robert M. Cluff, John C. Webb

					Piceance 510310391 Willow Ridge T63X-2G T63X-2G - 10633.6 ft (B) 8.68E-08 0.000088 3.0	Piceance 051063xxxx 21011-5 Moon Lake s905 - 790.3 ft (B) 9.87E-08 0.00010 5.0	Powder River 4900525627 1 Barlow 21-20 E393 - 6969.9 ft (B) 1.23E-03 1.25 20.4	Powder River 4900525627 1 Barlow 21-20 E393 - 6996 ft (B) 1.07E-06 0.00108 6.2	Powder River 4900525627 1 Barlow 21-20 E393 - 7053 ft (B) 5.90E-03 5.98 23.8	Powder River 4900525627 1 Barlow 21-20 E393 - 7060.4 ft (B) 6.61E-05 0.067 15.4	Powder River 4900525627 1 Barlow 21-20 E393 - 7076.6 ft (A) 1.02E-03 1.03 22.4	Powder River 4900905481 3 Shawnee S838 - 6998.5 ft (A) 1.19E-06 0.00121 5.8
					Ambient Cumulative Wetting Phase Saturation (% pore vol)	Ambient Cumulative Wetting Phase Saturation (% pore vol)	Ambient Cumulative Wetting Phase Saturation (% pore vol)	Ambient Cumulative Wetting Phase Saturation (% pore vol)	Ambient Cumulative Wetting Phase Saturation (% pore vol)	Ambient Cumulative Wetting Phase Saturation (% pore vol)	Ambient Cumulative Wetting Phase Saturation (% pore vol)	Ambient Cumulative Wetting Phase Saturation (% pore vol)
Mercury Injection Capillary Pressure (psia)	Mercury Injection Capillary Pressure (kPa)	Approx. Pore Entry Diameter (μ m)	Approx. Gas-Water Height Above Free Water Level (ft)	Approx. Gas-Water Height Above Free Water Level (m)								
2.0	13.8	107	0.10	0.03	100.0	100.0	100.0	100.0	100.0	100.0	100.0	100.0
2.5	17.2	86	0.64	0.20	100.0	100.0	100.0	100.0	100.0	100.0	100.0	100.0
3.3	22.8	65	0.80	0.24	100.0	100.0	100.0	100.0	99.8	100.0	100.0	100.0
4.3	29.6	50	1.06	0.32	100.0	100.0	100.0	100.0	99.7	100.0	100.0	100.0
5.5	37.9	39	1.38	0.42	100.0	100.0	100.0	100.0	99.6	100.0	100.0	100.0
7.2	49.6	30	1.76	0.54	100.0	100.0	100.0	100.0	99.6	100.0	100.0	100.0
9.3	64.1	23	2.31	0.70	100.0	100.0	100.0	100.0	99.5	100.0	99.9	100.0
12.0	82.7	18	2.98	0.91	100.0	100.0	100.0	100.0	99.5	100.0	99.9	100.0
15.5	106.9	14	3.85	1.17	100.0	100.0	100.0	100.0	99.4	100.0	99.8	100.0
20	137.9	11	4.97	1.51	100.0	100.0	99.9	100.0	99.3	100.0	99.8	100.0
25	172.4	8.6	6.41	2.0	100.0	100.0	99.8	100.0	99.2	99.9	99.8	100.0
35	241.3	6.1	8.01	2.4	100.0	100.0	99.8	100.0	92.5	99.9	99.7	100.0
45	310.3	4.8	11.2	3.4	100.0	100.0	99.7	100.0	92.5	99.9	99.7	100.0
55	379.2	3.9	14.4	4.4	100.0	100.0	99.6	100.0	75.5	99.8	99.5	100.0
75	517.1	2.9	17.6	5.4	100.0	100.0	99.4	100.0	70.3	99.7	99.7	100.0
95	655.0	2.3	24.0	7.3	100.0	100.0	79.5	100.0	65.3	99.7	82.1	100.0
120	827.4	1.8	30.5	9.3	100.0	100.0	71.9	100.0	62.4	99.4	69.8	100.0
150	1,034	1.4	38.5	11.7	100.0	100.0	66.2	100.0	59.3	98.1	62.4	100.0
200	1,379	1.1	48.1	14.7	100.0	100.0	63.3	100.0	57.4	95.7	59.3	100.0
260	1,793	0.82	64.1	19.5	100.0	100.0	60.1	99.6	54.9	92.2	55.5	100.0
350	2,413	0.61	83.4	25.4	100.0	100.0	57.3	99.2	52.4	87.1	52.0	100.0
430	2,965	0.50	112	34.1	100.0	100.0	54.1	98.1	49.3	78.3	47.4	99.8
550	3,792	0.39	138	42.1	100.0	100.0	51.7	93.9	46.9	70.1	44.0	99.5
725	4,999	0.30	176	53.6	100.0	100.0	48.8	80.7	43.6	60.2	39.5	98.8
925	6,378	0.23	232	70.7	100.0	99.9	45.2	63.9	39.4	51.3	34.3	97.1
1,200	8,274	0.18	297	90.5	100.0	99.8	41.8	53.8	35.5	45.1	30.0	95.4
1,550	10,687	0.14	385	117.3	98.5	99.5	37.9	48.6	30.9	38.3	26.0	91.6
2,000	13,790	0.11	497	151.5	96.8	99.3	33.4	44.1	24.5	33.2	21.8	88.6
2,600	17,926	0.08	641	195.4	88.8	98.9	28.7	40.9	17.6	28.4	18.3	85.0
3,350	23,097	0.06	834	254.2	79.4	98.5	23.3	37.4	12.9	24.1	14.9	80.6
4,300	29,647	0.05	1074	327.4	62.0	97.6	17.7	33.9	10.2	20.6	12.7	76.1
5,550	38,266	0.04	1378	420.0	49.8	96.6	13.2	31.0	8.4	17.6	11.3	70.4
7,200	49,642	0.03	1779	542.2	38.5	94.4	10.1	27.8	7.3	15.8	10.1	62.5
9,300	64,121	0.02	2308	703.5	29.2	91.0	8.0	25.6	6.6	13.8	9.3	53.7
			2981	908.6	19.7	78.1	6.9	23.4	5.9	12.2	8.5	25.1

All Hg calculations assume air-mercury $s=484$ dyne/cm, contact angle=140deg.

Gas-Brine Pc assumes insitu gas-brine $s_{osq}=40$ dyne/cm

Gas-Brine height assumes gas density gradient = 0.0935 psi/ft; 2.115 kPa/m

Gas-Brine height assumes brine density gradient 0.430 psi/ft; 9.727 kPa/m

Analysis of Critical Permeability, Capillary Pressure

and Electrical Properties for Mesaverde

Tight Gas Sandstones from Western U.S. Basins

US DOE # DE-FC26-05NT42660 Final Scientific Report

Alan P. Byrnes, Robert M. Cluff, John C. Webb

Appendix 4
Mercury Injection Capillary Pressure Analysis (Ambient Analyses)
US DOE #DE-FC26-05NT42660 Final Scientific/Technical Report
Alan P. Byrnes, Robert M. Cluff, John C. Webb

					Powder River 4900906335 2 Shawnee S835 - 6946.2 ft (B)	Powder River 4900906335 2 Shawnee S835 - 6979 ft (B)	Powder River 4900921513 2 Fred State E932 - 7538.0 ft (B)	Powder River 4900921513 2 Fred State E932 - 7550.1 ft (B)	Sand Wash 508106724 1-791-2613 Craig Dome T715 - 3469.2 ft (B)	Uinta 4304730545 2-7 Flat Mesa E946 - 6351.5 ft	Uinta 4304730545 2-7 Flat Mesa E946 - 6468.4 ft
<i>In situ</i> Klinkenberg Permeability (μm^2)=					1.07E-03	1.10E-03	1.99E-03	1.88E-07	2.68E-02	8.29E-06	3.82E-04
<i>In situ</i> Klinkenberg Permeability (mD) =					1.08	1.11	2.02	0.00019	27.2	0.0084	0.387
Routine Porosity (%) =					13.7	17.5	16.7	4.0	17.9	10.0	12.1
Mercury Injection Capillary Pressure (psia)	Mercury Injection Capillary Pressure (kPa)	Approx. Pore Entry Diameter (μm)	Approx. Gas-Water Height Above Free Water Level (ft)	Approx. Gas-Water Height Above Free Water Level (m)	Ambient Cumulative Wetting Phase Saturation (% pore vol)						
2.0	13.8	107	0.10	0.03	100.0	100.0	100.0	100.0	100.0	100.0	100.0
2.5	17.2	86	0.64	0.20	100.0	100.0	100.0	100.0	100.0	100.0	100.0
3.3	22.8	65	0.80	0.24	100.0	100.0	100.0	100.0	99.8	100.0	100.0
4.3	29.6	50	1.06	0.32	100.0	100.0	100.0	100.0	99.5	100.0	100.0
5.5	37.9	39	1.38	0.42	100.0	100.0	100.0	100.0	99.4	100.0	100.0
7.2	49.6	30	1.76	0.54	100.0	100.0	100.0	100.0	99.3	100.0	100.0
9.3	64.1	23	2.31	0.70	100.0	100.0	100.0	100.0	99.1	100.0	100.0
12.0	82.7	18	2.98	0.91	100.0	100.0	100.0	100.0	98.9	100.0	100.0
15.5	106.9	14	3.85	1.17	100.0	100.0	100.0	100.0	98.5	100.0	100.0
20	137.9	11	4.97	1.51	99.8	99.8	100.0	100.0	96.6	100.0	100.0
25	172.4	8.6	6.41	2.0	99.6	99.7	99.9	100.0	76.6	100.0	100.0
35	241.3	6.1	8.01	2.4	99.3	99.6	99.7	100.0	69.1	100.0	100.0
45	310.3	4.8	11.2	3.4	98.2	99.4	98.5	100.0	57.3	100.0	99.9
55	379.2	3.9	14.4	4.4	93.3	97.8	84.9	100.0	48.9	100.0	99.6
75	517.1	2.9	17.6	5.4	87.1	92.5	75.6	100.0	44.1	100.0	99.1
95	655.0	2.3	24.0	7.3	72.9	76.8	65.5	100.0	41.7	100.0	96.9
120	827.4	1.8	30.5	9.3	62.0	65.9	59.8	100.0	39.0	100.0	73.7
150	1,034	1.4	38.5	11.7	51.9	56.1	53.9	100.0	35.8	100.0	62.4
200	1,379	1.1	48.1	14.7	48.0	50.2	51.0	100.0	33.9	100.0	57.3
260	1,793	0.82	64.1	19.5	43.9	45.6	47.5	100.0	31.8	99.3	52.2
350	2,413	0.61	83.4	25.4	41.0	42.6	44.5	100.0	29.9	91.7	46.7
430	2,965	0.50	112	34.1	38.3	39.7	41.4	99.9	27.9	78.1	41.7
550	3,792	0.39	138	42.1	36.5	37.9	39.1	99.8	26.5	71.9	38.3
725	4,999	0.30	176	53.6	34.3	36.1	36.3	99.6	25.1	65.7	34.7
925	6,378	0.23	232	70.7	32.2	33.9	33.1	99.2	23.3	58.5	30.9
1,200	8,274	0.18	297	90.5	30.1	32.1	30.3	99.0	21.6	52.4	27.4
1,550	10,687	0.14	385	117.3	27.5	30.0	27.8	98.9	20.3	45.7	25.0
2,000	13,790	0.11	497	151.5	24.9	28.0	25.2	98.2	18.6	38.8	22.0
2,600	17,926	0.08	641	195.4	22.2	25.6	22.8	94.9	16.4	31.8	19.3
3,350	23,097	0.06	834	254.2	19.6	22.6	20.6	86.0	15.1	26.0	16.5
4,300	29,647	0.05	1074	327.4	17.4	19.7	18.4	75.8	14.0	20.3	13.8
5,550	38,266	0.04	1378	420.0	15.4	16.9	16.5	69.9	12.8	15.8	11.1
7,200	49,642	0.03	1779	542.2	14.0	14.4	14.4	62.6	11.5	11.2	8.7
9,300	64,121	0.02	2308	703.5	12.6	12.5	12.5	54.9	10.7	8.6	6.8
			2981	908.6	11.2	10.7	10.7	49.1	9.8	5.9	4.4

All Hg calculations assume air-mercury $s=484$ dyne/cm, contact angle=140deg.

Gas-Brine Pc assumes insitu gas-brine $\sigma\cos\theta=40$ dyne/cm

Gas-Brine height assumes gas density gradient = 0.0935 psi/ft; 2.115 kPa/m

Gas-Brine height assumes brine density gradient 0.430 psi/ft; 9.727 kPa/m

Analysis of Critical Permeability, Capillary Pressure

and Electrical Properties for Mesaverde

Tight Gas Sandstones from Western U.S. Basins

US DOE # DE-FC26-05NT42660 Final Scientific Report

Alan P. Byrnes, Robert M. Cluff, John C. Webb

Appendix 4
Mercury Injection Capillary Pressure Analysis (Ambient Analyses)
US DOE #De-FC26-05NT42660 Final Scientific/Technical Report
Alan P. Byrnes, Robert M. Cluff, John C. Webb

					Uinta 4304730545 2-7 Flat Mesa E946 - 6475.3 ft	Uinta 4304730545 2-7 Flat Mesa E946 - 6482 ft	Uinta 4304730545 2-7 Flat Mesa E946 - 6486.4 ft (B)	Uinta 4304730545 2-7 Flat Mesa E946 - 6486.7 ft (B)	Uinta 4304730545 2-7 Flat Mesa E946 - 6515.6 ft (B)	Uinta 4304730545 2-7 Flat Mesa E946 - 6515.6 ft (C)	Uinta 4304730545 2-7 Flat Mesa E946 - 6527.6 ft (B)	Uinta 4304730545 2-7 Flat Mesa E946 - 6530.3 ft (B)
<i>In situ</i> Klinkenberg Permeability (μm^2)=					4.73E-04	9.08E-08	6.29E-04	2.51E-04	1.59E-03	1.65E-03	5.05E-05	4.11E-05
<i>In situ</i> Klinkenberg Permeability (mD) =					0.479	0.000092	0.637	0.254	1.61	1.67	0.0512	0.0416
Routine Porosity (%) =					12.1	3.7	12.2	9.6	15.4	13.8	9.8	9.5
Mercury Injection Capillary Pressure (psia)	Mercury Injection Capillary Pressure (kPa)	Approx. Pore Entry Diameter (μm)	Approx. Gas-Water Height Above Free Water Level (ft)	Approx. Gas-Water Height Above Free Water Level (m)	Ambient Cumulative Wetting Phase Saturation (% pore vol)	Ambient Cumulative Wetting Phase Saturation (% pore vol)	Ambient Cumulative Wetting Phase Saturation (% pore vol)	Ambient Cumulative Wetting Phase Saturation (% pore vol)	Ambient Cumulative Wetting Phase Saturation (% pore vol)	Ambient Cumulative Wetting Phase Saturation (% pore vol)	Ambient Cumulative Wetting Phase Saturation (% pore vol)	Ambient Cumulative Wetting Phase Saturation (% pore vol)
2.0	13.8	107	0.10	0.03	100.0	100.0	100.0	100.0	100.0	100.0	100.0	100.0
2.5	17.2	86	0.64	0.20	100.0	100.0	100.0	100.0	100.0	100.0	100.0	100.0
3.3	22.8	65	0.80	0.24	100.0	100.0	100.0	100.0	100.0	100.0	100.0	100.0
4.3	29.6	50	1.06	0.32	100.0	100.0	100.0	100.0	100.0	100.0	100.0	100.0
5.5	37.9	39	1.38	0.42	100.0	100.0	100.0	100.0	100.0	100.0	100.0	100.0
7.2	49.6	30	1.76	0.54	100.0	100.0	100.0	100.0	100.0	100.0	100.0	100.0
9.3	64.1	23	2.31	0.70	100.0	100.0	100.0	100.0	100.0	100.0	100.0	100.0
12.0	82.7	18	2.98	0.91	100.0	100.0	100.0	100.0	100.0	100.0	100.0	100.0
15.5	106.9	14	3.85	1.17	100.0	100.0	99.8	100.0	100.0	100.0	100.0	100.0
20	137.9	11	4.97	1.51	100.0	100.0	99.5	100.0	99.7	97.5	100.0	100.0
25	172.4	8.6	6.41	2.0	100.0	100.0	99.4	100.0	99.4	97.1	100.0	100.0
35	241.3	6.1	8.01	2.4	100.0	100.0	99.2	100.0	98.9	96.5	100.0	100.0
45	310.3	4.8	11.2	3.4	99.7	100.0	98.8	100.0	97.1	93.9	100.0	100.0
55	379.2	3.9	14.4	4.4	99.3	99.8	98.0	100.0	91.3	75.2	100.0	99.8
75	517.1	2.9	17.6	5.4	98.6	99.6	96.1	99.9	82.8	65.8	100.0	99.6
95	655.0	2.3	24.0	7.3	89.3	99.4	84.8	99.4	74.2	59.3	99.9	99.5
120	827.4	1.8	30.5	9.3	75.4	98.7	68.7	91.0	69.8	54.7	99.3	99.1
150	1,034	1.4	38.5	11.7	65.2	97.9	60.7	74.9	63.0	48.8	82.3	88.4
200	1,379	1.1	48.1	14.7	60.4	97.5	56.3	67.4	59.8	45.9	71.8	79.7
260	1,793	0.82	64.1	19.5	54.7	97.3	51.5	60.3	55.9	42.2	64.5	72.2
350	2,413	0.61	83.4	25.4	50.3	96.9	47.5	55.1	52.8	39.1	59.5	66.9
430	2,965	0.50	112	34.1	45.2	96.4	43.2	50.0	49.3	35.7	53.7	61.7
550	3,792	0.39	138	42.1	42.2	95.6	40.3	46.7	46.7	33.4	49.7	58.0
725	4,999	0.30	176	53.6	38.8	94.4	37.3	42.9	44.4	31.1	45.4	54.4
925	6,378	0.23	232	70.7	34.9	91.7	33.6	39.3	41.4	28.1	40.3	50.2
1,200	8,274	0.18	297	90.5	31.9	90.1	31.2	35.1	38.9	25.8	35.9	46.4
1,550	10,687	0.14	385	117.3	28.4	86.8	28.4	31.0	36.7	23.2	31.3	42.4
2,000	13,790	0.11	497	151.5	25.4	85.0	25.3	26.9	34.1	20.3	26.6	38.1
2,600	17,926	0.08	641	195.4	23.0	84.0	22.7	23.3	31.2	17.6	23.0	33.7
3,350	23,097	0.06	834	254.2	20.3	82.1	20.3	19.5	27.4	14.1	19.5	29.4
4,300	29,647	0.05	1074	327.4	17.7	79.9	18.1	16.1	23.6	10.5	16.3	24.9
5,550	38,266	0.04	1378	420.0	15.5	77.2	16.3	13.5	21.1	8.2	14.0	21.0
7,200	49,642	0.03	1779	542.2	13.7	74.3	14.8	10.8	19.2	6.0	11.8	17.4
9,300	64,121	0.02	2308	703.5	11.9	71.3	13.3	8.8	17.6	5.4	10.1	14.5
			2981	908.6	10.0	66.3	11.7	6.3	16.2	4.0	8.3	11.7

All Hg calculations assume air-mercury $\sigma=484$ dyne/cm, contact angle=140deg.

Gas-Brine Pc assumes insitu gas-brine $\sigma\cos\theta=40$ dyne/cm

Gas-Brine height assumes gas density gradient = 0.0935 psi/ft; 2.115 kPa/m

Gas-Brine height assumes brine density gradient 0.430 psi/ft; 9.727 kPa/m

Analysis of Critical Permeability, Capillary Pressure

and Electrical Properties for Mesaverde

Tight Gas Sandstones from Western U.S. Basins

US DOE # DE-FC26-05NT42660 Final Scientific Report

Alan P. Byrnes, Robert M. Cluff, John C. Webb

Appendix 4

Mercury Injection Capillary Pressure Analysis (Ambient Analyses)

US DOE #DE-FC26-05NT42660 Final Scientific/Technical Report

Alan P. Byrnes, Robert M. Cluff, John C. Webb

					Uinta 4304730545 2-7 Flat Mesa E946 - 6550.5 ft (B)	Uinta 4304730545 2-7 Flat Mesa E946 - 6688.2 ft (B)	Uinta 4304730545 2-7 Flat Mesa E946 - 7276.2 ft (B)	Uinta 4304730545 2-7 Flat Mesa E946 - 7279.9 ft (B)	Uinta 4304730545 2-7 Flat Mesa E946 - 7293.5 ft (B)	Uinta 4304730545 2-7 Flat Mesa E946 - 7311.9 ft (B)	Uinta 4304730545 2-7 Flat Mesa E946 - 7312.7	Uinta 4304730545 2-7 Flat Mesa E946 - 7689.7 ft (B)	Uinta 4304730545 2-7 Flat Mesa R829 - 5638.8 ft (A)
<i>In situ</i> Klinkenberg Permeability (μm^2)=					1.09E-07	1.35E-06	2.27E-06	4.93E-07	5.72E-07	8.78E-07	2.49E-06	4.46E-06	3.29E-06
<i>In situ</i> Klinkenberg Permeability (mD) =					0.00011	0.00137	0.00230	0.00050	0.00058	0.00089	0.00252	0.00452	0.00333
Routine Porosity (%) =					1.5	7.2	7.3	6.6	3.1	5.9	8.3	7.6	5.0
Mercury Injection Capillary Pressure (psia)	Mercury Injection Capillary Pressure (kPa)	Approx. Pore Entry Diameter (μm)	Approx. Gas-Water Height Above Free Water Level (ft)	Approx. Gas-Water Height Above Free Water Level (m)	Ambient Cumulative Wetting Phase Saturation (% pore vol)								
2.0	13.8	107	0.10	0.03	100.0	100.0	100.0	100.0	100.0	100.0	100.0	100.0	100.0
2.5	17.2	86	0.64	0.20	100.0	100.0	100.0	100.0	100.0	100.0	100.0	100.0	100.0
3.3	22.8	65	0.80	0.24	100.0	100.0	100.0	100.0	100.0	100.0	100.0	100.0	100.0
4.3	29.6	50	1.06	0.32	100.0	100.0	100.0	100.0	100.0	100.0	100.0	100.0	100.0
5.5	37.9	39	1.38	0.42	100.0	100.0	100.0	100.0	100.0	100.0	100.0	100.0	100.0
7.2	49.6	30	1.76	0.54	100.0	100.0	100.0	100.0	100.0	100.0	100.0	100.0	100.0
9.3	64.1	23	2.31	0.70	100.0	100.0	100.0	100.0	100.0	100.0	100.0	100.0	100.0
12.0	82.7	18	2.98	0.91	100.0	100.0	100.0	100.0	100.0	100.0	100.0	100.0	100.0
15.5	106.9	14	3.85	1.17	100.0	100.0	100.0	100.0	100.0	100.0	100.0	100.0	100.0
20	137.9	11	4.97	1.51	100.0	100.0	100.0	100.0	100.0	100.0	100.0	100.0	100.0
25	172.4	8.6	6.41	2.0	100.0	100.0	100.0	100.0	100.0	100.0	100.0	100.0	100.0
35	241.3	6.1	8.01	2.4	100.0	100.0	100.0	100.0	100.0	100.0	100.0	100.0	100.0
45	310.3	4.8	11.2	3.4	100.0	100.0	100.0	100.0	100.0	100.0	100.0	100.0	100.0
55	379.2	3.9	14.4	4.4	100.0	100.0	100.0	100.0	100.0	100.0	100.0	100.0	100.0
75	517.1	2.9	17.6	5.4	100.0	100.0	100.0	100.0	100.0	100.0	100.0	100.0	100.0
95	655.0	2.3	24.0	7.3	100.0	100.0	100.0	100.0	100.0	100.0	100.0	100.0	100.0
120	827.4	1.8	30.5	9.3	100.0	99.7	100.0	99.6	100.0	98.7	99.4	100.0	100.0
150	1,034	1.4	38.5	11.7	100.0	99.5	100.0	99.3	100.0	98.2	99.4	99.6	100.0
200	1,379	1.1	48.1	14.7	100.0	99.2	100.0	99.3	100.0	97.9	99.2	99.6	100.0
260	1,793	0.82	64.1	19.5	100.0	98.8	100.0	98.8	100.0	97.1	99.1	99.3	99.9
350	2,413	0.61	83.4	25.4	100.0	94.2	100.0	98.8	100.0	97.1	98.8	99.2	99.7
430	2,965	0.50	112	34.1	100.0	85.5	99.6	98.4	99.6	95.6	87.3	91.6	98.2
550	3,792	0.39	138	42.1	100.0	79.8	97.6	98.0	99.1	92.3	79.9	78.0	70.1
725	4,999	0.30	176	53.6	100.0	73.7	87.0	95.0	98.7	87.5	69.9	67.0	60.3
925	6,378	0.23	232	70.7	100.0	66.7	81.1	76.1	95.7	83.8	64.7	57.7	52.7
1,200	8,274	0.18	297	90.5	100.0	61.0	76.2	65.9	91.6	76.6	60.6	51.4	49.6
1,550	10,687	0.14	385	117.3	100.0	54.5	70.2	56.5	87.1	73.0	55.8	44.5	45.0
2,000	13,790	0.11	497	151.5	100.0	47.7	63.2	48.6	83.0	70.0	51.7	37.0	41.2
2,600	17,926	0.08	641	195.4	97.3	41.8	56.5	42.1	78.0	67.2	47.8	29.9	38.2
3,350	23,097	0.06	834	254.2	95.4	35.4	43.6	35.9	74.2	63.7	43.6	23.7	35.3
4,300	29,647	0.05	1074	327.4	94.7	29.5	26.9	29.6	69.9	59.8	37.8	18.3	32.7
5,550	38,266	0.04	1378	420.0	93.2	24.4	16.5	23.8	66.9	53.4	30.2	14.5	30.5
7,200	49,642	0.03	1779	542.2	92.6	20.0	9.0	18.8	60.8	44.6	23.9	10.8	28.7
9,300	64,121	0.02	2308	703.5	88.7	15.2	4.4	13.7	51.7	29.5	17.9	8.4	27.3
			2981	908.6	85.4	11.5	0.8	8.9	37.5	17.7	14.7	6.5	26.4

All Hg calculations assume air-mercury $s=484$ dyne/cm, contact angle=140deg.

Gas-Brine Pc assumes insitu gas-brine $\sigma\cos\theta=40$ dyne/cm

Gas-Brine height assumes gas density gradient = 0.0935 psi/ft; 2.115 kPa/m

Gas-Brine height assumes brine density gradient 0.430 psi/ft; 9.727 kPa/m

Analysis of Critical Permeability, Capillary Pressure

and Electrical Properties for Mesaverde

Tight Gas Sandstones from Western U.S. Basins

US DOE # DE-FC26-05NT42660 Final Scientific Report

Alan P. Byrnes, Robert M. Cluff, John C. Webb

Appendix 4
Mercury Injection Capillary Pressure Analysis (Ambient Analyses)
US DOE #De-FC26-05NT42660 Final Scientific/Technical Report
Alan P. Byrnes, Robert M. Cluff, John C. Webb

					Uinta 4304730545 2-7 Flat Mesa E946 - 7712.7 ft (B)	Uinta 4304730545 2-7 Flat Mesa E946 - 7885.4 ft (B)	Uinta 4304730545 2-7 Flat Mesa E946 - 7885.4 ft (C)	Uinta 4304730852 4-5 US Lamco R829 - 5638.8 ft (A)	Uinta 4304730860 3-24 US Lamco R999 - 6812.2 ft	Uinta 4304730860 3-24 US Lamco R999 - 7158.9 ft (A)	Uinta 4304735788 NBU 9-20-360 State KM360 - 8279.5 ft	Uinta 4304736565 NBU 1022-1A Natural Butte KM1022 - 7808.7 ft (B)
					3.75E-07	1.87E-05	2.19E-05	3.29E-06	1.20E-05	1.68E-07	2.47E-07	3.75E-06
					0.00038	0.0189	0.0222	0.00333	0.0122	0.00017	0.00025	0.00380
					3.2	10.2	10.2	5.0	6.0	2.3	7.8	10.0
Mercury Injection Capillary Pressure (psia)	Mercury Injection Capillary Pressure (kPa)	Approx. Pore Entry Diameter (um)	Approx. Gas-Water Height Above Free Water Level (ft)	Approx. Gas-Water Height Above Free Water Level (m)	Ambient Cumulative Wetting Phase Saturation (% pore vol)	Ambient Cumulative Wetting Phase Saturation (% pore vol)	Ambient Cumulative Wetting Phase Saturation (% pore vol)	Ambient Cumulative Wetting Phase Saturation (% pore vol)	Ambient Cumulative Wetting Phase Saturation (% pore vol)	Ambient Cumulative Wetting Phase Saturation (% pore vol)	Ambient Cumulative Wetting Phase Saturation (% pore vol)	Ambient Cumulative Wetting Phase Saturation (% pore vol)
2.0	13.8	107	0.10	0.03	100.0	100.0	100.0	100.0	100.0	100.0	100.0	100.0
2.5	17.2	86	0.64	0.20	100.0	100.0	100.0	100.0	100.0	100.0	100.0	100.0
3.3	22.8	65	0.80	0.24	100.0	100.0	100.0	100.0	100.0	100.0	100.0	100.0
4.3	29.6	50	1.06	0.32	100.0	100.0	100.0	100.0	100.0	100.0	100.0	100.0
5.5	37.9	39	1.38	0.42	100.0	100.0	100.0	100.0	100.0	100.0	100.0	100.0
7.2	49.6	30	1.76	0.54	100.0	100.0	100.0	100.0	100.0	100.0	100.0	100.0
9.3	64.1	23	2.31	0.70	100.0	100.0	100.0	100.0	100.0	100.0	100.0	100.0
12.0	82.7	18	2.98	0.91	100.0	100.0	100.0	100.0	100.0	100.0	100.0	100.0
15.5	106.9	14	3.85	1.17	100.0	100.0	100.0	100.0	100.0	100.0	100.0	100.0
20	137.9	11	4.97	1.51	100.0	100.0	100.0	100.0	100.0	100.0	100.0	100.0
25	172.4	8.6	6.41	2.0	100.0	100.0	100.0	100.0	100.0	100.0	100.0	100.0
35	241.3	6.1	8.01	2.4	100.0	100.0	100.0	100.0	100.0	100.0	100.0	100.0
45	310.3	4.8	11.2	3.4	100.0	100.0	100.0	100.0	99.6	100.0	100.0	100.0
55	379.2	3.9	14.4	4.4	100.0	99.9	100.0	100.0	99.2	100.0	100.0	100.0
75	517.1	2.9	17.6	5.4	100.0	99.9	100.0	100.0	98.7	100.0	100.0	100.0
95	655.0	2.3	24.0	7.3	100.0	99.7	100.0	100.0	98.1	100.0	100.0	100.0
120	827.4	1.8	30.5	9.3	100.0	99.3	100.0	100.0	97.2	100.0	100.0	100.0
150	1,034	1.4	38.5	11.7	100.0	98.7	99.7	100.0	94.6	100.0	100.0	100.0
200	1,379	1.1	48.1	14.7	100.0	98.5	98.9	100.0	93.8	100.0	100.0	100.0
260	1,793	0.82	64.1	19.5	100.0	97.4	97.4	99.9	90.3	100.0	100.0	100.0
350	2,413	0.61	83.4	25.4	100.0	80.0	80.0	99.7	83.9	100.0	100.0	100.0
430	2,965	0.50	112	34.1	100.0	64.8	57.0	98.2	74.1	100.0	100.0	99.3
550	3,792	0.39	138	42.1	100.0	52.2	44.6	70.1	67.5	100.0	100.0	97.0
725	4,999	0.30	176	53.6	100.0	38.2	37.0	60.3	55.4	100.0	100.0	62.3
925	6,378	0.23	232	70.7	100.0	31.2	29.9	52.7	43.7	100.0	99.4	41.9
1,200	8,274	0.18	297	90.5	100.0	26.0	25.7	49.6	37.0	99.9	98.1	35.3
1,550	10,687	0.14	385	117.3	98.6	20.8	20.0	45.0	30.9	99.0	95.2	28.4
2,000	13,790	0.11	497	151.5	97.7	16.5	15.7	41.2	26.1	98.0	85.5	23.1
2,600	17,926	0.08	641	195.4	96.6	13.6	12.4	38.2	22.4	97.5	72.8	18.7
3,350	23,097	0.06	834	254.2	95.0	11.0	7.7	35.3	20.3	96.2	59.5	15.6
4,300	29,647	0.05	1074	327.4	89.4	8.5	5.6	32.7	17.5	94.1	50.3	12.9
5,550	38,266	0.04	1378	420.0	83.4	7.0	4.0	30.5	15.4	90.2	40.7	10.9
7,200	49,642	0.03	1779	542.2	69.2	5.8	2.4	28.7	13.3	80.3	32.5	9.3
9,300	64,121	0.02	2308	703.5	50.3	4.5	1.6	27.3	11.8	70.1	24.3	7.9
			2981	908.6	31.7	3.0	0.2	26.4	9.6	61.4	18.3	6.4

All Hg calculations assume air-mercury $\sigma=484$ dyne/cm, contact angle=140deg.

Gas-Brine Pc assumes insitu gas-brine $\sigma\cos\theta=40$ dyne/cm

Gas-Brine height assumes gas density gradient = 0.0935 psi/ft; 2.115 kPa/m

Gas-Brine height assumes brine density gradient 0.430 psi/ft; 9.727 kPa/m

Analysis of Critical Permeability, Capillary Pressure

and Electrical Properties for Mesaverde

Tight Gas Sandstones from Western U.S. Basins

US DOE # DE-FC26-05NT42660 Final Scientific Report

Alan P. Byrnes, Robert M. Cluff, John C. Webb

Appendix 4
Mercury Injection Capillary Pressure Analysis (Ambient Analyses)
US DOE #De-FC26-05NT42660 Final Scientific/Technical Report
Alan P. Byrnes, Robert M. Cluff, John C. Webb

					Uinta 43019xxxx1 3 Book Cliffs S172 - 175.3 ft (A1)	Uinta 43019xxxx1 3 Book Cliffs S172 - 392.5 ft (A1)	Uinta 43019xxxx2 4 Book Cliffs S174 - 161.7 ft (B)	Uinta 43019xxxx2 4 Book Cliffs S174 - 183.2 ft (B)	Uinta 43019xxxx2 4 Book Cliffs S174 - 183.4 ft (B)	Uinta 43019xxxx2 4 Book Cliffs S174 - 189.3 ft (B)	Washakie 4900721170 C-11 Fee T592 - 2340.7 ft (B)	Washakie 4903705683 65-1-7 Arch Unit S276 - 4728 ft (B)	Washakie 4903705683 65-1-7 Arch Unit S276 - 4729B ft
<i>In situ</i> Klinkenberg Permeability (μm^2)=					1.75E-02	7.60E-07	3.43E-05	2.83E-05	1.44E-04	6.41E-03	7.18E-05	2.57E-07	2.74E-05
<i>In situ</i> Klinkenberg Permeability (mD) =					17.7	0.00077	0.0348	0.0287	0.146	6.50	0.0728	0.00026	0.0278
Routine Porosity (%) =					21.2	11.6	11.6	8.8	10.1	21.5	14.1	6.8	13.0
Mercury Injection Capillary Pressure (psia)	Mercury Injection Capillary Pressure (kPa)	Approx. Pore Entry Diameter (μm)	Approx. Gas-Water Height Above Free Water Level (ft)	Approx. Gas-Water Height Above Free Water Level (m)	Ambient Cumulative Wetting Phase Saturation (% pore vol)	Ambient Cumulative Wetting Phase Saturation (% pore vol)	Ambient Cumulative Wetting Phase Saturation (% pore vol)	Ambient Cumulative Wetting Phase Saturation (% pore vol)	Ambient Cumulative Wetting Phase Saturation (% pore vol)	Ambient Cumulative Wetting Phase Saturation (% pore vol)	Ambient Cumulative Wetting Phase Saturation (% pore vol)	Ambient Cumulative Wetting Phase Saturation (% pore vol)	Ambient Cumulative Wetting Phase Saturation (% pore vol)
2.0	13.8	107	0.10	0.03	100.0	100.0	100.0	100.0	100.0	100.0	100.0	100.0	100.0
2.5	17.2	86	0.64	0.20	100.0	100.0	100.0	100.0	100.0	100.0	100.0	100.0	100.0
3.3	22.8	65	0.80	0.24	100.0	100.0	100.0	100.0	100.0	100.0	100.0	100.0	100.0
4.3	29.6	50	1.06	0.32	100.0	100.0	100.0	100.0	100.0	100.0	100.0	100.0	100.0
5.5	37.9	39	1.38	0.42	100.0	100.0	100.0	100.0	100.0	100.0	100.0	100.0	100.0
7.2	49.6	30	1.76	0.54	99.8	100.0	100.0	100.0	100.0	100.0	100.0	100.0	100.0
9.3	64.1	23	2.31	0.70	99.6	100.0	100.0	100.0	100.0	100.0	100.0	100.0	100.0
12.0	82.7	18	2.98	0.91	99.3	100.0	100.0	100.0	100.0	99.7	100.0	100.0	100.0
15.5	106.9	14	3.85	1.17	99.0	100.0	100.0	100.0	100.0	99.6	100.0	100.0	100.0
20	137.9	11	4.97	1.51	97.1	100.0	100.0	100.0	100.0	99.2	100.0	100.0	100.0
25	172.4	8.6	6.41	2.0	80.0	100.0	100.0	100.0	100.0	97.9	100.0	100.0	100.0
35	241.3	6.1	8.01	2.4	69.8	100.0	100.0	100.0	99.9	83.0	100.0	100.0	100.0
45	310.3	4.8	11.2	3.4	61.3	100.0	100.0	100.0	99.8	67.3	99.7	100.0	100.0
55	379.2	3.9	14.4	4.4	57.2	100.0	100.0	100.0	99.6	61.1	99.3	100.0	99.9
75	517.1	2.9	17.6	5.4	54.0	100.0	100.0	100.0	99.8	57.7	99.1	100.0	99.8
95	655.0	2.3	24.0	7.3	49.2	100.0	99.8	99.8	99.4	52.8	98.8	100.0	99.7
120	827.4	1.8	30.5	9.3	46.1	100.0	99.6	99.5	98.6	48.9	98.5	100.0	99.1
150	1,034	1.4	46.1	11.7	41.5	99.6	99.1	98.8	85.2	43.7	97.9	100.0	98.1
200	1,379	1.1	59.0	14.7	39.1	99.0	98.8	94.5	78.1	41.0	97.7	100.0	96.6
260	1,793	0.82	64.1	19.5	36.3	98.1	97.6	81.9	68.0	37.3	96.4	100.0	92.3
350	2,413	0.61	83.4	25.4	33.5	96.0	91.8	70.9	60.3	34.3	92.6	100.0	85.2
430	2,965	0.50	112	34.1	30.1	91.8	74.0	59.2	53.0	30.9	86.5	100.0	74.1
550	3,792	0.39	138	42.1	28.1	88.2	65.0	53.7	48.8	28.2	80.0	99.9	65.9
725	4,999	0.30	176	53.6	25.7	84.9	55.5	46.1	44.5	25.2	71.5	99.9	60.3
925	6,378	0.23	232	70.7	22.8	79.5	49.9	42.5	39.5	22.1	61.2	99.7	52.5
1,200	8,274	0.18	297	90.5	20.7	74.9	45.0	37.6	35.8	19.0	54.0	99.7	47.6
1,550	10,687	0.14	385	117.3	18.0	71.4	39.7	33.1	32.0	16.8	46.7	98.0	42.7
2,000	13,790	0.11	497	151.5	15.6	65.3	33.9	29.3	28.4	14.7	40.9	97.2	37.4
2,600	17,926	0.08	641	195.4	13.6	59.5	28.9	25.5	25.0	12.7	35.4	94.9	32.9
3,350	23,097	0.06	834	254.2	11.7	52.2	24.1	22.3	22.4	11.0	30.0	90.0	28.2
4,300	29,647	0.05	1074	327.4	10.1	45.8	19.5	19.2	19.6	9.4	25.1	82.2	23.9
5,550	38,266	0.04	1378	420.0	8.5	39.3	15.8	16.6	17.4	8.1	21.0	69.4	20.2
7,200	49,642	0.03	1779	542.2	7.6	34.0	12.5	14.5	15.8	7.1	17.4	55.1	16.7
9,300	64,121	0.02	2308	703.5	6.7	29.8	9.9	13.3	14.3	6.4	14.6	45.3	14.0
			2981	908.6	5.9	26.6	6.9	11.2	12.8	5.5	11.7	37.1	11.5

All Hg calculations assume air-mercury $s=484$ dyne/cm, contact angle=140deg.

Gas-Brine Pc assumes insitu gas-brine $s_{osq}=40$ dyne/cm

Gas-Brine height assumes gas density gradient = 0.0935 psi/ft; 2.115 kPa/m

Gas-Brine height assumes brine density gradient 0.430 psi/ft; 9.727 kPa/m

Analysis of Critical Permeability, Capillary Pressure

and Electrical Properties for Mesaverde

Tight Gas Sandstones from Western U.S. Basins

US DOE # DE-FC26-05NT42660 Final Scientific Report

Alan P. Byrnes, Robert M. Cluff, John C. Webb

Appendix 4
Mercury Injection Capillary Pressure Analysis (Ambient Analyses)
US DOE #De-FC26-05NT42660 Final Scientific/Technical Report
Alan P. Byrnes, Robert M. Cluff, John C. Webb

					Washakie 4903705683 65-1-7 Arch Unit S276 - 4757.9 ft (A)	Washakie 4903720033 102-7-10 Arch Unit S265 - 4878 ft (A)	Washakie 4903720033 102-7-10 Arch Unit S265 - 4899.0 ft (A)	Washakie 4903721053 Unit 3 Five Mile Gulch E489 - 10608.7 ft	Washakie 4903721053 Unit 3 Five Mile Gulch E489 - 10615.8 ft	Washakie 4903721053 Unit 3 Five Mile Gulch E489 - 10645 ft (A)	Washakie 4903721053 Unit 3 Five Mile Gulch E489 - 10666.3 ft (B)	Washakie 4903721053 Unit 3 Five Mile Gulch E489 - 10669.0 ft (B)
<i>In situ</i> Klinkenberg Permeability (μm^2)=					3.64E-05	3.03E-02	2.81E-02	4.93E-09	1.32E-05	2.86E-07	1.15E-06	2.86E-06
<i>In situ</i> Klinkenberg Permeability (mD) =					0.0369	30.7	28.5	0.000005	0.0134	0.00029	0.00117	0.00290
Routine Porosity (%) =					10.6	18.7	20.1	4.1	10.6	4.0	8.4	6.5
Mercury Injection Capillary Pressure (psia)	Mercury Injection Capillary Pressure (kPa)	Approx. Pore Entry Diameter (μm)	Approx. Gas-Water Height Above Free Water Level (ft)	Approx. Gas-Water Height Above Free Water Level (m)	Ambient Cumulative Wetting Phase Saturation (% pore vol)	Ambient Cumulative Wetting Phase Saturation (% pore vol)	Ambient Cumulative Wetting Phase Saturation (% pore vol)	Ambient Cumulative Wetting Phase Saturation (% pore vol)	Ambient Cumulative Wetting Phase Saturation (% pore vol)	Ambient Cumulative Wetting Phase Saturation (% pore vol)	Ambient Cumulative Wetting Phase Saturation (% pore vol)	Ambient Cumulative Wetting Phase Saturation (% pore vol)
2.0	13.8	107	0.10	0.03	100.0	100.0	100.0	100.0	100.0	100.0	100.0	100.0
2.5	17.2	86	0.64	0.20	100.0	100.0	100.0	100.0	100.0	100.0	100.0	100.0
3.3	22.8	65	0.80	0.24	100.0	99.8	100.0	100.0	100.0	100.0	100.0	100.0
4.3	29.6	50	1.06	0.32	100.0	99.6	100.0	100.0	100.0	100.0	100.0	100.0
5.5	37.9	39	1.38	0.42	100.0	99.4	100.0	100.0	100.0	100.0	100.0	100.0
7.2	49.6	30	1.76	0.54	100.0	99.2	100.0	100.0	100.0	100.0	100.0	100.0
9.3	64.1	23	2.31	0.70	100.0	99.0	100.0	100.0	100.0	100.0	100.0	100.0
12.0	82.7	18	2.98	0.91	100.0	98.7	100.0	100.0	100.0	100.0	100.0	100.0
15.5	106.9	14	3.85	1.17	100.0	98.3	99.8	100.0	100.0	100.0	100.0	100.0
20	137.9	11	4.97	1.51	100.0	94.1	98.8	100.0	100.0	100.0	100.0	100.0
25	172.4	8.6	6.41	2.0	100.0	78.2	70.1	100.0	100.0	100.0	100.0	100.0
35	241.3	6.1	8.01	2.4	100.0	69.2	62.8	100.0	100.0	100.0	100.0	100.0
45	310.3	4.8	11.2	3.4	99.8	61.7	55.3	100.0	100.0	100.0	100.0	99.9
55	379.2	3.9	14.4	4.4	99.6	56.4	50.4	100.0	100.0	100.0	100.0	99.8
75	517.1	2.9	17.6	5.4	99.5	52.7	47.1	100.0	100.0	99.8	100.0	99.7
95	655.0	2.3	24.0	7.3	99.3	47.1	42.1	100.0	99.9	99.4	100.0	99.7
120	827.4	1.8	30.5	9.3	99.0	43.1	38.3	100.0	99.8	99.0	100.0	99.2
150	1,034	1.4	38.5	11.7	97.9	37.9	34.2	100.0	99.5	97.8	100.0	99.0
200	1,379	1.1	48.1	14.7	93.4	34.9	31.4	100.0	99.5	97.8	100.0	98.9
260	1,793	0.82	64.1	19.5	77.7	30.9	27.9	100.0	99.0	97.0	100.0	98.4
350	2,413	0.61	83.4	25.4	65.8	28.0	25.0	100.0	95.3	97.0	100.0	98.1
430	2,965	0.50	112	34.1	57.0	24.8	21.6	100.0	72.4	96.8	99.9	96.5
550	3,792	0.39	138	42.1	51.8	22.7	19.5	100.0	66.8	96.6	99.9	84.1
725	4,999	0.30	176	53.6	46.8	19.9	17.0	100.0	62.3	96.6	99.8	49.8
925	6,378	0.23	232	70.7	41.4	17.8	14.5	99.9	57.9	95.9	98.7	39.4
1,200	8,274	0.18	297	90.5	37.3	16.0	13.4	99.8	54.5	91.2	78.8	34.4
1,550	10,687	0.14	385	117.3	33.3	14.1	11.4	98.9	51.0	83.7	66.7	29.7
2,000	13,790	0.11	497	151.5	29.7	12.5	8.6	98.0	48.1	77.7	59.3	26.4
2,600	17,926	0.08	641	195.4	26.1	11.0	6.2	96.8	45.5	73.9	54.4	24.0
3,350	23,097	0.06	834	254.2	22.8	9.7	4.9	93.7	42.8	70.0	49.3	22.1
4,300	29,647	0.05	1074	327.4	19.8	8.3	4.1	86.4	40.5	65.8	44.9	20.2
5,550	38,266	0.04	1378	420.0	17.4	7.3	3.0	75.6	38.5	61.3	41.1	18.7
7,200	49,642	0.03	1779	542.2	15.2	6.2	2.1	65.5	36.8	55.5	37.7	17.6
9,300	64,121	0.02	2308	703.5	13.1	5.4	0.8	59.6	35.2	49.8	34.7	16.8
			2981	908.6	11.7	4.7		54.4		43.4	31.6	15.7

All Hg calculations assume air-mercury $s=484$ dyne/cm, contact angle=140deg.

Gas-Brine Pc assumes insitu gas-brine $s_{\text{osq}}=40$ dyne/cm

Gas-Brine height assumes gas density gradient = 0.0935 psi/ft; 2.115 kPa/m

Gas-Brine height assumes brine density gradient 0.430 psi/ft; 9.727 kPa/m

Analysis of Critical Permeability, Capillary Pressure

and Electrical Properties for Mesaverde

Tight Gas Sandstones from Western U.S. Basins

US DOE # DE-FC26-05NT42660 Final Scientific Report

Alan P. Byrnes, Robert M. Cluff, John C. Webb

Appendix 4

Mercury Injection Capillary Pressure Analysis (Ambient Analyses)

US DOE #De-FC26-05NT42660 Final Scientific/Technical Report

Alan P. Byrnes, Robert M. Cluff, John C. Webb

					Washakie 4903721053 Unit 3 Five Mile Gulch E489 - 10681.2 ft	Washakie 4903722304 3 Dripping Rock DR3 - 12416.9 ft (A)	Washakie 4903722304 3 Dripping Rock DR3 - 12441.9 ft (A)	Washakie 4903722355 5 Dripping Rock DR5 - 12671.9 ft	Washakie 4903722355 5 Dripping Rock DR5 - 12673.6 ft	Washakie 9999999999 Wild Rose 1 (WLDR) - 9837.65 ft (A)	Washakie 9999999999 Wild Rose 1 (WLDR) - 9839.35 ft (A)	Wind River 4901320966 2-1 Chevron D031 - 15682.8 ft (A)
					7.90E-06	2.80E-05	9.44E-06	2.71E-06	7.40E-06		2.05E-06	2.44E-06
					0.00800	0.0284	0.00957	0.00275	0.00750		0.00208	0.00247
					10.5	13.2	10.2	10.9	12.7		6.4	9.7
					10.5	13.2	10.2	10.9	12.7		6.4	9.7
Mercury Injection Capillary Pressure (psia)	Mercury Injection Capillary Pressure (kPa)	Approx. Pore Entry Diameter (um)	Approx. Gas-Water Height Above Free Water Level (ft)	Approx. Gas-Water Height Above Free Water Level (m)	Ambient Cumulative Wetting Phase Saturation (% pore vol)	Ambient Cumulative Wetting Phase Saturation (% pore vol)	Ambient Cumulative Wetting Phase Saturation (% pore vol)	Ambient Cumulative Wetting Phase Saturation (% pore vol)	Ambient Cumulative Wetting Phase Saturation (% pore vol)	Ambient Cumulative Wetting Phase Saturation (% pore vol)	Ambient Cumulative Wetting Phase Saturation (% pore vol)	Ambient Cumulative Wetting Phase Saturation (% pore vol)
2.0	13.8	107	0.10	0.03	100.0	100.0	100.0	100.0	100.0	100.0	100.0	100.0
2.5	17.2	86	0.64	0.20	100.0	100.0	100.0	100.0	100.0	100.0	100.0	100.0
3.3	22.8	65	0.80	0.24	100.0	100.0	100.0	100.0	99.7	100.0	100.0	100.0
4.3	29.6	50	1.06	0.32	100.0	100.0	100.0	100.0	99.4	100.0	100.0	100.0
5.5	37.9	39	1.38	0.42	100.0	100.0	100.0	100.0	99.3	100.0	100.0	100.0
7.2	49.6	30	1.76	0.54	100.0	100.0	100.0	100.0	99.1	100.0	100.0	100.0
9.3	64.1	23	2.31	0.70	100.0	100.0	100.0	100.0	99.1	100.0	100.0	100.0
12.0	82.7	18	2.98	0.91	100.0	100.0	100.0	100.0	98.8	100.0	100.0	100.0
15.5	106.9	14	3.85	1.17	100.0	100.0	100.0	100.0	98.8	100.0	100.0	100.0
20	137.9	11	4.97	1.51	100.0	100.0	100.0	100.0	98.6	100.0	100.0	100.0
25	172.4	8.6	6.41	2.0	100.0	100.0	100.0	100.0	98.6	100.0	100.0	100.0
35	241.3	6.1	8.01	2.4	100.0	100.0	100.0	100.0	98.5	100.0	100.0	100.0
45	310.3	4.8	11.2	3.4	100.0	100.0	100.0	100.0	98.4	100.0	100.0	100.0
55	379.2	3.9	14.4	4.4	100.0	100.0	100.0	100.0	98.3	100.0	100.0	99.7
75	517.1	2.9	17.6	5.4	99.8	100.0	100.0	100.0	98.3	100.0	100.0	99.5
95	655.0	2.3	24.0	7.3	99.6	99.9	99.9	100.0	98.1	100.0	100.0	99.4
120	827.4	1.8	30.5	9.3	99.5	99.7	99.9	100.0	98.0	100.0	100.0	99.3
150	1,034	1.4	38.5	11.7	99.4	99.5	99.7	99.6	97.7	100.0	99.8	99.2
200	1,379	1.1	48.1	14.7	99.2	99.5	99.6	99.5	97.7	100.0	99.8	99.2
260	1,793	0.82	64.1	19.5	99.1	99.1	99.4	99.5	97.5	100.0	99.8	98.6
350	2,413	0.61	83.4	25.4	98.8	98.3	99.3	99.3	97.3	100.0	99.5	98.6
430	2,965	0.50	112	34.1	96.4	56.8	96.4	97.7	89.4	100.0	99.4	97.9
550	3,792	0.39	138	42.1	79.5	45.9	93.8	76.9	59.8	100.0	99.4	84.9
725	4,999	0.30	176	53.6	54.4	37.6	50.4	58.5	48.8	100.0	99.2	74.6
925	6,378	0.23	232	70.7	42.9	31.5	42.4	50.8	41.1	99.5	98.9	66.9
1,200	8,274	0.18	297	90.5	36.6	28.3	36.9	46.7	37.1	99.5	98.9	61.2
1,550	10,687	0.14	385	117.3	30.5	24.5	32.9	41.6	33.1	97.9	97.9	54.8
2,000	13,790	0.11	497	151.5	25.8	21.6	29.1	38.4	30.0	97.3	96.9	47.8
2,600	17,926	0.08	641	195.4	22.1	19.2	26.3	35.7	27.5	95.3	95.7	41.0
3,350	23,097	0.06	834	254.2	18.6	17.2	23.9	33.0	25.3	83.3	77.7	34.8
4,300	29,647	0.05	1074	327.4	15.5	15.9	21.5	30.3	22.9	61.9	55.1	29.4
5,550	38,266	0.04	1378	420.0	13.2	14.7	20.0	27.6	20.6	46.2	45.1	24.8
7,200	49,642	0.03	1779	542.2	11.1	13.3	18.3	25.2	18.3	38.5	36.9	21.1
9,300	64,121	0.02	2308	703.5	9.6	12.2	16.9	23.1	16.6	32.5	29.8	18.0
			2981	908.6	7.8	11.2	15.1	21.0	14.7	26.9	29.8	15.0

All Hg calculations assume air-mercury s=484 dyne/cm, contact angle=140deg.

Gas-Brine Pc assumes insitu gas-brine scosq= 40 dyne/cm

Gas-Brine height assumes gas density gradient = 0.0935 psi/ft; 2.115 kPa/m

Gas-Brine height assumes brine density gradient 0.430 psi/ft; 9.727 kPa/m

Analysis of Critical Permeability, Capillary Pressure

and Electrical Properties for Mesaverde

Tight Gas Sandstones from Western U.S. Basins

US DOE # DE-FC26-05NT42660 Final Scientific Report

Alan P. Byrnes, Robert M. Cluff, John C. Webb

Appendix 4
Mercury Injection Capillary Pressure Analysis (Ambient Analyses)
US DOE #De-FC26-05NT42660 Final Scientific/Technical Report
Alan P. Byrnes, Robert M. Cluff, John C. Webb

						Wind River 4901320836 1-27 Lookout (C899) - 16678.9 ft (A)
<i>In situ</i> Klinkenberg Permeability (μm^2)=						6.12E-07
<i>In situ</i> Klinkenberg Permeability (mD) =						0.00062
Routine Porosity (%) =						5.5
Mercury Injection Capillary Pressure (psia)	Mercury Injection Capillary Pressure (kPa)	Approx. Pore Entry Diameter (μm)	Approx. Gas-Water Height Above Free Water Level (ft)	Approx. Gas-Water Height Above Free Water Level (m)	Ambient Cumulative Wetting Phase Saturation (% pore vol)	
2.0	13.8	107	0.10	0.03	100.0	
2.5	17.2	86	0.64	0.20	100.0	
3.3	22.8	65	0.80	0.24	100.0	
4.3	29.6	50	1.06	0.32	100.0	
5.5	37.9	39	1.38	0.42	100.0	
7.2	49.6	30	1.76	0.54	100.0	
9.3	64.1	23	2.31	0.70	100.0	
12.0	82.7	18	2.98	0.91	100.0	
15.5	106.9	14	3.85	1.17	100.0	
20	137.9	11	4.97	1.51	100.0	
25	172.4	8.6	6.41	2.0	100.0	
35	241.3	6.1	8.01	2.4	100.0	
45	310.3	4.8	11.2	3.4	100.0	
55	379.2	3.9	14.4	4.4	100.0	
75	517.1	2.9	17.6	5.4	100.0	
95	655.0	2.3	24.0	7.3	100.0	
120	827.4	1.8	30.5	9.3	100.0	
150	1,034	1.4	38.5	11.7	100.0	
200	1,379	1.1	48.1	14.7	100.0	
260	1,793	0.82	64.1	19.5	100.0	
350	2,413	0.61	83.4	25.4	100.0	
430	2,965	0.50	112	34.1	100.0	
550	3,792	0.39	138	42.1	100.0	
725	4,999	0.30	176	53.6	98.9	
925	6,378	0.23	232	70.7	83.5	
1,200	8,274	0.18	297	90.5	76.7	
1,550	10,687	0.14	385	117.3	67.2	
2,000	13,790	0.11	497	151.5	60.7	
2,600	17,926	0.08	641	195.4	54.9	
3,350	23,097	0.06	834	254.2	48.7	
4,300	29,647	0.05	1074	327.4	42.4	
5,550	38,266	0.04	1378	420.0	37.5	
7,200	49,642	0.03	1779	542.2	33.3	
9,300	64,121	0.02	2308	703.5	29.7	
			2981	908.6	26.0	

All Hg calculations assume air-mercury $s=484$ dyne/cm, contact angle=140deg.

Gas-Brine Pc assumes insitu gas-brine $\sigma\cos\theta=40$ dyne/cm

Gas-Brine height assumes gas density gradient = 0.0935 psi/ft; 2.115 kPa/m

Gas-Brine height assumes brine density gradient 0.430 psi/ft; 9.727 kPa/m

Analysis of Critical Permeability, Capillary Pressure
and Electrical Properties for Mesaverde

Tight Gas Sandstones from Western U.S. Basins

US DOE # DE-FC26-05NT42660 Final Scientific Report

Alan P. Byrnes, Robert M. Cluff, John C. Webb

Appendix 4
Mercury Injection Capillary Pressure Analysis (In situ Analyses)
US DOE #DE-FC26-05NT42660 Final Scientific/Technical Report
Alan P. Byrnes, Robert M. Cluff, and John C. Webb

Net Confining Pressure = 4,000 psi (27.6 MPa)					Green River 4903505742 C-47 Tip Top Shallow R780 - 2699.7 ft (A)	Green River 4903505742 C-47 Tip Top Shallow R780 - 2717.1 ft (A)	Green River 4903505742 C-47 Tip Top Shallow R780 - 2729.9 ft (A)	Green River 4903506020 B-54 Big Piney E712 - 3403.9 ft (B)	Green River 4903506020 B-54 Big Piney E712 - 3433.8 ft (A)	Green River 4903506020 B-54 Big Piney E712 - 3461.5 A	Green River 4903506020 B-54 Big Piney E712 -3480.8 ft (B)	Green River 4903506020 B-54 Big Piney E712 - 3515.8 ft (B)
<i>In situ</i> Klinkenberg Permeability (mm ²)=					3.34E-02	1.12E-02	6.02E-03	1.88E-03	2.82E-02	1.69E-01	5.71E-06	1.96E-05
<i>In situ</i> Klinkenberg Permeability (mD) =					33.8	11.3	6.1	1.90	28.6	170.9	0.00579	0.0199
<i>Routine</i> Porosity =					21.7	20.0	18.7	16.0	17.4	18.2	8.9	12.0
Mercury Injection Capillary Pressure (psia)	Mercury Injection Capillary Pressure (kPa)	Approx. Pore Entry Diameter (mm)	Approx. Gas-Water Height Above Free Water Level (ft)	Approx. Gas-Water Height Above Free Water Level (m)	<i>In situ</i> Cumulative Wetting Phase Saturation (% pore vol)							
2.0	13.8	107	0.10	0.03	100.0	100.0	100.0	100.0	100.0	100.0	100.0	100.0
2.5	17.2	86	0.64	0.20	100.0	100.0	100.0	100.0	100.0	100.0	100.0	100.0
3.3	22.8	65	0.80	0.24	100.0	100.0	100.0	100.0	100.0	100.0	100.0	100.0
4.3	29.6	50	1.06	0.32	100.0	100.0	100.0	100.0	100.0	100.0	100.0	100.0
5.5	37.9	39	1.38	0.42	100.0	100.0	100.0	100.0	100.0	100.0	100.0	100.0
7.2	49.6	30	1.76	0.54	100.0	100.0	100.0	100.0	100.0	100.0	100.0	100.0
9.3	64.1	23	2.31	0.70	100.0	100.0	100.0	100.0	100.0	100.0	100.0	100.0
12.0	82.7	18	2.98	0.91	100.0	100.0	100.0	100.0	100.0	100.0	100.0	100.0
15.5	106.9	14	3.85	1.17	100.0	100.0	100.0	100.0	99.9	100.0	100.0	100.0
20	137.9	11	4.97	1.51	100.0	100.0	100.0	100.0	99.8	99.5	100.0	100.0
25	172.4	8.6	6.41	2.0	88.7	99.7	100.0	100.0	80.6	62.3	100.0	100.0
35	241.3	6.1	8.01	2.4	62.4	99.6	100.0	100.0	63.2	52.1	100.0	100.0
45	310.3	4.8	11.2	3.4	50.0	75.2	93.1	99.6	53.4	44.3	100.0	100.0
55	379.2	3.9	14.4	4.4	46.9	58.3	66.1	98.0	48.6	40.1	100.0	100.0
75	517.1	2.9	17.6	5.4	43.1	53.6	51.0	88.4	45.3	37.2	100.0	100.0
95	655.0	2.3	24.0	7.3	38.8	47.6	44.1	67.0	41.0	32.6	100.0	100.0
120	827.4	1.8	30.5	9.3	34.7	44.1	40.0	59.7	38.3	30.2	100.0	100.0
150	1,034	1.4	38.5	11.7	31.8	40.1	35.5	52.0	35.5	27.2	100.0	100.0
200	1,379	1.1	48.1	14.7	29.2	36.7	32.1	47.5	33.6	23.9	100.0	99.9
260	1,793	0.82	64.1	19.5	26.1	33.7	28.8	42.1	31.2	21.5	100.0	99.7
350	2,413	0.61	83.4	25.4	23.7	30.8	25.8	37.5	29.8	18.8	100.0	98.6
430	2,965	0.50	112	34.1	21.3	28.2	23.5	32.7	28.1	15.9	99.9	81.6
550	3,792	0.39	138	42.1	20.0	26.4	21.7	29.9	27.4	14.3	99.5	74.1
725	4,999	0.30	176	53.6	18.0	24.3	19.4	26.6	26.8	12.4	97.8	67.9
925	6,378	0.23	232	70.7	15.8	21.7	16.5	23.2	26.3	9.9	79.0	62.4
1,200	8,274	0.18	297	90.5	13.8	19.0	13.6	20.9	26.2	8.2	67.6	57.9
1,550	10,687	0.14	385	117.3	11.8	16.4	11.2	18.1	25.6	6.1	58.4	51.9
2,000	13,790	0.11	497	151.5	9.9	13.7	8.7	15.8	25.6	4.6	51.1	46.4
2,600	17,926	0.08	641	195.4	8.1	11.6	6.2	14.0	25.6	3.6	44.9	40.4
3,350	23,097	0.06	834	254.2	6.6	9.4	3.3	11.1	25.5	2.2	38.3	34.5
4,300	29,647	0.05	1074	327.4	5.3	7.6	1.7	7.6	25.5	0.9	32.2	29.4
5,550	38,266	0.04	1378	420.0	4.0	5.9	0.0	5.6	25.4	0.0	26.3	24.1
7,200	49,642	0.03	1779	542.2	3.1	4.7	0.0	3.6	25.3	0.0	20.6	20.4
9,300	64,121	0.02	2308	703.5	1.3	2.4	0.0	0.5	24.7	0.0	14.5	15.1

All Hg calculations assume air-mercury $\sigma=484$ dyne/cm, contact angle=140deg.

Gas-Brine Pc assumes insitu gas-brine $\sigma\cos\theta=40$ dyne/cm

Gas-Brine height assumes gas density gradient = 0.0935 psi/ft; 2.115 kPa/m

Gas-Brine height assumes brine density gradient 0.430 psi/ft; 9.727 kPa/m

Analysis of Critical Permeability, Capillary Pressure

and Electrical Properties for Mesaverde

Tight Gas Sandstones from Western U.S. Basins

US DOE # DE-FC26-05NT42660 Final Scientific Report

Alan P. Byrnes, Robert M. Cluff, John C. Webb

Appendix 4
Mercury Injection Capillary Pressure Analysis (In situ Analyses)
US DOE #DE-FC26-05NT42660 Final Scientific/Technical Report
Alan P. Byrnes, Robert M. Cluff, and John C. Webb

Net Confining Pressure = 4,000 psi (27.6 MPa)
In situ Klinkenberg Permeability (mm²)=
In situ Klinkenberg Permeability (mD) =
Routine Porosity =

Green River 4903506200 K-2 Mason S873 - 7703.7 ft (A2)	Green River 4903506200 K-2 Mason S873 - 9397.2 ft (A2)	Green River 4903520088 A-1 Wasp B029 - 11457.8 ft (C)	Green River 4903520088 A-1 Wasp B029 - 11460.6 ft (C)	Green River 4903520088 A-1 Wasp B029 - 11552.3 ft (C)	Green River 4903520088 A-1 Wasp B029 - 11587.2 ft (C)	Green River 4903520088 A-1 Wasp B029 - 11609.2 ft (C)
1.40E-04	6.32E-08	6.41E-08	2.76E-07	2.76E-07	4.26E-07	6.54E-06
0.142	0.000064	0.000065	0.00028	0.00028	0.000432	0.00663
11.5	8.2	2.6	4.2	4.2	4.4	6.0

Mercury Injection Capillary Pressure (psia)	Mercury Injection Capillary Pressure (kPa)	Approx. Pore Entry Diameter (mm)	Approx. Gas-Water Height Above Free Water Level (ft)	Approx. Gas-Water Height Above Free Water Level (m)	<i>In situ</i> Cumulative Wetting Phase Saturation (% pore vol)	<i>In situ</i> Cumulative Wetting Phase Saturation (% pore vol)	<i>In situ</i> Cumulative Wetting Phase Saturation (% pore vol)	<i>In situ</i> Cumulative Wetting Phase Saturation (% pore vol)	<i>In situ</i> Cumulative Wetting Phase Saturation (% pore vol)	<i>In situ</i> Cumulative Wetting Phase Saturation (% pore vol)	<i>In situ</i> Cumulative Wetting Phase Saturation (% pore vol)	<i>In situ</i> Cumulative Wetting Phase Saturation (% pore vol)
2.0	13.8	107	0.10	0.03	100.0	100.0	100.0	100.0	100.0	100.0	100.0	100.0
2.5	17.2	86	0.64	0.20	100.0	100.0	100.0	100.0	100.0	100.0	100.0	100.0
3.3	22.8	65	0.80	0.24	100.0	100.0	100.0	100.0	100.0	100.0	100.0	100.0
4.3	29.6	50	1.06	0.32	100.0	100.0	100.0	100.0	100.0	100.0	100.0	100.0
5.5	37.9	39	1.38	0.42	100.0	100.0	100.0	100.0	100.0	100.0	100.0	100.0
7.2	49.6	30	1.76	0.54	100.0	100.0	100.0	100.0	100.0	100.0	100.0	100.0
9.3	64.1	23	2.31	0.70	100.0	100.0	100.0	100.0	100.0	100.0	100.0	100.0
12.0	82.7	18	2.98	0.91	100.0	100.0	100.0	100.0	100.0	100.0	100.0	100.0
15.5	106.9	14	3.85	1.17	100.0	100.0	100.0	100.0	100.0	100.0	100.0	100.0
20	137.9	11	4.97	1.51	100.0	100.0	100.0	100.0	100.0	100.0	100.0	100.0
25	172.4	8.6	6.41	2.0	100.0	100.0	100.0	100.0	100.0	100.0	100.0	100.0
35	241.3	6.1	8.01	2.4	100.0	100.0	100.0	100.0	100.0	100.0	100.0	100.0
45	310.3	4.8	11.2	3.4	100.0	100.0	100.0	100.0	100.0	100.0	100.0	100.0
55	379.2	3.9	14.4	4.4	100.0	100.0	100.0	100.0	100.0	100.0	100.0	100.0
75	517.1	2.9	17.6	5.4	99.9	100.0	100.0	100.0	100.0	100.0	100.0	100.0
95	655.0	2.3	24.0	7.3	99.9	100.0	100.0	100.0	100.0	100.0	100.0	100.0
120	827.4	1.8	30.5	9.3	99.8	100.0	100.0	100.0	100.0	100.0	100.0	100.0
150	1,034	1.4	38.5	11.7	76.8	100.0	100.0	100.0	100.0	100.0	100.0	99.9
200	1,379	1.1	48.1	14.7	63.1	100.0	100.0	100.0	100.0	100.0	100.0	98.6
260	1,793	0.82	64.1	19.5	54.3	100.0	100.0	100.0	100.0	100.0	100.0	98.0
350	2,413	0.61	83.4	25.4	48.8	100.0	100.0	100.0	100.0	100.0	100.0	97.1
430	2,965	0.50	112	34.1	42.8	100.0	99.9	100.0	100.0	100.0	100.0	97.0
550	3,792	0.39	138	42.1	38.9	100.0	98.9	100.0	100.0	100.0	100.0	96.8
725	4,999	0.30	176	53.6	34.6	100.0	90.7	100.0	100.0	100.0	100.0	94.0
925	6,378	0.23	232	70.7	29.7	100.0	82.8	100.0	100.0	100.0	100.0	87.9
1,200	8,274	0.18	297	90.5	25.9	100.0	71.7	100.0	100.0	100.0	99.9	74.7
1,550	10,687	0.14	385	117.3	21.7	99.3	56.1	98.4	98.4	99.1	99.1	51.8
2,000	13,790	0.11	497	151.5	17.4	98.4	42.5	96.0	96.0	97.6	97.6	39.3
2,600	17,926	0.08	641	195.4	13.9	86.3	33.8	91.6	91.6	95.7	95.7	29.2
3,350	23,097	0.06	834	254.2	10.6	63.4	27.8	87.6	87.6	92.1	92.1	23.0
4,300	29,647	0.05	1074	327.4	8.5	54.3	21.8	79.3	79.3	89.9	89.9	17.6
5,550	38,266	0.04	1378	420.0	6.5	46.1	16.1	55.5	55.5	83.8	83.8	14.2
7,200	49,642	0.03	1779	542.2	4.9	38.6	11.8	28.8	28.8	65.8	65.8	9.8
9,300	64,121	0.02	2308	703.5	2.6	31.3	6.9	8.9	8.9	35.0	35.0	6.1

All Hg calculations assume air-mercury $\sigma=484$ dyne/cm, contact angle=140deg.

Gas-Brine Pc assumes insitu gas-brine $\sigma\cos\theta=40$ dyne/cm

Gas-Brine height assumes gas density gradient = 0.0935 psi/ft; 2.115 kPa/m

Gas-Brine height assumes brine density gradient 0.430 psi/ft; 9.727 kPa/m

Analysis of Critical Permeability, Capillary Pressure
and Electrical Properties for Mesaverde

Tight Gas Sandstones from Western U.S. Basins

US DOE # DE-FC26-05NT42660 Final Scientific Report

Alan P. Byrnes, Robert M. Cluff, John C. Webb

Appendix 4
Mercury Injection Capillary Pressure Analysis (In situ Analyses)
US DOE #DE-FC26-05NT42660 Final Scientific/Technical Report
Alan P. Byrnes, Robert M. Cluff, and John C. Webb

Net Confining Pressure = 4,000 psi (27.6 MPa)

In situ Klinkenberg Permeability (mm²)=

In situ Klinkenberg Permeability (mD) =

Routine Porosity =

Green River 4903520088 A-1 Wasp B029 - 11615.1 ft (C)	Green River 4903520088 A-1 Wasp B029 - 11706.8 ft (C)	Green River 4903520088 A-1 Wasp B029 - 13672.5 ft (B)	Green River 4903520622 1 Old Road E894 - 11936.3 A ft A	Piceance 504510927 PA 424-34 PA424 - 4578.8ft (A2)	Piceance 504510927 PA 424-34 PA424 - 4606.5 ft (A2)	Piceance 504510927 PA 424-34 PA424 - 5193.5 ft (A2)
9.57E-07	3.69E-07	3.55E-08	2.35E-06	1.68E-07	1.09E-06	6.12E-06
0.00097	0.000374	0.000036	0.00238	0.00017	0.00110	0.00620
4.9	3.7	2.8	9.8	4.5	12.8	7.3

Mercury Injection Capillary Pressure (psia)	Mercury Injection Capillary Pressure (kPa)	Approx. Pore Entry Diameter (mm)	Approx. Gas-Water Height Above Free Water Level (ft)	Approx. Gas-Water Height Above Free Water Level (m)	<i>In situ</i> Cumulative Wetting Phase Saturation (% pore vol)	<i>In situ</i> Cumulative Wetting Phase Saturation (% pore vol)	<i>In situ</i> Cumulative Wetting Phase Saturation (% pore vol)	<i>In situ</i> Cumulative Wetting Phase Saturation (% pore vol)	<i>In situ</i> Cumulative Wetting Phase Saturation (% pore vol)	<i>In situ</i> Cumulative Wetting Phase Saturation (% pore vol)	<i>In situ</i> Cumulative Wetting Phase Saturation (% pore vol)	<i>In situ</i> Cumulative Wetting Phase Saturation (% pore vol)
2.0	13.8	107	0.10	0.03	100.0	100.0	100.0	100.0	100.0	100.0	100.0	100.0
2.5	17.2	86	0.64	0.20	100.0	100.0	100.0	100.0	100.0	100.0	100.0	100.0
3.3	22.8	65	0.80	0.24	100.0	100.0	100.0	100.0	100.0	100.0	100.0	100.0
4.3	29.6	50	1.06	0.32	100.0	100.0	100.0	100.0	100.0	100.0	100.0	100.0
5.5	37.9	39	1.38	0.42	100.0	100.0	100.0	100.0	100.0	100.0	100.0	100.0
7.2	49.6	30	1.76	0.54	100.0	100.0	100.0	100.0	100.0	100.0	100.0	100.0
9.3	64.1	23	2.31	0.70	100.0	100.0	100.0	100.0	100.0	100.0	100.0	100.0
12.0	82.7	18	2.98	0.91	100.0	100.0	100.0	100.0	100.0	100.0	100.0	100.0
15.5	106.9	14	3.85	1.17	100.0	100.0	100.0	100.0	100.0	100.0	100.0	100.0
20	137.9	11	4.97	1.51	100.0	100.0	100.0	100.0	100.0	100.0	100.0	100.0
25	172.4	8.6	6.41	2.0	100.0	100.0	100.0	100.0	100.0	100.0	100.0	100.0
35	241.3	6.1	8.01	2.4	100.0	100.0	100.0	100.0	100.0	100.0	100.0	100.0
45	310.3	4.8	11.2	3.4	100.0	100.0	100.0	100.0	100.0	100.0	100.0	100.0
55	379.2	3.9	14.4	4.4	100.0	100.0	100.0	100.0	100.0	100.0	100.0	100.0
75	517.1	2.9	17.6	5.4	100.0	100.0	100.0	100.0	100.0	100.0	100.0	100.0
95	655.0	2.3	24.0	7.3	100.0	100.0	100.0	100.0	100.0	100.0	100.0	100.0
120	827.4	1.8	30.5	9.3	100.0	100.0	100.0	100.0	100.0	100.0	100.0	100.0
150	1,034	1.4	38.5	11.7	100.0	100.0	100.0	100.0	100.0	100.0	100.0	99.9
200	1,379	1.1	48.1	14.7	100.0	100.0	100.0	100.0	100.0	100.0	100.0	99.8
260	1,793	0.82	64.1	19.5	100.0	100.0	100.0	100.0	100.0	100.0	100.0	98.6
350	2,413	0.61	83.4	25.4	100.0	100.0	100.0	100.0	100.0	99.4	99.9	95.7
430	2,965	0.50	112	34.1	100.0	100.0	100.0	100.0	100.0	97.8	99.2	84.4
550	3,792	0.39	138	42.1	99.6	100.0	100.0	100.0	100.0	96.0	97.3	62.1
725	4,999	0.30	176	53.6	99.4	100.0	100.0	100.0	100.0	91.8	87.6	51.4
925	6,378	0.23	232	70.7	98.4	100.0	100.0	100.0	100.0	97.3	78.1	53.9
1,200	8,274	0.18	297	90.5	95.3	100.0	100.0	100.0	100.0	90.8	68.5	47.0
1,550	10,687	0.14	385	117.3	89.4	98.8	99.4	99.2	99.2	72.7	57.0	38.5
2,000	13,790	0.11	497	151.5	86.9	97.7	99.2	99.2	99.2	40.1	48.1	32.6
2,600	17,926	0.08	641	195.4	48.3	96.5	99.2	99.2	99.2	34.8	44.0	26.6
3,350	23,097	0.06	834	254.2	33.0	93.8	98.9	98.9	98.9	28.4	40.8	20.9
4,300	29,647	0.05	1074	327.4	22.7	88.2	95.6	95.6	95.6	23.2	38.5	16.5
5,550	38,266	0.04	1378	420.0	17.7	75.3	91.3	91.3	91.3	19.2	35.9	11.8
7,200	49,642	0.03	1779	542.2	14.1	61.8	78.6	78.6	78.6	15.4	34.7	7.0
9,300	64,121	0.02	2308	703.5	9.9	43.6	53.4	53.4	53.4	11.5	31.0	2.4

All Hg calculations assume air-mercury $\sigma=484$ dyne/cm, contact angle=140deg.

Gas-Brine Pc assumes insitu gas-brine $\sigma\cos\theta=40$ dyne/cm

Gas-Brine height assumes gas density gradient = 0.0935 psi/ft; 2.115 kPa/m

Gas-Brine height assumes brine density gradient 0.430 psi/ft; 9.727 kPa/m

Analysis of Critical Permeability, Capillary Pressure

and Electrical Properties for Mesaverde

Tight Gas Sandstones from Western U.S. Basins

US DOE # DE-FC26-05NT42660 Final Scientific Report

Alan P. Byrnes, Robert M. Cluff, John C. Webb

Appendix 4
Mercury Injection Capillary Pressure Analysis (In situ Analyses)
US DOE #DE-FC26-05NT42660 Final Scientific/Technical Report
Alan P. Byrnes, Robert M. Cluff, and John C. Webb

					Piceance 504510927 PA 424-34 PA424 - 6645.5 ft (A2)	Piceance 504511402 Last Dance 43C-3-792 B43C - 3544.85 ft (A)	Piceance 504511402 Last Dance 43C-3-792 B43C - 3555.4 ft (B)	Piceance 504511402 Last Dance 43C-3-792 B43C - 4004.3 ft (C)	Piceance 504511402 Last Dance 43C-3-792 B43C - 4013.25 ft (A)	Piceance 504511402 Last Dance 43C-3-792 B43C - 4416.6 ft (A)	Piceance 504511402 Last Dance 43C-3-792 B43C - 5715.4 ft (A)
Net Confining Pressure = 4,000 psi (27.6 MPa)					1.82E-06	4.64E-04	1.05E-03	2.59E-05	1.60E-04	1.74E-05	3.15E-06
<i>In situ</i> Klinkenberg Permeability (mm ²)=					0.00184	0.470	1.06	0.0262	0.1626	0.0176	0.00319
<i>In situ</i> Klinkenberg Permeability (mD) =					10.0	11.2	11.4	10.5	11.9	13.6	7.7
Routine Porosity =											
Mercury Injection Capillary Pressure (psia)	Mercury Injection Capillary Pressure (kPa)	Approx. Pore Entry Diameter (mm)	Approx. Gas-Water Height Above Free Water Level (ft)	Approx. Gas-Water Height Above Free Water Level (m)	<i>In situ</i> Cumulative Wetting Phase Saturation (% pore vol)	<i>In situ</i> Cumulative Wetting Phase Saturation (% pore vol)	<i>In situ</i> Cumulative Wetting Phase Saturation (% pore vol)	<i>In situ</i> Cumulative Wetting Phase Saturation (% pore vol)	<i>In situ</i> Cumulative Wetting Phase Saturation (% pore vol)	<i>In situ</i> Cumulative Wetting Phase Saturation (% pore vol)	<i>In situ</i> Cumulative Wetting Phase Saturation (% pore vol)
2.0	13.8	107	0.10	0.03	100.0	100.0	100.0	100.0	100.0	100.0	100.0
2.5	17.2	86	0.64	0.20	100.0	100.0	100.0	100.0	100.0	100.0	100.0
3.3	22.8	65	0.80	0.24	100.0	100.0	100.0	100.0	100.0	100.0	100.0
4.3	29.6	50	1.06	0.32	100.0	100.0	100.0	100.0	100.0	100.0	100.0
5.5	37.9	39	1.38	0.42	100.0	100.0	100.0	100.0	100.0	100.0	100.0
7.2	49.6	30	1.76	0.54	100.0	100.0	100.0	100.0	100.0	100.0	100.0
9.3	64.1	23	2.31	0.70	100.0	100.0	100.0	100.0	100.0	100.0	100.0
12.0	82.7	18	2.98	0.91	100.0	100.0	99.9	100.0	100.0	100.0	100.0
15.5	106.9	14	3.85	1.17	100.0	100.0	99.3	100.0	100.0	100.0	100.0
20	137.9	11	4.97	1.51	100.0	100.0	99.1	100.0	100.0	100.0	100.0
25	172.4	8.6	6.41	2.0	100.0	100.0	99.0	100.0	100.0	100.0	100.0
35	241.3	6.1	8.01	2.4	100.0	100.0	98.8	100.0	100.0	100.0	100.0
45	310.3	4.8	11.2	3.4	100.0	99.7	79.9	100.0	100.0	100.0	100.0
55	379.2	3.9	14.4	4.4	100.0	99.4	62.5	100.0	100.0	100.0	100.0
75	517.1	2.9	17.6	5.4	100.0	98.9	55.0	100.0	97.8	100.0	100.0
95	655.0	2.3	24.0	7.3	100.0	81.8	45.9	99.9	92.9	100.0	100.0
120	827.4	1.8	30.5	9.3	100.0	56.5	40.1	99.8	87.1	100.0	100.0
150	1,034	1.4	38.5	11.7	100.0	45.1	33.9	99.7	71.4	100.0	100.0
200	1,379	1.1	48.1	14.7	100.0	41.3	31.0	99.4	59.9	100.0	100.0
260	1,793	0.82	64.1	19.5	100.0	37.6	26.9	91.4	53.7	99.5	100.0
350	2,413	0.61	83.4	25.4	100.0	34.6	24.0	74.1	48.8	97.9	100.0
430	2,965	0.50	112	34.1	100.0	31.4	21.0	65.1	43.8	60.4	99.9
550	3,792	0.39	138	42.1	100.0	29.3	19.2	60.3	41.0	52.6	99.7
725	4,999	0.30	176	53.6	99.1	26.7	17.4	55.7	37.6	47.1	98.7
925	6,378	0.23	232	70.7	84.4	23.5	15.5	52.5	33.6	40.4	94.7
1,200	8,274	0.18	297	90.5	73.8	21.5	13.0	51.2	28.9	34.4	91.3
1,550	10,687	0.14	385	117.3	56.8	18.6	11.6	49.1	24.2	29.1	79.5
2,000	13,790	0.11	497	151.5	41.7	16.3	10.5	47.9	19.7	24.0	60.9
2,600	17,926	0.08	641	195.4	35.5	14.7	10.0	47.4	16.2	19.2	51.5
3,350	23,097	0.06	834	254.2	30.5	12.7	8.8	46.1	12.3	15.3	47.8
4,300	29,647	0.05	1074	327.4	25.1	11.3	8.3	45.4	9.3	11.3	43.6
5,550	38,266	0.04	1378	420.0	20.6	8.9	7.2	44.6	6.6	9.1	40.2
7,200	49,642	0.03	1779	542.2	16.2	6.2	6.6	43.9	4.3	7.1	37.0
9,300	64,121	0.02	2308	703.5	10.8	2.9	6.2	43.6	2.2	4.2	32.2

All Hg calculations assume air-mercury $\sigma=484$ dyne/cm, contact angle=140deg.

Gas-Brine Pc assumes insitu gas-brine $\sigma\cos\theta=40$ dyne/cm

Gas-Brine height assumes gas density gradient = 0.0935 psi/ft; 2.115 kPa/m

Gas-Brine height assumes brine density gradient 0.430 psi/ft; 9.727 kPa/m

Analysis of Critical Permeability, Capillary Pressure
and Electrical Properties for Mesaverde

Tight Gas Sandstones from Western U.S. Basins

US DOE # DE-FC26-05NT42660 Final Scientific Report

Alan P. Byrnes, Robert M. Cluff, John C. Webb

Appendix 4
Mercury Injection Capillary Pressure Analysis (In situ Analyses)
US DOE #DE-FC26-05NT42660 Final Scientific/Technical Report
Alan P. Byrnes, Robert M. Cluff, and John C. Webb

Net Confining Pressure = 4,000 psi (27.6 MPa)
In situ Klinkenberg Permeability (mm²)=
In situ Klinkenberg Permeability (mD) =
 Routine Porosity =

Piceance 504511402 Last Dance 43C-3-792 B43C - 6042.4 ft (B)	Piceance 05045xxxxx 1 Book Cliffs R091 - 255.9 ft (A2)	Powder River 4900525627 1 Barlow 21-20 E393 - 6994.1 ft (A)	Powder River 4900525627 1 Barlow 21-20 E393 - 7001.1 ft (A)	Powder River 4900525627 1 Barlow 21-20 E393 - 7027.2 ft (A)	Powder River 4900905481 3 Shawnee S838 - 6988.0 A	Powder River 4900906335 2 Shawnee S835 - 6991.2 ft (A)	Powder River 4900921513 2 Fred State E932 - 7544.1 ft (A)
6.71E-07	8.89E-02	3.60E-02	3.41E-02	2.50E-03	5.08E-03	7.53E-06	3.48E-03
0.00068	90.1	36.5	34.6	2.53	5.15	0.00763	3.53
6.1	24.3	18.1	17.0	14.7	17.3	9.0	16.6

Mercury Injection Capillary Pressure (psia)	Mercury Injection Capillary Pressure (kPa)	Approx. Pore Entry Diameter (mm)	Approx. Gas-Water Height Above Free Water Level (ft)	Approx. Gas-Water Height Above Free Water Level (m)	<i>In situ</i> Cumulative Wetting Phase Saturation (% pore vol)	<i>In situ</i> Cumulative Wetting Phase Saturation (% pore vol)	<i>In situ</i> Cumulative Wetting Phase Saturation (% pore vol)	<i>In situ</i> Cumulative Wetting Phase Saturation (% pore vol)	<i>In situ</i> Cumulative Wetting Phase Saturation (% pore vol)	<i>In situ</i> Cumulative Wetting Phase Saturation (% pore vol)	<i>In situ</i> Cumulative Wetting Phase Saturation (% pore vol)	<i>In situ</i> Cumulative Wetting Phase Saturation (% pore vol)	<i>In situ</i> Cumulative Wetting Phase Saturation (% pore vol)
2.0	13.8	107	0.10	0.03	100.0	100.0	100.0	100.0	100.0	100.0	100.0	100.0	100.0
2.5	17.2	86	0.64	0.20	100.0	100.0	100.0	100.0	100.0	100.0	100.0	100.0	100.0
3.3	22.8	65	0.80	0.24	100.0	100.0	100.0	100.0	100.0	100.0	100.0	100.0	100.0
4.3	29.6	50	1.06	0.32	100.0	100.0	100.0	100.0	100.0	100.0	100.0	100.0	100.0
5.5	37.9	39	1.38	0.42	100.0	100.0	100.0	100.0	100.0	100.0	100.0	100.0	100.0
7.2	49.6	30	1.76	0.54	100.0	100.0	100.0	100.0	100.0	100.0	100.0	100.0	100.0
9.3	64.1	23	2.31	0.70	100.0	100.0	100.0	100.0	100.0	100.0	100.0	100.0	100.0
12.0	82.7	18	2.98	0.91	100.0	99.8	100.0	100.0	100.0	100.0	100.0	100.0	100.0
15.5	106.9	14	3.85	1.17	100.0	68.3	99.9	100.0	100.0	100.0	100.0	100.0	100.0
20	137.9	11	4.97	1.51	100.0	58.2	98.2	99.9	100.0	100.0	100.0	100.0	100.0
25	172.4	8.6	6.41	2.0	100.0	50.2	59.2	86.6	100.0	100.0	100.0	100.0	100.0
35	241.3	6.1	8.01	2.4	100.0	47.3	52.1	56.4	100.0	100.0	100.0	100.0	99.9
45	310.3	4.8	11.2	3.4	100.0	44.0	44.6	44.7	100.0	88.9	100.0	100.0	94.2
55	379.2	3.9	14.4	4.4	100.0	41.2	40.7	40.0	99.9	60.7	100.0	100.0	63.7
75	517.1	2.9	17.6	5.4	100.0	39.5	38.1	37.3	86.6	50.2	100.0	100.0	56.7
95	655.0	2.3	24.0	7.3	100.0	36.7	34.9	33.8	55.5	41.7	100.0	100.0	49.9
120	827.4	1.8	30.5	9.3	99.8	34.6	32.5	31.2	49.1	37.9	100.0	100.0	45.8
150	1,034	1.4	38.5	11.7	98.3	31.9	31.2	28.3	45.0	33.5	100.0	100.0	41.9
200	1,379	1.1	48.1	14.7	98.2	29.9	27.8	26.0	41.4	30.7	99.9	99.9	38.9
260	1,793	0.82	64.1	19.5	98.2	27.2	25.6	23.4	37.6	28.2	99.8	99.8	36.0
350	2,413	0.61	83.4	25.4	98.0	24.7	23.5	21.0	34.3	26.3	99.3	99.3	33.1
430	2,965	0.50	112	34.1	98.0	21.9	21.0	18.2	30.5	24.1	95.3	95.3	30.4
550	3,792	0.39	138	42.1	98.0	19.9	19.6	16.6	28.2	22.3	90.2	90.2	28.6
725	4,999	0.30	176	53.6	97.8	17.5	17.5	14.8	25.5	21.3	82.7	82.7	26.4
925	6,378	0.23	232	70.7	96.5	15.1	15.3	12.7	22.7	19.5	69.1	69.1	23.7
1,200	8,274	0.18	297	90.5	95.8	13.0	13.4	11.2	20.3	17.9	59.0	59.0	20.7
1,550	10,687	0.14	385	117.3	92.6	10.8	11.6	9.5	17.5	15.9	59.0	59.0	18.0
2,000	13,790	0.11	497	151.5	81.6	8.2	9.7	8.1	15.5	13.2	59.0	59.0	14.9
2,600	17,926	0.08	641	195.4	74.2	6.8	8.0	6.8	14.1	10.6	59.0	59.0	12.6
3,350	23,097	0.06	834	254.2	63.0	5.7	6.1	5.7	12.0	8.1	59.0	59.0	10.1
4,300	29,647	0.05	1074	327.4	56.9	4.2	4.7	4.3	9.8	6.0	59.0	59.0	7.9
5,550	38,266	0.04	1378	420.0	52.4	3.3	3.3	3.0	7.3	4.3	59.0	59.0	5.4
7,200	49,642	0.03	1779	542.2	49.3	2.1	1.8	2.1	5.0	2.8	59.0	59.0	3.4
9,300	64,121	0.02	2308	703.5	43.2	0.8	0.0	0.7	2.2	0.3	59.0	59.0	0.3

All Hg calculations assume air-mercury $\sigma=484$ dyne/cm, contact angle=140deg.

Gas-Brine Pc assumes insitu gas-brine $\sigma\cos\theta=40$ dyne/cm

Gas-Brine height assumes gas density gradient = 0.0935 psi/ft; 2.115 kPa/m

Gas-Brine height assumes brine density gradient 0.430 psi/ft; 9.727 kPa/m

Analysis of Critical Permeability, Capillary Pressure

and Electrical Properties for Mesaverde

Tight Gas Sandstones from Western U.S. Basins

US DOE # DE-FC26-05NT42660 Final Scientific Report

Alan P. Byrnes, Robert M. Cluff, John C. Webb

Appendix 4
Mercury Injection Capillary Pressure Analysis (In situ Analyses)
US DOE #DE-FC26-05NT42660 Final Scientific/Technical Report
Alan P. Byrnes, Robert M. Cluff, and John C. Webb

					Powder River 4900921513 2 Fred State E932 - 7546.7 ft (A)	Powder River 4900921513 2 Fred State E932 - 7550.1 ft (A)	Sand Wash 508106718 1-691-0513 West Craig T717 - 1747.9 ft (A)	Sand Wash 508106718 1-691-0513 West Craig T717 - 1747.9 ft (B)	Sand Wash 508106718 1-691-0513 West Craig T717 - 1750.1 ft (A)	Sand Wash 508106724 1-791-2613 Craig Dome T715 - 3469.2 ft (A)	Uinta 4304730545 2-7 Flat Mesa E946 - 6468.4 ft (C)
Net Confining Pressure = 4,000 psi (27.6 MPa)					4.02E-05	1.48E-07	1.24E-06	1.68E-07	1.29E-06	2.98E-02	3.85E-04
<i>In situ</i> Klinkenberg Permeability (mm ²)=					0.0407	0.00015	0.00126	0.00017	0.00131	30.2	0.390
<i>In situ</i> Klinkenberg Permeability (mD) =					13.1	3.4	6.0	5.1	6.3	17.8	12.0
Routine Porosity =											
Mercury Injection Capillary Pressure (psia)	Mercury Injection Capillary Pressure (kPa)	Approx. Pore Entry Diameter (mm)	Approx. Gas-Water Height Above Free Water Level (ft)	Approx. Gas-Water Height Above Free Water Level (m)	<i>In situ</i> Cumulative Wetting Phase Saturation (% pore vol)	<i>In situ</i> Cumulative Wetting Phase Saturation (% pore vol)	<i>In situ</i> Cumulative Wetting Phase Saturation (% pore vol)	<i>In situ</i> Cumulative Wetting Phase Saturation (% pore vol)	<i>In situ</i> Cumulative Wetting Phase Saturation (% pore vol)	<i>In situ</i> Cumulative Wetting Phase Saturation (% pore vol)	<i>In situ</i> Cumulative Wetting Phase Saturation (% pore vol)
2.0	13.8	107	0.10	0.03	100.0	100.0	100.0	100.0	100.0	100.0	100.0
2.5	17.2	86	0.64	0.20	100.0	100.0	100.0	100.0	100.0	100.0	100.0
3.3	22.8	65	0.80	0.24	100.0	100.0	100.0	100.0	100.0	100.0	100.0
4.3	29.6	50	1.06	0.32	100.0	100.0	100.0	100.0	100.0	100.0	100.0
5.5	37.9	39	1.38	0.42	100.0	100.0	100.0	100.0	100.0	100.0	100.0
7.2	49.6	30	1.76	0.54	100.0	100.0	100.0	100.0	100.0	100.0	100.0
9.3	64.1	23	2.31	0.70	100.0	100.0	100.0	100.0	100.0	100.0	100.0
12.0	82.7	18	2.98	0.91	100.0	100.0	100.0	100.0	100.0	100.0	100.0
15.5	106.9	14	3.85	1.17	100.0	100.0	100.0	100.0	100.0	100.0	100.0
20	137.9	11	4.97	1.51	100.0	100.0	100.0	100.0	100.0	99.5	100.0
25	172.4	8.6	6.41	2.0	100.0	100.0	100.0	100.0	100.0	62.3	100.0
35	241.3	6.1	8.01	2.4	100.0	100.0	100.0	100.0	100.0	51.6	100.0
45	310.3	4.8	11.2	3.4	100.0	100.0	100.0	100.0	100.0	42.6	100.0
55	379.2	3.9	14.4	4.4	100.0	100.0	100.0	100.0	100.0	38.3	100.0
75	517.1	2.9	17.6	5.4	100.0	100.0	100.0	100.0	100.0	34.8	99.7
95	655.0	2.3	24.0	7.3	100.0	100.0	100.0	100.0	100.0	31.6	99.5
120	827.4	1.8	30.5	9.3	100.0	100.0	100.0	100.0	100.0	29.0	94.1
150	1,034	1.4	38.5	11.7	100.0	100.0	100.0	100.0	100.0	25.5	65.2
200	1,379	1.1	48.1	14.7	97.8	100.0	100.0	100.0	100.0	24.0	59.0
260	1,793	0.82	64.1	19.5	92.0	100.0	100.0	100.0	100.0	21.8	52.5
350	2,413	0.61	83.4	25.4	75.5	100.0	100.0	100.0	100.0	20.3	47.2
430	2,965	0.50	112	34.1	68.5	100.0	100.0	100.0	100.0	18.2	41.6
550	3,792	0.39	138	42.1	64.6	100.0	100.0	100.0	99.6	17.0	37.9
725	4,999	0.30	176	53.6	59.9	100.0	100.0	100.0	99.4	15.2	33.6
925	6,378	0.23	232	70.7	53.8	100.0	100.0	100.0	99.2	13.3	29.3
1,200	8,274	0.18	297	90.5	48.6	100.0	100.0	100.0	99.0	11.6	25.1
1,550	10,687	0.14	385	117.3	43.7	100.0	99.6	100.0	96.8	9.6	21.9
2,000	13,790	0.11	497	151.5	38.7	100.0	99.1	99.6	93.9	8.1	18.6
2,600	17,926	0.08	641	195.4	34.0	100.0	98.7	99.5	90.1	6.2	15.6
3,350	23,097	0.06	834	254.2	28.6	100.0	97.4	99.0	81.8	4.7	13.0
4,300	29,647	0.05	1074	327.4	23.7	99.1	91.6	98.4	56.3	3.7	10.1
5,550	38,266	0.04	1378	420.0	17.9	97.4	75.6	93.9	48.1	2.4	7.7
7,200	49,642	0.03	1779	542.2	12.8	94.7	60.8	88.7	40.5	1.5	5.7
9,300	64,121	0.02	2308	703.5	7.2	78.8	46.4	81.7	31.0	0.1	2.6

All Hg calculations assume air-mercury $\sigma=484$ dyne/cm, contact angle=140deg.

Gas-Brine Pc assumes insitu gas-brine $\sigma\cos\theta=40$ dyne/cm

Gas-Brine height assumes gas density gradient = 0.0935 psi/ft; 2.115 kPa/m

Gas-Brine height assumes brine density gradient 0.430 psi/ft; 9.727 kPa/m

Analysis of Critical Permeability, Capillary Pressure and Electrical Properties for Mesaverde

Tight Gas Sandstones from Western U.S. Basins

US DOE # DE-FC26-05NT42660 Final Scientific Report

Alan P. Byrnes, Robert M. Cluff, John C. Webb

Appendix 4
Mercury Injection Capillary Pressure Analysis (In situ Analyses)
US DOE #DE-FC26-05NT42660 Final Scientific/Technical Report
Alan P. Byrnes, Robert M. Cluff, and John C. Webb

					Uinta 4304730545 2-7 Flat Mesa E946 - 6486.4 ft (C)	Uinta 4304730545 2-7 Flat Mesa E946 - 6486.7 ft (C)	Uinta 4304730545 2-7 Flat Mesa E946 - 6527.6 ft (C)	Uinta 4304730545 2-7 Flat Mesa E946 - 6530.3 ft (C)	Uinta 4304730545 2-7 Flat Mesa E946 - 6550.5 ft (A)	Uinta 4304730545 2-7 Flat Mesa E946 - 7279.9 ft (C)	Uinta 4304730545 2-7 Flat Mesa E946 - 7293.5 ft (C)
Net Confining Pressure = 4,000 psi (27.6 MPa)					6.25E-04	1.80E-04	9.65E-05	3.59E-05	1.09E-07	2.32E-06	4.84E-07
<i>In situ</i> Klinkenberg Permeability (mm ²)=					0.633	0.182	0.0978	0.0364	0.00011	0.00235	0.00049
<i>In situ</i> Klinkenberg Permeability (mD) =					12.1	9.6	9.8	9.0	1.3	6.9	3.3
Routine Porosity =											
Mercury Injection Capillary Pressure (psia)	Mercury Injection Capillary Pressure (kPa)	Approx. Pore Entry Diameter (mm)	Approx. Gas-Water Height Above Free Water Level (ft)	Approx. Gas-Water Height Above Free Water Level (m)	<i>In situ</i> Cumulative Wetting Phase Saturation (% pore vol)	<i>In situ</i> Cumulative Wetting Phase Saturation (% pore vol)	<i>In situ</i> Cumulative Wetting Phase Saturation (% pore vol)	<i>In situ</i> Cumulative Wetting Phase Saturation (% pore vol)	<i>In situ</i> Cumulative Wetting Phase Saturation (% pore vol)	<i>In situ</i> Cumulative Wetting Phase Saturation (% pore vol)	<i>In situ</i> Cumulative Wetting Phase Saturation (% pore vol)
2.0	13.8	107	0.10	0.03	100.0	100.0	100.0	100.0	100.0	100.0	100.0
2.5	17.2	86	0.64	0.20	100.0	100.0	100.0	100.0	100.0	100.0	100.0
3.3	22.8	65	0.80	0.24	100.0	100.0	100.0	100.0	100.0	100.0	100.0
4.3	29.6	50	1.06	0.32	100.0	100.0	100.0	100.0	100.0	100.0	100.0
5.5	37.9	39	1.38	0.42	100.0	100.0	100.0	100.0	100.0	100.0	100.0
7.2	49.6	30	1.76	0.54	100.0	100.0	100.0	100.0	100.0	100.0	100.0
9.3	64.1	23	2.31	0.70	100.0	100.0	100.0	100.0	100.0	100.0	100.0
12.0	82.7	18	2.98	0.91	100.0	100.0	100.0	100.0	100.0	100.0	100.0
15.5	106.9	14	3.85	1.17	100.0	100.0	100.0	100.0	100.0	100.0	100.0
20	137.9	11	4.97	1.51	100.0	100.0	100.0	100.0	100.0	100.0	100.0
25	172.4	8.6	6.41	2.0	100.0	100.0	100.0	100.0	100.0	100.0	100.0
35	241.3	6.1	8.01	2.4	100.0	100.0	100.0	100.0	100.0	100.0	100.0
45	310.3	4.8	11.2	3.4	100.0	100.0	100.0	100.0	100.0	100.0	100.0
55	379.2	3.9	14.4	4.4	100.0	100.0	100.0	100.0	100.0	100.0	100.0
75	517.1	2.9	17.6	5.4	99.7	100.0	100.0	100.0	100.0	100.0	100.0
95	655.0	2.3	24.0	7.3	98.1	99.9	100.0	100.0	100.0	100.0	100.0
120	827.4	1.8	30.5	9.3	72.1	99.7	100.0	100.0	100.0	100.0	100.0
150	1,034	1.4	38.5	11.7	62.6	97.6	100.0	100.0	100.0	100.0	100.0
200	1,379	1.1	48.1	14.7	56.5	90.3	99.2	99.8	100.0	100.0	100.0
260	1,793	0.82	64.1	19.5	50.5	74.1	93.0	97.3	100.0	100.0	100.0
350	2,413	0.61	83.4	25.4	45.4	61.3	72.3	89.4	100.0	100.0	100.0
430	2,965	0.50	112	34.1	40.1	53.3	55.1	66.7	100.0	100.0	100.0
550	3,792	0.39	138	42.1	36.7	49.1	50.3	60.4	100.0	100.0	100.0
725	4,999	0.30	176	53.6	32.8	44.0	44.2	54.7	99.2	100.0	100.0
925	6,378	0.23	232	70.7	28.6	38.6	38.1	49.0	98.0	99.7	100.0
1,200	8,274	0.18	297	90.5	26.1	34.7	33.2	44.2	96.5	99.2	100.0
1,550	10,687	0.14	385	117.3	21.6	30.7	27.6	39.1	96.0	95.7	99.2
2,000	13,790	0.11	497	151.5	18.0	26.0	22.3	33.7	96.0	94.1	98.7
2,600	17,926	0.08	641	195.4	16.6	22.3	19.1	28.5	96.0	86.0	97.8
3,350	23,097	0.06	834	254.2	14.9	18.7	15.5	23.5	96.0	73.1	97.4
4,300	29,647	0.05	1074	327.4	13.0	15.3	12.8	18.4	89.9	39.1	95.1
5,550	38,266	0.04	1378	420.0	11.1	12.7	10.6	13.7	89.9	31.3	93.1
7,200	49,642	0.03	1779	542.2	10.2	10.5	8.9	11.0	89.9	27.2	88.7
9,300	64,121	0.02	2308	703.5	9.2	6.9	6.8	6.4	89.9	20.9	59.8

All Hg calculations assume air-mercury $\sigma=484$ dyne/cm, contact angle=140deg.

Gas-Brine Pc assumes insitu gas-brine $\sigma\cos\theta=40$ dyne/cm

Gas-Brine height assumes gas density gradient = 0.0935 psi/ft; 2.115 kPa/m

Gas-Brine height assumes brine density gradient 0.430 psi/ft; 9.727 kPa/m

Analysis of Critical Permeability, Capillary Pressure
and Electrical Properties for Mesaverde

Tight Gas Sandstones from Western U.S. Basins

US DOE # DE-FC26-05NT42660 Final Scientific Report

Alan P. Byrnes, Robert M. Cluff, John C. Webb

Appendix 4

Mercury Injection Capillary Pressure Analysis (In situ Analyses)

US DOE #DE-FC26-05NT42660 Final Scientific/Technical Report

Alan P. Byrnes, Robert M. Cluff, and John C. Webb

					Uinta 4304730545 2-7 Flat Mesa E946 - 7311.9 ft (C)	Uinta 4304730545 2-7 Flat Mesa E946 -7312.7 ft (C)	Uinta 4304730545 2-7 Flat Mesa E946 - 7689.7 ft (C)	Uinta 4304730852 4-5 US Lamco R829 - 5618.3 ft A	Uinta 4304730853 4-5 US Lamco R829 - 5633.1 ft (A)	Uinta 4304730860 3-24 US Lamco R999 - 6812.2 ft (A)	Uinta 4304735788 NBU 9-20-360 State KM360 - 8184.5 ft (A)	Uinta 4304735788 NBU 9-20-360 State KM360 - 8184.6 ft (A)
Net Confining Pressure = 4,000 psi (27.6 MPa)					1.51E-06	3.68E-06	6.10E-06	2.70E-04	8.39E-03	5.06E-06	2.25E-06	1.68E-06
<i>In situ</i> Klinkenberg Permeability (mm ²)=					0.00153	0.00373	0.00618	0.274	8.5	0.00513	0.00228	0.00170
<i>In situ</i> Klinkenberg Permeability (mD) =					5.9	8.4	7.8	9.0	11.7	5.1	7.0	6.9
Routine Porosity =												
Mercury Injection Capillary Pressure (psia)	Mercury Injection Capillary Pressure (kPa)	Approx. Pore Entry Diameter (mm)	Approx. Gas-Water Height Above Free Water Level (ft)	Approx. Gas-Water Height Above Free Water Level (m)	<i>In situ</i> Cumulative Wetting Phase Saturation (% pore vol)	<i>In situ</i> Cumulative Wetting Phase Saturation (% pore vol)	<i>In situ</i> Cumulative Wetting Phase Saturation (% pore vol)	<i>In situ</i> Cumulative Wetting Phase Saturation (% pore vol)	<i>In situ</i> Cumulative Wetting Phase Saturation (% pore vol)	<i>In situ</i> Cumulative Wetting Phase Saturation (% pore vol)	<i>In situ</i> Cumulative Wetting Phase Saturation (% pore vol)	<i>In situ</i> Cumulative Wetting Phase Saturation (% pore vol)
2.0	13.8	107	0.10	0.03	100.0	100.0	100.0	100.0	100.0	100.0	100.0	100.0
2.5	17.2	86	0.64	0.20	100.0	100.0	100.0	100.0	100.0	100.0	100.0	100.0
3.3	22.8	65	0.80	0.24	100.0	100.0	100.0	100.0	100.0	100.0	100.0	100.0
4.3	29.6	50	1.06	0.32	100.0	100.0	100.0	100.0	100.0	100.0	100.0	100.0
5.5	37.9	39	1.38	0.42	100.0	100.0	100.0	100.0	100.0	100.0	100.0	100.0
7.2	49.6	30	1.76	0.54	100.0	100.0	100.0	100.0	100.0	100.0	100.0	100.0
9.3	64.1	23	2.31	0.70	100.0	100.0	100.0	100.0	100.0	100.0	100.0	100.0
12.0	82.7	18	2.98	0.91	100.0	100.0	100.0	100.0	100.0	100.0	100.0	100.0
15.5	106.9	14	3.85	1.17	100.0	100.0	100.0	100.0	99.8	100.0	100.0	100.0
20	137.9	11	4.97	1.51	100.0	100.0	100.0	100.0	99.6	100.0	100.0	100.0
25	172.4	8.6	6.41	2.0	100.0	100.0	100.0	100.0	93.9	100.0	100.0	100.0
35	241.3	6.1	8.01	2.4	100.0	100.0	100.0	100.0	75.4	100.0	100.0	100.0
45	310.3	4.8	11.2	3.4	100.0	100.0	100.0	99.8	53.9	100.0	100.0	100.0
55	379.2	3.9	14.4	4.4	100.0	100.0	100.0	100.0	48.2	100.0	100.0	100.0
75	517.1	2.9	17.6	5.4	100.0	100.0	100.0	99.1	46.6	100.0	100.0	100.0
95	655.0	2.3	24.0	7.3	100.0	100.0	100.0	97.3	43.9	100.0	100.0	100.0
120	827.4	1.8	30.5	9.3	100.0	100.0	100.0	94.2	42.1	100.0	100.0	100.0
150	1,034	1.4	38.5	11.7	100.0	100.0	100.0	66.7	39.8	100.0	100.0	100.0
200	1,379	1.1	48.1	14.7	100.0	100.0	100.0	62.4	38.6	100.0	100.0	99.9
260	1,793	0.82	64.1	19.5	100.0	100.0	100.0	57.5	36.5	100.0	99.9	99.9
350	2,413	0.61	83.4	25.4	100.0	100.0	100.0	53.8	34.9	100.0	99.8	99.5
430	2,965	0.50	112	34.1	100.0	100.0	99.4	49.3	32.8	98.0	99.4	99.2
550	3,792	0.39	138	42.1	100.0	100.0	99.1	45.9	31.2	95.5	99.2	99.0
725	4,999	0.30	176	53.6	100.0	98.8	96.5	42.0	28.8	88.3	98.7	98.5
925	6,378	0.23	232	70.7	99.5	93.3	68.3	36.7	25.5	68.7	97.5	97.6
1,200	8,274	0.18	297	90.5	99.4	88.2	60.9	33.0	22.4	62.9	95.5	94.3
1,550	10,687	0.14	385	117.3	97.4	79.9	47.1	28.6	18.1	57.3	91.0	88.1
2,000	13,790	0.11	497	151.5	95.2	67.6	37.4	25.3	14.4	47.6	73.7	72.9
2,600	17,926	0.08	641	195.4	90.2	52.7	30.4	22.2	11.2	33.2	48.0	56.8
3,350	23,097	0.06	834	254.2	80.0	43.8	21.8	18.5	7.7	28.7	30.2	36.7
4,300	29,647	0.05	1074	327.4	70.9	35.7	16.6	15.9	6.1	25.0	24.7	30.7
5,550	38,266	0.04	1378	420.0	62.8	29.1	12.7	13.1	4.4	22.6	19.1	26.2
7,200	49,642	0.03	1779	542.2	49.3	22.2	9.8	10.6	3.1	20.8	16.3	22.8
9,300	64,121	0.02	2308	703.5	34.4	16.2	5.4	7.4	0.8	17.1	11.9	18.8

All Hg calculations assume air-mercury $\sigma=484$ dyne/cm, contact angle=140deg.

Gas-Brine Pc assumes insitu gas-brine $\sigma\cos\theta=40$ dyne/cm

Gas-Brine height assumes gas density gradient = 0.0935 psi/ft; 2.115 kPa/m

Gas-Brine height assumes brine density gradient 0.430 psi/ft; 9.727 kPa/m

Analysis of Critical Permeability, Capillary Pressure

and Electrical Properties for Mesaverde

Tight Gas Sandstones from Western U.S. Basins

US DOE # DE-FC26-05NT42660 Final Scientific Report

Alan P. Byrnes, Robert M. Cluff, John C. Webb

Appendix 4
Mercury Injection Capillary Pressure Analysis (In situ Analyses)
US DOE #DE-FC26-05NT42660 Final Scientific/Technical Report
Alan P. Byrnes, Robert M. Cluff, and John C. Webb

					Uinta 4304735788 NBU 9-20-360 State KM360 - 8185.7 ft (A)	Uinta 4304735788 NBU 9-20-360 State KM360 - 8279.5 ft (A)	Uinta 4304736565 NBU 1022-1A Natural Butte KM1022 - 7808.7 ft (A)	Uinta 4304736565 NBU 1022-1A Natural Butte KM1022 - 7825.5 ft (A)	Uinta 4304736565 NBU 1022-1A Natural Butte KM1022 - 7825.5 ft (B)	Uinta 4304736565 NBU 1022-1A Natural Butte KM1022 - 7853.5 ft (B)
Net Confining Pressure = 4,000 psi (27.6 MPa)					7.99E-07	2.57E-07	5.65E-06	1.88E-07	2.96E-07	7.40E-07
<i>In situ</i> Klinkenberg Permeability (mm ²)=					0.00081	0.00026	0.00573	0.00019	0.00030	0.00075
<i>In situ</i> Klinkenberg Permeability (mD) =					5.7	7.6	9.8	5.8	4.7	4.0
Routine Porosity =										
Mercury Injection Capillary Pressure (psia)	Mercury Injection Capillary Pressure (kPa)	Approx. Pore Entry Diameter (mm)	Approx. Gas-Water Height Above Free Water Level (ft)	Approx. Gas-Water Height Above Free Water Level (m)	<i>In situ</i> Cumulative Wetting Phase Saturation (% pore vol)	<i>In situ</i> Cumulative Wetting Phase Saturation (% pore vol)	<i>In situ</i> Cumulative Wetting Phase Saturation (% pore vol)	<i>In situ</i> Cumulative Wetting Phase Saturation (% pore vol)	<i>In situ</i> Cumulative Wetting Phase Saturation (% pore vol)	<i>In situ</i> Cumulative Wetting Phase Saturation (% pore vol)
2.0	13.8	107	0.10	0.03	100.0	100.0	100.0	100.0	100.0	100.0
2.5	17.2	86	0.64	0.20	100.0	100.0	100.0	100.0	100.0	100.0
3.3	22.8	65	0.80	0.24	100.0	100.0	100.0	100.0	100.0	100.0
4.3	29.6	50	1.06	0.32	100.0	100.0	100.0	100.0	100.0	100.0
5.5	37.9	39	1.38	0.42	100.0	100.0	100.0	100.0	100.0	100.0
7.2	49.6	30	1.76	0.54	100.0	100.0	100.0	100.0	100.0	100.0
9.3	64.1	23	2.31	0.70	100.0	100.0	100.0	100.0	100.0	100.0
12.0	82.7	18	2.98	0.91	100.0	100.0	100.0	100.0	100.0	100.0
15.5	106.9	14	3.85	1.17	100.0	100.0	100.0	100.0	100.0	100.0
20	137.9	11	4.97	1.51	100.0	100.0	100.0	100.0	100.0	100.0
25	172.4	8.6	6.41	2.0	100.0	100.0	100.0	100.0	100.0	100.0
35	241.3	6.1	8.01	2.4	100.0	100.0	100.0	100.0	100.0	100.0
45	310.3	4.8	11.2	3.4	100.0	100.0	100.0	100.0	100.0	100.0
55	379.2	3.9	14.4	4.4	100.0	100.0	100.0	100.0	100.0	100.0
75	517.1	2.9	17.6	5.4	100.0	100.0	100.0	100.0	100.0	100.0
95	655.0	2.3	24.0	7.3	100.0	100.0	100.0	100.0	100.0	100.0
120	827.4	1.8	30.5	9.3	100.0	100.0	100.0	100.0	100.0	100.0
150	1,034	1.4	38.5	11.7	100.0	100.0	100.0	100.0	100.0	100.0
200	1,379	1.1	48.1	14.7	100.0	100.0	100.0	100.0	100.0	100.0
260	1,793	0.82	64.1	19.5	100.0	100.0	100.0	100.0	100.0	100.0
350	2,413	0.61	83.4	25.4	99.9	100.0	100.0	100.0	100.0	100.0
430	2,965	0.50	112	34.1	99.9	100.0	100.0	100.0	100.0	100.0
550	3,792	0.39	138	42.1	99.8	100.0	99.7	100.0	100.0	100.0
725	4,999	0.30	176	53.6	99.6	100.0	98.7	100.0	100.0	100.0
925	6,378	0.23	232	70.7	98.2	100.0	87.8	100.0	100.0	100.0
1,200	8,274	0.18	297	90.5	96.9	100.0	81.6	99.9	100.0	100.0
1,550	10,687	0.14	385	117.3	95.6	99.9	34.5	99.6	99.4	99.6
2,000	13,790	0.11	497	151.5	94.0	99.8	25.6	99.2	98.5	98.7
2,600	17,926	0.08	641	195.4	90.9	99.7	20.1	98.6	96.2	96.3
3,350	23,097	0.06	834	254.2	85.3	99.4	15.6	97.4	94.1	91.5
4,300	29,647	0.05	1074	327.4	73.5	96.4	12.0	93.0	86.2	86.4
5,550	38,266	0.04	1378	420.0	57.0	90.1	9.3	86.0	79.5	75.8
7,200	49,642	0.03	1779	542.2	38.2	80.0	7.7	78.0	70.7	65.2
9,300	64,121	0.02	2308	703.5	27.1	62.3	5.4	63.0	54.3	58.0

All Hg calculations assume air-mercury $\sigma=484$ dyne/cm, contact angle=140deg.

Gas-Brine Pc assumes insitu gas-brine $\sigma\cos\theta=40$ dyne/cm

Gas-Brine height assumes gas density gradient = 0.0935 psi/ft; 2.115 kPa/m

Gas-Brine height assumes brine density gradient 0.430 psi/ft; 9.727 kPa/m

Analysis of Critical Permeability, Capillary Pressure

and Electrical Properties for Mesaverde

Tight Gas Sandstones from Western U.S. Basins

US DOE # DE-FC26-05NT42660 Final Scientific Report

Alan P. Byrnes, Robert M. Cluff, John C. Webb

Appendix 4
Mercury Injection Capillary Pressure Analysis (In situ Analyses)
US DOE #DE-FC26-05NT42660 Final Scientific/Technical Report
Alan P. Byrnes, Robert M. Cluff, and John C. Webb

					Uinta 43019xxxx1 3 Book Cliffs S172 - 175.3 ft (A2)	Uinta 43019xxxx1 3 Book Cliffs S172 - 389.8 ft (A)	Uinta 43019xxxx1 3 Book Cliffs S172 - 392.5 ft (A2)	Washakie 4903705683 65-1-7 Arch Unit S276 - 4743 ft (A)	Washakie 4903705683 65-1-7 Arch Unit S276 - 4745 ft (A)	Washakie 4903720033 102-7-10 Arch Unit S265 - 4899.0 ft (A)	Washakie 4903721053 Unit 3 Five Mile Gulch E489 - 10650 ft (B)	Washakie 4903721053 Unit 3 Five Mile Gulch E489 - 10669 ft (A)
Net Confining Pressure = 4,000 psi (27.6 MPa)					1.84E-02	5.38E-06	9.08E-07	4.81E-04	2.84E-04	2.81E-02	5.03E-07	2.57E-06
<i>In situ</i> Klinkenberg Permeability (mm ²)=					18.6	0.00545	0.00092	0.487	0.288	28.5	0.00051	0.00260
<i>In situ</i> Klinkenberg Permeability (mD) =					21.5	9.9	11.7	14.1	14.8	20.1	5.8	6.7
Routine Porosity =												
Mercury Injection Capillary Pressure (psia)	Mercury Injection Capillary Pressure (kPa)	Approx. Pore Entry Diameter (mm)	Approx. Gas-Water Height Above Free Water Level (ft)	Approx. Gas-Water Height Above Free Water Level (m)	<i>In situ</i> Cumulative Wetting Phase Saturation (% pore vol)	<i>In situ</i> Cumulative Wetting Phase Saturation (% pore vol)	<i>In situ</i> Cumulative Wetting Phase Saturation (% pore vol)	<i>In situ</i> Cumulative Wetting Phase Saturation (% pore vol)	<i>In situ</i> Cumulative Wetting Phase Saturation (% pore vol)	<i>In situ</i> Cumulative Wetting Phase Saturation (% pore vol)	<i>In situ</i> Cumulative Wetting Phase Saturation (% pore vol)	<i>In situ</i> Cumulative Wetting Phase Saturation (% pore vol)
2.0	13.8	107	0.10	0.03	100.0	100.0	100.0	100.0	100.0	100.0	100.0	100.0
2.5	17.2	86	0.64	0.20	100.0	100.0	100.0	100.0	100.0	100.0	100.0	100.0
3.3	22.8	65	0.80	0.24	100.0	100.0	100.0	100.0	100.0	100.0	100.0	100.0
4.3	29.6	50	1.06	0.32	100.0	100.0	100.0	100.0	100.0	100.0	100.0	100.0
5.5	37.9	39	1.38	0.42	100.0	100.0	100.0	100.0	100.0	100.0	100.0	100.0
7.2	49.6	30	1.76	0.54	100.0	100.0	100.0	100.0	100.0	100.0	100.0	100.0
9.3	64.1	23	2.31	0.70	100.0	100.0	100.0	100.0	100.0	100.0	100.0	100.0
12.0	82.7	18	2.98	0.91	100.0	100.0	100.0	100.0	100.0	100.0	100.0	100.0
15.5	106.9	14	3.85	1.17	100.0	100.0	100.0	100.0	100.0	99.8	100.0	100.0
20	137.9	11	4.97	1.51	99.9	100.0	100.0	100.0	100.0	98.8	100.0	100.0
25	172.4	8.6	6.41	2.0	79.6	100.0	100.0	100.0	100.0	70.1	100.0	100.0
35	241.3	6.1	8.01	2.4	67.0	100.0	100.0	100.0	100.0	62.8	100.0	100.0
45	310.3	4.8	11.2	3.4	57.5	100.0	100.0	100.0	100.0	55.3	100.0	100.0
55	379.2	3.9	14.4	4.4	53.3	100.0	100.0	100.0	100.0	50.4	100.0	100.0
75	517.1	2.9	17.6	5.4	50.3	100.0	100.0	100.0	100.0	47.1	100.0	100.0
95	655.0	2.3	24.0	7.3	45.6	100.0	100.0	100.0	99.9	42.1	100.0	100.0
120	827.4	1.8	30.5	9.3	42.1	100.0	100.0	100.0	99.9	38.3	100.0	100.0
150	1,034	1.4	38.5	11.7	38.3	100.0	100.0	100.0	66.3	34.2	100.0	100.0
200	1,379	1.1	48.1	14.7	34.9	100.0	100.0	100.0	58.6	31.4	100.0	99.9
260	1,793	0.82	64.1	19.5	32.3	100.0	99.7	50.6	55.3	27.9	100.0	99.5
350	2,413	0.61	83.4	25.4	29.1	99.5	99.1	44.7	47.4	25.0	100.0	99.0
430	2,965	0.50	112	34.1	25.9	96.9	93.2	38.6	40.6	21.6	100.0	97.2
550	3,792	0.39	138	42.1	23.3	94.1	87.4	35.2	36.6	19.5	100.0	84.5
725	4,999	0.30	176	53.6	20.7	90.5	82.0	30.9	32.0	17.0	100.0	49.3
925	6,378	0.23	232	70.7	17.5	86.8	76.9	26.5	27.4	14.5	100.0	38.4
1,200	8,274	0.18	297	90.5	14.3	82.5	72.4	23.0	25.1	13.4	99.9	33.1
1,550	10,687	0.14	385	117.3	12.8	77.4	67.0	19.7	20.4	11.4	99.8	28.4
2,000	13,790	0.11	497	151.5	10.4	66.4	60.6	16.0	16.4	8.6	99.5	25.3
2,600	17,926	0.08	641	195.4	7.9	57.1	54.5	12.9	12.6	6.2	99.5	23.6
3,350	23,097	0.06	834	254.2	6.0	48.2	46.8	10.1	9.9	4.9	98.7	21.8
4,300	29,647	0.05	1074	327.4	4.4	40.4	39.6	7.6	7.7	4.1	95.7	20.2
5,550	38,266	0.04	1378	420.0	2.4	33.2	32.9	5.2	5.6	3.0	85.3	18.8
7,200	49,642	0.03	1779	542.2	1.4	27.1	26.6	3.7	4.0	2.1	65.3	18.2
9,300	64,121	0.02	2308	703.5	0.6	20.3	20.4	1.4	1.3	0.8	51.3	17.6

All Hg calculations assume air-mercury $\sigma=484$ dyne/cm, contact angle=140deg.

Gas-Brine Pc assumes insitu gas-brine $\sigma\cos\theta=40$ dyne/cm

Gas-Brine height assumes gas density gradient = 0.0935 psi/ft; 2.115 kPa/m

Gas-Brine height assumes brine density gradient 0.430 psi/ft; 9.727 kPa/m

Analysis of Critical Permeability, Capillary Pressure and Electrical Properties for Mesaverde

Tight Gas Sandstones from Western U.S. Basins

US DOE # DE-FC26-05NT42660 Final Scientific Report

Alan P. Byrnes, Robert M. Cluff, John C. Webb

Appendix 4
Mercury Injection Capillary Pressure Analysis (In situ Analyses)
US DOE #DE-FC26-05NT42660 Final Scientific/Technical Report
Alan P. Byrnes, Robert M. Cluff, and John C. Webb

					Washakie 4903722355 5 Dripping Rock DR5 - 12671.9 A	Washakie 4903722355 5 Dripping Rock DR5 - 12673.6 ft (A)	Washakie 4903722355 5 Dripping Rock DR5 - 12686.5 ft (A)	Washakie 9999999999 Wild Rose 1 (WLDR) - 10133.5 ft (A)	Washakie 9999999999 Wild Rose 1 (WLDR) - 10207.8 ft (A)
Net Confining Pressure = 4,000 psi (27.6 MPa)					3.15E-06	8.47E-06	1.18E-05	2.40E-06	1.89E-04
<i>In situ</i> Klinkenberg Permeability (mm ²)=					0.00319	0.00858	0.01191	0.00243	0.192
<i>In situ</i> Klinkenberg Permeability (mD) =					10.7	11.8	11.7	6.1	11.1
Routine Porosity =									
Mercury Injection Capillary Pressure (psia)	Mercury Injection Capillary Pressure (kPa)	Approx. Pore Entry Diameter (mm)	Approx. Gas-Water Height Above Free Water Level (ft)	Approx. Gas-Water Height Above Free Water Level (m)	<i>In situ</i> Cumulative Wetting Phase Saturation (% pore vol)	<i>In situ</i> Cumulative Wetting Phase Saturation (% pore vol)	<i>In situ</i> Cumulative Wetting Phase Saturation (% pore vol)	<i>In situ</i> Cumulative Wetting Phase Saturation (% pore vol)	<i>In situ</i> Cumulative Wetting Phase Saturation (% pore vol)
2.0	13.8	107	0.10	0.03	100.0	100.0	100.0	100.0	100.0
2.5	17.2	86	0.64	0.20	100.0	100.0	100.0	100.0	100.0
3.3	22.8	65	0.80	0.24	100.0	100.0	100.0	100.0	100.0
4.3	29.6	50	1.06	0.32	100.0	100.0	100.0	100.0	100.0
5.5	37.9	39	1.38	0.42	100.0	100.0	100.0	100.0	100.0
7.2	49.6	30	1.76	0.54	100.0	100.0	100.0	100.0	100.0
9.3	64.1	23	2.31	0.70	100.0	100.0	100.0	100.0	100.0
12.0	82.7	18	2.98	0.91	100.0	100.0	100.0	100.0	100.0
15.5	106.9	14	3.85	1.17	100.0	100.0	100.0	100.0	100.0
20	137.9	11	4.97	1.51	100.0	100.0	100.0	100.0	100.0
25	172.4	8.6	6.41	2.0	100.0	100.0	100.0	100.0	100.0
35	241.3	6.1	8.01	2.4	100.0	100.0	100.0	100.0	100.0
45	310.3	4.8	11.2	3.4	100.0	100.0	100.0	100.0	100.0
55	379.2	3.9	14.4	4.4	100.0	100.0	100.0	100.0	100.0
75	517.1	2.9	17.6	5.4	100.0	100.0	100.0	100.0	100.0
95	655.0	2.3	24.0	7.3	100.0	100.0	100.0	100.0	99.8
120	827.4	1.8	30.5	9.3	100.0	100.0	100.0	100.0	98.7
150	1,034	1.4	38.5	11.7	100.0	100.0	100.0	100.0	56.4
200	1,379	1.1	48.1	14.7	100.0	100.0	100.0	100.0	44.9
260	1,793	0.82	64.1	19.5	100.0	99.9	100.0	100.0	35.9
350	2,413	0.61	83.4	25.4	100.0	99.9	99.9	100.0	30.9
430	2,965	0.50	112	34.1	100.0	99.6	99.9	100.0	26.0
550	3,792	0.39	138	42.1	100.0	93.7	81.0	100.0	22.8
725	4,999	0.30	176	53.6	97.0	73.4	51.4	100.0	20.0
925	6,378	0.23	232	70.7	94.0	31.8	30.4	98.0	17.1
1,200	8,274	0.18	297	90.5	41.3	27.8	24.9	89.9	15.7
1,550	10,687	0.14	385	117.3	35.5	22.5	20.2	47.2	13.1
2,000	13,790	0.11	497	151.5	31.8	18.6	16.5	35.4	11.1
2,600	17,926	0.08	641	195.4	28.5	16.1	13.5	31.4	9.6
3,350	23,097	0.06	834	254.2	25.5	13.2	10.4	27.6	7.1
4,300	29,647	0.05	1074	327.4	21.8	10.4	8.4	23.1	5.4
5,550	38,266	0.04	1378	420.0	18.7	7.8	5.6	21.1	4.3
7,200	49,642	0.03	1779	542.2	15.5	5.1	3.6	19.1	3.5
9,300	64,121	0.02	2308	703.5	12.0	1.5	1.0	16.1	0.9

All Hg calculations assume air-mercury $\sigma=484$ dyne/cm, contact angle=140deg.

Gas-Brine Pc assumes insitu gas-brine $\sigma\cos\theta=40$ dyne/cm

Gas-Brine height assumes gas density gradient = 0.0935 psi/ft; 2.115 kPa/m

Gas-Brine height assumes brine density gradient 0.430 psi/ft; 9.727 kPa/m

Analysis of Critical Permeability, Capillary Pressure
and Electrical Properties for Mesaverde

Tight Gas Sandstones from Western U.S. Basins

US DOE # DE-FC26-05NT42660 Final Scientific Report

Alan P. Byrnes, Robert M. Cluff, John C. Webb

Appendix 4

US DOE #DE-FC26-05NT42660 Final Scientific/Technical Report

Alan P. Byrnes, Robert M. Cluff and John C. Webb

Mercury Injection Drainage-Imbibition Capillary Pressure Analysis

AMERICAN HUNTER EXPL: 1 OLD ROAD - E894 - 11936.3 ft (B)

In situ Klinkenberg Permeability (μm^2) =

2.27E-07

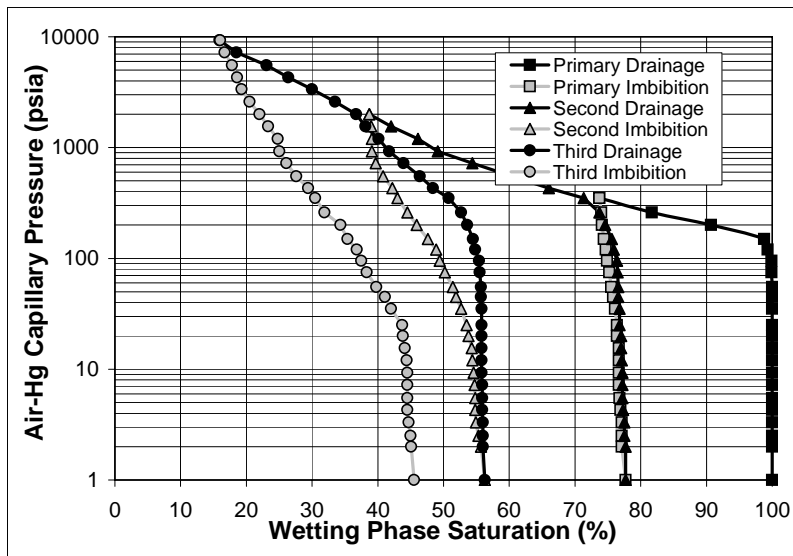
In situ Klinkenberg Permeability (mD) =

0.000230

Routine Porosity (%)=

5.0

Mercury Injection Capillary Pressure (psia)	Mercury Injection Capillary Pressure (kPa)	Approx. Pore Entry Diameter (μm)	Approx. Gas-Water Height Above Free Water Level (ft)	Approx. Gas-Water Height Above Free Water Level (m)	Drainage 1 Cumulative Wetting Phase Saturation (% pore vol)	Imbibition 1 Cumulative Wetting Phase Saturation (% pore vol)	Drainage 2 Cumulative Wetting Phase Saturation (% pore vol)	Imbibition 2 Cumulative Wetting Phase Saturation (% pore vol)	Drainage 3 Cumulative Wetting Phase Saturation (% pore vol)	Imbibition 3 Cumulative Wetting Phase Saturation (% pore vol)
2.0	13.8	107	0.10	0.03	100.0	88.3	88.3	76.0	76.0	71.6
2.5	17.2	86	0.64	0.20	100.0	87.3	88.2	75.1	75.6	71.1
3.3	22.8	65	0.80	0.24	100.0	87.1	87.6	74.9	75.4	71.1
4.3	29.6	50	1.06	0.32	100.0	87.1	87.3	74.9	74.9	71.0
5.5	37.9	39	1.38	0.42	100.0	86.6	86.8	74.5	74.5	70.8
7.2	49.6	30	1.76	0.54	100.0	86.3	86.4	74.3	74.3	70.8
9.3	64.1	23	2.31	0.70	100.0	86.2	86.3	74.0	74.1	70.7
12.0	82.7	18	2.98	0.91	100.0	85.7	86.1	74.0	73.9	70.5
15.5	106.9	14	3.85	1.17	100.0	85.5	85.8	73.7	73.7	70.2
20	137.9	11	4.97	1.51	100.0	85.4	85.5	73.4	73.4	70.1
25	172.4	8.6	6.41	2.0	100.0	85.1	85.3	73.2	73.2	70.0
35	241.3	6.1	8.01	2.4	100.0	84.8	85.2	73.1	73.2	69.9
45	310.3	4.8	11.2	3.4	100.0	84.7	85.1	73.0	73.0	69.7
55	379.2	3.9	14.4	4.4	100.0	84.5	85.0	72.8	72.7	69.4
75	517.1	2.9	17.6	5.4	100.0	84.1	85.0	72.5	72.7	69.0
95	655.0	2.3	24.0	7.3	100.0	84.0	84.8	72.3	72.4	69.0
120	827.4	1.8	30.5	9.3	100.0	83.6	84.7	71.9	72.4	68.9
150	1,034	1.4	38.5	11.7	100.0	83.6	84.5	71.9	72.4	68.7
200	1,379	1.1	48.1	14.7	100.0	83.5	84.5	71.8	72.4	68.6
260	1,793	0.82	64.1	19.5	100.0	82.8	84.4	71.8	72.2	68.4
350	2,413	0.61	83.4	25.4	100.0	82.8	84.3	71.8	72.2	68.4
430	2,965	0.50	112	34.1	99.9	82.8	84.2	71.0	72.2	68.4
550	3,792	0.39	138	42.1	99.5	82.4	84.0	70.8	72.2	68.4
725	4,999	0.30	176	53.6	99.4	82.2	83.9	70.6	72.2	68.4
925	6,378	0.23	232	70.7	98.9	82.0	83.9	69.8	72.0	68.4
1200	8,274	0.18	297	90.5	98.8	81.4	83.9	69.0	71.8	68.4
1550	10,687	0.14	385	117.3	97.6	81.4	83.5	69.0	71.2	68.4
2000	13,790	0.11	497	151.5	96.5	80.7	82.6	67.6	70.4	67.1
2600	17,926	0.08	641	195.4	96.2	79.6	82.6	66.2	70.3	65.7
3350	23,097	0.06	834	254.2	94.3	78.9	81.5	64.6	69.3	64.3
4300	29,647	0.05	1074	327.4	91.8	77.9	80.0	63.1	67.9	62.8
5550	38,266	0.04	1378	420.0	87.2	77.2	78.6	62.1	65.6	61.3
7200	49,642	0.03	1779	542.2	76.7	76.7	74.0	60.9	63.3	60.0
9300	64,121	0.02	2308	703.5			64.1	59.1	60.3	58.5
			2981	908.6			57.7	57.7	56.8	56.8

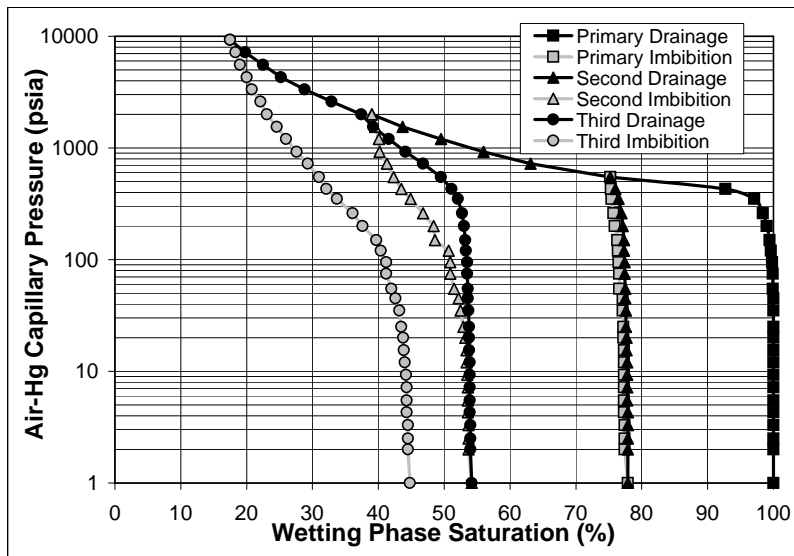


Mercury Injection Drainage-Imbibition Capillary Pressure Analysis

AMERICAN HUNTER EXPL: 1 OLD ROAD - E894 - 11936.3 ft (B)

In situ Klinkenberg Permeability (μm^2) = 2.86E-06
In situ Klinkenberg Permeability (mD) = 0.0029
 Routine Porosity (%) = 10.3

Mercury Injection Capillary Pressure (psia)	Mercury Injection Capillary Pressure (kPa)	Approx. Pore Entry Diameter (μm)	Approx. Gas-Water Height Above Free Water Level (ft)	Approx. Gas-Water Height Above Free Water Level (m)	Drainage 1 Cumulative Wetting Phase Saturation (% pore vol)	Imbibition 1 Cumulative Wetting Phase Saturation (% pore vol)	Drainage 2 Cumulative Wetting Phase Saturation (% pore vol)	Imbibition 2 Cumulative Wetting Phase Saturation (% pore vol)	Drainage 3 Cumulative Wetting Phase Saturation (% pore vol)	Imbibition 3 Cumulative Wetting Phase Saturation (% pore vol)
2.0	13.8	107	0.10	0.03	100.0	77.9	77.9	54.2	54.2	44.8
2.5	17.2	86	0.64	0.20	100.0	77.4	77.9	53.7	54.0	44.5
3.3	22.8	65	0.80	0.24	100.0	77.4	77.9	53.7	54.0	44.5
4.3	29.6	50	1.06	0.32	100.0	77.4	77.9	53.7	54.0	44.5
5.5	37.9	39	1.38	0.42	100.0	77.3	77.8	53.6	53.9	44.3
7.2	49.6	30	1.76	0.54	100.0	77.3	77.8	53.6	53.9	44.3
9.3	64.1	23	2.31	0.70	100.0	77.3	77.8	53.5	53.9	44.2
12.0	82.7	18	2.98	0.91	100.0	77.3	77.8	53.5	53.9	44.2
15.5	106.9	14	3.85	1.17	100.0	77.3	77.7	53.4	53.8	43.9
20	137.9	11	4.97	1.51	100.0	77.3	77.7	53.4	53.8	43.9
25	172.4	8.6	6.41	2.0	100.0	77.2	77.7	53.2	53.8	43.8
35	241.3	6.1	8.01	2.4	100.0	77.2	77.6	52.9	53.8	43.5
45	310.3	4.8	11.2	3.4	100.0	77.1	77.6	52.5	53.7	43.2
55	379.2	3.9	14.4	4.4	100.0	77.1	77.5	52.2	53.6	42.6
75	517.1	2.9	17.6	5.4	99.9	76.6	77.5	51.5	53.6	42.0
95	655.0	2.3	24.0	7.3	99.9	76.6	77.4	50.9	53.5	41.2
120	827.4	1.8	30.5	9.3	99.8	76.5	77.4	50.9	53.5	41.2
150	1,034	1.4	38.5	11.7	99.6	76.4	77.3	50.7	53.3	40.4
200	1,379	1.1	48.1	14.7	99.4	76.3	77.3	48.6	53.2	39.7
260	1,793	0.82	64.1	19.5	99.0	75.9	77.1	48.4	53.0	37.6
350	2,413	0.61	83.4	25.4	98.4	75.7	76.9	46.8	52.7	36.1
430	2,965	0.50	112	34.1	97.1	75.4	76.5	44.9	52.1	33.7
550	3,792	0.39	138	42.1	92.7	75.3	76.0	43.5	51.1	32.1
725	4,999	0.30	176	53.6	75.2	75.2	75.2	42.3	49.5	31.0
925	6,378	0.23	232	70.7			63.1	41.3	46.8	29.3
1200	8,274	0.18	297	90.5			56.0	40.2	44.1	27.6
1550	10,687	0.14	385	117.3			49.5	40.1	41.6	26.0
2000	13,790	0.11	497	151.5			43.7	39.5	39.2	24.6
2600	17,926	0.08	641	195.4			39.0	39.0	37.4	23.1
3350	23,097	0.06	834	254.2					32.9	22.1
4300	29,647	0.05	1074	327.4					28.8	20.8
5550	38,266	0.04	1378	420.0					25.2	20.0
7200	49,642	0.03	1779	542.2					22.5	19.0
9300	64,121	0.02	2308	703.5					19.8	18.3
			2981	908.6					17.5	17.5

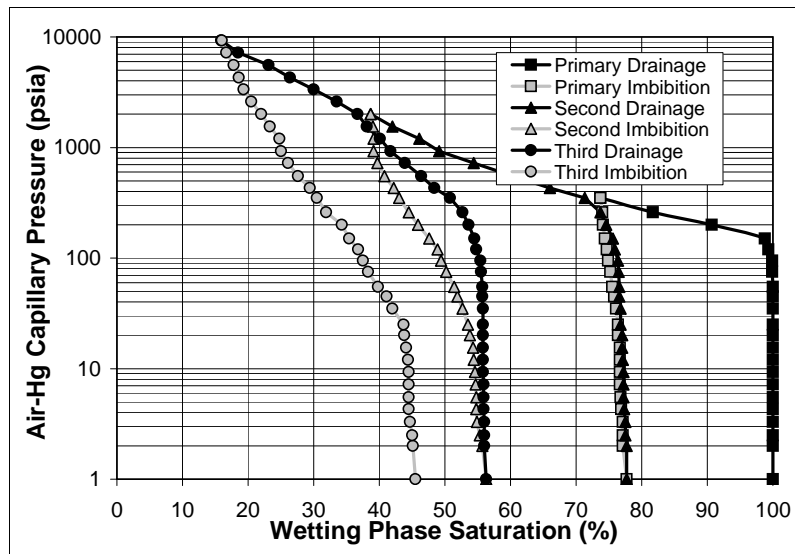


Mercury Injection Drainage-Imbibition Capillary Pressure Analysis

CER CORPORATION: MWX-2 SUPERIOR - T649 - 5734.1 ft (B)

In situ Klinkenberg Permeability (μm^2) = 5.03E-06
In situ Klinkenberg Permeability (mD) = 0.0051
 Routine Porosity (%) = 8.7

Mercury Injection Capillary Pressure (psia)	Mercury Injection Capillary Pressure (kPa)	Approx. Pore Entry Diameter (μm)	Approx. Gas-Water Height Above Free Water Level (ft)	Approx. Gas-Water Height Above Free Water Level (m)	Drainage 1 Cumulative Wetting Phase Saturation (% pore vol)	Imbibition 1 Cumulative Wetting Phase Saturation (% pore vol)	Drainage 2 Cumulative Wetting Phase Saturation (% pore vol)	Imbibition 2 Cumulative Wetting Phase Saturation (% pore vol)	Drainage 3 Cumulative Wetting Phase Saturation (% pore vol)	Imbibition 3 Cumulative Wetting Phase Saturation (% pore vol)
2.0	13.8	107	0.10	0.03	100.0	77.7	77.7	56.3	56.3	45.5
2.5	17.2	86	0.64	0.20	100.0	77.1	77.7	55.7	56.0	45.1
3.3	22.8	65	0.80	0.24	100.0	77.1	77.5	55.3	56.0	45.0
4.3	29.6	50	1.06	0.32	100.0	77.1	77.5	54.9	56.0	44.7
5.5	37.9	39	1.38	0.42	100.0	76.9	77.3	54.8	55.9	44.5
7.2	49.6	30	1.76	0.54	100.0	76.8	77.2	54.8	55.9	44.5
9.3	64.1	23	2.31	0.70	100.0	76.7	77.2	54.7	55.9	44.5
12.0	82.7	18	2.98	0.91	100.0	76.7	77.2	54.6	55.8	44.5
15.5	106.9	14	3.85	1.17	100.0	76.7	77.1	54.4	55.8	44.4
20	137.9	11	4.97	1.51	100.0	76.7	77.0	54.3	55.8	44.1
25	172.4	8.6	6.41	2.0	100.0	76.4	77.0	53.8	55.8	43.8
35	241.3	6.1	8.01	2.4	100.0	76.4	76.8	53.5	55.8	43.7
45	310.3	4.8	11.2	3.4	100.0	76.1	76.8	52.7	55.8	42.0
55	379.2	3.9	14.4	4.4	100.0	75.8	76.6	51.9	55.7	41.1
75	517.1	2.9	17.6	5.4	100.0	75.5	76.6	51.4	55.7	39.8
95	655.0	2.3	24.0	7.3	99.9	75.2	76.5	50.2	55.5	38.3
120	827.4	1.8	30.5	9.3	99.9	74.9	76.4	49.4	55.4	37.5
150	1,034	1.4	38.5	11.7	99.3	74.7	75.9	48.9	54.8	36.8
200	1,379	1.1	48.1	14.7	98.8	74.4	75.6	47.6	54.5	35.4
260	1,793	0.82	64.1	19.5	90.7	74.1	74.6	45.9	53.6	34.3
350	2,413	0.61	83.4	25.4	81.7	74.0	73.7	44.5	52.7	31.9
430	2,965	0.50	112	34.1	73.7	73.7	71.3	43.0	50.8	30.5
550	3,792	0.39	138	42.1			66.0	42.2	48.4	29.4
725	4,999	0.30	176	53.6			60.4	40.8	46.4	27.6
925	6,378	0.23	232	70.7			54.4	39.7	43.9	26.1
1200	8,274	0.18	297	90.5			49.1	39.1	41.7	25.0
1550	10,687	0.14	385	117.3			46.1	39.1	40.1	24.8
2000	13,790	0.11	497	151.5			42.0	39.0	38.1	23.3
2600	17,926	0.08	641	195.4			38.7	38.7	36.7	22.0
3350	23,097	0.06	834	254.2					33.5	20.5
4300	29,647	0.05	1074	327.4					30.0	19.3
5550	38,266	0.04	1378	420.0					26.4	18.6
7200	49,642	0.03	1779	542.2					23.1	17.8
9300	64,121	0.02	2308	703.5					18.5	16.7
			2981	908.6					15.9	16.0



Appendix 4

US DOE #DE-FC26-05NT42660 Final Scientific/Technical Report

Alan P. Byrnes, Robert M. Cluff and John C. Webb

Mercury Injection Drainage-Imbibition Capillary Pressure Analysis

CER CORPORATION: MWX-2 SUPERIOR - T649 - 6554.3 ft (A2)

In situ Klinkenberg Permeability (μm^2) =

1.09E-06

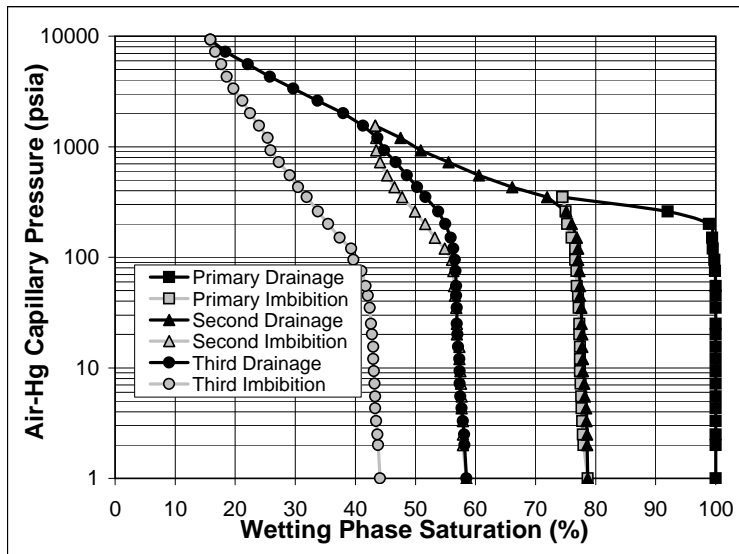
In situ Klinkenberg Permeability (mD) =

0.0011

Routine Porosity (%) =

6.1

Mercury Injection Capillary Pressure (psia)	Mercury Injection Capillary Pressure (kPa)	Approx. Pore Entry Diameter (μm)	Approx. Gas-Water Height Above Free Water Level (ft)	Approx. Gas-Water Height Above Free Water Level (m)	Drainage 1 Cumulative Wetting Phase Saturation (% pore vol)	Imbibition 1 Cumulative Wetting Phase Saturation (% pore vol)	Drainage 2 Cumulative Wetting Phase Saturation (% pore vol)	Imbibition 2 Cumulative Wetting Phase Saturation (% pore vol)	Drainage 3 Cumulative Wetting Phase Saturation (% pore vol)	Imbibition 3 Cumulative Wetting Phase Saturation (% pore vol)
2.0	13.8	107	0.10	0.03	100.0	78.7	78.7	58.5	58.5	44.1
2.5	17.2	86	0.64	0.20	100.0	78.0	78.6	57.9	58.2	43.8
3.3	22.8	65	0.80	0.24	100.0	77.9	78.6	57.9	58.1	43.7
4.3	29.6	50	1.06	0.32	100.0	77.8	78.5	57.9	57.9	43.5
5.5	37.9	39	1.38	0.42	100.0	77.7	78.4	57.7	57.7	43.3
7.2	49.6	30	1.76	0.54	100.0	77.6	78.2	57.7	57.5	43.3
9.3	64.1	23	2.31	0.70	100.0	77.5	78.1	57.6	57.4	43.2
12.0	82.7	18	2.98	0.91	100.0	77.4	77.9	57.5	57.4	43.1
15.5	106.9	14	3.85	1.17	100.0	77.4	77.9	57.3	57.3	43.0
20	137.9	11	4.97	1.51	100.0	77.4	77.8	57.3	57.1	43.0
25	172.4	8.6	6.41	2.0	100.0	77.3	77.8	56.9	57.0	42.8
35	241.3	6.1	8.01	2.4	100.0	77.3	77.7	56.9	56.9	42.6
45	310.3	4.8	11.2	3.4	100.0	77.2	77.6	56.8	56.9	42.4
55	379.2	3.9	14.4	4.4	100.0	77.1	77.4	56.6	56.8	42.1
75	517.1	2.9	17.6	5.4	100.0	76.9	77.4	56.4	56.8	41.7
95	655.0	2.3	24.0	7.3	99.9	76.8	77.3	56.3	56.7	41.0
120	827.4	1.8	30.5	9.3	99.8	76.6	77.1	56.1	56.6	39.7
150	1,034	1.4	38.5	11.7	99.5	76.6	77.1	54.9	56.3	39.3
200	1,379	1.1	48.1	14.7	99.4	76.0	76.9	53.2	55.9	37.4
260	1,793	0.82	64.1	19.5	98.9	75.3	76.0	51.6	55.0	35.5
350	2,413	0.61	83.4	25.4	92.0	75.0	75.1	49.9	53.8	33.8
430	2,965	0.50	112	34.1	74.5	74.5	71.9	47.8	51.7	31.9
550	3,792	0.39	138	42.1			66.1	46.5	50.3	30.5
725	4,999	0.30	176	53.6			60.6	45.3	48.6	29.1
925	6,378	0.23	232	70.7			55.5	44.1	46.7	27.3
1200	8,274	0.18	297	90.5			50.9	43.5	44.8	25.9
1550	10,687	0.14	385	117.3			47.5	43.5	43.7	25.4
2000	13,790	0.11	497	151.5			43.3	43.3	41.3	24.0
2600	17,926	0.08	641	195.4					38.0	22.5
3350	23,097	0.06	834	254.2					33.7	21.2
4300	29,647	0.05	1074	327.4					29.7	19.7
5550	38,266	0.04	1378	420.0					25.8	18.6
7200	49,642	0.03	1779	542.2					22.1	17.7
9300	64,121	0.02	2308	703.5					18.4	16.7
			2981	908.6					15.9	15.9

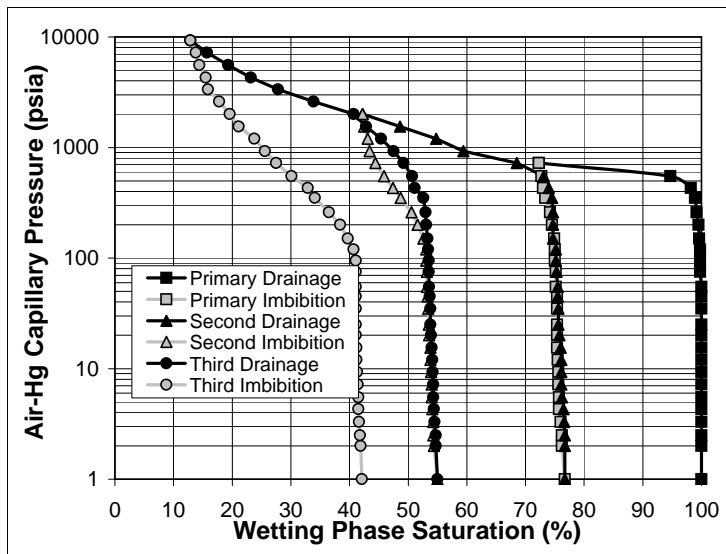


Mercury Injection Drainage-Imbibition Capillary Pressure Analysis

CER CORPORATION: MWX-2 SUPERIOR - T649 - 7877.6 ft (A)

In situ Klinkenberg Permeability (μm^2) = 1.48E-06
In situ Klinkenberg Permeability (mD) = 0.0015
 Routine Porosity (%) = 7.6

Mercury Injection Capillary Pressure (psia)	Mercury Injection Capillary Pressure (kPa)	Approx. Pore Entry Diameter (μm)	Approx. Gas-Water Height Above Free Water Level (ft)	Approx. Gas-Water Height Above Free Water Level (m)	Drainage 1 Cumulative Wetting Phase Saturation (% pore vol)	Imbibition 1 Cumulative Wetting Phase Saturation (% pore vol)	Drainage 2 Cumulative Wetting Phase Saturation (% pore vol)	Imbibition 2 Cumulative Wetting Phase Saturation (% pore vol)	Drainage 3 Cumulative Wetting Phase Saturation (% pore vol)	Imbibition 3 Cumulative Wetting Phase Saturation (% pore vol)
2.0	13.8	107	0.10	0.03	100.0	76.7	76.7	55.0	55.0	42.1
2.5	17.2	86	0.64	0.20	100.0	76.2	76.7	54.4	54.7	41.9
3.3	22.8	65	0.80	0.24	100.0	76.2	76.7	54.3	54.7	41.8
4.3	29.6	50	1.06	0.32	100.0	76.0	76.6	54.3	54.5	41.6
5.5	37.9	39	1.38	0.42	100.0	75.7	76.5	54.1	54.4	41.5
7.2	49.6	30	1.76	0.54	100.0	75.7	76.2	54.0	54.3	41.5
9.3	64.1	23	2.31	0.70	100.0	75.6	76.1	54.0	54.3	41.4
12.0	82.7	18	2.98	0.91	100.0	75.6	76.1	53.9	54.2	41.3
15.5	106.9	14	3.85	1.17	100.0	75.5	76.1	53.8	54.1	41.2
20	137.9	11	4.97	1.51	100.0	75.4	76.0	53.8	54.0	41.2
25	172.4	8.6	6.41	2.0	100.0	75.4	75.8	53.6	53.9	41.1
35	241.3	6.1	8.01	2.4	100.0	75.4	75.6	53.5	53.8	41.1
45	310.3	4.8	11.2	3.4	100.0	75.4	75.6	53.4	53.8	41.1
55	379.2	3.9	14.4	4.4	100.0	75.4	75.5	53.3	53.7	41.1
75	517.1	2.9	17.6	5.4	100.0	75.2	75.5	53.2	53.6	41.1
95	655.0	2.3	24.0	7.3	99.8	75.2	75.3	53.2	53.5	41.1
120	827.4	1.8	30.5	9.3	99.8	75.0	75.2	53.1	53.5	41.1
150	1,034	1.4	38.5	11.7	99.8	75.0	75.2	53.1	53.4	40.7
200	1,379	1.1	48.1	14.7	99.6	74.9	74.7	52.6	53.3	39.7
260	1,793	0.82	64.1	19.5	99.5	74.5	74.7	51.6	53.1	38.4
350	2,413	0.61	83.4	25.4	99.2	74.2	74.7	50.6	53.0	36.5
430	2,965	0.50	112	34.1	98.9	73.4	74.5	48.7	52.6	34.1
550	3,792	0.39	138	42.1	98.2	73.0	74.0	47.4	51.1	32.9
725	4,999	0.30	176	53.6	94.7	72.7	73.1	45.9	50.7	30.1
925	6,378	0.23	232	70.7	72.3	72.3	68.5	44.4	49.2	27.5
1200	8,274	0.18	297	90.5			59.4	43.4	47.5	25.6
1550	10,687	0.14	385	117.3			54.8	43.1	45.4	23.8
2000	13,790	0.11	497	151.5			48.6	42.5	42.8	21.1
2600	17,926	0.08	641	195.4			42.2	42.2	40.7	19.6
3350	23,097	0.06	834	254.2					33.9	17.8
4300	29,647	0.05	1074	327.4					27.8	15.9
5550	38,266	0.04	1378	420.0					23.2	15.5
7200	49,642	0.03	1779	542.2					19.3	14.4
9300	64,121	0.02	2308	703.5					15.7	13.8
			2981	908.6					12.9	12.9



Mercury Injection Drainage-Imbibition Capillary Pressure Analysis

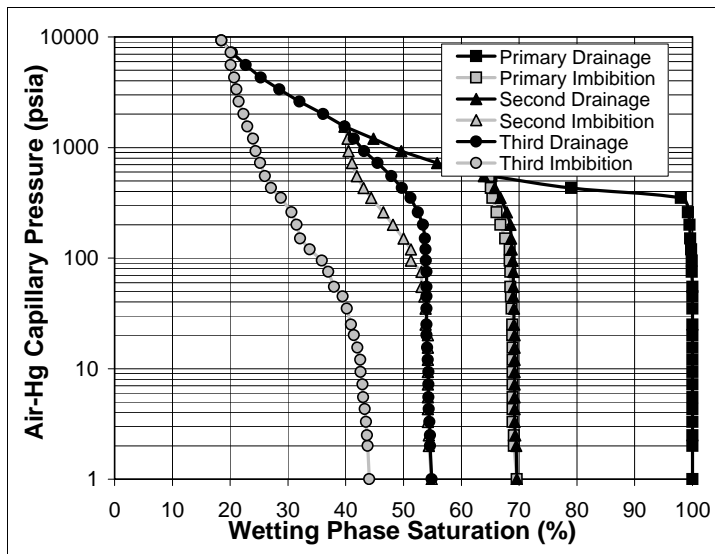
FUEL RESOURCES DEV: M-30-2-96W /D-037934 - E458 - 6404.8 ft (A)

In situ Klinkenberg Permeability (μm^2) = 1.88E-06

In situ Klinkenberg Permeability (mD) = 0.0019

Routine Porosity (%) = 9.5

Mercury Injection Capillary Pressure (psia)	Mercury Injection Capillary Pressure (kPa)	Approx. Pore Entry Diameter (μm)	Approx. Gas-Water Height Above Free Water Level (ft)	Approx. Gas-Water Height Above Free Water Level (m)	Drainage 1 Cumulative Wetting Phase Saturation (% pore vol)	Imbibition 1 Cumulative Wetting Phase Saturation (% pore vol)	Drainage 2 Cumulative Wetting Phase Saturation (% pore vol)	Imbibition 2 Cumulative Wetting Phase Saturation (% pore vol)	Drainage 3 Cumulative Wetting Phase Saturation (% pore vol)	Imbibition 3 Cumulative Wetting Phase Saturation (% pore vol)
2.0	13.8	107	0.10	0.03	100.0	69.6	69.6	54.9	54.9	44.1
2.5	17.2	86	0.64	0.20	100.0	69.1	69.5	54.4	54.6	43.8
3.3	22.8	65	0.80	0.24	100.0	69.1	69.3	54.4	54.6	43.7
4.3	29.6	50	1.06	0.32	100.0	68.9	69.2	54.2	54.5	43.5
5.5	37.9	39	1.38	0.42	100.0	68.9	69.2	54.2	54.4	43.3
7.2	49.6	30	1.76	0.54	100.0	68.9	69.2	54.2	54.3	43.0
9.3	64.1	23	2.31	0.70	100.0	68.9	69.2	54.2	54.3	42.9
12.0	82.7	18	2.98	0.91	100.0	68.9	69.2	54.2	54.3	42.6
15.5	106.9	14	3.85	1.17	100.0	68.9	69.2	54.2	54.2	42.5
20	137.9	11	4.97	1.51	100.0	68.9	69.2	54.2	54.1	42.0
25	172.4	8.6	6.41	2.0	100.0	68.8	69.2	54.2	54.0	41.4
35	241.3	6.1	8.01	2.4	100.0	68.8	69.1	53.8	54.0	40.9
45	310.3	4.8	11.2	3.4	100.0	68.7	69.1	53.8	54.0	40.2
55	379.2	3.9	14.4	4.4	100.0	68.6	69.0	53.6	54.0	39.5
75	517.1	2.9	17.6	5.4	100.0	68.5	69.0	53.1	54.0	38.0
95	655.0	2.3	24.0	7.3	99.9	68.5	69.0	53.1	54.0	37.0
120	827.4	1.8	30.5	9.3	99.9	68.4	68.9	51.3	53.9	35.9
150	1,034	1.4	38.5	11.7	99.8	68.4	68.7	51.3	53.8	33.8
200	1,379	1.1	48.1	14.7	99.6	67.6	68.6	50.0	53.7	32.1
260	1,793	0.82	64.1	19.5	99.5	66.8	68.5	48.2	53.4	31.5
350	2,413	0.61	83.4	25.4	99.2	66.1	67.9	46.5	52.5	30.6
430	2,965	0.50	112	34.1	98.0	65.4	66.8	44.4	51.2	28.8
550	3,792	0.39	138	42.1	79.0	65.1	65.8	43.1	49.7	27.1
725	4,999	0.30	176	53.6	65.2	64.8	63.9	41.9	47.9	26.0
925	6,378	0.23	232	70.7			55.8	41.1	45.5	25.2
1200	8,274	0.18	297	90.5			49.6	40.5	43.2	24.4
1550	10,687	0.14	385	117.3			44.8	40.3	41.4	24.0
2000	13,790	0.11	497	151.5			39.8	39.8	39.8	23.0
2600	17,926	0.08	641	195.4					36.1	22.3
3350	23,097	0.06	834	254.2					32.0	21.5
4300	29,647	0.05	1074	327.4					28.5	21.1
5550	38,266	0.04	1378	420.0					25.3	20.7
7200	49,642	0.03	1779	542.2					22.7	20.1
9300	64,121	0.02	2308	703.5					20.3	20.1
			2981	908.6					18.5	18.5

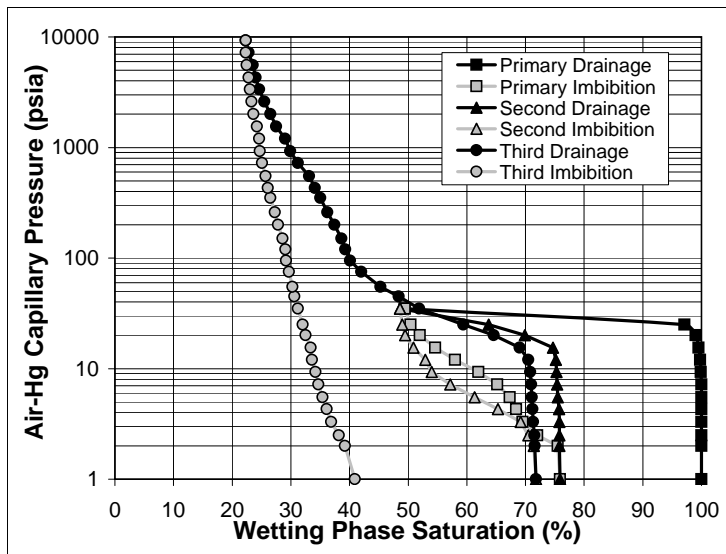


Mercury Injection Drainage-Imbibition Capillary Pressure Analysis

WESTERN FUELS ASSOC: 21011-5 MOON LAKE - S905 - 812.9 ft (B)

In situ Klinkenberg Permeability (μm^2) = 2.43E-02
In situ Klinkenberg Permeability (mD) = 24.6
 Routine Porosity (%) = 17.9

Mercury Injection Capillary Pressure (psia)	Mercury Injection Capillary Pressure (kPa)	Approx. Pore Entry Diameter (μm)	Approx. Gas-Water Height Above Free Water Level (ft)	Approx. Gas-Water Height Above Free Water Level (m)	Drainage 1 Cumulative Wetting Phase Saturation (% pore vol)	Imbibition 1 Cumulative Wetting Phase Saturation (% pore vol)	Drainage 2 Cumulative Wetting Phase Saturation (% pore vol)	Imbibition 2 Cumulative Wetting Phase Saturation (% pore vol)	Drainage 3 Cumulative Wetting Phase Saturation (% pore vol)	Imbibition 3 Cumulative Wetting Phase Saturation (% pore vol)
2.0	13.8	107	0.10	0.03	100.0	75.9	75.9	71.8	71.8	40.9
2.5	17.2	86	0.64	0.20	100.0	75.5	75.8	71.4	71.6	39.2
3.3	22.8	65	0.80	0.24	100.0	72.0	75.8	70.5	71.5	38.2
4.3	29.6	50	1.06	0.32	100.0	69.5	75.8	69.2	71.3	36.9
5.5	37.9	39	1.38	0.42	100.0	68.4	75.7	65.3	71.2	36.1
7.2	49.6	30	1.76	0.54	100.0	67.3	75.5	61.3	71.1	35.4
9.3	64.1	23	2.31	0.70	100.0	65.2	75.4	57.2	71.0	34.7
12.0	82.7	18	2.98	0.91	99.9	62.0	75.3	54.0	70.8	34.2
15.5	106.9	14	3.85	1.17	99.8	58.0	75.2	52.9	70.5	33.6
20	137.9	11	4.97	1.51	99.5	54.6	74.7	50.9	69.0	33.4
25	172.4	8.6	6.41	2.0	99.0	52.0	69.9	49.5	64.6	32.5
35	241.3	6.1	8.01	2.4	97.1	50.4	63.7	49.0	59.4	32.0
45	310.3	4.8	11.2	3.4	49.4	49.4	48.6	48.6	51.9	31.2
55	379.2	3.9	14.4	4.4					48.4	30.6
75	517.1	2.9	17.6	5.4					45.3	30.3
95	655.0	2.3	24.0	7.3					42.0	29.7
120	827.4	1.8	30.5	9.3					40.1	29.2
150	1,034	1.4	38.5	11.7					39.3	29.1
200	1,379	1.1	48.1	14.7					38.6	28.6
260	1,793	0.82	64.1	19.5					37.4	27.8
350	2,413	0.61	83.4	25.4					36.2	27.3
430	2,965	0.50	112	34.1					35.0	26.5
550	3,792	0.39	138	42.1					34.1	26.1
725	4,999	0.30	176	53.6					33.1	25.7
925	6,378	0.23	232	70.7					31.2	25.1
1200	8,274	0.18	297	90.5					29.9	24.7
1550	10,687	0.14	385	117.3					29.0	24.6
2000	13,790	0.11	497	151.5					27.5	24.2
2600	17,926	0.08	641	195.4					26.5	23.6
3350	23,097	0.06	834	254.2					25.5	23.3
4300	29,647	0.05	1074	327.4					24.6	23.0
5550	38,266	0.04	1378	420.0					24.0	22.8
7200	49,642	0.03	1779	542.2					23.5	22.5
9300	64,121	0.02	2308	703.5					22.8	22.3
			2981	908.6					22.3	22.3



Appendix 4

US DOE #DE-FC26-05NT42660 Final Scientific/Technical Report

Alan P. Byrnes, Robert M. Cluff and John C. Webb

Mercury Injection Drainage-Imbibition Capillary Pressure Analysis

LOUISIANA LAND & EXP: 1 BARLOW 21-20 - E393 - 6994.1 ft (B)

In situ Klinkenberg Permeability (μm^2) =

2.96E-02

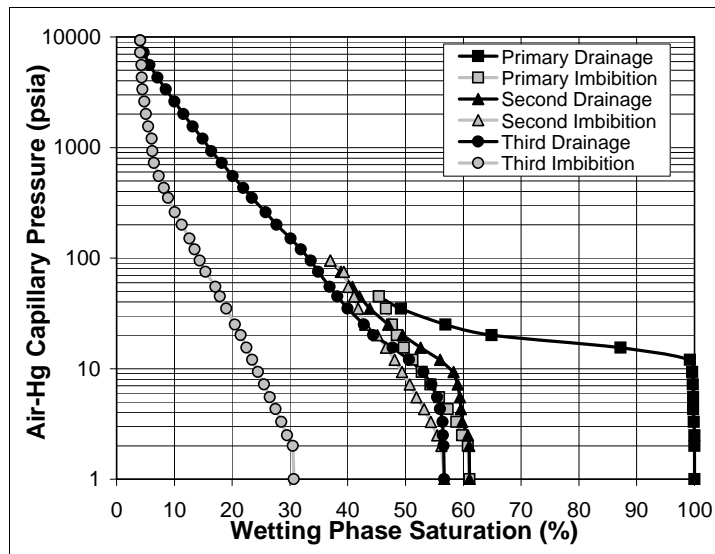
In situ Klinkenberg Permeability (mD) =

30.0

Routine Porosity (%) =

18.0

Mercury Injection Capillary Pressure (psia)	Mercury Injection Capillary Pressure (kPa)	Approx. Pore Entry Diameter (μm)	Approx. Gas-Water Height Above Free Water Level (ft)	Approx. Gas-Water Height Above Free Water Level (m)	Drainage 1 Cumulative Wetting Phase Saturation (% pore vol)	Imbibition 1 Cumulative Wetting Phase Saturation (% pore vol)	Drainage 2 Cumulative Wetting Phase Saturation (% pore vol)	Imbibition 2 Cumulative Wetting Phase Saturation (% pore vol)	Drainage 3 Cumulative Wetting Phase Saturation (% pore vol)	Imbibition 3 Cumulative Wetting Phase Saturation (% pore vol)
2.0	13.8	107	0.10	0.03	100.0	61.1	61.1	56.7	56.7	30.7
2.5	17.2	86	0.64	0.20	100.0	60.8	61.0	56.2	56.6	30.5
3.3	22.8	65	0.80	0.24	100.0	59.8	60.8	55.5	56.5	29.5
4.3	29.6	50	1.06	0.32	99.9	58.8	59.8	54.4	56.4	28.5
5.5	37.9	39	1.38	0.42	99.8	57.3	59.6	53.2	56.0	27.5
7.2	49.6	30	1.76	0.54	99.8	55.8	59.4	51.9	55.5	26.5
9.3	64.1	23	2.31	0.70	99.7	54.3	59.0	50.7	54.5	25.5
12.0	82.7	18	2.98	0.91	99.6	52.8	58.3	49.4	53.1	24.5
15.5	106.9	14	3.85	1.17	99.2	51.2	56.0	48.1	50.6	23.5
20	137.9	11	4.97	1.51	87.2	49.7	52.6	46.6	47.8	22.5
25	172.4	8.6	6.41	2.0	64.9	48.5	49.5	45.1	44.4	21.5
35	241.3	6.1	8.01	2.4	56.9	47.7	47.0	43.0	42.8	20.5
45	310.3	4.8	11.2	3.4	49.2	46.6	43.8	41.8	40.0	19.0
55	379.2	3.9	14.4	4.4	45.4	45.4	42.0	41.1	38.2	17.9
75	517.1	2.9	17.6	5.4			40.8	40.1	36.9	17.1
95	655.0	2.3	24.0	7.3			38.8	39.3	34.9	15.4
120	827.4	1.8	30.5	9.3			37.0	37.0	33.6	14.4
150	1,034	1.4	38.5	11.7					31.9	13.5
200	1,379	1.1	48.1	14.7					30.1	12.6
260	1,793	0.82	64.1	19.5					27.7	11.3
350	2,413	0.61	83.4	25.4					25.8	10.1
430	2,965	0.50	112	34.1					23.4	8.9
550	3,792	0.39	138	42.1					21.9	8.2
725	4,999	0.30	176	53.6					20.1	7.3
925	6,378	0.23	232	70.7					18.2	6.5
1200	8,274	0.18	297	90.5					16.4	6.2
1550	10,687	0.14	385	117.3					14.9	6.1
2000	13,790	0.11	497	151.5					13.2	5.5
2600	17,926	0.08	641	195.4					11.6	5.1
3350	23,097	0.06	834	254.2					10.0	4.8
4300	29,647	0.05	1074	327.4					8.5	4.5
5550	38,266	0.04	1378	420.0					7.1	4.4
7200	49,642	0.03	1779	542.2					5.7	4.3
9300	64,121	0.02	2308	703.5					4.7	4.1
			2981	908.6					4.1	4.1



Mercury Injection Drainage-Imbibition Capillary Pressure Analysis

LOUISIANA LAND & EXP: 1 BARLOW 21-20 - E393 - 7027.2 ft

In situ Klinkenberg Permeability (μm^2) =

1.90E-03

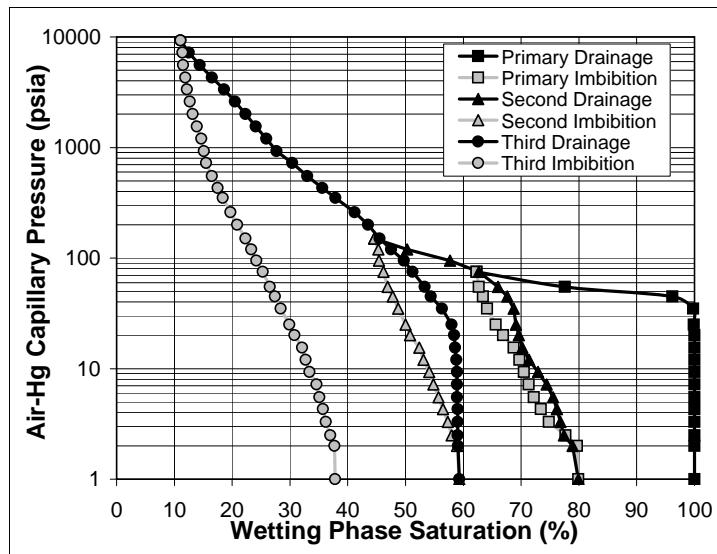
In situ Klinkenberg Permeability (mD) =

1.93

Routine Porosity (%) =

15.0

Mercury Injection Capillary Pressure (psia)	Mercury Injection Capillary Pressure (kPa)	Approx. Pore Entry Diameter (μm)	Approx. Gas-Water Height Above Free Water Level (ft)	Approx. Gas-Water Height Above Free Water Level (m)	Drainage 1 Cumulative Wetting Phase Saturation (% pore vol)	Imbibition 1 Cumulative Wetting Phase Saturation (% pore vol)	Drainage 2 Cumulative Wetting Phase Saturation (% pore vol)	Imbibition 2 Cumulative Wetting Phase Saturation (% pore vol)	Drainage 3 Cumulative Wetting Phase Saturation (% pore vol)	Imbibition 3 Cumulative Wetting Phase Saturation (% pore vol)
2.0	13.8	107	0.10	0.03	100.0	79.9	79.9	59.3	59.3	37.8
2.5	17.2	86	0.64	0.20	100.0	79.7	78.9	58.9	59.1	37.7
3.3	22.8	65	0.80	0.24	100.0	77.7	77.4	58.0	59.0	37.0
4.3	29.6	50	1.06	0.32	100.0	74.8	76.8	57.3	59.0	36.2
5.5	37.9	39	1.38	0.42	100.0	73.4	76.2	56.5	59.0	35.7
7.2	49.6	30	1.76	0.54	100.0	72.2	75.5	55.7	58.9	35.1
9.3	64.1	23	2.31	0.70	100.0	71.3	74.4	54.8	58.9	34.6
12.0	82.7	18	2.98	0.91	100.0	70.5	72.9	54.1	58.9	33.4
15.5	106.9	14	3.85	1.17	100.0	69.7	71.4	53.1	58.8	32.7
20	137.9	11	4.97	1.51	100.0	68.7	70.2	52.4	58.6	32.1
25	172.4	8.6	6.41	2.0	100.0	66.9	69.6	50.8	58.4	30.8
35	241.3	6.1	8.01	2.4	99.9	65.6	69.1	50.0	58.0	29.9
45	310.3	4.8	11.2	3.4	99.8	64.1	68.7	48.7	56.3	28.4
55	379.2	3.9	14.4	4.4	96.2	63.4	67.6	47.8	54.4	27.4
75	517.1	2.9	17.6	5.4	77.6	62.7	66.0	46.9	53.3	26.5
95	655.0	2.3	24.0	7.3	62.3	62.3	62.7	46.2	51.2	25.3
120	827.4	1.8	30.5	9.3			57.7	45.4	49.7	24.2
150	1,034	1.4	38.5	11.7			50.3	45.3	47.5	23.3
200	1,379	1.1	48.1	14.7			44.6	44.6	45.5	22.3
260	1,793	0.82	64.1	19.5					43.5	20.9
350	2,413	0.61	83.4	25.4					41.2	19.7
430	2,965	0.50	112	34.1					37.9	18.4
550	3,792	0.39	138	42.1					35.6	17.5
725	4,999	0.30	176	53.6					33.0	16.5
925	6,378	0.23	232	70.7					30.4	15.5
1200	8,274	0.18	297	90.5					27.7	15.1
1550	10,687	0.14	385	117.3					25.9	14.7
2000	13,790	0.11	497	151.5					24.1	13.9
2600	17,926	0.08	641	195.4					22.3	13.2
3350	23,097	0.06	834	254.2					20.5	12.7
4300	29,647	0.05	1074	327.4					18.6	12.2
5550	38,266	0.04	1378	420.0					16.5	11.9
7200	49,642	0.03	1779	542.2					14.4	11.5
9300	64,121	0.02	2308	703.5					12.5	11.4
			2981	908.6					11.1	11.1



Appendix 4

US DOE #DE-FC26-05NT42660 Final Scientific/Technical Report

Alan P. Byrnes, Robert M. Cluff and John C. Webb

Mercury Injection Drainage-Imbibition Capillary Pressure Analysis

BELCO PETROLEUM: 3 SHAWNEE - S838 - 6988 ft (B)

In situ Klinkenberg Permeability (μm^2) =

5.54E-03

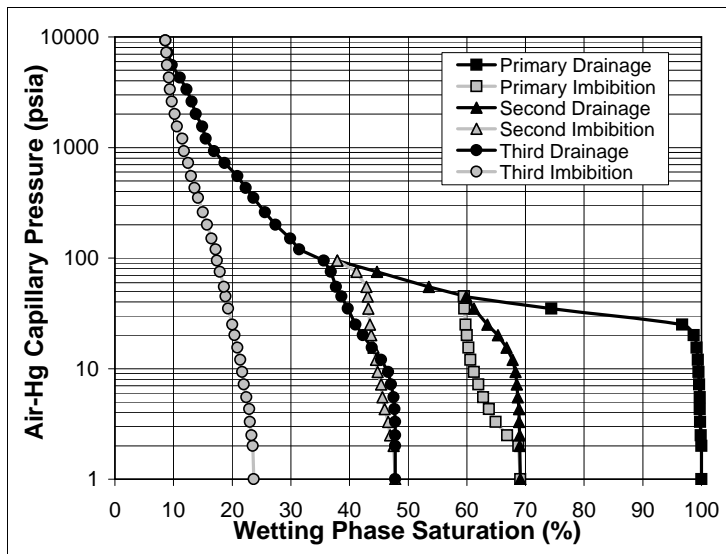
In situ Klinkenberg Permeability (mD) =

5.61

Routine Porosity (%) =

18.3

Mercury Injection Capillary Pressure (psia)	Mercury Injection Capillary Pressure (kPa)	Approx. Pore Entry Diameter (μm)	Approx. Gas-Water Height Above Free Water Level (ft)	Approx. Gas-Water Height Above Free Water Level (m)	Drainage 1 Cumulative Wetting Phase Saturation (% pore vol)	Imbibition 1 Cumulative Wetting Phase Saturation (% pore vol)	Drainage 2 Cumulative Wetting Phase Saturation (% pore vol)	Imbibition 2 Cumulative Wetting Phase Saturation (% pore vol)	Drainage 3 Cumulative Wetting Phase Saturation (% pore vol)	Imbibition 3 Cumulative Wetting Phase Saturation (% pore vol)
2.0	13.8	107	0.10	0.03	100.0	69.1	69.1	47.8	47.8	23.7
2.5	17.2	86	0.64	0.20	100.0	68.8	69.0	47.5	47.8	23.5
3.3	22.8	65	0.80	0.24	99.9	66.9	69.0	46.9	47.8	23.3
4.3	29.6	50	1.06	0.32	99.8	64.9	68.9	46.6	47.8	23.0
5.5	37.9	39	1.38	0.42	99.7	63.8	68.9	46.0	47.7	22.9
7.2	49.6	30	1.76	0.54	99.7	62.8	68.7	45.6	47.5	22.4
9.3	64.1	23	2.31	0.70	99.6	62.0	68.5	45.4	47.1	22.0
12.0	82.7	18	2.98	0.91	99.5	61.2	68.3	44.8	46.6	21.7
15.5	106.9	14	3.85	1.17	99.4	60.6	67.8	44.5	45.4	21.4
20	137.9	11	4.97	1.51	99.2	60.3	66.8	44.1	43.8	20.9
25	172.4	8.6	6.41	2.0	98.7	60.0	65.3	43.7	42.3	20.4
35	241.3	6.1	8.01	2.4	96.7	59.8	63.5	43.5	41.0	20.0
45	310.3	4.8	11.2	3.4	74.4	59.6	61.2	43.2	39.7	19.3
55	379.2	3.9	14.4	4.4	59.5	59.5	59.9	43.1	38.6	18.9
75	517.1	2.9	17.6	5.4			53.5	42.9	37.7	18.6
95	655.0	2.3	24.0	7.3			44.7	41.2	36.8	17.9
120	827.4	1.8	30.5	9.3			37.9	37.9	35.6	17.4
150	1,034	1.4	38.5	11.7					31.4	17.2
200	1,379	1.1	48.1	14.7					29.9	16.5
260	1,793	0.82	64.1	19.5					27.4	15.7
350	2,413	0.61	83.4	25.4					25.6	15.0
430	2,965	0.50	112	34.1					23.6	14.2
550	3,792	0.39	138	42.1					22.3	13.6
725	4,999	0.30	176	53.6					20.9	13.0
925	6,378	0.23	232	70.7					18.7	12.5
1200	8,274	0.18	297	90.5					16.9	11.8
1550	10,687	0.14	385	117.3					15.5	11.5
2000	13,790	0.11	497	151.5					14.9	10.6
2600	17,926	0.08	641	195.4					13.8	10.2
3350	23,097	0.06	834	254.2					13.1	9.7
4300	29,647	0.05	1074	327.4					12.2	9.4
5550	38,266	0.04	1378	420.0					11.1	9.2
7200	49,642	0.03	1779	542.2					9.7	8.9
9300	64,121	0.02	2308	703.5					9.0	8.8
			2981	908.6					8.6	8.6



Appendix 4

US DOE #DE-FC26-05NT42660 Final Scientific/Technical Report

Alan P. Byrnes, Robert M. Cluff and John C. Webb

Mercury Injection Drainage-Imbibition Capillary Pressure Analysis

BELCO PETROLEUM: 2 SHAWNEE - S835 - 6991.2 ft (B)

In situ Klinkenberg Permeability (μm^2) =

6.22E-06

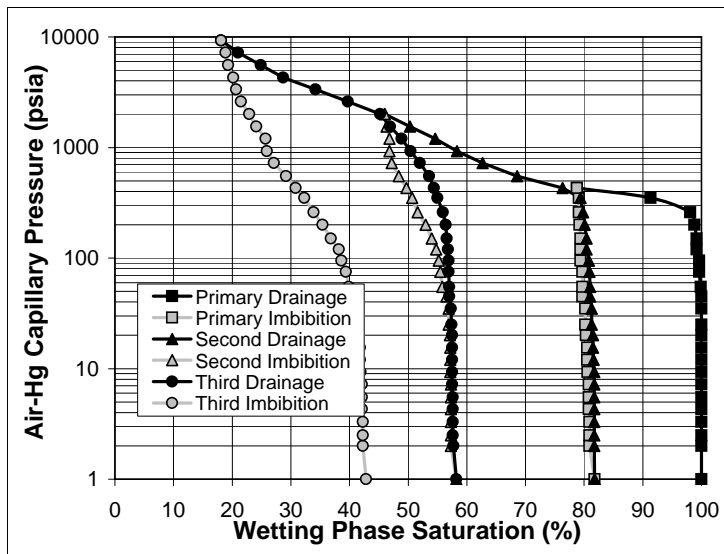
In situ Klinkenberg Permeability (mD) =

0.0063

Routine Porosity (%) =

8.6

Mercury Injection Capillary Pressure (psia)	Mercury Injection Capillary Pressure (kPa)	Approx. Pore Entry Diameter (μm)	Approx. Gas-Water Height Above Free Water Level (ft)	Approx. Gas-Water Height Above Free Water Level (m)	Drainage 1 Cumulative Wetting Phase Saturation (% pore vol)	Imbibition 1 Cumulative Wetting Phase Saturation (% pore vol)	Drainage 2 Cumulative Wetting Phase Saturation (% pore vol)	Imbibition 2 Cumulative Wetting Phase Saturation (% pore vol)	Drainage 3 Cumulative Wetting Phase Saturation (% pore vol)	Imbibition 3 Cumulative Wetting Phase Saturation (% pore vol)
2.0	13.8	107	0.10	0.03	100.0	81.8	81.8	58.2	58.2	42.8
2.5	17.2	86	0.64	0.20	100.0	80.9	81.7	57.3	57.7	42.3
3.3	22.8	65	0.80	0.24	100.0	80.9	81.7	57.3	57.6	42.3
4.3	29.6	50	1.06	0.32	100.0	80.8	81.7	57.3	57.6	42.3
5.5	37.9	39	1.38	0.42	100.0	80.8	81.7	57.3	57.6	42.1
7.2	49.6	30	1.76	0.54	100.0	80.8	81.7	57.3	57.6	42.1
9.3	64.1	23	2.31	0.70	100.0	80.8	81.7	57.3	57.5	42.1
12.0	82.7	18	2.98	0.91	100.0	80.6	81.7	57.2	57.5	41.9
15.5	106.9	14	3.85	1.17	100.0	80.5	81.6	57.2	57.5	41.8
20	137.9	11	4.97	1.51	100.0	80.5	81.5	57.2	57.5	41.8
25	172.4	8.6	6.41	2.0	100.0	80.3	81.5	57.1	57.5	41.6
35	241.3	6.1	8.01	2.4	100.0	80.2	81.3	56.9	57.4	41.4
45	310.3	4.8	11.2	3.4	100.0	80.2	81.3	56.9	57.3	41.2
55	379.2	3.9	14.4	4.4	100.0	79.7	81.0	56.5	57.0	40.5
75	517.1	2.9	17.6	5.4	99.9	79.7	81.0	55.8	57.0	39.9
95	655.0	2.3	24.0	7.3	99.6	79.7	80.9	55.5	56.9	39.4
120	827.4	1.8	30.5	9.3	99.6	79.4	80.8	55.2	56.9	38.6
150	1,034	1.4	38.5	11.7	99.2	79.4	80.4	54.8	56.8	38.2
200	1,379	1.1	48.1	14.7	99.2	79.4	80.4	54.0	56.6	36.8
260	1,793	0.82	64.1	19.5	98.8	79.2	80.1	53.0	56.4	35.4
350	2,413	0.61	83.4	25.4	98.1	79.1	79.8	51.6	55.9	33.9
430	2,965	0.50	112	34.1	91.3	79.1	79.4	50.7	55.0	32.3
550	3,792	0.39	138	42.1	78.8	78.8	76.3	49.7	54.4	30.8
725	4,999	0.30	176	53.6			68.6	48.4	53.6	29.2
925	6,378	0.23	232	70.7			62.7	47.2	52.0	27.1
1200	8,274	0.18	297	90.5			58.3	46.8	50.4	25.9
1550	10,687	0.14	385	117.3			54.6	46.8	48.9	25.7
2000	13,790	0.11	497	151.5			50.3	46.3	46.9	24.1
2600	17,926	0.08	641	195.4			46.0	46.0	45.2	22.9
3350	23,097	0.06	834	254.2					39.7	21.5
4300	29,647	0.05	1074	327.4					34.2	20.7
5550	38,266	0.04	1378	420.0					28.7	20.2
7200	49,642	0.03	1779	542.2					24.9	19.3
9300	64,121	0.02	2308	703.5					21.0	18.9
			2981	908.6					18.1	18.1



Mercury Injection Drainage-Imbibition Capillary Pressure Analysis

DAVIS OIL COMPANY: 2 FRED STATE - E932 - 7544.1 ft (B)

In situ Klinkenberg Permeability (μm^2) =

3.31E-03

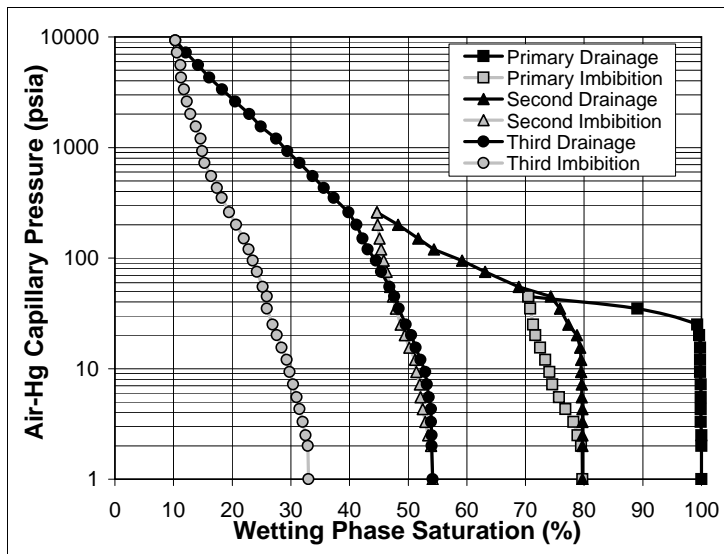
In situ Klinkenberg Permeability (mD) =

3.3500

Routine Porosity (%) =

16.7

Mercury Injection Capillary Pressure (psia)	Mercury Injection Capillary Pressure (kPa)	Approx. Pore Entry Diameter (μm)	Approx. Gas-Water Height Above Free Water Level (ft)	Approx. Gas-Water Height Above Free Water Level (m)	Drainage 1 Cumulative Wetting Phase Saturation (% pore vol)	Imbibition 1 Cumulative Wetting Phase Saturation (% pore vol)	Drainage 2 Cumulative Wetting Phase Saturation (% pore vol)	Imbibition 2 Cumulative Wetting Phase Saturation (% pore vol)	Drainage 3 Cumulative Wetting Phase Saturation (% pore vol)	Imbibition 3 Cumulative Wetting Phase Saturation (% pore vol)
2.0	13.8	107	0.10	0.03	100.0	79.7	79.7	54.2	54.2	33.0
2.5	17.2	86	0.64	0.20	100.0	79.5	79.7	53.9	54.0	32.9
3.3	22.8	65	0.80	0.24	100.0	78.9	79.7	53.4	54.0	32.5
4.3	29.6	50	1.06	0.32	99.9	78.2	79.7	52.9	53.9	32.0
4.3	29.6	50	1.38	0.42	99.9	76.8	79.7	52.5	53.9	31.5
5.5	37.9	39	1.76	0.54	99.9	75.7	79.6	52.1	53.5	31.0
7.2	49.6	30	2.31	0.70	99.9	74.6	79.6	52.0	53.2	30.4
9.3	64.1	23	2.98	0.91	99.8	74.1	79.5	51.4	52.9	29.8
12.0	82.7	18	3.85	1.17	99.8	73.4	79.5	51.2	52.1	29.3
15.5	106.9	14	4.97	1.51	99.8	72.5	79.3	50.2	51.3	28.4
20	137.9	11	6.41	2.0	99.6	71.7	78.8	49.4	50.5	27.6
25	172.4	8.6	8.01	2.4	99.3	71.3	77.3	48.7	49.6	26.9
35	241.3	6.1	11.2	3.4	89.1	70.8	75.9	47.9	48.4	25.9
45	310.3	4.8	14.4	4.4	70.5	70.5	74.3	47.4	47.6	25.9
55	379.2	3.9	17.6	5.4			68.9	46.9	46.8	25.2
75	517.1	2.9	24.0	7.3			63.1	46.3	45.4	24.2
95	655.0	2.3	30.5	9.3			59.2	45.8	44.5	23.5
120	827.4	1.8	38.5	11.7			54.4	45.4	43.1	22.8
150	1,034	1.4	48.1	14.7			51.7	45.1	42.2	22.0
200	1,379	1.1	64.1	19.5			48.3	44.8	41.2	20.7
260	1,793	0.82	83.4	25.4			44.7	44.7	39.8	19.5
350	2,413	0.61	112	34.1					37.3	18.2
430	2,965	0.50	138	42.1					35.6	17.4
550	3,792	0.39	176	53.6					33.7	16.4
725	4,999	0.30	232	70.7					31.5	15.3
925	6,378	0.23	297	90.5					29.4	14.9
1200	8,274	0.18	385	117.3					27.5	14.6
1550	10,687	0.14	497	151.5					24.9	13.8
2000	13,790	0.11	641	195.4					22.9	12.9
2600	17,926	0.08	834	254.2					20.5	12.3
3350	23,097	0.06	1074	327.4					18.3	11.8
4300	29,647	0.05	1378	420.0					16.1	11.3
5550	38,266	0.04	1779	542.2					14.2	11.2
7200	49,642	0.03	2308	703.5					12.1	10.6
9300	64,121	0.02	2981	908.6					10.3	10.3



Appendix 4

US DOE #DE-FC26-05NT42660 Final Scientific/Technical Report

Alan P. Byrnes, Robert M. Cluff and John C. Webb

Mercury Injection Drainage-Imbibition Capillary Pressure Analysis

DAVIS OIL COMPANY: 2 FRED STATE - E932 - 7546.7 ft (B)

In situ Klinkenberg Permeability (μm^2) =

5.53E-05

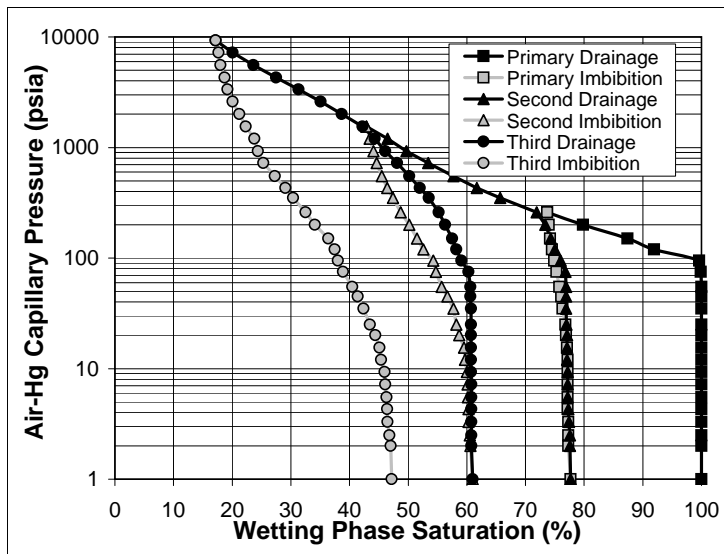
In situ Klinkenberg Permeability (mD) =

0.0560

Routine Porosity (%) =

13.4

Mercury Injection Capillary Pressure (psia)	Mercury Injection Capillary Pressure (kPa)	Approx. Pore Entry Diameter (μm)	Approx. Gas-Water Height Above Free Water Level (ft)	Approx. Gas-Water Height Above Free Water Level (m)	Drainage 1 Cumulative Wetting Phase Saturation (% pore vol)	Imbibition 1 Cumulative Wetting Phase Saturation (% pore vol)	Drainage 2 Cumulative Wetting Phase Saturation (% pore vol)	Imbibition 2 Cumulative Wetting Phase Saturation (% pore vol)	Drainage 3 Cumulative Wetting Phase Saturation (% pore vol)	Imbibition 3 Cumulative Wetting Phase Saturation (% pore vol)
2.0	13.8	107	0.10	0.03	100.0	77.7	77.7	61.0	61.0	47.2
2.5	17.2	86	0.64	0.20	100.0	77.3	77.6	60.6	60.8	47.0
3.3	22.8	65	0.80	0.24	100.0	77.3	77.6	60.5	60.8	46.8
4.3	29.6	50	1.06	0.32	100.0	77.3	77.4	60.3	60.8	46.5
5.5	37.9	39	1.38	0.42	100.0	77.2	77.3	60.3	60.8	46.4
7.2	49.6	30	1.76	0.54	100.0	77.2	77.2	60.2	60.8	46.3
9.3	64.1	23	2.31	0.70	100.0	77.2	77.2	60.1	60.8	46.1
12.0	82.7	18	2.98	0.91	100.0	77.2	77.2	60.0	60.7	46.0
15.5	106.9	14	3.85	1.17	100.0	77.2	77.1	59.7	60.7	45.4
20	137.9	11	4.97	1.51	100.0	77.1	77.1	59.5	60.7	45.1
25	172.4	8.6	6.41	2.0	100.0	76.9	77.1	58.7	60.7	44.4
35	241.3	6.1	8.01	2.4	100.0	76.8	77.0	58.2	60.7	43.5
45	310.3	4.8	11.2	3.4	100.0	76.3	76.9	57.7	60.7	42.4
55	379.2	3.9	14.4	4.4	100.0	76.1	76.9	56.7	60.6	41.4
75	517.1	2.9	17.6	5.4	100.0	75.8	76.9	55.7	60.6	40.5
95	655.0	2.3	24.0	7.3	99.9	75.3	76.8	54.7	60.3	38.9
120	827.4	1.8	30.5	9.3	99.6	74.9	76.0	54.3	59.1	38.0
150	1,034	1.4	38.5	11.7	91.9	74.5	75.0	52.6	58.2	37.5
200	1,379	1.1	48.1	14.7	87.4	74.2	74.3	51.5	57.5	36.4
260	1,793	0.82	64.1	19.5	79.8	74.0	73.4	50.2	56.3	34.1
350	2,413	0.61	83.4	25.4	73.7	73.7	71.9	48.7	55.2	32.5
430	2,965	0.50	112	34.1			65.7	47.4	53.5	30.4
550	3,792	0.39	138	42.1			61.7	46.4	52.0	29.1
725	4,999	0.30	176	53.6			57.7	45.5	50.2	27.3
925	6,378	0.23	232	70.7			53.4	44.6	48.1	25.3
1200	8,274	0.18	297	90.5			49.7	44.1	46.1	24.4
1550	10,687	0.14	385	117.3			46.5	43.4	44.3	23.8
2000	13,790	0.11	497	151.5			42.9	42.9		22.3
2600	17,926	0.08	641	195.4					38.7	21.2
3350	23,097	0.06	834	254.2					35.1	20.1
4300	29,647	0.05	1074	327.4					31.3	19.2
5550	38,266	0.04	1378	420.0					27.5	18.7
7200	49,642	0.03	1779	542.2					23.6	18.0
9300	64,121	0.02	2308	703.5					20.1	17.7
			2981	908.6					17.2	17.2



Mercury Injection Drainage-Imbibition Capillary Pressure Analysis

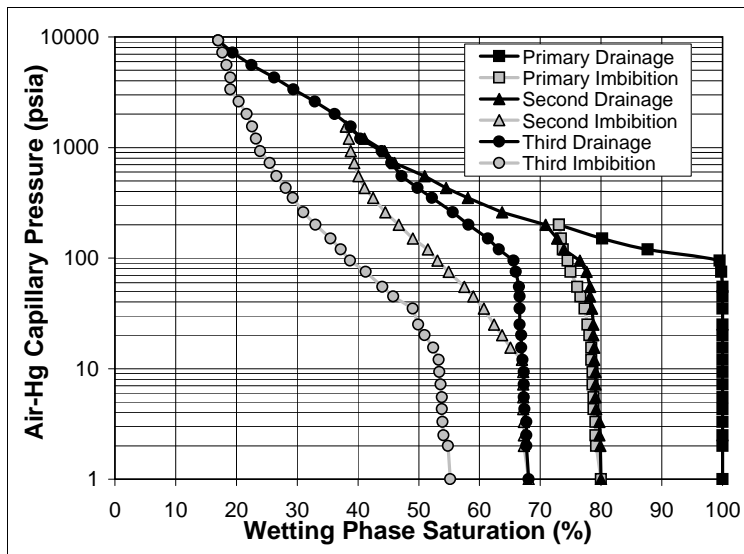
MAPCO INCORPORATED: 11-17F RIVER BEND UNIT - B646 - 8294.4 ft (B)

In situ Klinkenberg Permeability (μm^2) = 2.17E-05

In situ Klinkenberg Permeability (mD) = 0.0220

Routine Porosity (%) = 7.6

Mercury Injection Capillary Pressure (psia)	Mercury Injection Capillary Pressure (kPa)	Approx. Pore Entry Diameter (μm)	Approx. Gas-Water Height Above Free Water Level (ft)	Approx. Gas-Water Height Above Free Water Level (m)	Drainage 1 Cumulative Wetting Phase Saturation (% pore vol)	Imbibition 1 Cumulative Wetting Phase Saturation (% pore vol)	Drainage 2 Cumulative Wetting Phase Saturation (% pore vol)	Imbibition 2 Cumulative Wetting Phase Saturation (% pore vol)	Drainage 3 Cumulative Wetting Phase Saturation (% pore vol)	Imbibition 3 Cumulative Wetting Phase Saturation (% pore vol)
2.0	13.8	107	0.10	0.03	100.0	80.0	80.0	68.1	68.1	55.2
2.5	17.2	86	0.64	0.20	100.0	79.2	79.9	67.3	67.7	54.8
3.3	22.8	65	0.80	0.24	100.0	79.1	79.7	67.3	67.7	54.1
4.3	29.6	50	1.06	0.32	100.0	78.8	79.2	67.2	67.4	53.8
5.5	37.9	39	1.38	0.42	100.0	78.8	79.1	67.2	67.3	53.8
7.2	49.6	30	1.76	0.54	100.0	78.8	79.1	67.2	67.3	53.6
9.3	64.1	23	2.31	0.70	100.0	78.6	79.1	67.2	67.3	53.4
12.0	82.7	18	2.98	0.91	100.0	78.6	79.1	67.2	67.3	53.4
15.5	106.9	14	3.85	1.17	100.0	78.4	78.9	67.0	67.1	53.3
20	137.9	11	4.97	1.51	100.0	78.4	78.9	65.1	66.9	52.4
25	172.4	8.6	6.41	2.0	100.0	78.1	78.7	63.7	66.9	51.0
35	241.3	6.1	8.01	2.4	100.0	77.8	78.7	62.4	66.6	49.9
45	310.3	4.8	11.2	3.4	100.0	77.3	78.5	60.7	66.6	49.0
55	379.2	3.9	14.4	4.4	100.0	76.6	78.2	59.0	66.6	48.8
75	517.1	2.9	17.6	5.4	100.0	76.1	78.2	57.5	66.5	44.0
95	655.0	2.3	24.0	7.3	99.8	75.0	77.6	54.9	66.0	41.3
120	827.4	1.8	30.5	9.3	99.5	74.5	76.5	53.1	65.6	38.7
150	1,034	1.4	38.5	11.7	87.7	73.7	73.9	51.5	63.2	37.2
200	1,379	1.1	48.1	14.7	80.2	73.4	72.8	49.0	61.4	35.5
260	1,793	0.82	64.1	19.5	73.1	73.1	70.9	46.7	58.2	33.0
350	2,413	0.61	83.4	25.4			63.7	44.5	55.6	31.0
430	2,965	0.50	112	34.1			58.1	42.5	52.2	29.3
550	3,792	0.39	138	42.1			54.5	41.1	49.8	28.1
725	4,999	0.30	176	53.6			51.0	40.1	47.2	26.6
925	6,378	0.23	232	70.7			46.0	39.4	45.5	25.5
1200	8,274	0.18	297	90.5			44.4	38.8	43.9	23.9
1550	10,687	0.14	385	117.3			41.1	38.5	40.4	23.2
2000	13,790	0.11	497	151.5			38.0	38.0	38.8	22.6
2600	17,926	0.08	641	195.4					36.2	21.7
3350	23,097	0.06	834	254.2					32.9	20.4
4300	29,647	0.05	1074	327.4					29.4	19.0
5550	38,266	0.04	1378	420.0					26.2	19.0
7200	49,642	0.03	1779	542.2					22.5	18.4
9300	64,121	0.02	2308	703.5					19.4	17.7
			2981	908.6					17.0	17.0

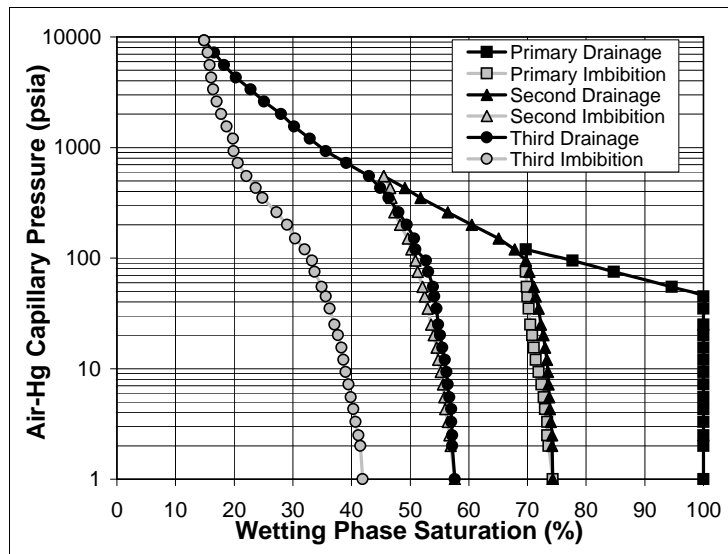


Mercury Injection Drainage-Imbibition Capillary Pressure Analysis

ENSERCH EXPLORATION: 4-5 US LAMCO - R829 - 5618.3 ft (B)

In situ Klinkenberg Permeability (μm^2) = 2.83E-04
In situ Klinkenberg Permeability (mD) = 0.2870
 Routine Porosity (%) = 9.2

Mercury Injection Capillary Pressure (psia)	Mercury Injection Capillary Pressure (kPa)	Approx. Pore Entry Diameter (μm)	Approx. Gas-Water Height Above Free Water Level (ft)	Approx. Gas-Water Height Above Free Water Level (m)	Drainage 1 Cumulative Wetting Phase Saturation (% pore vol)	Imbibition 1 Cumulative Wetting Phase Saturation (% pore vol)	Drainage 2 Cumulative Wetting Phase Saturation (% pore vol)	Imbibition 2 Cumulative Wetting Phase Saturation (% pore vol)	Drainage 3 Cumulative Wetting Phase Saturation (% pore vol)	Imbibition 3 Cumulative Wetting Phase Saturation (% pore vol)
2.0	13.8	107	0.10	0.03	100.0	74.3	74.3	57.6	57.6	41.9
2.5	17.2	86	0.64	0.20	100.0	73.6	74.2	56.9	57.2	41.5
3.3	22.8	65	0.80	0.24	100.0	73.4	74.2	56.7	57.2	41.2
4.3	29.6	50	1.06	0.32	100.0	73.4	74.0	56.4	57.0	40.7
5.5	37.9	39	1.38	0.42	100.0	73.0	73.8	56.0	57.0	40.3
7.2	49.6	30	1.76	0.54	100.0	72.8	73.7	55.8	56.7	39.9
9.3	64.1	23	2.31	0.70	100.0	72.4	73.6	55.6	56.4	39.5
12.0	82.7	18	2.98	0.91	100.0	71.9	73.5	55.2	56.2	39.0
15.5	106.9	14	3.85	1.17	100.0	71.4	73.3	54.8	55.9	38.6
20	137.9	11	4.97	1.51	100.0	71.1	73.0	54.5	55.5	38.3
25	172.4	8.6	6.41	2.0	100.0	70.8	72.7	54.0	55.1	37.7
35	241.3	6.1	8.01	2.4	100.0	70.5	72.3	53.6	54.8	37.1
45	310.3	4.8	11.2	3.4	100.0	70.2	71.9	53.0	54.5	36.3
55	379.2	3.9	14.4	4.4	100.0	70.0	71.4	52.5	54.1	35.6
75	517.1	2.9	17.6	5.4	94.6	69.9	71.1	52.1	53.9	34.9
95	655.0	2.3	24.0	7.3	84.7	69.7	70.3	51.3	53.1	33.7
120	827.4	1.8	30.5	9.3	77.7		69.7	50.9	52.7	33.3
150	1,034	1.4	38.5	11.7	69.7		67.8	50.2	50.9	32.0
200	1,379	1.1	48.1	14.7			65.1	49.6	50.7	30.4
260	1,793	0.82	64.1	19.5			60.5	48.3	49.4	29.0
350	2,413	0.61	83.4	25.4			56.4	47.3	48.0	27.2
430	2,965	0.50	112	34.1			51.8	46.8	46.3	24.8
550	3,792	0.39	138	42.1			49.1	46.6	44.9	23.7
725	4,999	0.30	176	53.6			45.5	45.5	43.0	22.1
925	6,378	0.23	232	70.7					39.1	20.6
1200	8,274	0.18	297	90.5					35.6	19.9
1550	10,687	0.14	385	117.3					32.9	19.8
2000	13,790	0.11	497	151.5					30.2	18.7
2600	17,926	0.08	641	195.4					28.0	17.8
3350	23,097	0.06	834	254.2					25.1	17.0
4300	29,647	0.05	1074	327.4					22.8	16.4
5550	38,266	0.04	1378	420.0					20.3	16.1
7200	49,642	0.03	1779	542.2					18.3	15.8
9300	64,121	0.02	2308	703.5					16.6	15.5
			2981	908.6					14.9	14.9



Appendix 4

US DOE #DE-FC26-05NT42660 Final Scientific/Technical Report

Alan P. Byrnes, Robert M. Cluff and John C. Webb

Mercury Injection Drainage-Imbibition Capillary Pressure Analysis

ENSERCH EXPLORATION: 4-5 US LAMCO - R829 - 5633.1 ft (B)

In situ Klinkenberg Permeability (μm^2) =

6.03E-03

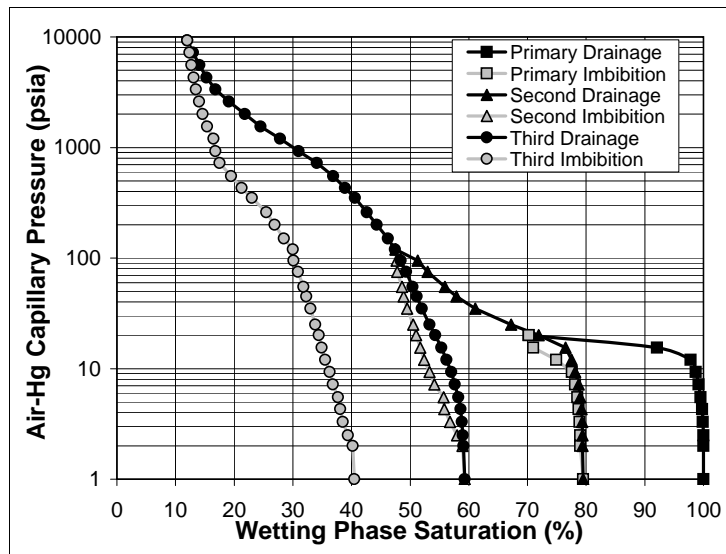
In situ Klinkenberg Permeability (mD) =

6.1100

Routine Porosity (%) =

11.8

Mercury Injection Capillary Pressure (psia)	Mercury Injection Capillary Pressure (kPa)	Approx. Pore Entry Diameter (μm)	Approx. Gas-Water Height Above Free Water Level (ft)	Approx. Gas-Water Height Above Free Water Level (m)	Drainage 1 Cumulative Wetting Phase Saturation (% pore vol)	Imbibition 1 Cumulative Wetting Phase Saturation (% pore vol)	Drainage 2 Cumulative Wetting Phase Saturation (% pore vol)	Imbibition 2 Cumulative Wetting Phase Saturation (% pore vol)	Drainage 3 Cumulative Wetting Phase Saturation (% pore vol)	Imbibition 3 Cumulative Wetting Phase Saturation (% pore vol)
2.0	13.8	107	0.10	0.03	100.0	79.5	79.5	59.3	59.3	40.5
2.5	17.2	86	0.64	0.20	100.0	79.0	79.4	58.9	59.1	40.2
3.3	22.8	65	0.80	0.24	100.0	79.0	79.4	58.0	59.0	39.4
4.3	29.6	50	1.06	0.32	99.9	78.9	79.3	56.8	58.8	38.5
5.5	37.9	39	1.38	0.42	99.8	78.7	79.2	55.8	58.6	38.1
7.2	49.6	30	1.76	0.54	99.5	78.5	79.0	55.7	58.2	37.7
9.3	64.1	23	2.31	0.70	99.2	78.1	78.7	54.1	57.6	36.8
12.0	82.7	18	2.98	0.91	98.7	77.6	78.1	53.3	57.0	36.3
15.5	106.9	14	3.85	1.17	97.8	74.9	77.5	52.4	56.2	35.5
20	137.9	11	4.97	1.51	92.1	71.0	76.5	51.7	55.3	34.9
25	172.4	8.6	6.41	2.0	70.2	70.2	71.9	51.0	54.3	34.4
35	241.3	6.1	8.01	2.4			67.2	50.5	53.3	33.8
45	310.3	4.8	11.2	3.4			61.1	49.5	52.0	33.0
55	379.2	3.9	14.4	4.4			57.9	48.9	51.1	32.3
75	517.1	2.9	17.6	5.4			55.9	48.6	50.4	31.8
95	655.0	2.3	24.0	7.3			53.0	47.8	49.3	30.9
120	827.4	1.8	30.5	9.3			51.3	47.7	48.4	30.1
150	1,034	1.4	38.5	11.7			47.5	47.5	47.4	30.0
200	1,379	1.1	48.1	14.7					46.2	28.5
260	1,793	0.82	64.1	19.5					44.3	26.9
350	2,413	0.61	83.4	25.4					42.6	25.5
430	2,965	0.50	112	34.1					40.6	23.0
550	3,792	0.39	138	42.1					38.9	21.3
725	4,999	0.30	176	53.6					36.9	19.5
925	6,378	0.23	232	70.7					34.1	17.5
1200	8,274	0.18	297	90.5					31.0	16.8
1550	10,687	0.14	385	117.3					27.8	16.5
2000	13,790	0.11	497	151.5					24.5	15.4
2600	17,926	0.08	641	195.4					21.8	14.6
3350	23,097	0.06	834	254.2					19.1	14.0
4300	29,647	0.05	1074	327.4					16.8	13.5
5550	38,266	0.04	1378	420.0					15.3	13.1
7200	49,642	0.03	1779	542.2					14.1	12.7
9300	64,121	0.02	2308	703.5					13.0	12.4
			2981	908.6					12.0	12.0

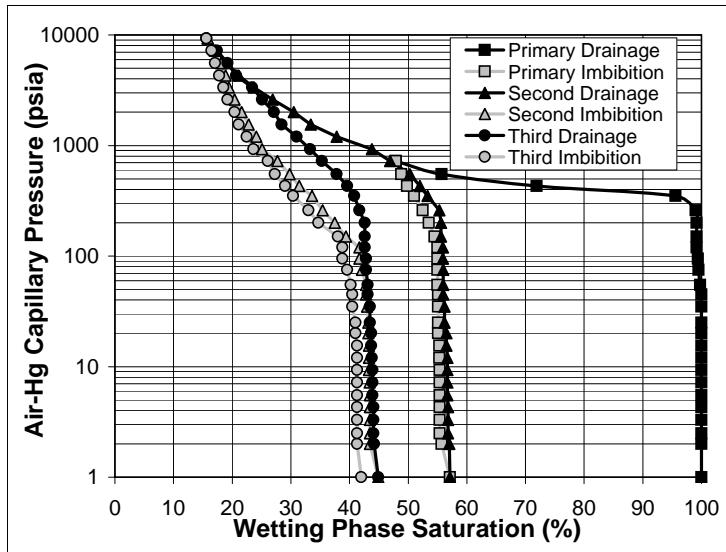


Mercury Injection Drainage-Imbibition Capillary Pressure Analysis

ENSERCH EXPLORATION: 4-5 US LAMCO - R829 - 5638.8 ft (B)

In situ Klinkenberg Permeability (μm^2) = 3.75E-06
In situ Klinkenberg Permeability (mD) = 0.0038
 Routine Porosity (%) = 5.0

Mercury Injection Capillary Pressure (psia)	Mercury Injection Capillary Pressure (kPa)	Approx. Pore Entry Diameter (μm)	Approx. Gas-Water Height Above Free Water Level (ft)	Approx. Gas-Water Height Above Free Water Level (m)	Drainage 1 Cumulative Wetting Phase Saturation (% pore vol)	Imbibition 1 Cumulative Wetting Phase Saturation (% pore vol)	Drainage 2 Cumulative Wetting Phase Saturation (% pore vol)	Imbibition 2 Cumulative Wetting Phase Saturation (% pore vol)	Drainage 3 Cumulative Wetting Phase Saturation (% pore vol)	Imbibition 3 Cumulative Wetting Phase Saturation (% pore vol)
2.0	13.8	107	0.10	0.03	100.0	57.1	57.1	44.9	44.9	42.0
2.5	17.2	86	0.64	0.20	100.0	55.7	57.0	43.5	44.2	41.3
3.3	22.8	65	0.80	0.24	100.0	55.4	56.8	43.5	44.1	41.3
4.3	29.6	50	1.06	0.32	100.0	55.4	56.8	43.5	44.1	41.3
5.5	37.9	39	1.38	0.42	100.0	55.4	56.7	43.5	43.9	41.3
7.2	49.6	30	1.76	0.54	100.0	55.4	56.7	43.4	43.9	41.3
9.3	64.1	23	2.31	0.70	100.0	55.4	56.7	43.3	43.9	41.3
12.0	82.7	18	2.98	0.91	100.0	55.4	56.7	43.3	43.9	41.3
15.5	106.9	14	3.85	1.17	100.0	55.3	56.7	43.3	43.8	41.3
20	137.9	11	4.97	1.51	100.0	55.3	56.5	43.3	43.7	41.3
25	172.4	8.6	6.41	2.0	100.0	55.1	56.5	43.2	43.7	41.0
35	241.3	6.1	8.01	2.4	100.0	55.1	56.2	43.2	43.5	41.0
45	310.3	4.8	11.2	3.4	100.0	55.1	56.2	43.0	43.5	40.5
55	379.2	3.9	14.4	4.4	100.0	55.1	56.0	42.8	43.1	40.5
75	517.1	2.9	17.6	5.4	99.8	55.0	56.0	42.8	43.1	40.2
95	655.0	2.3	24.0	7.3	99.5	55.0	56.0	42.1	42.8	39.6
120	827.4	1.8	30.5	9.3	99.4	55.0	55.9	41.7	42.8	38.8
150	1,034	1.4	38.5	11.7	99.2	55.0	55.9	41.7	42.6	38.8
200	1,379	1.1	48.1	14.7	99.2	54.5	55.6	39.4	42.6	38.0
260	1,793	0.82	64.1	19.5	99.2	53.5	55.6	37.5	42.6	34.7
350	2,413	0.61	83.4	25.4	99.0	52.5	55.3	35.4	41.7	33.0
430	2,965	0.50	112	34.1	95.6	51.0	53.3	33.6	40.8	30.4
550	3,792	0.39	138	42.1	71.9	49.8	52.0	31.4	39.6	29.0
725	4,999	0.30	176	53.6	55.7	48.8	50.3	29.8	37.8	27.3
925	6,378	0.23	232	70.7	47.9	47.9	46.9	27.7	35.3	26.1
1200	8,274	0.18	297	90.5			43.8	25.1	33.3	23.6
1550	10,687	0.14	385	117.3			37.8	24.1	31.0	22.5
2000	13,790	0.11	497	151.5			33.4	22.8	28.4	21.1
2600	17,926	0.08	641	195.4			30.5	21.6	27.1	20.4
3350	23,097	0.06	834	254.2			26.9	20.4	25.1	19.2
4300	29,647	0.05	1074	327.4			23.7	19.4	23.4	18.5
5550	38,266	0.04	1378	420.0			21.1	18.9	20.7	17.8
7200	49,642	0.03	1779	542.2			19.1	18.1	19.2	17.1
9300	64,121	0.02	2308	703.5			17.1	17.0	17.4	16.5
			2981	908.6			15.8	15.8	15.6	15.6



Mercury Injection Drainage-Imbibition Capillary Pressure Analysis

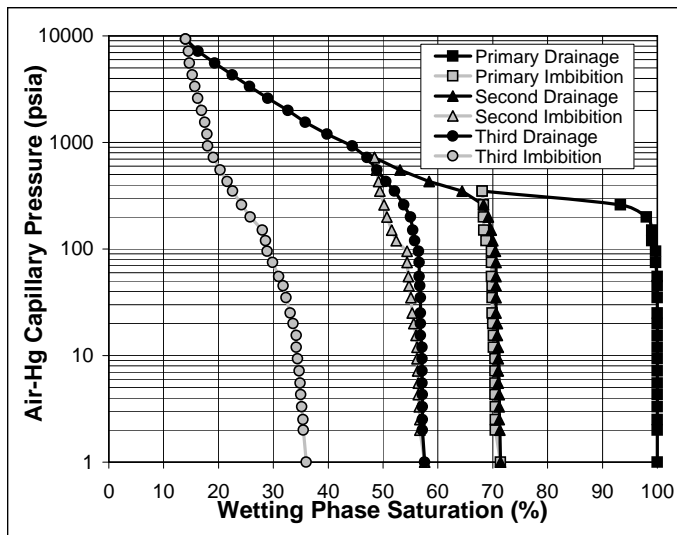
KERR-MCGEE OIL&GAS ONSHORE: NBU 920-360 - KM360 -8184.5 ft (B)

In situ Klinkenberg Permeability (μm^2) = 2.37E-06

In situ Klinkenberg Permeability (mD) = 0.0024

Routine Porosity (%) = 7.1

Mercury Injection Capillary Pressure (psia)	Mercury Injection Capillary Pressure (kPa)	Approx. Pore Entry Diameter (μm)	Approx. Gas-Water Height Above Free Water Level (ft)	Approx. Gas-Water Height Above Free Water Level (m)	Drainage 1 Cumulative Wetting Phase Saturation (% pore vol)	Imbibition 1 Cumulative Wetting Phase Saturation (% pore vol)	Drainage 2 Cumulative Wetting Phase Saturation (% pore vol)	Imbibition 2 Cumulative Wetting Phase Saturation (% pore vol)	Drainage 3 Cumulative Wetting Phase Saturation (% pore vol)	Imbibition 3 Cumulative Wetting Phase Saturation (% pore vol)
2.0	13.8	107	0.10	0.03	100.0	71.4	71.4	57.6	57.6	36.0
2.5	17.2	86	0.64	0.20	100.0	70.5	71.3	56.7	57.2	35.5
3.3	22.8	65	0.80	0.24	100.0	70.5	71.2	56.7	57.2	35.4
4.3	29.6	50	1.06	0.32	100.0	70.5	71.2	56.6	57.2	35.2
5.5	37.9	39	1.38	0.42	100.0	70.4	71.2	56.4	57.2	35.0
7.2	49.6	30	1.76	0.54	100.0	70.4	71.0	56.4	57.1	34.9
9.3	64.1	23	2.31	0.70	100.0	70.4	71.0	56.3	57.1	34.7
12.0	82.7	18	2.98	0.91	100.0	70.4	71.0	56.2	57.1	34.4
15.5	106.9	14	3.85	1.17	100.0	70.1	71.0	56.2	57.1	34.2
20	137.9	11	4.97	1.51	100.0	70.1	70.8	56.0	56.8	34.2
25	172.4	8.6	6.41	2.0	100.0	70.0	70.8	55.6	56.8	33.6
35	241.3	6.1	8.01	2.4	100.0	69.9	70.6	55.3	56.8	33.1
45	310.3	4.8	11.2	3.4	100.0	69.9	70.6	55.1	56.8	32.3
55	379.2	3.9	14.4	4.4	100.0	69.9	70.6	54.7	56.7	31.8
75	517.1	2.9	17.6	5.4	100.0	69.8	70.6	54.6	56.6	31.0
95	655.0	2.3	24.0	7.3	99.7	69.8	70.6	54.4	56.6	29.9
120	827.4	1.8	30.5	9.3	99.7	69.8	70.5	54.4	56.5	28.9
150	1,034	1.4	38.5	11.7	99.0	68.8	70.0	52.4	55.8	28.6
200	1,379	1.1	48.1	14.7	99.0	68.4	69.7	51.6	55.4	28.0
260	1,793	0.82	64.1	19.5	98.0	68.3	69.2	50.7	55.0	25.8
350	2,413	0.61	83.4	25.4	93.3	68.3	68.3	50.2	53.8	24.2
430	2,965	0.50	112	34.1	68.1	68.1	64.4	49.4	52.1	22.6
550	3,792	0.39	138	42.1			58.4	49.2	50.5	21.6
725	4,999	0.30	176	53.6			53.1	48.8	48.9	20.3
925	6,378	0.23	232	70.7			48.4	48.4	47.1	19.1
1200	8,274	0.18	297	90.5					44.4	18.0
1550	10,687	0.14	385	117.3					39.8	17.9
2000	13,790	0.11	497	151.5					35.8	17.5
2600	17,926	0.08	641	195.4					32.7	16.9
3350	23,097	0.06	834	254.2					29.0	16.2
4300	29,647	0.05	1074	327.4					25.7	15.7
5550	38,266	0.04	1378	420.0					22.5	15.2
7200	49,642	0.03	1779	542.2					19.3	14.7
9300	64,121	0.02	2308	703.5					16.3	14.5
			2981	908.6					14.0	14.0



Mercury Injection Drainage-Imbibition Capillary Pressure Analysis

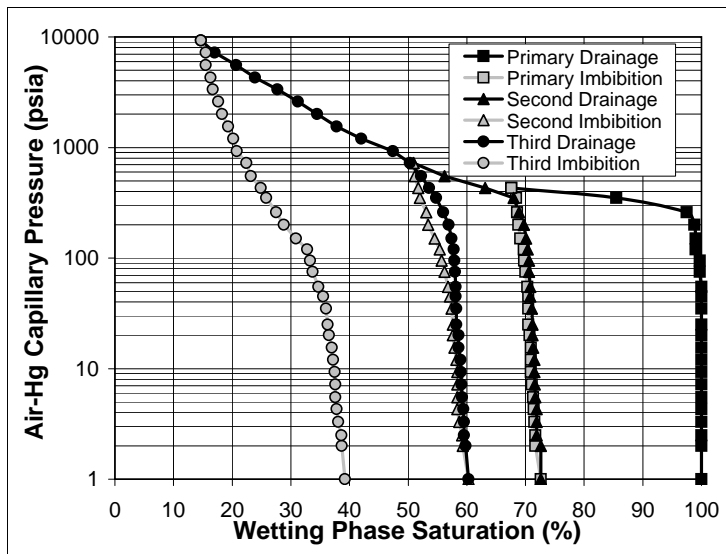
KERR-MCGEE OIL&GAS ONSHORE: NBU 920-360 - KM360 - 8184.6 ft (B)

In situ Klinkenberg Permeability (μm^2) = 2.27E-06

In situ Klinkenberg Permeability (mD) = 0.0023

Routine Porosity (%) = 6.7

Mercury Injection Capillary Pressure (psia)	Mercury Injection Capillary Pressure (kPa)	Approx. Pore Entry Diameter (μm)	Approx. Gas-Water Height Above Free Water Level (ft)	Approx. Gas-Water Height Above Free Water Level (m)	Drainage 1 Cumulative Wetting Phase Saturation (% pore vol)	Imbibition 1 Cumulative Wetting Phase Saturation (% pore vol)	Drainage 2 Cumulative Wetting Phase Saturation (% pore vol)	Imbibition 2 Cumulative Wetting Phase Saturation (% pore vol)	Drainage 3 Cumulative Wetting Phase Saturation (% pore vol)	Imbibition 3 Cumulative Wetting Phase Saturation (% pore vol)
2.0	13.8	107	0.10	0.03	100.0	72.6	72.6	60.3	60.3	39.2
2.5	17.2	86	0.64	0.20	100.0	71.7	72.6	59.3	59.8	38.7
3.3	22.8	65	0.80	0.24	100.0	71.7	71.9	59.2	59.5	38.6
4.3	29.6	50	1.06	0.32	100.0	71.5	71.9	58.7	59.5	38.1
5.5	37.9	39	1.38	0.42	100.0	71.4	71.9	58.4	59.4	37.8
7.2	49.6	30	1.76	0.54	100.0	71.3	71.7	58.4	59.2	37.6
9.3	64.1	23	2.31	0.70	100.0	71.1	71.6	58.4	59.1	37.6
12.0	82.7	18	2.98	0.91	100.0	70.9	71.5	58.4	59.0	37.5
15.5	106.9	14	3.85	1.17	100.0	70.9	71.5	58.2	58.9	37.2
20	137.9	11	4.97	1.51	100.0	70.9	71.3	57.9	58.6	37.0
25	172.4	8.6	6.41	2.0	100.0	70.7	71.2	57.6	58.6	36.5
35	241.3	6.1	8.01	2.4	100.0	70.5	71.2	57.6	58.2	36.3
45	310.3	4.8	11.2	3.4	100.0	70.5	71.1	57.4	58.2	36.0
55	379.2	3.9	14.4	4.4	100.0	70.5	70.8	57.1	58.1	35.5
75	517.1	2.9	17.6	5.4	100.0	70.3	70.8	56.8	58.1	34.7
95	655.0	2.3	24.0	7.3	99.7	70.0	70.6	56.2	58.0	33.7
120	827.4	1.8	30.5	9.3	99.7	69.8	70.6	55.7	57.9	33.3
150	1,034	1.4	38.5	11.7	99.0	69.7	70.4	55.4	57.8	32.8
200	1,379	1.1	48.1	14.7	99.0	69.1	70.1	54.5	57.4	30.9
260	1,793	0.82	64.1	19.5	98.8	68.8	69.7	53.4	56.9	28.8
350	2,413	0.61	83.4	25.4	97.5	68.6	68.9	53.1	56.0	27.5
430	2,965	0.50	112	34.1	85.5	68.4	68.0	52.0	54.8	25.8
550	3,792	0.39	138	42.1	67.6	67.6	63.1	51.7	53.6	24.9
725	4,999	0.30	176	53.6			56.2	51.1	52.2	23.2
925	6,378	0.23	232	70.7			50.9	50.9	50.3	22.4
1200	8,274	0.18	297	90.5					47.4	20.8
1550	10,687	0.14	385	117.3					42.0	20.2
2000	13,790	0.11	497	151.5					37.8	19.3
2600	17,926	0.08	641	195.4					34.5	18.3
3350	23,097	0.06	834	254.2					31.2	17.6
4300	29,647	0.05	1074	327.4					27.7	16.7
5550	38,266	0.04	1378	420.0					23.9	16.3
7200	49,642	0.03	1779	542.2					20.7	15.5
9300	64,121	0.02	2308	703.5					17.0	15.5
			2981	908.6					14.7	14.7

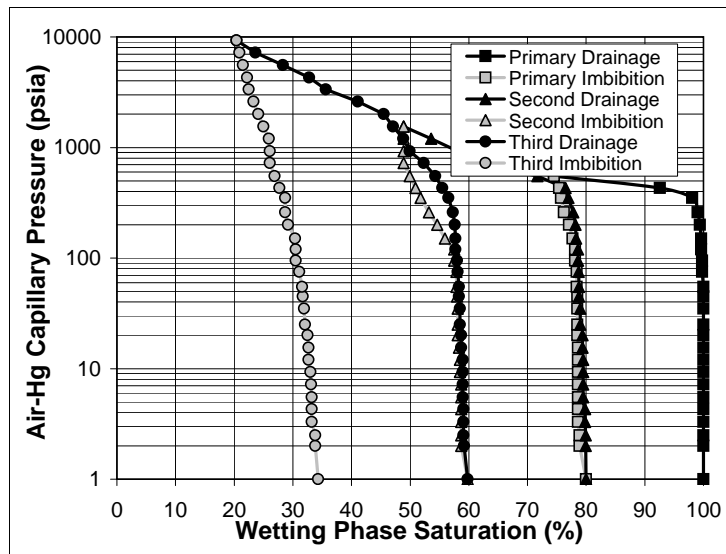


Mercury Injection Drainage-Imbibition Capillary Pressure Analysis

KERR-MCGEE OIL&GAS ONSHORE: NBU 920-360 - KM360 -8185.7 ft (B)

In situ Klinkenberg Permeability (μm^2) = 6.91E-07
In situ Klinkenberg Permeability (mD) = 0.0007
 Routine Porosity (%) = 5.9

Mercury Injection Capillary Pressure (psia)	Mercury Injection Capillary Pressure (kPa)	Approx. Pore Entry Diameter (μm)	Approx. Gas-Water Height Above Free Water Level (ft)	Approx. Gas-Water Height Above Free Water Level (m)	Drainage 1 Cumulative Wetting Phase Saturation (% pore vol)	Imbibition 1 Cumulative Wetting Phase Saturation (% pore vol)	Drainage 2 Cumulative Wetting Phase Saturation (% pore vol)	Imbibition 2 Cumulative Wetting Phase Saturation (% pore vol)	Drainage 3 Cumulative Wetting Phase Saturation (% pore vol)	Imbibition 3 Cumulative Wetting Phase Saturation (% pore vol)
2.0	13.8	107	0.10	0.03	100.0	80.0	80.0	59.8	59.8	34.3
2.5	17.2	86	0.64	0.20	100.0	78.9	79.9	58.7	59.2	33.8
3.3	22.8	65	0.80	0.24	100.0	78.9	79.9	58.7	59.1	33.8
4.3	29.6	50	1.06	0.32	100.0	78.6	79.8	58.7	59.1	33.2
5.5	37.9	39	1.38	0.42	100.0	78.6	79.5	58.7	59.0	33.2
7.2	49.6	30	1.76	0.54	100.0	78.6	79.5	58.7	59.0	33.1
9.3	64.1	23	2.31	0.70	100.0	78.6	79.5	58.5	59.0	33.0
12.0	82.7	18	2.98	0.91	100.0	78.6	79.5	58.5	59.0	32.7
15.5	106.9	14	3.85	1.17	100.0	78.6	79.4	58.5	59.0	32.7
20	137.9	11	4.97	1.51	100.0	78.6	79.4	58.3	58.7	32.5
25	172.4	8.6	6.41	2.0	100.0	78.5	79.4	58.1	58.7	32.5
35	241.3	6.1	8.01	2.4	100.0	78.5	79.0	58.1	58.5	32.1
45	310.3	4.8	11.2	3.4	100.0	78.5	79.0	58.1	58.5	31.9
55	379.2	3.9	14.4	4.4	100.0	78.5	78.8	58.0	58.3	31.7
75	517.1	2.9	17.6	5.4	100.0	78.4	78.8	57.9	58.3	31.6
95	655.0	2.3	24.0	7.3	99.8	78.4	78.7	57.9	58.1	31.1
120	827.4	1.8	30.5	9.3	99.8	78.1	78.6	57.5	58.0	30.5
150	1,034	1.4	38.5	11.7	99.6	78.1	78.6	57.5	57.7	30.5
200	1,379	1.1	48.1	14.7	99.6	77.7	78.3	55.9	57.7	30.4
260	1,793	0.82	64.1	19.5	99.4	77.1	78.2	54.6	57.6	29.2
350	2,413	0.61	83.4	25.4	99.0	76.2	77.8	53.2	57.3	28.7
430	2,965	0.50	112	34.1	98.1	75.7	77.0	51.8	56.5	28.7
550	3,792	0.39	138	42.1	92.6	75.4	76.5	50.9	55.5	27.7
725	4,999	0.30	176	53.6	74.5	74.5	71.7	49.9	54.3	26.9
925	6,378	0.23	232	70.7			62.9	48.9	52.3	26.1
1200	8,274	0.18	297	90.5			58.1	48.9	49.9	26.1
1550	10,687	0.14	385	117.3			53.6	48.9	48.8	25.9
2000	13,790	0.11	497	151.5			48.9	48.9	47.1	25.0
2600	17,926	0.08	641	195.4					45.5	24.1
3350	23,097	0.06	834	254.2					41.1	23.3
4300	29,647	0.05	1074	327.4					35.6	22.5
5550	38,266	0.04	1378	420.0					32.8	22.2
7200	49,642	0.03	1779	542.2					28.3	21.5
9300	64,121	0.02	2308	703.5					23.6	20.9
			2981	908.6					20.4	20.4



Appendix 4

US DOE #DE-FC26-05NT42660 Final Scientific/Technical Report

Alan P. Byrnes, Robert M. Cluff and John C. Webb

Mercury Injection Drainage-Imbibition Capillary Pressure Analysis

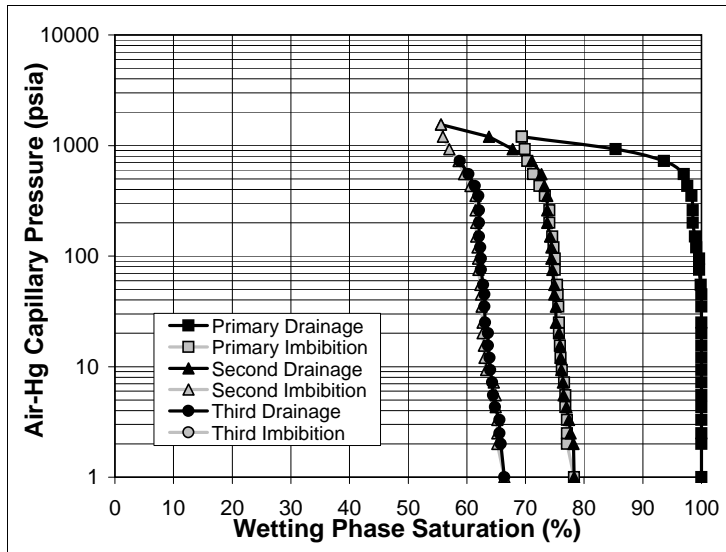
KERR-MCGEE OIL&GAS ONSHORE: NBU 1022-1A - KM1022 - 7853.5 ft (A)

In situ Klinkenberg Permeability (μm^2) = 8.88E-07

In situ Klinkenberg Permeability (mD) = 0.0009

Routine Porosity (%) = 3.8

Mercury Injection Capillary Pressure (psia)	Mercury Injection Capillary Pressure (kPa)	Approx. Pore Entry Diameter (μm)	Approx. Gas-Water Height Above Free Water Level (ft)	Approx. Gas-Water Height Above Free Water Level (m)	Drainage 1 Cumulative Wetting Phase Saturation (% pore vol)	Imbibition 1 Cumulative Wetting Phase Saturation (% pore vol)	Drainage 2 Cumulative Wetting Phase Saturation (% pore vol)	Imbibition 2 Cumulative Wetting Phase Saturation (% pore vol)	Drainage 3 Cumulative Wetting Phase Saturation (% pore vol)	Imbibition 3 Cumulative Wetting Phase Saturation (% pore vol)
2.0	13.8	107	0.10	0.03	100.0	78.3	78.3	66.4	66.4	
2.5	17.2	86	0.64	0.20	100.0	77.1	78.2	65.2	65.8	
3.3	22.8	65	0.80	0.24	100.0	77.1	77.7	65.2	65.6	
4.3	29.6	50	1.06	0.32	100.0	77.1	77.4	65.2	65.6	
5.5	37.9	39	1.38	0.42	100.0	76.8	77.0	64.9	64.8	
7.2	49.6	30	1.76	0.54	100.0	76.8	76.5	64.9	64.5	
9.3	64.1	23	2.31	0.70	100.0	76.6	76.4	64.6	64.3	
12.0	82.7	18	2.98	0.91	100.0	76.2	76.1	63.3	64.0	
15.5	106.9	14	3.85	1.17	100.0	76.0	76.0	63.0	63.9	
20	137.9	11	4.97	1.51	100.0	75.9	75.9	62.9	63.6	
25	172.4	8.6	6.41	2.0	100.0	75.7	75.7	62.7	63.6	
35	241.3	6.1	8.01	2.4	100.0	75.7	75.2	62.7	63.1	
45	310.3	4.8	11.2	3.4	100.0	75.6	75.2	62.5	63.0	
55	379.2	3.9	14.4	4.4	100.0	75.5	74.9	62.4	63.0	
75	517.1	2.9	17.6	5.4	99.9	75.4	74.9	62.3	62.8	
95	655.0	2.3	24.0	7.3	99.6	75.0	74.6	62.0	62.4	
120	827.4	1.8	30.5	9.3	99.6	75.0	74.4	61.9	62.4	
150	1,034	1.4	38.5	11.7	99.1	74.8	74.4	61.8	62.3	
200	1,379	1.1	48.1	14.7	98.9	74.6	74.2	61.6	62.1	
260	1,793	0.82	64.1	19.5	98.5	74.1	73.7	61.6	62.1	
350	2,413	0.61	83.4	25.4	98.5	74.1	73.7	61.5	62.1	
430	2,965	0.50	112	34.1	98.3	73.3	73.7	61.5	62.0	
550	3,792	0.39	138	42.1	97.6	72.4	73.2	60.6	61.4	
725	4,999	0.30	176	53.6	97.0	71.3	72.7	59.5	60.3	
925	6,378	0.23	232	70.7	93.6	70.3	71.1	58.6	58.8	
1200	8,274	0.18	297	90.5	85.4	69.9	67.8	57.0		
1550	10,687	0.14	385	117.3	69.4	69.4	63.8	55.9		
2000	13,790	0.11	497	151.5			55.6	55.6		
2600	17,926	0.08	641	195.4						
3350	23,097	0.06	834	254.2						
4300	29,647	0.05	1074	327.4						
5550	38,266	0.04	1378	420.0						
7200	49,642	0.03	1779	542.2						
9300	64,121	0.02	2308	703.5						
			2981	908.6						



Appendix 4

US DOE #DE-FC26-05NT42660 Final Scientific/Technical Report

Alan P. Byrnes, Robert M. Cluff and John C. Webb

Mercury Injection Drainage-Imbibition Capillary Pressure Analysis

USGS-CG: 3 BOOK CLIFFS - S172 - 124.7 ft (A)

In situ Klinkenberg Permeability (μm^2) =

4.90E-04

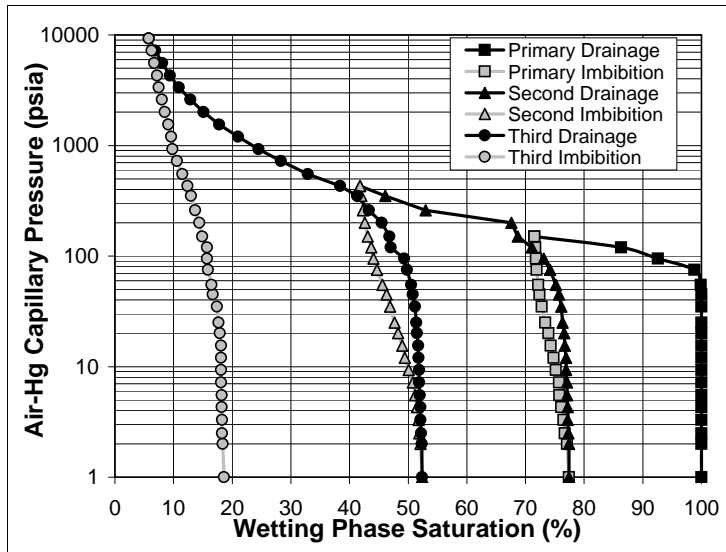
In situ Klinkenberg Permeability (mD) =

0.4960

Routine Porosity (%) =

18.9

Mercury Injection Capillary Pressure (psia)	Mercury Injection Capillary Pressure (kPa)	Approx. Pore Entry Diameter (μm)	Approx. Gas-Water Height Above Free Water Level (ft)	Approx. Gas-Water Height Above Free Water Level (m)	Drainage 1 Cumulative Wetting Phase Saturation (% pore vol)	Imbibition 1 Cumulative Wetting Phase Saturation (% pore vol)	Drainage 2 Cumulative Wetting Phase Saturation (% pore vol)	Imbibition 2 Cumulative Wetting Phase Saturation (% pore vol)	Drainage 3 Cumulative Wetting Phase Saturation (% pore vol)	Imbibition 3 Cumulative Wetting Phase Saturation (% pore vol)
2.0	13.8	107	0.10	0.03	100.0	77.4	77.4	52.4	52.4	18.6
2.5	17.2	86	0.64	0.20	100.0	77.1	77.4	52.3	52.3	18.4
3.3	22.8	65	0.80	0.24	100.0	76.7	77.3	51.9	52.2	18.3
4.3	29.6	50	1.06	0.32	100.0	76.5	77.2	51.8	52.1	18.3
5.5	37.9	39	1.38	0.42	100.0	76.1	77.2	51.5	52.1	18.2
7.2	49.6	30	1.76	0.54	100.0	75.8	77.1	51.2	52.0	18.2
9.3	64.1	23	2.31	0.70	100.0	75.7	77.1	50.8	51.9	18.1
12.0	82.7	18	2.98	0.91	100.0	75.2	76.9	50.1	51.9	18.1
15.5	106.9	14	3.85	1.17	100.0	74.8	76.9	49.4	51.8	18.1
20	137.9	11	4.97	1.51	100.0	74.3	76.7	49.0	51.7	18.1
25	172.4	8.6	6.41	2.0	100.0	73.9	76.6	48.3	51.5	17.9
35	241.3	6.1	8.01	2.4	100.0	73.4	76.3	47.7	51.4	17.7
45	310.3	4.8	11.2	3.4	100.0	72.8	76.1	46.9	51.2	17.4
55	379.2	3.9	14.4	4.4	100.0	72.4	75.7	46.3	50.8	16.7
75	517.1	2.9	17.6	5.4	99.9	72.2	75.2	45.6	50.5	16.5
95	655.0	2.3	24.0	7.3	98.8	71.9	74.2	44.7	49.8	15.9
120	827.4	1.8	30.5	9.3	92.6	71.8	73.1	44.1	49.3	15.7
150	1,034	1.4	38.5	11.7	86.3	71.7	71.1	43.7	47.0	15.7
200	1,379	1.1	48.1	14.7	71.5	71.5	68.7	43.1	46.8	14.9
260	1,793	0.82	64.1	19.5			67.6	42.6	45.5	14.4
350	2,413	0.61	83.4	25.4			53.0	42.3	43.3	13.7
430	2,965	0.50	112	34.1			46.1	42.0	41.3	13.0
550	3,792	0.39	138	42.1			41.8	41.8	38.4	12.4
725	4,999	0.30	176	53.6					32.9	11.5
925	6,378	0.23	232	70.7					28.3	10.6
1200	8,274	0.18	297	90.5					24.5	9.8
1550	10,687	0.14	385	117.3					21.0	9.6
2000	13,790	0.11	497	151.5					17.8	9.1
2600	17,926	0.08	641	195.4					15.1	8.5
3350	23,097	0.06	834	254.2					12.9	8.0
4300	29,647	0.05	1074	327.4					10.9	7.5
5550	38,266	0.04	1378	420.0					9.4	7.2
7200	49,642	0.03	1779	542.2					8.1	6.7
9300	64,121	0.02	2308	703.5					6.9	6.3
			2981	908.6					5.8	5.8



Appendix 4

US DOE #DE-FC26-05NT42660 Final Scientific/Technical Report

Alan P. Byrnes, Robert M. Cluff and John C. Webb

Mercury Injection Drainage-Imbibition Capillary Pressure Analysis

FOREST OIL CORP: 65-1-7 ARCH UNIT - S276 - 4743 ft (B)

In situ Klinkenberg Permeability (μm^2) =

5.77E-04

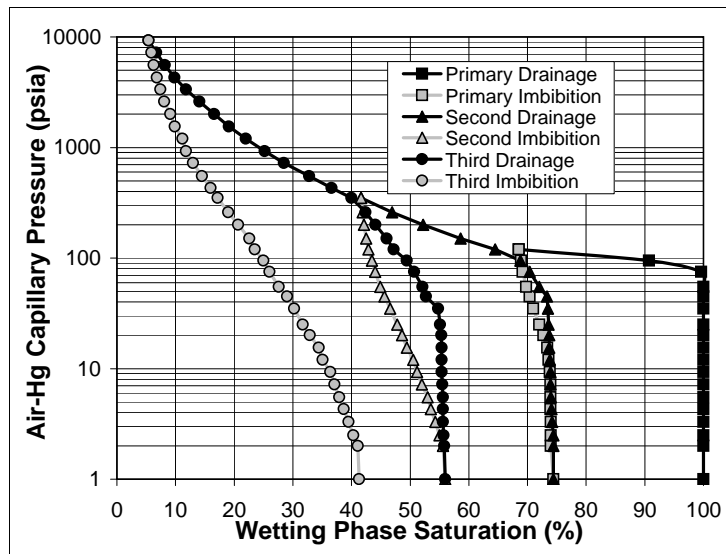
In situ Klinkenberg Permeability (mD) =

0.5850

Routine Porosity (%) =

14.7

Mercury Injection Capillary Pressure (psia)	Mercury Injection Capillary Pressure (kPa)	Approx. Pore Entry Diameter (μm)	Approx. Gas-Water Height Above Free Water Level (ft)	Approx. Gas-Water Height Above Free Water Level (m)	Drainage 1 Cumulative Wetting Phase Saturation (% pore vol)	Imbibition 1 Cumulative Wetting Phase Saturation (% pore vol)	Drainage 2 Cumulative Wetting Phase Saturation (% pore vol)	Imbibition 2 Cumulative Wetting Phase Saturation (% pore vol)	Drainage 3 Cumulative Wetting Phase Saturation (% pore vol)	Imbibition 3 Cumulative Wetting Phase Saturation (% pore vol)
2.0	13.8	107	0.10	0.03	100.0	74.4	74.4	56.0	56.0	41.3
2.5	17.2	86	0.64	0.20	100.0	74.0	74.4	55.6	55.8	41.1
3.3	22.8	65	0.80	0.24	100.0	74.0	74.4	55.0	55.7	40.3
4.3	29.6	50	1.06	0.32	100.0	74.0	74.2	54.3	55.6	39.5
5.5	37.9	39	1.38	0.42	100.0	73.9	74.1	53.5	55.6	38.7
7.2	49.6	30	1.76	0.54	100.0	73.9	74.0	53.0	55.6	37.9
9.3	64.1	23	2.31	0.70	100.0	73.9	73.9	52.0	55.5	37.1
12.0	82.7	18	2.98	0.91	100.0	73.8	73.9	51.2	55.4	36.4
15.5	106.9	14	3.85	1.17	100.0	73.6	73.8	50.5	55.4	35.1
20	137.9	11	4.97	1.51	100.0	73.4	73.7	49.4	55.4	34.4
25	172.4	8.6	6.41	2.0	100.0	72.7	73.7	48.6	55.3	32.9
35	241.3	6.1	8.01	2.4	100.0	72.0	73.6	47.8	55.1	31.7
45	310.3	4.8	11.2	3.4	100.0	71.0	73.5	46.6	54.8	30.2
55	379.2	3.9	14.4	4.4	100.0	70.4	73.3	45.6	52.7	29.0
75	517.1	2.9	17.6	5.4	100.0	69.8	72.0	44.9	52.1	27.6
95	655.0	2.3	24.0	7.3	99.6	69.2	70.4	44.0	50.7	26.0
120	827.4	1.8	30.5	9.3	90.7	68.9	68.8	43.5	49.4	25.0
150	1,034	1.4	38.5	11.7	68.5	68.5	64.5	42.9	47.2	23.5
200	1,379	1.1	48.1	14.7			58.6	42.5	46.0	22.6
260	1,793	0.82	64.1	19.5			52.2	42.1	44.1	20.7
350	2,413	0.61	83.4	25.4			46.9	41.9	42.4	19.0
430	2,965	0.50	112	34.1			41.6	41.6	40.0	17.2
550	3,792	0.39	138	42.1					40.0	16.0
725	4,999	0.30	176	53.6					32.8	14.5
925	6,378	0.23	232	70.7					28.5	13.0
1200	8,274	0.18	297	90.5					25.2	11.8
1550	10,687	0.14	385	117.3					22.0	11.2
2000	13,790	0.11	497	151.5					19.1	9.9
2600	17,926	0.08	641	195.4					16.6	9.1
3350	23,097	0.06	834	254.2					14.1	8.1
4300	29,647	0.05	1074	327.4					11.8	7.4
5550	38,266	0.04	1378	420.0					9.8	6.8
7200	49,642	0.03	1779	542.2					8.2	6.3
9300	64,121	0.02	2308	703.5					6.7	5.9
			2981	908.6					5.4	5.4



Appendix 4

US DOE #DE-FC26-05NT42660 Final Scientific/Technical Report

Alan P. Byrnes, Robert M. Cluff and John C. Webb

Mercury Injection Drainage-Imbibition Capillary Pressure Analysis

FOREST OIL CORP: 65-1-7 ARCH UNIT - S276 - 4745 ft (B)

In situ Klinkenberg Permeability (μm^2) =

3.88E-04

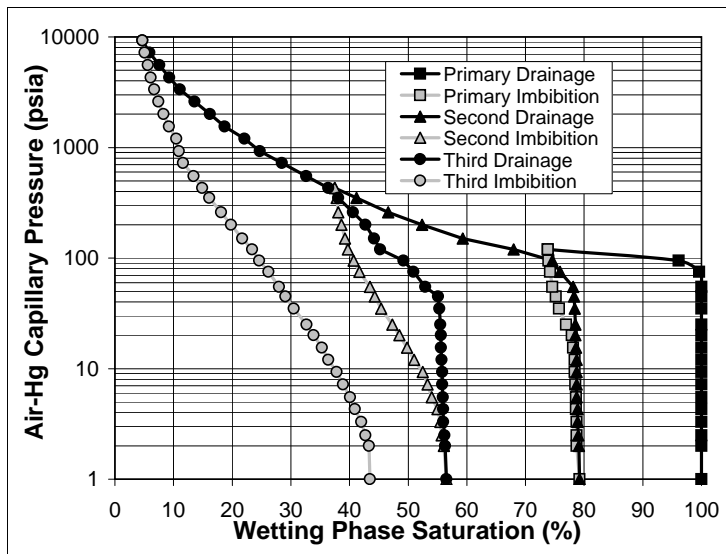
In situ Klinkenberg Permeability (mD) =

0.3930

Routine Porosity (%) =

14.6

Mercury Injection Capillary Pressure (psia)	Mercury Injection Capillary Pressure (kPa)	Approx. Pore Entry Diameter (μm)	Approx. Gas-Water Height Above Free Water Level (ft)	Approx. Gas-Water Height Above Free Water Level (m)	Drainage 1 Cumulative Wetting Phase Saturation (% pore vol)	Imbibition 1 Cumulative Wetting Phase Saturation (% pore vol)	Drainage 2 Cumulative Wetting Phase Saturation (% pore vol)	Imbibition 2 Cumulative Wetting Phase Saturation (% pore vol)	Drainage 3 Cumulative Wetting Phase Saturation (% pore vol)	Imbibition 3 Cumulative Wetting Phase Saturation (% pore vol)
2.0	13.8	107	0.10	0.03	100.0	79.2	79.2	56.5	56.5	43.5
2.5	17.2	86	0.64	0.20	100.0	78.7	79.1	56.1	56.3	43.3
3.3	22.8	65	0.80	0.24	100.0	78.7	79.0	55.7	56.2	42.7
4.3	29.6	50	1.06	0.32	100.0	78.7	78.9	55.5	56.0	42.0
5.5	37.9	39	1.38	0.42	100.0	78.6	78.9	55.0	56.0	40.9
7.2	49.6	30	1.76	0.54	100.0	78.6	78.7	54.0	55.9	40.1
9.3	64.1	23	2.31	0.70	100.0	78.5	78.7	53.3	55.8	38.9
12.0	82.7	18	2.98	0.91	100.0	78.4	78.7	52.5	55.8	37.8
15.5	106.9	14	3.85	1.17	100.0	78.4	78.7	51.0	55.7	36.4
20	137.9	11	4.97	1.51	100.0	78.1	78.6	49.8	55.6	35.3
25	172.4	8.6	6.41	2.0	100.0	77.9	78.5	48.5	55.6	33.9
35	241.3	6.1	8.01	2.4	100.0	76.9	78.5	47.3	55.5	32.7
45	310.3	4.8	11.2	3.4	100.0	75.7	78.4	45.4	55.3	30.5
55	379.2	3.9	14.4	4.4	100.0	75.2	78.3	44.3	55.1	29.1
75	517.1	2.9	17.6	5.4	100.0	74.6	78.1	43.5	52.9	28.0
95	655.0	2.3	24.0	7.3	99.6	74.2	75.9	41.7	50.9	26.2
120	827.4	1.8	30.5	9.3	96.1	73.9	74.6	40.7	49.2	24.6
150	1,034	1.4	38.5	11.7	73.8	73.8	68.0	39.7	45.2	23.4
200	1,379	1.1	48.1	14.7			59.3	39.2	44.2	21.7
260	1,793	0.82	64.1	19.5			52.4	38.6	42.7	19.8
350	2,413	0.61	83.4	25.4			46.6	38.1	40.6	18.1
430	2,965	0.50	112	34.1			41.2	37.8	38.1	16.1
550	3,792	0.39	138	42.1			37.5	37.5	36.4	14.9
725	4,999	0.30	176	53.6					32.6	13.4
925	6,378	0.23	232	70.7					28.5	11.6
1200	8,274	0.18	297	90.5					24.7	10.9
1550	10,687	0.14	385	117.3					22.1	10.5
2000	13,790	0.11	497	151.5					18.7	9.2
2600	17,926	0.08	641	195.4					16.2	8.3
3350	23,097	0.06	834	254.2					13.6	7.4
4300	29,647	0.05	1074	327.4					11.1	6.7
5550	38,266	0.04	1378	420.0					9.3	6.1
7200	49,642	0.03	1779	542.2					7.6	5.6
9300	64,121	0.02	2308	703.5					5.9	5.1
			2981	908.6					4.7	4.7



Appendix 4

US DOE #DE-FC26-05NT42660 Final Scientific/Technical Report

Alan P. Byrnes, Robert M. Cluff and John C. Webb

Mercury Injection Drainage-Imbibition Capillary Pressure Analysis

FOREST OIL CORP: 65-1-7 ARCH UNIT - S276 - 4757.9 ft (B)

In situ Klinkenberg Permeability (μm^2) =

3.65E-05

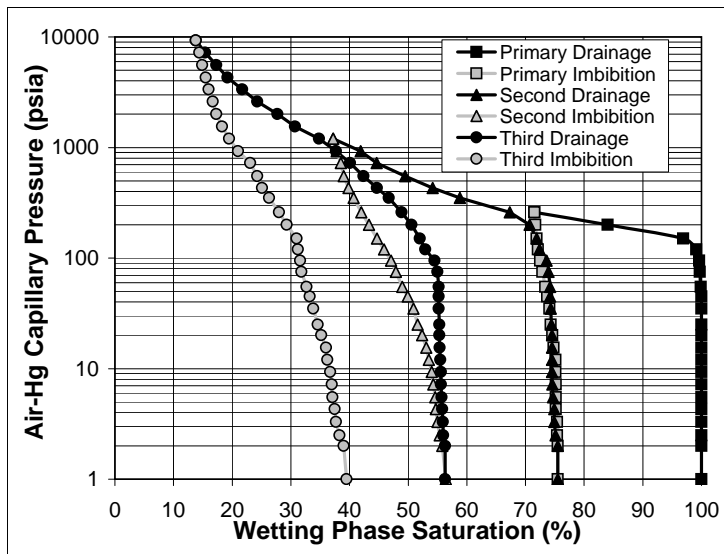
In situ Klinkenberg Permeability (mD) =

0.0370

Routine Porosity (%) =

11.1

Mercury Injection Capillary Pressure (psia)	Mercury Injection Capillary Pressure (kPa)	Approx. Pore Entry Diameter (μm)	Approx. Gas-Water Height Above Free Water Level (ft)	Approx. Gas-Water Height Above Free Water Level (m)	Drainage 1 Cumulative Wetting Phase Saturation (% pore vol)	Imbibition 1 Cumulative Wetting Phase Saturation (% pore vol)	Drainage 2 Cumulative Wetting Phase Saturation (% pore vol)	Imbibition 2 Cumulative Wetting Phase Saturation (% pore vol)	Drainage 3 Cumulative Wetting Phase Saturation (% pore vol)	Imbibition 3 Cumulative Wetting Phase Saturation (% pore vol)
2.0	13.8	107	0.10	0.03	100.0	75.5	75.5	56.4	56.3	39.5
2.5	17.2	86	0.64	0.20	100.0	75.5	75.5	55.8	56.3	39.0
3.3	22.8	65	0.80	0.24	100.0	75.4	75.1	55.4	56.0	38.3
4.3	29.6	50	1.06	0.32	100.0	75.2	74.9	55.0	55.9	37.7
5.5	37.9	39	1.38	0.42	100.0	75.2	74.9	54.7	55.8	37.5
7.2	49.6	30	1.76	0.54	100.0	75.2	74.7	54.6	55.7	37.1
9.3	64.1	23	2.31	0.70	100.0	75.2	74.6	54.3	55.6	37.0
12.0	82.7	18	2.98	0.91	100.0	75.1	74.5	54.0	55.6	36.7
15.5	106.9	14	3.85	1.17	100.0	75.1	74.5	53.5	55.5	36.2
20	137.9	11	4.97	1.51	100.0	74.8	74.5	53.1	55.4	36.0
25	172.4	8.6	6.41	2.0	100.0	74.6	74.5	52.4	55.3	35.2
35	241.3	6.1	8.01	2.4	100.0	74.3	74.4	51.6	55.3	34.6
45	310.3	4.8	11.2	3.4	100.0	74.1	74.3	50.9	55.2	33.8
55	379.2	3.9	14.4	4.4	100.0	73.7	74.2	49.9	55.2	33.2
75	517.1	2.9	17.6	5.4	99.9	73.4	74.2	49.0	55.2	32.7
95	655.0	2.3	24.0	7.3	99.7	72.9	73.9	47.9	55.0	31.8
120	827.4	1.8	30.5	9.3	99.6	72.5	73.6	47.1	54.5	31.6
150	1,034	1.4	38.5	11.7	99.1	72.1	72.4	45.9	52.9	31.2
200	1,379	1.1	48.1	14.7	96.9	71.9	71.9	44.7	52.0	31.0
260	1,793	0.82	64.1	19.5	84.0	71.7	70.7	43.3	50.6	29.3
350	2,413	0.61	83.4	25.4	71.5	71.5	67.3	42.0	48.9	28.0
430	2,965	0.50	112	34.1			58.8	40.7	46.7	26.3
550	3,792	0.39	138	42.1			54.2	39.8	44.7	25.1
725	4,999	0.30	176	53.6			49.5	39.0	42.4	24.3
925	6,378	0.23	232	70.7			44.6	38.5	40.1	23.1
1200	8,274	0.18	297	90.5			41.9	37.8	37.7	21.0
1550	10,687	0.14	385	117.3			37.2	37.2	34.8	19.5
2000	13,790	0.11	497	151.5					30.7	18.3
2600	17,926	0.08	641	195.4					27.7	17.3
3350	23,097	0.06	834	254.2					24.3	16.7
4300	29,647	0.05	1074	327.4					21.7	16.0
5550	38,266	0.04	1378	420.0					19.2	15.5
7200	49,642	0.03	1779	542.2					17.3	14.9
9300	64,121	0.02	2308	703.5					15.4	14.4
			2981	908.6					13.8	13.8



Appendix 4

US DOE #DE-FC26-05NT42660 Final Scientific/Technical Report

Alan P. Byrnes, Robert M. Cluff and John C. Webb

Mercury Injection Drainage-Imbibition Capillary Pressure Analysis

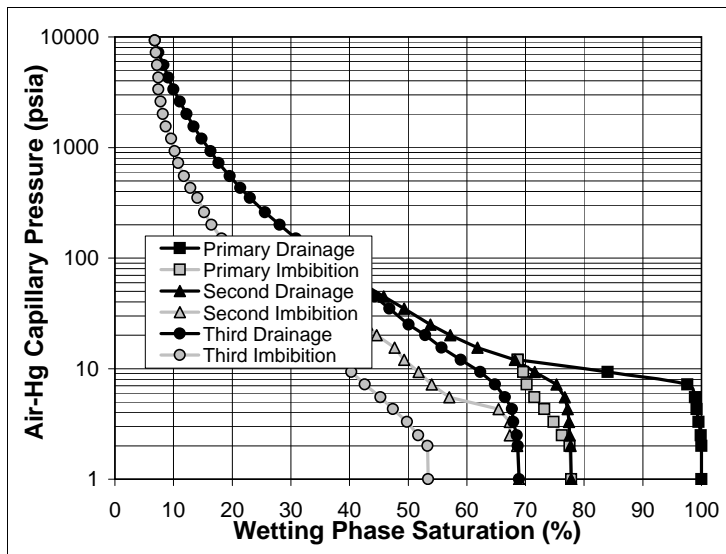
ANADARKO E&P CO. LP: ARCH UNIT UPRR #102-7-10 - S265 - 4899 ft (D)

In situ Klinkenberg Permeability (μm^2) = 5.65E-02

In situ Klinkenberg Permeability (mD) = 57.3000

Routine Porosity (%) = 21.6

Mercury Injection Capillary Pressure (psia)	Mercury Injection Capillary Pressure (kPa)	Approx. Pore Entry Diameter (μm)	Approx. Gas-Water Height Above Free Water Level (ft)	Approx. Gas-Water Height Above Free Water Level (m)	Drainage 1 Cumulative Wetting Phase Saturation (% pore vol)	Imbibition 1 Cumulative Wetting Phase Saturation (% pore vol)	Drainage 2 Cumulative Wetting Phase Saturation (% pore vol)	Imbibition 2 Cumulative Wetting Phase Saturation (% pore vol)	Drainage 3 Cumulative Wetting Phase Saturation (% pore vol)	Imbibition 3 Cumulative Wetting Phase Saturation (% pore vol)
2.0	13.8	107	0.10	0.03	100.0	77.8	77.8	68.9	68.9	53.4
2.5	17.2	86	0.64	0.20	100.0	77.5	77.5	68.6	68.7	53.3
3.3	22.8	65	0.80	0.24	99.9	76.2	77.5	67.3	68.5	51.7
4.3	29.6	50	1.06	0.32	99.5	74.8	77.4	67.3	67.9	49.8
5.5	37.9	39	1.38	0.42	99.2	73.2	77.2	65.4	67.7	47.4
7.2	49.6	30	1.76	0.54	98.9	71.5	76.7	57.0	66.5	45.3
9.3	64.1	23	2.31	0.70	97.6	70.2	75.3	54.0	64.8	42.6
12.0	82.7	18	2.98	0.91	84.0	69.6	71.6	51.8	62.3	40.3
15.5	106.9	14	3.85	1.17	68.7	68.7	68.2	49.3	59.0	38.5
20	137.9	11	4.97	1.51			61.8	47.7	55.7	37.3
25	172.4	8.6	6.41	2.0			57.2	44.6	52.9	34.2
35	241.3	6.1	8.01	2.4			53.8	43.0	50.1	32.2
45	310.3	4.8	11.2	3.4			49.3	40.1	46.8	28.5
55	379.2	3.9	14.4	4.4			45.8	38.3	44.3	26.4
75	517.1	2.9	17.6	5.4			43.1	37.2	42.3	24.7
95	655.0	2.3	24.0	7.3			38.9	36.0	39.3	22.1
120	827.4	1.8	30.5	9.3			35.8	35.8	37.0	20.6
150	1,034	1.4	38.5	11.7					33.0	19.7
200	1,379	1.1	48.1	14.7					30.9	18.2
260	1,793	0.82	64.1	19.5					28.1	16.5
350	2,413	0.61	83.4	25.4					25.6	15.2
430	2,965	0.50	112	34.1					23.0	14.1
550	3,792	0.39	138	42.1					21.4	12.9
725	4,999	0.30	176	53.6					19.6	11.8
925	6,378	0.23	232	70.7					17.7	10.8
1200	8,274	0.18	297	90.5					16.3	10.2
1550	10,687	0.14	385	117.3					14.8	9.6
2000	13,790	0.11	497	151.5					13.4	8.7
2600	17,926	0.08	641	195.4					12.2	8.2
3350	23,097	0.06	834	254.2					11.1	7.8
4300	29,647	0.05	1074	327.4					10.0	7.4
5550	38,266	0.04	1378	420.0					9.1	7.4
7200	49,642	0.03	1779	542.2					8.3	7.2
9300	64,121	0.02	2308	703.5					7.4	7.0
			2981	908.6					6.8	6.8



Appendix 4

US DOE #DE-FC26-05NT42660 Final Scientific/Technical Report

Alan P. Byrnes, Robert M. Cluff and John C. Webb

Mercury Injection Drainage-Imbibition Capillary Pressure Analysis

CELSIUS: DRIPPING ROCK #5 - DR5 - 12686.5 ft

In situ Klinkenberg Permeability (μm^2) =

1.19E-05

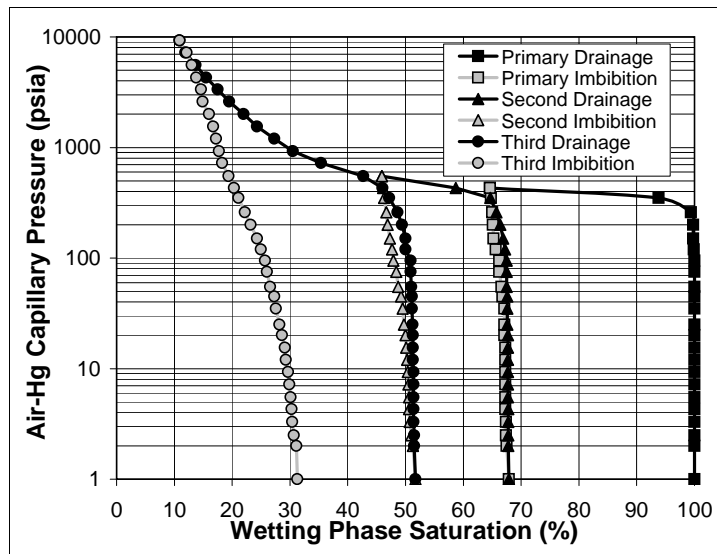
In situ Klinkenberg Permeability (mD) =

0.0121

Routine Porosity (%) =

12.5

Mercury Injection Capillary Pressure (psia)	Mercury Injection Capillary Pressure (kPa)	Approx. Pore Entry Diameter (μm)	Approx. Gas-Water Height Above Free Water Level (ft)	Approx. Gas-Water Height Above Free Water Level (m)	Drainage 1 Cumulative Wetting Phase Saturation (% pore vol)	Imbibition 1 Cumulative Wetting Phase Saturation (% pore vol)	Drainage 2 Cumulative Wetting Phase Saturation (% pore vol)	Imbibition 2 Cumulative Wetting Phase Saturation (% pore vol)	Drainage 3 Cumulative Wetting Phase Saturation (% pore vol)	Imbibition 3 Cumulative Wetting Phase Saturation (% pore vol)
2.0	13.8	107	0.10	0.03	100.0	67.9	67.9	51.7	51.7	31.3
2.5	17.2	86	0.64	0.20	100.0	67.5	67.8	51.3	51.5	31.1
3.3	22.8	65	0.80	0.24	100.0	67.4	67.8	51.0	51.5	30.7
4.3	29.6	50	1.06	0.32	100.0	67.3	67.8	50.7	51.4	30.4
5.5	37.9	39	1.38	0.42	100.0	67.3	67.7	50.6	51.4	30.3
7.2	49.6	30	1.76	0.54	100.0	67.3	67.7	50.6	51.4	30.1
9.3	64.1	23	2.31	0.70	100.0	67.3	67.7	50.5	51.4	29.9
12.0	82.7	18	2.98	0.91	100.0	67.3	67.7	50.4	51.4	29.7
15.5	106.9	14	3.85	1.17	100.0	67.3	67.7	50.3	51.3	29.3
20	137.9	11	4.97	1.51	100.0	67.3	67.7	50.1	51.3	29.1
25	172.4	8.6	6.41	2.0	100.0	67.1	67.7	50.0	51.3	28.6
35	241.3	6.1	8.01	2.4	100.0	67.1	67.6	49.7	51.2	28.2
45	310.3	4.8	11.2	3.4	100.0	67.1	67.6	49.5	51.1	27.6
55	379.2	3.9	14.4	4.4	100.0	66.8	67.6	49.2	51.1	27.3
75	517.1	2.9	17.6	5.4	100.0	66.6	67.5	48.7	51.0	26.6
95	655.0	2.3	24.0	7.3	100.0	66.2	67.5	48.4	50.9	26.0
120	827.4	1.8	30.5	9.3	100.0	66.2	67.5	47.9	50.9	25.7
150	1,034	1.4	38.5	11.7	99.9	65.6	67.2	47.7	50.0	25.0
200	1,379	1.1	48.1	14.7	99.8	65.2	66.9	47.3	50.0	24.3
260	1,793	0.82	64.1	19.5	99.8	65.1	66.4	46.9	49.4	23.2
350	2,413	0.61	83.4	25.4	99.4	65.0	65.7	46.7	48.6	22.2
430	2,965	0.50	112	34.1	93.8	64.8	64.7	46.3	47.2	21.1
550	3,792	0.39	138	42.1	64.6	64.6	58.7	46.1	46.0	20.3
725	4,999	0.30	176	53.6			45.9	45.9	42.7	19.4
925	6,378	0.23	232	70.7					35.4	18.3
1200	8,274	0.18	297	90.5					30.5	17.7
1550	10,687	0.14	385	117.3					27.3	17.2
2000	13,790	0.11	497	151.5					24.3	16.7
2600	17,926	0.08	641	195.4					22.0	16.0
3350	23,097	0.06	834	254.2					19.5	14.9
4300	29,647	0.05	1074	327.4					17.5	14.6
5550	38,266	0.04	1378	420.0					15.5	13.8
7200	49,642	0.03	1779	542.2					13.7	13.0
9300	64,121	0.02	2308	703.5					11.9	12.1
			2981	908.6					10.9	10.9



Mercury Injection Drainage-Imbibition Capillary Pressure Analysis

CER CORPORATION: MWX-2 SUPERIOR - T649 - 6554.3 ft (A2)

In situ Klinkenberg Permeability (μm^2) =

6.65E-03

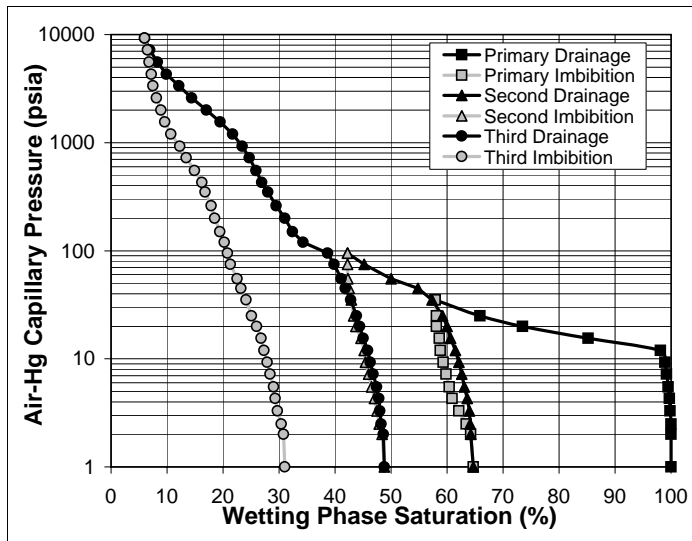
In situ Klinkenberg Permeability (mD) =

6.7400

Routine Porosity (%) =

12.3

Mercury Injection Capillary Pressure (psia)	Mercury Injection Capillary Pressure (kPa)	Approx. Pore Entry Diameter (μm)	Approx. Gas-Water Height Above Free Water Level (ft)	Approx. Gas-Water Height Above Free Water Level (m)	Drainage 1 Cumulative Wetting Phase Saturation (% pore vol)	Imbibition 1 Cumulative Wetting Phase Saturation (% pore vol)	Drainage 2 Cumulative Wetting Phase Saturation (% pore vol)	Imbibition 2 Cumulative Wetting Phase Saturation (% pore vol)	Drainage 3 Cumulative Wetting Phase Saturation (% pore vol)	Imbibition 3 Cumulative Wetting Phase Saturation (% pore vol)
2.0	13.8	107	0.10	0.03	100.0	64.7	64.7	48.8	48.8	31.0
2.5	17.2	86	0.64	0.20	100.0	64.2	64.2	48.4	48.6	30.8
3.3	22.8	65	0.80	0.24	100.0	63.4	64.1	47.9	48.2	30.4
4.3	29.6	50	1.06	0.32	99.8	62.1	64.0	47.5	48.0	29.7
5.5	37.9	39	1.38	0.42	99.7	60.9	63.6	47.0	47.8	29.3
7.2	49.6	30	1.76	0.54	99.5	60.4	63.1	46.5	47.4	29.0
9.3	64.1	23	2.31	0.70	99.2	59.8	62.6	46.0	46.8	28.4
12.0	82.7	18	2.98	0.91	98.9	59.3	62.1	45.4	46.3	27.9
15.5	106.9	14	3.85	1.17	98.1	58.8	61.5	45.2	45.8	27.3
20	137.9	11	4.97	1.51	85.2	58.6	60.6	44.6	45.0	26.8
25	172.4	8.6	6.41	2.0	73.5	58.1	60.0	43.7	44.4	26.0
35	241.3	6.1	8.01	2.4	65.9	58.1	59.2	43.3	43.8	25.1
45	310.3	4.8	11.2	3.4	57.9	57.9	57.3	42.9	42.8	24.1
55	379.2	3.9	14.4	4.4			54.8	42.5	41.8	23.2
75	517.1	2.9	17.6	5.4			50.0	42.3	41.1	22.5
95	655.0	2.3	24.0	7.3			45.2	42.2	39.8	21.3
120	827.4	1.8	30.5	9.3			42.2	42.2	38.7	20.8
150	1,034	1.4	38.5	11.7					34.3	20.2
200	1,379	1.1	48.1	14.7					32.4	19.4
260	1,793	0.82	64.1	19.5					31.0	18.5
350	2,413	0.61	83.4	25.4					29.5	17.9
430	2,965	0.50	112	34.1					28.0	16.8
550	3,792	0.39	138	42.1					26.9	16.2
725	4,999	0.30	176	53.6					25.9	14.9
925	6,378	0.23	232	70.7					24.7	13.4
1200	8,274	0.18	297	90.5					23.4	12.3
1550	10,687	0.14	385	117.3					21.7	10.7
2000	13,790	0.11	497	151.5					19.5	9.6
2600	17,926	0.08	641	195.4					17.0	8.9
3350	23,097	0.06	834	254.2					14.4	8.1
4300	29,647	0.05	1074	327.4					12.1	7.5
5550	38,266	0.04	1378	420.0					9.9	7.2
7200	49,642	0.03	1779	542.2					8.3	6.8
9300	64,121	0.02	2308	703.5					6.9	6.5
			2981	908.6					6.0	6.0



Appendix 5
Summary Multisalinity Archie Porosity Exponent Data
Analysis of Critical Permeability, Capillary Pressure and Electrical Properties for Mesaverde Tight Gas Sandstones from Western U.S. Basins
US DOE # DE-FC26-05NT42660 Final Scientific/Technical Report
Alan P. Byrnes, Robert M. Cluff, John C. Webb
website: <http://www.kgs.ku.edu/mesaverde>

USGS Library Number	Basin	API Number	Well Name	Operator	Depth ft	A/B/C	Rock Type Code	Routine Porosity %	Est. In situ Porosity %	Klinkenberg Gas Permeability mD	20K ppm brine salinity			40K ppm brine salinity			80K ppm brine salinity			200K ppm brine salinity		
											brine salinity (Kppm) > 20			40			80			200		
											Cw (rhos) > 0.302			5.73			10.50			20.4		
											Rw (ohmm) > 0.331			0.17452			0.09524			0.049		
Formation Resistivity Factor	Co	Archie Porosity Exponent m, As=1	Formation Resistivity Factor	Co	Archie Porosity Exponent m, As=1	Formation Resistivity Factor	Co	Archie Porosity Exponent m, As=1	Formation Resistivity Factor	Co	Archie Porosity Exponent m, As=1	Formation Resistivity Factor	Co	Archie Porosity Exponent m, As=1								
R091	Piceance	05045XXXX4	BOOK CLIFFS 1	USGS-CG	213.0	A	1223	6.4	4.9	0.000225	12.90	0.0617	1.50	92.9	0.0775	1.57	14.8	0.7078	1.86	83.6	0.2441	1.61
R091	Piceance	05045XXXX4	BOOK CLIFFS 1	USGS-CG	242.4	A	13219	6.7	6.4	0.000164	67.3	0.0449	1.40	74.0	0.0775	1.57	14.8	0.7078	1.86	83.6	0.2441	1.61
R091	Piceance	05045XXXX4	BOOK CLIFFS 1	USGS-CG	255.8	A	15567	24.9	23.4	0.000082	112	0.0501	1.78	72.8	0.0787	1.86	77.3	0.1358	1.89	75.3	0.2710	1.56
R091	Piceance	05045XXXX4	BOOK CLIFFS 1	USGS-CG	256.5	A	13258	11.0	10.0	0.000082	60.3	0.0501	1.78	72.8	0.0787	1.86	77.3	0.1358	1.89	75.3	0.2710	1.56
R091	Piceance	05045XXXX4	BOOK CLIFFS 1	USGS-CG	257.3	A	11219	6.9	6.3	0.000167	14.1	0.2150	1.82	74.0	0.0775	1.57	14.8	0.7078	1.86	83.6	0.2441	1.61
R091	Piceance	05045XXXX4	BOOK CLIFFS 1	USGS-CG	307.3	A	12219	9.6	8.8	0.000096	67.3	0.0449	1.40	74.0	0.0775	1.57	14.8	0.7078	1.86	83.6	0.2441	1.61
R091	Piceance	05045XXXX4	BOOK CLIFFS 1	USGS-CG	512.2	A	12236	10.6	9.8	0.000094	67.3	0.0449	1.40	74.0	0.0775	1.57	14.8	0.7078	1.86	83.6	0.2441	1.61
S905	Piceance	05103XXXX3	2101-1-5 MOON LAKE	WESTERN FUELS ASSOC	788.0	A	12225	1.9	1.6	0.000067	22.6	0.1337	1.79	21.8	0.2630	1.77	22.8	0.4607	1.78	21.9	0.9319	1.75
S905	Piceance	05103XXXX3	2101-1-5 MOON LAKE	WESTERN FUELS ASSOC	790.3	A	12239	5.0	4.5	0.000209	32.9	0.0918	1.77	38.4	0.1491	1.59	52.4	0.2003	1.65	58.8	0.3471	1.70
S905	Piceance	05103XXXX3	2101-1-5 MOON LAKE	WESTERN FUELS ASSOC	812.6	B	13236	18.4	17.5	0.000172	115.8	0.0261	1.67	128.1	0.0447	1.91	177.5	0.0591	1.91	255.2	0.0800	1.97
S905	Piceance	05103XXXX3	2101-1-5 MOON LAKE	WESTERN FUELS ASSOC	812.7	A	13276	18.1	17.2	0.000172	115.8	0.0261	1.67	128.1	0.0447	1.91	177.5	0.0591	1.91	255.2	0.0800	1.97
S905	Piceance	05103XXXX3	2101-1-5 MOON LAKE	WESTERN FUELS ASSOC	812.9	A	14577	17.0	15.8	0.000172	115.8	0.0261	1.67	128.1	0.0447	1.91	177.5	0.0591	1.91	255.2	0.0800	1.97
S905	Piceance	05103XXXX3	2101-1-5 MOON LAKE	WESTERN FUELS ASSOC	816.5	A	12239	10.6	9.1	0.000205	32.9	0.0918	1.77	38.4	0.1491	1.59	52.4	0.2003	1.65	58.8	0.3471	1.70
S905	Piceance	05103XXXX3	2101-1-5 MOON LAKE	WESTERN FUELS ASSOC	817.6	B	11239	2.7	1.3	0.000441	32.9	0.0918	1.77	38.4	0.1491	1.59	52.4	0.2003	1.65	58.8	0.3471	1.70
S905	Piceance	05103XXXX3	2101-1-5 MOON LAKE	WESTERN FUELS ASSOC	817.8	A	11239	8.7	7.7	0.000118	32.9	0.0918	1.77	38.4	0.1491	1.59	52.4	0.2003	1.65	58.8	0.3471	1.70
T63X2G	Piceance	0510310391	T63X-2G	EXXON-MOBIL	10556.8	B	15286	7.1	6.8	0.000155	108.6	0.0278	1.74	138.7	0.0413	1.83	215.3	0.0488	1.89	367.1	0.0556	1.43
T63X2G	Piceance	0510310391	T63X-2G	EXXON-MOBIL	10572.9	B	15265	4.3	4.1	0.000244	108.6	0.0278	1.74	138.7	0.0413	1.83	215.3	0.0488	1.89	367.1	0.0556	1.43
T63X2G	Piceance	0510310391	T63X-2G	EXXON-MOBIL	10615.6	B	15225	6.1	5.8	0.000176	115.8	0.0261	1.67	124.6	0.0234	1.94	176.5	0.0595	1.93	227.7	0.8960	1.69
T63X2G	Piceance	0510310391	T63X-2G	EXXON-MOBIL	10615.6	B	15225	6.3	5.9	0.000178	115.8	0.0261	1.67	124.6	0.0234	1.94	176.5	0.0595	1.93	227.7	0.8960	1.69
T63X2G	Piceance	0510310391	T63X-2G	EXXON-MOBIL	10619.7	A	15276	7.3	6.8	0.000247	108.6	0.0278	1.74	138.7	0.0413	1.83	215.3	0.0488	1.89	367.1	0.0556	1.43
T63X2G	Piceance	0510310391	T63X-2G	EXXON-MOBIL	10636.3	A	13265	2.5	2.4	0.000038	108.6	0.0278	1.74	138.7	0.0413	1.83	215.3	0.0488	1.89	367.1	0.0556	1.43
T649	Piceance	0504560011	MWX-2	CER CORPORATION	4885.4	B	4939	4.3	4.1	0.000427	131.6	0.0230	1.52	181.0	0.0317	1.62	299.0	0.0351	1.78	367.1	0.0556	1.43
T649	Piceance	0504560011	MWX-2	CER CORPORATION	4945.1	B	5276	10.1	9.6	0.000750	64.8	0.0466	1.78	88.8	0.0645	1.91	112.3	0.0935	2.01	157.9	0.1292	2.00
T649	Piceance	0504560011	MWX-2	CER CORPORATION	5734.1	A	16276	8.7	8.0	0.00471	78.0	0.0388	1.61	128.1	0.0447	1.79	177.5	0.0591	1.91	255.2	0.0800	1.97
T649	Piceance	0504560011	MWX-2	CER CORPORATION	5737.3	A	16276	9.4	8.7	0.00220	78.0	0.0388	1.61	128.1	0.0447	1.79	177.5	0.0591	1.91	255.2	0.0800	1.97
T649	Piceance	0504560011	MWX-2	CER CORPORATION	5757.0	A	13225	0.8	0.6	0.000014	78.0	0.0388	1.61	128.1	0.0447	1.79	177.5	0.0591	1.91	255.2	0.0800	1.97
T649	Piceance	0504560011	MWX-2	CER CORPORATION	5836.8	B	7.1	6.7	0.000146	78.0	0.0388	1.61	128.1	0.0447	1.79	177.5	0.0591	1.91	255.2	0.0800	1.97	
T649	Piceance	0504560011	MWX-2	CER CORPORATION	5838.7	A	6.6	6.0	0.000146	78.0	0.0388	1.61	128.1	0.0447	1.79	177.5	0.0591	1.91	255.2	0.0800	1.97	
T649	Piceance	0504560011	MWX-2	CER CORPORATION	6536.3	A	8.2	7.8	0.000318	97.8	0.0309	1.61	136.5	0.0420	1.93	162.6	0.0647	1.99	190.0	0.1074	2.05	
T649	Piceance	0504560011	MWX-2	CER CORPORATION	6550.3	A	7.2	6.3	0.000870	97.8	0.0309	1.61	136.5	0.0420	1.93	162.6	0.0647	1.99	190.0	0.1074	2.05	
T649	Piceance	0504560011	MWX-2	CER CORPORATION	6554.3	B	6.3	5.8	0.000227	97.8	0.0309	1.61	136.5	0.0420	1.93	162.6	0.0647	1.99	190.0	0.1074	2.05	
T649	Piceance	0504560011	MWX-2	CER CORPORATION	7082.5	A	0.9	0.8	0.000024	97.8	0.0309	1.61	136.5	0.0420	1.93	162.6	0.0647	1.99	190.0	0.1074	2.05	
T649	Piceance	0504560011	MWX-2	CER CORPORATION	7124.7	A	11.1	10.2	0.000345	97.8	0.0309	1.61	136.5	0.0420	1.93	162.6	0.0647	1.99	190.0	0.1074	2.05	
T649	Piceance	0504560011	MWX-2	CER CORPORATION	7133.5	A	10.2	9.7	0.000670	97.8	0.0309	1.61	136.5	0.0420	1.93	162.6	0.0647	1.99	190.0	0.1074	2.05	
T649	Piceance	0504560011	MWX-2	CER CORPORATION	7136.8	A	6.9	6.1	0.000219	97.8	0.0309	1.61	136.5	0.0420	1.93	162.6	0.0647	1.99	190.0	0.1074	2.05	
T649	Piceance	0504560011	MWX-2	CER CORPORATION	7141.9	A	3.9	3.8	0.000065	97.8	0.0309	1.61	136.5	0.0420	1.93	162.6	0.0647	1.99	190.0	0.1074	2.05	
T649	Piceance	0504560011	MWX-2	CER CORPORATION	7218.7	B	3.6	3.3	0.000385	214.7	0.0141	1.57	279.5	0.0205	1.65	372.9	0.0282	1.73	527.4	0.0387	1.31	
T649	Piceance	0504560011	MWX-2	CER CORPORATION	7227.8	A	13285	8.9	8.2	0.000234	214.7	0.0141	1.57	279.5	0.0205	1.65	372.9	0.0282	1.73	527.4	0.0387	1.31
T649	Piceance	0504560011	MWX-2	CER CORPORATION	7276.5	A	15295	8.4	8.1	0.000173	214.7	0.0141	1.57	279.5	0.0205	1.65	372.9	0.0282	1.73	527.4	0.0387	1.31
T649	Piceance	0504560011	MWX-2	CER CORPORATION	7319.7	A	13257	5.7	5.4	0.000183	113.9	0.0265	1.81	129.7	0.0442	1.94	157.0	0.0669	2.01	154.1	0.1324	2.01
T649	Piceance	0504560011	MWX-2	CER CORPORATION	7340.4	A	15275	2.1	1.8	0.000106	113.9	0.0265	1.81	129.7	0.0442	1.94	157.0	0.0669	2.01	154.1	0.1324	2.01
T649	Piceance	0504560011	MWX-2	CER CORPORATION	7350.4	A	15265	4.5	4.0	0.000372	113.9	0.0265	1.81	129.7	0.0442	1.94	157.0	0.0669	2.01	154.1	0.1324	2.01
T649	Piceance	0504560011	MWX-2	CER CORPORATION	7381.3	A	3.8	3.7	0.000244	113.9	0.0265	1.81	129.7	0.0442	1.94	157.0	0.0669	2.01	154.1	0.1324	2.01	
T649	Piceance	0504560011	MWX-2	CER CORPORATION	7385.8	B	7.6	7.3	0.000595	113.9	0.0265	1.81	129.7	0.0442	1.94	157.0	0.0669	2.01	154.1	0.1324	2.01	
T649	Piceance	0504560011	MWX-2	CER CORPORATION	7877.5	A	7.6	7.4	0.000910	113.9	0.0265	1.81	129.7	0.0442	1.94	157.0	0.0669	2.01	154.1	0.1324	2.01	
T649	Piceance	0504560011	MWX-2	CER CORPORATION	7880.1	A	7.6	7.0	0.000179	113.9	0.0265	1.81	129.7	0.0442	1.94	157.0	0.0669	2.01	154.1	0.1324	2.01	
T649	Piceance	0504560011	MWX-2	CER CORPORATION	8117.9	A	6.5	5.9	0.000227	113												

Appendix 5
Summary Multisatinity Waxman-Smits Data
Analysis of Critical Permeability, Capillary Pressure and Electrical Properties for Mesaverde Tight Gas Sandstones from Western U.S. Basins
US DOE # DE-FC26-05NT42660 Final Scientific/Technical Report
Alan P. Byrnes, Robert M. Cluff, John C. Webb
website: <http://www.kgs.ku.edu/mesaverde>

USGS Library Number	Basin	API Number	Well Name	Operator	Depth ft	A/B/C	Rock Type Code	Routine Porosity %	Est. In situ Porosity %	In situ Klinkenberg Gas Permeability mD	20K ppm				F* 1/slope of Co vs Cw	Salinity-independent Archie cementation exponent m*	B _{max} Qv/F ² Co vs Cw	B _{max} Qv	Qv Approximate Caclon Exchange Capacity per unit PV B _{max} =3.83 (1/ohmm)(e/l)	Correlation Co vs Cw r ²				
											20K ppm		40K ppm								80K ppm		200K ppm	
											Co	Co	Co	Co							Co	Co	Co	Co
R091	Piceance	05045XXXX4	BOOK CLIFFS 1	USGS-CG	213.0	A	12293	6.4	4.9	0.000225	0.0449	0.0617		161.3	1.69	0.0262	4.23	1.10	1.00					
R091	Piceance	05045XXXX4	BOOK CLIFFS 1	USGS-CG	242.4	A	13219	6.7	6.4	0.000164		0.0775		88.1	1.63	0.0124	1.09	0.29	1.00					
R091	Piceance	05045XXXX4	BOOK CLIFFS 1	USGS-CG	255.8	A	15567	24.9	23.4	0.000112	0.2150	0.3922	0.7078	15.2	1.87	0.0154	0.23	0.06	1.00					
R091	Piceance	05045XXXX4	BOOK CLIFFS 1	USGS-CG	256.5	A	13258	11.0	10.0	0.000082	0.0501	0.0787	0.1358	86.8	1.94	0.0143	1.24	0.32	1.00					
R091	Piceance	05045XXXX4	BOOK CLIFFS 1	USGS-CG	257.3	A	11219	6.9	6.3	0.000167		0.2710												
R091	Piceance	05045XXXX4	BOOK CLIFFS 1	USGS-CG	387.3	A	12219	9.6	8.8	0.000095		0.3947												
R091	Piceance	05045XXXX4	BOOK CLIFFS 1	USGS-CG	512.2	A	12236	10.6	9.8	0.000904		0.3302												
S905	Piceance	05103XXXX3	21011-S MOON LAKE	WESTERN FUELS ASSOC	788.0	A	13225	1.9	1.6	0.000067		0.0556	0.0459	1020.6	1.68	0.0356	36.33	9.49	1.00					
S905	Piceance	05103XXXX3	21011-S MOON LAKE	WESTERN FUELS ASSOC	790.3	A	12239	5.0	4.5	0.000209		0.1288												
S905	Piceance	05103XXXX3	21011-S MOON LAKE	WESTERN FUELS ASSOC	812.6	B	13238	18.4	17.5	0.000117	0.1337	0.2630		21.0	1.75	0.0050	0.11	0.03	1.00					
S905	Piceance	05103XXXX3	21011-S MOON LAKE	WESTERN FUELS ASSOC	812.7	A	13276	18.1	17.2	0.000120		0.2569	0.4607	21.6	1.75	0.0050	0.11	0.03	1.00					
S905	Piceance	05103XXXX3	21011-S MOON LAKE	WESTERN FUELS ASSOC	812.9	A	14577	17.0	15.8	0.000129		0.8990												
S905	Piceance	05103XXXX3	21011-S MOON LAKE	WESTERN FUELS ASSOC	816.5	A	12239	10.6	9.1	0.000205		0.1142	0.2003	63.6	1.73	0.0286	1.82	0.48	1.00					
S905	Piceance	05103XXXX3	21011-S MOON LAKE	WESTERN FUELS ASSOC	817.6	B	11239	2.7	1.3	0.000441	0.0918	0.1491		47.3	0.89	0.0279	1.32	0.34	1.00					
S905	Piceance	05103XXXX3	21011-S MOON LAKE	WESTERN FUELS ASSOC	817.8	A	11239	8.7	7.7	0.000118		0.0958		62.6	1.61	0.0042	0.26	0.07	1.00					
T63X2G	Piceance	0510310391	T63X-2G	EXXON-MOBIL	10556.6	B	15286	7.1	6.8	0.00155	0.0278	0.0413		200.7	1.97	0.0128	2.57	0.67	1.00					
T63X2G	Piceance	0510310391	T63X-2G	EXXON-MOBIL	10572.9	B	15265	4.3	4.1	0.000214		0.0276												
T63X2G	Piceance	0510310391	T63X-2G	EXXON-MOBIL	10615.6	A	15225	6.1	5.8	0.00175	0.0261	0.0313	0.0488	321.8	2.03	0.0155	4.99	1.30	0.99					
T63X2G	Piceance	0510310391	T63X-2G	EXXON-MOBIL	10615.6	B	15225	6.3	5.9	0.00178		0.0234												
T63X2G	Piceance	0510310391	T63X-2G	EXXON-MOBIL	10619.7	A	15276	7.3	6.8	0.00247		0.0297	0.0595											
T63X2G	Piceance	0510310391	T63X-2G	EXXON-MOBIL	10636.3	A	13265	2.5	2.4	0.000308		0.0142												
T649	Piceance	0504560011	MWX-2	CER CORPORATION	4885.4	A	12239	4.3	4.1	0.000427	0.0230	0.0337		160.4	2.03	0.0202	13.34	3.48	0.92					
T649	Piceance	0504560011	MWX-2	CER CORPORATION	4939.8	A	9.0	8.6	0.000426	0.0462	0.0628	0.0351	163.3	2.08	0.0277	4.52	1.18	1.00						
T649	Piceance	0504560011	MWX-2	CER CORPORATION	4945.1	B	10.1	9.6	0.000750	0.0466	0.0645	0.0935	160.0	2.17	0.0281	4.50	1.17	1.00						
T649	Piceance	0504560011	MWX-2	CER CORPORATION	5734.1	A	16276	8.7	8.0	0.00471		0.1292												
T649	Piceance	0504560011	MWX-2	CER CORPORATION	5737.3	A	16276	9.4	8.7	0.00220		0.0637	0.1022	166.4	2.09	0.0332	5.53	1.44	0.99					
T649	Piceance	0504560011	MWX-2	CER CORPORATION	5757.0	A	13225	0.8	0.6	0.000014		0.0126												
T649	Piceance	0504560011	MWX-2	CER CORPORATION	5838.6	B	7.1	6.7	0.00160	0.0388	0.0447	0.0591	363.8	2.18	0.0299	10.88	2.84	1.00						
T649	Piceance	0504560011	MWX-2	CER CORPORATION	5838.7	A	6.6	6.0	0.00146		0.0146	0.0800												
T649	Piceance	0504560011	MWX-2	CER CORPORATION	6336.3	A	8.2	7.8	0.00318		0.0420	0.0647	1074	2.25	0.0172	3.88	1.01	1.00						
T649	Piceance	0504560011	MWX-2	CER CORPORATION	6550.3	A	7.2	6.3	0.000870	0.0431	0.0837	0.1314	171.3	1.86	0.0148	2.54	0.66	0.99						
T649	Piceance	0504560011	MWX-2	CER CORPORATION	6554.3	B	6.3	5.8	0.000227	0.0309	0.0493	0.0595	3125.3	1.97	0.0233	6.42	1.68	0.95						
T649	Piceance	0504560011	MWX-2	CER CORPORATION	7082.5	A	0.9	0.8	0.000024		0.0387		275.4	1.67	0.0322	10.51	26.24	1.00						
T649	Piceance	0504560011	MWX-2	CER CORPORATION	7124.7	A	11.1	10.2	0.000345		0.1564													
T649	Piceance	0504560011	MWX-2	CER CORPORATION	7133.5	A	10.2	9.7	0.00670		0.0656	0.0876	1412	1.92	0.0257	6.88	1.74	1.00						
T649	Piceance	0504560011	MWX-2	CER CORPORATION	7136.8	A	6.9	6.1	0.00219	0.0561	0.0924	0.1781	119.5	1.71	0.0067	0.80	0.21	1.00						
T649	Piceance	0504560011	MWX-2	CER CORPORATION	7141.9	A	3.9	3.8	0.000065	0.0410	0.0629	0.0629	669.9	1.99	0.0324	21.70	5.67	1.00						
T649	Piceance	0504560011	MWX-2	CER CORPORATION	7218.7	B	3.6	3.3	0.000385	0.0141	0.0205	0.0282	53.3	1.84	0.0090	4.85	1.27	0.99						
T649	Piceance	0504560011	MWX-2	CER CORPORATION	7272.8	A	13285	8.9	8.2	0.00234		0.1324												
T649	Piceance	0504560011	MWX-2	CER CORPORATION	7276.2	A	15295	8.4	8.1	0.00173		0.0442	0.0669	306.9	2.28	0.0284	8.72	2.28	0.99					
T649	Piceance	0504560011	MWX-2	CER CORPORATION	7319.7	A	13257	5.7	5.4	0.00193	0.0395	0.0717		455.6	2.10	0.0269	12.26	3.20	1.00					
T649	Piceance	0504560011	MWX-2	CER CORPORATION	7340.4	A	15275	2.1	1.8	0.000106		0.0326												
T649	Piceance	0504560011	MWX-2	CER CORPORATION	7350.4	A	15265	4.5	4.0	0.000372		0.0599												
T649	Piceance	0504560011	MWX-2	CER CORPORATION	7851.3	A	3.8	3.7	0.000244		0.0328	0.0463	385.3	1.78	0.0166	5.87	1.53	1.00						
T649	Piceance	0504560011	MWX-2	CER CORPORATION	7865.6	B	7.6	7.3	0.000505	0.0265	0.0535		100.4	1.76	0.0050	0.50	0.13	1.00						
T649	Piceance	0504560011	MWX-2	CER CORPORATION	7877.5	A	6.6	5.4	0.000910		0.0339	0.0632	1112	1.92	0.0205	1.13	0.30	1.00						
T649	Piceance	0504560011	MWX-2	CER CORPORATION	7880.1	A	7.6	7.0	0.00179	0.0502	0.0812		153.9	1.89	0.0190	2.00	0.52	1.00						
T649	Piceance	0504560011	MWX-2	CER CORPORATION	8117.9	A	6.5	5.9	0.00227		0.0699													
E393	Powder River	4900252627	1 BARLOW 21-20	LOUISIANA LAND & EXP	6969.7	B	15287	20.7	19.6	0.00118	0.1179	0.2064	0.3465	32.9	2.14	0.0284	0.93	0.24	1.00					
E393	Powder River	4900252627	1 BARLOW 21-20	LOUISIANA LAND & EXP	6969.9	A	15287	20.2	19.1	0.00120		0.1952	0.3420	32.1	2.10	0.0159	0.51	0.13	1.00					
E393	Powder River	4900252627	1 BARLOW 21-20	LOUISIANA LAND & EXP	6965.8	B	15295	5.4	5.0	0.00111		0.0288	0.0595	477.9	2.06	0.0168	8.03	2.10	1.00					
E393	Powder River	4900252627	1 BARLOW 21-20	LOUISIANA LAND & EXP	6995.8	A	15295	5.1	4.6	0.00115	0.0159	0.0251	0.0311	514.5	2.03	0.0116	5.97	1.56	0.96					
E393	Powder River	4900252627	1 BARLOW 21-20	LOUISIANA LAND & EXP	6996.0	A	15295	5.9	5.4	0.00143		0.0629												
E393	Powder River	4900252627	1 BARLOW 21-20	LOUISIANA LAND & EXP	6996.2	A	15295	7.1	6.2	0.00473	0.0290	0.0408	0.0548	294.9	2.05	0.0198	5.84	1.52	0.99					
E393	Powder River	4900252627	1 BARLOW 21-20	LOUISIANA LAND & EXP	7000.9	B	15587	17.4	16.3	0.000110	0.1041	0.1934	0.3271	33.8	1.94	0.0182	0.62	0.16	1.00					
E393	Powder River	4900252627	1 BARLOW 21-20	LOUISIANA LAND & EXP	7012.0	A	14276	6.2	6.1	0.000068		0.0577	0.0753	904.1	2.43	0.0563	50.90	13.29	0.79					
E393	Powder River	4900252627	1 BARLOW 21-20	LOUISIANA LAND & EXP	7039.2	B	14286	17.1	15.9	0.00011		0.621												
E393	Powder River	4900252627	1 BARLOW 21-20	LOUISIANA LAND & EXP	7039.4	A	14286	16.6	15.7	0.00011	0.1211	0.1842	0.3165	38.0	1.96	0.0385	1.46	0.38	1.00					
E393	Powder River	4900252627	1 BARLOW 21-20	LOUISIANA LAND & EXP	7053.0	A	14597	23.7	22.4															

Appendix 5
Summary Multisatinity Waxman-Smits Data
Analysis of Critical Permeability, Capillary Pressure and Electrical Properties for Mesaverde Tight Gas Sandstones from Western U.S. Basins
US DOE # DE-FC26-05NT42660 Final Scientific/Technical Report
Alan P. Byrnes, Robert M. Cluff, John C. Webb
website: <http://www.kgs.ku.edu/mesaverde>

USGS Library Number	Basin	API Number	Well Name	Operator	Depth ft	A/B/C	Rock Type Code	Routine Porosity %	Est. In situ Porosity %	Klinkenberg Gas Permeability mD	Brine salinity (Kppm) > Cw (rhhos) > Rw (ohmm) >				F* 1/slope of Co vs Cw	Salinity-independent Archie cementation exponent m*	BmaxQv/F* Co vs Cw	BmaxQv	Qv Approximate Caion Exchange Capacity per unit PV Bmax=3.83 (1/ohmm)(e/l)	Correlation Coefficient Co vs Cw r ²
											20	40	80	200						
											3.02	5.73	10.50	20.4						
S172	Uinta	43019XXX1	3 BOOK CLIFFS	USGS-CG	124.1	A	13219	15.2	13.8	0.1027	0.1105	0.2012	0.3456	0.2314	32.0	1.75	0.0183	0.59	0.15	1.00
S172	Uinta	43019XXX1	3 BOOK CLIFFS	USGS-CG	174.0	A	12217	7.0	6.4	0.000416										
S172	Uinta	43019XXX1	3 BOOK CLIFFS	USGS-CG	175.2	A	13257	19.9	18.5	0.00486										
S172	Uinta	43019XXX1	3 BOOK CLIFFS	USGS-CG	206.0	A	11219	10.6	9.8	0.00486										
S172	Uinta	43019XXX1	3 BOOK CLIFFS	USGS-CG	252.1	A	12217	14.9	13.8	0.1326										
S372	Uinta	43019XXX1	3 BOOK CLIFFS	USGS-CG	334.5	A	11219	3.6	3.2	0.000142										
S172	Uinta	43019XXX1	3 BOOK CLIFFS	USGS-CG	398.8	A	12239	10.9	9.5	0.0463		0.1219	0.1927	0.1391	71.6	1.81	0.0436	3.12	0.82	1.00
S174	Uinta	43019XXX2	4 BOOK CLIFFS	USGS-CG	161.7	A	12	11.2	11.2	0.0313				0.3724						
S174	Uinta	43019XXX2	4 BOOK CLIFFS	USGS-CG	183.4	A	12	9.8	9.0	0.1115				0.2327						
S174	Uinta	43019XXX2	4 BOOK CLIFFS	USGS-CG	184.5	A	14.2	13.5	13.5	0.2104	0.0832	0.1418	0.2436		46.7	1.92	0.0187	0.87	0.23	1.00
S174	Uinta	43019XXX2	4 BOOK CLIFFS	USGS-CG	189.2	A	21.0	19.5	19.5	5.65	0.1658	0.2541	1.0972		30.7	2.19	0.0674	2.07	0.54	1.00
S174	Uinta	43019XXX2	4 BOOK CLIFFS	USGS-CG	189.2	B	22.2	20.9	20.9	9.31	0.1658	0.2541	1.0972		30.7	2.19	0.0674	2.07	0.54	1.00
S174	Uinta	43019XXX2	4 BOOK CLIFFS	USGS-CG	189.3	A	21.9	20.6	20.6	6.12	0.1658	0.2541	1.0972		18.0	1.83	0.0050	0.09	0.02	1.00
DR3	Washakie	4903722304	3 DRIPPING ROCK	CELSIUS	12415.1	A	14.1	13.0	13.0	0.0276				0.2049						
DR3	Washakie	4903722304	3 DRIPPING ROCK	CELSIUS	12416.8	A	13.7	12.7	12.7	0.0271	0.0485	0.0731			110.2	2.28	0.0211	2.32	0.61	1.00
DR3	Washakie	4903722304	3 DRIPPING ROCK	CELSIUS	12422.2	A	7.5	6.9	6.9	0.000418			0.1049							
DR3	Washakie	4903722304	3 DRIPPING ROCK	CELSIUS	12428.1	A	12.0	11.1	11.1	0.00500			0.1524							
DR3	Washakie	4903722304	3 DRIPPING ROCK	CELSIUS	12439.1	A	10.8	10.3	10.3	0.00386	0.0391	0.0570	0.0884		151.7	2.21	0.0192	2.91	0.76	1.00
DR3	Washakie	4903722304	3 DRIPPING ROCK	CELSIUS	12441.8	A	10.3	9.2	9.2	0.00791			0.1204		216.2	2.25	0.0265	5.74	1.50	1.00
DR3	Washakie	4903722304	3 DRIPPING ROCK	CELSIUS	12448.3	A	9.4	9.2	9.2	0.00107			0.1280		242.1	2.30	0.0437	10.58	2.76	1.00
DR3	Washakie	4903722304	3 DRIPPING ROCK	CELSIUS	12452.8	A	7.6	7.3	7.3	0.00002	0.0254	0.0379	0.0539		266.1	2.13	0.0150	3.99	1.04	1.00
DR3	Washakie	4903722304	3 DRIPPING ROCK	CELSIUS	12453.7	A	5.5	5.3	5.3	0.000107	0.0305	0.0393			308.0	1.95	0.0207	6.38	1.66	1.00
DR5	Washakie	4903722355	5 DRIPPING ROCK	CELSIUS	12688.7	A	12.8	11.8	11.8	0.0120				0.1847						
DR5	Washakie	4903722355	5 DRIPPING ROCK	CELSIUS	12693.3	B	13.2	12.4	12.4	0.0151	0.0467	0.0740			99.3	2.20	0.0263	1.62	0.42	1.00
DR5	Washakie	4903722355	5 DRIPPING ROCK	CELSIUS	12704.2	B	10.6	10.1	10.1	0.00283	0.0534	0.0727	0.1130		124.6	2.10	0.0282	3.52	0.92	1.00
DR5	Washakie	4903722355	5 DRIPPING ROCK	CELSIUS	12704.2	A	11.4	11.1	11.1	0.00348			0.1666		175.9	2.35	0.0506	8.90	2.32	1.00
DR5	Washakie	4903722355	5 DRIPPING ROCK	CELSIUS	12713.7	A	8.7	8.2	8.2	0.000191	0.0359	0.0473	0.0831		155.1	2.02	0.0141	2.19	0.57	0.99
E489	Washakie	4903721053	3 UNIT FIVE MILE GULCH	AMOCO PRODUCTION	10608.7	A	4.3	3.9	3.9	0.00079			0.0562							
E489	Washakie	4903721053	3 UNIT FIVE MILE GULCH	AMOCO PRODUCTION	10610.2	A	6.6	6.4	6.4	0.000011			0.0775		428.9	2.21	0.0299	12.83	3.35	1.00
E489	Washakie	4903721053	3 UNIT FIVE MILE GULCH	AMOCO PRODUCTION	10612.0	B	6.3	6.1	6.1	0.000719	0.0305	0.0409			260.6	1.99	0.0189	4.93	1.29	1.00
E489	Washakie	4903721053	3 UNIT FIVE MILE GULCH	AMOCO PRODUCTION	10612.3	A	5.6	5.5	5.5	0.000145			0.0545		382.5	2.05	0.0249	9.52	2.49	0.96
E489	Washakie	4903721053	3 UNIT FIVE MILE GULCH	AMOCO PRODUCTION	10613.8	A	9.5	9.1	9.1	0.00140			0.1238		206.0	2.22	0.0235	4.84	1.26	1.00
E489	Washakie	4903721053	3 UNIT FIVE MILE GULCH	AMOCO PRODUCTION	10615.6	A	11.0	10.0	10.0	0.00814			0.1417		157.1	2.20	0.0120	1.89	0.49	1.00
E489	Washakie	4903721053	3 UNIT FIVE MILE GULCH	AMOCO PRODUCTION	10615.6	B	10.1	9.1	9.1	0.0117	0.0284	0.0437			177.1	2.16	0.0113	2.00	0.52	1.00
E489	Washakie	4903721053	3 UNIT FIVE MILE GULCH	AMOCO PRODUCTION	10615.8	A	4.3	4.0	4.0	0.00187			0.1393		171.2	2.18	0.0201	3.44	0.90	1.00
E489	Washakie	4903721053	3 UNIT FIVE MILE GULCH	AMOCO PRODUCTION	10627.0	A	2.3	2.0	2.0	0.00069			0.1393		115.1	1.80	0.0246	28.1	7.42	0.97
E489	Washakie	4903721053	3 UNIT FIVE MILE GULCH	AMOCO PRODUCTION	10634.0	A	3.3	3.1	3.1	0.000139			0.0301		210.4	2.20	0.0209	43.98	11.48	0.94
E489	Washakie	4903721053	3 UNIT FIVE MILE GULCH	AMOCO PRODUCTION	10634.0	B	2.2	2.0	2.0	0.000184	0.0128	0.0180	0.0274		504.8	1.62	0.0076	4.26	1.11	1.00
E489	Washakie	4903721053	3 UNIT FIVE MILE GULCH	AMOCO PRODUCTION	10636.2	A	5.4	5.2	5.2	0.00145			0.0673		345.6	1.98	0.0081	2.80	0.73	1.00
E489	Washakie	4903721053	3 UNIT FIVE MILE GULCH	AMOCO PRODUCTION	10650.0	A	6.2	6.0	6.0	0.00309			0.0370		432.2	2.16	0.0211	9.12	2.38	0.98
E489	Washakie	4903721053	3 UNIT FIVE MILE GULCH	AMOCO PRODUCTION	10651.0	A	4.3	4.0	4.0	0.00187			0.0622		508.8	1.94	0.0230	11.70	3.06	0.98
E489	Washakie	4903721053	3 UNIT FIVE MILE GULCH	AMOCO PRODUCTION	10658.1	A	8.4	7.7	7.7	0.00541			0.0882		253.9	2.16	0.0074	1.88	0.49	1.00
E489	Washakie	4903721053	3 UNIT FIVE MILE GULCH	AMOCO PRODUCTION	10662.1	A	6.2	5.9	5.9	0.00147			0.0732		354.3	2.07	0.0145	5.14	1.34	0.99
E489	Washakie	4903721053	3 UNIT FIVE MILE GULCH	AMOCO PRODUCTION	10662.5	A	4.7	4.4	4.4	0.000234			0.0455		503.8	1.99	0.0196	9.88	2.58	0.96
E489	Washakie	4903721053	3 UNIT FIVE MILE GULCH	AMOCO PRODUCTION	10666.3	A	8.4	8.2	8.2	0.000785			0.0903		324.6	2.31	0.0274	8.89	2.32	1.00
E489	Washakie	4903721053	3 UNIT FIVE MILE GULCH	AMOCO PRODUCTION	10668.2	A	7.9	7.5	7.5	0.00215			0.0447		284.6	2.18	0.0033	8.62	2.25	0.96
E489	Washakie	4903721053	3 UNIT FIVE MILE GULCH	AMOCO PRODUCTION	10668.2	B	7.9	7.4	7.4	0.00232	0.0241	0.0391	0.0612		203.1	2.04	0.0099	2.01	0.53	1.00
E489	Washakie	4903721053	3 UNIT FIVE MILE GULCH	AMOCO PRODUCTION	10669.0	A	6.7	6.1	6.1	0.00281			0.0570		476.2	2.31	0.0152	7.27	1.90	0.99
E489	Washakie	4903721053	3 UNIT FIVE MILE GULCH	AMOCO PRODUCTION	10670.9	A	8.7	7.6	7.6	0.0309			0.0341		187.8	2.03	0.0033	6.62	0.16	1.00
E489	Washakie	4903721053	3 UNIT FIVE MILE GULCH	AMOCO PRODUCTION	10675.3	A	10.4	9.6	9.6	0.0299			0.0533		187.1	2.23	0.0227	4.25	1.11	1.00
E489	Washakie	4903721053	3 UNIT FIVE MILE GULCH	AMOCO PRODUCTION	10675.4	A	10.1	9.1	9.1	0.0327			0.0497		178.0	2.16	0.0175	3.12	0.81	1.00
E489	Washakie	4903721053	3 UNIT FIVE MILE GULCH	AMOCO PRODUCTION	10675.5	A	10.2	9.2	9.2	0.0328			0.0429		219.5	2.26	0.0150	3.29	0.86	1.00
E489	Washakie	4903721053	3 UNIT FIVE MILE GULCH	AMOCO PRODUCTION	10675.8	A	10.1	9.4	9.4	0.0255			0.0428		163.4	2.16	0.0095	1.55	0.41	1.00
E489	Washakie	4903721053	3 UNIT FIVE MILE GULCH	AMOCO PRODUCTION	10682.0	A	10.2	9.8	9.8	0.00243			0.0812		221.2	2.32	0.0316	6.99	1.83	0.99
E489	Washakie	4903721053	3 UNIT FIVE MILE GULCH	AMOCO PRODUCTION	10682.3	A	9.2	8.9	8.9	0.00420			0.0537		217.6	2.23	0.0270	5.88	1.53	1.00
E489	Washakie	4903721053	3 UNIT FIVE MILE GULCH	AMOCO PRODUCTION	10683.4	A	2.6	2.5	2.5	0.000140			0.0166		3860.5	2.24	0.0151	58.29	15.22	1.00
E489	Washakie	4903721053																		

National Energy Technology Laboratory

626 Cochrans Mill Road
P.O. Box 10940
Pittsburgh, PA 15236-0940

3610 Collins Ferry Road
P.O. Box 880
Morgantown, WV 26507-0880

One West Third Street, Suite 1400
Tulsa, OK 74103-3519

1450 Queen Avenue SW
Albany, OR 97321-2198

2175 University Ave. South
Suite 201
Fairbanks, AK 99709

Visit the NETL website at:
www.netl.doe.gov

Customer Service:
1-800-553-7681

